Investigation on Neuroprotective Potential of Proteins Extracted from Leaves of *Orthosiphon stamineus*

CHUNG YIN SIR
Master of Biomedical Science, Monash University Malaysia

A thesis submitted for the degree of Doctor of Philosophy at
Monash University in 2020
Jeffrey Cheah School of Medicine and Health Sciences, Monash University Malaysia

Copyright notice

Abstract

Many of the central nervous system disorders lack complete cure and the management of these conditions is still a challenging task. The key hallmarks in most of these conditions are neurotoxicity and neurodegeneration. Consequently, neuroprotection is being explored as an alternative treatment strategy. *Orthosiphon stamineus* (OS; cat's whiskers; "misai kucing") is a medicinal plant with its primary metabolites remain unexplored. This study investigates the neuroprotective potential of proteins extracted from OS leaves (OSLP) on human SH-SY5Y cell model and adult zebrafish (*Danio rerio*). OSLP was successfully extracted using One-Tube Method. Proteomics analysis has identified the different protein compositions present in OSLP. Functional annotation analysis has classified them into 49 protein families, 21 cellular components and 23 types of molecular function. They involved in diverse biological processes encompassing protein homeostasis, trafficking, signalling, metabolic processes, energy metabolism, defence responses and gene transcriptions. Findings of the SH-SY5Y cell model induced by hydrogen peroxide (H_2O_2) have demonstrated the neuroprotective potential of OSLP. OSLP pre-treatment (1000 µg/mL; 24-h) increased the survival of H_2O_2-induced cells (57%; 150 µM H_2O_2). Mass spectrometry (MS)-based proteomics and bioinformatics analysis have proposed OSLP neuroprotective potential is modulated by three pathways, namely the "Signaling of Interleukin-4 and Interleukin-13", "Attenuation Phase" and "HSP90 Chaperone Cycle for Steroid Hormone Receptors". Findings of the zebrafish model induced by pentylenetetrazol (PTZ, 170 mg/kg) have demonstrated the neuroprotective potential of OSLP as an anticonvulsant. OSLP was safe up to 800 µg/kg. OSLP-treated PTZ-induced zebrafish (800 µg/kg, i.p., 30 min) had improvements in the seizure profile (lower score and prolonged onset time) and locomotor behaviors. OSLP modulated excitatory glutamate (Glu) and had increased brain protein Complexin 2 (Cplx2) expressions. MS-based proteomics and bioinformatics analysis have proposed the role of Cplx2 involved in the regulation of calcium-dependent synaptic vesicle exocytosis via "Synaptic Vesicle Cycle" pathway for the neuroprotective potential of OSLP. Whilst, OSLP pre-treatment (800 µg/kg i.p., 30 min) had demonstrated a subtle anticonvulsive effect in the zebrafish model of double challenge (hypoxia induction, 15-18 min on average; PTZ injection, 170 mg/kg). OSLP pre-treatment showed

improvements in seizure profile, locomotor behaviors, neurotransmitter profile (lower Glu levels), and increased brain protein glutamine synthetase (Glula) expression. Glula encodes for glutamine synthetase which is required to keep the GABA-Glu-Gln (glutamine) cycle in check. OSLP also increased Enolase 2 and Isocitrate dehydrogenase 2 expressions in the hypoxic but seizure-free zebrafish. These proteins promote anaerobic metabolism in neurons under hypoxic conditions. Taken together, OSLP is suggested to influence the synaptic transmission by providing hypoxic-ischaemic tolerance to the synapses via the “Glutamatergic Synapse” and “GABAergic Synapse” pathways, in addition to modulating cellular energy metabolism via the “HIF-1 Signalling” and “Citrate Cycle” pathways. Overall, this study provides evidence on the neuroprotective potential of OSLP in neuronal cells and adult zebrafish.

Publications during enrolment

1. **Yin-Sir Chung**, Brandon Kar-Meng Choo, Pervaiz Khalid Ahmed, Iekhsan Othman, Mohd. Farooq Shaikh. *Orthosiphon stamineus* Proteins Alleviate Pentylenetetrazol-Induced Seizures in Zebrafish. *Biomedicines*. 2020; 8(7):191.
2. **Yin-Sir Chung**, Brandon Kar-Meng Choo, Pervaiz Khalid Ahmed, Iekhsan Othman, Mohd. Farooq Shaikh (2020). A Systematic Review of the Protective Actions of Cat's Whiskers (Misai Kucing) on the Central Nervous System. *Frontiers in Pharmacology*, 11, 692. https://doi.org/10.3389/fphar.2020.00692
3. Lin-Lin Lee V, Kar-Meng Choo B, **Yin-Sir Chung,** Kundap UP, Kumari Y, Shaikh M (2018). Treatment, Therapy and Management of Metabolic Epilepsy: A Systematic Review. International Journal of Molecular Sciences. 19(3):871. https://doi.org/10.3390/ijms19030871

Declaration

I hereby declare that this thesis contains no material which has been accepted for the award of any other degree or diploma at any university or equivalent institution and that, to the best of my knowledge and belief, this thesis contains no material previously published or written by another person, except where due reference is made in the text of the thesis.

This thesis includes (2) original papers published in peer-reviewed journals and (3) submitted publications. The core theme of the thesis is Investigation on Neuroprotective Potential of Proteins Extracted from Leaves of *Orthosiphon stamineus*. The ideas, development and writing up of all the papers in the thesis were the principal responsibility of myself, the student, working within the Jeffrey Cheah School of Medicine and Health Sciences under the supervision of Dr. Mohd. Farooq Shaikh, Prof. Iekhsan Othman, and Prof. Pervaiz Khalid Ahmed.

The inclusion of co-authors reflects the fact that the work came from active collaboration between researchers and acknowledges input into team-based research.

In the case of Chapters 1 and 5, my contributions to the work involved the following:

Thesis Chapter	**Publication Title**	**Status** *(published, in press, accepted or returned for revision, submitted)*	**Nature and % of student contribution**	**Co-author name(s) Nature and % of Co-author's contribution***	**Co-author(s), Monash student Y/N***
1	*A Systematic Review of the Protective Actions of Cat's Whiskers (Misai Kucing) on the Central Nervous System*	*Published*	*60%. designed, collected and analysed the data, and wrote the manuscript*	*1) Brandon Kar Meng Choo, contributed to data collection and analysis as well as writing and revising the manuscript, 25%* *2) Mohd. Farooq Shaikh, conceptualised, edited and revised the review, and supervised all aspects of the study, 5%* *3) Iekhsan Othman supervised all*	*Yes* *No* *No*

				aspects of the study and edited the review, 5% *4) Pervaiz Khalid Ahmed supervised all aspects of the study and edited the review, 5%*	
2	*Extraction and Characterisation of Orthosiphon stamineus Proteins*	*Submitted*	*70%. designed, performed all the experiments, analysed all the data, wrote and reviewed the manuscript*	*1) Syafiq Asnawi Zainal Abidin, helped edited the final manuscript as submitted, 5%* *2) Mohd. Farooq Shaikh, supervised all aspects of the study, edited and reviewed the final manuscript as submitted, 10%* *3) Iekhsan Othman supervised all aspects of the study, edited and reviewed the final manuscript as submitted, 10%* *4) Pervaiz Khalid Ahmed, aided in supervision and helped edit the final manuscript as submitted, 5%*	*No* *No* *No* *No*
3	*Orthosiphon stamineus Proteins Alleviate Hydrogen Peroxide Stress in SH-SY5Y Cells*	*Submitted*	*70%. designed, performed all the experiments, analysed all the data, wrote and reviewed the manuscript*	*1) Mohd. Farooq Shaikh, supervised all aspects of the study, edited and reviewed the final manuscript as submitted, 15%* *2) Iekhsan Othman supervised all aspects of the study and edited the final manuscript as submitted, 10%* *3) Pervaiz Khalid Ahmed, aided in supervision and helped edit the final manuscript as submitted, 5%*	*No* *No* *No*
4	*Orthosiphon stamineus Proteins Alleviate Pentylenetetrazol-Induced Seizures in Zebrafish*	*Published*	*60%. designed, performed all the experiments, analysed all the data, wrote and*	*1) Brandon Kar Meng Choo, helped in the behavioural experiments, edited and reviewed the final manuscript submitted, 25%* *2) Mohd. Farooq Shaikh, contributed*	*Yes* *No*

			reviewed the manuscript	*to the design of research, supervised all aspects of the study and edited the final manuscript as submitted, 5%* *3) Iekhsan Othman supervised all aspects of the study and edited the final manuscript as submitted, 5%* *4) Pervaiz Khalid Ahmed, aided in supervision and helped edit the final manuscript as submitted, 5%*	*No* *No*
5	*Orthosiphon stamineus Proteins Provide Hypoxic-Ischaemic Tolerance to Zebrafish Challenged by Hypoxia and Pentylenetetrazol-Induced Seizures*	*Submitted*	*60%. designed, performed all the experiments, analysed all the data, wrote and reviewed the manuscript*	*1) Brandon Kar Meng Choo, helped in the behavioural experiments, edited and reviewed the final manuscript submitted, 25%* *2) Mohd. Farooq Shaikh, contributed to the design of research, supervised all aspects of the study and edited the final manuscript as submitted, 5%* *3) Iekhsan Othman supervised all aspects of the study and edited the final manuscript as submitted, 5%* *4) Pervaiz Khalid Ahmed, aided in supervision and helped edit the final manuscript as submitted, 5%*	*Yes* *No* *No* *No*

**If no co-authors, leave fields blank*

I have renumbered sections of submitted or published papers in order to generate a consistent presentation within the thesis.

Student name: Chung Yin Sir

Student signature: Date: 30 June 2020

I hereby certify that the above declaration correctly reflects the nature and extent of the student's and co-authors' contributions to this work. In instances where I am not the responsible author, I have consulted with the responsible author to agree on the respective contributions of the authors.

Main Supervisor name: Mohmad Farooq Shaikh

Main Supervisor signature: **Date:** 10 July 2020

Acknowledgements

My deepest gratitude and love to my family whom I am most indebted to. They have been supporting me unconditionally throughout the years. I would like to especially pen down the forbearance of my beloved late father who tolerated my imperfection. You remain a wonderful father to me and no words can best depict my love and appreciation for all you had done for me. Because of you, I am who I am today. Time flies but we all have never ceased missing you since your decease in last 2013. In loving memories, father, you will always be part of me.

My deepest appreciation for my main supervisor, Dr. Mohmad Farooq Shaikh, and my co-supervisors, Professor Iekhsan Othman and Professor Pervaiz Khalid Ahmed. They have been there for me all the ways, patiently advising and pushing me along the way until I have finally reached this critical end. They offered their constant support and guidance in my research endeavors. Without their care, love, assistance and supervision, this dissertation would not have been possible. They remain as the best mentors in my life. Also, I would like to especially thank Associate Professor Rakesh Naidu and Dr. Tang Kim-Sang for their constant encouragement and help throughout the years in my research endeavors.

Another wonderful soul is Brandon KM Choo who never failed to lend me his helping hand at the time I needed most. Thank you for your unconditional support, both spiritual and physical, throughout my research endeavors. Not forgetting Wesley See Zhi-Chung, Vanessa Lee Lin-Lin, Ooi Man-Kwan, Tan Yiing-Jye, Lee Yee-Qian, Sugita Kunalan and Dr. Tan Jey-Sern. Working with you all was a valuable experience with loads of fond memories.

I especially appreciate Dr. Syafiq Asnawi Bin Zainal Abidin, Nurziana Sharmilla Binti Nawawi and Tee Ting-Yee (former) of LC-MS/MS platform of Monash University Malaysia who have been supportive in the proteomics work. Thanked for technical assistance and experience sharing. It is also a pleasure to acknowledge Dr. Muhamad Rusdi Bin Haji Ahmad Rusmili, Associate Professor Sharifah Syed Hassan and Dr. Kyi-Kyi Thar. All of you have given me great inspiration and help throughout the years.

I also thank my colleagues in the Medical Research Laboratories 1, 2, 3 and 5 or their kind-hearted help and lovely friendship. I especially appreciate the Neuropharmacology Laboratory members. Special thanks also go to Camelia Minoot and the School Research Office - Kong Li San and the staff. Not forgetting Mr. Ragavan s/o Murugiah (School of Science), Mr. Andrew Leong Kum-Loong and Mr. Zulkhaili bin Zainal Abidin from the animal facility of Monash University Malaysia. The technical team is also thanked for their support throughout the years.

Last but not least, I would like to convey my gratitude to Monash University Malaysia for the scholarships and financial support respectively.

This Ph.D. thesis is dedicated to my late father whom I am most indebted to. Time flies but I could never cease missing you since your decease in 2013. In loving memories, father, you will always be part of me.

Table of Contents

List of Abbreviations

B.W.	Body weight
CHAPS	3-[(3-cholamidopropyl)dimethylammonio]-1-propanesulfonate
DZP	Diazepam
ESI	Electrospray ionisation
FDR	False Discovery rate
GABA	Gamma-Aminobutyric acid,
Glu	Glutamate
Gln	Glutamine
GO	Gene Ontology
H_2O_2	Hydrogen peroxide
I.P.	Intraperitoneal injection
KAAS	KEGG Automatic Annotation Server
KEGG	Kyoto Encyclopedia of Genes and Genomes
KO	KEGG Orthology
LC-MS/MS	Liquid-chromatography tandem mass spectrometry
LFQ	Label-free proteomics quantification
LN_2	Liquid nitrogen
M.W.	Molecular weight
M/Z	Mass to charge ratio
MALDI	Matrix assisted laser desorption ionisation
MTBE	Methyl tert-butyl ether
MTT	3-[4,5-dimethylthiazole-2-yl]-2,5-diphenyltetrazolium bromide
$NADP^+$	Oxidised nicotinamide adenine dinucleotide phosphate
NADPH	Reduced nicotinamide adenine dinucleotide phosphate
NCBInr	National Center for Biotechnology Information non-reduntant sequence database
OSLP	*Orthosiphon stamineus* leaf protein
OTM	One-Tube Method
PTZ	Pentylenetetrazol

QQQ	Triple quadrupole
QTOF	Quadrupole time-of-flight
RT	Retention time
UniProt	Universal Protein Resource
UniProtKB	Universal Protein Knowledgebase
ZFIN	Zebrafish Information Network

Chapter 1

General Introduction and Literature Review

1.1 Introduction

Neurological disorders are the leading cause of disability and the second leading cause of death worldwide. Over the past 25 years, the absolute number of people affected by or remaining disabled from neurological disorders has surged globally (Feigin et al., 2017; G. B. D. Neurology Collaborators, 2019). Although there are many conventional drugs available however, some patients fail to respond adequately to the treatment, or they have tolerability issues due to adverse effects. Some of them have turned to alternative interventions especially traditional and complementary medicine (T&CM) as well as herbal medicine. Owing to their health protection backed by well-established evidence, herbal medicines have come under the limelight in the search for novel central nervous system (CNS) treatment.

Orthosiphon stamineus (OS) or *Orthosiphon aristatus var. aristatus* (OAA) is commonly known as cat's whiskers or "misai kucing". As a folk medicine in Southeast Asia, the aerial leaves of OS are dried and used as a herbal remedy (Gan et al., 2017). In modern medicine, hundreds of bioactive phytochemicals of OS are successfully characterized. Amongst, the most prominent are flavonoids (i.e. sinensetin, eupatorin, 3'-hydroxy-5,6,7,4'-tetramethoxyflavones), phenylpropanoids (i.e. rosmarinic acid, caffeic acid) and terpenoids (i.e. orthosiphols A-Z, orthosiphones A-D, siphonols A-E, ursolic acid, hydroxybetullinic acid). These secondary metabolites, justified by the plethora of pharmacological studies, are shown to have diverse biological activities such as cognitive-enhancing (Z.-L. Huang et al., 2005), anti-inflammatory and antioxidative, to name a few (Adnyana, Setiawan, & Insanu, 2013; Ameer, Salman, Asmawi, Ibraheem, & Yam, 2012; Ashraf, Sultan, & Adam, 2018).

Neurological disorders may occur through a single or a wide variety of mechanisms, sharing some commonalities such as abnormal protein behavior, oxidative stress, mitochondrial dysfunction, neuroinflammation, neuroexcitation and others (Jellinger, 2010). These varied mechanisms result in an equally varied array of disorders such as epilepsy, motor neuron disease, multiple sclerosis and neurodegenerative diseases including Parkinson's and Alzheimer's, to name a few (Vajda, 2004). Although there remain gaps in understanding the complex interactions underlying neurological disorders, the ultimate goal is to better preserve CNS functions. In view of that, neuroprotection worth being considered as a possible

treatment strategy for CNS dysfunctions. For centuries, OS has widely been trusted as an important medicinal plant with substantial natural goodness on health in many traditional medicine systems (Adnyana et al., 2013; Sawaya & Poupelloz, 2011). With all the science-backed evidence, OS is worthwhile to be explored as a dietary complement to supporting a healthy lifestyle or used as an alternative to mitigate ailments of which the conventional medicine cannot meet the expected clinical effectiveness.

The present chapter is a comprehensive systematic literature review of the neuroprotective potential of OS on the CNS disorders. Hence, the objectives of this chapter are:

1. To explore the pharmacological actions underlying the neuroprotective potential of OS on various neurological disorders
2. To propose the future discovery of novel neuroprotection of OS using its primary metabolites

References:

Adnyana, I. K., Setiawan, F., & Insanu, M. (2013). From ethnopharmacology to clinical study of *Orthosiphon stamineus* Benth. *Int. J. Pharm. Pharm. Sci., 5*(3), 66.

Ameer, O. Z., Salman, I. M., Asmawi, M. Z., Ibraheem, Z. O., & Yam, M. F. (2012). *Orthosiphon stamineus*: traditional uses, phytochemistry, pharmacology, and toxicology. *J. Med. Food., 15*. doi:10.1089/jmf.2011.1973

Ashraf, K., Sultan, S., & Adam, A. (2018). Orthosiphon stamineus Benth. is an Outstanding Food Medicine: Review of Phytochemical and Pharmacological Activities. *Journal of pharmacy & bioallied sciences, 10*(3), 109-118. doi:10.4103/jpbs.JPBS_253_17

Feigin, V. L., Abajobir, A. A., Abate, K. H., Abd-Allah, F., Abdulle, A. M., Abera, S. F., . . . Aichour, I. (2017). Global, regional, and national burden of neurological disorders during 1990–2015: a systematic analysis for the Global Burden of Disease Study 2015. *The lancet neurology, 16*(11), 877-897.

G. B. D. Neurology Collaborators. (2019). Global, regional, and national burden of neurological disorders, 1990-2016: a systematic analysis for the Global Burden of Disease Study 2016. *The Lancet. Neurology, 18*(5), 459-480. doi:10.1016/S1474-4422(18)30499-X

Gan, S. H., Chua, L. S., Aziz, R., Baba, M. R., Abdullah, L. C., Ong, S. P., & Law, C. L. (2017). Drying Characteristics of *Orthosiphon stamineus* Benth by Solar Assisted Heat Pump Drying. *Drying Technology*, null-null. doi:10.1080/07373937.2016.1275673

Huang, Z.-L., Qu, W.-M., Eguchi, N., Chen, J.-F., Schwarzschild, M. A., Fredholm, B. B., . . . Hayaishi, O. (2005). Adenosine A2A, but not A1, receptors mediate the arousal effect of caffeine. *Nature neuroscience, 8*(7), 858-859.

Jellinger, K. A. (2010). Basic mechanisms of neurodegeneration: a critical update. *Journal of cellular and molecular medicine, 14*(3), 457-487. doi:10.1111/j.1582-4934.2010.01010.x

Sawaya, R. A., & Poupelloz, J. V. (2011). Assessment report on Orthosiphon stamineus Benth., folium. *UK: European Medicines Agency, European Union*.

Vajda, F. J. E. (2004). Neuroprotection and neurodegenerative disease. In *Alzheimer's Disease* (pp. 235-243): Springer.

frontiers in Pharmacology

SYSTEMATIC REVIEW
published: 13 May 2020
doi: 10.3389/fphar.2020.00692

A Systematic Review of the Protective Actions of Cat's Whiskers (Misai Kucing) on the Central Nervous System

*Yin-Sir Chung[1,2], Brandon Kar Meng Choo[1], Pervaiz Khalid Ahmed[3,4], Iekhsan Othman[1,2] and Mohd. Farooq Shaikh[1]**

[1] Neuropharmacology Research Strength, Jeffrey Cheah School of Medicine and Health Sciences, Monash University Malaysia, Bandar Sunway, Malaysia, [2] Liquid Chromatography-Mass Spectrometry (LCMS) Platform, Jeffrey Cheah School of Medicine and Health Sciences, Monash University Malaysia, Bandar Sunway, Malaysia, [3] School of Business, Monash University Malaysia, Bandar Sunway, Malaysia, [4] Global Asia in the 21st Century (GA21), Monash University Malaysia, Bandar Sunway, Malaysia

OPEN ACCESS

Edited by:
Adolfo Andrade-Cetto, National Autonomous University of Mexico, Mexico

Reviewed by:
Sayeed Ahmad, Jamia Hamdard University, India
Andy Wai Kan Yeung, The University of Hong Kong, Hong Kong

***Correspondence:**
Mohd. Farooq Shaikh
farooq.shaikh@monash.edu

Specialty section:
This article was submitted to Ethnopharmacology, a section of the journal Frontiers in Pharmacology

Received: *28 February 2020*
Accepted: *27 April 2020*
Published: *13 May 2020*

Citation:
Chung Y-S, Choo BKM, Ahmed PK, Othman I and Shaikh MF (2020) A Systematic Review of the Protective Actions of Cat's Whiskers (Misai Kucing) on the Central Nervous System. Front. Pharmacol. 11:692. doi: 10.3389/fphar.2020.00692

Orthosiphon stamineus (OS) or *Orthosiphon aristatus* var. *aristatus* (OAA) is commonly known as cat's whiskers or "misai kucing". It is an herbaceous shrub that is popular in many different traditional and complementary medicinal systems. Its popularity has been justified by the plethora of studies that have shown that the secondary metabolites of the plant has effects that range from anti-inflammatory and gastroprotective to anorexic and antihypertensive. As such, OS could also be a potential treatment for Central Nervous System (CNS) disorders. However, a cohesive synthesis of the protective actions of OS was lacking. This systematic review was therefore commenced to elaborate on the various protective mechanisms of OS in the CNS. The PRISMA model was used and five databases (Google Scholar, SCOPUS, SpringerLink, ScienceDirect, and PubMed) were searched with relevant keywords to finally identify four articles that met the inclusion criteria. The articles described the protective effects of OS extracts on Alzheimer's disease, epilepsy, learning and memory, oxidative stress, and neurotoxicity. All the articles found were experimental or preclinical studies on animal models or *in vitro* systems. The reported activities demonstrated that OS could be a potential neuroprotective agent and might improve CNS conditions like neurodegeneration, neuroinflammation, and oxidative stress.

Keywords: *Orthosiphon stamineus*, central nervous system, neuroprotection, neurotoxicity, oxidative stress

INTRODUCTION

Neuroprotection is a relatively new concept in neuroscience research, coined to incorporate a great variety of mechanisms that aim to prevent neuronal injury and loss of various brain functions with an ultimate goal to better preserve brain function (Schapira, 2010). Thus, neuroprotection is being explored as a possible treatment strategy for Central Nervous System (CNS) disorders such as neurodegeneration, stroke, or trauma that result in CNS injuries (Lalkovičová and Danielisová, 2016). These disorders may

occur through a wide variety of mechanisms, although some common themes include abnormal protein behavior, oxidative stress, mitochondrial dysfunction, neuroinflammation, excitotoxicity, and others (Jellinger, 2010). These varied mechanisms result in an equally varied array of disorders such as epilepsy, motor neuron disease, Parkinson's disease, multiple sclerosis, and Alzheimer's disease (Vajda, 2004). Neurological disorders remain as one of the greatest threats to public health. There are several gaps in understanding the many issues related to neurological disorders, but we already know enough about their nature and treatment to be able to shape effective intervention responses to some of the most prevalent among them.

In the search for novel CNS treatments, medicinal plants are worthy of attention as they have been used as natural remedies since the dawn of civilization due to their substantial protective effects on human health. Thus, the different traditional medicinal systems practiced by the diverse communities worldwide may contain clues pointing towards natural remedies or an effective cure. Among these systems are the Sowa Rigba in Bhutan, Jamu in Indonesia, Ayuverda and Unani in India, Bangladesh, Nepal and Sri Lanka, homeopathy practices in European societies, Islamic Traditional Medicine among Muslims, Traditional Chinese Medicine among the Chinese, and Koryo Medicine among the Koreans (World Health Organization, 2013). Even today, medicinal plants still have significant roles to play in not only addressing various health issues, but also in supporting a healthy lifestyle. In modern medicine, extensive research evidence has shown that many plant-derived secondary metabolites have notable protective effects on the CNS (Edeoga et al., 2005; Rabiei, 2017; Manchishi, 2018). For instance, discovered in the 1940s, reserpine which is an indole alkaloid (Gurib-Fakim, 2006; Abdelfatah and Efferth, 2015) isolated from the roots of *Rauwolfia serpentina* (Indian snakeroot) was an antipsychotic used to treat schizophrenia in the past (Nur and Adams, 2016) and has heralded the beginning of a new era of drug treatment for mental disorders. Cannabis-based products such as cannabidiol (CBD) is another candidate in the spotlight for its efficacy and safety for treating different forms of epilepsy (See completed cannabidiol clinical trials in epilepsy https://clinicaltrials.gov/) (Perucca, 2017; Silvestro et al., 2019).

Orthosiphon stamineus (OS) or *Orthosiphon aristatus* var. *aristatus* (OAA), is commonly known as cat's whiskers or "misai kucing". Belonging to the *Lamiaceae* family, it is a perennial, herbaceous medicinal shrub that stands 30 to 150 cm tall and is ubiquitous in the temperate and tropical areas of Asia, Australia, and the Pacific. The stamens and pistil can grow as far as 2 cm beyond the flower clusters during full bloom to form a shape that is reminiscent of cat whiskers (Sawaya and Poupelloz, 2011; Ameer et al., 2012; Adnyana et al., 2013). OS is believed to originate in South East Asia and is unsurprisingly known by a myriad of local names such as java tea (English common name), "neko no hige" (Japan), "mao xu cao" (China), "se-cho" or "myit-shwe" (Myanmar); "rau-meo" (Vietnam) and "yaa-nuad-maew" or "pa-yab-mek" (Thailand), "misai kucing", "ruku hutan", or cat's whisker (Malaysia), "kumis kucing", "kutum", "mamam", "bunga laba-laba", "remuk jung/remujung", "songot koceng" and "sesalaseyan" (Indonesia); "kabling gubat/kabling parang" (Philippines). It is a popular medicinal plant due to its widespread and prolonged used in many traditional and complementary medicinal systems across many South East Asian and European countries for the prevention and treatment of disorders such as rheumatism, diabetes, hypertension, and epilepsy among many others (Sawaya and Poupelloz, 2011; Adnyana et al., 2013). OS has been reported to be anorexic (Son et al., 2011), diuretic, hypouriceamic and antiurolithic; anti-inflammatory, analgesic and antipyretic; antioxidative, hepatoprotective, nephroprotective, gastroprotective, cardiovascular-protective, hypolipidaemic, antihypertensive and anti-obesity; hypoglycaemic, antiproliferative, cytotoxic and anti-angiogenic; antimicrobial and also has anti-sebum activity (Ameer et al., 2012; Adnyana et al., 2013). Given its traditional use as a treatment for epilepsy (which is a CNS disorder) and that the ability of OS to counteract oxidative stress and inflammation [which are both implicated in CNS disorders (Kamat et al., 2008; Amor et al., 2010)], OS could have the potential to be neuroprotective. However, while there are extensive reviews of OS, both narrative and systematic, reviews on neuroprotective potential of OS was however found to be lacking. Hence, a comprehensive systematic literature review was commenced to address this shortcoming and to elaborate on the protective actions of OS on the CNS.

MATERIALS AND METHODS

Search Method

Five databases (Google Scholar, SCOPUS, SpringerLink, ScienceDirect, and PubMed) were searched to identify relevant articles using the keywords "*Orthosiphon stamineus* AND Brain Protection" and "*Orthosiphon stamineus* AND CNS". The common term *Orthosiphon stamineus* was used as the alternative name for *Orthosiphon aristatus* as this term typically produces more search results. The results were then filtered to include only studies between January 2009 and December 2019 to maximise the inclusion of more recent publications in this review, while minimizing the possibility of inadvertently excluding older studies. SCOPUS and ScienceDirect results were exported as RIS files, Google Scholar results were exported using Harzing's Publish or Perish 7 into RIS files, SpringerLink results were individually exported as RIS files and PubMed results were exported as nbib files. All the exported files were then imported into EndNote X9.2 to generate a library, which was then exported as a text file in the EndNote Export style. The text file was then imported into Rayyan (Ouzzani et al., 2016) and the generated list of unique entries (software identified duplicates were automatically excluded) were screened for their relevance based on their title and abstract.

Study Selection and Inclusion Criteria

Only original research articles were considered for their content for this systematic review as other publication types would not have provided sufficient information for evaluation and comparison. Any duplicated results that were missed by Rayyan were also removed, as well as those that have no

relevance to OS or the field of neuroscience. The result selection process was conducted as per the PRISMA guidelines (Moher et al., 2015).

RESULTS

Searching the aforementioned databases using the chosen keywords resulted in a total of 781 records. Of the 781 records, 737 records were from Google Scholar, 0 from SCOPUS, 20 from SpringerLink and 24 Science Direct and 0 from PubMed. After applying exclusion criteria, 777 records were removed, which includes 101 duplicates and 676 articles not related to the scope of the review (**Figure 1**). The remaining four records underwent full text evaluation and no further records were removed as all four records were found to be relevant. The four articles are summarized in **Table 1** and discussed in the present systematic review.

HPLC analysis of an ethanolic OS extract for seven reference compounds by George et al. (2015) showed that their standardised extract contained ombuin (3,3′,5-trihydroxy-4′,7-dimethoxyflavone) (0.14%), 3′-hydroxy-4′,5,6,7-tetramethoxyflavone (0.10%), sinensetin (0.07%), orthosiphol B (0.26%), orthosiphol A (0.67%), staminol A (0.45%), and orthosiphonone A (0.12%) as shown in **Figure 2**. A summary of the preparations used in each of the selected articles is given in **Table 2**.

OS and Alzheimer's Disease

Alzheimer's disease (AD) is an age-related neurodegenerative disorder that leads to cognitive, functional and behavioral alterations (Cummings et al., 2018). The cause of Alzheimer's disease is currently unknown, but is believed to result from a variety of factors such as an abnormal accumulation of beta-amyloid, death of cholinergic neurons, aggregation of microtubule tau proteins, metal dyshomeostasis, and metal-induced oxidative stress (Simunkova et al., 2019). As compared to rats given only 1 mg/kg of scopolamine, an ethanolic extract of OS has been shown by Retinasamy et al. (2019) to enhance memory when given to rats in a scopolamine-induced amnesia model which mimics the memory impairment in human Alzheimer's patients. They believed that the effects of the extract could be due to its positive modulation of the *CREB1* (cAMP response element-binding protein), *BDNF* (Brain-derived neurotrophic factor), and *TrKB* (Tropomyosin receptor kinase B) genes which are involved in memory, as BDNF binds to the TrKB receptor with a high affinity.

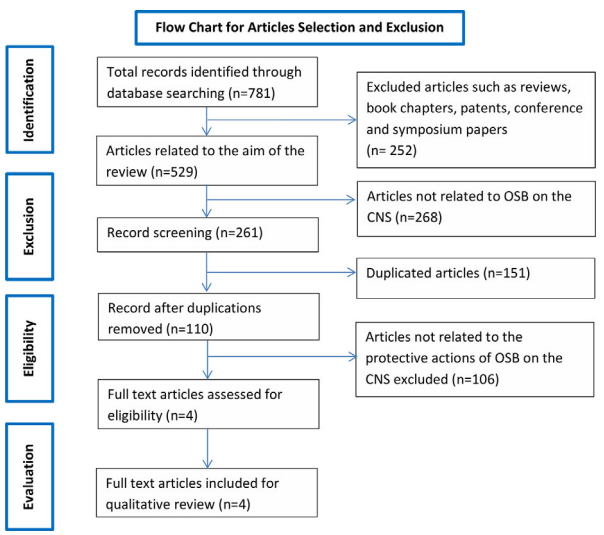

FIGURE 1 | Flow chart of the study selection criteria based on the Preferred Reporting Items for Systematic Reviews and Meta-Analyses (PRISMA) guidelines.

Epilepsy

Epilepsy is a CNS disorder that afflicts approximately one in every hundred people, with about half of those cases being idiopathic (Holland, 2014). Epileptic seizures are a short-term appearance of various signs and/or symptoms due to unusually excessive or concurrent brain activity (Fisher et al., 2014). Seizures can affect memory, cognition, behavior, or emotional state among others, though not always in tandem (Fisher et al., 2005). As compared to zebrafish given 170 mg/kg of the pro-convulsant pentylenetetrazol only, OS extract has been shown by Choo et al. (2018) to have anti-seizure properties in an adult zebrafish model of pentylenetetrazol induced acute seizures. Choo et al. (2018) remarked that OS extract appears to prevent the upregulation of NF-*kB* (Nuclear Factor kappa-light-chain-enhancer of activated B cells) and *NPY* (Neuropeptide Y), which was puzzling as the upregulation of both genes is associated with a decrease in seizure threshold (Lubin et al., 2007; Wickham et al., 2019). Choo et al. (2018) postulated that these two pathways were not activated in the presence of OS as it exerted its anti-seizure activity *via* one or more other mechanisms. They suggested that one of these mechanisms could be at least partially due to the downregulation of *TNFα* (Tumor Necrosis Factor alpha).

Learning and Memory

In the CNS, endogenous adenosine receptors have been associated with an array of functions including sleep and arousal, cognition, learning and memory, protection from neuronal damage and degeneration as well as influencing neuronal maturation (Chen et al., 2007). Adenosine receptors (AR) belong to the G-protein-coupled receptor family (Fredholm et al., 1999) and their antagonism can produce CNS-enhancing effects. Adenosine is known to modulate cognitive functions through the adenosine receptors A_1 (A1R) and adenosine A_{2A} (A2AR). The selective blockade of A1R and A2AR can facilitate learning and memory in *in vivo* models (Pereira et al., 2002; Takahashi et al., 2008). A proprietary standardized ethanolic OS leaf extract has been shown to have memory-enhancing properties in Sprague Dawley rats possibly by reversing age-related deficits in short-term social memory and due to involvement of adenosine A_1 and adenosine A_{2A} as a target bioactivity site in the restoration of memory (George et al., 2015). They determined this *via in vitro* binding assays (A2A binding assay, A1 and A2A functional agonist and antagonist activity assays) which showed that an OS concentration of 150 μg/ml was

TABLE 1 | Summary of studies reported for neuroprotective effects of *Orthosiphon stamineus* Benth.

Study details	Study design and model	Testing dose	Active constituents	Administration route	Pharmacological actions	Summary of findings
Retinasamy et al. (2019)	*in vivo* (adult Sprague Dawley rats)	50, 100 and 200 mg/kg	Not mentioned	Oral and intraperitoneal (i.p., at a volume corresponding to 0.1 mL/100 g of b.w.)	Anti-AD *via* the BDNF-TrKB and CREB-BDNF pathways and can promote hippocampal neurogenesis	Ethanolic extract of OS might be a promising candidate as a memory enhancer or as a therapeutic treatment for neurodegenerative diseases like AD
Choo et al. (2018)	*in vivo* (adult *Danio rerio*)	50, 100 and 200 mg/L	Not mentioned	Oral	Anti-convulsive and anti-inflammatory *via* TNFα pathway	Ethanolic leaf extract of OS has the potential to be a novel symptomatic treatment for epileptic seizures as it is pharmacologically active against seizures in the zebrafish
George et al. (2015)	For *in vitro* adenosine receptors $A2_A$ and A_1 assays: • human recombinant HEK-293 cells and Wistar rat vas deferens For *in vivo* work: • adult male Sprague Dawley (3-mo, 200 – 250 g) and juvenile male SD rats (35–40-do, 75 –100 g)	$A2_A$ binding assay: 15 and 150 μg/mL; $A2_A$ and A_1 functional assay antagonist and agonist: 3, 30 and 300 μg/mL 200, 300 and 600 mg/kg (p.o.) 60 and 120 mg/kg (i.p.)	ombuin (3,3′,5-trihydroxy-4′,7-dimethoxyflavone) (0.14%),3′-hydroxy-4′,5,6,7-tetramethoxyflavone (0.10%), sinensetin (0.07%), orthosiphol B (0.26%), orthosiphol A (0.67%), staminol A (0.45%), orthosiphonone A (0.12%)	Oral and intraperitoneal	Enhanced learning and memory *via* blockade of receptors A_1 and A_{2A}	Standardised ethanolic extract of OS may reverse age-related deficits in short-term social memory and can be considered to prevent or decrease the rate of neurodegeneration
Sree et al. (2015)	*in vitro* (human neuroblastoma cell line, SH-SY5Y)	0.01 to 1 mg/mL	Not mentioned	N/A	Antioxidative, antiapoptotic and neuroprotective to alleviate ROS-mediated dysfunction of dopamenergic neurons and neuronal cell death	OS methanol bioactive guided fraction (OMF) can attenuate the H_2O_2 induced oxidative stress by improving the antioxidant status, cell viability, ROS formation, mitochondrial membrane integrity and regulation of gene expression in the neuronal cells. OMF can be considered as an alternative to some of the toxic synthetic antioxidants which are used in food, cosmetics and pharmaceutical applications

AD, Alzheimer's Disease; BDNF, brain-derived neurotrophic factor; b.w., body weight; CREB, cAMP response element binding protein; do, day-old; i.p., intraperitoneal; mo, month-old; OS, Orthosiphon stamineus; p.o., per oral; SD, Sprague Dawley; TrKB, Tropomyosin receptor kinase B.

sufficient to produce 74% inhibition of the A2AR and 300 μg/ml essentially produced complete inhibition of the A1R and A2AR. They measured social memory *via* the social recognition tests which compares the time spent by an adult rat in investigating a juvenile rat, with the assumption that a second successive encounter should produce a shorter investigation time if the juvenile rat is recognised by the adult. By comparing the successive investigation times before and after treatment with OS, George et al. (2015) concluded that the standardized ethanolic extract of OS can be considered to prevent or to decrease the rate of neurodegeneration as compared to a rats given the vehicle control of distilled water.

Oxidative Stress-Induced Neurotoxicity

Oxidative stress has been shown to play a key role in regulating redox reactions in the CNS. Elevated levels of oxidative stress as a result of increased generation of free radicals such as reactive oxygen species (ROS), have been linked to apoptosis in neuronal cells which in turn leads to various neurological disorders (Hensley et al., 2000). As compared to an unspecified vehicle control, a methanolic fraction extracted from OS leaves (OMF) has been shown by Sree et al. (2015) to have neuroprotective and cytoprotective effects in the human SH-SY5Y cell model. When 1,000 μg of OMF was given to SH-SY5Y cells, H_2O_2-induced oxidative stress (increased cell viability, decreased ROS formation, and lipid peroxidation) and the loss of mitochondrial membrane integrity (decreased amounts of lactate dehydrogenase leakage and increased mitochondrial membrane potential) was prevented. Lactate dehydrogenase leakage can also be indirectly used as a measure for cell death (Smith et al., 2011) and the decreased level found by Sree et al. (2015) also suggests that OMF is not cytotoxic to SH-SY5Y cells. SH-SY5Y cells given 1,000 μg of OMF also had improved

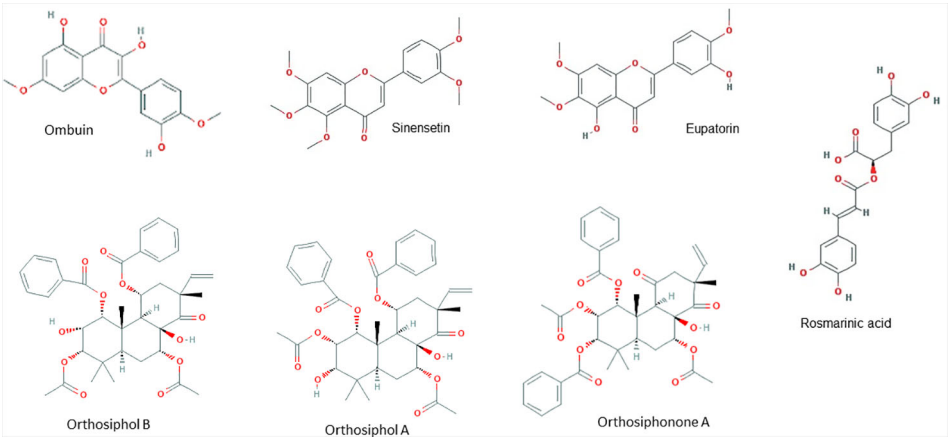

FIGURE 2 | Principal chemical constituents of *Orthosiphon stamineus*.

TABLE 2 | Summary table of the preparations used by the studies in the present systematic literature review.

Study	Formulation	Source	Species, concentration	Quality control reported? (Y/N)	Chemical analysis reported? (Y/N)
Retinasamy et al. (2019)	50% ethanolic extract	NatureCeuticals Sdn Bhd, Kedah DA, Malaysia	*Orthosiphon stamineus*, Unknown concentration	Y- Prepared in a Good Manufacturing Practice (GMP) based environment	N
Choo et al. (2018)	50% ethanolic extract	NatureCeuticals Sdn Bhd, Kedah DA, Malaysia	*Orthosiphon stamineus* Unknown concentration	N	N
George et al. (2015)	70% ethanolic extract	Prepared by George et al. (2015)	*Orthosiphon stamineus* [Biotropics Malaysia Berhad, Malaysia], 1000g	Y - Plant material identified by a taxonomist on the basis of exomorphic characters and literature review	Y - HPLC
Sree et al. (2015)	Methanolic fraction	Prepared by Sree et al. (2015)	*Orthosiphon stamineus* [Western Ghats, India], 3 mg/m	Y - Plant material authenticated at Acharya Nagarjuna University, Guntur, India	Y - HPLC

antioxidant status (increased SOD, CAT and GPx expressions). Superoxide dismutase (SOD), catalase (CAT), and glutathione peroxidase (GPx) are active scavengers of superoxide ($O_2 \cdot^-$) and hydrogen peroxide (H_2O_2). Additionally, OMF enhanced the expression of neuronal biomarker genes (increased levels of *BDNF*, *TH,* and *AADC*) in SH-SY5Y cells. *BDNF*, *TH* (Tyrosine hydroxylase), and *AADC* (Amino acid decarboxylase) are genes that play a pivotal role in the survival and differentiation of dopaminergic neurons. This increase occurred both in the presence or absence of H_2O_2 oxidative stress, though to a greater degree when H_2O_2 was present, even though H_2O_2 alone downregulates these genes. Based on their findings, Sree et al. (2015) proposed that the neuroprotective potential of OMF could possibly be *via* antioxidative mechanisms.

DISCUSSION

Various forms of CNS disorders may not be caused by only a single factor, but may also be a combination of multiple factors. For instance, the synaptic dysfunction and memory impairment detected in AD (McGeer and McGeer, 2010; Gomes et al., 2011) are also components commonly found in epilepsy (Wen et al., 2010; Holmes, 2015) and oxidative stress-induced neurological conditions (Aguiar et al., 2012; Ho et al., 2015; Chitnis and Weiner, 2017; Walker, 2018). There exists an interplay between oxidative stress, neurodegeneration, and neuroinflammation. The studies elaborated in this systematic review have collectively proposed that OS has a protective role to play in the CNS. OS has demonstrated its ability to intercept the cross-talk between neurodegeneration, neuroinflammation, and oxidative stress, and hence contributes to neuroprotection *via* four mechanisms: enhancing memory, anti-inflammation, anti-seizure, and antioxidative as depicted in **Figure 3**.

Modulation of BDNF Signalling and Neurogenesis

All neurodegenerative processes are evolving conditions (Gomes et al., 2011). Based on the studies in this systematic review, OS contributes to the prevention of evolving memory impairment by modulating the BDNF-TrkB and CREB-BDNF signalling pathways as well as promoting neurogenesis. These three

pathways serve to counteract the progressive impairment of memory as a result of neurodegeneration (Toledo and Inestrosa, 2010); with BDNF together with its major receptor TrkB being involved in synaptic plasticity in the form of long term potentiation and also long term memory formation and consolidation (Cunha et al., 2010). Modulation of these signalling pathways results in the initiation of three major signalling pathway cascades, namely phospholipase Cγ (PLCγ), phosphatidylinositol 3-kinase (PI3K), and extracellular signal-regulated kinases (ERK) (Cunha et al., 2010). All three of these pathways and the transcription factor CREB1 have been associated with learning and memory, though the exact role of BDNF and any interactions between these pathways have yet to be fully uncovered (Barco et al., 2003; Thomas and Huganir, 2004; Liu et al., 2006; Gruart et al., 2007). The upregulation of CREB also has positive effects on memory consolidation and performance as CREB modulates BDNF expression and thus upregulates it in turn (Suzuki et al., 2011). In addition, the transcription factor CREB, is also capable of promoting anti-inflammatory responses. These anti-inflammatory responses could be neuroprotective by inhibiting unwanted inflammation, tissue damage, and autoimmune response (Wen et al., 2010) in the CNS. Owing to the anti-inflammatory potential of OS, this may also enhance its capability to prevent neurodegeneration due to a decrease in CREB. OS extract could also reverse the scopolamine induced suppression of neurogenesis in the dentate gyrus of the hippocampus, which again plays a role in spatial memory. The role of the dentate gyrus in spatial memory is postulated to be in the alignment of an internally memorized spatial map with external landmarks as determined by sensory information and thus an impaired dentate gyrus would also impair spatial memory if the external landmarks change (Won Lee et al., 2009).

Antagonism of A1R and A2AR

OS contributes to enhancing learning and memory by modulating the adenosine receptors, A1R and A2AR in the CNS, as discovered by George et al. (2015). In a human study using positron emission tomography (PET) and 8-dicyclopropylmethyl-1-[11C] methyl-3-propylxanthine, Fukumitsu et al. (2008) showed a significant reduction in A1R binding potential in the temporal cortex and thalamus of AD patients as compared with elderly normal subjects. Cunha (2005) also reported a decrease of A1R density and efficiency in neurodegenerative disorders. Canas et al. (2009) and Dall'lgna et al. (2003) have showed that A2AR antagonism prevents synaptic loss as well as neuronal death triggered by Aβ synthetic peptides and thus suggests that modulation of A2AR antagonism could have neuroprotective effects in AD. One interesting finding by Prediger and Takahashi (2005) is that antagonising either adenosine

FIGURE 3 | Mechanism of action of *Orthosiphon stamineus* in CNS disorders.

receptor, A1R or A2AR, can still result in an enhancement of social memory. An experiment by Kaster et al. (2015) proposed that caffeine acts through neuronal adenosine A2A receptors to prevent mood and memory dysfunction triggered by chronic stress. This finding may suggest that OS could be working in a similar manner. By acting on these adenosine receptors, synaptic degeneration and subsequent neuronal death can be improved. This enhances learning and memory to help in arresting neurodegeneration at the early stages (Gomes et al., 2011).

Modulation of Dopaminergic Neurotransmission

OS contributes to the prevention of neurodegeneration by modulating dopaminergic neurotransmission (Sree et al., 2015). This suggests that OS could be preventing dopamine neuron dysfunction or loss as a consequence of neurodegeneration, oxidative stress, neuroinflammation, or a combination of the aforementioned. There is a large body of evidence that associates BDNF, TH, and AADC with the survival, differentiation, and regulation of dopaminergic neurons (Baquet et al., 2005; Bathina and Das, 2015; Lima Giacobbo et al., 2019). Additionally, OS may also be capable of enhancing memory, besides preventing memory loss. Dopamine together with noradrenaline, are two key enzymes in catecholamine neurotransmitter synthesis. Catecholamine neurotransmission is important as it is implicated in working memory performance (Cools and D'Esposito, 2011).

TNFα Signalling

OS contributes to the prevention of seizures and epilepsy by downregulating *TNFα* (Choo et al. (2018). *TNFα* has been shown to play a part in not only systemic inflammation, but also in epilepsy (Rana and Musto, 2018) and oxidative stress (Aguiar et al., 2012). Sinha et al. (2008) have found a decrease in cytokines, including *TNFα*, in patients with epilepsy. An experiment by Ho et al. (2015) has also reported an increased seizure susceptibility due to the induction of neuroinflammation and oxidative stress in the hippocampus. Perhaps the anti-convulsive potential of OS could be acting against neuroinflammation owing to its anti-inflammatory properties (Yam et al., 2008; Yam et al., 2010). The downregulation of *TNFα* also reduces AMPA (α-amino-3-hydroxy-5-methyl-4-isoxazolepropionic acid) glutamatergic receptor trafficking in turn and hence decreases excitatory synaptic transmission (Patel et al., 2017). In addition, the downregulation of TNFα also decrease glutamate release through the downregulation of glutaminase and microglia gap junctions (Takeuchi et al., 2006) and also reduces the endocytosis of inhibitory γ-aminobutyric acid (GABA) receptors (Stellwagen et al., 2005).

Redox Signalling

Oxidative stress, alone or in combination, plays a pivotal role in various CNS disorders and can also damage essential macromolecules (Čolak, 2008; Pizzino et al., 2017). For instance, post-mortem samples from patients with AD revealed that there were elevated markers of oxidative stress including protein carbonylation and lipid peroxidation within the tissue (Butterfield and Lauderback, 2002; Sultana et al., 2006). Based on the studies in this systematic review, OS has demonstrated its capability in modulating the redox signalling cascade by regulating SOD, CAT, and GPx, to scavenge ROS. These enzymatic antioxidants collectively known as the first line defense antioxidants (Ighodaro and Akinloye, 2018). They act very fast to suppress or prevent the formation of free radicals or reactive species in cells by neutralizing any molecule with the potential of developing into a free radical or any free radical with the ability to induce the production of other radicals. An experiment by Akowuah et al. (2005) has reported that an OS leaf extract containing major components including sinensetin, eupatorine, 3′-hydroxy-5,6,7,4′-tetramethoxyflavone, rosmarinic acid, and quercetin, shows significant free radical scavenging and antioxidant abilities. In another experiment by Yam et al. (2007), a standardized OS extract has also demonstrated anti-oxidant and free-radical scavenging abilities. With these science-backed evidence, OS has been suggested to play a fundamental role in the redox signalling cascade—by activating the first line enzymatic antioxidants defense, it is able to scavenge and prevent the accumulation of free radicals (pro-oxidants such as $O_2{\cdot}^-$, H_2O_2 and hydroxyl, ·OH) and thus, reducing the deleterious effects of oxidative stress. OS can thereby contribute to the delay of the onset and progression of neurodegeneration such as neuronal death, AD, and dementia induced by oxidative stress (Uberti et al., 2002; Zhang et al., 2010; Barsukova et al., 2011).

In the face of increased oxidative stress, the inability of antioxidant defense systems to counter the proinflammatory response is key to the onset and progression of neurodegeneration and neuroinflammation (Bakunina et al., 2015). There exists large amount of evidence suggesting that several basic mechanisms which drive neurodegeneration may be triggered by inflammatory cells and their mediators at various stages of the neurodegenerative cascade (Wyss-Coray and Mucke, 2002; Chitnis and Weiner, 2017; Kinney et al., 2018; Walker, 2018). In AD, for instance, the two most common mechanisms are mitochondrial dysfunction and inflammation mediated by cytokines and activated immune cells. de la Monte and Wands (2006) found that the neurons of AD patients have a high percentage of damaged mitochondria, which may be due to the increased presence of mutations in the mitochondrial DNA. Oxidative damage of mitochondrial proteins and DNA is found even in early stages of AD, suggesting a role of oxidative stress in disease progression (Nunomura et al., 2001; de la Monte and Wands, 2006). In both astrocytes and microglia, toll-like receptor (TLR)-mediated activation can release cytokines and chemokines (i.e. TNFα, IL-1, -3, -6, CCL2/MCP-1) as well as ROS, which can either promote neuronal survival or, in case of massive damage as in AD (Lee et al., 2018), ischemia or spinal cord injury, may promote inflammation and aggravate neuronal damage (van Noort and Bsibsi, 2009; Hinojosa et al., 2011). Activated immune cells, particularly macrophages, can produce ROS which also contributes to mitochondrial dysfunction and ultimately neuronal apoptosis (Chitnis and Weiner, 2017). In two separate experiments by Yam and colleagues (Yam et al., 2008; Yam et al., 2010), the components of OS leaves which are responsible for its anti-inflammatory effect were found to be the

polymethoxylated flavones sinensetin, eupatorine and 30-hydroxy-5,6,7,40-tetramethoxyflavone.

Safety and Toxicity of OS

According to the Assessment Report on *Orthosiphon stamineus* Benth. (EMA/HMPC/135701/2009), clinical safety data is limited. The report concludes that no safety problems concerning the traditional use of OS or its preparations overall. OS preparations are considered not harmful when used in the recommended dosages for specified preparations. Its use however, can only be limited to the adults and elderly as no data on the use in children and adolescents is available. As there is no information on reproductive and developmental toxicity, its use during pregnancy and lactation cannot be recommended.

Pharmacokinetics of OS

Recently, selected secondary metabolites of OS have been investigated for their pharmacokinetics. Guo et al. (2019) studied the plasma pharmacokinetics of an OS extract with selected nine analytes (protocatechuic acid, PCA; danshensu, DSS; caffeic acid, CAA; rosmarinic acid, RA; sinensetin, SIN; eupatorine, EUP; cichoric acid, CA; salvianolic acid A, Sal A and salvianolic acid B, Sal B) in rats after oral administration at 10 g/kg. The maximum plasma time (T_{max}, h) ranged between 0.36–2.79 and the maximum concentration (C_{max}, ng/ml) was between 2.05–1008.02. The half-life ($t_{1/2z}$, h) ranged from 0.59-13.50, area under the plasma concentration versus time curve from zero to last sampling time (AUC_{0-t}, h) was 1.66–9421.62 and mean residence time (MRT_{0-t}, h) was 0.79–9.02. In another study by Shafaei et al. (2017), the plasma pharmacokinetics of an ethanolic OS extract with four marker compounds (RA, SIN, EUP and 3′-hydroxy-5,6,7,4′-tetramethoxyflavone, TMF) in rats after oral administration at 1,000 mg/kg and intravenous administration at 250 mg/kg *via* the tail vein was elucidated. After oral administration, T_{max} was ranged between 2.83–3.17 h and C_{max} was between 0.77–1.89 μg/ml, AUC (0–24, μg h/ml) ranged between 0.91–4.37 and bioavailability was between 15.28–26.45%. After IV administration, the estimated volume of distribution (V_d, l/kg h) ranged between 0.09–1.06, mean clearance value (CL, l/kg h) was 0.12–0.66, elimination rate constant (K_e, h-1) was 0.62–1.44, biological half-life ($t_{1/2}$, h) 0.49–1.13 and AUC (24-∞, μg h/ml) ranged between 1.73–4.13. These studies suggested that different OS extracts display a varying pharmacokinetic profiles dependent upon the route of administration.

Future Directions

All the four articles discussed in this review share one major limitation, that is all the studies were in the pre-clinical stage and were conducted on animals or in isolated cells rather than in humans. While the results are nevertheless encouraging, it should be noted that it is far from certain that the results would be translatable to humans (Cahill et al., 2011) if and when clinical trials are conducted in humans. However, there is one other limitation, in that all the studies in this review used various extracts of OS rather than pure compounds. This could be problematic when comparing the various studies as the levels of certain secondary metabolites can vary depending on the place in which the plant is grown, even within the same country, and hence their properties can differ as well (Akowuah et al., 2004). If OS is to be developed into drugs for treating CNS disorders, either the extract properties need to be standardized or the interactions between the constituents need to be established. While there have been limited studies conducted on pure compounds of OS constituents (Erkan et al., 2008; Laavola et al., 2012; Shin et al., 2012), this however creates another issue as there could be synergistic effects between the constituents.

Besides secondary metabolites, OS is also naturally bestowed with rich primary metabolites encompassing proteins, lipids, and carbohydrates. Yet, they are not as popularly sought after, especially the OS proteins. However, the pharmaceutical demand for plant-derived proteins is tremendous, with one third of all approved pharmaceuticals being glycoproteins (Solá and Griebenow, 2010). Plant-derived proteins have emerged as a favourable therapeutic alternative mainly owing to their product safety. For instance, topical applications of plant-derived glycoproteins in humans was reported to have no significant side effects (Yao et al., 2015). Additionally, plant-based proteins eliminates potential contamination of the therapeutic drug with animal pathogens (i.e. prions, viruses, mycoplasmas) (Yao et al., 2015). Perhaps, the primary metabolites of OS such as proteins, lipids, and carbohydrates, may also hold valuable therapeutic rationale. These primary metabolites are therefore worthy of future exploration particularly in the search for a more promising treatment to a wide array of CNS disorders.

CONCLUSION

The studies elaborated in current systematic review have collectively proposed that OS plays a protective role in the CNS. OS has demonstrated its ability, notably *via* its secondary metabolites (small molecules), to intercept the cross-talk between neurodegeneration, neuroinflammation, and oxidative stress, and hence contributing to neuroprotection. However, all these studies were at the pre-clinical phase and it remains to be seen if OS will be as effective in humans.

AUTHOR CONTRIBUTIONS

Y-SC designed, performed literature research, screened articles, and wrote the final manuscript with the help of BC. MS conceptualized, edited, and revised the final manuscript. MS, PA, and IO supervised all aspects of the research and edited the final manuscript. All authors read and approved the final manuscript.

FUNDING

This work is supported by the NKEA Research Grant Scheme (NRGS), Ministry of Agriculture and Agro-Based Industry Malaysia (Grant No. NH1014D066).

REFERENCES

Abdelfatah, S. A., and Efferth, T. (2015). Cytotoxicity of the indole alkaloid reserpine from Rauwolfia serpentina against drug-resistant tumor cells. *Phytomedicine* 22 (2), 308–318. doi: 10.1016/j.phymed.2015.01.002

Adnyana, I. K., Setiawan, F., and Insanu, M. (2013). From ethnopharmacology to clinical study of *Orthosiphon stamineus* Benth. *Int. J. Pharm. Pharm. Sci.* 5 (3), 66.

Agency, E. M. (2011). *Assessment report on Orthosiphon stamineus Benth., folium*, Retrieved from.

Aguiar, C. C. T., Almeida, A. B., Araújo, P. V. P., de Abreu, R. N. D. C., Chaves, E. M. C., do Vale, O. C., et al. (2012). Oxidative stress and epilepsy: literature review. *Oxid. Med. Cell. Longevity* 2012, 795259–795259. doi: 10.1155/2012/795259

Akowuah, G., Zhari, I., Norhayati, I., Sadikun, A., and Khamsah, S. (2004). Sinensetin, eupatorin, 3′-hydroxy-5, 6, 7, 4′-tetramethoxyflavone and rosmarinic acid contents and antioxidative effect of Orthosiphon stamineus from Malaysia. *Food Chem.* 87 (4), 559–566. doi: 10.1016/j.foodchem.2004.01.008

Akowuah, G., Ismail, Z., Norhayati, I., and Sadikun, A. (2005). The effects of different extraction solvents of varying polarities on polyphenols of Orthosiphon stamineus and evaluation of the free radical-scavenging activity. *Food Chem.* 93 (2), 311–317. doi: 10.1016/j.foodchem.2004.09.028

Ameer, O. Z., Salman, I. M., Asmawi, M. Z., Ibraheem, Z. O., and Yam, M. F. (2012). *Orthosiphon stamineus*: traditional uses, phytochemistry, pharmacology, and toxicology. *J. Med. Food.* 15 (8), 678–690. doi: 10.1089/jmf.2011.1973

Amor, S., Puentes, F., Baker, D., and van der Valk, P. (2010). Inflammation in neurodegenerative diseases. *Immunology* 129 (2), 154–169. doi: 10.1111/j.1365-2567.2009.03225.x

Bakunina, N., Pariante, C. M., and Zunszain, P. A. (2015). Immune mechanisms linked to depression via oxidative stress and neuroprogression. *Immunology* 144 (3), 365–373. doi: 10.1111/imm.12443

Baquet, Z. C., Bickford, P. C., and Jones, K. R. (2005). Brain-Derived Neurotrophic Factor Is Required for the Establishment of the Proper Number of Dopaminergic Neurons in the Substantia Nigra Pars Compacta. *J. Neurosci.* 25 (26), 6251–6259. doi: 10.1523/jneurosci.4601-04.2005

Barco, A., Pittenger, C., and Kandel, E. R. (2003). CREB, memory enhancement and the treatment of memory disorders: promises, pitfalls and prospects. *Expert Opin. Ther. Targets* 7 (1), 101–114. doi: 10.1517/14728222.7.1.101

Barsukova, A. G., Bourdette, D., and Forte, M. (2011). Mitochondrial calcium and its regulation in neurodegeneration induced by oxidative stress. *Eur. J. Neurosci.* 34 (3), 437–447. doi: 10.1111/j.1460-9568.2011.07760.x

Bathina, S., and Das, U. N. (2015). Brain-derived neurotrophic factor and its clinical implications. *Arch. Med. Sci. : AMS* 11 (6), 1164–1178. doi: 10.5114/aoms.2015.56342

Butterfield, D. A., and Lauderback, C. M. (2002). Lipid peroxidation and protein oxidation in Alzheimer's disease brain: potential causes and consequences involving amyloid β-peptide-associated free radical oxidative stress. *Free Radical Biol. Med.* 32 (11), 1050–1060. doi: 10.1016/S0891-5849(02)00794-3

Cahill, H., Rattner, A., and Nathans, J. (2011). Preclinical assessment of CNS drug action using eye movements in mice. *J. Clin. Invest.* 121 (9), 3528–3541. doi: 10.1172/JCI45557

Canas, P. M., Porciúncula, L. O., Cunha, G. M., Silva, C. G., Machado, N. J., Oliveira, J. M., et al. (2009). Adenosine A2A receptor blockade prevents synaptotoxicity and memory dysfunction caused by β-amyloid peptides via p38 mitogen-activated protein kinase pathway. *J. Neurosci.* 29 (47), 14741–14751. doi: 10.1523/JNEUROSCI.3728-09.2009

Chen, J.-F., Sonsalla, P. K., Pedata, F., Melani, A., Domenici, M. R., Popoli, P., et al. (2007). Adenosine A2A receptors and brain injury: Broad spectrum of neuroprotection, multifaceted actions and "fine tuning" modulation. *Prog. Neurobiol.* 83 (5), 310–331. doi: 10.1016/j.pneurobio.2007.09.002

Chitnis, T., and Weiner, H. L. (2017). CNS inflammation and neurodegeneration. *J. Clin. Invest.* 127 (10), 3577–3587. doi: 10.1172/JCI90609

Choo, B. K. M., Kundap, U. P., Kumari, Y., Hue, S.-M., Othman, I., and Shaikh, M. F. (2018). Orthosiphon stamineus Leaf Extract Affects TNF-α and Seizures in a Zebrafish Model. *Front. Pharmacol.* 9 (139), 1–11. doi: 10.3389/fphar.2018.00139

Čolak, E. (2008). New markers of oxidative damage to macromolecules. *J. Med. Biochem.* 27 (1), 1–16. doi: 10.2478/v10011-007-0049-x

Cools, R., and D'Esposito, M. (2011). Inverted-U–Shaped Dopamine Actions on Human Working Memory and Cognitive Control. *Biol. Psychiatry* 69 (12), e113–e125. doi: 10.1016/j.biopsych.2011.03.028

Cummings, J., Lee, G., Ritter, A., and Zhong, K. (2018). Alzheimer's disease drug development pipeline: 2018. *Alzheimer's Dementia: Trans. Res. Clin. Interventions* 4, 195–214. doi: 10.1016/j.trci.2018.03.009

Cunha, C., Brambilla, R., and Thomas, K. (2010). A simple role for BDNF in learning and memory? *Front. Mol. Neurosci.* 3 (1), 1–14. doi: 10.3389/neuro.02.001.2010

Cunha, R. A. (2005). Neuroprotection by adenosine in the brain: from A 1 receptor activation to A 2A receptor blockade. *Purinergic Signall.* 1 (2), 111–134. doi: 10.1007/s11302-005-0649-1

Dall'lgna, O. P., Porciúncula, L. O., Souza, D. O., Cunha, R. A., and Lara, D. R. (2003). Neuroprotection by caffeine and adenosine A2A receptor blockade of β-amyloid neurotoxicity. *Br. J. Pharmacol.* 138 (7), 1207–1209. doi: 10.1038/sj.bjp.0705185

de la Monte, S. M., and Wands, J. R. (2006). Molecular indices of oxidative stress and mitochondrial dysfunction occur early and often progress with severity of Alzheimer's disease. *J. Alzheimer's Dis.* 9 (2), 167–181. doi: 10.3233/JAD-2006-9209

Edeoga, H., Okwu, D., and Mbaebie, B. (2005). Phytochemical Constituents of Some Nigerian Medicinal Plants. *Afr. J. Biotechnol.* 4 (7), 685–688. doi: 10.5897/AJB2005.000-3127

Erkan, N., Ayranci, G., and Ayranci, E. (2008). Antioxidant activities of rosemary (Rosmarinus Officinalis L.) extract, blackseed (Nigella sativa L.) essential oil, carnosic acid, rosmarinic acid and sesamol. *Food Chem.* 110 (1), 76–82. doi: 10.1016/j.foodchem.2008.01.058

Fisher, R. S., Boas, W. v. E., Blume, W., Elger, C., Genton, P., et al. (2005). Epileptic Seizures and Epilepsy: Definitions Proposed by the International League Against Epilepsy (ILAE) and the International Bureau for Epilepsy (IBE). *Epilepsia* 46 (4), 470–472. doi: 10.1111/j.0013-9580.2005.66104.x

Fisher, R. S., Acevedo, C., Arzimanoglou, A., Bogacz, A., Cross, J. H., Elger, C. E., et al. (2014). ILAE Official Report: A Practical Clinical Definition of Epilepsy. *Epilepsia* 55 (4), 475–482. doi: 10.1111/epi.12550

Fredholm, B. B., Bättig, K., Holmén, J., Nehlig, A., and Zvartau, E. E. (1999). Actions of caffeine in the brain with special reference to factors that contribute to its widespread use. *Pharmacol. Rev.* 51 (1), 83–133.

Fukumitsu, N., Ishii, K., Kimura, Y., Oda, K., Hashimoto, M., Suzuki, M., et al. (2008). Adenosine A1 receptors using 8-dicyclopropylmethyl-1-[11C]methyl-3-propylxanthine PET in Alzheimer's disease. *Ann. Nuclear Med.* 22 (10), 841–847. doi: 10.1007/s12149-008-0185-5

George, A., Chinnappan, S., Choudhary, Y., Choudhary, V. K., Bommu, P., and Wong, H. J. (2015). Effects of a Proprietary Standardized Orthosiphon stamineus Ethanolic Leaf Extract on Enhancing Memory in Sprague Dawley Rats Possibly via Blockade of Adenosine A2a Receptors. *Evidence-Based Complement. Altern. Med.* 375837, 1–9. doi: 10.1155/2015/375837

Gomes, C. V., Kaster, M. P., Tomé, A. R., Agostinho, P. M., and Cunha, R. A. (2011). Adenosine receptors and brain diseases: Neuroprotection and neurodegeneration. *Biochim. Biophys. Acta (BBA) Biomembranes* 1808 (5), 1380–1399. doi: 10.1016/j.bbamem.2010.12.001

Gruart, A., Sciarretta, C., Valenzuela-Harrington, M., Delgado-García, J. M., and Minichiello, L. (2007). Mutation at the TrkB PLC{gamma}-docking site affects hippocampal LTP and associative learning in conscious mice. *Learn. Memory (Cold Spring Harbor N.Y.)* 14 (1), 54–62. doi: 10.1101/lm.428307

Guo, Z., Li, B., Gu, J., Zhu, P., Su, F., Bai, R., et al. (2019). Simultaneous Quantification and Pharmacokinetic Study of Nine Bioactive Components of Orthosiphon stamineus Benth. Extract in Rat Plasma by UHPLC-MS/MS. *Mol. (Basel Switzerland)* 24 (17), 3057. doi: 10.3390/molecules24173057

Gurib-Fakim, A. (2006). Medicinal plants: traditions of yesterday and drugs of tomorrow. *Mol. Aspects Med.* 27 (1), 1–93. doi: 10.1016/j.mam.2005.07.008

Hensley, K., Robinson, K. A., Gabbita, S. P., Salsman, S., and Floyd, R. A. (2000). Reactive oxygen species, cell signaling, and cell injury. *Free Radical Biol. Med.* 28 (10), 1456–1462. doi: 10.1016/S0891-5849(00)00252-5

Hinojosa, A. E., Garcia-Bueno, B., Leza, J. C., and Madrigal, J. L. (2011). CCL2/MCP-1 modulation of microglial activation and proliferation. *J. Neuroinflamm.* 8 (1), 77. doi: 10.1186/1742-2094-8-77

Ho, Y.-H., Lin, Y.-T., Wu, C.-W. J., Chao, Y.-M., Chang, A. Y. W., and Chan, J. Y. H. (2015). Peripheral inflammation increases seizure susceptibility via the induction of neuroinflammation and oxidative stress in the hippocampus. *J. Biomed. Sci.* 22 (1), 46–46. doi: 10.1186/s12929-015-0157-8

Holland, K. (2014). *Epilepsy by the Numbers: Facts, Statistics, and You*. Healthline.com. Retrieved from http://www.healthline.com/health/epilepsy/facts-statistics-infographic.

Holmes, G. L. (2015). Cognitive impairment in epilepsy: the role of network abnormalities. *Epileptic Disord. : Int. Epilepsy J. Videotape* 17 (2), 101–116. doi: 10.1684/epd.2015.0739

Ighodaro, O. M., and Akinloye, O. A. (2018). First line defence antioxidants-superoxide dismutase (SOD), catalase (CAT) and glutathione peroxidase (GPX): Their fundamental role in the entire antioxidant defence grid. *Alexandria J. Med.* 54 (4), 287–293. doi: 10.1016/j.ajme.2017.09.001

Jellinger, K. A. (2010). Basic mechanisms of neurodegeneration: a critical update. *J. Cell. Mol. Med.* 14 (3), 457–487. doi: 10.1111/j.1582-4934.2010.01010.x

Kamat, C. D., Gadal, S., Mhatre, M., Williamson, K. S., Pye, Q. N., and Hensley, K. (2008). Antioxidants in central nervous system diseases: preclinical promise and translational challenges. *J. Alzheimer's Dis. : JAD* 15 (3), 473–493. doi: 10.3233/jad-2008-15314

Kaster, M. P., Machado, N. J., Silva, H. B., Nunes, A., Ardais, A. P., Santana, M., et al. (2015). Caffeine acts through neuronal adenosine A2A receptors to prevent mood and memory dysfunction triggered by chronic stress. *Proc. Natl. Acad. Sci.* 112 (25), 7833–7838. doi: 10.1073/pnas.1423088112

Kinney, J. W., Bemiller, S. M., Murtishaw, A. S., Leisgang, A. M., Salazar, A. M., and Lamb, B. T. (2018). Inflammation as a central mechanism in Alzheimer's disease. *Alzheimer's Dementia (New York N. Y.)* 4, 575–590. doi: 10.1016/j.trci.2018.06.014

Laavola, M., Nieminen, R., Yam, M. F., Sadikun, A., Asmawi, M. Z., Basir, R., et al. (2012). Flavonoids Eupatorin and Sinensetin Present in Orthosiphon stamineus Leaves Inhibit Inflammatory Gene Expression and STAT1 Activation. *Planta Med.* 78 (08), 779–786. doi: 10.1055/s-0031-1298458

Lalkovičová, M., and Danielisová, V. (2016). Neuroprotection and antioxidants. *Neural Regeneration Res.* 11 (6), 865–874. doi: 10.4103/1673-5374.184447

Lee, W.-J., Liao, Y.-C., Wang, Y.-F., Lin, I. F., Wang, S.-J., and Fuh, J.-L. (2018). Plasma MCP-1 and Cognitive Decline in Patients with Alzheimer's Disease and Mild Cognitive Impairment: A Two-year Follow-up Study. *Sci. Rep.* 8 (1), 1280. doi: 10.1038/s41598-018-19807-y

Lima Giacobbo, B., Doorduin, J., Klein, H. C., Dierckx, R. A. J. O., Bromberg, E., and de Vries, E. F. J. (2019). Brain-Derived Neurotrophic Factor in Brain Disorders: Focus on Neuroinflammation. *Mol. Neurobiol.* 56 (5), 3295–3312. doi: 10.1007/s12035-018-1283-6

Liu, Q.-R., Lu, L., Zhu, X.-G., Gong, J.-P., Shaham, Y., and Uhl, G. R. (2006). Rodent BDNF genes, novel promoters, novel splice variants, and regulation by cocaine. *Brain Res.* 1067 (1), 1–12. doi: 10.1016/j.brainres.2005.10.004

Lubin, F. D., Ren, Y., Xu, X., and Anderson, A. E. (2007). Nuclear factor-κB regulates seizure threshold and gene transcription following convulsant stimulation. *J. Neurochem.* 103 (4), 1381–1395. doi: 10.1111/j.1471-4159.2007.04863.x

Manchishi, S. M. (2018). Recent Advances in Antiepileptic Herbal Medicine. *Curr. Neuropharmacol.* 16 (1), 79–83. doi: 10.2174/1570159X15666170518151809

McGeer, E. G., and McGeer, P. L. (2010). Neuroinflammation in Alzheimer's disease and mild cognitive impairment: a field in its infancy. *J. Alzheimer's Dis.* 19 (1), 355–361. doi: 10.3233/JAD-2010-1219

Moher, D., Shamseer, L., Clarke, M., Ghersi, D., Liberati, A., Petticrew, M., et al. (2015). Preferred reporting items for systematic review and meta-analysis protocols (PRISMA-P) 2015 statement. *Syst. Rev.* 4 (1), 1. doi: 10.1186/2046-4053-4-1

Nunomura, A., Perry, G., Aliev, G., Hirai, K., Takeda, A., Balraj, E. K., et al. (2001). Oxidative damage is the earliest event in Alzheimer disease. *J. Neuropathol. Exp. Neurol.* 60 (8), 759–767. doi: 10.1093/jnen/60.8.759

Nur, S., and Adams, C. E. (2016). Chlorpromazine versus reserpine for schizophrenia. *Cochrane Database Syst. Rev.* 2016 (4), CD012122, 1–47. doi: 10.1002/14651858.CD012122.pub2

Ouzzani, M., Hammady, H., Fedorowicz, Z., and Elmagarmid, A. (2016). Rayyan—a web and mobile app for systematic reviews. *Syst. Rev.* 5 (1), 210. doi: 10.1186/s13643-016-0384-4

Patel, D. C., Wallis, G., Dahle, E. J., McElroy, P. B., Thomson, K. E., Tesi, R. J., et al. (2017). Hippocampal TNFα Signaling Contributes to Seizure Generation in an Infection-Induced Mouse Model of Limbic Epilepsy. *eNeuro* 4 (2), e0105-17.2017 1–20. doi: 10.1523/ENEURO.0105-17.2017

Pereira, G. S., Mello e Souza, T., Vinadé, E. R. C., Choi, H., Rodrigues, C., Battastini, A. M. O., et al. (2002). Blockade of adenosine A1 receptors in the posterior cingulate cortex facilitates memory in rats. *Eur. J. Pharmacol.* 437 (3), 151–154. doi: 10.1016/S0014-2999(02)01307-9

Perucca, E. (2017). Cannabinoids in the Treatment of Epilepsy: Hard Evidence at Last? *J. Epilepsy Res.* 7 (2), 61–76. doi: 10.14581/jer.17012

Pizzino, G., Irrera, N., Cucinotta, M., Pallio, G., Mannino, F., Arcoraci, V., et al. (2017). Oxidative stress: harms and benefits for human health. *Oxid. Med. Cell. Longevity* 2017, 8416763, 1–13. doi: 10.1155/2017/8416763

Prediger, R. D. S., and Takahashi, R. N. (2005). Modulation of short-term social memory in rats by adenosine A1 and A2A receptors. *Neurosci. Lett.* 376 (3), 160–165. doi: 10.1016/j.neulet.2004.11.049

Rabiei, Z. (2017). Anticonvulsant effects of medicinal plants with emphasis on mechanisms of action. *Asian Pacific J. Trop. Biomed.* 7 (2), 166–172. doi: 10.1016/j.apjtb.2016.11.028

Rana, A., and Musto, A. E. (2018). The role of inflammation in the development of epilepsy. *J. Neuroinflamm.* 15 (1), 144. doi: 10.1186/s12974-018-1192-7

Retinasamy, T., Shaikh, M. F., Kumari, Y., and Othman, I. (2019). Ethanolic Extract of Orthosiphon stamineus Improves Memory in Scopolamine-Induced Amnesia Model. *Front. Pharmacol.* 10 (1216), 1–11. doi: 10.3389/fphar.2019.01216

Sawaya, R. A., and Poupelloz, J. V. (2011). *Assessment report on Orthosiphon stamineus Benth., folium.* UK:European Medicines Agency, European Union

Schapira, A. H. V. (2010). Neuroprotection in Parkinson's disease. *Parkinsonism Relat. Disord.* 15, S41–S43. doi: 10.1016/S1353-8020(09)70834-X

Shafaei, A., Saeed, M., Aisha, A. F., and Ismail, Z. (2017). Pharmacokinetics and bioavailability of Orthosiphon stamineus ethanolic extract and its nano liposomes in Sprague–Dawley rats. *Int. J. Pharm. Pharmaceut. Sci.* 9, 199–206. doi: 10.22159/ijpps.2017v9i1.12407

Shin, H.-S., Kang, S.-I., Yoon, S.-A., Ko, H.-C., and Kim, S.-J. (2012). Sinensetin attenuates LPS-induced inflammation by regulating the protein level of IκB-α. *Biosci. Biotechnol. Biochem.* 76 (4), 847–849. doi: 10.1271/bbb.110908

Silvestro, S., Mammana, S., Cavalli, E., Bramanti, P., and Mazzon, E. (2019). Use of Cannabidiol in the Treatment of Epilepsy: Efficacy and Security in Clinical Trials. *Mol. (Basel Switzerland)* 24 (8), 1459. doi: 10.3390/molecules24081459

Simunkova, M., Alwasel, S. H., Alhazza, I. M., Jomova, K., Kollar, V., Rusko, M., et al. (2019). Management of oxidative stress and other pathologies in Alzheimer's disease. *Arch. Toxicol.* 93 (9), 2491–2513. doi: 10.1007/s00204-019-02538-y

Sinha, S., Patil, S. A., Jayalekshmy, V., and Satishchandra, P. (2008). Do cytokines have any role in epilepsy? *Epilepsy Res.* 82 (2), 171–176. doi: 10.1016/j.eplepsyres.2008.07.018

Smith, S. M., Wunder, M. B., Norris, D. A., and Shellman, Y. G. (2011). A simple protocol for using a LDH-based cytotoxicity assay to assess the effects of death and growth inhibition at the same time. *PloS One* 6 (11), e26908–e26908. doi: 10.1371/journal.pone.0026908

Solá, R. J., and Griebenow, K. (2010). Glycosylation of therapeutic proteins. *BioDrugs* 24 (1), 9–21. doi: 10.2165/11530550-000000000-00000

Son, J.-Y., Park, S.-Y., Kim, J.-Y., Won, K.-C., Kim, Y.-D., Choi, Y.-J., et al. (2011). *Orthosiphon stamineus* reduces appetite and visceral fat in rats. *J. Korean Soc Appl. Biol. Chem.* 54 (2), 200–205. doi: 10.3839/jksabc.2011.033

Sree, N. V., Sri, P. U., and Ramarao, N. (2015). Neuro-protective properties of Orthosiphon stamineus (Benth) leaf methanolic fraction through antioxidant mechanisms on SH-SY5Y cells: an in-vitro evaluation. *Int. J. Pharm. Sci. Res.* 6 (3), 1115–1125. doi: 10.13040/IJPSR.0975-8232.6(3).1115-25

Stellwagen, D., Beattie, E. C., Seo, J. Y., and Malenka, R. C. (2005). Differential regulation of AMPA receptor and GABA receptor trafficking by tumor necrosis factor-alpha. *J. Neurosci. : Off. J. Soc. Neurosci.* 25 (12), 3219–3228. doi: 10.1523/JNEUROSCI.4486-04.2005

Sultana, R., Perluigi, M., and Butterfield, D. A. (2006). Protein oxidation and lipid peroxidation in brain of subjects with Alzheimer's disease: insights into mechanism of neurodegeneration from redox proteomics. *Antioxid. Redox Signaling* 8 (11-12), 2021–2037. doi: 10.1089/ars.2006.8.2021

Suzuki, A., Fukushima, H., Mukawa, T., Toyoda, H., Wu, L.-J., Zhao, M.-G., et al. (2011). Upregulation of CREB-Mediated Transcription Enhances Both Short- and Long-Term Memory. *J. Neurosci.* 31 (24), 8786–8802. doi: 10.1523/jneurosci.3257-10.2011

Takahashi, R. N., Pamplona, F. A., and Prediger, R. (2008). Adenosine receptor antagonists for cognitive dysfunction: a review of animal studies. *Front. Biosci.* 13 (26), 2614–2632. doi: 10.2741/2870

Takeuchi, H., Jin, S., Wang, J., Zhang, G., Kawanokuchi, J., Kuno, R., et al. (2006). Tumor Necrosis Factor-α Induces Neurotoxicity via Glutamate Release from Hemichannels of Activated Microglia in an Autocrine Manner. *J. Biol. Chem.* 281 (30), 21362–21368. doi: 10.1074/jbc.M600504200

Thomas, G. M., and Huganir, R. L. (2004). MAPK cascade signalling and synaptic plasticity. *Nat. Rev. Neurosci.* 5 (3), 173–183. doi: 10.1038/nrn1346

Toledo, E. M., and Inestrosa, N. C. (2010). Activation of Wnt signaling by lithium and rosiglitazone reduced spatial memory impairment and neurodegeneration in brains of an APPswe/PSEN1ΔE9 mouse model of Alzheimer's disease. *Mol. Psychiatry* 15 (3), 272–285. doi: 10.1038/mp.2009.72

Uberti, D., Piccioni, L., Colzi, A., Bravi, D., Canonico, P. L., and Memo, M. (2002). Pergolide protects SH-SY5Y cells against neurodegeneration induced by H2O2. *Eur. J. Pharmacol.* 434 (1), 17–20. doi: 10.1016/S0014-2999(01)01537-0

Vajda, F. J. E. (2004). "Neuroprotection and neurodegenerative disease," in *Alzheimer"s Disease* (Springer), 235–243.

van Noort, J. M., and Bsibsi, M. (2009). Toll-like receptors in the CNS: implications for neurodegeneration and repair. *Prog. Brain Res.* 175, 139–148. doi: 10.1016/S0079-6123(09)17509-X

Walker, K. A. (2018). Inflammation and neurodegeneration: chronicity matters. *Aging* 11 (1), 3–4. doi: 10.18632/aging.101704

Wen, A. Y., Sakamoto, K. M., and Miller, L. S. (2010). The role of the transcription factor CREB in immune function. *J. Immunol. (Baltimore Md. : 1950)* 185 (11), 6413–6419. doi: 10.4049/jimmunol.1001829

Wickham, J., Ledri, M., Bengzon, J., Jespersen, B., Pinborg, L. H., Englund, E., et al. (2019). Inhibition of epileptiform activity by neuropeptide Y in brain tissue from drug-resistant temporal lobe epilepsy patients. *Sci. Rep.* 9 (1), 19393. doi: 10.1038/s41598-019-56062-1

Won Lee, J., Kim, W. R., Sun, W., and Jung, M. W. (2009). Role of dentate gyrus in aligning internal spatial map to external landmark. *Learn. Memory* 16 (9), 530–536. doi: 10.1101/lm.1483709

World Health Organization (2013). WHO traditional medicine strategy: 2014-2023. *World Health Organisation*. Available at: https://apps.who.int/iris/bitstream/handle/10665/92455/9789241506090_eng.pdf?sequence=1 dated 7 May 2020

Wyss-Coray, T., and Mucke, L. (2002). Inflammation in Neurodegenerative Disease—A Double-Edged Sword. *Neuron* 35 (3), 419–432. doi: 10.1016/S0896-6273(02)00794-8

Yam, M. F., Basir, R., Asmawi, M. Z., and Ismail, Z. (2007). Antioxidant and hepatoprotective effects of Orthosiphon stamineus Benth. standardized extract. *Am. J. Chin. Med.* 35 (01), 115–126. doi: 10.1142/S0192415X07004679

Yam, M. F., Asmawi, M. Z., and Basir, R. (2008). An investigation of the anti-inflammatory and analgesic effects of Orthosiphon stamineus leaf extract. *J. Med. Food* 11 (2), 362–368. doi: 10.1089/jmf.2006.065

Yam, M. F., Lim, V., Salman, I. M., Ameer, O. Z., Ang, L. F., Rosidah, N., et al. (2010). HPLC and anti-inflammatory studies of the flavonoid rich chloroform extract fraction of Orthosiphon stamineus leaves. *Mol. (Basel Switzerland)* 15 (6), 4452–4466. doi: 10.3390/molecules15064452

Yao, J., Weng, Y., Dickey, A., and Wang, K. Y. (2015). Plants as Factories for Human Pharmaceuticals: Applications and Challenges. *Int. J. Mol. Sci.* 16 (12), 28549–28565. doi: 10.3390/ijms161226122

Zhang, L., Yu, H., Zhao, X., Lin, X., Tan, C., Cao, G., et al. (2010). Neuroprotective effects of salidroside against beta-amyloid-induced oxidative stress in SH-SY5Y human neuroblastoma cells. *Neurochem. Int.* 57 (5), 547–555. doi: 10.1016/j.neuint.2010.06.021

Conflict of Interest: The authors declare that the research was conducted in the absence of any commercial or financial relationships that could be construed as a potential conflict of interest.

Chapter 2

Extraction and Characterisation of *Orthosiphon stamineus* Proteins

2.1 Introduction

The Lamiaceae family represents one of the twenty largest plant families with a significant proportion of medicinal values, with 13.7% of species in the family used for medicinal purposes (Allkin, 2017). *Orthosiphon stamineus* (OS) or *Orthosiphon aristatus var. aristatus* (OAA) is a member of the Lamiaceae family, and more popularly known as cat's whiskers or "misai kucing". OS has since attracted extensive research focus, particularly on its secondary metabolites (small molecules), as evidenced by a substantial volume of investigation devoted to it (Adnyana et al., 2013; George et al., 2015; Z.-L. Huang et al., 2005; Son et al., 2011). Whilst on the market, OS continues to draw tremendous attention. There are corporate patents filed for the use of OS extracts such as in lymph drainage (Aboca S.P.A Società Agricola, WO2016110794A1) patented by a French group, in cosmetic use (US20110244063A1, BASF Beauty Care Solutions France Sas) and as cognition enhancer patented by a Malaysian corporate (US20110151033A, Biotropics Malaysia Berhad), to name a few. Typically, they all used various secondary metabolites extracted from OS.

Up to date, literature search found only a paper published by Saidan and colleagues (Saidan et al., 2015) which reported the anti-oxidative potential (DPPH and FRAP assays) and anti-proliferative activities (in MCF7 and HCT116 cells) of a combination of primary metabolites extracted from OS leaves. This thus shed light on the possibility of primary metabolites possessing protective potential. Additional literature search has found one existing use of a medicinal plant-derived protein (a component of primary metabolites) in pharmaceutical: thaumatin (also known as talin) extracted from *Thaumatococcus daniellii* (Benn.) Benth. ex Eichler is widely used as a substitute of synthetic sweetener in pharmaceutical products for its low-calorie nature and intense sweetness (Yeboah, Hilger, & Kroschel, 2003). Recently, another medicinal plant-derived protein, protein osmotin (24 kDa) extracted from *Nicotiana tabacum* L., has been reported to potentially improve Alzheimer's disease (Niu, Chen, & Gao, 2019; S. A. Shah et al., 2017). This sees that the rationale of OS primary metabolites being used for pharmaceutical application may be under-utilized (and often under-researched), particularly the proteins. The OS proteins, similar to the two medicinal plant-derived proteins aforementioned, may be a possible source of a drug cadidate.

Proteomics is defined as large-scale analysis of proteome. Proteome is a highly structured entity formed by a set of constituent proteins of which carry out their functions at specific times and locations in a cell, in physical or functional association with other proteins or biomolecules (Aebersold & Mann, 2016). Proteomics facilitates the identification, quantification and characterization of proteins present in a complex crude, in terms of expression, localization, interactions and post-translational modifications (Y. Liu et al., 2019; Zhang, Fonslow, Shan, Baek, & Yates III, 2013). Proteomics has been described as an important approach to obtain biological information as many biological activities are attributed by proteins, thus enhancing our understanding of biological systems (Patterson & Aebersold, 2003).

Liquid chromatography-mass spectrometry (LC-MS) based proteomics can analyze large-scale proteomics owing to its rapid advancement in resolution, sensitivity, mass accuracy and protein analysis scan rate (Zhang et al., 2013). It also provides the quantitative state of a proteome (Aebersold & Mann, 2016). In recent decades, with the availability of online protein databases, LC-MS has accelerated the research on plant proteomics particularly in medicinal plants. Detection of homologous proteins in the medicinal plants obtained from mass spectrometry analysis is assisted by the protein sequences databases available online such as The Universal Protein Resource (UniProt) and The National Center for Biotechnology Information (NCBI) (Xu & Xu, 2004). Nevertheless, the richness of plant protein databases remains lower when compared to the other databases such as human, yeast, bacterium, and snake, to name a few. Nonetheless, LC-MS based proteomics is still an essential component in the comprehensive characterization of medicinal plants. Moreover, it may contribute to the discovery of novel proteins with potential therapeutic applications or as an important research tool. In fact, the pharmaceutical demand for plant-derived proteins is high. It is estimated that about one third of all the approved pharmaceuticals comes from glycoproteins (Solá & Griebenow, 2010). Plant-derived proteins have since emerged as a favorable therapeutic alternative mainly owing to their product safety. For instance, Yao, Weng, Dickey, & Wang (2015) has reported that topical applications of plant-derived glycoproteins in humans was found no significant side effects. Therefore, it is worthwhile to explore OS proteins as a therapeutic source from medicinal plants.

The present chapter investigates an optimal protein extraction method achievable at laboratory scale and analysed the proteins extracted using mass spectrometry-based proteomics (shotgun-LC-MS/MS approach). The protein compositions of OSLP are determined using automated *de novo* protein sequencing software (PEAKS® Studio). Functional annotation analysis is applied to characterize the protein family, cellular component and molecular functions Hence, the objectives of this chapter are:

1. To develop an optimal protein extraction method for OS
2. To identify the protein compositions of OS
3. To characterize the protein compositions of OS

The flowchart outlining the overview of experimental design to achieve the objectives is summarized in Figure 2.1 below:

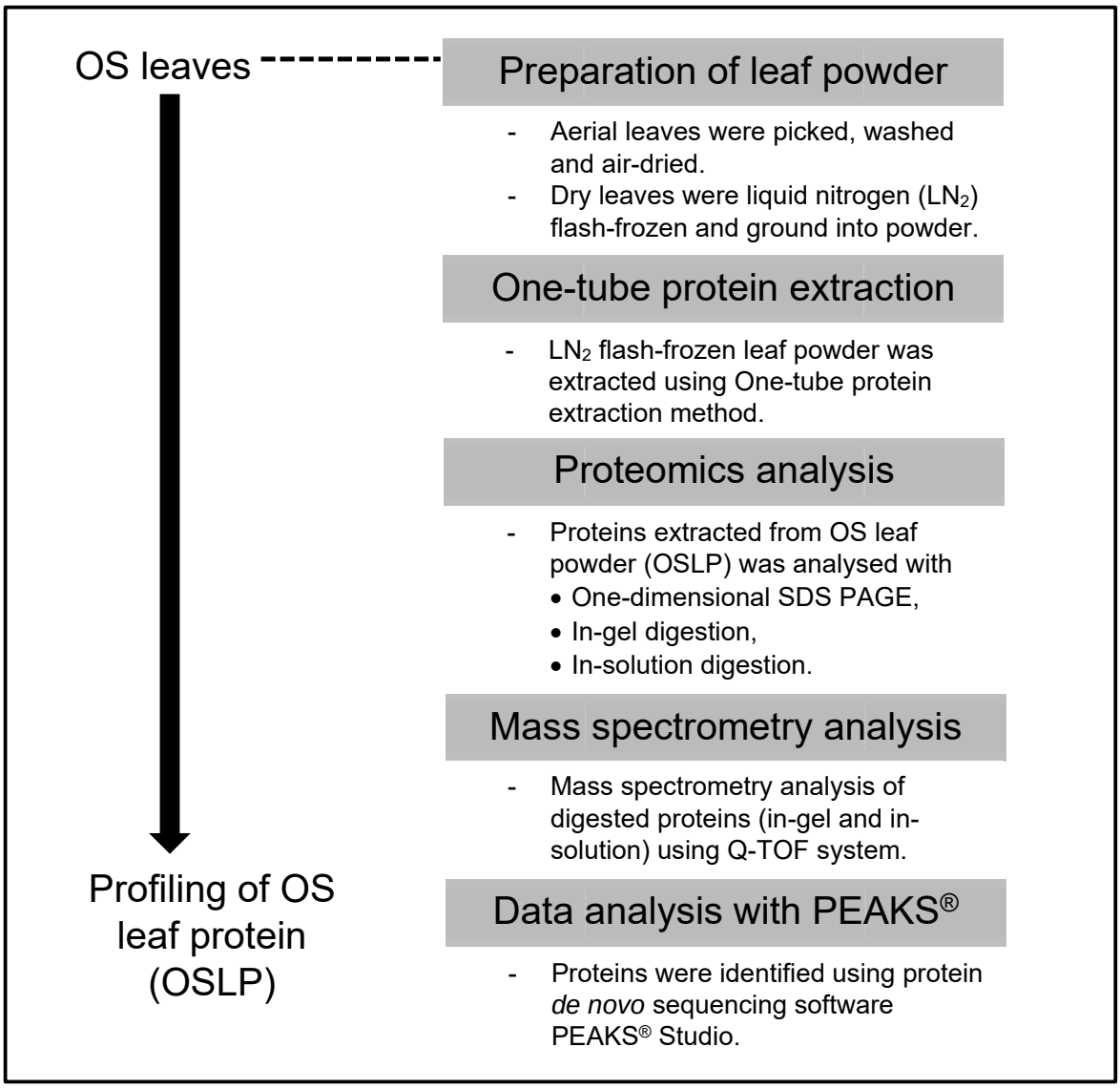

Figure 2.1: Flowchart summarizing the overview of experimental design.

References:

Adnyana, I. K., Setiawan, F., & Insanu, M. (2013). From ethnopharmacology to clinical study of *Orthosiphon stamineus* Benth. *Int. J. Pharm. Pharm. Sci., 5*(3), 66.

Aebersold, R., & Mann, M. (2016). Mass-spectrometric exploration of proteome structure and function. *Nature, 537*(7620), 347-355. doi:10.1038/nature19949

Allkin, B. (2017). Useful plants–medicines: at least 28,187 plant species are currently recorded as being of medicinal use.

George, A., Chinnappan, S., Choudhary, Y., Choudhary, V. K., Bommu, P., & Wong, H. J. (2015). Effects of a Proprietary Standardized *Orthosiphon stamineus* Ethanolic Leaf Extract on Enhancing Memory in Sprague Dawley Rats Possibly via Blockade of Adenosine A(2A) Receptors. *J. Evid. Based Complementary Altern. Med. : eCAM, 2015*, 375837. doi:10.1155/2015/375837

Huang, Z.-L., Qu, W.-M., Eguchi, N., Chen, J.-F., Schwarzschild, M. A., Fredholm, B. B., . . . Hayaishi, O. (2005). Adenosine A2A, but not A1, receptors mediate the arousal effect of caffeine. *Nature neuroscience, 8*(7), 858-859.

Liu, Y., Lu, S., Liu, K., Wang, S., Huang, L., & Guo, L. (2019). Proteomics: a powerful tool to study plant responses to biotic stress. *Plant Methods, 15*(1), 135. doi:10.1186/s13007-019-0515-8

Niu, X., Chen, J., & Gao, J. (2019). Nanocarriers as a powerful vehicle to overcome blood-brain barrier in treating neurodegenerative diseases: Focus on recent advances. *Asian Journal of Pharmaceutical Sciences, 14*(5), 480-496. doi:https://doi.org/10.1016/j.ajps.2018.09.005

Patterson, S. D., & Aebersold, R. H. (2003). Proteomics: the first decade and beyond. *Nat Genet, 33 Suppl*, 311-323. doi:10.1038/ng1106

Saidan, N. H., Hamil, M. S. R., Memon, A. H., Abdelbari, M. M., Hamdan, M. R., Mohd, K. S., . . . Ismail, Z. (2015). Selected metabolites profiling of Orthosiphon stamineus Benth leaves extracts combined with chemometrics analysis and correlation with biological activities. *BMC Complementary and Alternative Medicine, 15*, 350. doi:10.1186/s12906-015-0884-0

Shah, S. A., Yoon, G. H., Chung, S. S., Abid, M. N., Kim, T. H., Lee, H. Y., & Kim, M. O. (2017). Novel osmotin inhibits SREBP2 via the AdipoR1/AMPK/SIRT1 pathway to improve Alzheimer's disease neuropathological deficits. *Mol. Psychiatry, 22*(3), 407-416. doi:10.1038/mp.2016.23

Solá, R. J., & Griebenow, K. (2010). Glycosylation of therapeutic proteins. *BioDrugs, 24*(1), 9-21.

Son, J.-Y., Park, S.-Y., Kim, J.-Y., Won, K.-C., Kim, Y.-D., Choi, Y.-J., . . . Kim, Y.-W. (2011). *Orthosiphon stamineus* reduces appetite and visceral fat in rats. *J. Korean Soc. Appl. Biol. Chem. , 54*(2), 200-205.

Xu, D., & Xu, Y. (2004). Protein databases on the internet. *Current protocols in molecular biology, Chapter 19*, Unit-19.14. doi:10.1002/0471142727.mb1904s68

Yao, J., Weng, Y., Dickey, A., & Wang, K. Y. (2015). Plants as Factories for Human Pharmaceuticals: Applications and Challenges. *International Journal of Molecular Sciences, 16*(12), 28549-28565. doi:10.3390/ijms161226122

Yeboah, S., Hilger, T., & Kroschel, J. (2003). Thaumatococcus daniellii (Benn.) Benth.–a Natural Sweetener from the Rain Forest Zone in West Africa with Potential for Income Generation in Small Scale Farming. *Proceedings of international research on food security, National Resource Management and Rural Development. Georg-August-Universitat Gottingen. http://www.tropentag. de/2003/abstracts/full/305. pdf*.

Zhang, Y., Fonslow, B. R., Shan, B., Baek, M.-C., & Yates, J. R., 3rd. (2013). Protein analysis by shotgun/bottom-up proteomics. *Chemical reviews, 113*(4), 2343-2394. doi:10.1021/cr3003533

EXTRACTION AND CHARACTERISATION OF *ORTHOSIPHON STAMINEUS* PROTEINS

Yin-Sir Chung[1,2], Syafiq Asnawi Zainal Abidin[1,2], Mohd. Farooq Shaikh[1], Pervaiz Khalid Ahmed[3,4], Iekhsan Othman[1,2*]

[1] Neuropharmacology Research Laboratory, Jeffrey Cheah School of Medicine and Health Sciences, Monash University Malaysia, Bandar Sunway 47500, Malaysia; chung.yinsir@monash.edu (Y.-S.C.); syafiq.asnawi@monash.edu (S.A.Z.A.); farooq.shaikh@monash.edu (M.F.S.); Iekhsan.Othman@monash.edu (I.O.)
[2] Liquid Chromatography-Mass Spectrometry (LCMS) Platform, Jeffrey Cheah School of Medicine and Health Sciences, Monash University Malaysia, Bandar Sunway 47500, Malaysia.
[3] School of Business, Monash University Malaysia, Bandar Sunway 47500, Malaysia; pervaiz.ahmed@monash.edu
[4] Global Asia in the 21st Century (GA21), Monash University Malaysia, Bandar Sunway 47500, Malaysia.
Correspondence: Iekhsan.othman@monash.edu

ABSTRACT

Orthosiphon stamineus (OS) is a medicinal plant in the Lamiaceae family commonly found in Malaysia. Substantial research evidence on OS secondary metabolites have suggested their contributions to many drug discoveries. Nonetheless, OS primary metabolites remain unexplored, let alone its proteins. This study attempts to extract proteins from OS leaves (OSLP) with the One-Tube Method (OTM) at laboratory scale and characterize the protein compositions of OSLP. Fresh OS leaves were flash-frozen by liquid nitrogen (LN_2). OTM used sequential extraction strategy to separate the non-protein constituents from OSLP. OSLP extracted were analysed using mass spectrometry-based proteomics. OTM successfully extracted OSLP from the LN_2 flash-frozen leaf sample, with a total yield of 3 mg/g (about 0.3%). Proteomics analysis detected the different protein compositions present in OSLP and they were classified into 49 protein families. The protein compositions were found to localized at 21 different cellular components, from cytoplasm and nucleus to chloroplast and plastid. The three major protein compositions were lyases (14%), oxidoreductases (28%) and monooxygenases (10%). Using functional annotation analysis, they were categorised into 23 classes based on their molecular functions, ranging from biosynthesis of metabolites and enzymatic activities to protein homeostasis and gene transcriptions. Findings in this study contribute to understanding the protein compositions of OSLP which could be helpful in the exploration of protein with important therapeutic potential.

Keywords *Orthosiphon stamineus*; leaf proteins; plant-derived proteins; medicinal plants

DECLARATIONS

Funding

This research was supported by the NKEA EPP#1 Research Grant Scheme (NRGS) (NH1014D066), Ministry of Agriculture and Agro-based Industry, Malaysia. The authors would like to thank Tee Ting-Yee and Nurziana Sharmilla Binti Nawawi for ESI-LCMS/MS technical support (LC-MS laboratory of Jeffrey Cheah School of Medicine and Health Sciences); Sugita Kunalan (Jeffrey Cheah School of Medicine and Health Sciences) for providing guidance to proteomics work.

Conflicts of interest

The authors declare that this research was conducted in the absence of any commercial or financial relationships that could be construed as a potential conflict of interest.

Availability of data and material

The data used to support the findings of this study are available from the corresponding author upon request.

Code availability

Not applicable.

Authors' contributions

Y.S.C designed, performed all the experiments and prepared the final manuscript; S.A.Z.A. helped edited the final manuscript; P.K.A aided in supervision and helped edit the final manuscript; M.F.S and I.O contributed to the design of research, supervised all aspects of the study and edited the final manuscript as submitted. All authors have read and agreed to the published version of the manuscript.

1 INTRODUCTION

Orthosiphon stamineus (OS) or *Orthosiphon aristatus var. aristatus* (OAA), popular known as cat's whiskers (in English), "misai kucing" (in Malay), "mao xu cao" (in Mandarin) and "Java tea" (across European countries), is a medicinal plant in the Lamiaceae family. Aerial leaves and stem tips collected during the flowering season are key components used in various herbal preparations as natural remedies or folk medicine across Southeast Asian countries (Adnyana, Setiawan, & Insanu, 2013; Agency, 2011; George et al., 2015). For instance, OS leaves are used as a traditional medicine to manage seizures and epilepsy (Gan et al., 2017). Extensive modern pharmacological studies, notably on the secondary metabolites (small molecules) of OS, have since been in the limelight owing to their well-known health benefits such as cognitive-enhancing (George et al., 2015; Huang et al., 2005), antioxidative and anti-inflammatory (Adnyana et al., 2013; Ameer, Salman, Asmawi, Ibraheem, & Yam, 2012), to name a few. The primary metabolites of OS however, are not as popularly sought after. In recent years, plant-derived proteins have emerged as a favorable therapeutic alternative mainly owing to their product safety with a low risk of contamination by animal pathogens (Yao, Weng, Dickey, & Wang, 2015). It is reported that nearly one third of all the approved pharmaceuticals derived from glycoproteins (Solá & Griebenow, 2010).

Proteomics study permits the identification, quantification and characterization of proteins present in a complex mixture. This information is particularly useful in studying the expression, localization, interactions and post-translational modifications of a protein (Liu et al., 2019; Y. Zhang, Fonslow, Shan, Baek, & Yates, 2013). Proteomics has been described as an important approach to obtain biological information as most biological activities are attributed by proteins, thus enhancing our conception of a biological system (Aebersold & Mann, 2016; Patterson & Aebersold, 2003). In recent decades, with the availability of online protein databases, liquid chromatography-mass spectrometry (LC-MS) based proteomics has accelerated the research on plant proteomics particularly in medicinal plants. Detection of homologous proteins in the medicinal plant obtained from mass spectrometry spectra analysis is assisted by the protein sequences databases deposited online such as The Universal Protein Resource (UniProt) and The National Center for Biotechnology Information (NCBI) (Xu & Xu, 2004). Nevertheless, the richness of plant protein databases remains lower when compared to the other databases available for human, snake, bird and yeast, to name a few. Nonetheless, LC-MS based proteomics is still an

essential tool in the investigation of medicinal plants, contributing to the discovery of novel proteins with potential therapeutic applications or as an important research approach.

This study attempts to extract proteins from OS leaves (OSLP) with a method achievable at laboratory scale and characterize the protein compositions of OSLP extracted using mass spectrometry-based proteomics.

2 MATERIALS AND METHODS

2.1 Preparation of plant material

The OS plants aged about 12 months old (voucher specimen 11009) were collected from Kampung Repuh, Batu Kurau (GPS coordinates: 4.52°N, 100.48°E; Perak, Malaysia). The fresh leaves were collected, cleaned, flash-frozen using liquid nitrogen and grounded into fine, homogeneous powder using pre-chilled grinder and ultrasonic cell crusher. The leaf powder was then weighed (50 mg) and kept in sterile 2.0 mL protein lo-bind (Eppendorf) microtubes.

2.2 Preparation of reagents

Non-protein extraction buffer (M1) was prepared in 100 mL of methyl tert-butyl ether (MTBE)/methanol (MeOH): 75 mL of MTBE to 25 mL of MeOH (3:1, vol/vol). The M1 buffer was kept at -20°C. Phase separation-inducing solvent (M2) was prepared in 100 mL of Milli-Q ultrapure water (MQUPW) /MeOH: 75 mL of MQUPW was added to 25 mL of MeOH (3:1, vol/vol). The M2 solvent was kept at 4°C. Protein extraction (PE) buffer was freshly prepared in 10 mL which contained 6 M urea, 2 M thiourea, 15 mM dithiothreitol (DTT), 3-[(3-cholamidopropyl) dimethylammonio]-1-propanesulfonate (CHAPS, 2%), protease and phosphatase inhibitors. The PE buffer was kept at room temperature (r.t.).

2.3 Protein extraction by One-Tube Method (OTM)

One-Tube Method (OTM) was modified from previous studies (Isaacson et al., 2006; Salem, Jüppner, Bajdzienko, & Giavalisco, 2016; Smaczniak et al., 2012). 1.0 mL of pre-cooled M1 was added into each aliquot (50 mg of LN_2 flash-frozen OS leaf powder in individual microtube). All microtubes were thoroughly vortexed (1 min; 2000 rpm) and then incubated on orbital shaker (60 min; 70 rpm; 4°C). Following that, all the microtubes were subjected to sonication (ice water; 30 min; 4°C). Next, pre-cold M2 (650 µL) was added into each aliquot, thoroughly vortexed (1 min; 2000 rpm) and centrifuged at 18,000 g for 10

minutes; at 4°C. The aqueous phases were carefully pipetted off without disturbing the insoluble pellet formed at the bottom. 500 µL of pre-cooled (4°C) MeOH was added and vortexed thoroughly (30 s; 1400 rpm). Following that, all the microtubes were centrifuged (18,000 x g; 10 min; 4°C). This washing step was repeated for two times. The washed pellet from each aliquot was re-suspended in 200 µL of freshly prepared PE (1:4; wt/vol) followed by sonication (ice water; 10 min; 4°C) and then incubated on orbital shaker (60 min; 70 rpm; r.t.). Finally, all the microtubes were centrifuged (10,000 g; 5 min; 4°C). The supernatants produced were then harvested and subjected to vacuum concentration (300 rpm; 24 h; 40°C).

2.4 Protein estimation by Bradford protein assay

Protein concentration was estimated using Quick Start™ Bradford Protein Assay with bovine serum albumin as standard (Bio-Rad, USA). Briefly, 5µL of the protein sample (OSLP) or standard was separately loaded onto a sterile 96-well plate in triplicate. 250 µL of dye reagent was then added into each well. The plate was incubated (25-27°C; 5 min) and the absorbance was read at 595 nm (Bio-Rad Benchmark Plus Microplate Reader with Microplate Manager 5.2.1 software, Bio-Rad, USA). The percentage (%) of yield for OSLP was calculated:

$$Yield\ of\ OSLP\ (\%) = \frac{weight\ of\ \ extract}{weight\ of liquid\ nitrogen\ flash - frozen\ OSB\ leaf\ powder}$$

2.5 Protein separation by one-dimensional sodium dodecyl sulphate-polyacrylamide gel electrophoresis (1-D SDS-PAGE)

One-dimensional SDS-PAGE (1-D SDS-PAGE, 12% polyacrylamide gel) was performed according to the Laemmli method (Laemmli, 1970) with modifications. Briefly, OSLP was re-suspended in MQUPW, boiled at 95°C (5 min) and cooled to room temperature. Then, 50 µg of solubilized OSLP was well mixed with loading buffers in a 1:1 ratio and separated on 12% (w/v) resolving gel and 4% (w/v) stacking gel using the Laemmli buffer system. This procedure was conducted at room temperature. Thermo Scientific PageRuler^{TM} Plus Pre-stained Protein Ladder was used as the molecular weight marker. Bio-

Rad mini-Protean II electrophoresis set was used to perform the protein separation under constant 200V for 60 min until the loading dye front reached the bottom of gel.

2.6 Silver nitrate staining of protein in 1-D SDS-PAGE

After completion of electrophoresis, the gel was subjected to ultrafast silver nitrate staining as previously described (Chevallet, Luche, & Rabilloud, 2006) with modifications. Briefly, the gel was rinsed with MQUPW followed by the addition of fixation solution and incubated with gentle shaking (overnight). Next, the gel was collected and washed with ethanol (50%, 20 min; 20%, 20 min) with gentle shaking. The gel was rinsed with MQUPW (20 s; twice) and was soaked in sensitizing solution (1 min). Then, the gel was rinsed with MQUPW (20 s; thrice) followed by silver nitrate impregnation (20 min; r.t.) with gentle shaking and then was washed off using MQUPW (20 s; twice). Developing solution was added until clear protein bands appeared and then was rinsed off with MQUPW (2 min; twice). Finally, the staining process was terminated by adding in 10% glacial acetic acid. The gel image was scanned using Epson Expression 10,000XL coupled with Epson Scan Utility software (Seiko Epson Co., Japan).

2.7 De-staining 1-D SDS-PAGE

The gel was de-stained prior to in-gel protein digestion. Firstly, the silver nitrate stained SDS-PAGE gel was soaked overnight in MQUPW. Next, selected visible gel bands were carefully excised and transferred to sterile 2.0 mL Protein lo-bind microtubes and de-stained using 0.4 g of potassium ferricyanide in 200 mL sodium thiosulphate (0.2 g/L water). The gel bands were incubated at room temperature in the de-staining solution with gentle shaking for 15 minutes or until completely de-stained. Then, the gel bands were rinsed for 15 minutes with MQUPW. The washing step was repeated for a total of 5 times with gentle shaking.

2.8 In-gel protein digestion

In-gel protein digestion was carried out based on manufacturer's instructions (Mass Spec Grade Promega, USA). Briefly, the gel bands were washed in 25 mM ammonium bicarbonate (ABC) and dehydrated in acetonitrile (ACN) (4 times; r.t.). Herein, this washing and dehydration was termed as Step 1. Next, the gel bands were reduced in 10 mM DTT (65°C; 30 minutes). Following that, Step 1 as aforementioned was repeated. The gel bands were then alkylated in 10 mM IAA in 25 mM ABC and incubated in the dark (45 min; 37°C).

Step 1 as aforementioned was repeated. After that, 20 µL of 20 ng/µL Trypsin/Lys-C Mix in 25 mM ABC was added and the mixture was incubated for 10 min. Next, the mixture was incubated overnight at 37°C (Mass Spec Grade Promega, USA). Finally, the digestion was terminated by adding in 1% formic acid (FA). The extracted peptides were vacuum-concentrated (300 rpm; 24 h; 40°C) and de-salted using C-18 spin column following the manufacturer's instructions (Thermo Scientific, USA). 8 µL of MQUPW with 0.1 % FA was used to reconstitute the de-salted peptides prior to Agilent ESI-LCMS/MS analysis.

2.9 In-solution protein digestion

In-solution protein digestion was carried out based on manufacturer's instructions (Mass Spec Grade Promega, USA). Briefly, 20 µg of OSLP was digested by Trypsin/Lys-C Mix (ratio 25 protein:1 protease; w/w) buffered in 50 mM Tris (hydroxymethyl) aminomethane (THAM) hydrochloride (Tris-HCl, pH 8) and then incubated in the dark (overnight; 37°C). FA (1%) was added to cease the enzyme activity. Following that, the digested peptides were spun down (16,000 x g; 4°C; 10 min) to collect the supernatant. The supernatant was vacuum-concentrated (300 rpm; 24 h; 40°C). They were de-salted using C-18 spin column (Thermo Scientific, USA). Finally, the de-salted peptides were reconstituted in 10 µL of FA (0.1%), briefly vortexed and centrifuged prior to Agilent LCMS/MS analysis.

2.10 Protein analysis of nanoflow liquid chromatography electrospray-ionization coupled with tandem mass spectrometry/mass spectrometry (Nanoflow-ESI-LCMS/MS)

The digested peptides were loaded onto C-18 300Å Large Capacity Chip (Agilent, USA) and separated using a binary buffer system. The column was equilibrated by Buffer 1 (0.1% FA in MQUPW) and Buffer 2 (60% ACN containing 0.1% FA). The digested peptides were eluted with a linear gradient: 50 min in 0-40% Buffer 2 followed by 40-80% Buffer 2 for additional 30 minute. Quadrupole-time of flight (Q-TOF) was set at positive polarity, capillary voltage at 2050 V, fragmentor voltage at 300 V, drying gas flow 5 L/min and gas temperature of 300°C. The peptide spectrum was analyzed in auto MS mode ranging from 110-3000 m/z for MS scan and 50-3000 m/z for MS/MS scan, followed by up to 15 data-dependent MS/MS scans (Top 15 approach) with higher-energy collisional dissociation (HCD) at a resolution of 17,500 at 200 m/z. Dynamic exclusion was set to 30 seconds. Agilent MassHunter data acquisition software (version B.07.00, Agilent Technologies,

Santa Clara, CA, USA) and PEAKS®Studio software (version 7.5, Bioinformatics Solutions Inc., Waterloo, ON, Canada) were used for the spectrum analysis.

2.11 Identification of protein and peptide by automated *de novo* sequencing

The Lamiaceae protein databases (March 2018) of UniProtKB (http://www.uniprot.org/uniprot/) and NCBInr (https://www.ncbi.nlm.nih.gov/) were downloaded. Protein identification and homology search by comparing the *de novo* sequence tag were assisted by the PEAKS®Studio (Version B.07.00). The settings applied were as follow: both parent mass and precursor mass tolerance was set at 0.1 Da with monoisotopic as the precursor mass search type, carbamidomethylation was set as fixed modification with maximum missed cleavage was set at 3, maximum variable post-translational modification was set at 3 and Trypsin/Lys-C was selected as the digestion enzyme. The other parameters were set as default by Agilent. The filtration parameters were set at a significant score (-10logP) of protein ≥ 20 and number of peptides ≥ 20 to exclude inaccurate proteins. PEAKS® indicated that a -10logP score of greater than 20 is of relatively high in confidence as it targets very few decoy matches above the threshold (J. Zhang et al., 2012). Separately, the different protein compositions of OSLP detected were searched in the databases of UniProtKB, NCBInr and InterPro Classification of Protein Families (https://www.ebi.ac.uk/interpro/protein/) for their annotated protein family, cellular component and molecular function, and the percentage (%) of each category was calculated (Eq. 1 – 3):

$$\%\ protein\ family = \frac{no.\ of\ protein\ \text{compositions}\ in\ same\ protein\ family}{total\ detected\ protein\ compositions} x\ 100 \quad \text{....Eq.1}$$

$$\%\ cellular\ component = \frac{no.\ of\ protein\ \text{compositions}\ in\ same\ cellular\ component}{total\ detected\ protein\ compositions} x\ 100 \quad \text{....Eq.2}$$

$$\%\ molecular\ function = \frac{no.\ of\ protein\ \text{compositions}\ with\ same\ molecular function}{total\ detected\ protein\ compositions} x\ 100 \quad \text{.... Eq.3}$$

3 RESULTS AND DISCUSSION

3.1 Yield of OSLP from OTM

Extraction of protein from medicinal plants represents a great challenge, especially from the green leaf tissues. Plant cells are enveloped by a rigid and tough structure constituted of two layers of cell wall, primary and secondary. The primary cell is thinner and harder than the secondary cell wall. This wall structure is constructed by a complex network of pectins, cross-linking glycans, cellulose microfibrils and lignins, all of which are present substantially and ubiquitously. In addition, the middle lamella structure is rich in pectins. These structures make the plant cell walls to be significantly thicker and more difficult to be completely ruptured. To harvest the proteins embedded deeply beyond the cell walls, an optimal protein extraction strategy is required.

In this study, OTM employed the sequential extraction strategy to extract OSLP from the LN_2 flash-frozen leaf sample. Buffer M1 separated the "non-protein contaminants" including polar-, semi-polar and hydrophobic metabolites. Buffer M2 precipitated the insoluble compounds including proteins, starch and plant cell wall components (Salem et al., 2016). The protein compositions of OSLP were harvested by the PE buffer. OTM has successfully produced a total yield of 3 mg of OSLP per 1 g of LN_2 flash-frozen leaf sample (about 0.3%). This yield was relatively higher when compared to the previous studies reported (N. Wang et al., 2015; W. Wang et al., 2003); the former extracted proteins from aged olive leaf sample (total yield was 2.49 mg/g) and the latter extracted proteins from maize leaf midrib (total yield was 1.86 mg/g), wherein the phenol-based and trichloroacetic acid (TCA) precipitation-based protocols were employed respectively. Plant protein extractions, conventionally, were either phenol-based or TCA precipitation-based. In some cases, a combination of both was used depending on the sample type and experimental requirements (N. Wang, Wu, Ku, Chen, & Wang, 2016; W. Wang et al., 2003; Xiang et al., 2010). These common methods used organic solvents especially acetone, TCA, phenol and SDS (sodium dodecyl sulphate). The phenol-based method is more time-consuming and laborious than the TCA precipitation-based protocol, but it is more preferred rendered by its potential to separate and precipitate proteins more efficiently from the recalcitrant plant tissues (Isaacson et al., 2006; N. Wang et al., 2016; W. Wang et al., 2003; Xiang et al., 2010). However, organic solvents especially SDS and phenol are denaturant agents that may introduce chemical modifications to proteins and thereby, affect the folding and structures

(Bhuyan, 2010). Conformational changes cause a protein to lose its specific actions (Hashiguchi & Komatsu, 2017). Thus, concern arises on the preservation of biological actions of a protein. The preservation of plant-derived bioactive proteins is essential as they also possess important pharmaceutical values (Shah et al., 2017; Yeboah, Hilger, & Kroschel, 2003). In comparison, OTM did not use denaturant agents. This might reduce the damage to the protein structures and thereby, contribute to the slight increase in the total protein yield obtained in this study. As such, OTM used in this study can be considered as an optimal extraction alternative at laboratory scale particularly in a fundamental research laboratory which often is equipped with limited resources.

3.2 One-dimensional SDS-PAGE (1-D SDS-PAGE)

1-D SDS-PAGE was used to accessed the protein compositions of OSLP (Fig. 2). As seen, OSLP constituted of protein compositions with varying electrophoretic (molecular weight-distribution) protein profiles. Silver nitrate-stained OSLP bands were displayed in several regions, ranging from 10, 25-35, 55-250 to above 250 kDa. The separation pattern was sufficiently distinctive and with low backgrounds. In 1-D SDS-PAGE, visible bands are indicative of the presence of a protein sample whereas a low-backgrounds staining is indicative of a clean protein sample with the interfering substances including non-protein contaminants, salts, detergents, denaturants and organic solvents are sufficiently removed (Evans, Romero, & Westoby, 2009). 1-D SDS-PAGE has confirmed the presence of OSLP extracted with OTM. A visual representation of the OSLP pattern illustrates the complexity of the sample being investigated.

Leaf is considered as a type of recalcitrant tissue which the protein contents inside are difficult to be extracted mainly due to high levels of interfering compounds (W. Wang et al., 2003). In line with that, a study by Rehman and Adnan (2018) on medicinal plants from different families have found the majority is especially low in protein contents. Conversely, they are naturally rich in secondary metabolites such as phenolic compounds, pigments, oils, starches and cell wall polysaccharides. In proteomics study, these components are known as "non-protein contaminants" which may contaminate a protein sample and thereby, interfere protein separations (Isaacson et al., 2006; Saha & Bhattacharya, 2017; Xiang et al., 2010). Additional limitations from green leaf tissues are the high levels of proteases (e.g. Serine and Cysteine) and oxidative enzymes (e.g. Catalase), which may be detrimental to the stability and function of a protein (Isaacson et al., 2006; Mónico, Martínez-Senra, Zorrilla,

& Pérez-Sala, 2017). In view of this, as an attempt to lower the degradation of OSLP as much as possible, both protease and phosphatase inhibitors as well as CHAPS were included in the PE buffer. Protease inhibitors suppress a broad spectrum of proteolytic activities whilst phosphatase inhibitors suppress various cellular protein phosphatases (e.g. alkaline phosphatase, serine/threonine (Ser/Thr) phosphatase, tyrosine (Tyr) phosphatase and dual specificity, Tyr and Ser/Thr phosphatase). This is helpful in freezing the phosphorylation state of a protein at a selected time point (Gleiser I, 2010) and improving the stability of proteins (Cook, 1993; Wenger, O'Dorisio, & Campolito, 1991). CHAPS is a mild and non-denaturing zwitterionic sulfobetaine detergent. It solubilizes membrane proteins and receptors, useful for breaking protein-protein interactions (Chattopadhyay & Harikumar, 1996; Singh et al., 2015). 1-D SDS-PAGE has visualised the OSLP bands of varying molecular weights (Fig. 2). This might be attributed to the improved protein recovery rate, in line with the findings reported by Salem et al. (2016). However, Salem and colleagues (Salem et al., 2016) did not visualise the proteins extracted from *Arabidopsis thaliana* rosette leaves (Brassicaceae family) with any gel electrophoresis applications.

3.3 Proteomic identification and characterization of OSLP

In this study, shotgun-proteomics and tandem mass spectrometry were employed in the identification of protein compositions present in OSLP. The protein compositions identified were matched to the Lamiaceae family protein databases in UniProtKB and NCBInr. A total of 904 protein compositions were detected from the in-gel and in-solution samples (See Supplementary Data). The detected protein compositions were then filtered by PEAKS® Studio software. After removing duplications and grouping them accordingly, a total of 336 of protein compositions were found (Table 1).

Orthosiphon stamineus (OS) is a medicinal plant in the Lamiaceae family. Therefore, matching to the Lamiaceae databases increased the identification of unique protein compositions which shares highly homologous or identical peptides. Similar homology-driven proteomics approach has been adopted by Salem et al. (2016) wherein the detected proteins from *Arabidopsis thaliana* rosette leaves were matched to the Brassicaceae database and in a study by Saha and Bhattacharya (2017), the allergens from *Phoenix sylvestris* was compared to the Arecaceae database. Homology-driven proteomics is a powerful tool in protein identification as it allows multiple mismatches in a sequence stretch by using peptide sequences that are highly homologous or genetically similar (Junqueira et al., 2008;

Shevchenko, Valcu, & Junqueira, 2009). Nonetheless, matching to the same family database may limit the number of proteins detected. The richness of a plant family database remains lower when compared to the Viridiplantae kingdom database wherein the data is made up of the green algae, aquatic and the land plants. This is one of the limitations in this study.

Table 1 List of protein compositions identified from OSLP with annotations based on UniProtKB (http://www.uniprot.org/uniprot/) and NCBInr (https://www.ncbi.nlm.nih.gov/).

No.	Protein Accession No.	Average Mass	Max-10logP	Max Coverage (%)	Max# Peptides	Max# Unique Peptides	Protein Description
1	gi|403399409|sp|E2E2P0|GTPS_ORIVU	69063	534.29	33	26	26	Gamma-terpinene synthase, chloroplastic [Origanum vulgare] (Wild marjoram)
2	gi|75306222|sp|Q947B7|MFS_MENPI	55360	272	28	15	15	(+)-menthofuran synthase [Mentha piperita](Peppermint) (Mentha aquatica x Mentha spicata)
3	gi|75251483|sp|Q5SBP6|GDS_OCIBA	63395	178.18	5	3	3	Germacrene-D synthase [Ocimum basilicum] (Sweet basil)
4	gi|29839421|sp|Q9XGW0|COMT1_OCIBA	39529	566.71	50	22	12	Caffeic acid 3-O-methyltransferase 1 [Ocimum basilicum] (Sweet basil)
5	gi|29839420|sp|Q9XGV9|COMT2_OCIBA	39613	500.82	56	25	17	Caffeic acid 3-O-methyltransferase 2 [Ocimum basilicum] (Sweet basil)
6	gi|75315260|sp|Q9XHE7|C71DD_MENPI	56601	227.54	14	7	7	Cytochrome P450 71D13 [Mentha piperita](Peppermint) (Mentha aquatica x Mentha spicata)
7	gi|75129878|sp|Q6WAU0|PULR_MENPI	37915	1021.98	65	33	33	(+)-pulegone reductase [Mentha piperita](Peppermint) (Mentha aquatica x Mentha spicata)
8	gi|75251484|sp|Q5SBP7|SELS_OCIBA	63125	415.32	27	15	14	Selinene synthase [Ocimum basilicum] (Sweet basil)
9	gi|75251481|sp|Q5SBP4|AZIS_OCIBA	62858	93.41	6	3	3	Alpha-zingiberene synthase [Ocimum basilicum] (Sweet basil)
10	gi|5915814|sp|O04164|C71A6_NEPRA	57955	486.08	31	18	18	Cytochrome P450 71A6 [Nepeta racemosa] (Catmint) (Raceme catnip)
11	gi|62899675|sp|O81192|BPPS_SALOF	69292	327.6	17	10	8	(+)-bornyl diphosphate synthase, chloroplastic [Salvia officinalis] (Sage)
12	gi|122210943|sp|Q2XSC5|LALIN_LAVAN	65654	189.93	8	4	4	R-linalool synthase [Lavandula angustifolia] (Lavender)
13	gi|75180331|sp|Q9LRC8|BAGLU_SCUBA	58772	289.62	21	9	9	Baicalin-beta-D-glucuronidase [Scutellaria baicalensis] (Baical skullcap)
14	gi|122233627|sp|Q4JF75|RBR_SCUBA	111795	881.95	67	78	78	Retinoblastoma-related protein [Scutellaria baicalensis] (Baical skullcap)
15	gi|75251477|sp|Q5SBP0|TPSD_OCIBA	70000	400.55	30	22	16	Terpinolene synthase, chloroplastic [Ocimum basilicum] (Sweet basil)

No.	Protein Accession No.	Average Mass	Max-10logP	Max Coverage (%)	Max# Peptides	Max# Unique Peptides	Protein Description
16	gi|5921781|sp|O04111|CHSY_PERFR	42686	253	54	38	38	Chalcone synthase [Perilla frutescens] (Beefsteak mint) (Perilla ocymoides)
17	gi|75251482|sp|Q5SBP5|GCS1_OCIBA	63566	305.93	15	9	8	Gamma-cadinene synthase [Ocimum basilicum] (Sweet basil)
18	gi|910312590|ref|YP_009162251.1|	158800	75.7	2	2	2	DNA-directed RNA polymerase beta subunit-2 (chloroplast) [Scutellaria baicalensis]
19	gi|916442749|gb|AKZ23931.1|	157974	98.65	4	4	4	RNA polymerase beta" subunit (plastid) [Salvia nemorosa]
20	gi|836643373|ref|YP_009144505.1|	158291	68.68	2	2	2	DNA-directed RNA polymerase beta" subunit (chloroplast) [Rosmarinus officinalis]
21	gi|401879732|gb|AFQ30919.1|	158403	68.68	2	2	2	DNA-directed RNA polymerase beta subunit-2 (chloroplast) [Salvia miltiorrhiza]
22	gi|827345865|gb|AKJ77166.1|	25335	49.94	8	2	2	NAD(P)H-quinone oxidoreductase subunit K, chloroplastic [Scutellaria baicalensis]
23	gi|122219295|sp|Q49SP7|TPSCS_POGCB	63586	356.54	31	17	17	Gamma-curcumene synthase [Pogostemon cablin] (Patchouli) (Mentha cablin)
24	gi|8134569|sp|Q42662|METE_PLESU	84590	567.24	29	24	24	5-methyltetrahydropteroyltriglutamate--homocysteine methyltransferase [Plectranthus scutellarioides] (Coleus) (Solenostemon scutellarioides)
25	gi|122237148|sp|Q15GI4|EGS1_OCIBA	35607	88.09	6	2	2	Eugenol synthase 1 [Ocimum basilicum] (Sweet basil)
26	gi|75227033|sp|Q76MR7|UBGAT_SCUBA	48654	294.42	33	14	14	Baicalein 7-O-glucuronosyltransferase [Scutellaria baicalensis] (Baical skullcap)
27	gi|75161989|sp|Q8W1W9|5MAT1_SALSN	50724	335.2	14	7	7	Malonyl-coenzyme:anthocyanin 5-O-glucoside-6'''-O-malonyltransferase [Salvia splendens] (Scarlet sage)
28	gi|84027871|sp|Q93WU2|EOMT1_OCIBA	40237	128.93	8	3	3	Eugenol O-methyltransferase [Ocimum basilicum] (Sweet basil)
29	gi|403399735|sp|E2E2N7|BCGS_ORIVU	64443	172.34	6	4	4	Bicyclogermacrene synthase [Origanum vulgare] (Wild marjoram)
30	gi|75338882|sp|Q9ZR27|5GT1_PERFR	50974	177.13	10	5	5	Anthocyanidin 3-O-glucoside 5-O-glucosyltransferase 1 [Perilla frutescens] (Beefsteak mint) (Perilla ocymoides)
31	gi|75338881|sp|Q9ZR26|5GT2_PERFR	49110	125.23	8	4	4	Anthocyanidin 3-O-glucoside 5-O-glucosyltransferase 2 [Perilla frutescens] (Beefsteak mint) (Perilla ocymoides)

No.	Protein Accession No.	Average Mass	Max-10logP	Max Coverage (%)	Max# Peptides	Max# Unique Peptides	Protein Description
32	gi|75288825|sp|Q65CJ7|HPPR_PLESU	34128	72.51	6	2	2	Hydroxyphenylpyruvate reductase [Plectranthus scutellarioides] (Coleus) (Solenostemon scutellarioides)
33	gi|748013964|gb|AJE28434.1|	225117	274.52	14	32	24	Protein TIC 214 [Premna microphylla]
34	gi|827346602|gb|AKJ77788.1|	181164	149.72	7	9	6	Protein TIC 214 [Perilla frutescens]
35	gi|401879732|gb|AFQ30919.1|	158403	111.71	4	4	4	DNA-directed RNA polymerase subunit beta" [Salvia miltiorrhiza]
36	gi|836643373|ref|YP_009144505.1|	158291	86.06	4	4	4	DNA-directed RNA polymerase subunit beta" [Rosmarinus officinalis]
37	gi|827345132|gb|AKJ76716.1|	218366	180.02	6	6	6	Protein TIC 214 [Rosmarinus officinalis]
38	gi|510794432|gb|AGN52182.1|	27098	22.41	3	1	1	MYB-related transcription factor [Salvia miltiorrhiza]
39	gi|510794526|gb|AGN52229.1|	28066	22.41	3	1	1	MYB-related transcription factor [Salvia miltiorrhiza]
40	gi|510794500|gb|AGN52216.1|	35378	22.41	3	1	1	MYB-related transcription factor [Salvia miltiorrhiza]
41	gi|510794478|gb|AGN52205.1|	38440	22.41	2	1	1	MYB-related transcription factor [Salvia miltiorrhiza]
42	gi|844572791|gb|AKN09590.1|	34611	22.35	4	1	1	basic helix-loop-helix transcription factor [Salvia miltiorrhiza]
43	gi|844572722|gb|AKN09568.1|	41656	105.33	8	4	4	basic helix-loop-helix transcription factor [Salvia miltiorrhiza]
44	gi|908373664|gb|AKT44364.1|	81096	41.79	2	2	2	heat shock protein 2 [Tectona grandis]
45	gi|56749087|sp|Q85XY6|MATK_OCIBA	60282	345.11	36	20	20	Maturase K [Ocimum basilicum] (Sweet basil)
46	gi|75290511|sp|Q6IV13|C7D95_MENSP	56322	408.04	32	17	11	Cytochrome P450 71D95 [Mentha spicata] (Spearmint)
47	gi|75293242|sp|Q6WKY9|C7D95_MENGR	56365	239.93	23	11	10	Cytochrome P450 71D95 [Mentha gracilis] (Gingermint)
48	gi|75219538|sp|O48935|TPSBF_MENPI	63830	330.11	36	21	20	Beta-farnesene synthase [Mentha piperita] (Peppermint) (Mentha aquatica x Mentha spicata)
49	gi|75293243|sp|Q6WKZ0|C7D94_MENGR	56308	524.59	75	53	50	Cytochrome P450 71D94 [Mentha gracilis] (Gingermint)
50	gi|62900763|sp|O81191|SCS_SALOF	69369	124.9	12	7	7	1,8-cineole synthase, chloroplastic [Salvia officinalis] (Sage)
51	gi|75251479|sp|Q5SBP2|FES_OCIBA	69866	37.38	2	1	1	(-)-endo-fenchol synthase, chloroplastic [Ocimum basilicum] (Sweet basil)

No.	Protein Accession No.	Average Mass	Max-10logP	Max Coverage (%)	Max# Peptides	Max# Unique Peptides	Protein Description
52	gi|75224312|sp|Q6USK1|GERS_OCIBA	64933	117.7	4	2	2	Geraniol synthase, chloroplastic [Ocimum basilicum] (Sweet basil)
53	gi|3914545|sp|Q31655|RBL_AJUCH	52455	118.97	10	5	5	Ribulose bisphosphate carboxylase large chain [Ajuga chamaepitys] (Yellow bugle) (Teucrium chamaepitys)
54	gi|548687|sp|P36483|RBL_CALDI	49209	29.59	2	1	1	Ribulose bisphosphate carboxylase large chain [Callicarpa dichotoma] (Purple beautyberry) (Porphyra dichotoma)
55	gi|132044|sp|P28453|RBL_SCUBO	51794	175.85	22	10	10	Ribulose bisphosphate carboxylase large chain [Scutellaria bolanderi] (Sierra skullcap)
56	gi|122219292|sp|Q49SP4|TPGD1_POGCB	64197	183.33	10	7	4	Germacrene D synthase 1 [Pogostemon cablin] (Patchouli) (Mentha cablin)
57	gi|510785777|sp|G0LD36|RAS_MELOI	47161	205.33	18	8	8	Rosmarinate synthase [Melissa officinalis] (Lemon balm)
58	gi|17366672|sp|Q9ARF9|HPPD_PLESU	47736	48.63	4	2	2	4-hydroxyphenylpyruvate dioxygenase [Plectranthus scutellarioides] (Coleus) (Solenostemon scutellarioides)
59	gi|753709941|gb|AJI44435.1|	41648	38.44	2	1	1	Oxoglutarate-dependent flavone 7-O-demethylase [Ocimum basilicum]
60	gi|745791067|gb|AJD25242.1|	53008	48.25	6	2	2	cytochrome P450 CYP707A102 [Salvia miltiorrhiza]
61	gi|745790971|gb|AJD25194.1|	55908	22.03	2	1	1	cytochrome P450 CYP81B62 [Salvia miltiorrhiza]
62	gi|410176144|gb|AFV61803.1|	26773	110.53	20	4	4	30S ribosomal protein S2 (chloroplast) [Origanum vulgare subsp. vulgare]
63	gi|916442902|gb|AKZ23975.1|	26773	132.1	25	5	5	ribosomal protein S2 (plastid) [Monarda fistulosa var. mollis]
64	gi|916442908|gb|AKZ23977.1|	26686	132.1	25	5	5	ribosomal protein S2 (plastid) [Nepeta cataria]
65	gi|827346574|gb|AKJ77760.1|	26722	132.1	25	5	5	30S ribosomal protein S2 (chloroplast) [Perilla frutescens]
66	gi|827345166|gb|AKJ76750.1|	26770	43.14	10	2	2	30S ribosomal protein S2 (chloroplast) [Rosmarinus officinalis]
67	gi|401879731|gb|AFQ30918.1|	26744	43.14	10	2	2	30S ribosomal protein S2 (chloroplast) [Salvia miltiorrhiza]
68	gi|916442905|gb|AKZ23976.1|	26758	132.1	25	5	5	ribosomal protein S2 (plastid) [Salvia nemorosa]
69	gi|442775714|gb|AGC73980.1|	19816	20.22	6	1	1	jasmonate ZIM-domain protein 1 [Salvia miltiorrhiza]
70	gi|745791091|gb|AJD25254.1|	55430	48.55	2	2	2	cytochrome P450 CYP728D17 [Salvia miltiorrhiza]

No.	Protein Accession No.	Average Mass	Max-10logP	Max Coverage (%)	Max# Peptides	Max# Unique Peptides	Protein Description
71	gi|735679295|gb|AJA39985.1|	82378	100.26	5	4	4	(E)-4-hydroxy-3-methylbut-2-enyl diphosphate synthase [Salvia miltiorrhiza f. alba]
72	gi|122249145|sp|Q49SP3|TPSPS_POGCB	64199	456.1	51	31	29	Patchoulol synthase [Pogostemon cablin] (Patchouli) (Mentha cablin)
73	gi|116256299|sp|Q9XES0|DXR_MENPI	51034	129.28	15	9	9	1-deoxy-D-xylulose 5-phosphate reductoisomerase, chloroplastic [Mentha piperita] (Peppermint) (Mentha aquatica x Mentha spicata)
74	gi|75192856|sp|Q9MBC1|3AT_PERFR	50675	179.09	15	7	7	Anthocyanidin 3-O-glucoside 6"-O-acyltransferase [Perilla frutescens] (Beefsteak mint) (Perilla ocymoides)
75	gi|75129654|sp|Q6VMW0|Q8OMT_MENPI	40849	43.32	6	2	2	8-hydroxyquercetin 8-O-methyltransferase [Mentha piperita] (Peppermint) (Mentha aquatica x Mentha spicata)
76	gi|916438881|gb|AKZ22145.1|	84354	99.12	3	3	3	NADH dehydrogenase subunit 5 (plastid) [Monarda fistulosa var. mollis]
77	gi|410176201|gb|AFV61860.1|	84295	99.12	3	3	3	NADH dehydrogenase subunit 5 (chloroplast) [Origanum vulgare subsp. vulgare]
78	gi|669254287|gb|AII20583.1|	77022	93.96	6	3	3	NADH dehydrogenase subunit F, partial (chloroplast) [Holocheila longipedunculata]
79	gi|669254291|gb|AII20585.1|	79070	93.96	6	3	3	NADH dehydrogenase subunit F, partial (chloroplast) [Petraeovitex multiflora]
80	gi|669254283|gb|AII20581.1|	77991	93.96	6	3	3	NADH dehydrogenase subunit F, partial (chloroplast) [Holocheila longipedunculata]
81	gi|395484522|gb|AFN66518.1|	76105	93.96	6	3	3	NADH dehydrogenase subunit F, partial (plastid) [Teucrium subspinosum]
82	gi|669254293|gb|AII20586.1|	79081	125.9	7	4	4	NADH dehydrogenase subunit F, partial (chloroplast) [Hymenopyramis cana]
83	gi|401879790|gb|AFQ30977.1|	83587	247.04	12	10	8	NADH dehydrogenase subunit 5 (chloroplast) [Salvia miltiorrhiza]
84	gi|395484502|gb|AFN66509.1|	75956	93.96	6	3	3	NADH dehydrogenase subunit F, partial (plastid) [Teucrium divaricatum]
85	gi|395484481|gb|AFN66500.1|	76061	93.96	6	3	3	NADH dehydrogenase subunit F, partial (plastid) [Teucrium flavum subsp. glaucum]
86	gi|395484475|gb|AFN66497.1|	78510	93.96	6	3	3	NADH dehydrogenase subunit F, partial (plastid) [Rubiteucris palmata]
87	gi|836643377|ref|YP_009144562.1|	84218	187.92	6	6	6	NADH dehydrogenase subunit 5 (chloroplast) [Rosmarinus officinalis]
88	gi|916438885|gb|AKZ22147.1|	84443	93.96	3	3	3	NADH dehydrogenase subunit 5 (plastid) [Salvia nemorosa]

No.	Protein Accession No.	Average Mass	Max-10logP	Max Coverage (%)	Max# Peptides	Max# Unique Peptides	Protein Description
89	gi|395484513|gb|AFN66514.1|	76814	86.22	6	3	3	NADH dehydrogenase subunit F, partial (plastid) [Teucrium pyrenaicum]
90	gi|827346594|gb|AKJ77780.1|	84248	93.96	3	3	3	NADH dehydrogenase subunit 5 (chloroplast) [Perilla frutescens]
91	gi|827345833|gb|AKJ77134.1|	85675	156.12	6	6	6	NADH dehydrogenase subunit 5 (chloroplast) [Scutellaria baicalensis]
92	gi|395484511|gb|AFN66513.1|	76860	86.22	6	3	3	NADH dehydrogenase subunit F, partial (plastid) [Teucrium oxylepis]
93	gi|752789835|ref|YP_009117269.1|	85385	187.92	6	6	6	NADH-plastoquinone oxidoreductase subunit 5 (chloroplast) [Premna microphylla]
94	gi|395484489|gb|AFN66504.1|	76910	86.22	6	3	3	NADH dehydrogenase subunit F, partial (plastid) [Teucrium betonicum]
95	gi|916438887|gb|AKZ22148.1|	83254	86.22	3	3	3	NADH dehydrogenase subunit 5 (plastid) [Teucrium canadense]
96	gi|395484495|gb|AFN66506.1|	76993	86.22	6	3	3	NADH dehydrogenase subunit F, partial (plastid) [Teucrium eriocephalum subsp. almeriense]
97	gi|395484500|gb|AFN66508.1|	77065	86.22	6	3	3	NADH dehydrogenase subunit F, partial (plastid) [Teucrium stocksianum subsp. incanum]
98	gi|395484526|gb|AFN66520.1|	76596	86.22	6	3	3	NADH dehydrogenase subunit F, partial (plastid) [Teucrium bicolor]
99	gi|395484515|gb|AFN66515.1|	76501	121.16	8	4	4	NADH dehydrogenase subunit F, partial (plastid) [Teucrium racemosum]
100	gi|395484473|gb|AFN66496.1|	78531	127.61	9	5	4	NADH dehydrogenase subunit F, partial (plastid) [Teucridium parvifolium]
101	gi|395484524|gb|AFN66519.1|	75723	51.28	4	2	2	NADH dehydrogenase subunit F, partial (plastid) [Teucrium kotschyanum]
102	gi|395484477|gb|AFN66498.1|	76293	86.22	6	3	3	NADH dehydrogenase subunit F, partial (plastid) [Spartothamnella puberula]
103	gi|395484517|gb|AFN66516.1|	76688	86.22	6	3	3	NADH dehydrogenase subunit F, partial (plastid) [Teucrium salviastrum]
104	gi|395484520|gb|AFN66517.1|	76892	86.22	6	3	3	NADH dehydrogenase subunit F, partial (plastid) [Teucrium spinosum]
105	gi|395484483|gb|AFN66501.1|	77431	128.1	9	5	4	NADH dehydrogenase subunit F, partial (plastid) [Teucrium albicaule]
106	gi|395484504|gb|AFN66510.1|	77454	86.22	6	3	3	NADH dehydrogenase subunit F, partial (plastid) [Teucrium laciniatum]
107	gi|395484530|gb|AFN66522.1|	76725	86.22	6	3	3	NADH dehydrogenase subunit F, partial (plastid) [Teucrium viscidum var. miquelianum]

No.	Protein Accession No.	Average Mass	Max-10logP	Max Coverage (%)	Max# Peptides	Max# Unique Peptides	Protein Description
108	gi|395484528|gb|AFN66521.1|	76705	86.22	6	3	3	NADH dehydrogenase subunit F, partial (plastid) [Teucrium japonicum]
109	gi|395484537|gb|AFN66525.1|	78210	86.22	6	3	3	NADH dehydrogenase subunit F, partial (plastid) [Teucrium decipiens]
110	gi|395484533|gb|AFN66523.1|	75763	78.06	6	3	3	NADH dehydrogenase subunit F, partial (plastid) [Teucrium montbretii subsp. heliotropiifolium]
111	gi|395484507|gb|AFN66511.1|	77434	86.22	6	3	3	NADH dehydrogenase subunit F, partial (plastid) [Teucrium nudicaule]
112	gi|395484479|gb|AFN66499.1|	34714	78.06	12	3	3	NADH dehydrogenase subunit F, partial (plastid) [Oncinocalyx betchei]
113	gi|395484535|gb|AFN66524.1|	76413	78.06	6	3	3	NADH dehydrogenase subunit F, partial (plastid) [Teucrium antitauricum]
114	gi|395484493|gb|AFN66505.1|	77203	86.22	6	3	3	NADH dehydrogenase subunit F, partial (plastid) [Teucrium pseudochamaepitys]
115	gi|395484487|gb|AFN66503.1|	77172	86.22	6	3	3	NADH dehydrogenase subunit F, partial (plastid) [Teucrium aroanium]
116	gi|395484509|gb|AFN66512.1|	77251	86.22	6	3	3	NADH dehydrogenase subunit F, partial (plastid) [Teucrium orientale subsp. gloeotrichum]
117	gi|395484485|gb|AFN66502.1|	77595	86.22	6	3	3	NADH dehydrogenase subunit F, partial (plastid) [Teucrium aristatum]
118	gi|395484497|gb|AFN66507.1|	77873	86.22	6	3	3	NADH dehydrogenase subunit F, partial (plastid) [Teucrium fruticans]
119	gi|827345131|gb|AKJ76715.1|	266537	154.6	0	4	4	Protein Ycf2 [Rosmarinus officinalis]
120	gi|573462016|emb|CCQ71685.1|	267080	154.6	0	4	4	Protein Ycf2 [Salvia miltiorrhiza]
121	gi|748013968|gb|AJE28438.1|	268103	154.6	0	4	4	Protein Ycf2 [Premna microphylla]
122	gi|910312663|ref|YP_009162324.1|	268069	154.6	0	4	4	Protein Ycf2 [Scutellaria baicalensis]
123	gi|827346597|gb|AKJ77783.1|	266476	77.3	0	2	2	Protein Ycf2 [Perilla frutescens]
124	gi|749489569|emb|CEO43479.1|	50534	28.93	2	1	1	unnamed protein product [Lavandula angustifolia] - patented sequence
125	gi|787592954|gb|AKA27904.1|	30582	23.75	4	1	1	WRKY protein [Salvia miltiorrhiza]
126	gi|659902912|gb|AID69536.1|	58940	22.81	2	1	1	phenylalanine ammonia-lyase, partial [Phlomoides rotata]
127	gi|735665579|gb|AJA38250.1|	90993	40.08	4	2	2	copalyl diphosphate synthase, partial [Salvia fruticosa]
128	gi|62900766|sp|O81193|SSS_SALOF	68942	92.38	9	5	4	(+)-sabinene synthase, chloroplastic [Salvia officinalis] (Sage)

No.	Protein Accession No.	Average Mass	Max-10logP	Max Coverage (%)	Max# Peptides	Max# Unique Peptides	Protein Description
129	gi|510785778|sp|A0PDV5|RAS_PLESU	47902	81.71	8	5	5	Rosmarinate synthase [Plectranthus scutellarioides] (Coleus) (Solenostemon scutellarioides)
130	gi|122219294|sp|Q49SP6|TPGD2_POGCB	64149	543.51	53	36	31	Germacrene D synthase 2 [Pogostemon cablin] (Patchouli) (Mentha cablin)
131	gi|75315261|sp|Q9XHE8|C71DI_MENSP	56149	74.62	8	4	2	Cytochrome P450 71D18 [Mentha piperita] (Peppermint) (Mentha aquatica x Mentha spicata)
132	gi|75315259|sp|Q9XHE6|C71DF_MENPI	56532	94.94	6	3	3	Cytochrome P450 71D15 [Mentha piperita] (Peppermint) (Mentha aquatica x Mentha spicata)
133	gi|704000326|sp|S4UX02|CYPH1_SALMI	55520	114.72	5	3	3	Ferruginol synthase [Salvia miltiorrhiza] (Chinese sage)
134	gi|122200954|sp|Q2KNL5|CADH1_OCIBA	38769	23.05	4	1	1	Cinnamyl alcohol dehydrogenase 1 [Ocimum basilicum] (Sweet basil)
135	gi|401879801|gb|AFQ30988.1|	218699	154.47	4	6	5	Photosystem I assembly protein Ycf1 (chloroplast) [Salvia miltiorrhiza]
136	gi|573462011|emb|CCQ71680.1|	218685	152.08	4	6	5	Photosystem I assembly protein Ycf1 (chloroplast) [Salvia miltiorrhiza]
137	gi|836643389|ref|YP_009144556.1|	29997	113.08	12	4	4	ribosomal protein L2 (chloroplast) [Rosmarinus officinalis]
138	gi|401879808|gb|AFQ30995.1|	29997	56.54	6	2	2	ribosomal protein L2 (chloroplast) [Salvia miltiorrhiza]
139	gi|916441525|gb|AKZ23467.1|	29921	28.27	3	1	1	ribosomal protein L2 (plastid) [Nepeta cataria]
140	gi|410176218|gb|AFV61877.1|	29997	56.54	6	2	2	ribosomal protein L2 (chloroplast) [Origanum vulgare subsp. vulgare]
141	gi|916441521|gb|AKZ23465.1|	29997	28.27	3	1	1	ribosomal protein L2 (plastid) [Monarda fistulosa var. mollis]
142	gi|916441523|gb|AKZ23466.1|	29997	28.27	3	1	1	ribosomal protein L2 (plastid) [Salvia nemorosa]
143	gi|752789852|ref|YP_009117286.1|	30084	56.54	6	2	2	ribosomal protein L2 (chloroplast) [Premna microphylla]
144	gi|827346587|gb|AKJ77773.1|	31403	28.27	3	1	1	ribosomal protein L2 (chloroplast) [Perilla frutescens]
145	gi|827346537|gb|AKJ77723.1|	31391	28.27	3	1	1	ribosomal protein L2 (chloroplast) [Perilla frutescens]
146	gi|910312642|ref|YP_009162303.1|	30114	113.08	12	4	4	ribosomal protein L2 (chloroplast) [Scutellaria baicalensis]
147	gi|916441533|gb|AKZ23471.1|	30010	28.27	3	1	1	ribosomal protein L2 (plastid) [Teucrium canadense]
148	gi|916441821|gb|AKZ23615.1|	17837	25.53	7	1	1	ribosomal protein L22 (plastid) [Salvia nemorosa]

No.	Protein Accession No.	Average Mass	Max-10logP	Max Coverage (%)	Max# Peptides	Max# Unique Peptides	Protein Description
149	gi|913341377|gb|AKU77131.1|	121334	23.61	1	1	1	Structural maintenance of chromosomes protein 1, partial [Callicarpa bodinieri]
150	gi|762060299|gb|AJQ20621.1|	41314	21.58	2	1	1	Enoyl-ACP Reductase [Salvia miltiorrhiza]
151	gi|661525312|gb|AIE15763.1|	216665	106.44	4	4	4	Dicer-like protein 1 [Salvia miltiorrhiza]
152	gi|5915815|sp|Q42716|C71A8_MENPI	57213	188.9	28	15	15	Cytochrome P450 71A8 [Mentha piperita] (Peppermint) (Mentha aquatica x Mentha spicata)
153	gi|661525316|gb|AIE15765.1|	184302	229.83	7	7	7	Dicer-like protein 3 [Salvia miltiorrhiza]
154	gi|827345132|gb|AKJ76716.1|	218366	62.38	2	2	2	Ycf1 (chloroplast) [Rosmarinus officinalis]
155	gi|787592932|gb|AKA27893.1|	37310	25.11	4	1	1	WRKY protein [Salvia miltiorrhiza]
156	gi|662170387|gb|AIE45494.1|	44939	24.14	3	1	1	CONSTANS-like protein 9 [Tectona grandis]
157	gi|745790929|gb|AJD25173.1|	57680	43.97	2	2	2	Cytochrome P450 CYP73A120 [Salvia miltiorrhiza]
158	gi|630057998|gb|AHY94893.1|	57803	22.85	1	1	1	Cinnamate-4-hydroxylase [Prunella vulgaris]
159	gi|725812545|gb|AIY32618.1|	57979	43.97	2	2	2	Cinnamate-4-hydroxylase [Perilla frutescens]
160	gi|745791023|gb|AJD25220.1|	56140	22.76	2	1	1	Cytochrome P450 CYP94B50 [Salvia miltiorrhiza]
161	gi|762060309|gb|AJQ20626.1|	51963	21.88	4	1	1	Ketoacyl-ACP Synthase I [Salvia miltiorrhiza]
162	gi|844572842|gb|AKN09607.1|	76725	43.94	2	2	2	Basic helix-loop-helix transcription factor [Salvia miltiorrhiza]
163	gi|762060281|gb|AJQ20612.1|	13344	20.65	12	1	1	Acyl Carrier Protein [Salvia miltiorrhiza]
164	gi|822603217|emb|CQR79430.1|	35399	20.39	3	1	1	Maturase K, partial (chloroplast) [Clerodendrum bracteatum]
165	gi|630058023|gb|AHY94894.1|	51993	41.41	4	2	2	4-coumarate:CoA ligase, partial [Prunella vulgaris]
166	gi|122219293|sp|Q49SP5|TPGAS_POGCB	64232	302.47	24	15	15	Germacrene A synthase [Pogostemon cablin] (Patchouli) (Mentha cablin)
167	gi|75283876|sp|Q5C9I9|ISPD_MENPI	27191	102.75	18	5	5	(-)-isopiperitenol/(-)-carveol dehydrogenase, mitochondrial [Mentha piperita] (Peppermint) (Mentha aquatica x Mentha spicata)
168	gi|75252096|sp|Q5W283|TPSCM_MENPI	63839	254.94	15	9	9	Cis-muuroladiene synthase [Mentha piperita] (Peppermint) (Mentha aquatica x Mentha spicata)
169	gi|748013964|gb|AJE28434.1|	225117	248.42	8	18	16	hypothetical chloroplast RF19 (chloroplast) [Premna microphylla]
170	gi|916443350|gb|AKZ24105.1|	17446	55.83	10	2	2	ribosomal protein S7 (plastid) [Teucrium canadense]

No.	Protein Accession No.	Average Mass	Max-10logP	Max Coverage (%)	Max# Peptides	Max# Unique Peptides	Protein Description
171	gi|827345872|gb|AKJ77173.1|	17389	223.32	40	8	8	ribosomal protein S7 (chloroplast) [Scutellaria baicalensis]
172	gi|827345177|gb|AKJ76761.1|	17379	223.32	40	8	8	ribosomal protein S7 (chloroplast) [Rosmarinus officinalis]
173	gi|916443332|gb|AKZ24099.1|	17391	55.83	10	2	2	ribosomal protein S7 (plastid) [Monarda fistulosa var. mollis]
174	gi|573462013|emb|CCQ71682.1|	17361	133.84	20	4	4	ribosomal protein S7 (chloroplast) [Salvia miltiorrhiza]
175	gi|410176200|gb|AFV61859.1|	17361	111.66	20	4	4	ribosomal protein S7 (chloroplast) [Origanum vulgare subsp. vulgare]
176	gi|752789834|ref|YP_009117268.1|	17361	223.68	40	8	8	ribosomal protein S7 (chloroplast) [Premna microphylla]
177	gi|827346599|gb|AKJ77785.1|	17361	111.66	20	4	4	ribosomal protein S7 (chloroplast) [Perilla frutescens]
178	gi|916443335|gb|AKZ24100.1|	17379	55.83	10	2	2	ribosomal protein S7 (plastid) [Salvia nemorosa]
179	gi|916443338|gb|AKZ24101.1|	17361	55.83	10	2	2	ribosomal protein S7 (plastid) [Nepeta cataria]
180	gi|910312663|ref|YP_009162324.1|	268069	381.43	3	11	11	Hypothetical chloroplast RF2 (chloroplast) [Scutellaria baicalensis]
181	gi|748013968|gb|AJE28438.1|	268103	329.96	4	8	8	Hypothetical chloroplast RF21 (chloroplast) [Premna microphylla]
182	gi|827346597|gb|AKJ77783.1|	266476	159.62	2	4	4	Ycf2 (chloroplast) [Perilla frutescens]
183	gi|836643370|ref|YP_009144558.1|	266537	306.8	4	8	8	Ycf2 (chloroplast) [Rosmarinus officinalis]
184	gi|573462016|emb|CCQ71685.1|	267080	159.62	2	4	4	Ycf2 (chloroplast) [Salvia miltiorrhiza]
185	gi|401879785|gb|AFQ30972.1|	267080	72.34	0	2	2	Hypothetical chloroplast RF2 (chloroplast) [Salvia miltiorrhiza]
186	gi|410176216|gb|AFV61875.1|	264781	153.4	2	4	4	Ycf2 (chloroplast) [Origanum vulgare subsp. vulgare]
187	gi|585636485|gb|AHJ59322.1|	90900	24.77	1	1	1	Copalyl diphosphate synthase [Salvia miltiorrhiza f. alba]
188	gi|751414476|gb|AJF93403.1|	58880	24.19	2	1	1	Ent-kaurene oxidase [Salvia miltiorrhiza]
189	gi|745791049|gb|AJD25233.1|	58838	24.19	2	1	1	Cytochrome P450 CYP701A40 [Salvia miltiorrhiza]
190	gi|787592958|gb|AKA27906.1|	38850	20.03	3	1	1	WRKY protein [Salvia miltiorrhiza]
191	gi|75251480|sp|Q5SBP3|LLOS_OCIBA	65822	178.43	14	8	8	R-linalool synthase (chloroplastic) [Ocimum basilicum] (Sweet basil)

No.	Protein Accession No.	Average Mass	Max-10logP	Max Coverage (%)	Max# Peptides	Max# Unique Peptides	Protein Description
192	gi|6919914|sp|P56848|ISPE_MENPI	44603	63.19	5	2	2	4-diphosphocytidyl-2-C-methyl-D-erythritol kinase (chloroplastic) [Mentha piperita] (Peppermint) (Mentha aquatica x Mentha spicata)
193	gi|916439925|gb|AKZ22667.1|	82427	21.45	1	1	1	photosystem I P700 chlorophyll a apoprotein A2 (plastid) [Nepeta cataria]
194	gi|410176154|gb|AFV61813.1|	82441	21.45	1	1	1	photosystem I P700 chlorophyll a apoprotein A2 (chloroplast) [Origanum vulgare subsp. vulgare]
195	gi|916439921|gb|AKZ22665.1|	82459	21.45	1	1	1	photosystem I P700 chlorophyll a apoprotein A2 (plastid) [Monarda fistulosa var. mollis]
196	gi|827345836|gb|AKJ77137.1|	82407	42.9	2	2	2	photosystem I P700 apoprotein A2 (chloroplast) [Scutellaria baicalensis]
197	gi|836643380|ref|YP_009144514.1|	82458	42.9	2	2	2	photosystem I P700 chlorophyll a apoprotein A2 (chloroplast) [Rosmarinus officinalis]
198	gi|916439923|gb|AKZ22666.1|	82440	21.45	1	1	1	photosystem I P700 chlorophyll a apoprotein A2 (plastid) [Salvia nemorosa]
199	gi|752789785|ref|YP_009117220.1|	82392	42.9	2	2	2	photosystem I P700 apoprotein A2 (chloroplast) [Premna microphylla]
200	gi|573461950|emb|CCQ71619.1|	82459	21.45	1	1	1	photosystem I P700 chlorophyll a apoprotein A2 (chloroplast) [Salvia miltiorrhiza]
201	gi|916439933|gb|AKZ22671.1|	82411	21.45	1	1	1	photosystem I P700 chlorophyll a apoprotein A2 (plastid) [Teucrium canadense]
202	gi|401879741|gb|AFQ30928.1|	82459	21.45	1	1	1	photosystem I P700 apoprotein A2 (chloroplast) [Salvia miltiorrhiza]
203	gi|827346564|gb|AKJ77750.1|	82379	21.45	1	1	1	photosystem I P700 chlorophyll a apoprotein A2 (chloroplast) [Perilla frutescens]
204	gi|75244696|sp|Q8H2B4|LLOS_MENAQ	70535	274.95	25	20	18	R-linalool synthase (chloroplastic) [Mentha aquatica] (Water mint)
205	gi|762060711|gb|AJQ20633.1|	73689	38.32	2	1	1	Long-Chain Acyl-CoA Synthetase [Salvia miltiorrhiza]
206	gi|913341331|gb|AKU77108.1|	104619	30.23	1	1	1	Structural maintenance of chromosomes protein 2, partial [Callicarpa bodinieri]
207	gi|827346602|gb|AKJ77788.1|	181164	29.32	1	1	1	Ycf1, partial (chloroplast) [Perilla frutescens]
208	gi|691200620|gb|AIR77798.1|	26940	25.37	4	1	1	TCP transcription factor, partial [Perovskia atriplicifolia]
209	gi|691200582|gb|AIR77779.1|	29756	25.37	4	1	1	TCP transcription factor, partial [Tectona grandis]
210	gi|691200714|gb|AIR77845.1|	29953	25.37	4	1	1	TCP transcription factor, partial [Gmelina arborea]
211	gi|691200580|gb|AIR77778.1|	30438	25.37	4	1	1	TCP transcription factor, partial [Congea tomentosa]

No.	Protein Accession No.	Average Mass	Max-10logP	Max Coverage (%)	Max# Peptides	Max# Unique Peptides	Protein Description
212	gi|691200590|gb|AIR77783.1|	26615	32.97	4	1	1	TCP transcription factor, partial [Origanum vulgare]
213	gi|691200584|gb|AIR77780.1|	30608	25.37	4	1	1	TCP transcription factor, partial [Callicarpa cathayana]
214	gi|691200708|gb|AIR77842.1|	29615	25.37	4	1	1	TCP transcription factor, partial [Congea tomentosa]
215	gi|691200712|gb|AIR77844.1|	29757	25.37	4	1	1	TCP transcription factor, partial [Holmskioldia sanguinea]
216	gi|691200594|gb|AIR77785.1|	25444	25.37	4	1	1	TCP transcription factor, partial [Mentha longifolia]
217	gi|691200596|gb|AIR77786.1|	25755	25.37	4	1	1	TCP transcription factor, partial [Mentha longifolia]
218	gi|691200624|gb|AIR77800.1|	29841	25.37	4	1	1	TCP transcription factor, partial [Mentha longifolia]
219	gi|691200622|gb|AIR77799.1|	29930	25.37	4	1	1	TCP transcription factor, partial [Premna fulva]
220	gi|691200630|gb|AIR77803.1|	26302	25.37	4	1	1	TCP transcription factor, partial [Ocimum basilicum]
221	gi|510794468|gb|AGN52200.1|	23112	24.18	3	1	1	MYB-related transcription factor [Salvia miltiorrhiza]
222	gi|662858700|gb|AIE77092.1|	90197	20.42	1	1	1	(+)-copalyl diphosphate synthase [Marrubium vulgare]
223	gi|837370038|gb|AKM94187.1|	20521	20.13	6	1	1	Maturase K, partial (chloroplast) [Leonotis nepetifolia]
224	gi|837370329|gb|AKM94283.1|	28841	20.13	4	1	1	Maturase K, partial (chloroplast) [Leonotis nepetifolia]
225	gi|837372516|gb|AKM95003.1|	28942	20.13	4	1	1	Maturase K, partial (chloroplast) [Leonotis nepetifolia]
226	gi|837371203|gb|AKM94570.1|	20329	20.13	6	1	1	Maturase K, partial (chloroplast) [Leonotis nepetifolia]
227	gi|75251478|sp|Q5SBP1|MYRS_OCIBA	69964	210.84	21	15	10	Beta-myrcene synthase (chloroplastic) [Ocimum basilicum] (Sweet basil)
228	gi|3914571|sp|Q33600|RBL_LAVLA	52404	86.13	8	4	4	Ribulose bisphosphate carboxylase large chain [Salvia divinorum] (Maria pastora) (Diviner's sage)
229	gi|1352807|sp|P36485|RBL_SALDI	52005	80.31	8	4	4	Ribulose bisphosphate carboxylase large chain [Salvia divinorum] (Maria pastora) (Diviner's sage)
230	gi|122200955|sp|Q2KNL6|GEDH1_OCIBA	39044	41.75	4	1	1	Geraniol dehydrogenase 1 [Ocimum basilicum] (Sweet basil)
231	gi|122210942|sp|Q2XSC4|LABER_LAVAN	62405	29.22	2	1	1	Exo-alpha-bergamotene synthase [Lavandula angustifolia] (Lavender)

No.	Protein Accession No.	Average Mass	Max-10logP	Max Coverage (%)	Max# Peptides	Max# Unique Peptides	Protein Description
232	gi|84029472|sp|Q93WU3|CVMT1_OCIBA	39916	40.43	6	2	2	Chavicol O-methyltransferase [Ocimum basilicum] (Sweet basil)
233	gi|752789776|ref|YP_009117211.1|	158193	96.12	2	2	2	RNA polymerase beta' subunit (chloroplast) [Premna microphylla]
234	gi|827346527|gb|AKJ77713.1|	158467	83.3	3	3	3	RNA polymerase beta" subunit (chloroplast) [Perilla frutescens]
235	gi|916442767|gb|AKZ23937.1|	155842	83.3	3	3	3	RNA polymerase beta" subunit (plastid) [Teucrium canadense]
236	gi|844572778|gb|AKN09586.1|	68167	22.47	1	1	1	Basic helix-loop-helix transcription factor [Salvia miltiorrhiza]
237	gi|844572715|gb|AKN09566.1|	67854	22.47	1	1	1	Basic helix-loop-helix transcription factor [Salvia miltiorrhiza]
238	gi|748013960|gb|AJE28430.1|	19533	85.42	24	4	4	NADH-plastoquinone oxidoreductase subunit I (chloroplast) [Premna microphylla]
239	gi|766946303|gb|AJT36912.1|	32806	20.06	3	1	1	Ycf1, partial (chloroplast) [Vitex negundo var. negundo]
240	gi|751663101|gb|AJF98632.1	51505	48.13	4	2	2	Ribulose-1,5-bisphosphate carboxylase/oxygenase large subunit, partial (chloroplast) [Nepeta cataria]
241	gi|916441445|gb|AKZ23427.1|	52869	48.13	4	2	2	Ribulose-1,5-bisphosphate carboxylase/oxygenase large subunit, partial (chloroplast) [Nepeta cataria]
242	gi|751663177|gb|AJF98669.1|	51810	48.13	4	2	2	Ribulose-1,5-bisphosphate carboxylase/oxygenase large subunit, partial (chloroplast) [Stachys byzantina]
243	gi|751663109|gb|AJF98636.1|	51713	45.5	4	2	2	Ribulose-1,5-bisphosphate carboxylase/oxygenase large subunit, partial (chloroplast) [Mentha x piperita]
244	gi|817992263|gb|AKG25296.1|	52111	45.5	4	2	2	Ribulose-1,5-bisphosphate carboxylase/oxygenase large subunit, partial (plastid) [Prunella vulgaris]
245	gi|817992309|gb|AKG25319.1|	51956	45.5	4	2	2	Ribulose-1,5-bisphosphate carboxylase/oxygenase large subunit, partial (plastid) [Salvia pratensis]
246	gi|817991831|gb|AKG25080.1|	51983	45.5	4	2	2	Ribulose-1,5-bisphosphate carboxylase/oxygenase large subunit, partial (plastid) [Clinopodium vulgare]
247	gi|751663103|gb|AJF98633.1|	51988	45.5	4	2	2	Ribulose-1,5-bisphosphate carboxylase/oxygenase large subunit, partial (chloroplast) [Mentha spicata]
248	gi|751663105|gb|AJF98634.1|	52345	45.5	4	2	2	Ribulose-1,5-bisphosphate carboxylase/oxygenase large subunit, partial (chloroplast) [Mentha suaveolens]

No.	Protein Accession No.	Average Mass	Max-10logP	Max Coverage (%)	Max# Peptides	Max# Unique Peptides	Protein Description
249	gi|827345151|gb|AKJ76735.1|	52873	91	8	4	4	Ribulose-1,5-bisphosphate carboxylase/oxygenase large subunit (chloroplast) [Rosmarinus officinalis]
250	gi|916441443|gb|AKZ23426.1|	52850	45.5	4	2	2	Ribulose-1,5-bisphosphate carboxylase/oxygenase large subunit (plastid) [Salvia nemorosa]
251	gi|410176163|gb|AFV61822.1|	52889	45.5	4	2	2	Ribulose-1,5-bisphosphate carboxylase/oxygenase large subunit (chloroplast) [Origanum vulgare subsp. vulgare]
252	gi|916441441|gb|AKZ23425.1|	52888	45.5	4	2	2	Ribulose-1,5-bisphosphate carboxylase/oxygenase large subunit (plastid) [Monarda fistulosa var. mollis]
253	gi|817991973|gb|AKG25151.1|	52020	45.5	4	2	2	Ribulose-1,5-bisphosphate carboxylase/oxygenase large subunit, partial (plastid) [Galeopsis bifida]
254	gi|751663168|gb|AJF98665.1|	51966	45.5	4	2	2	Ribulose-1,5-bisphosphate carboxylase/oxygenase large subunit, partial (chloroplast) [Ocimum tenuiflorum]
255	gi|817992375|gb|AKG25352.1|	52022	45.5	4	2	2	Ribulose-1,5-bisphosphate carboxylase/oxygenase large subunit, partial (plastid) [Stachys sylvatica]
256	gi|817992237|gb|AKG25283.1|	52058	45.5	4	2	2	Ribulose-1,5-bisphosphate carboxylase/oxygenase large subunit, partial (plastid) [Phlomis fruticosa]
257	gi|751663097|gb|AJF98630.1|	52095	45.5	4	2	2	Ribulose-1,5-bisphosphate carboxylase/oxygenase large subunit, partial (chloroplast) [Ocimum basilicum]
258	gi|817992335|gb|AKG25332.1|	51941	45.5	4	2	2	Ribulose-1,5-bisphosphate carboxylase/oxygenase large subunit, partial (plastid) [Scutellaria galericulata]
259	gi|817992071|gb|AKG25200.1|	51959	45.5	4	2	2	Ribulose-1,5-bisphosphate carboxylase/oxygenase large subunit, partial (plastid) [Lavandula x intermedia]
260	gi|817992059|gb|AKG25194.1|	51961	45.5	4	2	2	Ribulose-1,5-bisphosphate carboxylase/oxygenase large subunit, partial (plastid) [Lamium galeobdolon]
261	gi|751663113|gb|AJF98638.1|	52702	45.5	4	2	2	Ribulose-1,5-bisphosphate carboxylase/oxygenase large subunit, partial (chloroplast) [Ajuga bracteosa]
262	gi|401879750|gb|AFQ30937.1|	52887	45.5	4	2	2	Ribulose-1,5-bisphosphate carboxylase/oxygenase large subunit (chloroplast) [Salvia miltiorrhiza]
263	gi|916441453|gb|AKZ23431.1|	53169	45.5	4	2	2	Ribulose-1,5-bisphosphate carboxylase/oxygenase large subunit (plastid) [Teucrium canadense]

No.	Protein Accession No.	Average Mass	Max-10logP	Max Coverage (%)	Max# Peptides	Max# Unique Peptides	Protein Description
264	gi|910312608|ref|YP_009162269.1|	53663	91	8	4	4	Ribulose-1,5-bisphosphate carboxylase/oxygenase large subunit (chloroplast) [Scutellaria baicalensis]
265	gi|827346558|gb|AKJ77744.1|	53955	45.5	4	2	2	Ribulose-1 (chloroplast) [Perilla frutescens]
266	gi|573461959|emb|CCQ71628.1|	53698	45.5	4	2	2	Ribulose-1 (chloroplast) [Salvia miltiorrhiza]
267	gi|599079565|dbj|BAO57028.1|	49007	44.57	4	2	2	Ribulose-1,5-bisphosphate carboxylase/oxygenase large subunit, partial (chloroplast) [Sideritis cretica subsp. spicata]
268	gi|817992077|gb|AKG25203.1|	49757	44.57	4	2	2	Ribulose-1,5-bisphosphate carboxylase/oxygenase large subunit, partial (plastid) [Leonurus cardiaca]
269	gi|817992301|gb|AKG25315.1|	49431	41.41	4	2	2	Ribulose-1,5-bisphosphate carboxylase/oxygenase large subunit, partial (plastid) [Rosmarinus officinalis]
270	gi|602690611|gb|AHN96261.1|	27410	165.64	28	8	8	Ribulose-1,5-bisphosphatecarboxylase/oxygenase large subunit, partial (chloroplast) [Zhumeria majdae]
271	gi|602690623|gb|AHN96267.1|	27409	124.23	21	6	6	Ribulose-1,5-bisphosphatecarboxylase/oxygenase large subunit, partial (chloroplast) [Zhumeria majdae]
272	gi|602690627|gb|AHN96269.1|	27428	82.82	14	4	4	Ribulose-1,5-bisphosphatecarboxylase/oxygenase large subunit, partial (chloroplast) [Zhumeria majdae]
273	gi|602690615|gb|AHN96263.1|	27394	124.23	21	6	6	Ribulose-1,5-bisphosphatecarboxylase/oxygenase large subunit, partial (chloroplast) [Zhumeria majdae]
274	gi|751663115|gb|AJF98639.1|	27926	41.41	7	2	2	Ribulose-1,5-bisphosphatecarboxylase/oxygenase large subunit, partial (chloroplast) [Zhumeria majdae]
275	gi|602690633|gb|AHN96272.1|	27525	124.23	21	6	6	Ribulose-1,5-bisphosphatecarboxylase/oxygenase large subunit, partial (chloroplast) [Zhumeria majdae]
276	gi|752789794|ref|YP_009117229.1|	53224	82.82	8	4	4	Ribulose-1,5-bisphosphate carboxylase/oxygenase large subunit (chloroplast) [Premna microphylla]
277	gi|599079563|dbj|BAO57027.1|	48957	41.41	4	2	2	Ribulose-1,5-bisphosphate carboxylase/oxygenase large subunit, partial (chloroplast) [Teucrium heterophyllum]
278	gi|910312590|ref|YP_009162251.1|	158800	176.64	4	6	6	RNA polymerase beta subunit-2 (chloroplast) [Scutellaria baicalensis]

No.	Protein Accession No.	Average Mass	Max-10logP	Max Coverage (%)	Max# Peptides	Max# Unique Peptides	Protein Description
279	gi|521953395|gb|AGQ04156.1|	82464	28.81	2	1	1	4-hydroxy-3-methylbut-2-enyl diphosphate synthase [Lavandula angustifolia]
280	gi|796406070|gb|AKA59790.1|	28575	24.94	4	1	1	MYB19 [Scutellaria playfairii]
281	gi|670606706|gb|AII31147.1|	9275	20.48	11	1	1	Adenosine kinase, partial [Micromeria hyssopifolia var. hyssopifolia]
282	gi|670606710|gb|AII31149.1|	9520	20.48	10	1	1	Adenosine kinase, partial [Micromeria hyssopifolia var. kuegleri]
283	gi|670606712|gb|AII31150.1|	10786	20.48	9	1	1	Adenosine kinase, partial [Micromeria teneriffae var. cordifolia]
284	gi|670606714|gb|AII31151.1|	11074	20.48	9	1	1	Adenosine kinase, partial [Micromeria teneriffae var. cordifolia]
285	gi|670606704|gb|AII31146.1|	10951	20.48	9	1	1	Adenosine kinase, partial [Micromeria lepida subsp. lepida]
286	gi|670606708|gb|AII31148.1|	11164	20.48	9	1	1	Adenosine kinase, partial [Micromeria hyssopifolia var. kuegleri]
287	gi|670606716|gb|AII31152.1|	11349	20.48	9	1	1	Adenosine kinase, partial [Micromeria hyssopifolia var. glabrescens]
288	gi|670606702|gb|AII31145.1|	11506	20.48	9	1	1	Adenosine kinase, partial [Micromeria hyssopifolia var. glabrescens]
289	gi|401879785|gb|AFQ30972.1|	267080	87.28	2	2	2	Hypothetical chloroplast RF2 (chloroplast) [Salvia miltiorrhiza]
290	gi|510794472|gb|AGN52202.1|	40938	24.14	2	1	1	MYB-related transcription factor [Salvia miltiorrhiza]
291	gi|573462009|emb|CCQ71678.1|	45534	46.36	8	2	2	NADH dehydrogenase subunit 7 (chloroplast) [Salvia miltiorrhiza]
292	gi|836643397|ref|YP_009144571.1|	45642	46.36	8	2	2	NADH dehydrogenase subunit 7 (chloroplast) [Rosmarinus officinalis]
293	gi|410176210|gb|AFV61869.1|	45519	23.18	4	1	1	NADH dehydrogenase subunit 7 (chloroplast) [Origanum vulgare subsp. vulgare]
294	gi|916439041|gb|AKZ22225.1|	45538	23.18	4	1	1	NADH dehydrogenase subunit 7 (plastid) [Monarda fistulosa var. mollis]
295	gi|916439045|gb|AKZ22227.1|	45533	23.18	4	1	1	NADH dehydrogenase subunit 7 (plastid) [Salvia nemorosa]
296	gi|916439043|gb|AKZ22226.1|	45734	23.18	4	1	1	NADH dehydrogenase subunit 7 (plastid) [Nepeta cataria]
297	gi|916439047|gb|AKZ22228.1|	45476	23.18	4	1	1	NADH dehydrogenase subunit 7 (plastid) [Teucrium canadense]
298	gi|827346580|gb|AKJ77766.1|	45539	23.18	4	1	1	NADH dehydrogenase subunit 7 (chloroplast) [Perilla frutescens]

No.	Protein Accession No.	Average Mass	Max-10logP	Max Coverage (%)	Max# Peptides	Max# Unique Peptides	Protein Description
299	gi|827345853|gb|AKJ77154.1|	45491	46.36	8	2	2	NADH dehydrogenase subunit 7 (chloroplast) [Scutellaria baicalensis]
300	gi|752789844|ref|YP_009117278.1|	45401	46.36	8	2	2	NADH-plastoquinone oxidoreductase subunit 7 (chloroplast) [Premna microphylla]
301	gi|916438099|gb|AKZ21755.1|	37677	21.34	2	1	1	cytochrome c biogenesis protein (plastid) [Nepeta cataria]
302	gi|836643373|ref|YP_009144505.1|	158291	68.68	2	2	2	RNA polymerase beta" subunit (chloroplast) [Rosmarinus officinalis]
303	gi|410176145|gb|AFV61804.1|	158559	21.28	1	1	1	RNA polymerase beta" subunit (chloroplast) [Origanum vulgare subsp. vulgare]
304	gi|916442746|gb|AKZ23930.1|	158642	21.28	1	1	1	RNA polymerase beta" subunit (plastid) [Monarda fistulosa var. mollis]
305	gi|75244696|sp|Q8H2B4.1|LLOS_MENAQ	267080	137.47	5	14	14	R-linalool synthase (chloroplastic) [Mentha aquatica] (Water mint)
306	gi|122210942|sp|Q2XSC4|LABER_LAVAN	84218	34.94	1	1	1	Exo-alpha-bergamotene synthase [Lavandula angustifolia] (Lavender)
307	gi|122200954|sp|Q2KNL5|CADH1_OCIBA	84443	34.94	1	1	1	Cinnamyl alcohol dehydrogenase 1 [Ocimum basilicum] (Sweet basil)
308	gi|401879785|gb|AFQ30972.1|	267080	274.94	10	28	28	Hypothetical chloroplast RF2 (chloroplast) [Salvia miltiorrhiza]
309	gi|844572794|gb|AKN09591.1|	22976	53.82	8	2	2	Basic helix-loop-helix transcription factor [Salvia miltiorrhiza]
310	gi|916441767|gb|AKZ23588.1|	15470	24.02	6	1	1	Ribosomal protein L20 (plastid) [Teucrium canadense]
311	gi|827345878|gb|AKJ77179.1|	15363	48.04	12	2	2	Ribosomal protein L20 (chloroplast) [Scutellaria baicalensis]
312	gi|916441755|gb|AKZ23582.1|	15554	24.02	6	1	1	Ribosomal protein L20 (plastid) [Nepeta cataria]
313	gi|916441757|gb|AKZ23583.1|	15566	24.02	6	1	1	Ribosomal protein L20 (plastid) [Salvia nemorosa]
314	gi|410176177|gb|AFV61836.1|	15446	24.02	6	1	1	Ribosomal protein L20 (chloroplast) [Origanum vulgare subsp. vulgare]
315	gi|916441753|gb|AKZ23581.1|	15522	24.02	6	1	1	Ribosomalprotein L20 (plastid) [Monarda fistulosa var. mollis]
316	gi|827345181|gb|AKJ76765.1|	15446	48.04	12	2	2	Ribosomal protein L20 (chloroplast) [Rosmarinus officinalis]
317	gi|827346543|gb|AKJ77729.1|	15537	24.02	6	1	1	Ribosomal protein L20 (chloroplast) [Perilla frutescens]
318	gi|748013927|gb|AJE28397.1|	15724	48.04	12	2	2	Ribosomal protein L20 (chloroplast) [Premna microphylla]

No.	Protein Accession No.	Average Mass	Max-10logP	Max Coverage (%)	Max# Peptides	Max# Unique Peptides	Protein Description
319	gi|573461974|emb|CCQ71643.1|	15541	48.04	12	2	2	Ribosomal protein L20 (chloroplast) [Salvia miltiorrhiza]
320	gi|745791013|gb|AJD25215.1|	56512	21.31	2	1	1	Cytochrome P450 CYP92B28 [Salvia miltiorrhiza]
321	gi|14423898|sp|Q9M573|RL31_PERFR	13894	64.2	7	1	1	60S ribosomal protein L31 [Perilla frutescens] (Beefsteak mint)
322	gi|410176212|gb|AFV61871.1|	217739	129.41	11	24	23	Protein Ycf1 (chloroplast) [Origanum vulgare subsp. vulgare]
323	gi|661525318|gb|AIE15766.1|	183633	46.23	0	1	1	Dicer-like protein 4a [Salvia miltiorrhiza]
324	gi|410176197|gb|AFV61856.1|	264781	80.62	2	4	4	Protein Ycf2 (chloroplast) [Origanum vulgare subsp. vulgare]
325	gi|844572640|gb|AKN09541.1|	34841	39.74	3	1	1	Basic helix-loop-helix transcription factor [Salvia miltiorrhiza]
326	gi|602690681|gb|AHN96278.1|	37139	264.67	21	7	7	Maturase K, partial (chloroplast) [Zhumeria majdae]
327	gi|602690683|gb|AHN96279.1|	37138	75.62	6	2	2	Maturase K, partial (chloroplast) [Zhumeria majdae]
328	gi|602690687|gb|AHN96281.1|	37105	113.43	9	3	3	Maturase K, partial (chloroplast) [Zhumeria majdae]
329	gi|745790967|gb|AJD25192.1|	58706	32.46	2	1	1	Cytochrome P450 CYP79D40 [Salvia miltiorrhiza]
330	gi|844572703|gb|AKN09562.1|	36568	32.19	2	1	1	Basic helix-loop-helix transcription factor [Salvia miltiorrhiza]
331	gi|910312590|ref|YP_009162251.1|	158800	54.02	2	2	2	Hypothetical chloroplast RF2 (chloroplast) [Salvia miltiorrhiza]
332	gi|745791003|gb|AJD25210.1|	57675	23.31	2	1	1	Cytochrome P450 CYP89A115 [Salvia miltiorrhiza]
333	gi|521953403|gb|AGQ04160.1|	40132	21.67	3	1	1	Farnesyl diphosphate synthase [Lavandula angustifolia]
334	gi|762060297|gb|AJQ20620.1|	48394	21.05	2	1	1	Dihydrolipoamide Acetyltransferase [Salvia miltiorrhiza]
335	gi|548918017|gb|AGX15389.1|	56042	20.86	2	1	1	Flavonoid 3' monooxygenase [Plectranthus barbatus]
336	gi|661525320|gb|AIE15767.1|	174990	20.37	1	1	1	Dicer-like protein 4b [Salvia miltiorrhiza]

Additionally, the InterPro Classification of Protein Families and UniProtKB databases were used to characterize the respective protein class (Fig.3), cellular component (Fig.4) and molecular function (Fig.5).

The protein compositions of OSLP were categorized into 49 protein families (Fig.3). The two major protein families (13%) were ribulose bisphosphate carboxylase large chain (RuBisCo large chain) and nicotinamide adenine dinucleotide (NADH)-plastoquinone oxidoreductase, chain 5. A number of the protein compositions was annotated as "none predicted" in the databases at the time this study was commenced. They represent the second large family (10%). 9% of the protein compositions belongs to the terpene synthase family and 8% of them was found in the family of cytochrome P450. The remaining protein families was displayed in Fig.3.

The protein compositions of OSLP were found at 21 different cellular components encompassing cytoplasm within which various organelles and particles are localised; intracellular organelles such as cytosol, chloroplast, plastid, ribosome, chromosome and mitochondrion, to name a few. The identified protein compositions were also found at the nucleus (Fig.4).

The protein compositions of OSLP were also analyzed using functional annotation; majority of them were involved in the biosynthesis of metabolites, both primary and secondary. For instance, DNA (Deoxyribonucleic Acid) and RNA (Ribonucleic Acid) bindings are essential for controlling protein synthesis and functions whereas, a wide spectrum of enzymatic activities regulate the production of different small molecules. The three major enzymes were found to be lyases (14%), oxidoreductases (28%) and monooxygenases (10%). The others were found to be involved in ATP (Adenosine-5'-triphosphate) bindings; kinases which regulate the phosphorylation of proteins (Avendaño & Menéndez, 2008) and transport proteins that involved in both active and passive cellular transports of many substrates (e.g. ions; glucose; proteins and messenger molecules) (Fig.5). In a plant cell, these protein compositions regulate diverse biological processes encompassing protein homeostasis, trafficking, signalling, metabolic processes, energy metabolism, defence responses and gene transcriptions.

On a separate note, the protein compositions of OSLP may hold important therapeutic potential. Seeing that the pharmaceutical demand for plant-derived proteins as a

favourable therapeutic alternative is on the rise (Solá & Griebenow, 2010; Yao et al., 2015), the protein compositions of OSLP is especially worthy of future investigation. For instance, heat shock protein 2 (HSP2) of the heat shock protein (Hsp90) family. HSP 2 may be potentially protective for neurons in a similar way like the other HSPs such as HSP27, 60, 70 and 90, which have been reported for inhibiting neuronal excitability (Akbar et al., 2003; Bidmon et al., 2004; Gammazza et al., 2015; Hu et al., 2019; Kamel, Mounir, Okaily, Abdelzaher, & Hassan, 2018; Kandratavicius, Hallak, Carlotti Jr, Assirati Jr, & Leite, 2014). Baicalein 7-O-glucuronosyltransferase (Cytochrome P450 family) and baicalin-beta-D-glucuronidase (Glycosyl hydrolase 79 family) are responsible the biosynthesis of baicalein and baicalin respectively. R-linalool synthase and Beta-mycrene synthase, belonging to the terpene synthase family, are proteins involved in the biosynthesis of linalool and myrcene respectively. These small molecules have been reported for their anticonvulsant effects (Hill et al., 2013; Karniol, Shirakawa, Takahashi, Knobel, & Musty, 1975; Z. Zhang, Lian, Li, & Stringer, 2009) and anti-tumour activities (Nagashima, Hirotani, & Yoshikawa, 2000). Rosmarinate synthase (Transferase family) catalyzes the production of rosmarinic acid (Weitzel & Petersen, 2011). Rosmarinic acid and its analogs have been demonstrated to inhibit neuroexcitation (Choo et al., 2018; Coelho et al., 2015) and to inhibit macrophage-mediated lung inflammatory diseases, such as chronic obstructive pulmonary disease (COPD) (Thammason, Khetkam, Pabuprapap, Suksamrarn, & Kunthalert, 2018).

In this study, OTM has successfully extracted OSLP from the different cellular components with different molecular functions. This suggests that OTM is an optimal protein extraction method and hence, could be adopted as a routine procedure at laboratory scale. Mass spectrometry-based proteomics has successfully identified the protein compositions of OSLP extracted by OTM. Functional annotation analysis has characterized the protein compositions of OSLP in terms of protein families, cellular components and molecular functions. Some of the small molecules synthesized have demonstrated protective effects as aforementioned. OSLP alone has never been extracted for investigation before. There is no prior published scientific evidence on OSLP. A prior literature search only yielded one study wherein Saidan and colleagues (Saidan et al., 2015) examined a mixture of primary metabolites (not proteins alone) extracted from OS leaves for their antioxidative and anti-proliferative activities. As such, this study represents the first of its kind.

4 Concluding remarks

OTM has successfully extracted OSLP from OS leaves. OTM could be considered as a routine procedure useful in plant protein extraction achievable at laboratory scale. The protein compositions of OSLP merit for future investigation for their therapeutic potential.

REFERENCES

Adnyana, I. K., Setiawan, F., & Insanu, M. (2013). From ethnopharmacology to clinical study of *Orthosiphon stamineus* Benth. *Int. J. Pharm. Pharm. Sci., 5*(3), 66.

Aebersold, R., & Mann, M. (2016). Mass-spectrometric exploration of proteome structure and function. *Nature, 537*(7620), 347-355. doi:10.1038/nature19949

Agency, E. M. (2011). *Assessment report on Orthosiphon stamineus Benth., folium*. Retrieved from

Akbar, M. T., Lundberg, A. M., Liu, K., Vidyadaran, S., Wells, K. E., Dolatshad, H., . . . de Belleroche, J. (2003). The neuroprotective effects of heat shock protein 27 overexpression in transgenic animals against kainate-induced seizures and hippocampal cell death. *Journal of Biological Chemistry, 278*(22), 19956-19965.

Ameer, O. Z., Salman, I. M., Asmawi, M. Z., Ibraheem, Z. O., & Yam, M. F. (2012). *Orthosiphon stamineus*: traditional uses, phytochemistry, pharmacology, and toxicology. *J. Med. Food., 15*. doi:10.1089/jmf.2011.1973

Avendaño, C., & Menéndez, J. C. (2008). Chapter 9 - Drugs That Inhibit Signalling Pathways for Tumor Cell Growth and Proliferation. In C. Avendaño & J. C. Menéndez (Eds.), *Medicinal Chemistry of Anticancer Drugs* (pp. 251-305). Amsterdam: Elsevier.

Bhuyan, A. K. (2010). On the mechanism of SDS-induced protein denaturation. *Biopolymers, 93*(2), 186-199. doi:10.1002/bip.21318

Bidmon, H.-J., Görg, B., Palomero-Gallagher, N., Behne, F., Lahl, R., Pannek, H. W., . . . Zilles, K. (2004). Heat Shock Protein-27 Is Upregulated in the Temporal Cortex of Patients with Epilepsy. *Epilepsia, 45*(12), 1549-1559. doi:10.1111/j.0013-9580.2004.14904.x

Chattopadhyay, A., & Harikumar, K. (1996). Dependence of critical micelle concentration of a zwitterionic detergent on ionic strength: implications in receptor solubilization. *FEBS letters, 391*(1-2), 199-202.

Chevallet, M., Luche, S., & Rabilloud, T. (2006). Silver staining of proteins in polyacrylamide gels. *Nat. Protocols, 1*(4), 1852-1858. Retrieved from http://dx.doi.org/10.1038/nprot.2006.288

Choo, B. K. M., Kundap, U. P., Kumari, Y., Hue, S.-M., Othman, I., & Shaikh, M. F. (2018). Orthosiphon stamineus Leaf Extract Affects TNF-α and Seizures in a Zebrafish Model. *Frontiers in Pharmacology, 9*, 139. doi:10.3389/fphar.2018.00139

Coelho, V. R., Vieira, C. G., de Souza, L. P., Moysés, F., Basso, C., Papke, D. K. M., . . . Pereira, P. (2015). Antiepileptogenic, antioxidant and genotoxic evaluation of rosmarinic acid and its metabolite caffeic acid in mice. *Life sciences, 122*, 65-71. doi:10.1016/j.lfs.2014.11.009

Cook, N. J. (1993). 19 - Simultaneous Purification and Characterization of the cGMP-Gated Cation Channel and the Na+/Ca2+,K+-Exchanger. In P. A. Hargrave (Ed.), *Methods in Neurosciences* (Vol. 15, pp. 271-282): Academic Press.

Evans, D. R., Romero, J. K., & Westoby, M. (2009). Concentration of proteins and removal of solutes. *Methods Enzymol, 463*, 97-120. doi:10.1016/s0076-6879(09)63009-3

Gammazza, A. M., Colangeli, R., Orban, G., Pierucci, M., Di Gennaro, G., Bello, M. L., . . . Valentino, M. (2015). Hsp60 response in experimental and human temporal lobe epilepsy. *Scientific Reports, 5*, 9434.

Gan, S. H., Chua, L. S., Aziz, R., Baba, M. R., Abdullah, L. C., Ong, S. P., & Law, C. L. (2017). Drying Characteristics of *Orthosiphon stamineus* Benth by Solar Assisted Heat Pump Drying. *Drying Technology*, null-null. doi:10.1080/07373937.2016.1275673

George, A., Chinnappan, S., Choudhary, Y., Choudhary, V. K., Bommu, P., & Wong, H. J. (2015). Effects of a Proprietary Standardized *Orthosiphon stamineus* Ethanolic Leaf Extract on Enhancing Memory in Sprague Dawley Rats Possibly via Blockade of Adenosine A(2A) Receptors. *J. Evid. Based Complementary Altern. Med. : eCAM, 2015*, 375837. doi:10.1155/2015/375837

Gleiser I, Y. P., Barnea-Gedalyahu E, Zharhary D. . (2010). *In: Biowire, Volume 10,* (Article 1,). Retrieved from http://www.sigmaaldrich.com/technical-documents/articles/biowire/phosphatase inhibitor.html. (accessed 10/07/2017)

Hashiguchi, A., & Komatsu, S. (2017). Chapter Six - Posttranslational Modifications and Plant–Environment Interaction. In A. K. Shukla (Ed.), *Methods in Enzymology* (Vol. 586, pp. 97-113): Academic Press.

Hill, T. D. M., Cascio, M.-G., Romano, B., Duncan, M., Pertwee, R. G., Williams, C. M., . . . Hill, A. J. (2013). Cannabidivarin-rich cannabis extracts are anticonvulsant in mouse and rat via a CB1 receptor-independent mechanism. *British Journal of Pharmacology, 170*(3), 679-692. doi:10.1111/bph.12321

Hu, F., Zhou, J., Lu, Y., Guan, L., Wei, N.-N., Tang, Y.-Q., & Wang, K. (2019). Inhibition of Hsp70 Suppresses Neuronal Hyperexcitability and Attenuates Epilepsy by Enhancing A-Type Potassium Current. *Cell Reports, 26*(1), 168-181.e164. doi:https://doi.org/10.1016/j.celrep.2018.12.032

Huang, Z.-L., Qu, W.-M., Eguchi, N., Chen, J.-F., Schwarzschild, M. A., Fredholm, B. B., . . . Hayaishi, O. (2005). Adenosine A2A, but not A1, receptors mediate the arousal effect of caffeine. *Nature neuroscience, 8*(7), 858-859.

Isaacson, T., Damasceno, C. M., Saravanan, R. S., He, Y., Catalá, C., Saladié, M., & Rose, J. K. (2006). Sample extraction techniques for enhanced proteomic analysis of plant tissues. *Nature Protocols, 1*(2), 769.

Junqueira, M., Spirin, V., Balbuena, T. S., Thomas, H., Adzhubei, I., Sunyaev, S., & Shevchenko, A. (2008). Protein identification pipeline for the homology-driven proteomics. *Journal of proteomics, 71*(3), 346-356. doi:10.1016/j.jprot.2008.07.003

Kamel, M. M., Mounir, S. M., Okaily, N. I., Abdelzaher, M. H., & Hassan, M. H. (2018). Possible Role of Heat Shock Protein 70 in Childhood Seizures. *International Journal of Epilepsy, 05*(02), 087-091. doi:10.1055/s-0038-1676907

Kandratavicius, L., Hallak, J. E., Carlotti Jr, C. G., Assirati Jr, J. A., & Leite, J. P. (2014). Hippocampal expression of heat shock proteins in mesial temporal lobe epilepsy with psychiatric comorbidities and their relation to seizure outcome. *Epilepsia, 55*(11), 1834-1843. doi:10.1111/epi.12787

Karniol, I. G., Shirakawa, I., Takahashi, R. N., Knobel, E., & Musty, R. E. (1975). Effects of Δ⁹-Tetrahydrocannabinol and Cannabinol in Man. *Pharmacology, 13*(6), 502-512. doi:10.1159/000136944

Laemmli, U. (1970). Cleavage of structural proteins during the assembly of the head of bacteriophage T4 *Nature, 227*, 680–685.

Liu, Y., Lu, S., Liu, K., Wang, S., Huang, L., & Guo, L. (2019). Proteomics: a powerful tool to study plant responses to biotic stress. *Plant Methods, 15*(1), 135. doi:10.1186/s13007-019-0515-8

Mónico, A., Martínez-Senra, E., Zorrilla, S., & Pérez-Sala, D. (2017). Drawbacks of Dialysis Procedures for Removal of EDTA. *PloS one, 12*(1), e0169843.

Nagashima, S., Hirotani, M., & Yoshikawa, T. (2000). Purification and characterization of UDP-glucuronate: baicalein 7-O-glucuronosyltransferase from Scutellaria baicalensis Georgi. cell suspension cultures. *Phytochemistry, 53*(5), 533-538. doi:https://doi.org/10.1016/S0031-9422(99)00593-2

Patterson, S. D., & Aebersold, R. H. (2003). Proteomics: the first decade and beyond. *Nat Genet, 33 Suppl*, 311-323. doi:10.1038/ng1106

Rehman, A., & Adnan, M. (2018). Nutritional potential of Pakistani medicinal plants and their contribution to human health in times of climate change and food insecurity. *Pakistan Journal of Botany, 50*(1), 287-300.

Saha, B., & Bhattacharya, S. G. (2017). Charting novel allergens from date palm pollen (Phoenix sylvestris) using homology driven proteomics. *Journal of proteomics, 165*, 1-10. doi:http://dx.doi.org/10.1016/j.jprot.2017.05.021

Saidan, N. H., Hamil, M. S. R., Memon, A. H., Abdelbari, M. M., Hamdan, M. R., Mohd, K. S., . . . Ismail, Z. (2015). Selected metabolites profiling of Orthosiphon stamineus Benth leaves extracts combined with chemometrics analysis and correlation with biological activities. *BMC Complementary and Alternative Medicine, 15*, 350. doi:10.1186/s12906-015-0884-0

Salem, M. A., Jüppner, J., Bajdzienko, K., & Giavalisco, P. (2016). Protocol: a fast, comprehensive and reproducible one-step extraction method for the rapid preparation of polar and semi-polar metabolites, lipids, proteins, starch and cell wall polymers from a single sample. *Plant Methods, 12*(1), 45.

Shah, S., Yoon, G., Chung, S., Abid, M., Kim, T., Lee, H., & Kim, M. (2017). Novel osmotin inhibits SREBP2 via the AdipoR1/AMPK/SIRT1 pathway to improve Alzheimer's disease neuropathological deficits. *Molecular psychiatry, 22*(3), 407.

Shevchenko, A., Valcu, C.-M., & Junqueira, M. (2009). Tools for exploring the proteomosphere. *Journal of proteomics, 72*(2), 137-144. doi:10.1016/j.jprot.2009.01.012

Singh, N., Jain, N., Kumar, R., Jain, A., Singh, N. K., & Rai, V. (2015). A comparative method for protein extraction and 2-D gel electrophoresis from different tissues of Cajanus cajan. *Frontiers in plant science, 6*, 606.

Smaczniak, C., Li, N., Boeren, S., America, T., van Dongen, W., Goerdayal, S. S., . . . Kaufmann, K. (2012). Proteomics-based identification of low-abundance signaling and regulatory protein complexes in native plant tissues. *Nat. Protocols, 7*(12), 2144-2158. doi:http://www.nature.com/nprot/journal/v7/n12/abs/nprot.2012.129.html#supplementary-information

Solá, R. J., & Griebenow, K. (2010). Glycosylation of Therapeutic Proteins: An Effective Strategy to Optimize Efficacy. *BioDrugs : clinical immunotherapeutics, biopharmaceuticals and gene therapy, 24*(1), 9-21. doi:10.2165/11530550-000000000-00000

Thammason, H., Khetkam, P., Pabuprapap, W., Suksamrarn, A., & Kunthalert, D. (2018). Ethyl rosmarinate inhibits lipopolysaccharide-induced nitric oxide and prostaglandin E2 production in alveolar macrophages. *European Journal of Pharmacology, 824*, 17-23. doi:https://doi.org/10.1016/j.ejphar.2018.01.042

Wang, N., Cao, D., Gong, F., Ku, L., Chen, Y., & Wang, W. (2015). Differences in properties and proteomes of the midribs contribute to the size of the leaf angle in two near-isogenic maize lines. *Journal of proteomics, 128*, 113-122.

Wang, N., Wu, X., Ku, L., Chen, Y., & Wang, W. (2016). Evaluation of Three Protein-Extraction Methods for Proteome Analysis of Maize Leaf Midrib, a Compound Tissue Rich in Sclerenchyma Cells. *Front. Plant Sci., 7*, 856. doi:10.3389/fpls.2016.00856

Wang, W., Scali, M., Vignani, R., Spadafora, A., Sensi, E., Mazzuca, S., & Cresti, M. (2003). Protein extraction for two-dimensional electrophoresis from olive leaf, a plant tissue containing high levels of interfering compounds. *Electrophoresis, 24*(14), 2369-2375. doi:10.1002/elps.200305500

Weitzel, C., & Petersen, M. (2011). Cloning and characterisation of rosmarinic acid synthase from Melissa officinalis L. *Phytochemistry, 72*(7), 572-578. doi:https://doi.org/10.1016/j.phytochem.2011.01.039

Wenger, G. D., O'Dorisio, M. S., & Campolito, L. B. (1991). 24 - Assays for Vasoactive Intestinal Peptide Receptor. In P. M. Conn (Ed.), *Methods in Neurosciences* (Vol. 5, pp. 362-385): Academic Press.

Xiang, X., Ning, S., Jiang, X., Gong, X., Zhu, R., Zhu, L., & Wei, D. (2010). Protein extraction from rice (Oryza sativa L.) root for two-dimensional electrophresis. *Frontiers of Agriculture in China, 4*(4), 416-421. doi:10.1007/s11703-010-1031-9

Xu, D., & Xu, Y. (2004). Protein databases on the internet. *Current protocols in molecular biology, Chapter 19*, Unit-19.14. doi:10.1002/0471142727.mb1904s68

Yao, J., Weng, Y., Dickey, A., & Wang, K. Y. (2015). Plants as Factories for Human Pharmaceuticals: Applications and Challenges. *International Journal of Molecular Sciences, 16*(12), 28549-28565. doi:10.3390/ijms161226122

Yeboah, S., Hilger, T., & Kroschel, J. (2003). Thaumatococcus daniellii (Benn.) Benth.–a Natural Sweetener from the Rain Forest Zone in West Africa with Potential for Income Generation in Small Scale Farming. *Proceedings of international research on food security, National Resource Management and Rural Development. Georg-August-Universitat Gottingen. http://www.tropentag. de/2003/abstracts/full/305. pdf*.

Zhang, J., Xin, L., Shan, B., Chen, W., Xie, M., Yuen, D., . . . Ma, B. (2012). PEAKS DB: De Novo Sequencing Assisted Database Search for Sensitive and Accurate Peptide Identification. *Molecular & Cellular Proteomics, 11*(4). doi:10.1074/mcp.M111.010587

Zhang, Y., Fonslow, B. R., Shan, B., Baek, M.-C., & Yates, J. R., 3rd. (2013). Protein analysis by shotgun/bottom-up proteomics. *Chemical reviews, 113*(4), 2343-2394. doi:10.1021/cr3003533

Zhang, Z., Lian, X.-y., Li, S., & Stringer, J. L. (2009). Characterization of chemical ingredients and anticonvulsant activity of American skullcap (Scutellaria lateriflora). *Phytomedicine, 16*(5), 485-493. doi:https://doi.org/10.1016/j.phymed.2008.07.011

List of Figures and Captions

- Fig.1 Procedure for One-Tube Method (OTM) showing the extraction of proteins from OS leaves (OSLP).
- Fig.2 One-dimension electrophoretic profile of OSLP. 12% (w/v) SDS-PAGE gel picture produced by 50 µg of OSLP. "M" represents the molecular weight standard in kDa (Thermo Scientific PageRulerTM Plus Pre-stained Protein Ladder.
- Fig.3 Bar graph represents the protein family (expressed in percentage, %) of the protein compositions identified in OSLP. A total of 49 protein families were identified.
- Fig.4 Bar graph represents the cellular component (expressed in percentage, %) of the protein compositions identified in OSLP. They were localised at 21 different cellular components.
- Fig.5 Bar graph represents the molecular function (expressed in percentage, %) of the protein compositions identified in OSLP. A total of 23 molecular functions were annotated.

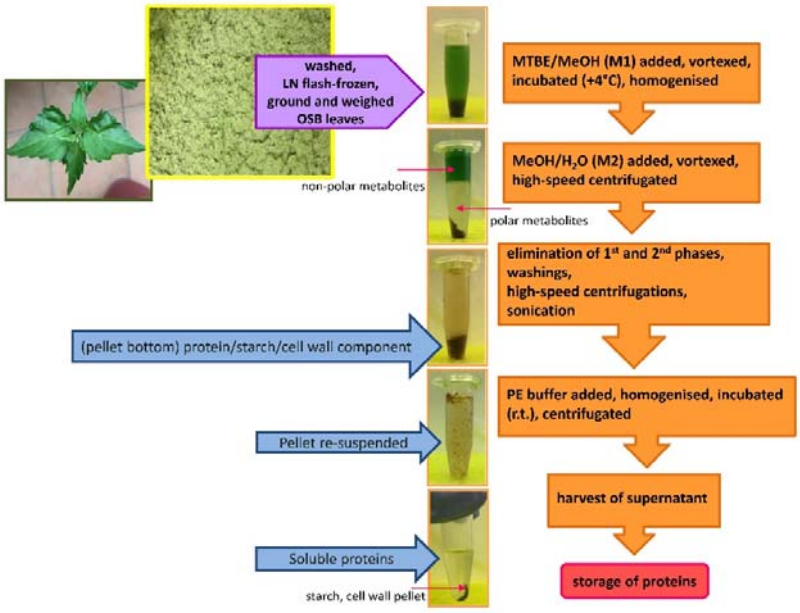

Fig.1 Procedure for One-Tube Method (OTM) showing the extraction of proteins from OS leaves (OSLP).

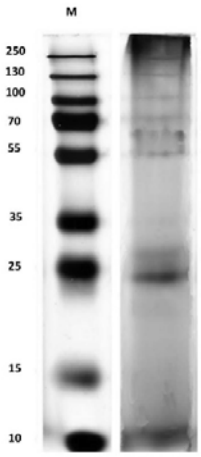

Fig.2 One-dimension electrophoretic profile of OSLP. 12% (w/v) SDS-PAGE gel picture produced by 50 µg of OSLP. "M" represents the molecular weight standard in kDa (Thermo Scientific PageRulerTM Plus Pre-stained Protein Ladder.

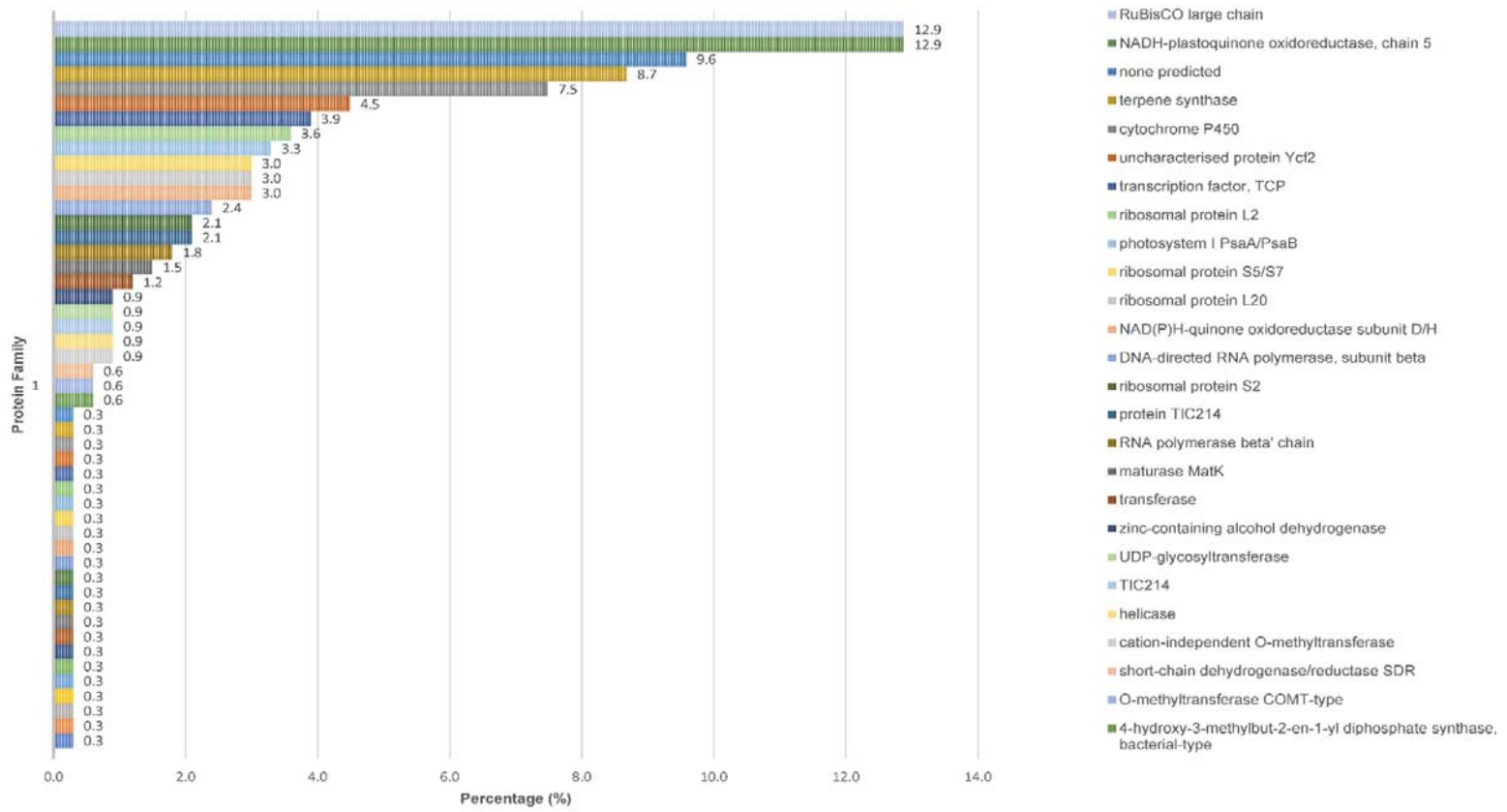

Fig.3 Bar graph represents the protein family (expressed in percentage, %) of the protein compositions identified in OSLP. A total of 49 protein families were identified.

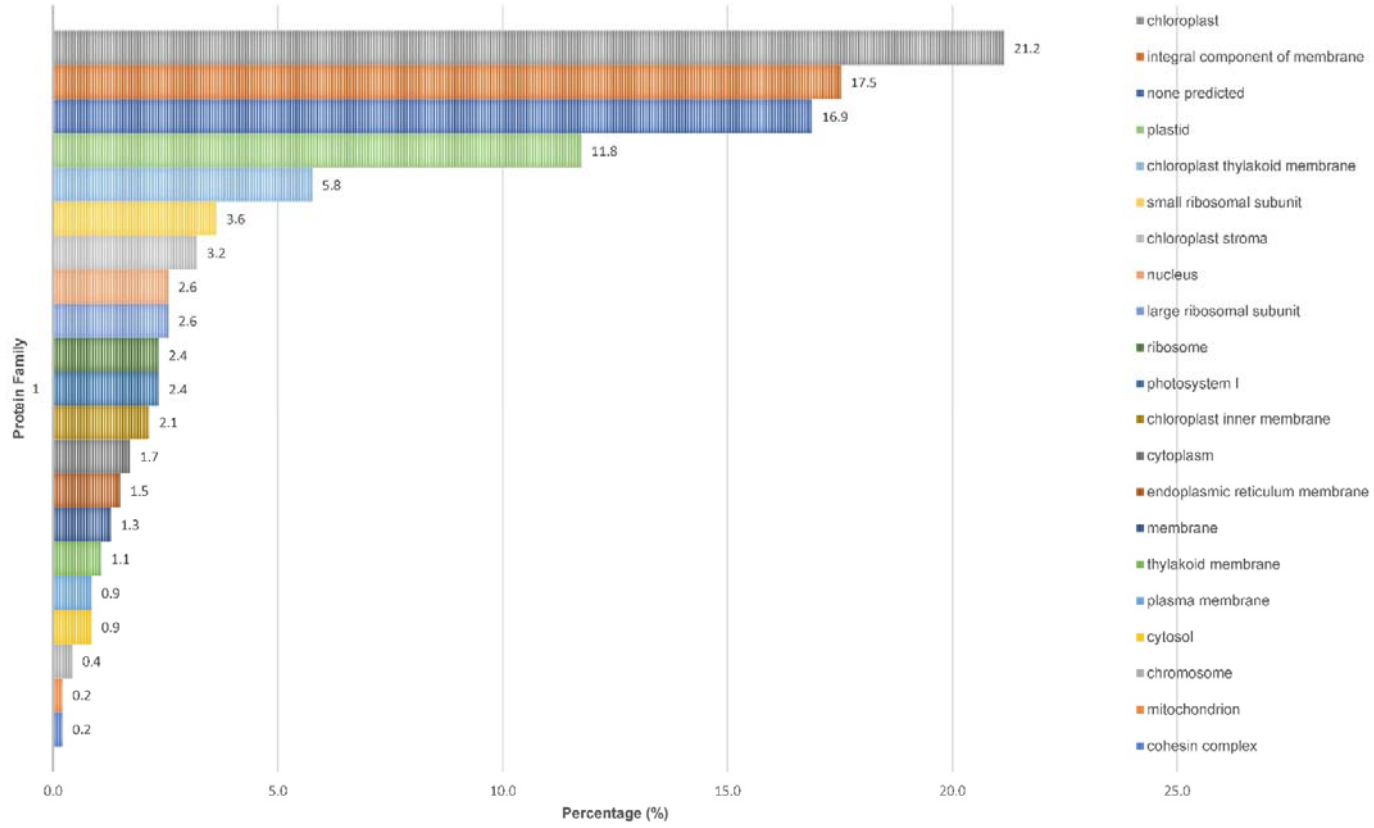

Fig.4 Bar graph represents the cellular component (expressed in percentage, %) of the protein compositions identified in OSLP. They were localised at 21 different cellular components.

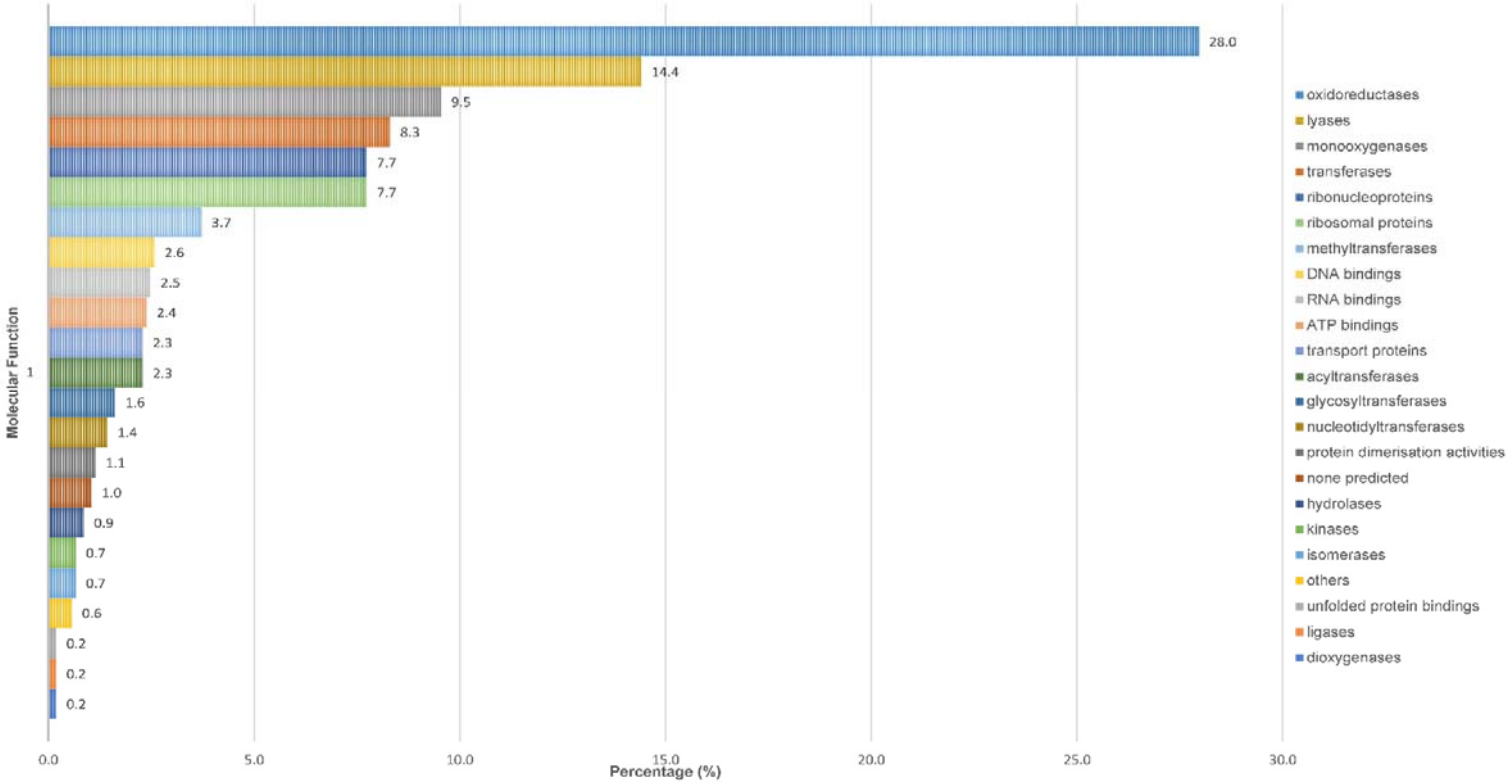

Fig.5 Bar graph represents the molecular function (expressed in percentage, %) of the protein compositions identified in OSLP. A total of 23 molecular functions were annotated.

SUPPLEMENTARY DATA

Table SD-1. List of the total identified protein compositions of OSLP (both in-solution and in-gel digestions) using shotgun-ESI-LC-MS/MS approach. The annotations were retrieved from the databases of UniProtKB (http://www.uniprot.org/uniprot/) and NCBInr (https://www.ncbi.nlm.nih.gov/).

No.	Accession Number	Average Mass	Max-10logP	Max Coverage (%)	Max# Peptides	Max# Unique	Description
1	gi|403399409|sp|E2E2P0.1|GTPS_ORIVU	69063	95.94	7	6	6	Gamma-terpinene synthase, chloroplastic; Short=Ovtps2; AltName: Full=Alpha-terpinene synthase; Flags: Precursor
2	gi|75306222|sp|Q947B7.1|MFS_MENPI	55360	85.61	4	2	2	(+)-menthofuran synthase; AltName: Full=(+)-pulegone 9-hydroxylase
3	gi|75251483|sp|Q5SBP6.1|GDS_OCIBA	63395	77.82	2	1	1	Germacrene-D synthase; AltName: Full=(-)-germacrene D synthase
4	gi|29839421|sp|Q9XGW0.1|COMT1_OCIBA	39529	73.20	2	1	1	Caffeic acid 3-O-methyltransferase 1; Short=CAOMT-1; Short=COMT-1; AltName: Full=S-adenosysl-L-methionine:caffeic acid 3-O-methyltransferase 1
5	gi|29839420|sp|Q9XGV9.1|COMT2_OCIBA	39613	71.77	2	1	1	Caffeic acid 3-O-methyltransferase 2; Short=CAOMT-2; Short=COMT-2; AltName: Full=S-adenosysl-L-methionine:caffeic acid 3-O-methyltransferase 2
6	gi|75315260|sp|Q9XHE7.1|C71DD_MENPI	56601	72.69	2	1	1	Cytochrome P450 71D13; AltName: Full=(-)-(4S)-Limonene-3-hydroxylase; AltName: Full=Cytochrome P450 isoform PM17
7	gi|75129878|sp|Q6WAU0.1|PULR_MENPI	37915	68.99	6	3	3	(+)-pulegone reductase
8	gi|75251484|sp|Q5SBP7.1|SELS_OCIBA	63125	68.51	3	2	2	Selinene synthase
9	gi|75251481|sp|Q5SBP4.1|AZIS_OCIBA	62858	67.78	4	2	2	Alpha-zingiberene synthase
10	gi|5915814|sp|O04164.1|C71A6_NEPRA	57955	66.16	2	1	1	Cytochrome P450 71A6
11	gi|62899675|sp|O81192.1|BPPS_SALOF	69292	49.27	2	1	1	(+)-bornyl diphosphate synthase, chloroplastic; Short=BPPS; AltName: Full=(+)-alpha-pinene synthase; AltName: Full=(+)-camphene synthase; AltName: Full=SBS; Flags: Precursor

No.	Accession Number	Average Mass	Max-10logP	Max Coverage (%)	Max# Peptides	Max# Unique	Description
12	gi|122210943|sp|Q2XSC5.1|LALIN_LAVAN	65654	47.80	2	1	1	R-linalool synthase; Short=LaLINS
13	gi|75180331|sp|Q9LRC8.1|BAGLU_SCUBA	58772	46.95	1	1	1	Baicalin-beta-D-glucuronidase; AltName: Full=Baicalinase; Flags: Precursor
14	gi|122233627|sp|Q4JF75.1|RBR_SCUBA	111795	39.51	1	1	1	Retinoblastoma-related protein
15	gi|75251477|sp|Q5SBP0.1|TPSD_OCIBA	70000	39.42	1	1	1	Terpinolene synthase, chloroplastic; Flags: Precursor
16	gi|5921781|sp|O04111.1|CHSY_PERFR	42686	36.23	3	1	1	Chalcone synthase; AltName: Full=Naringenin-chalcone synthase
17	gi|75251482|sp|Q5SBP5.1|GCS1_OCIBA	63566	26.10	1	1	1	Gamma-cadinene synthase; AltName: Full=(+)-gamma-cadinene synthase
18	gi|910312590|ref|YP_009162251.1|	158800	37.85	1	1	1	DNA-directed RNA polymerase beta subunit-2 (chloroplast) [Scutellaria baicalensis]
19	gi|827345829|gb|AKJ77130.1|	158800	37.85	1	1	1	DNA-directed RNA polymerase beta subunit-2 (chloroplast) [Scutellaria baicalensis]
20	gi|916442749|gb|AKZ23931.1|	157974	34.34	1	1	1	RNA polymerase beta" subunit (plastid) [Salvia nemorosa]
21	gi|836643373|ref|YP_009144505.1|	158291	34.34	1	1	1	DNA-directed RNA polymerase beta" subunit (chloroplast) [Rosmarinus officinalis]
22	gi|827345133|gb|AKJ76717.1|	158291	34.34	1	1	1	DNA-directed RNA polymerase beta" subunit (chloroplast) [Rosmarinus officinalis]
23	gi|401879732|gb|AFQ30919.1|	158403	34.34	1	1	1	DNA-directed RNA polymerase beta subunit-2 (chloroplast) [Salvia miltiorrhiza]
24	gi|573461941|emb|CCQ71610.1|	158403	34.34	1	1	1	DNA-directed RNA polymerase beta" subunit (chloroplast) [Salvia miltiorrhiza]
25	gi|827345865|gb|AKJ77166.1|	25335	24.97	4	1	1	NAD(P)H-quinone oxidoreductase subunit K, chloroplastic [Scutellaria baicalensis]

No.	Accession Number	Average Mass	Max-10logP	Max Coverage (%)	Max# Peptides	Max# Unique	Description
26	gi|910312604|ref|YP_009162265.1|	25335	24.97	4	1	1	NAD(P)H-quinone oxidoreductase subunit K, chloroplastic [Scutellaria baicalensis]
27	gi|75129878|sp|Q6WAU0.1|PULR_MENPI	37915	20.85	2	1	1	(+)-pulegone reductase
28	gi|5915814|sp|O04164.1|C71A6_NEPRA	57955	20.22	2	1	1	Cytochrome P450 71A6
29	gi|122219295|sp|Q49SP7.1|TPSCS_POGCB	63586	136.21	11	7	7	Gamma-curcumene synthase; AltName: Full=PatTpsA
30	gi|5915814|sp|O04164.1|C71A6_NEPRA	57955	113.24	3	4	4	Cytochrome P450 71A6
31	gi|75129878|sp|Q6WAU0.1|PULR_MENPI	37915	91.51	3	2	2	(+)-pulegone reductase
32	gi|403399409|sp|E2E2P0.1|GTPS_ORIVU	69063	86.99	2	1	1	Gamma-terpinene synthase, chloroplastic; Short=Ovtps2; AltName: Full=Alpha-terpinene synthase; Flags: Precursor
33	gi|8134569|sp|Q42662.2|METE_PLESU	84590	83.05	1	1	1	5-methyltetrahydropteroyltriglutamate--homocysteine methyltransferase; AltName: Full=Cobalamin-independent methionine synthase isozyme; AltName: Full=Vitamin-B12-independent methionine synthase isozyme
34	gi|122237148|sp|Q15GI4.1|EGS1_OCIBA	35607	65.94	3	1	1	Eugenol synthase 1 [Ocimum basilicum] (Sweet basil)
35	gi|75227033|sp|Q76MR7.1|UBGAT_SCUBA	48654	63.01	2	1	1	Baicalein 7-O-glucuronosyltransferase; AltName: Full=UDP-glucuronate:baicalein 7-O-glucuronosyltransferase
36	gi|75251483|sp|Q5SBP6.1|GDS_OCIBA	63395	59.78	1	1	1	Germacrene-D synthase; AltName: Full=(-)-germacrene D synthase
37	gi|75161989|sp|Q8W1W9.1|5MAT1_SALSN	50724	56.73	3	1	1	Malonyl-coenzyme:anthocyanin 5-O-glucoside-6'''-O-malonyltransferase; Short=Malonyl CoA:anthocyanin 5-O-glucoside-6'''-O-malonyltransferase; Short=Ss5MaT1
38	gi|84027871|sp|Q93WU2.1|EOMT1_OCIBA	40237	48.94	2	1	1	Eugenol O-methyltransferase; AltName: Full=(Iso)eugenol O-methyltransferase EOMT1;

No.	Accession Number	Average Mass	Max-10logP	Max Coverage (%)	Max# Peptides	Max# Unique	Description
							AltName: Full=S-adenosysl-L-methionine:(Iso)eugenol O-methyltransferase EOMT1
39	gi|75251482|sp|Q5SBP5.1|GCS1_OCIBA	63566	48.14	1	1	1	Gamma-cadinene synthase; AltName: Full=(+)-gamma-cadinene synthase
40	gi|403399735|sp|E2E2N7.1|BCGS_ORIVU	64443	45.36	2	1	1	Bicyclogermacrene synthase; Short=Ovtps4
41	gi|75338882|sp|Q9ZR27.1|5GT1_PERFR	50974	44.00	2	1	1	Anthocyanidin 3-O-glucoside 5-O-glucosyltransferase 1; AltName: Full=UDP-glucose:anthocyanin 5-O-glucosyltransferase 3R4; Short=p3R4; Flags: Precursor
42	gi|75338881|sp|Q9ZR26.1|5GT2_PERFR	49110	37.36	2	1	1	Anthocyanidin 3-O-glucoside 5-O-glucosyltransferase 2; AltName: Full=UDP-glucose:anthocyanin 5-O-glucosyltransferase 3R6; Short=p3R6; Flags: Precursor
43	gi|75180331|sp|Q9LRC8.1|BAGLU_SCUBA	58772	34.79	1	1	1	Baicalin-beta-D-glucuronidase; AltName: Full=Baicalinase; Flags: Precursor
44	gi|75288825|sp|Q65CJ7.2|HPPR_PLESU	34128	29.75	3	1	1	Hydroxyphenylpyruvate reductase; Short=HPPR
45	gi|748013964|gb|AJE28434.1|	225117	108.02	6	15	11	Protein TIC 214 [Premna microphylla]
46	gi|752789846|ref|YP_009117280.1|	225117	108.02	6	15	11	Protein TIC 214 [Premna microphylla]
47	gi|827346602|gb|AKJ77788.1|	181164	97.80	5	7	4	Protein TIC 214 [Perilla frutescens]
48	gi|916442749|gb|AKZ23931.1|	157974	43.03	2	2	2	RNA polymerase beta" subunit (plastid) [Salvia nemorosa]
49	gi|401879732|gb|AFQ30919.1|	158403	43.03	2	2	2	DNA-directed RNA polymerase subunit beta" [Salvia miltiorrhiza]
50	gi|836643373|ref|YP_009144505.1|	158291	43.03	2	2	2	DNA-directed RNA polymerase subunit beta" [Rosmarinus officinalis]
51	gi|827345133|gb|AKJ76717.1|	158291	43.03	2	2	2	DNA-directed RNA polymerase subunit beta" [Rosmarinus officinalis]

No.	Accession Number	Average Mass	Max-10logP	Max Coverage (%)	Max# Peptides	Max# Unique	Description
52	gi|827345132|gb|AKJ76716.1|	218366	30.45	1	1	1	Protein TIC 214 [Rosmarinus officinalis]
53	gi|836643372|ref|YP_009144573.1|	218366	30.45	1	1	1	Protein TIC 214 [Rosmarinus officinalis]
54	gi|5915814|sp|O04164.1|C71A6_NEPRA	57955	29.66	2	1	1	Cytochrome P450 71A6
55	gi|75129878|sp|Q6WAU0.1|PULR_MENPI	37915	25.41	2	1	1	(+)-pulegone reductase
56	gi|510794432|gb|AGN52182.1|	27098	22.41	3	1	1	MYB-related transcription factor [Salvia miltiorrhiza]
57	gi|510794526|gb|AGN52229.1|	28066	22.41	3	1	1	MYB-related transcription factor [Salvia miltiorrhiza]
58	gi|510794500|gb|AGN52216.1|	35378	22.41	3	1	1	MYB-related transcription factor [Salvia miltiorrhiza]
59	gi|510794478|gb|AGN52205.1|	38440	22.41	2	1	1	MYB-related transcription factor [Salvia miltiorrhiza]
60	gi|844572791|gb|AKN09590.1|	34611	22.35	4	1	1	basic helix-loop-helix transcription factor [Salvia miltiorrhiza]
61	gi|844572722|gb|AKN09568.1|	41656	20.96	2	1	1	basic helix-loop-helix transcription factor [Salvia miltiorrhiza]
62	gi|908373664|gb|AKT44364.1|	81096	21.38	1	1	1	heat shock protein 2 [Tectona grandis]
63	gi|5921781|sp|O04111.1|CHSY_PERFR	42686	131.05	46	35	35	Chalcone synthase; AltName: Full=Naringenin-chalcone synthase
64	gi|75306222|sp|Q947B7.1|MFS_MENPI	55360	96.60	19	10	10	(+)-menthofuran synthase; AltName: Full=(+)-pulegone 9-hydroxylase
65	gi|56749087|sp|Q85XY6.1|MATK_OCIBA	60282	91.89	20	12	12	Maturase K; AltName: Full=Intron maturase
66	gi|122219295|sp|Q49SP7.1|TPSCS_POGCB	63586	91.44	13	6	6	Gamma-curcumene synthase; AltName: Full=PatTpsA
67	gi|75227033|sp|Q76MR7.1|UBGAT_SCUBA	48654	82.13	15	8	8	Baicalein 7-O-glucuronosyltransferase; AltName: Full=UDP-glucuronate:baicalein 7-O-glucuronosyltransferase

No.	Accession Number	Average Mass	Max-10logP	Max Coverage (%)	Max# Peptides	Max# Unique	Description
68	gi|75290511|sp|Q6IV13.1|C7D95_MENSP	56322	73.91	15	7	7	Cytochrome P450 71D95; AltName: Full=(-)-(4S)-Limonene-3-hydroxylase
69	gi|75293242|sp|Q6WKY9.1|C7D95_MENGR	56365	73.91	15	7	7	Cytochrome P450 71D95; AltName: Full=(-)-(4S)-Limonene-3-hydroxylase
70	gi|75251482|sp|Q5SBP5.1|GCS1_OCIBA	63566	64.20	5	3	3	Gamma-cadinene synthase; AltName: Full=(+)-gamma-cadinene synthase
71	gi|62899675|sp|O81192.1|BPPS_SALOF	69292	45.92	2	1	1	(+)-bornyl diphosphate synthase, chloroplastic; Short=BPPS; AltName: Full=(+)-alpha-pinene synthase; AltName: Full=(+)-camphene synthase; AltName: Full=SBS; Flags: Precursor
72	gi|75219538|sp|O48935.1|TPSBF_MENPI	63830	45.64	4	2	2	Beta-farnesene synthase
73	gi|75338881|sp|Q9ZR26.1|5GT2_PERFR	49110	43.65	2	1	1	Anthocyanidin 3-O-glucoside 5-O-glucosyltransferase 2; AltName: Full=UDP-glucose:anthocyanin 5-O-glucosyltransferase 3R6; Short=p3R6; Flags: Precursor
74	gi|75293243|sp|Q6WKZ0.1|C7D94_MENGR	56308	41.18	2	1	1	Cytochrome P450 71D94
75	gi|62900763|sp|O81191.1|SCS_SALOF	69369	40.37	2	1	1	1,8-cineole synthase, chloroplastic; Short=SCS; Flags: Precursor
76	gi|403399409|sp|E2E2P0.1|GTPS_ORIVU	69063	39.33	3	2	2	Gamma-terpinene synthase, chloroplastic; Short=Ovtps2; AltName: Full=Alpha-terpinene synthase; Flags: Precursor
77	gi|403399735|sp|E2E2N7.1|BCGS_ORIVU	64443	37.93	1	1	1	Bicyclogermacrene synthase; Short=Ovtps4
78	gi|75338882|sp|Q9ZR27.1|5GT1_PERFR	50974	37.58	2	1	1	Anthocyanidin 3-O-glucoside 5-O-glucosyltransferase 1; AltName: Full=UDP-glucose:anthocyanin 5-O-glucosyltransferase 3R4; Short=p3R4; Flags: Precursor
79	gi|75251477|sp|Q5SBP0.1|TPSD_OCIBA	70000	37.03	2	1	1	Terpinolene synthase, chloroplastic; Flags: Precursor
80	gi|75251478|sp|Q5SBP1.1|MYRS_OCIBA	69964	37.38	2	1	1	Beta-myrcene synthase, chloroplastic; Flags: Precursor

No.	Accession Number	Average Mass	Max-10logP	Max Coverage (%)	Max# Peptides	Max# Unique	Description
81	gi|75251479|sp|Q5SBP2.1|FES_OCIBA	69866	37.38	2	1	1	(-)-endo-fenchol synthase, chloroplastic; Flags: Precursor
82	gi|75224312|sp|Q6USK1.1|GERS_OCIBA	64933	32.96	2	1	1	Geraniol synthase, chloroplastic; Short=ObGES; Flags: Precursor
83	gi|3914545|sp|Q31655.1|RBL_AJUCH	52455	29.59	2	1	1	Ribulose bisphosphate carboxylase large chain; Short=RuBisCO large subunit; Flags: Precursor
84	gi|548687|sp|P36483.1|RBL_CALDI	49209	29.59	2	1	1	Ribulose bisphosphate carboxylase large chain; Short=RuBisCO large subunit; Flags: Precursor
85	gi|132044|sp|P28453.1|RBL_SCUBO	51794	21.37	2	1	1	Ribulose bisphosphate carboxylase large chain; Short=RuBisCO large subunit
86	gi|122219292|sp|Q49SP4.1|TPGD1_POGCB	64197	24.21	1	1	1	Germacrene D synthase 1; AltName: Full=PatTpsB15
87	gi|510785777|sp|G0LD36.1|RAS_MELOI	47161	21.06	2	1	1	Rosmarinate synthase; Short=MoRAS; AltName: Full=Hydroxycinnamoyl-CoA:hydroxyphenyllactate hydroxycinnamoyltransferase
88	gi|17366672|sp|Q9ARF9.1|HPPD_PLESU	47736	20.60	2	1	1	4-hydroxyphenylpyruvate dioxygenase; AltName: Full=4-hydroxyphenylpyruvic acid oxidase; Short=4HPPD; Short=HPD; Short=HPPDase
89	gi|753709941|gb|AJI44435.1|	41648	38.44	2	1	1	Oxoglutarate-dependent flavone 7-O-demethylase [Ocimum basilicum]
90	gi|827345132|gb|AKJ76716.1|	218366	38.05	1	1	1	Protein TIC 214 [Rosmarinus officinalis]
91	gi|836643372|ref|YP_009144573.1|	218366	38.05	1	1	1	Protein TIC 214 [Rosmarinus officinalis]
92	gi|827346602|gb|AKJ77788.1|	181164	21.27	1	1	1	Protein TIC 214 [Perilla frutescens]
93	gi|745791067|gb|AJD25242.1|	53008	22.18	3	1	1	cytochrome P450 CYP707A102 [Salvia miltiorrhiza]
94	gi|745790971|gb|AJD25194.1|	55908	22.03	2	1	1	cytochrome P450 CYP81B62 [Salvia miltiorrhiza]

No.	Accession Number	Average Mass	Max-10logP	Max Coverage (%)	Max# Peptides	Max# Unique	Description
95	gi|410176144|gb|AFV61803.1|	26773	21.57	5	1	1	30S ribosomal protein S2 (chloroplast) [Origanum vulgare subsp. vulgare]
96	gi|916442902|gb|AKZ23975.1|	26773	21.57	5	1	1	ribosomal protein S2 (plastid) [Monarda fistulosa var. mollis]
97	gi|916442908|gb|AKZ23977.1|	26686	21.57	5	1	1	ribosomal protein S2 (plastid) [Nepeta cataria]
98	gi|827346574|gb|AKJ77760.1|	26722	21.57	5	1	1	30S ribosomal protein S2 (chloroplast) [Perilla frutescens]
99	gi|827345166|gb|AKJ76750.1|	26770	21.57	5	1	1	30S ribosomal protein S2 (chloroplast) [Rosmarinus officinalis]
100	gi|836643406|ref|YP_009144504.1|	26770	21.57	5	1	1	30S ribosomal protein S2 (chloroplast) [Rosmarinus officinalis]
101	gi|401879731|gb|AFQ30918.1|	26744	21.57	5	1	1	30S ribosomal protein S2 (chloroplast) [Salvia miltiorrhiza]
102	gi|573461940|emb|CCQ71609.1|	26744	21.57	5	1	1	30S ribosomal protein S2 (chloroplast) [Salvia miltiorrhiza]
103	gi|916442905|gb|AKZ23976.1|	26758	21.57	5	1	1	ribosomal protein S2 (plastid) [Salvia nemorosa]
104	gi|442775714|gb|AGC73980.1|	19816	20.22	6	1	1	jasmonate ZIM-domain protein 1 [Salvia miltiorrhiza]
105	gi|745791091|gb|AJD25254.1|	55430	20.07	1	1	1	cytochrome P450 CYP728D17 [Salvia miltiorrhiza]
106	gi|8134569|sp|Q42662.2|METE_PLESU	84590	20.07	1	1	1	5-methyltetrahydropteroyltriglutamate--homocysteine methyltransferase; AltName: Full=Cobalamin-independent methionine synthase isozyme; AltName: Full=Vitamin-B12-independent methionine synthase isozyme
107	gi|29839421|sp|Q9XGW0.1|COMT1_OCIBA	39529	20.07	1	1	1	Caffeic acid 3-O-methyltransferase 1; Short=CAOMT-1; Short=COMT-1; AltName: Full=S-adenosysl-L-methionine:caffeic acid 3-O-methyltransferase 1

No.	Accession Number	Average Mass	Max-10logP	Max Coverage (%)	Max# Peptides	Max# Unique	Description
108	gi|29839420|sp|Q9XGV9.1|COMT2_OCIBA	39613	20.07	1	1	1	Caffeic acid 3-O-methyltransferase 2; Short=CAOMT-2; Short=COMT-2; AltName: Full=S-adenosysl-L-methionine:caffeic acid 3-O-methyltransferase 2
109	gi|735679295|gb|AJA39985.1|	82378	20.07	1	1	1	(E)-4-hydroxy-3-methylbut-2-enyl diphosphate synthase [Salvia miltiorrhiza f. alba]
110	gi|75219538|sp|O48935.1|TPSBF_MENPI	63830	109.4	23	14	13	Beta-farnesene synthase
111	gi|122249145|sp|Q49SP3.1|TPSPS_POGCB	64199	102.97	22	14	13	Patchoulol synthase; Short=PatTps177; AltName: Full=Alpha-guaiene synthase; AltName: Full=Delta-guaiene synthase
112	gi|116256299|sp|Q9XES0.2|DXR_MENPI	51034	80.68	11	7	7	1-deoxy-D-xylulose 5-phosphate reductoisomerase, chloroplastic; Short=1-deoxyxylulose-5-phosphate reductoisomerase; Short=DXP reductoisomerase; AltName: Full=2-C-methyl-D-erythritol 4-phosphate synthase; F...
113	gi|75192856|sp|Q9MBC1.1|3AT_PERFR	50675	78.82	8	4	4	Anthocyanidin 3-O-glucoside 6''-O-acyltransferase; Short=3AT
114	gi|29839420|sp|Q9XGV9.1|COMT2_OCIBA	39613	77.93	6	3	1	Caffeic acid 3-O-methyltransferase 2; Short=CAOMT-2; Short=COMT-2; AltName: Full=S-adenosysl-L-methionine:caffeic acid 3-O-methyltransferase 2
115	gi|75293243|sp|Q6WKZ0.1|C7D94_MENGR	56308	76.56	7	4	4	Cytochrome P450 71D94
116	gi|403399409|sp|E2E2P0.1|GTPS_ORIVU	69063	74.1	5	4	4	Gamma-terpinene synthase, chloroplastic; Short=Ovtps2; AltName: Full=Alpha-terpinene synthase; Flags: Precursor
117	gi|29839421|sp|Q9XGW0.1|COMT1_OCIBA	39529	72.15	6	3	1	Caffeic acid 3-O-methyltransferase 1; Short=CAOMT-1; Short=COMT-1; AltName: Full=S-adenosysl-L-methionine:caffeic acid 3-O-methyltransferase 1
118	gi|132044|sp|P28453.1|RBL_SCUBO	51794	68.35	12	5	5	Ribulose bisphosphate carboxylase large chain; Short=RuBisCO large subunit

No.	Accession Number	Average Mass	Max-10logP	Max Coverage (%)	Max# Peptides	Max# Unique	Description
119	gi|8134569|sp|Q42662.2|METE_PLESU	84590	56.89	4	3	3	5-methyltetrahydropteroyltriglutamate--homocysteine methyltransferase; AltName: Full=Cobalamin-independent methionine synthase isozyme; AltName: Full=Vitamin-B12-independent methionine synthase isozyme
120	gi|75129654|sp|Q6VMW0.1|Q8OMT_MENPI	40849	43.32	6	2	2	8-hydroxyquercetin 8-O-methyltransferase; AltName: Full=Flavonol 8-O-methyltransferase
121	gi|75293242|sp|Q6WKY9.1|C7D95_MENGR	56365	42.08	2	1	1	Cytochrome P450 71D95; AltName: Full=(-)-(4S)-Limonene-3-hydroxylase
122	gi|75290511|sp|Q6IV13.1|C7D95_MENSP	56322	42.08	2	1	1	Cytochrome P450 71D95; AltName: Full=Limonene-3-hydroxylase
123	gi|75306222|sp|Q947B7.1|MFS_MENPI	55360	30.62	2	1	1	(+)-menthofuran synthase; AltName: Full=(+)-pulegone 9-hydroxylase
124	gi|17366672|sp|Q9ARF9.1|HPPD_PLESU	47736	28.03	2	1	1	4-hydroxyphenylpyruvate dioxygenase; AltName: Full=4-hydroxyphenylpyruvic acid oxidase; Short=4HPPD; Short=HPD; Short=HPPDase
125	gi|510785777|sp|G0LD36.1|RAS_MELOI	47161	26.9	2	1	1	Rosmarinate synthase; Short=MoRAS; AltName: Full=Hydroxycinnamoyl-CoA:hydroxyphenyllactate hydroxycinnamoyltransferase
126	gi|75129878|sp|Q6WAU0.1|PULR_MENPI	37915	26.37	2	1	1	(+)-pulegone reductase
127	gi|122237148|sp|Q15GI4.1|EGS1_OCIBA	35607	22.15	3	1	1	Eugenol synthase 1 [Ocimum basilicum] (Sweet basil)
128	gi|56749087|sp|Q85XY6.1|MATK_OCIBA	60282	20.19	2	1	1	Maturase K; AltName: Full=Intron maturase
129	gi|29839421|sp|Q9XGW0.1|COMT1_OCIBA	39529	28.48	1	1	1	Caffeic acid 3-O-methyltransferase 1; Short=CAOMT-1; Short=COMT-1; AltName: Full=S-adenosysl-L-methionine:caffeic acid 3-O-methyltransferase 1
130	gi|8134569|sp|Q42662.2|METE_PLESU	84590	37.07	1	1	1	5-methyltetrahydropteroyltriglutamate--homocysteine methyltransferase; AltName: Full=Cobalamin-independent methionine synthase isozyme; AltName:

No.	Accession Number	Average Mass	Max-10logP	Max Coverage (%)	Max# Peptides	Max# Unique	Description
							Full=Vitamin-B12-independent methionine synthase isozyme
131	gi|29839420|sp|Q9XGV9.1|COMT2_OCIBA	39613	28.48	1	1	1	Caffeic acid 3-O-methyltransferase 2; Short=CAOMT-2; Short=COMT-2; AltName: Full=S-adenosysl-L-methionine:caffeic acid 3-O-methyltransferase 2
132	gi|735679295|gb|AJA39985.1|	82378	28.48	1	1	1	(E)-4-hydroxy-3-methylbut-2-enyl diphosphate synthase [Salvia miltiorrhiza f. alba]
133	gi|745791091|gb|AJD25254.1|	55430	28.48	1	1	1	cytochrome P450 CYP728D17 [Salvia miltiorrhiza]
134	gi|916438881|gb|AKZ22145.1|	84354	39.87	1	1	1	NADH dehydrogenase subunit 5 (plastid) [Monarda fistulosa var. mollis]
135	gi|410176201|gb|AFV61860.1|	84295	39.87	1	1	1	NADH dehydrogenase subunit 5 (chloroplast) [Origanum vulgare subsp. vulgare]
136	gi|669254287|gb|AII20583.1|	77022	34.71	2	1	1	NADH dehydrogenase subunit F, partial (chloroplast) [Holocheila longipedunculata]
137	gi|669254291|gb|AII20585.1|	79070	34.71	2	1	1	NADH dehydrogenase subunit F, partial (chloroplast) [Petraeovitex multiflora]
138	gi|669254285|gb|AII20582.1|	74815	34.71	2	1	1	NADH dehydrogenase subunit F, partial (chloroplast) [Holocheila longipedunculata]
139	gi|669254283|gb|AII20581.1|	77991	34.71	2	1	1	NADH dehydrogenase subunit F, partial (chloroplast) [Holocheila longipedunculata]
140	gi|395484522|gb|AFN66518.1|	76105	34.71	2	1	1	NADH dehydrogenase subunit F, partial (plastid) [Teucrium subspinosum]
141	gi|669254293|gb|AII20586.1|	79081	34.71	2	1	1	NADH dehydrogenase subunit F, partial (chloroplast) [Hymenopyramis cana]
142	gi|401879790|gb|AFQ30977.1|	83587	34.70	1	1	1	NADH dehydrogenase subunit 5 (chloroplast) [Salvia miltiorrhiza]

No.	Accession Number	Average Mass	Max-10logP	Max Coverage (%)	Max# Peptides	Max# Unique	Description
143	gi|573462000|emb|CCQ71669.1|	83587	34.70	1	1	1	NADH dehydrogenase subunit 5 (chloroplast) [Salvia miltiorrhiza]
144	gi|395484502|gb|AFN66509.1|	75956	34.71	2	1	1	NADH dehydrogenase subunit F, partial (plastid) [Teucrium divaricatum]
145	gi|395484481|gb|AFN66500.1|	76061	34.71	2	1	1	NADH dehydrogenase subunit F, partial (plastid) [Teucrium flavum subsp. glaucum]
146	gi|395484475|gb|AFN66497.1|	78510	34.71	2	1	1	NADH dehydrogenase subunit F, partial (plastid) [Rubiteucris palmata]
147	gi|836643377|ref|YP_009144562.1|	84218	34.71	1	1	1	NADH dehydrogenase subunit 5 (chloroplast) [Rosmarinus officinalis]
148	gi|827345137|gb|AKJ76721.1|	84218	34.71	1	1	1	NADH dehydrogenase subunit 5 (chloroplast) [Rosmarinus officinalis]
149	gi|916438885|gb|AKZ22147.1|	84443	34.71	1	1	1	NADH dehydrogenase subunit 5 (plastid) [Salvia nemorosa]
150	gi|395484513|gb|AFN66514.1|	76814	26.97	2	1	1	NADH dehydrogenase subunit F, partial (plastid) [Teucrium pyrenaicum]
151	gi|827346594|gb|AKJ77780.1|	84248	34.71	1	1	1	NADH dehydrogenase subunit 5 (chloroplast) [Perilla frutescens]
152	gi|827345833|gb|AKJ77134.1|	85675	26.97	1	1	1	NADH dehydrogenase subunit 5 (chloroplast) [Scutellaria baicalensis]
153	gi|910312648|ref|YP_009162309.1|	85675	26.97	1	1	1	NADH dehydrogenase subunit 5 (chloroplast) [Scutellaria baicalensis]
154	gi|395484511|gb|AFN66513.1|	76860	26.97	2	1	1	NADH dehydrogenase subunit F, partial (plastid) [Teucrium oxylepis]
155	gi|752789835|ref|YP_009117269.1|	85385	34.71	1	1	1	NADH-plastoquinone oxidoreductase subunit 5 (chloroplast) [Premna microphylla]

No.	Accession Number	Average Mass	Max-10logP	Max Coverage (%)	Max# Peptides	Max# Unique	Description
156	gi|748013953|gb|AJE28423.1|	85385	34.71	1	1	1	NADH-plastoquinone oxidoreductase subunit 5 (chloroplast) [Premna microphylla]
157	gi|395484489|gb|AFN66504.1|	76910	26.97	2	1	1	NADH dehydrogenase subunit F, partial (plastid) [Teucrium betonicum]
158	gi|916438887|gb|AKZ22148.1|	83254	26.97	1	1	1	NADH dehydrogenase subunit 5 (plastid) [Teucrium canadense]
159	gi|395484495|gb|AFN66506.1|	76993	26.97	2	1	1	NADH dehydrogenase subunit F, partial (plastid) [Teucrium eriocephalum subsp. almeriense]
160	gi|395484500|gb|AFN66508.1|	77065	26.97	2	1	1	NADH dehydrogenase subunit F, partial (plastid) [Teucrium stocksianum subsp. incanum]
161	gi|395484526|gb|AFN66520.1|	76596	26.97	2	1	1	NADH dehydrogenase subunit F, partial (plastid) [Teucrium bicolor]
162	gi|395484515|gb|AFN66515.1|	76501	26.97	2	1	1	NADH dehydrogenase subunit F, partial (plastid) [Teucrium racemosum]
163	gi|395484473|gb|AFN66496.1|	78531	26.97	2	1	1	NADH dehydrogenase subunit F, partial (plastid) [Teucridium parvifolium]
164	gi|395484524|gb|AFN66519.1|	75723	26.97	2	1	1	NADH dehydrogenase subunit F, partial (plastid) [Teucrium kotschyanum]
165	gi|395484477|gb|AFN66498.1|	76293	26.97	2	1	1	NADH dehydrogenase subunit F, partial (plastid) [Spartothamnella puberula]
166	gi|395484517|gb|AFN66516.1|	76688	26.97	2	1	1	NADH dehydrogenase subunit F, partial (plastid) [Teucrium salviastrum]
167	gi|395484520|gb|AFN66517.1|	76892	26.97	2	1	1	NADH dehydrogenase subunit F, partial (plastid) [Teucrium spinosum]
168	gi|395484483|gb|AFN66501.1|	77431	26.97	2	1	1	NADH dehydrogenase subunit F, partial (plastid) [Teucrium albicaule]

No.	Accession Number	Average Mass	Max-10logP	Max Coverage (%)	Max# Peptides	Max# Unique	Description
169	gi|395484504|gb|AFN66510.1|	77454	26.97	2	1	1	NADH dehydrogenase subunit F, partial (plastid) [Teucrium laciniatum]
170	gi|395484530|gb|AFN66522.1|	76725	26.97	2	1	1	NADH dehydrogenase subunit F, partial (plastid) [Teucrium viscidum var. miquelianum]
171	gi|395484528|gb|AFN66521.1|	76705	26.97	2	1	1	NADH dehydrogenase subunit F, partial (plastid) [Teucrium japonicum]
172	gi|395484537|gb|AFN66525.1|	78210	26.97	2	1	1	NADH dehydrogenase subunit F, partial (plastid) [Teucrium decipiens]
173	gi|395484533|gb|AFN66523.1|	75763	26.97	2	1	1	NADH dehydrogenase subunit F, partial (plastid) [Teucrium montbretii subsp. heliotropiifolium]
174	gi|395484507|gb|AFN66511.1|	77434	26.97	2	1	1	NADH dehydrogenase subunit F, partial (plastid) [Teucrium nudicaule]
175	gi|395484479|gb|AFN66499.1|	34714	26.97	4	1	1	NADH dehydrogenase subunit F, partial (plastid) [Oncinocalyx betchei]
176	gi|395484535|gb|AFN66524.1|	76413	26.97	2	1	1	NADH dehydrogenase subunit F, partial (plastid) [Teucrium antitauricum]
177	gi|395484493|gb|AFN66505.1|	77203	26.97	2	1	1	NADH dehydrogenase subunit F, partial (plastid) [Teucrium pseudochamaepitys]
178	gi|395484487|gb|AFN66503.1|	77172	26.97	2	1	1	NADH dehydrogenase subunit F, partial (plastid) [Teucrium aroanium]
179	gi|395484509|gb|AFN66512.1|	77251	26.97	2	1	1	NADH dehydrogenase subunit F, partial (plastid) [Teucrium orientale subsp. gloeotrichum]
180	gi|395484485|gb|AFN66502.1|	77595	26.97	2	1	1	NADH dehydrogenase subunit F, partial (plastid) [Teucrium aristatum]
181	gi|395484497|gb|AFN66507.1|	77873	26.97	2	1	1	NADH dehydrogenase subunit F, partial (plastid) [Teucrium fruticans]

No.	Accession Number	Average Mass	Max-10logP	Max Coverage (%)	Max# Peptides	Max# Unique	Description
182	gi|827345131|gb|AKJ76715.1|	266537	38.65	0	1	1	Protein Ycf2 [Rosmarinus officinalis]
183	gi|827345130|gb|AKJ76714.1|	266537	38.65	0	1	1	Protein Ycf2 [Rosmarinus officinalis]
184	gi|836643371|ref|YP_009144577.1|	266537	38.65	0	1	1	Protein Ycf2 [Rosmarinus officinalis]
185	gi|836643370|ref|YP_009144558.1|	266537	38.65	0	1	1	Protein Ycf2 [Rosmarinus officinalis]
186	gi|573462016|emb|CCQ71685.1|	267080	38.65	0	1	1	Protein Ycf2 [Salvia miltiorrhiza]
187	gi|573461995|emb|CCQ71664.1|	267080	38.65	0	1	1	Protein Ycf2 [Salvia miltiorrhiza]
188	gi|401879785|gb|AFQ30972.1|	267080	38.65	0	1	1	Protein Ycf2 [Salvia miltiorrhiza]
189	gi|401879806|gb|AFQ30993.1|	267080	38.65	0	1	1	Protein Ycf2 [Salvia miltiorrhiza]
190	gi|748013968|gb|AJE28438.1|	268103	38.65	0	1	1	Protein Ycf2 [Premna microphylla]
191	gi|752789850|ref|YP_009117284.1|	268103	38.65	0	1	1	Protein Ycf2 [Premna microphylla]
192	gi|752789831|ref|YP_009117265.1|	268103	38.65	0	1	1	Protein Ycf2 [Premna microphylla]
193	gi|748013949|gb|AJE28419.1|	268103	38.65	0	1	1	Protein Ycf2 [Premna microphylla]
194	gi|910312663|ref|YP_009162324.1|	268069	38.65	0	1	1	Protein Ycf2 [Scutellaria baicalensis]
195	gi|827345827|gb|AKJ77128.1|	268069	38.65	0	1	1	Protein Ycf2 [Scutellaria baicalensis]
196	gi|910312644|ref|YP_009162305.1|	268069	38.65	0	1	1	Protein Ycf2 [Scutellaria baicalensis]
197	gi|827345826|gb|AKJ77127.1|	268069	38.65	0	1	1	Protein Ycf2 [Scutellaria baicalensis]
198	gi|827346597|gb|AKJ77783.1|	266476	38.65	0	1	1	Protein Ycf2 [Perilla frutescens]
199	gi|827346579|gb|AKJ77765.1|	266476	38.65	0	1	1	Protein Ycf2 [Perilla frutescens]
200	gi|827346602|gb|AKJ77788.1|	181164	30.65	1	1	1	Protein TIC 214 [Perilla frutescens]
201	gi|827345132|gb|AKJ76716.1|	218366	21.51	1	1	1	Protein TIC 214 [Rosmarinus officinalis]

No.	Accession Number	Average Mass	Max-10logP	Max Coverage (%)	Max# Peptides	Max# Unique	Description
202	gi|836643372|ref|YP_009144573.1|	218366	21.51	1	1	1	Protein TIC 214 [Rosmarinus officinalis]
203	gi|748013964|gb|AJE28434.1|	225117	29.24	1	1	1	Protein TIC 214 [Premna microphylla]
204	gi|752789846|ref|YP_009117280.1|	225117	29.24	1	1	1	Protein TIC 214 [Premna microphylla]
205	gi|75192856|sp|Q9MBC1.1|3AT_PERFR	50675	28.93	2	1	1	Anthocyanidin 3-O-glucoside 6''-O-acyltransferase; Short=3AT
206	gi|749489569|emb|CEO43479.1|	50534	28.93	2	1	1	unnamed protein product [Lavandula angustifolia] - patented sequence
207	gi|745791067|gb|AJD25242.1|	53008	26.07	3	1	1	cytochrome P450 CYP707A102 [Salvia miltiorrhiza]
208	gi|410176144|gb|AFV61803.1|	26773	25.72	5	1	1	ribosomal protein S2 (chloroplast) [Origanum vulgare subsp. vulgare]
209	gi|916442902|gb|AKZ23975.1|	26773	25.72	5	1	1	ribosomal protein S2 (plastid) [Monarda fistulosa var. mollis]
210	gi|916442908|gb|AKZ23977.1|	26686	25.72	5	1	1	ribosomal protein S2 (plastid) [Nepeta cataria]
211	gi|827346574|gb|AKJ77760.1|	26722	25.72	5	1	1	ribosomal protein S2 (chloroplast) [Perilla frutescens]
212	gi|827345166|gb|AKJ76750.1|	26770	25.72	5	1	1	ribosomal protein S2 (chloroplast) [Rosmarinus officinalis]
213	gi|836643406|ref|YP_009144504.1|	26770	25.72	5	1	1	ribosomal protein S2 (chloroplast) [Rosmarinus officinalis]
214	gi|401879731|gb|AFQ30918.1|	26744	25.72	5	1	1	ribosomal protein S2 (chloroplast) [Salvia miltiorrhiza]
215	gi|573461940|emb|CCQ71609.1|	26744	25.72	5	1	1	ribosomal protein S2 (chloroplast) [Salvia miltiorrhiza]
216	gi|916442905|gb|AKZ23976.1|	26758	25.72	5	1	1	ribosomal protein S2 (plastid) [Salvia nemorosa]
217	gi|787592954|gb|AKA27904.1|	30582	23.75	4	1	1	WRKY protein [Salvia miltiorrhiza]

No.	Accession Number	Average Mass	Max-10logP	Max Coverage (%)	Max# Peptides	Max# Unique	Description
218	gi|659902912|gb|AID69536.1|	58940	22.81	2	1	1	phenylalanine ammonia-lyase, partial [Phlomoides rotata]
219	gi|735665579|gb|AJA38250.1|	90993	20.04	2	1	1	copalyl diphosphate synthase, partial [Salvia fruticosa]
220	gi|763711578|gb|AJQ30184.1|	90993	20.04	2	1	1	copalyl diphosphate synthase, partial [Salvia fruticosa]
221	gi|122233627|sp|Q4JF75.1|RBR_SCUBA	111795	107.9	14	16	16	Retinoblastoma-related protein
222	gi|62900766|sp|O81193.1|SSS_SALOF	68942	92.38	9	5	4	(+)-sabinene synthase, chloroplastic; Short=SSS; Flags: Precursor
223	gi|29839420|sp|Q9XGV9.1|COMT2_OCIBA	39613	89.09	15	7	4	Caffeic acid 3-O-methyltransferase 2; Short=CAOMT-2; Short=COMT-2; AltName: Full=S-adenosysl-L-methionine:caffeic acid 3-O-methyltransferase 2
224	gi|122249145|sp|Q49SP3.1|TPSPS_POGCB	64199	88.62	15	8	7	Patchoulol synthase; Short=PatTps177; AltName: Full=Alpha-guaiene synthase; AltName: Full=Delta-guaiene synthase
225	gi|62900763|sp|O81191.1|SCS_SALOF	69369	84.53	10	6	6	1,8-cineole synthase, chloroplastic; Short=SCS; Flags: Precursor
226	gi|510785778|sp|A0PDV5.1|RAS_PLESU	47902	81.71	8	5	5	Rosmarinate synthase; Short=CbRAS; AltName: Full=Hydroxycinnamoyl transferase; Short=CbHCT1
227	gi|29839421|sp|Q9XGW0.1|COMT1_OCIBA	39529	78.79	11	5	2	Caffeic acid 3-O-methyltransferase 1; Short=CAOMT-1; Short=COMT-1; AltName: Full=S-adenosysl-L-methionine:caffeic acid 3-O-methyltransferase 1
228	gi|75251477|sp|Q5SBP0.1|TPSD_OCIBA	70000	72.11	9	5	4	Terpinolene synthase, chloroplastic; Flags: Precursor
229	gi|8134569|sp|Q42662.2|METE_PLESU	84590	71.27	6	5	5	5-methyltetrahydropteroyltriglutamate--homocysteine methyltransferase; AltName: Full=Cobalamin-independent methionine synthase isozyme; AltName: Full=Vitamin-B12-independent methionine synthase isozyme

No.	Accession Number	Average Mass	Max-10logP	Max Coverage (%)	Max# Peptides	Max# Unique	Description
230	gi|75251484|sp|Q5SBP7.1|SELS_OCIBA	63125	71.11	7	4	4	Selinene synthase
231	gi|122219294|sp|Q49SP6.1|TPGD2_POGCB	64149	67.75	4	2	1	Germacrene D synthase 2; AltName: Full=PatTpsBF2
232	gi|62899675|sp|O81192.1|BPPS_SALOF	69292	65.17	3	2	1	(+)-bornyl diphosphate synthase, chloroplastic; Short=BPPS; AltName: Full=(+)-alpha-pinene synthase; AltName: Full=(+)-camphene synthase; AltName: Full=SBS; Flags: Precursor
233	gi|122210943|sp|Q2XSC5.1|LALIN_LAVAN	65654	56.70	2	1	1	R-linalool synthase; Short=LaLINS
234	gi|75251482|sp|Q5SBP5.1|GCS1_OCIBA	63566	48.42	1	1	1	Gamma-cadinene synthase; AltName: Full=(+)-gamma-cadinene synthase
235	gi|75129878|sp|Q6WAU0.1|PULR_MENPI	37915	46.22	2	1	1	(+)-pulegone reductase
236	gi|75315261|sp|Q9XHE8.1|C71DI_MENSP	56149	37.31	4	2	1	Cytochrome P450 71D18; AltName: Full=(-)-(4S)-Limonene-6-hydroxylase
237	gi|75293244|sp|Q6WKZ1.1|C71DI_MENGR	56149	37.31	4	2	1	Cytochrome P450 71D18; AltName: Full=(-)-(4S)-Limonene-6-hydroxylase
238	gi|75180331|sp|Q9LRC8.1|BAGLU_SCUBA	58772	33.32	6	2	2	Baicalin-beta-D-glucuronidase; AltName: Full=Baicalinase; Flags: Precursor
239	gi|75315259|sp|Q9XHE6.1|C71DF_MENPI	56532	32.17	4	2	2	Cytochrome P450 71D15; AltName: Full=(-)-(4S)-Limonene-3-hydroxylase; AltName: Full=Cytochrome P450 isoform PM2
240	gi|75161989|sp|Q8W1W9.1|5MAT1_SALSN	50724	31.33	2	1	1	Malonyl-coenzyme:anthocyanin 5-O-glucoside-6'''-O-malonyltransferase; Short=Malonyl CoA:anthocyanin 5-O-glucoside-6'''-O-malonyltransferase; Short=Ss5MaT1
241	gi|75293243|sp|Q6WKZ0.1|C7D94_MENGR	56308	31.28	4	2	1	Cytochrome P450 71D94
242	gi|704000326|sp|S4UX02.1|CYPH1_SALMI	55520	31.06	1	1	1	Ferruginol synthase; AltName: Full=Cytochrome P450 76AH1

No.	Accession Number	Average Mass	Max-10logP	Max Coverage (%)	Max# Peptides	Max# Unique	Description
243	gi|75338882|sp|Q9ZR27.1|5GT1_PERFR	50974	31.00	2	1	1	Anthocyanidin 3-O-glucoside 5-O-glucosyltransferase 1; AltName: Full=UDP-glucose:anthocyanin 5-O-glucosyltransferase 3R4; Short=p3R4; Flags: Precursor
244	gi|75338881|sp|Q9ZR26.1|5GT2_PERFR	49110	22.61	2	1	1	Anthocyanidin 3-O-glucoside 5-O-glucosyltransferase 2; AltName: Full=UDP-glucose:anthocyanin 5-O-glucosyltransferase 3R6; Short=p3R6; Flags: Precursor
245	gi|122200954|sp|Q2KNL5.1|CADH1_OCIBA	38769	23.05	4	1	1	Cinnamyl alcohol dehydrogenase 1; Short=CAD 1; Short=ObaCAD1
246	gi|75227033|sp|Q76MR7.1|UBGAT_SCUBA	48654	22.49	5	1	1	Baicalein 7-O-glucuronosyltransferase [Scutellaria baicalensis](Baical skullcap)
247	gi|84029472|sp|Q93WU3.1|CVMT1_OCIBA	39916	20.44	3	1	1	Chavicol O-methyltransferase [Ocimum basilicum] (Sweet basil) Status
248	gi|84027871|sp|Q93WU2.1|EOMT1_OCIBA	40237	20.44	3	1	1	Eugenol O-methyltransferase; AltName: Full=(Iso)eugenol O-methyltransferase EOMT1; AltName: Full=S-adenosysl-L-methionine:(Iso)eugenol O-methyltransferase EOMT1
249	gi|401879801|gb|AFQ30988.1|	218699	41.13	1	2	2	Photosystem I assembly protein Ycf1 (chloroplast) [Salvia miltiorrhiza]
250	gi|573462011|emb|CCQ71680.1|	218685	41.13	1	2	2	Photosystem I assembly protein Ycf1 (chloroplast) [Salvia miltiorrhiza]
251	gi|836643389|ref|YP_009144556.1|	29997	28.27	3	1	1	ribosomal protein L2 (chloroplast) [Rosmarinus officinalis]
252	gi|827345149|gb|AKJ76733.1|	29997	28.27	3	1	1	ribosomal protein L2 (chloroplast) [Rosmarinus officinalis]
253	gi|827345150|gb|AKJ76734.1|	29997	28.27	3	1	1	ribosomal protein L2 (chloroplast) [Rosmarinus officinalis]

No.	Accession Number	Average Mass	Max-10logP	Max Coverage (%)	Max# Peptides	Max# Unique	Description
254	gi|836643390|ref|YP_009144579.1|	29997	28.27	3	1	1	ribosomal protein L2 (chloroplast) [Rosmarinus officinalis]
255	gi|401879808|gb|AFQ30995.1|	29997	28.27	3	1	1	ribosomal protein L2 (chloroplast) [Salvia miltiorrhiza]
256	gi|401879783|gb|AFQ30970.1|	29997	28.27	3	1	1	ribosomal protein L2 (chloroplast) [Salvia miltiorrhiza]
257	gi|916441525|gb|AKZ23467.1|	29921	28.27	3	1	1	ribosomal protein L2 (plastid) [Nepeta cataria]
258	gi|410176218|gb|AFV61877.1|	29997	28.27	3	1	1	ribosomal protein L2 (chloroplast) [Origanum vulgare subsp. vulgare]
259	gi|410176195|gb|AFV61854.1|	29997	28.27	3	1	1	ribosomal protein L2 (chloroplast) [Origanum vulgare subsp. vulgare]
260	gi|916441521|gb|AKZ23465.1|	29997	28.27	3	1	1	ribosomal protein L2 (plastid) [Monarda fistulosa var. mollis]
261	gi|916441523|gb|AKZ23466.1|	29997	28.27	3	1	1	ribosomal protein L2 (plastid) [Salvia nemorosa]
262	gi|752789852|ref|YP_009117286.1|	30084	28.27	3	1	1	ribosomal protein L2 (chloroplast) [Premna microphylla]
263	gi|752789829|ref|YP_009117263.1|	30084	28.27	3	1	1	ribosomal protein L2 (chloroplast) [Premna microphylla]
264	gi|827346587|gb|AKJ77773.1|	31403	28.27	3	1	1	ribosomal protein L2 (chloroplast) [Perilla frutescens]
265	gi|827346537|gb|AKJ77723.1|	31391	28.27	3	1	1	ribosomal protein L2 (chloroplast) [Perilla frutescens]
266	gi|910312642|ref|YP_009162303.1|	30114	28.27	3	1	1	ribosomal protein L2 (chloroplast) [Scutellaria baicalensis]
267	gi|910312665|ref|YP_009162326.1|	30114	28.27	3	1	1	ribosomal protein L2 (chloroplast) [Scutellaria baicalensis]
268	gi|827345846|gb|AKJ77147.1|	30114	28.27	3	1	1	ribosomal protein L2 (chloroplast) [Scutellaria baicalensis]

No.	Accession Number	Average Mass	Max-10logP	Max Coverage (%)	Max# Peptides	Max# Unique	Description
269	gi|827345845|gb|AKJ77146.1|	30114	28.27	3	1	1	ribosomal protein L2 (chloroplast) [Scutellaria baicalensis]
270	gi|916441533|gb|AKZ23471.1|	30010	28.27	3	1	1	ribosomal protein L2 (plastid) [Teucrium canadense]
271	gi|836643406|ref|YP_009144504.1|	26770	27.53	5	1	1	ribosomal protein S2 (chloroplast) [Rosmarinus officinalis]
272	gi|827345166|gb|AKJ76750.1|	26770	27.53	5	1	1	ribosomal protein S2 (chloroplast) [Rosmarinus officinalis]
273	gi|401879731|gb|AFQ30918.1|	26744	27.53	5	1	1	ribosomal protein S2 (chloroplast) [Salvia miltiorrhiza]
274	gi|573461940|emb|CCQ71609.1|	26744	27.53	5	1	1	ribosomal protein S2 (chloroplast) [Salvia miltiorrhiza]
275	gi|827346574|gb|AKJ77760.1|	26722	27.53	5	1	1	ribosomal protein S2 (chloroplast) [Perilla frutescens]
276	gi|410176144|gb|AFV61803.1|	26773	27.53	5	1	1	ribosomal protein S2 (chloroplast) [Origanum vulgare subsp. vulgare]
277	gi|916442905|gb|AKZ23976.1|	26758	27.53	5	1	1	ribosomal protein S2 (plastid) [Salvia nemorosa]
278	gi|916442902|gb|AKZ23975.1|	26773	27.53	5	1	1	ribosomal protein S2 (plastid) [Monarda fistulosa var. mollis]
279	gi|916442908|gb|AKZ23977.1|	26686	27.53	5	1	1	ribosomal protein S2 (plastid) [Nepeta cataria]
280	gi|916441821|gb|AKZ23615.1|	17837	25.53	7	1	1	ribosomal protein L22 (plastid) [Salvia nemorosa]
281	gi|913341377|gb|AKU77131.1|	121334	23.61	1	1	1	Structural maintenance of chromosomes protein 1, partial [Callicarpa bodinieri]
282	gi|735679295|gb|AJA39985.1|	82378	22.90	1	1	1	(E)-4-hydroxy-3-methylbut-2-enyl diphosphate synthase [Salvia miltiorrhiza f. alba]
283	gi|762060299|gb|AJQ20621.1|	41314	21.58	2	1	1	Enoyl-ACP Reductase [Salvia miltiorrhiza]
284	gi|661525312|gb|AIE15763.1|	216665	20.56	1	1	1	Dicer-like protein 1 [Salvia miltiorrhiza]

No.	Accession Number	Average Mass	Max-10logP	Max Coverage (%)	Max# Peptides	Max# Unique	Description
285	gi|908373664|gb|AKT44364.1|	81096	20.41	1	1	1	Heat shock protein 2 [Tectona grandis]
286	gi|8134569|sp|Q42662.2|METE_PLESU	84590	115.32	8	7	7	5-methyltetrahydropteroyltriglutamate--homocysteine methyltransferase; AltName: Full=Cobalamin-independent methionine synthase isozyme; AltName: Full=Vitamin-B12-independent methionine synthase isozyme
287	gi|5915814|sp|O04164.1|C71A6_NEPRA	57955	92.61	5	3	3	Cytochrome P450 71A6
288	gi|29839421|sp|Q9XGW0.1|COMT1_OCIBA	39529	90.64	6	3	1	Caffeic acid 3-O-methyltransferase 1; Short=CAOMT-1; Short=COMT-1; AltName: Full=S-adenosysl-L-methionine:caffeic acid 3-O-methyltransferase 1
289	gi|5915815|sp|Q42716.1|C71A8_MENPI	57213	90.02	5	3	3	Cytochrome P450 71A8
290	gi|122219292|sp|Q49SP4.1|TPGD1_POGCB	64197	86.02	3	2	2	Germacrene D synthase 1; AltName: Full=PatTpsB15
291	gi|5921781|sp|O04111.1|CHSY_PERFR	42686	85.72	5	2	2	Chalcone synthase; AltName: Full=Naringenin-chalcone synthase
292	gi|122233627|sp|Q4JF75.1|RBR_SCUBA	111795	73.59	3	2	2	Retinoblastoma-related protein
293	gi|84027871|sp|Q93WU2.1|EOMT1_OCIBA	40237	59.55	3	1	1	Eugenol O-methyltransferase; AltName: Full=(Iso)eugenol O-methyltransferase EOMT1; AltName: Full=S-adenosysl-L-methionine:(Iso)eugenol O-methyltransferase EOMT1
294	gi|122219294|sp|Q49SP6.1|TPGD2_POGCB	64149	59.19	3	1	1	Germacrene D synthase 2; AltName: Full=PatTpsBF2
295	gi|75161989|sp|Q8W1W9.1|5MAT1_SALSN	50724	46.86	2	1	1	Malonyl-coenzyme:anthocyanin 5-O-glucoside-6'''-O-malonyltransferase; Short=Malonyl CoA:anthocyanin 5-O-glucoside-6'''-O-malonyltransferase; Short=Ss5MaT1
296	gi|75251484|sp|Q5SBP7.1|SELS_OCIBA	63125	43.61	2	1	1	Selinene synthase

No.	Accession Number	Average Mass	Max-10logP	Max Coverage (%)	Max# Peptides	Max# Unique	Description
297	gi|122249145|sp|Q49SP3.1|TPSPS_POGCB	64199	42.70	4	1	1	Patchoulol synthase; Short=PatTps177; AltName: Full=Alpha-guaiene synthase; AltName: Full=Delta-guaiene synthase
298	gi|75293243|sp|Q6WKZ0.1|C7D94_MENGR	56308	40.60	3	1	1	Cytochrome P450 71D94
299	gi|75338882|sp|Q9ZR27.1|5GT1_PERFR	50974	37.18	2	1	1	Anthocyanidin 3-O-glucoside 5-O-glucosyltransferase 1; AltName: Full=UDP-glucose:anthocyanin 5-O-glucosyltransferase 3R4; Short=p3R4; Flags: Precursor
300	gi|75180331|sp|Q9LRC8.1|BAGLU_SCUBA	58772	37.03	5	1	1	Baicalin-beta-D-glucuronidase; AltName: Full=Baicalinase; Flags: Precursor
301	gi|704000326|sp|S4UX02.1|CYPH1_SALMI	55520	35.26	1	1	1	Ferruginol synthase; AltName: Full=Cytochrome P450 76AH1
302	gi|75129878|sp|Q6WAU0.1|PULR_MENPI	37915	33.26	2	1	1	(+)-pulegone reductase
303	gi|75227033|sp|Q76MR7.1|UBGAT_SCUBA	48654	27.59	5	1	1	Baicalein 7-O-glucuronosyltransferase; AltName: Full=UDP-glucuronate:baicalein 7-O-glucuronosyltransferase
304	gi|661525316|gb|AIE15765.1|	184302	48.48	1	1	1	Dicer-like protein 3 [Salvia miltiorrhiza]
305	gi|836643406|ref|YP_009144504.1|	26770	34.08	5	1	1	Ribosomal protein S2 (chloroplast) [Rosmarinus officinalis]
306	gi|827345166|gb|AKJ76750.1|	26770	34.08	5	1	1	Ribosomal protein S2 (chloroplast) [Rosmarinus officinalis]
307	gi|401879731|gb|AFQ30918.1|	26744	34.08	5	1	1	Ribosomal protein S2 (chloroplast) [Salvia miltiorrhiza]
308	gi|573461940|emb|CCQ71609.1|	26744	34.08	5	1	1	Ribosomal protein S2 (chloroplast) [Salvia miltiorrhiza]
309	gi|410176144|gb|AFV61803.1|	26773	34.08	5	1	1	Ribosomal protein S2 (chloroplast) [Origanum vulgare subsp. vulgare]

No.	Accession Number	Average Mass	Max-10logP	Max Coverage (%)	Max# Peptides	Max# Unique	Description
310	gi|916442902|gb|AKZ23975.1|	26773	34.08	5	1	1	Ribosomal protein S2 (plastid) [Monarda fistulosa var. mollis]
311	gi|916442905|gb|AKZ23976.1|	26758	34.08	5	1	1	Ribosomal protein S2 (plastid) [Salvia nemorosa]
312	gi|916442908|gb|AKZ23977.1|	26686	34.08	5	1	1	Ribosomal protein S2 (plastid) [Nepeta cataria]
313	gi|827346574|gb|AKJ77760.1|	26722	34.08	5	1	1	Ribosomal protein S2 (chloroplast) [Perilla frutescens]
314	gi|827345132|gb|AKJ76716.1|	218366	31.19	1	1	1	Ycf1 (chloroplast) [Rosmarinus officinalis]
315	gi|836643372|ref|YP_009144573.1|	218366	31.19	1	1	1	Ycf1 (chloroplast) [Rosmarinus officinalis]
316	gi|401879801|gb|AFQ30988.1|	218699	30.62	1	1	1	Photosystem I assembly protein Ycf1 (chloroplast) [Salvia miltiorrhiza]
317	gi|573462011|emb|CCQ71680.1|	218685	30.62	1	1	1	Ycf1 (chloroplast) [Salvia miltiorrhiza]
318	gi|787592932|gb|AKA27893.1|	37310	25.11	4	1	1	WRKY protein [Salvia miltiorrhiza]
319	gi|662170387|gb|AIE45494.1|	44939	24.14	3	1	1	CONSTANS-like protein 9 [Tectona grandis]
320	gi|745790929|gb|AJD25173.1|	57680	22.85	1	1	1	Cytochrome P450 CYP73A120 [Salvia miltiorrhiza]
321	gi|630057998|gb|AHY94893.1|	57803	22.85	1	1	1	Cinnamate-4-hydroxylase [Prunella vulgaris]
322	gi|725812545|gb|AIY32618.1|	57979	22.85	1	1	1	Cinnamate-4-hydroxylase [Perilla frutescens]
323	gi|745791023|gb|AJD25220.1|	56140	22.76	2	1	1	Cytochrome P450 CYP94B50 [Salvia miltiorrhiza]
324	gi|762060309|gb|AJQ20626.1|	51963	21.88	4	1	1	Ketoacyl-ACP Synthase I [Salvia miltiorrhiza]
325	gi|844572842|gb|AKN09607.1|	76725	21.06	1	1	1	Basic helix-loop-helix transcription factor [Salvia miltiorrhiza]
326	gi|762060281|gb|AJQ20612.1|	13344	20.65	12	1	1	Acyl Carrier Protein [Salvia miltiorrhiza]
327	gi|822603217|emb|CQR79430.1|	35399	20.39	3	1	1	Maturase K, partial (chloroplast) [Clerodendrum bracteatum]

No.	Accession Number	Average Mass	Max-10logP	Max Coverage (%)	Max# Peptides	Max# Unique	Description
328	gi|630058023|gb|AHY94894.1|	51993	20.11	2	1	1	4-coumarate:CoA ligase, partial [Prunella vulgaris]
329	gi|29839421|sp|Q9XGW0.1|COMT1_OCIBA	39529	20.10	2	1	1	Caffeic acid 3-O-methyltransferase 1; Short=CAOMT-1; Short=COMT-1; AltName: Full=S-adenosysl-L-methionine:caffeic acid 3-O-methyltransferase 1
330	gi|29839420|sp|Q9XGV9.1|COMT2_OCIBA	39613	20.10	2	1	1	Caffeic acid 3-O-methyltransferase 2; Short=CAOMT-2; Short=COMT-2; AltName: Full=S-adenosysl-L-methionine:caffeic acid 3-O-methyltransferase 2
331	gi|122219293|sp|Q49SP5.1|TPGAS_POGCB	64232	129.73	17	10	10	Germacrene A synthase; AltName: Full=PatTpsCF2
332	gi|75283876|sp|Q5C9I9.1|ISPD_MENPI	27191	102.75	18	5	5	(-)-isopiperitenol/(-)-carveol dehydrogenase, mitochondrial; Flags: Precursor
333	gi|8134569|sp|Q42662.2|METE_PLESU	84590	91.09	3	2	2	5-methyltetrahydropteroyltriglutamate--homocysteine methyltransferase; AltName: Full=Cobalamin-independent methionine synthase isozyme; AltName: Full=Vitamin-B12-independent methionine synthase isozyme
334	gi|75219538|sp|O48935.1|TPSBF_MENPI	63830	90.41	4	2	2	Beta-farnesene synthase
335	gi|75252096|sp|Q5W283.1|TPSCM_MENPI	63839	85.44	4	2	2	Cis-muuroladiene synthase; Short=MxpSS1
336	gi|75129878|sp|Q6WAU0.1|PULR_MENPI	37915	89.97	6	3	3	(+)-pulegone reductase
337	gi|75224312|sp|Q6USK1.1|GERS_OCIBA	64933	84.74	2	1	1	Geraniol synthase, chloroplastic; Short=ObGES; Flags: Precursor
338	gi|75293243|sp|Q6WKZ0.1|C7D94_MENGR	56308	75.65	4	2	2	Cytochrome P450 71D94
339	gi|403399409|sp|E2E2P0.1|GTPS_ORIVU	69063	74.54	2	1	1	Gamma-terpinene synthase, chloroplastic; Short=Ovtps2; AltName: Full=Alpha-terpinene synthase; Flags: Precursor

No.	Accession Number	Average Mass	Max-10logP	Max Coverage (%)	Max# Peptides	Max# Unique	Description
340	gi|75161989|sp|Q8W1W9.1|5MAT1_SALSN	50724	49.68	2	1	1	Malonyl-coenzyme:anthocyanin 5-O-glucoside-6'''-O-malonyltransferase; Short=Malonyl CoA:anthocyanin 5-O-glucoside-6'''-O-malonyltransferase; Short=Ss5MaT1
341	gi|122210943|sp|Q2XSC5.1|LALIN_LAVAN	65654	48.77	2	1	1	R-linalool synthase; Short=LaLINS
342	gi|75251481|sp|Q5SBP4.1|AZIS_OCIBA	62858	25.63	2	1	1	Alpha-zingiberene synthase
343	gi|748013964|gb|AJE28434.1|	225117	38.72	1	2	1	hypothetical chloroplast RF19 (chloroplast) [Premna microphylla]
344	gi|752789846|ref|YP_009117280.1|	225117	38.72	1	2	1	hypothetical chloroplast RF19 (chloroplast) [Premna microphylla]
345	gi|916443350|gb|AKZ24105.1|	17446	33.46	5	1	1	ribosomal protein S7 (plastid) [Teucrium canadense]
346	gi|827345872|gb|AKJ77173.1|	17389	33.46	5	1	1	ribosomal protein S7 (chloroplast) [Scutellaria baicalensis]
347	gi|910312647|ref|YP_009162308.1|	17389	33.46	5	1	1	ribosomal protein S7 (chloroplast) [Scutellaria baicalensis]
348	gi|827345873|gb|AKJ77174.1|	17389	33.46	5	1	1	ribosomal protein S7 (chloroplast) [Scutellaria baicalensis]
349	gi|827345177|gb|AKJ76761.1|	17379	33.46	5	1	1	ribosomal protein S7 (chloroplast) [Rosmarinus officinalis]
350	gi|827345176|gb|AKJ76760.1|	17379	33.46	5	1	1	ribosomal protein S7 (chloroplast) [Rosmarinus officinalis]
351	gi|836643417|ref|YP_009144574.1|	17379	33.46	5	1	1	ribosomal protein S7 (chloroplast) [Rosmarinus officinalis]
352	gi|836643416|ref|YP_009144561.1|	17379	33.46	5	1	1	ribosomal protein S7 (chloroplast) [Rosmarinus officinalis]

No.	Accession Number	Average Mass	Max-10logP	Max Coverage (%)	Max# Peptides	Max# Unique	Description
353	gi|916443332|gb|AKZ24099.1|	17391	33.46	5	1	1	ribosomal protein S7 (plastid) [Monarda fistulosa var. mollis]
354	gi|573462013|emb|CCQ71682.1|	17361	33.46	5	1	1	ribosomal protein S7 (chloroplast) [Salvia miltiorrhiza]
355	gi|401879803|gb|AFQ30990.1|	17361	33.46	5	1	1	ribosomal protein S7 (chloroplast) [Salvia miltiorrhiza]
356	gi|573461998|emb|CCQ71667.1|	17361	33.46	5	1	1	ribosomal protein S7 (chloroplast) [Salvia miltiorrhiza]
357	gi|401879788|gb|AFQ30975.1|	17361	33.46	5	1	1	ribosomal protein S7 (chloroplast) [Salvia miltiorrhiza]
358	gi|410176200|gb|AFV61859.1|	17361	33.46	5	1	1	ribosomal protein S7 (chloroplast) [Origanum vulgare subsp. vulgare]
359	gi|410176213|gb|AFV61872.1|	17361	33.46	5	1	1	ribosomal protein S7 (chloroplast) [Origanum vulgare subsp. vulgare]
360	gi|752789834|ref|YP_009117268.1|	17361	33.46	5	1	1	ribosomal protein S7 (chloroplast) [Premna microphylla]
361	gi|748013965|gb|AJE28435.1|,	17361	33.46	5	1	1	ribosomal protein S7 (chloroplast) [Premna microphylla]
362	gi|752789847|ref|YP_009117281.1|	17361	33.46	5	1	1	ribosomal protein S7 (chloroplast) [Premna microphylla]
363	gi|748013952|gb|AJE28422.1|	17361	33.46	5	1	1	ribosomal protein S7 (chloroplast) [Premna microphylla]
364	gi|827346599|gb|AKJ77785.1|	17361	33.46	5	1	1	ribosomal protein S7 (chloroplast) [Perilla frutescens]
365	gi|827346590|gb|AKJ77776.1|	17361	33.46	5	1	1	ribosomal protein S7 (chloroplast) [Perilla frutescens]
366	gi|916443335|gb|AKZ24100.1|	17379	33.46	5	1	1	ribosomal protein S7 (plastid) [Salvia nemorosa]
367	gi|910312660|ref|YP_009162321.1|	17389	33.46	5	1	1	ribosomal protein S7 (chloroplast) [Scutellaria baicalensis]
368	gi|916443338|gb|AKZ24101.1|	17361	33.46	5	1	1	ribosomal protein S7 (plastid) [Nepeta cataria]
369	gi|661525316|gb|AIE15765.1|	184302	22.76	1	1	1	Dicer-like protein 3 [Salvia miltiorrhiza]

No.	Accession Number	Average Mass	Max-10logP	Max Coverage (%)	Max# Peptides	Max# Unique	Description
370	gi|75290511|sp|Q6IV13.1|C7D95_MENSP	56322	168.40	9	6	1	Cytochrome P450 71D95; AltName: Full=Limonene-3-hydroxylase
371	gi|122233627|sp|Q4JF75.1|RBR_SCUBA	111795	136.20	1	1	1	Retinoblastoma-related protein
372	gi|75129878|sp|Q6WAU0.1|PULR_MENPI	37915	114.35	6	3	3	(+)-pulegone reductase
373	gi|122249145|sp|Q49SP3.1|TPSPS_POGCB	64199	106.65	3	2	2	Patchoulol synthase; Short=PatTps177; AltName: Full=Alpha-guaiene synthase; AltName: Full=Delta-guaiene synthase
374	gi|403399735|sp|E2E2N7.1|BCGS_ORIVU	64443	54.15	2	1	1	Bicyclogermacrene synthase; Short=Ovtps4
375	gi|661525316|gb|AIE15765.1|	184302	47.70	1	1	1	Dicer-like protein 3 [Salvia miltiorrhiza]
376	gi|910312663|ref|YP_009162324.1|	268069	41.48	0	1	1	Hypothetical chloroplast RF2 (chloroplast) [Scutellaria baicalensis]
377	gi|827345827|gb|AKJ77128.1|	268069	41.48	0	1	1	Hypothetical chloroplast RF2 (chloroplast) [Scutellaria baicalensis]
378	gi|910312644|ref|YP_009162305.1|	268069	41.48	0	1	1	Hypothetical chloroplast RF2 (chloroplast) [Scutellaria baicalensis]
379	gi|827345826|gb|AKJ77127.1|	268069	41.48	0	1	1	Hypothetical chloroplast RF2 (chloroplast) [Scutellaria baicalensis]
380	gi|748013968|gb|AJE28438.1|	268103	36.17	0	1	1	Hypothetical chloroplast RF21 (chloroplast) [Premna microphylla]
381	gi|752789850|ref|YP_009117284.1|	268103	36.17	0	1	1	Hypothetical chloroplast RF21 (chloroplast) [Premna microphylla]
382	gi|752789831|ref|YP_009117265.1|	268103	36.17	0	1	1	Hypothetical chloroplast RF21 (chloroplast) [Premna microphylla]
383	gi|748013949|gb|AJE28419.1|	268103	36.17	0	1	1	Hypothetical chloroplast RF21 (chloroplast) [Premna microphylla]

No.	Accession Number	Average Mass	Max-10logP	Max Coverage (%)	Max# Peptides	Max# Unique	Description
384	gi|827346597|gb|AKJ77783.1|	266476	36.17	0	1	1	Ycf2 (chloroplast) [Perilla frutescens]
385	gi|827346579|gb|AKJ77765.1|	266476	36.17	0	1	1	Ycf2 (chloroplast) [Perilla frutescens]
386	gi|836643370|ref|YP_009144558.1|	266537	36.17	0	1	1	Ycf2 (chloroplast) [Rosmarinus officinalis]
387	gi|827345131|gb|AKJ76715.1|	266537	36.17	0	1	1	Ycf2 (chloroplast) [Rosmarinus officinalis]
388	gi|827345130|gb|AKJ76714.1|	266537	36.17	0	1	1	Ycf2 (chloroplast) [Rosmarinus officinalis]
389	gi|836643371|ref|YP_009144577.1|	266537	36.17	0	1	1	Ycf2 (chloroplast) [Rosmarinus officinalis]
390	gi|573462016|emb|CCQ71685.1|	267080	36.17	0	1	1	Ycf2 (chloroplast) [Salvia miltiorrhiza]
391	gi|573461995|emb|CCQ71664.1|	267080	36.17	0	1	1	Ycf2 (chloroplast) [Salvia miltiorrhiza]
392	gi|401879785|gb|AFQ30972.1|	267080	36.17	0	1	1	Hypothetical chloroplast RF2 (chloroplast) [Salvia miltiorrhiza]
393	gi|401879806|gb|AFQ30993.1|	267080	36.17	0	1	1	Hypothetical chloroplast RF2 (chloroplast) [Salvia miltiorrhiza]
394	gi|410176216|gb|AFV61875.1|	264781	36.17	0	1	1	Ycf2 (chloroplast) [Origanum vulgare subsp. vulgare]
395	gi|410176197|gb|AFV61856.1|	264781	36.17	0	1	1	Ycf2 (chloroplast) [Origanum vulgare subsp. vulgare]
396	gi|661525312|gb|AIE15763.1|	216665	28.26	1	1	1	Dicer-like protein 1 [Salvia miltiorrhiza]
397	gi|585636485|gb|AHJ59322.1|	90900	24.77	1	1	1	Copalyl diphosphate synthase [Salvia miltiorrhiza f. alba]
398	gi|751414476|gb|AJF93403.1|	58880	24.19	2	1	1	Ent-kaurene oxidase [Salvia miltiorrhiza]
399	gi|745791049|gb|AJD25233.1|	58838	24.19	2	1	1	Cytochrome P450 CYP701A40 [Salvia miltiorrhiza]
400	gi|410176144|gb|AFV61803.1|	26773	23.20	5	1	1	ribosomal protein S2 (chloroplast) [Origanum vulgare subsp. vulgare]
401	gi|916442902|gb|AKZ23975.1|	26773	23.20	5	1	1	ribosomal protein S2 (plastid) [Monarda fistulosa var. mollis]

No.	Accession Number	Average Mass	Max-10logP	Max Coverage (%)	Max# Peptides	Max# Unique	Description
402	gi|916442908|gb|AKZ23977.1|	26686	23.20	5	1	1	ribosomal protein S2 (plastid) [Nepeta cataria]
403	gi|827346574|gb|AKJ77760.1|	26722	23.20	5	1	1	ribosomal protein S2 (chloroplast) [Perilla frutescens]
404	gi|836643406|ref|YP_009144504.1|	26770	23.20	5	1	1	ribosomal protein S2 (chloroplast) [Rosmarinus officinalis]
405	gi|827345166|gb|AKJ76750.1|	26770	23.20	5	1	1	ribosomal protein S2 (chloroplast) [Rosmarinus officinalis]
406	gi|401879731|gb|AFQ30918.1|	26744	23.20	5	1	1	ribosomal protein S2 (chloroplast) [Salvia miltiorrhiza]
407	gi|573461940|emb|CCQ71609.1|	26744	23.20	5	1	1	ribosomal protein S2 (chloroplast) [Salvia miltiorrhiza]
408	gi|916442905|gb|AKZ23976.1|	26758	23.20	5	1	1	ribosomal protein S2 (plastid) [Salvia nemorosa]
409	gi|75129878|sp|Q6WAU0.1|PULR_MENPI	37915	21.98	2	1	1	(+)-pulegone reductase
410	gi|787592958|gb|AKA27906.1|	38850	20.03	3	1	1	WRKY protein [Salvia miltiorrhiza]
411	gi|122219294|sp|Q49SP6.1|TPGD2_POGCB	64149	107.08	8	5	5	Germacrene D synthase 2; AltName: Full=PatTpsBF2
412	gi|122233627|sp|Q4JF75.1|RBR_SCUBA	111795	101.83	4	4	4	Retinoblastoma-related protein
413	gi|56749087|sp|Q85XY6.1|MATK_OCIBA	60282	86.78	4	2	2	Maturase K; AltName: Full=Intron maturase
414	gi|75219538|sp|O48935.1|TPSBF_MENPI	63830	84.66	5	3	3	Beta-farnesene synthase
415	gi|75252096|sp|Q5W283.1|TPSCM_MENPI	63839	81.24	5	3	3	Cis-muuroladiene synthase; Short=MxpSS1
416	gi|122219293|sp|Q49SP5.1|TPGAS_POGCB	64232	80.48	1	1	1	Germacrene A synthase; AltName: Full=PatTpsCF2
417	gi|510785777|sp|G0LD36.1|RAS_MELOI	47161	71.10	7	3	3	Rosmarinate synthase; Short=MoRAS; AltName: Full=Hydroxycinnamoyl-CoA:hydroxyphenyllactate hydroxycinnamoyltransferase
418	gi|75251480|sp|Q5SBP3.1|LLOS_OCIBA	65822	67.77	3	2	2	R-linalool synthase, chloroplastic; Flags: Precursor

No.	Accession Number	Average Mass	Max-10logP	Max Coverage (%)	Max# Peptides	Max# Unique	Description
419	gi|6919914|sp|P56848.1|ISPE_MENPI	44603	63.19	5	2	2	4-diphosphocytidyl-2-C-methyl-D-erythritol kinase, chloroplastic; AltName: Full=4-(cytidine-5'-diphospho)-2-C-methyl-D-erythritol kinase; Short=CMK; Flags: Precursor
420	gi|75251484|sp|Q5SBP7.1|SELS_OCIBA	63125	53.85	2	1	1	Selinene synthase
421	gi|122219295|sp|Q49SP7.1|TPSCS_POGCB	63586	46.67	2	1	1	Gamma-curcumene synthase; AltName: Full=PatTpsA
422	gi|75129878|sp|Q6WAU0.1|PULR_MENPI	37915	29.75	2	1	1	(+)-pulegone reductase
423	gi|75293243|sp|Q6WKZ0.1|C7D94_MENGR	56308	26.13	2	1	1	Cytochrome P450 71D94
424	gi|75251480|sp|Q5SBP3.1|LLOS_OCIBA	65822	44.02	5	3	3	R-linalool synthase, chloroplastic; Flags: Precursor
425	gi|844572842|gb|AKN09607.1|	76725	22.88	1	1	1	Basic helix-loop-helix transcription factor [Salvia miltiorrhiza]
426	gi|916443332|gb|AKZ24099.1|	17391	22.37	5	1	1	ribosomal protein S7 (plastid) [Monarda fistulosa var. mollis]
427	gi|916443350|gb|AKZ24105.1|	17446	22.37	5	1	1	ribosomal protein S7 (plastid) [Teucrium canadense]
428	gi|827345872|gb|AKJ77173.1|	17389	22.37	5	1	1	ribosomal protein S7 (chloroplast) [Scutellaria baicalensis]
429	gi|910312647|ref|YP_009162308.1|	17389	22.37	5	1	1	ribosomal protein S7 (chloroplast) [Scutellaria baicalensis]
430	gi|827345177|gb|AKJ76761.1|	17379	22.37	5	1	1	ribosomal protein S7 (chloroplast) [Rosmarinus officinalis]
431	gi|827345176|gb|AKJ76760.1|	17379	22.37	5	1	1	ribosomal protein S7 (chloroplast) [Rosmarinus officinalis]
432	gi|836643417|ref|YP_009144574.1|	17379	22.37	5	1	1	ribosomal protein S7 (chloroplast) [Rosmarinus officinalis]

No.	Accession Number	Average Mass	Max-10logP	Max Coverage (%)	Max# Peptides	Max# Unique	Description
433	gi|836643416|ref|YP_009144561.1|	17379	22.37	5	1	1	ribosomal protein S7 (chloroplast) [Rosmarinus officinalis]
434	gi|573462013|emb|CCQ71682.1|	17361	22.37	5	1	1	ribosomal protein S7 (chloroplast) [Salvia miltiorrhiza]
435	gi|401879803|gb|AFQ30990.1|	17361	22.37	5	1	1	ribosomal protein S7 (chloroplast) [Salvia miltiorrhiza]
436	gi|573461998|emb|CCQ71667.1|	17361	22.37	5	1	1	ribosomal protein S7 (chloroplast) [Salvia miltiorrhiza]
437	gi|401879788|gb|AFQ30975.1|	17361	22.37	5	1	1	ribosomal protein S7 (chloroplast) [Salvia miltiorrhiza]
438	gi|410176200|gb|AFV61859.1|	17361	22.37	5	1	1	ribosomal protein S7 (chloroplast) [Origanum vulgare subsp. vulgare]
439	gi|752789834|ref|YP_009117268.1|	17361	22.37	5	1	1	ribosomal protein S7 (chloroplast) [Premna microphylla]
440	gi|748013965|gb|AJE28435.1|	17361	22.37	5	1	1	ribosomal protein S7 (chloroplast) [Premna microphylla]
441	gi|752789847|ref|YP_009117281.1|	17361	22.37	5	1	1	ribosomal protein S7 (chloroplast) [Premna microphylla]
442	gi|748013952|gb|AJE28422.1|	17361	22.37	5	1	1	ribosomal protein S7 (chloroplast) [Premna microphylla]
443	gi|827345873|gb|AKJ77174.1|	17389	22.37	5	1	1	ribosomal protein S7 (chloroplast) [Scutellaria baicalensis]
444	gi|910312660|ref|YP_009162321.1|	17389	22.37	5	1	1	ribosomal protein S7 (chloroplast) [Scutellaria baicalensis]
445	gi|827346599|gb|AKJ77785.1|	17361	22.37	5	1	1	ribosomal protein S7 (chloroplast) [Perilla frutescens]
446	gi|827346590|gb|AKJ77776.1|	17361	22.37	5	1	1	ribosomal protein S7 (chloroplast) [Perilla frutescens]
447	gi|410176213|gb|AFV61872.1|	17361	22.37	5	1	1	ribosomal protein S7 (chloroplast) [Origanum vulgare subsp. vulgare]
448	gi|916443335|gb|AKZ24100.1|	17379	22.37	5	1	1	ribosomal protein S7 (plastid) [Salvia nemorosa]
449	gi|916443338|gb|AKZ24101.1|	17361	22.37	5	1	1	ribosomal protein S7 (plastid) [Nepeta cataria]

No.	Accession Number	Average Mass	Max-10logP	Max Coverage (%)	Max# Peptides	Max# Unique	Description
450	gi|916439925|gb|AKZ22667.1|	82427	21.45	1	1	1	photosystem I P700 chlorophyll a apoprotein A2 (plastid) [Nepeta cataria]
451	gi|410176154|gb|AFV61813.1|	82441	21.45	1	1	1	photosystem I P700 chlorophyll a apoprotein A2 (chloroplast) [Origanum vulgare subsp. vulgare]
452	gi|916439921|gb|AKZ22665.1|	82459	21.45	1	1	1	photosystem I P700 chlorophyll a apoprotein A2 (plastid) [Monarda fistulosa var. mollis]
453	gi|827345836|gb|AKJ77137.1|	82407	21.45	1	1	1	photosystem I P700 apoprotein A2 (chloroplast) [Scutellaria baicalensis]
454	gi|910312599|ref|YP_009162260.1|	82407	21.45	1	1	1	photosystem I P700 apoprotein A2 (chloroplast) [Scutellaria baicalensis]
455	gi|836643380|ref|YP_009144514.1|	82458	21.45	1	1	1	photosystem I P700 chlorophyll a apoprotein A2 (chloroplast) [Rosmarinus officinalis]
456	gi|827345140|gb|AKJ76724.1|	82458	21.45	1	1	1	photosystem I P700 chlorophyll a apoprotein A2 (chloroplast) [Rosmarinus officinalis]
457	gi|916439923|gb|AKZ22666.1|	82440	21.45	1	1	1	photosystem I P700 chlorophyll a apoprotein A2 (plastid) [Salvia nemorosa]
458	gi|752789785|ref|YP_009117220.1|	82392	21.45	1	1	1	photosystem I P700 apoprotein A2 (chloroplast) [Premna microphylla]
459	gi|573461950|emb|CCQ71619.1|	82459	21.45	1	1	1	photosystem I P700 chlorophyll a apoprotein A2 (chloroplast) [Salvia miltiorrhiza]
460	gi|916439933|gb|AKZ22671.1|	82411	21.45	1	1	1	photosystem I P700 chlorophyll a apoprotein A2 (plastid) [Teucrium canadense]
461	gi|401879741|gb|AFQ30928.1|	82459	21.45	1	1	1	photosystem I P700 apoprotein A2 (chloroplast) [Salvia miltiorrhiza]
462	gi|748013903|gb|AJE28373.1|	82392	21.45	1	1	1	photosystem I P700 apoprotein A2 (chloroplast) [Premna microphylla]

No.	Accession Number	Average Mass	Max-10logP	Max Coverage (%)	Max# Peptides	Max# Unique	Description
463	gi|827346564|gb|AKJ77750.1|	82379	21.45	1	1	1	photosystem I P700 chlorophyll a apoprotein A2 (chloroplast) [Perilla frutescens]
464	gi|122219294|sp|Q49SP6.1|TPGD2_POGCB	64149	163.8	30	23	22	Germacrene D synthase 2; AltName: Full=PatTpsBF2
465	gi|403399409|sp|E2E2P0.1|GTPS_ORIVU	69063	113.8	11	10	10	Gamma-terpinene synthase, chloroplastic; Short=Ovtps2; AltName: Full=Alpha-terpinene synthase; Flags: Precursor
466	gi|75315260|sp|Q9XHE7.1|C71DD_MENPI	56601	111.98	10	5	5	Cytochrome P450 71D13; AltName: Full=(-)-(4S)-Limonene-3-hydroxylase; AltName: Full=Cytochrome P450 isoform PM17
467	gi|29839420|sp|Q9XGV9.1|COMT2_OCIBA	39613	108.84	23	9	6	Caffeic acid 3-O-methyltransferase 2; Short=CAOMT-2; Short=COMT-2; AltName: Full=S-adenosysl-L-methionine:caffeic acid 3-O-methyltransferase 2
468	gi|29839421|sp|Q9XGW0.1|COMT1_OCIBA	39529	100.08	15	5	2	Caffeic acid 3-O-methyltransferase 1; Short=CAOMT-1; Short=COMT-1; AltName: Full=S-adenosysl-L-methionine:caffeic acid 3-O-methyltransferase 1
469	gi|8134569|sp|Q42662.2|METE_PLESU	84590	92.48	5	4	4	5-methyltetrahydropteroyltriglutamate--homocysteine methyltransferase; AltName: Full=Cobalamin-independent methionine synthase isozyme; AltName: Full=Vitamin-B12-independent methionine synthase isozyme
470	gi|75180331|sp|Q9LRC8.1|BAGLU_SCUBA	58772	74.70	6	3	3	Baicalin-beta-D-glucuronidase; AltName: Full=Baicalinase; Flags: Precursor
471	gi|75244696|sp|Q8H2B4.1|LLOS_MENAQ	70535	72.02	1	1	1	R-linalool synthase, chloroplastic; Flags: Precursor
472	gi|75192856|sp|Q9MBC1.1|3AT_PERFR	50675	71.34	5	2	2	Anthocyanidin 3-O-glucoside 6"-O-acyltransferase; Short=3AT
473	gi|122219295|sp|Q49SP7.1|TPSCS_POGCB	63586	49.89	2	1	1	Gamma-curcumene synthase; AltName: Full=PatTpsA
474	gi|75251484|sp|Q5SBP7.1|SELS_OCIBA	63125	47.56	2	1	1	Selinene synthase

No.	Accession Number	Average Mass	Max-10logP	Max Coverage (%)	Max# Peptides	Max# Unique	Description
475	gi|75293243|sp|Q6WKZ0.1|C7D94_MENGR	56308	40.29	2	1	1	Cytochrome P450 71D94
476	gi|75306222|sp|Q947B7.1|MFS_MENPI	55360	38.64	2	1	1	(+)-menthofuran synthase; AltName: Full=(+)-pulegone 9-hydroxylase
477	gi|75129878|sp|Q6WAU0.1|PULR_MENPI	37915	28.57	2	1	1	(+)-pulegone reductase
478	gi|75227033|sp|Q76MR7.1|UBGAT_SCUBA	48654	25.41	2	1	1	Baicalein 7-O-glucuronosyltransferase; AltName: Full=UDP-glucuronate:baicalein 7-O-glucuronosyltransferase
479	gi|395484483|gb|AFN66501.1|	77431	41.88	3	2	1	NADH dehydrogenase subunit F, partial (plastid) [Teucrium albicaule]
480	gi|401879790|gb|AFQ30977.1|	83587	37.73	3	2	1	NADH dehydrogenase subunit 5 (chloroplast) [Salvia miltiorrhiza]
481	gi|573462000|emb|CCQ71669.1|	83587	37.73	3	2	1	NADH dehydrogenase subunit 5 (chloroplast) [Salvia miltiorrhiza]
482	gi|395484473|gb|AFN66496.1|	78531	41.39	3	2	1	NADH dehydrogenase subunit F, partial (plastid) [Teucridium parvifolium]
483	gi|762060711|gb|AJQ20633.1|	73689	38.32	2	1	1	Long-Chain Acyl-CoA Synthetase [Salvia miltiorrhiza]
484	gi|913341331|gb|AKU77108.1|	104619	30.23	1	1	1	Structural maintenance of chromosomes protein 2, partial [Callicarpa bodinieri]
485	gi|827346602|gb|AKJ77788.1|	181164	29.32	1	1	1	Ycf1, partial (chloroplast) [Perilla frutescens]
486	gi|844572722|gb|AKN09568.1|	41656	28.76	2	1	1	Basic helix-loop-helix transcription factor [Salvia miltiorrhiza]
487	gi|691200620|gb|AIR77798.1|	26940	25.37	4	1	1	TCP transcription factor, partial [Perovskia atriplicifolia]
488	gi|691200582|gb|AIR77779.1|	29756	25.37	4	1	1	TCP transcription factor, partial [Tectona grandis]
489	gi|691200714|gb|AIR77845.1|	29953	25.37	4	1	1	TCP transcription factor, partial [Gmelina arborea]

No.	Accession Number	Average Mass	Max-10logP	Max Coverage (%)	Max# Peptides	Max# Unique	Description
490	gi|691200580|gb|AIR77778.1|	30438	25.37	4	1	1	TCP transcription factor, partial [Congea tomentosa]
491	gi|691200590|gb|AIR77783.1|	26615	32.97	4	1	1	TCP transcription factor, partial [Origanum vulgare]
492	gi|691200584|gb|AIR77780.1|	30608	25.37	4	1	1	TCP transcription factor, partial [Callicarpa cathayana]
493	gi|691200708|gb|AIR77842.1|	29615	25.37	4	1	1	TCP transcription factor, partial [Congea tomentosa]
494	gi|691200712|gb|AIR77844.1|	29757	25.37	4	1	1	TCP transcription factor, partial [Holmskioldia sanguinea]
495	gi|691200594|gb|AIR77785.1|	25444	25.37	4	1	1	TCP transcription factor, partial [Mentha longifolia]
496	gi|691200596|gb|AIR77786.1|	25755	25.37	4	1	1	TCP transcription factor, partial [Mentha longifolia]
497	gi|691200624|gb|AIR77800.1|	29841	25.37	4	1	1	TCP transcription factor, partial [Mentha longifolia]
498	gi|691200622|gb|AIR77799.1|	29930	25.37	4	1	1	TCP transcription factor, partial [Premna fulva]
499	gi|691200630|gb|AIR77803.1|	26302	25.37	4	1	1	TCP transcription factor, partial [Ocimum basilicum]
500	gi|75251484|sp|Q5SBP7.1|SELS_OCIBA	63125	24.81	2	1	1	Selinene synthase
501	gi|510794468|gb|AGN52200.1|	23112	24.18	3	1	1	MYB-related transcription factor [Salvia miltiorrhiza]
502	gi|662858700|gb|AIE77092.1|	90197	20.42	1	1	1	(+)-copalyl diphosphate synthase [Marrubium vulgare]
503	gi|837370038|gb|AKM94187.1|	20521	20.13	6	1	1	Maturase K, partial (chloroplast) [Leonotis nepetifolia]
504	gi|837370329|gb|AKM94283.1|	28841	20.13	4	1	1	Maturase K, partial (chloroplast) [Leonotis nepetifolia]
505	gi|837372516|gb|AKM95003.1|	28942	20.13	4	1	1	Maturase K, partial (chloroplast) [Leonotis nepetifolia]
506	gi|837371203|gb|AKM94570.1|	20329	20.13	6	1	1	Maturase K, partial (chloroplast) [Leonotis nepetifolia]
507	gi|122233627|sp|Q4JF75.1|RBR_SCUBA	111795	128.39	19	22	22	Retinoblastoma-related protein
508	gi|75244696|sp|Q8H2B4.1|LLOS_MENAQ	70535	102.21	17	14	13	R-linalool synthase, chloroplastic; Flags: Precursor

No.	Accession Number	Average Mass	Max-10logP	Max Coverage (%)	Max# Peptides	Max# Unique	Description
509	gi|5915815|sp|Q42716.1|C71A8_MENPI	57213	98.88	23	12	12	Cytochrome P450 71A8
510	gi|75251478|sp|Q5SBP1.1|MYRS_OCIBA	69964	98.67	16	12	8	Beta-myrcene synthase, chloroplastic; Flags: Precursor
511	gi|75251477|sp|Q5SBP0.1|TPSD_OCIBA	70000	75.90	7	6	2	Terpinolene synthase, chloroplastic; Flags: Precursor
512	gi|75251480|sp|Q5SBP3.1|LLOS_OCIBA	65822	66.64	6	3	3	R-linalool synthase, chloroplastic; Flags: Precursor
513	gi|62899675|sp|O81192.1|BPPS_SALOF	69292	55.98	4	3	3	(+)-bornyl diphosphate synthase, chloroplastic; Short=BPPS; AltName: Full=(+)-alpha-pinene synthase; AltName: Full=(+)-camphene synthase; AltName: Full=SBS; Flags: Precursor
514	gi|403399409|sp|E2E2P0.1|GTPS_ORIVU	69063	49.59	3	2	2	Gamma-terpinene synthase, chloroplastic; Short=Ovtps2; AltName: Full=Alpha-terpinene synthase; Flags: Precursor
515	gi|116256299|sp|Q9XES0.2|DXR_MENPI	51034	48.60	4	2	2	1-deoxy-D-xylulose 5-phosphate reductoisomerase, chloroplastic; Short=1-deoxyxylulose-5-phosphate reductoisomerase; Short=DXP reductoisomerase; AltName: Full=2-C-methyl-D-erythritol 4-phosphate synthase; F...
516	gi|75129878|sp|Q6WAU0.1|PULR_MENPI	37915	47.66	2	1	1	(+)-pulegone reductase
517	gi|122219294|sp|Q49SP6.1|TPGD2_POGCB	64149	45.43	2	1	1	Germacrene D synthase 2; AltName: Full=PatTpsBF2
518	gi|3914571|sp|Q33600.1|RBL_LAVLA	52404	43.88	4	2	2	Ribulose bisphosphate carboxylase large chain; Short=RuBisCO large subunit; Flags: Precursor
519	gi|3914545|sp|Q31655.1|RBL_AJUCH	52455	43.88	4	2	2	Ribulose bisphosphate carboxylase large chain; Short=RuBisCO large subunit; Flags: Precursor
520	gi|132044|sp|P28453.1|RBL_SCUBO	51794	43.88	4	2	2	Ribulose bisphosphate carboxylase large chain; Short=RuBisCO large subunit
521	gi|1352807|sp|P36485.2|RBL_SALDI	52005	38.06	4	2	2	Ribulose bisphosphate carboxylase large chain; Short=RuBisCO large subunit

No.	Accession Number	Average Mass	Max-10logP	Max Coverage (%)	Max# Peptides	Max# Unique	Description
522	gi|75288825|sp|Q65CJ7.2|HPPR_PLESU	34128	42.76	3	1	1	Hydroxyphenylpyruvate reductase; Short=HPPR
523	gi|122200955|sp|Q2KNL6.1|GEDH1_OCIBA	39044	41.75	4	1	1	Geraniol dehydrogenase 1; Short=ObaGEDH1
524	gi|122219293|sp|Q49SP5.1|TPGAS_POGCB	64232	41.24	3	2	2	Germacrene A synthase; AltName: Full=PatTpsCF2
525	gi|5915814|sp|O04164.1|C71A6_NEPRA	57955	40.18	3	1	1	Cytochrome P450 71A6
526	gi|122210943|sp|Q2XSC5.1|LALIN_LAVAN	65654	36.66	2	1	1	R-linalool synthase; Short=LaLINS
527	gi|403399735|sp|E2E2N7.1|BCGS_ORIVU	64443	34.90	1	1	1	Bicyclogermacrene synthase; Short=Ovtps4
528	gi|56749087|sp|Q85XY6.1|MATK_OCIBA	60282	34.86	2	1	1	Maturase K; AltName: Full=Intron maturase
529	gi|122219295|sp|Q49SP7.1|TPSCS_POGCB	63586	32.33	3	2	2	Gamma-curcumene synthase; AltName: Full=PatTpsA
530	gi|122210942|sp|Q2XSC4.1|LABER_LAVAN	62405	29.22	2	1	1	Exo-alpha-bergamotene synthase; Short=LaBERS; AltName: Full=Trans-alpha-bergamotene synthase
531	gi|75227033|sp|Q76MR7.1|UBGAT_SCUBA	48654	28.98	2	1	1	Baicalein 7-O-glucuronosyltransferase; AltName: Full=UDP-glucuronate:baicalein 7-O-glucuronosyltransferase
532	gi|75251484|sp|Q5SBP7.1|SELS_OCIBA	63125	23.05	2	1	1	Selinene synthase
533	gi|84029472|sp|Q93WU3.1|CVMT1_OCIBA	39916	22.03	3	1	1	Chavicol O-methyltransferase; AltName: Full=(Iso)eugenol O-methyltransferase CVOMT1; AltName: Full=S-adenosysl-L-methionine:(Iso)eugenol O-methyltransferase CVOMT1
534	gi|75338881|sp|Q9ZR26.1|5GT2_PERFR	49110	21.61	2	1	1	Anthocyanidin 3-O-glucoside 5-O-glucosyltransferase 2; AltName: Full=UDP-glucose:anthocyanin 5-O-glucosyltransferase 3R6; Short=p3R6; Flags: Precursor
535	gi|75306222|sp|Q947B7.1|MFS_MENPI	55360	20.53	1	1	1	(+)-menthofuran synthase; AltName: Full=(+)-pulegone 9-hydroxylase

No.	Accession Number	Average Mass	Max-10logP	Max Coverage (%)	Max# Peptides	Max# Unique	Description
536	gi|752789776|ref|YP_009117211.1|	158193	48.06	1	1	1	RNA polymerase beta' subunit (chloroplast) [Premna microphylla]
537	gi|748013894|gb|AJE28364.1|	158193	48.06	1	1	1	RNA polymerase beta' subunit (chloroplast) [Premna microphylla]
538	gi|827346527|gb|AKJ77713.1|	158467	47.83	1	1	1	RNA polymerase beta'' subunit (chloroplast) [Perilla frutescens]
539	gi|910312590|ref|YP_009162251.1|	158800	47.83	1	1	1	RNA polymerase beta subunit-2 (chloroplast) [Scutellaria baicalensis]
540	gi|827345829|gb|AKJ77130.1|	158800	47.83	1	1	1	RNA polymerase beta subunit-2 (chloroplast) [Scutellaria baicalensis]
541	gi|916442767|gb|AKZ23937.1|	155842	47.83	1	1	1	RNA polymerase beta'' subunit (plastid) [Teucrium canadense]
542	gi|844572722|gb|AKN09568.1|	41656	30.64	2	1	1	Basic helix-loop-helix transcription factor [Salvia miltiorrhiza]
543	gi|844572778|gb|AKN09586.1|	68167	22.47	1	1	1	Basic helix-loop-helix transcription factor [Salvia miltiorrhiza]
544	gi|844572715|gb|AKN09566.1|	67854	22.47	1	1	1	Basic helix-loop-helix transcription factor [Salvia miltiorrhiza]
545	gi|748013960|gb|AJE28430.1|	19533	20.98	6	1	1	NADH-plastoquinone oxidoreductase subunit I (chloroplast) [Premna microphylla]
546	gi|752789842|ref|YP_009117276.1|	19533	20.98	6	1	1	NADH-plastoquinone oxidoreductase subunit I (chloroplast) [Premna microphylla]
547	gi|75251484|sp|Q5SBP7.1|SELS_OCIBA	63125	20.86	2	1	1	Selinene synthase
548	gi|766946303|gb|AJT36912.1|	32806	20.06	3	1	1	Ycf1, partial (chloroplast) [Vitex negundo var. negundo]
549	gi|122233627|sp|Q4JF75.1|RBR_SCUBA	111795	120.77	8	9	9	Retinoblastoma-related protein

No.	Accession Number	Average Mass	Max-10logP	Max Coverage (%)	Max# Peptides	Max# Unique	Description
550	gi|122219294|sp|Q49SP6.1|TPGD2_POGCB	64149	100.26	6	4	1	Germacrene D synthase 2; AltName: Full=PatTpsBF2
551	gi|122219292|sp|Q49SP4.1|TPGD1_POGCB	64197	73.10	6	4	1	Germacrene D synthase 1; AltName: Full=PatTpsB15
552	gi|75251482|sp|Q5SBP5.1|GCS1_OCIBA	63566	72.41	3	2	1	Gamma-cadinene synthase; AltName: Full=(+)-gamma-cadinene synthase
553	gi|62899675|sp|O81192.1|BPPS_SALOF	69292	70.24	3	2	1	(+)-bornyl diphosphate synthase, chloroplastic; Short=BPPS; AltName: Full=(+)-alpha-pinene synthase; AltName: Full=(+)-camphene synthase; AltName: Full=SBS; Flags: Precursor
554	gi|75180331|sp|Q9LRC8.1|BAGLU_SCUBA	58772	62.83	2	1	1	Baicalin-beta-D-glucuronidase; AltName: Full=Baicalinase; Flags: Precursor
555	gi|75251484|sp|Q5SBP7.1|SELS_OCIBA	63125	61.96	5	3	2	Selinene synthase
556	gi|122219293|sp|Q49SP5.1|TPGAS_POGCB	64232	51.02	3	2	2	Germacrene A synthase; AltName: Full=PatTpsCF2
557	gi|704000326|sp|S4UX02.1|CYPH1_SALMI	55520	48.40	3	1	1	Ferruginol synthase; AltName: Full=Cytochrome P450 76AH1
558	gi|75293242|sp|Q6WKY9.1|C7D95_MENGR	56365	42.87	2	1	1	Cytochrome P450 71D95; AltName: Full=(-)-(4S)-Limonene-3-hydroxylase
559	gi|75290511|sp|Q6IV13.1|C7D95_MENSP	56322	42.58	2	1	1	Cytochrome P450 71D95; AltName: Full=Limonene-3-hydroxylase
560	gi|75315260|sp|Q9XHE7.1|C71DD_MENPI	56601	42.87	2	1	1	Cytochrome P450 71D13; AltName: Full=(-)-(4S)-Limonene-3-hydroxylase; AltName: Full=Cytochrome P450 isoform PM17
561	gi|56749087|sp|Q85XY6.1|MATK_OCIBA	60282	35.91	2	1	1	Maturase K; AltName: Full=Intron maturase
562	gi|75129878|sp|Q6WAU0.1|PULR_MENPI	37915	30.97	2	1	1	(+)-pulegone reductase

No.	Accession Number	Average Mass	Max-10logP	Max Coverage (%)	Max# Peptides	Max# Unique	Description
563	gi|75338882|sp|Q9ZR27.1|5GT1_PERFR	50974	27.37	2	1	1	Anthocyanidin 3-O-glucoside 5-O-glucosyltransferase 1; AltName: Full=UDP-glucose:anthocyanin 5-O-glucosyltransferase 3R4; Short=p3R4; Flags: Precursor
564	gi|510785777|sp|G0LD36.1|RAS_MELOI	47161	25.33	2	1	1	Rosmarinate synthase; Short=MoRAS; AltName: Full=Hydroxycinnamoyl-CoA:hydroxyphenyllactate hydroxycinnamoyltransferase
565	gi|748013964|gb|AJE28434.1|	225117	85.49	3	7	7	Hypothetical chloroplast RF19 (chloroplast) [Premna microphylla]
566	gi|752789846|ref|YP_009117280.1|	225117	85.49	3	7	7	Hypothetical chloroplast RF19 (chloroplast) [Premna microphylla]
567	gi|751663101|gb|AJF98632.1	51505	48.13	4	2	2	Ribulose-1,5-bisphosphate carboxylase/oxygenase large subunit, partial (chloroplast) [Nepeta cataria]
568	gi|916441445|gb|AKZ23427.1|	52869	48.13	4	2	2	Ribulose-1,5-bisphosphate carboxylase/oxygenase large subunit, partial (chloroplast) [Nepeta cataria]
569	gi|751663177|gb|AJF98669.1|	51810	48.13	4	2	2	Ribulose-1,5-bisphosphate carboxylase/oxygenase large subunit, partial (chloroplast) [Stachys byzantina]
570	gi|751663109|gb|AJF98636.1|	51713	45.5	4	2	2	Ribulose-1,5-bisphosphate carboxylase/oxygenase large subunit, partial (chloroplast) [Mentha x piperita]
571	gi|817992263|gb|AKG25296.1|	52111	45.5	4	2	2	Ribulose-1,5-bisphosphate carboxylase/oxygenase large subunit, partial (plastid) [Prunella vulgaris]
572	gi|817992309|gb|AKG25319.1|	51956	45.5	4	2	2	Ribulose-1,5-bisphosphate carboxylase/oxygenase large subunit, partial (plastid) [Salvia pratensis]
573	gi|817991831|gb|AKG25080.1|	51983	45.5	4	2	2	Ribulose-1,5-bisphosphate carboxylase/oxygenase large subunit, partial (plastid) [Clinopodium vulgare]
574	gi|751663103|gb|AJF98633.1|	51988	45.5	4	2	2	Ribulose-1,5-bisphosphate carboxylase/oxygenase large subunit, partial (chloroplast) [Mentha spicata]

No.	Accession Number	Average Mass	Max-10logP	Max Coverage (%)	Max# Peptides	Max# Unique	Description
575	gi|751663105|gb|AJF98634.1|	52345	45.5	4	2	2	Ribulose-1,5-bisphosphate carboxylase/oxygenase large subunit, partial (chloroplast) [Mentha suaveolens]
576	gi|827345151|gb|AKJ76735.1|	52873	45.5	4	2	2	Ribulose-1,5-bisphosphate carboxylase/oxygenase large subunit (chloroplast) [Rosmarinus officinalis]
577	gi|836643391|ref|YP_009144523.1|	52873	45.5	4	2	2	Ribulose-1,5-bisphosphate carboxylase/oxygenase large subunit (chloroplast) [Rosmarinus officinalis]
578	gi|916441443|gb|AKZ23426.1|	52850	45.5	4	2	2	Ribulose-1,5-bisphosphate carboxylase/oxygenase large subunit (plastid) [Salvia nemorosa]
579	gi|410176163|gb|AFV61822.1|	52889	45.5	4	2	2	Ribulose-1,5-bisphosphate carboxylase/oxygenase large subunit (chloroplast) [Origanum vulgare subsp. vulgare]
580	gi|916441441|gb|AKZ23425.1|	52888	45.5	4	2	2	Ribulose-1,5-bisphosphate carboxylase/oxygenase large subunit (plastid) [Monarda fistulosa var. mollis]
581	gi|817991973|gb|AKG25151.1|	52020	45.5	4	2	2	Ribulose-1,5-bisphosphate carboxylase/oxygenase large subunit, partial (plastid) [Galeopsis bifida]
582	gi|751663168|gb|AJF98665.1|	51966	45.5	4	2	2	Ribulose-1,5-bisphosphate carboxylase/oxygenase large subunit, partial (chloroplast) [Ocimum tenuiflorum]
583	gi|817992375|gb|AKG25352.1|	52022	45.5	4	2	2	Ribulose-1,5-bisphosphate carboxylase/oxygenase large subunit, partial (plastid) [Stachys sylvatica]
584	gi|817992237|gb|AKG25283.1|	52058	45.5	4	2	2	Ribulose-1,5-bisphosphate carboxylase/oxygenase large subunit, partial (plastid) [Phlomis fruticosa]
585	gi|751663097|gb|AJF98630.1|	52095	45.5	4	2	2	Ribulose-1,5-bisphosphate carboxylase/oxygenase large subunit, partial (chloroplast) [Ocimum basilicum]
586	gi|817992335|gb|AKG25332.1|	51941	45.5	4	2	2	Ribulose-1,5-bisphosphate carboxylase/oxygenase large subunit, partial (plastid) [Scutellaria galericulata]

No.	Accession Number	Average Mass	Max-10logP	Max Coverage (%)	Max# Peptides	Max# Unique	Description
587	gi|817992071|gb|AKG25200.1|	51959	45.5	4	2	2	Ribulose-1,5-bisphosphate carboxylase/oxygenase large subunit, partial (plastid) [Lavandula x intermedia]
588	gi|817992059|gb|AKG25194.1|	51961	45.5	4	2	2	Ribulose-1,5-bisphosphate carboxylase/oxygenase large subunit, partial (plastid) [Lamium galeobdolon]
589	gi|3914545|sp|Q31655.1|RBL_AJUCH	52455	45.5	4	2	2	Ribulose bisphosphate carboxylase large chain; Short=RuBisCO large subunit; Flags: Precursor
590	gi|751663113|gb|AJF98638.1|	52702	45.5	4	2	2	Ribulose-1,5-bisphosphate carboxylase/oxygenase large subunit, partial (chloroplast) [Ajuga bracteosa]
591	gi|401879750|gb|AFQ30937.1|	52887	45.5	4	2	2	Ribulose-1,5-bisphosphate carboxylase/oxygenase large subunit (chloroplast) [Salvia miltiorrhiza]
592	gi|916441453|gb|AKZ23431.1|	53169	45.5	4	2	2	Ribulose-1,5-bisphosphate carboxylase/oxygenase large subunit (plastid) [Teucrium canadense]
593	gi|910312608|ref|YP_009162269.1|	53663	45.5	4	2	2	Ribulose-1,5-bisphosphate carboxylase/oxygenase large subunit (chloroplast) [Scutellaria baicalensis]
594	gi|827345848|gb|AKJ77149.1|	53663	45.5	4	2	2	Ribulose-1,5-bisphosphate carboxylase/oxygenase large subunit (chloroplast) [Scutellaria baicalensis]
595	gi|827346558|gb|AKJ77744.1|	53955	45.5	4	2	2	Ribulose-1 (chloroplast) [Perilla frutescens]
596	gi|573461959|emb|CCQ71628.1|	53698	45.5	4	2	2	Ribulose-1 (chloroplast) [Salvia miltiorrhiza]
597	gi|1352807|sp|P36485.2|RBL_SALDI	52005	42.25	4	2	2	Ribulose bisphosphate carboxylase large chain; Short=RuBisCO large subunit
598	gi|3914571|sp|Q33600.1|RBL_LAVLA	52404	42.25	4	2	2	Ribulose bisphosphate carboxylase large chain; Short=RuBisCO large subunit
599	gi|132044|sp|P28453.1|RBL_SCUBO	51794	42.25	4	2	2	Ribulose bisphosphate carboxylase large chain; Short=RuBisCO large subunit

No.	Accession Number	Average Mass	Max-10logP	Max Coverage (%)	Max# Peptides	Max# Unique	Description
600	gi|599079565|dbj|BAO57028.1|	49007	44.57	4	2	2	Ribulose-1,5-bisphosphate carboxylase/oxygenase large subunit, partial (chloroplast) [Sideritis cretica subsp. spicata]
601	gi|817992077|gb|AKG25203.1|	49757	44.57	4	2	2	Ribulose-1,5-bisphosphate carboxylase/oxygenase large subunit, partial (plastid) [Leonurus cardiaca]
602	gi|817992301|gb|AKG25315.1|	49431	41.41	4	2	2	Ribulose-1,5-bisphosphate carboxylase/oxygenase large subunit, partial (plastid) [Rosmarinus officinalis]
603	gi|602690611|gb|AHN96261.1|	27410	41.41	7	2	2	Ribulose-1,5-bisphosphatecarboxylase/oxygenase large subunit, partial (chloroplast) [Zhumeria majdae]
604	gi|602690609|gb|AHN96260.1|	27410	41.41	7	2	2	Ribulose-1,5-bisphosphatecarboxylase/oxygenase large subunit, partial (chloroplast) [Zhumeria majdae]
605	gi|602690607|gb|AHN96259.1|	27410	41.41	7	2	2	Ribulose-1,5-bisphosphatecarboxylase/oxygenase large subunit, partial (chloroplast) [Zhumeria majdae]
606	gi|602690629|gb|AHN96270.1|	27410	41.41	7	2	2	Ribulose-1,5-bisphosphatecarboxylase/oxygenase large subunit, partial (chloroplast) [Zhumeria majdae]
607	gi|602690623|gb|AHN96267.1|	27409	41.41	7	2	2	Ribulose-1,5-bisphosphatecarboxylase/oxygenase large subunit, partial (chloroplast) [Zhumeria majdae]
608	gi|602690619|gb|AHN96265.1|	27409	41.41	7	2	2	Ribulose-1,5-bisphosphatecarboxylase/oxygenase large subunit, partial (chloroplast) [Zhumeria majdae]
609	gi|602690617|gb|AHN96264.1|	27409	41.41	7	2	2	Ribulose-1,5-bisphosphatecarboxylase/oxygenase large subunit, partial (chloroplast) [Zhumeria majdae]
610	gi|602690627|gb|AHN96269.1|	27428	41.41	7	2	2	Ribulose-1,5-bisphosphatecarboxylase/oxygenase large subunit, partial (chloroplast) [Zhumeria majdae]
611	gi|602690625|gb|AHN96268.1|	27428	41.41	7	2	2	Ribulose-1,5-bisphosphatecarboxylase/oxygenase large subunit, partial (chloroplast) [Zhumeria majdae]

No.	Accession Number	Average Mass	Max-10logP	Max Coverage (%)	Max# Peptides	Max# Unique	Description
612	gi|602690615|gb|AHN96263.1|	27394	41.41	7	2	2	Ribulose-1,5-bisphosphatecarboxylase/oxygenase large subunit, partial (chloroplast) [Zhumeria majdae]
613	gi|602690613|gb|AHN96262.1|	27394	41.41	7	2	2	Ribulose-1,5-bisphosphatecarboxylase/oxygenase large subunit, partial (chloroplast) [Zhumeria majdae]
614	gi|602690621|gb|AHN96266.1|	27394	41.41	7	2	2	Ribulose-1,5-bisphosphatecarboxylase/oxygenase large subunit, partial (chloroplast) [Zhumeria majdae]
615	gi|751663115|gb|AJF98639.1|	27926	41.41	7	2	2	Ribulose-1,5-bisphosphatecarboxylase/oxygenase large subunit, partial (chloroplast) [Zhumeria majdae]
616	gi|602690633|gb|AHN96272.1|	27525	41.41	7	2	2	Ribulose-1,5-bisphosphatecarboxylase/oxygenase large subunit, partial (chloroplast) [Zhumeria majdae]
617	gi|602690631|gb|AHN96271.1|	27525	41.41	7	2	2	Ribulose-1,5-bisphosphatecarboxylase/oxygenase large subunit, partial (chloroplast) [Zhumeria majdae]
618	gi|602690635|gb|AHN96273.1|	27525	41.41	7	2	2	Ribulose-1,5-bisphosphatecarboxylase/oxygenase large subunit, partial (chloroplast) [Zhumeria majdae]
619	gi|752789794|ref|YP_009117229.1|	53224	41.41	4	2	2	Ribulose-1,5-bisphosphate carboxylase/oxygenase large subunit (chloroplast) [Premna microphylla]
620	gi|748013912|gb|AJE28382.1|	53224	41.41	4	2	2	Ribulose-1,5-bisphosphate carboxylase/oxygenase large subunit (chloroplast) [Premna microphylla]
621	gi|599079563|dbj|BAO57027.1|	48957	41.41	4	2	2	Ribulose-1,5-bisphosphate carboxylase/oxygenase large subunit, partial (chloroplast) [Teucrium heterophyllum]
622	gi|910312590|ref|YP_009162251.1|	158800	40.49	1	2	2	RNA polymerase beta subunit-2 (chloroplast) [Scutellaria baicalensis]
623	gi|827345829|gb|AKJ77130.1|	158800	40.49	1	2	2	RNA polymerase beta subunit-2 (chloroplast) [Scutellaria baicalensis]

No.	Accession Number	Average Mass	Max-10logP	Max Coverage (%)	Max# Peptides	Max# Unique	Description
624	gi|827346527|gb|AKJ77713.1|	158467	35.47	2	2	2	RNA polymerase beta" subunit (chloroplast) [Perilla frutescens]
625	gi|916442767|gb|AKZ23937.1|	155842	35.47	2	2	2	RNA polymerase beta" subunit (plastid) [Teucrium canadense]
626	gi|669254293|gb|AII20586.1|	79081	31.94	1	1	1	NADH dehydrogenase subunit F, partial (chloroplast) [Hymenopyramis cana]
627	gi|521953395|gb|AGQ04156.1|	82464	28.81	2	1	1	4-hydroxy-3-methylbut-2-enyl diphosphate synthase [Lavandula angustifolia]
628	gi|735679295|gb|AJA39985.1|	82378	28.81	2	1	1	(E)-4-hydroxy-3-methylbut-2-enyl diphosphate synthase [Salvia miltiorrhiza f. alba]
629	gi|796406070|gb|AKA59790.1|	28575	24.94	4	1	1	MYB19 [Scutellaria playfairii]
630	gi|661525316|gb|AIE15765.1|	184302	21.75	1	1	1	Dicer-like protein 3 [Salvia miltiorrhiza]
631	gi|910312663|ref|YP_009162324.1|	268069	21.56	0	1	1	Hypothetical chloroplast RF2 (chloroplast) [Scutellaria baicalensis]
632	gi|827345826|gb|AKJ77127.1|	268069	21.56	0	1	1	Hypothetical chloroplast RF2 (chloroplast) [Scutellaria baicalensis]
633	gi|827345827|gb|AKJ77128.1|	268069	21.56	0	1	1	Hypothetical chloroplast RF2 (chloroplast) [Scutellaria baicalensis]
634	gi|910312644|ref|YP_009162305.1|	268069	21.56	0	1	1	Hypothetical chloroplast RF2 (chloroplast) [Scutellaria baicalensis]
635	gi|670606706|gb|AII31147.1|	9275	20.48	11	1	1	Adenosine kinase, partial [Micromeria hyssopifolia var. hyssopifolia]
636	gi|670606710|gb|AII31149.1|	9520	20.48	10	1	1	Adenosine kinase, partial [Micromeria hyssopifolia var. kuegleri]

No.	Accession Number	Average Mass	Max-10logP	Max Coverage (%)	Max# Peptides	Max# Unique	Description
637	gi|670606712|gb|AII31150.1|	10786	20.48	9	1	1	Adenosine kinase, partial [Micromeria teneriffae var. cordifolia]
638	gi|670606714|gb|AII31151.1|	11074	20.48	9	1	1	Adenosine kinase, partial [Micromeria teneriffae var. cordifolia]
639	gi|670606704|gb|AII31146.1|	10951	20.48	9	1	1	Adenosine kinase, partial [Micromeria lepida subsp. lepida]
640	gi|670606708|gb|AII31148.1|	11164	20.48	9	1	1	Adenosine kinase, partial [Micromeria hyssopifolia var. kuegleri]
641	gi|670606716|gb|AII31152.1|	11349	20.48	9	1	1	Adenosine kinase, partial [Micromeria hyssopifolia var. glabrescens]
642	gi|670606702|gb|AII31145.1|	11506	20.48	9	1	1	Adenosine kinase, partial [Micromeria hyssopifolia var. glabrescens]
643	gi|75129878|sp|Q6WAU0.1|PULR_MENPI	37915	20.03	2	1	1	(+)-pulegone reductase
644	gi|75293243|sp|Q6WKZ0.1|C7D94_MENGR	56308	192.9	51	41	39	Cytochrome P450 71D94
645	gi|122233627|sp|Q4JF75.1|RBR_SCUBA	111795	173.76	17	23	23	Retinoblastoma-related protein
646	gi|122249145|sp|Q49SP3.1|TPSPS_POGCB	64199	115.16	7	6	6	Patchoulol synthase; Short=PatTps177; AltName: Full=Alpha-guaiene synthase; AltName: Full=Delta-guaiene synthase
647	gi|75251477|sp|Q5SBP0.1|TPSD_OCIBA	70000	111	6	6	6	Terpinolene synthase, chloroplastic; Flags: Precursor
648	gi|75129878|sp|Q6WAU0.1|PULR_MENPI	37915	107.88	8	4	4	(+)-pulegone reductase
649	gi|75252096|sp|Q5W283.1|TPSCM_MENPI	63839	88.26	6	4	4	Cis-muuroladiene synthase; Short=MxpSS1
650	gi|75290511|sp|Q6IV13.1|C7D95_MENSP	56322	81.07	4	2	1	Cytochrome P450 71D95; AltName: Full=Limonene-3-hydroxylase

No.	Accession Number	Average Mass	Max-10logP	Max Coverage (%)	Max# Peptides	Max# Unique	Description
651	gi|75293242|sp|Q6WKY9.1|C7D95_MENGR	56365	81.07	4	2	1	Cytochrome P450 71D95; AltName: Full=(-)-(4S)-Limonene-3-hydroxylase
652	gi|75161989|sp|Q8W1W9.1|5MAT1_SALSN	50724	46.62	2	1	1	Malonyl-coenzyme:anthocyanin 5-O-glucoside-6'''-O-malonyltransferase; Short=Malonyl CoA:anthocyanin 5-O-glucoside-6'''-O-malonyltransferase; Short=Ss5MaT1
653	gi|62899675|sp|O81192.1|BPPS_SALOF	69292	41.02	3	1	1	(+)-bornyl diphosphate synthase, chloroplastic; Short=BPPS; AltName: Full=(+)-alpha-pinene synthase; AltName: Full=(+)-camphene synthase; AltName: Full=SBS; Flags: Precursor
654	gi|75251483|sp|Q5SBP6.1|GDS_OCIBA	63395	40.58	2	1	1	Germacrene-D synthase; AltName: Full=(-)-germacrene D synthase
655	gi|748013968|gb|AJE28438.1|	268103	46.32	1	1	1	Hypothetical chloroplast RF21 (chloroplast) [Premna microphylla]
656	gi|752789850|ref|YP_009117284.1|	268103	46.32	1	1	1	Hypothetical chloroplast RF21 (chloroplast) [Premna microphylla]
657	gi|752789831|ref|YP_009117265.1|	268103	46.32	1	1	1	Hypothetical chloroplast RF21 (chloroplast) [Premna microphylla]
658	gi|748013949|gb|AJE28419.1|	268103	46.32	1	1	1	Hypothetical chloroplast RF21 (chloroplast) [Premna microphylla]
659	gi|573462016|emb|CCQ71685.1|	267080	43.64	1	1	1	Ycf2 (chloroplast) [Salvia miltiorrhiza]
660	gi|573461995|emb|CCQ71664.1|	267080	43.64	1	1	1	Ycf2 (chloroplast) [Salvia miltiorrhiza]
661	gi|401879785|gb|AFQ30972.1|	267080	43.64	1	1	1	Hypothetical chloroplast RF2 (chloroplast) [Salvia miltiorrhiza]
662	gi|401879806|gb|AFQ30993.1|	267080	43.64	1	1	1	Hypothetical chloroplast RF2 (chloroplast) [Salvia miltiorrhiza]
663	gi|827346579|gb|AKJ77765.1|	266476	43.64	1	1	1	Ycf2 (chloroplast) [Perilla frutescens]

No.	Accession Number	Average Mass	Max-10logP	Max Coverage (%)	Max# Peptides	Max# Unique	Description
664	gi|827346597|gb|AKJ77783.1|	266476	43.64	1	1	1	Ycf2 (chloroplast) [Perilla frutescens]
665	gi|836643370|ref|YP_009144558.1|	266537	40.53	1	1	1	Ycf2 (chloroplast) [Rosmarinus officinalis]
666	gi|827345131|gb|AKJ76715.1|	266537	40.53	1	1	1	Ycf2 (chloroplast) [Rosmarinus officinalis]
667	gi|827345130|gb|AKJ76714.1|	266537	40.53	1	1	1	Ycf2 (chloroplast) [Rosmarinus officinalis]
668	gi|836643371|ref|YP_009144577.1|	266537	40.53	1	1	1	Ycf2 (chloroplast) [Rosmarinus officinalis]
669	gi|410176216|gb|AFV61875.1|	264781	40.53	1	1	1	Ycf2 (chloroplast) [Origanum vulgare subsp. vulgare]
670	gi|410176197|gb|AFV61856.1|	264781	40.53	1	1	1	Ycf2 (chloroplast) [Origanum vulgare subsp. vulgare]
671	gi|827345827|gb|AKJ77128.1|	268069	43.09	1	1	1	Hypothetical chloroplast RF2 (chloroplast) [Scutellaria baicalensis]
672	gi|827345826|gb|AKJ77127.1|	268069	43.09	1	1	1	Hypothetical chloroplast RF2 (chloroplast) [Scutellaria baicalensis]
673	gi|910312644|ref|YP_009162305.1|	268069	43.09	1	1	1	Hypothetical chloroplast RF2 (chloroplast) [Scutellaria baicalensis]
674	gi|661525316|gb|AIE15765.1|	184302	31.49	1	1	1	Dicer-like protein 3 [Salvia miltiorrhiza]
675	gi|75129878|sp|Q6WAU0.1|PULR_MENPI	37915	31.47	2	1	1	(+)-pulegone reductase
676	gi|844572722|gb|AKN09568.1|	41656	24.97	2	1	1	Basic helix-loop-helix transcription factor [Salvia miltiorrhiza]
677	gi|395484497|gb|AFN66507.1|	77873	24.31	2	1	1	NADH dehydrogenase subunit F, partial (plastid) [Teucrium fruticans]
678	gi|395484493|gb|AFN66505.1|	77203	24.31	2	1	1	NADH dehydrogenase subunit F, partial (plastid) [Teucrium pseudochamaepitys]
679	gi|395484487|gb|AFN66503.1|	77172	24.31	2	1	1	NADH dehydrogenase subunit F, partial (plastid) [Teucrium aroanium]

No.	Accession Number	Average Mass	Max-10logP	Max Coverage (%)	Max# Peptides	Max# Unique	Description
680	gi|395484509|gb|AFN66512.1|	77251	24.31	2	1	1	NADH dehydrogenase subunit F, partial (plastid) [Teucrium orientale subsp. gloeotrichum]
681	gi|395484485|gb|AFN66502.1|	77595	24.31	2	1	1	NADH dehydrogenase subunit F, partial (plastid) [Teucrium aristatum]
682	gi|836643377|ref|YP_009144562.1|	84218	24.31	1	1	1	NADH dehydrogenase subunit 5 (chloroplast) [Rosmarinus officinalis]
683	gi|827345137|gb|AKJ76721.1|	84218	24.31	1	1	1	NADH dehydrogenase subunit 5 (chloroplast) [Rosmarinus officinalis]
684	gi|916438885|gb|AKZ22147.1|	84443	24.31	1	1	1	NADH dehydrogenase subunit 5 (plastid) [Salvia nemorosa]
685	gi|395484473|gb|AFN66496.1|	78531	24.31	2	1	1	NADH dehydrogenase subunit F, partial (plastid) [Teucridium parvifolium]
686	gi|827346594|gb|AKJ77780.1|	84248	24.31	1	1	1	NADH dehydrogenase subunit 5 (chloroplast) [Perilla frutescens]
687	gi|395484489|gb|AFN66504.1|	76910	24.31	2	1	1	NADH dehydrogenase subunit F, partial (plastid) [Teucrium betonicum]
688	gi|395484515|gb|AFN66515.1|	76501	24.31	2	1	1	NADH dehydrogenase subunit F, partial (plastid) [Teucrium racemosum]
689	gi|395484524|gb|AFN66519.1|	75723	24.31	2	1	1	NADH dehydrogenase subunit F, partial (plastid) [Teucrium kotschyanum]
690	gi|395484517|gb|AFN66516.1|	76688	24.31	2	1	1	NADH dehydrogenase subunit F, partial (plastid) [Teucrium salviastrum]
691	gi|395484511|gb|AFN66513.1|	76860	24.31	2	1	1	NADH dehydrogenase subunit F, partial (plastid) [Teucrium oxylepis]
692	gi|401879790|gb|AFQ30977.1|	83587	24.31	1	1	1	NADH dehydrogenase subunit 5 (chloroplast) [Salvia miltiorrhiza]

No.	Accession Number	Average Mass	Max-10logP	Max Coverage (%)	Max# Peptides	Max# Unique	Description
693	gi|573462000|emb|CCQ71669.1|	83587	24.31	1	1	1	NADH dehydrogenase subunit 5 (chloroplast) [Salvia miltiorrhiza]
694	gi|395484522|gb|AFN66518.1|	76105	24.31	2	1	1	NADH dehydrogenase subunit F, partial (plastid) [Teucrium subspinosum]
695	gi|752789835|ref|YP_009117269.1|	85385	24.31	1	1	1	NADH-plastoquinone oxidoreductase subunit 5 (chloroplast) [Premna microphylla]
696	gi|748013953|gb|AJE28423.1|	85385	24.31	1	1	1	NADH-plastoquinone oxidoreductase subunit 5 (chloroplast) [Premna microphylla]
697	gi|395484475|gb|AFN66497.1|	78510	24.31	2	1	1	NADH dehydrogenase subunit F, partial (plastid) [Rubiteucris palmata]
698	gi|916438887|gb|AKZ22148.1|	83254	24.31	1	1	1	NADH dehydrogenase subunit 5 (plastid) [Teucrium canadense]
699	gi|395484502|gb|AFN66509.1|	75956	24.31	2	1	1	NADH dehydrogenase subunit F, partial (plastid) [Teucrium divaricatum]
700	gi|395484481|gb|AFN66500.1|	76061	24.31	2	1	1	NADH dehydrogenase subunit F, partial (plastid) [Teucrium flavum subsp. glaucum]
701	gi|395484520|gb|AFN66517.1|	76892	24.31	2	1	1	NADH dehydrogenase subunit F, partial (plastid) [Teucrium spinosum]
702	gi|395484477|gb|AFN66498.1|	76293	24.31	2	1	1	NADH dehydrogenase subunit F, partial (plastid) [Spartothamnella puberula]
703	gi|395484483|gb|AFN66501.1|	77431	24.31	2	1	1	NADH dehydrogenase subunit F, partial (plastid) [Teucrium albicaule]
704	gi|669254293|gb|AII20586.1|	79081	24.31	2	1	1	NADH dehydrogenase subunit F, partial (chloroplast) [Hymenopyramis cana]
705	gi|669254291|gb|AII20585.1|	79070	24.31	2	1	1	NADH dehydrogenase subunit F, partial (chloroplast) [Petraeovitex multiflora]

No.	Accession Number	Average Mass	Max-10logP	Max Coverage (%)	Max# Peptides	Max# Unique	Description
706	gi|916438881|gb|AKZ22145.1|	84354	24.31	1	1	1	NADH dehydrogenase subunit 5 (plastid) [Monarda fistulosa var. mollis]
707	gi|410176201|gb|AFV61860.1|	84295	24.31	1	1	1	NADH dehydrogenase subunit 5 (chloroplast) [Origanum vulgare subsp. vulgare]
708	gi|395484537|gb|AFN66525.1|	78210	24.31	2	1	1	NADH dehydrogenase subunit F, partial (plastid) [Teucrium decipiens]
709	gi|395484530|gb|AFN66522.1|	76725	24.31	2	1	1	NADH dehydrogenase subunit F, partial (plastid) [Teucrium viscidum var. miquelianum]
710	gi|395484528|gb|AFN66521.1|	76705	24.31	2	1	1	NADH dehydrogenase subunit F, partial (plastid) [Teucrium japonicum]
711	gi|395484507|gb|AFN66511.1|	77434	24.31	2	1	1	NADH dehydrogenase subunit F, partial (plastid) [Teucrium nudicaule]
712	gi|395484504|gb|AFN66510.1|	77454	24.31	2	1	1	NADH dehydrogenase subunit F, partial (plastid) [Teucrium laciniatum]
713	gi|395484526|gb|AFN66520.1|	76596	24.31	2	1	1	NADH dehydrogenase subunit F, partial (plastid) [Teucrium bicolor]
714	gi|827345833|gb|AKJ77134.1|	85675	24.31	1	1	1	NADH dehydrogenase subunit 5 (chloroplast) [Scutellaria baicalensis]
715	gi|910312648|ref|YP_009162309.1|	85675	24.31	1	1	1	NADH dehydrogenase subunit 5 (chloroplast) [Scutellaria baicalensis]
716	gi|669254285|gb|AII20582.1|	74815	24.31	2	1	1	NADH dehydrogenase subunit F, partial (chloroplast) [Holocheila longipedunculata]
717	gi|669254287|gb|AII20583.1|	77022	24.31	2	1	1	NADH dehydrogenase subunit F, partial (chloroplast) [Holocheila longipedunculata]
718	gi|669254283|gb|AII20581.1|	77991	24.31	2	1	1	NADH dehydrogenase subunit F, partial (chloroplast) [Holocheila longipedunculata]

No.	Accession Number	Average Mass	Max-10logP	Max Coverage (%)	Max# Peptides	Max# Unique	Description
719	gi|395484513|gb|AFN66514.1|	76814	24.31	2	1	1	NADH dehydrogenase subunit F, partial (plastid) [Teucrium pyrenaicum]
720	gi|395484495|gb|AFN66506.1|	76993	24.31	2	1	1	NADH dehydrogenase subunit F, partial (plastid) [Teucrium eriocephalum subsp. almeriense]
721	gi|395484500|gb|AFN66508.1|	77065	24.31	2	1	1	NADH dehydrogenase subunit F, partial (plastid) [Teucrium stocksianum subsp. incanum]
722	gi|395484479|gb|AFN66499.1|	34714	24.31	4	1	1	NADH dehydrogenase subunit F, partial (plastid) [Oncinocalyx betchei]
723	gi|395484533|gb|AFN66523.1|	75763	24.31	2	1	1	NADH dehydrogenase subunit F, partial (plastid) [Teucrium montbretii subsp. heliotropiifolium]
724	gi|395484535|gb|AFN66524.1|	76413	24.31	2	1	1	NADH dehydrogenase subunit F, partial (plastid) [Teucrium antitauricum]
725	gi|510794472|gb|AGN52202.1|	40938	24.14	2	1	1	MYB-related transcription factor [Salvia miltiorrhiza]
726	gi|573462009|emb|CCQ71678.1|	45534	23.18	4	1	1	NADH dehydrogenase subunit 7 (chloroplast) [Salvia miltiorrhiza]
727	gi|401879799|gb|AFQ30986.1|	45534	23.18	4	1	1	NADH dehydrogenase subunit 7 (chloroplast) [Salvia miltiorrhiza]
728	gi|836643397|ref|YP_009144571.1|	45642	23.18	4	1	1	NADH dehydrogenase subunit 7 (chloroplast) [Rosmarinus officinalis]
729	gi|827345157|gb|AKJ76741.1|	45642	23.18	4	1	1	NADH dehydrogenase subunit 7 (chloroplast) [Rosmarinus officinalis]
730	gi|410176210|gb|AFV61869.1|	45519	23.18	4	1	1	NADH dehydrogenase subunit 7 (chloroplast) [Origanum vulgare subsp. vulgare]
731	gi|916439041|gb|AKZ22225.1|	45538	23.18	4	1	1	NADH dehydrogenase subunit 7 (plastid) [Monarda fistulosa var. mollis]

No.	Accession Number	Average Mass	Max-10logP	Max Coverage (%)	Max# Peptides	Max# Unique	Description
732	gi|916439045|gb|AKZ22227.1|	45533	23.18	4	1	1	NADH dehydrogenase subunit 7 (plastid) [Salvia nemorosa]
733	gi|916439043|gb|AKZ22226.1|	45734	23.18	4	1	1	NADH dehydrogenase subunit 7 (plastid) [Nepeta cataria]
734	gi|916439047|gb|AKZ22228.1|	45476	23.18	4	1	1	NADH dehydrogenase subunit 7 (plastid) [Teucrium canadense]
735	gi|827346580|gb|AKJ77766.1|	45539	23.18	4	1	1	NADH dehydrogenase subunit 7 (chloroplast) [Perilla frutescens]
736	gi|827345853|gb|AKJ77154.1|	45491	23.18	4	1	1	NADH dehydrogenase subunit 7 (chloroplast) [Scutellaria baicalensis]
737	gi|910312657|ref|YP_009162318.1|	45491	23.18	4	1	1	NADH dehydrogenase subunit 7 (chloroplast) [Scutellaria baicalensis]
738	gi|752789844|ref|YP_009117278.1|	45401	23.18	4	1	1	NADH-plastoquinone oxidoreductase subunit 7 (chloroplast) [Premna microphylla]
739	gi|748013962|gb|AJE28432.1|	45401	23.18	4	1	1	NADH-plastoquinone oxidoreductase subunit 7 (chloroplast) [Premna microphylla]
740	gi|748013960|gb|AJE28430.1|	19533	21.73	6	1	1	NADH-plastoquinone oxidoreductase subunit I (chloroplast) [Premna microphylla]
741	gi|752789842|ref|YP_009117276.1|	19533	21.73	6	1	1	NADH-plastoquinone oxidoreductase subunit I (chloroplast) [Premna microphylla]
742	gi|916438099|gb|AKZ21755.1|	37677	21.34	2	1	1	cytochrome c biogenesis protein (plastid) [Nepeta cataria]
743	gi|916442749|gb|AKZ23931.1|	157974	21.28	1	1	1	RNA polymerase beta" subunit (plastid) [Salvia nemorosa]
744	gi|836643373|ref|YP_009144505.1|	158291	21.28	1	1	1	RNA polymerase beta" subunit (chloroplast) [Rosmarinus officinalis]

No.	Accession Number	Average Mass	Max-10logP	Max Coverage (%)	Max# Peptides	Max# Unique	Description
745	gi|827345133|gb|AKJ76717.1|	158291	21.28	1	1	1	RNA polymerase beta" subunit (chloroplast) [Rosmarinus officinalis]
746	gi|410176145|gb|AFV61804.1|	158559	21.28	1	1	1	RNA polymerase beta" subunit (chloroplast) [Origanum vulgare subsp. vulgare]
747	gi|916442746|gb|AKZ23930.1|	158642	21.28	1	1	1	RNA polymerase beta" subunit (plastid) [Monarda fistulosa var. mollis]
748	gi|75244696|sp|Q8H2B4.1|LLOS_MENAQ	267080	137.47	5	14	14	R-linalool synthase, chloroplastic; Flags: Precursor
749	gi|75251477|sp|Q5SBP0.1|TPSD_OCIBA	267080	137.47	5	14	14	Terpinolene synthase, chloroplastic; Flags: Precursor
750	gi|8134569|sp|Q42662.2|METE_PLESU	267080	137.19	5	14	14	5-methyltetrahydropteroyltriglutamate--homocysteine methyltransferase; AltName: Full=Cobalamin-independent methionine synthase isozyme; AltName: Full=Vitamin-B12-independent methionine synthase isozyme
751	gi|75251482|sp|Q5SBP5.1|GCS1_OCIBA	267080	137.47	5	14	14	Gamma-cadinene synthase; AltName: Full=(+)-gamma-cadinene synthase
752	gi|122249145|sp|Q49SP3.1|TPSPS_POGCB	78531	34.94	2	1	1	Patchoulol synthase; Short=PatTps177; AltName: Full=Alpha-guaiene synthase; AltName: Full=Delta-guaiene synthase
753	gi|75251481|sp|Q5SBP4.1|AZIS_OCIBA	76501	34.94	2	1	1	Alpha-zingiberene synthase
754	gi|75129878|sp|Q6WAU0.1|PULR_MENPI	84218	34.94	1	1	1	(+)-pulegone reductase
755	gi|122210942|sp|Q2XSC4.1|LABER_LAVAN	84218	34.94	1	1	1	Exo-alpha-bergamotene synthase; Short=LaBERS; AltName: Full=Trans-alpha-bergamotene synthase
756	gi|122200954|sp|Q2KNL5.1|CADH1_OCIBA	84443	34.94	1	1	1	Cinnamyl alcohol dehydrogenase 1; Short=CAD 1; Short=ObaCAD1
757	gi|122219295|sp|Q49SP7.1|TPSCS_POGCB	77203	34.94	2	1	1	Gamma-curcumene synthase; AltName: Full=PatTpsA

No.	Accession Number	Average Mass	Max-10logP	Max Coverage (%)	Max# Peptides	Max# Unique	Description
758	gi|122233627|sp|Q4JF75.1|RBR_SCUBA	84354	34.94	1	1	1	Retinoblastoma-related protein
759	gi|75161989|sp|Q8W1W9.1|5MAT1_SALSN	79081	34.94	2	1	1	Malonyl-coenzyme:anthocyanin 5-O-glucoside-6'''-O-malonyltransferase; Short=Malonyl CoA:anthocyanin 5-O-glucoside-6'''-O-malonyltransferase; Short=Ss5MaT1
760	gi|510785777|sp|G0LD36.1|RAS_MELOI	84295	34.94	1	1	1	Rosmarinate synthase; Short=MoRAS; AltName: Full=Hydroxycinnamoyl-CoA:hydroxyphenyllactate hydroxycinnamoyltransferase
761	gi|573461995|emb|CCQ71664.1|	267080	137.47	5	14	14	Ycf2 (chloroplast) [Salvia miltiorrhiza]
762	gi|573462016|emb|CCQ71685.1|	267080	137.47	5	14	14	Ycf2 (chloroplast) [Salvia miltiorrhiza]
763	gi|401879785|gb|AFQ30972.1|	267080	137.47	5	14	14	Hypothetical chloroplast RF2 (chloroplast) [Salvia miltiorrhiza]
764	gi|401879806|gb|AFQ30993.1|	267080	137.47	5	14	14	Hypothetical chloroplast RF2 (chloroplast) [Salvia miltiorrhiza]
765	gi|395484473|gb|AFN66496.1|	78531	34.94	2	1	1	NADH dehydrogenase subunit F, partial (plastid) [Teucridium parvifolium]
766	gi|395484515|gb|AFN66515.1|	76501	34.94	2	1	1	NADH dehydrogenase subunit F, partial (plastid) [Teucrium racemosum]
767	gi|836643377|ref|YP_009144562.1|	84218	34.94	1	1	1	NADH dehydrogenase subunit 5 (chloroplast) [Rosmarinus officinalis]
768	gi|827345137|gb|AKJ76721.1|	84218	34.94	1	1	1	NADH dehydrogenase subunit 5 (chloroplast) [Rosmarinus officinalis]
769	gi|916438885|gb|AKZ22147.1|	84443	34.94	1	1	1	NADH dehydrogenase subunit 5 (plastid) [Salvia nemorosa]
770	gi|395484493|gb|AFN66505.1|	77203	34.94	2	1	1	NADH dehydrogenase subunit F, partial (plastid) [Teucrium pseudochamaepitys]

No.	Accession Number	Average Mass	Max-10logP	Max Coverage (%)	Max# Peptides	Max# Unique	Description
771	gi|916438881|gb|AKZ22145.1|	84354	34.94	1	1	1	NADH dehydrogenase subunit 5 (plastid) [Monarda fistulosa var. mollis]
772	gi|669254293|gb|AII20586.1|	79081	34.94	2	1	1	NADH dehydrogenase subunit F, partial (chloroplast) [Hymenopyramis cana]
773	gi|410176201|gb|AFV61860.1|	84295	34.94	1	1	1	NADH dehydrogenase subunit 5 (chloroplast) [Origanum vulgare subsp. vulgare]
774	gi|395484517|gb|AFN66516.1|	76688	34.94	2	1	1	NADH dehydrogenase subunit F, partial (plastid) [Teucrium salviastrum]
775	gi|395484511|gb|AFN66513.1|	76860	34.94	2	1	1	NADH dehydrogenase subunit F, partial (plastid) [Teucrium oxylepis]
776	gi|395484489|gb|AFN66504.1|	76910	34.94	2	1	1	NADH dehydrogenase subunit F, partial (plastid) [Teucrium betonicum]
777	gi|669254285|gb|AII20582.1|	74815	34.94	2	1	1	NADH dehydrogenase subunit F, partial (chloroplast) [Holocheila longipedunculata]
778	gi|669254287|gb|AII20583.1|	77022	34.94	2	1	1	NADH dehydrogenase subunit F, partial (chloroplast) [Holocheila longipedunculata]
779	gi|669254283|gb|AII20581.1|	77991	34.94	2	1	1	NADH dehydrogenase subunit F, partial (chloroplast) [Holocheila longipedunculata]
780	gi|395484483|gb|AFN66501.1|	77431	34.94	2	1	1	NADH dehydrogenase subunit F, partial (plastid) [Teucrium albicaule]
781	gi|395484520|gb|AFN66517.1|	76892	34.94	2	1	1	NADH dehydrogenase subunit F, partial (plastid) [Teucrium spinosum]
782	gi|395484495|gb|AFN66506.1|	76993	34.94	2	1	1	NADH dehydrogenase subunit F, partial (plastid) [Teucrium eriocephalum subsp. almeriense]
783	gi|395484500|gb|AFN66508.1|	77065	34.94	2	1	1	NADH dehydrogenase subunit F, partial (plastid) [Teucrium stocksianum subsp. incanum]

No.	Accession Number	Average Mass	Max-10logP	Max Coverage (%)	Max# Peptides	Max# Unique	Description
784	gi|395484526|gb|AFN66520.1|	76596	34.94	2	1	1	NADH dehydrogenase subunit F, partial (plastid) [Teucrium bicolor]
785	gi|395484507|gb|AFN66511.1|	77434	34.94	2	1	1	NADH dehydrogenase subunit F, partial (plastid) [Teucrium nudicaule]
786	gi|395484504|gb|AFN66510.1|	77454	34.94	2	1	1	NADH dehydrogenase subunit F, partial (plastid) [Teucrium laciniatum]
787	gi|395484477|gb|AFN66498.1|	76293	34.94	2	1	1	NADH dehydrogenase subunit F, partial (plastid) [Spartothamnella puberula]
788	gi|395484513|gb|AFN66514.1|	76814	34.94	2	1	1	NADH dehydrogenase subunit F, partial (plastid) [Teucrium pyrenaicum]
789	gi|395484502|gb|AFN66509.1|	75956	34.94	2	1	1	NADH dehydrogenase subunit F, partial (plastid) [Teucrium divaricatum]
790	gi|395484522|gb|AFN66518.1|	76105	34.94	2	1	1	NADH dehydrogenase subunit F, partial (plastid) [Teucrium subspinosum]
791	gi|669254291|gb|AII20585.1|	79070	34.94	2	1	1	NADH dehydrogenase subunit F, partial (chloroplast) [Petraeovitex multiflora]
792	gi|395484475|gb|AFN66497.1|	78510	34.94	2	1	1	NADH dehydrogenase subunit F, partial (plastid) [Rubiteucris palmata]
793	gi|395484481|gb|AFN66500.1|	76061	34.94	2	1	1	NADH dehydrogenase subunit F, partial (plastid) [Teucrium flavum subsp. glaucum]
794	gi|916438887|gb|AKZ22148.1|	83254	34.94	1	1	1	NADH dehydrogenase subunit 5 (plastid) [Teucrium canadense]
795	gi|748013953|gb|AJE28423.1|	85385	34.94	1	1	1	NADH-plastoquinone oxidoreductase subunit 5 (chloroplast) [Premna microphylla]
796	gi|752789835|ref|YP_009117269.1|	85385	34.94	1	1	1	NADH-plastoquinone oxidoreductase subunit 5 (chloroplast) [Premna microphylla]

No.	Accession Number	Average Mass	Max-10logP	Max Coverage (%)	Max# Peptides	Max# Unique	Description
797	gi|395484530|gb|AFN66522.1|	76725	34.94	2	1	1	NADH dehydrogenase subunit F, partial (plastid) [Teucrium viscidum var. miquelianum]
798	gi|395484528|gb|AFN66521.1|	76705	34.94	2	1	1	NADH dehydrogenase subunit F, partial (plastid) [Teucrium japonicum]
799	gi|827346594|gb|AKJ77780.1|	84248	34.94	1	1	1	NADH dehydrogenase subunit 5 (chloroplast) [Perilla frutescens]
800	gi|395484497|gb|AFN66507.1|	77873	34.94	2	1	1	NADH dehydrogenase subunit F, partial (plastid) [Teucrium fruticans]
801	gi|395484509|gb|AFN66512.1|	77251	34.94	2	1	1	NADH dehydrogenase subunit F, partial (plastid) [Teucrium orientale subsp. gloeotrichum]
802	gi|395484485|gb|AFN66502.1|	77595	34.94	2	1	1	NADH dehydrogenase subunit F, partial (plastid) [Teucrium aristatum]
803	gi|395484487|gb|AFN66503.1|	77172	34.94	2	1	1	NADH dehydrogenase subunit F, partial (plastid) [Teucrium aroanium]
804	gi|395484537|gb|AFN66525.1|	78210	34.94	2	1	1	NADH dehydrogenase subunit F, partial (plastid) [Teucrium decipiens]
805	gi|573462000|emb|CCQ71669.1|	83587	26.78	1	1	1	NADH dehydrogenase subunit 5 (chloroplast) [Salvia miltiorrhiza]
806	gi|401879790|gb|AFQ30977.1|	83587	26.78	1	1	1	NADH dehydrogenase subunit 5 (chloroplast) [Salvia miltiorrhiza]
807	gi|395484533|gb|AFN66523.1|	75763	26.78	2	1	1	NADH dehydrogenase subunit F, partial (plastid) [Teucrium montbretii subsp. heliotropiifolium]
808	gi|395484535|gb|AFN66524.1|	76413	26.78	2	1	1	NADH dehydrogenase subunit F, partial (plastid) [Teucrium antitauricum]
809	gi|827345833|gb|AKJ77134.1|	85675	26.78	1	1	1	NADH dehydrogenase subunit 5 (chloroplast) [Scutellaria baicalensis]

No.	Accession Number	Average Mass	Max-10logP	Max Coverage (%)	Max# Peptides	Max# Unique	Description
810	gi|910312648|ref|YP_009162309.1|	85675	26.78	1	1	1	NADH dehydrogenase subunit 5 (chloroplast) [Scutellaria baicalensis]
811	gi|395484479|gb|AFN66499.1|	34714	26.78	4	1	1	NADH dehydrogenase subunit F, partial (plastid) [Oncinocalyx betchei]
812	gi|75129878|sp|Q6WAU0.1|PULR_MENPI	37915	34.40	2	1	1	(+)-pulegone reductase
813	gi|5915814|sp|O04164.1|C71A6_NEPRA	57955	124.01	14	7	7	Cytochrome P450 71A6
814	gi|75161989|sp|Q8W1W9.1|5MAT1_SALSN	50724	103.98	3	2	2	Malonyl-coenzyme:anthocyanin 5-O-glucoside-6'''-O-malonyltransferase; Short=Malonyl CoA:anthocyanin 5-O-glucoside-6'''-O-malonyltransferase; Short=Ss5MaT1
815	gi|75244696|sp|Q8H2B4.1|LLOS_MENAQ	70535	100.72	7	5	4	R-linalool synthase, chloroplastic; Flags: Precursor
816	gi|75129878|sp|Q6WAU0.1|PULR_MENPI	37915	86.57	6	3	3	(+)-pulegone reductase
817	gi|56749087|sp|Q85XY6.1|MATK_OCIBA	60282	75.48	6	3	3	Maturase K; AltName: Full=Intron maturase
818	gi|75251478|sp|Q5SBP1.1|MYRS_OCIBA	69964	74.79	3	2	1	Beta-myrcene synthase, chloroplastic; Flags: Precursor
819	gi|75251477|sp|Q5SBP0.1|TPSD_OCIBA	70000	65.09	5	3	2	Terpinolene synthase, chloroplastic; Flags: Precursor
820	gi|75315259|sp|Q9XHE6.1|C71DF_MENPI	56532	62.77	2	1	1	Cytochrome P450 71D15; AltName: Full=(-)-(4S)-Limonene-3-hydroxylase; AltName: Full=Cytochrome P450 isoform PM2
821	gi|510785777|sp|G0LD36.1|RAS_MELOI	47161	60.94	5	2	2	Rosmarinate synthase; Short=MoRAS; AltName: Full=Hydroxycinnamoyl-CoA:hydroxyphenyllactate hydroxycinnamoyltransferase
822	gi|29839421|sp|Q9XGW0.1|COMT1_OCIBA	39529	59.08	3	1	1	Caffeic acid 3-O-methyltransferase 1; Short=CAOMT-1; Short=COMT-1; AltName: Full=S-adenosysl-L-methionine:caffeic acid 3-O-methyltransferase 1

No.	Accession Number	Average Mass	Max-10logP	Max Coverage (%)	Max# Peptides	Max# Unique	Description
823	gi|29839420|sp|Q9XGV9.1|COMT2_OCIBA	39613	52.73	3	1	1	Caffeic acid 3-O-methyltransferase 2; Short=CAOMT-2; Short=COMT-2; AltName: Full=S-adenosysl-L-methionine:caffeic acid 3-O-methyltransferase 2
824	gi|75251482|sp|Q5SBP5.1|GCS1_OCIBA	63566	46.66	4	1	1	Gamma-cadinene synthase; AltName: Full=(+)-gamma-cadinene synthase
825	gi|75227033|sp|Q76MR7.1|UBGAT_SCUBA	48654	44.81	2	1	1	Baicalein 7-O-glucuronosyltransferase; AltName: Full=UDP-glucuronate:baicalein 7-O-glucuronosyltransferase
826	gi|401879801|gb|AFQ30988.1|	218699	34.68	1	1	1	Photosystem I assembly protein Ycf1 (chloroplast) [Salvia miltiorrhiza]
827	gi|573462011|emb|CCQ71680.1|	218685	32.29	1	1	1	Ycf1 (chloroplast) [Salvia miltiorrhiza]
828	gi|661525316|gb|AIE15765.1|	184302	32.29	1	1	1	Dicer-like protein 3 [Salvia miltiorrhiza]
829	gi|844572794|gb|AKN09591.1|	22976	26.64	4	1	1	Basic helix-loop-helix transcription factor [Salvia miltiorrhiza]
830	gi|661525312|gb|AIE15763.1|	216665	24.47	1	1	1	Dicer-like protein 1 [Salvia miltiorrhiza]
831	gi|916441767|gb|AKZ23588.1|	15470	24.02	6	1	1	Ribosomal protein L20 (plastid) [Teucrium canadense]
832	gi|827345878|gb|AKJ77179.1|	15363	24.02	6	1	1	Ribosomal protein L20 (chloroplast) [Scutellaria baicalensis]
833	gi|910312623|ref|YP_009162284.1|	15363	24.02	6	1	1	Ribosomal protein L20 (chloroplast) [Scutellaria baicalensis]
834	gi|916441755|gb|AKZ23582.1|	15554	24.02	6	1	1	Ribosomal protein L20 (plastid) [Nepeta cataria]
835	gi|916441757|gb|AKZ23583.1|	15566	24.02	6	1	1	Ribosomal protein L20 (plastid) [Salvia nemorosa]
836	gi|410176177|gb|AFV61836.1|	15446	24.02	6	1	1	Ribosomal protein L20 (chloroplast) [Origanum vulgare subsp. vulgare]

No.	Accession Number	Average Mass	Max-10logP	Max Coverage (%)	Max# Peptides	Max# Unique	Description
837	gi|916441753|gb|AKZ23581.1|	15522	24.02	6	1	1	Ribosomalprotein L20 (plastid) [Monarda fistulosa var. mollis]
838	gi|827345181|gb|AKJ76765.1|	15446	24.02	6	1	1	Ribosomal protein L20 (chloroplast) [Rosmarinus officinalis]
839	gi|836643421|ref|YP_009144537.1|	15446	24.02	6	1	1	Ribosomal protein L20 (chloroplast) [Rosmarinus officinalis]
840	gi|827346543|gb|AKJ77729.1|	15537	24.02	6	1	1	Ribosomal protein L20 (chloroplast) [Perilla frutescens]
841	gi|748013927|gb|AJE28397.1|	15724	24.02	6	1	1	Ribosomal protein L20 (chloroplast) [Premna microphylla]
842	gi|752789809|ref|YP_009117244.1|	15724	24.02	6	1	1	Ribosomal protein L20 (chloroplast) [Premna microphylla]
843	gi|573461974|emb|CCQ71643.1|	15541	24.02	6	1	1	Ribosomal protein L20 (chloroplast) [Salvia miltiorrhiza]
844	gi|401879765|gb|AFQ30952.1|	15541	24.02	6	1	1	Ribosomal protein L20 (chloroplast) [Salvia miltiorrhiza]
845	gi|75129878|sp|Q6WAU0.1|PULR_MENPI	37915	23.86	2	1	1	(+)-pulegone reductase
846	gi|745791013|gb|AJD25215.1|	56512	21.31	2	1	1	Cytochrome P450 CYP92B28 [Salvia miltiorrhiza]
847	gi|75161989|sp|Q8W1W9.1|5MAT1_SALSN	101.20	10	5	5	50724	Malonyl-coenzyme:anthocyanin 5-O-glucoside-6'''-O-malonyltransferase; Short=Malonyl CoA:anthocyanin 5-O-glucoside-6'''-O-malonyltransferase; Short=Ss5MaT1
848	gi|75129878|sp|Q6WAU0.1|PULR_MENPI	96.90	6	3	3	37915	(+)-pulegone reductase
849	gi|8134569|sp|Q42662.2|METE_PLESU	92.21	4	4	4	84590	5-methyltetrahydropteroyltriglutamate--homocysteine methyltransferase; AltName: Full=Cobalamin-independent methionine synthase isozyme; AltName: Full=Vitamin-B12-independent methionine synthase isozyme

No.	Accession Number	Average Mass	Max-10logP	Max Coverage (%)	Max# Peptides	Max# Unique	Description
850	gi|5921781|sp|O04111.1|CHSY_PERFR	88.85	2	1	1	42686	Chalcone synthase; AltName: Full=Naringenin-chalcone synthase
851	gi|75288825|sp|Q65CJ7.2|HPPR_PLESU	79.89	3	1	1	34128	Hydroxyphenylpyruvate reductase; Short=HPPR
852	gi|75180331|sp|Q9LRC8.1|BAGLU_SCUBA	77.84	4	2	2	58772	Baicalin-beta-D-glucuronidase; AltName: Full=Baicalinase; Flags: Precursor
853	gi|75219538|sp|O48935.1|TPSBF_MENPI	73.42	4	2	2	63830	Beta-farnesene synthase
854	gi|122219294|sp|Q49SP6.1|TPGD2_POGCB	72.68	2	1	1	64149	Germacrene D synthase 2; AltName: Full=PatTpsBF2
855	gi|75244696|sp|Q8H2B4.1|LLOS_MENAQ	71.83	2	1	1	70535	R-linalool synthase, chloroplastic; Flags: Precursor
856	gi|62899675|sp|O81192.1|BPPS_SALOF	70.92	2	1	1	69292	(+)-bornyl diphosphate synthase, chloroplastic; Short=BPPS; AltName: Full=(+)-alpha-pinene synthase; AltName: Full=(+)-camphene synthase; AltName: Full=SBS; Flags: Precursor
857	gi|14423898|sp|Q9M573.1|RL31_PERFR	64.2	7	1	1	13894	60S ribosomal protein L31
858	gi|75251477|sp|Q5SBP0.1|TPSD_OCIBA	59.95	2	1	1	70000	Terpinolene synthase, chloroplastic; Flags: Precursor
859	gi|75251482|sp|Q5SBP5.1|GCS1_OCIBA	41.49	4	1	1	63566	Gamma-cadinene synthase; AltName: Full=(+)-gamma-cadinene synthase
860	gi|56749087|sp|Q85XY6.1|MATK_OCIBA	40.87	2	1	1	60282	Maturase K; AltName: Full=Intron maturase
861	gi|122210943|sp|Q2XSC5.1|LALIN_LAVAN	39.51	1	1	1	65654	R-linalool synthase; Short=LaLINS
862	gi|510785777|sp|G0LD36.1|RAS_MELOI	38.69	2	1	1	47161	Rosmarinate synthase; Short=MoRAS; AltName: Full=Hydroxycinnamoyl-CoA:hydroxyphenyllactate hydroxycinnamoyltransferase
863	gi|75306222|sp|Q947B7.1|MFS_MENPI	34.67	5	1	1	55360	(+)-menthofuran synthase; AltName: Full=(+)-pulegone 9-hydroxylase

No.	Accession Number	Average Mass	Max-10logP	Max Coverage (%)	Max# Peptides	Max# Unique	Description
864	gi|410176212|gb|AFV61871.1|	217739	129.41	11	24	23	Protein Ycf1 (chloroplast) [Origanum vulgare subsp. vulgare]; Protein TIC 214
865	gi|401879801|gb|AFQ30988.1|	218699	48.04	1	2	1	Photosystem I assembly protein Ycf1 (chloroplast) [Salvia miltiorrhiza]; Protein TIC 214
866	gi|573462011|emb|CCQ71680.1|	218685	48.04	1	2	1	Protein Ycf1 (chloroplast) [Salvia miltiorrhiza]; Protein TIC 214
867	gi|661525318|gb|AIE15766.1|	183633	46.23	0	1	1	Dicer-like protein 4a [Salvia miltiorrhiza]
868	gi|75129878|sp|Q6WAU0.1|PULR_MENPI	37915	41.91	2	1	1	(+)-pulegone reductase
869	gi|410176197|gb|AFV61856.1|	264781	40.31	1	2	2	Protein Ycf2 (chloroplast) [Origanum vulgare subsp. vulgare]
870	gi|410176216|gb|AFV61875.1|	264781	40.31	1	2	2	Protein Ycf2 (chloroplast) [Origanum vulgare subsp. vulgare]
871	gi|836643370|ref|YP_009144558.1|	266537	40.31	1	2	2	Protein Ycf2 (chloroplast) [Rosmarinus officinalis]
872	gi|827345131|gb|AKJ76715.1|	266537	40.31	1	2	2	Protein Ycf2 (chloroplast) [Rosmarinus officinalis]
873	gi|827345130|gb|AKJ76714.1|	266537	40.31	1	2	2	Protein Ycf2 (chloroplast) [Rosmarinus officinalis]
874	gi|836643371|ref|YP_009144577.1|	266537	40.31	1	2	2	Protein Ycf2 (chloroplast) [Rosmarinus officinalis]
875	gi|844572640|gb|AKN09541.1|	34841	39.74	3	1	1	Basic helix-loop-helix transcription factor [Salvia miltiorrhiza]
876	gi|602690681|gb|AHN96278.1|	37139	37.81	3	1	1	Marurase K, partial (chloroplast) [Zhumeria majdae]
877	gi|602690679|gb|AHN96277.1|	37139	37.81	3	1	1	Marurase K, partial (chloroplast) [Zhumeria majdae]
878	gi|602690689|gb|AHN96282.1|	37139	37.81	3	1	1	Marurase K, partial (chloroplast) [Zhumeria majdae]
879	gi|602690701|gb|AHN96288.1|	37139	37.81	3	1	1	Marurase K, partial (chloroplast) [Zhumeria majdae]
880	gi|602690697|gb|AHN96286.1|	37139	37.81	3	1	1	Marurase K, partial (chloroplast) [Zhumeria majdae]

No.	Accession Number	Average Mass	Max-10logP	Max Coverage (%)	Max# Peptides	Max# Unique	Description
881	gi|602690673|gb|AHN96274.1|	37139	37.81	3	1	1	Marurase K, partial (chloroplast) [Zhumeria majdae]
882	gi|602690675|gb|AHN96275.1|	37139	37.81	3	1	1	Marurase K, partial (chloroplast) [Zhumeria majdae]
883	gi|602690683|gb|AHN96279.1|	37138	37.81	3	1	1	Marurase K, partial (chloroplast) [Zhumeria majdae]
884	gi|602690699|gb|AHN96287.1|	37138	37.81	3	1	1	Marurase K, partial (chloroplast) [Zhumeria majdae]
885	gi|602690687|gb|AHN96281.1|	37105	37.81	3	1	1	Marurase K, partial (chloroplast) [Zhumeria majdae]
886	gi|602690685|gb|AHN96280.1|	37105	37.81	3	1	1	Marurase K, partial (chloroplast) [Zhumeria majdae]
887	gi|602690677|gb|AHN96276.1|	37105	37.81	3	1	1	Marurase K, partial (chloroplast) [Zhumeria majdae]
888	gi|661525312|gb|AIE15763.1|	216665	33.15	1	1	1	Dicer-like protein 1 [Salvia miltiorrhiza]
889	gi|745790967|gb|AJD25192.1|	58706	32.46	2	1	1	Cytochrome P450 CYP79D40 [Salvia miltiorrhiza]
890	gi|844572703|gb|AKN09562.1|	36568	32.19	2	1	1	Basic helix-loop-helix transcription factor [Salvia miltiorrhiza]
891	gi|29839420|sp|Q9XGV9.1|COMT2_OCIBA	39613	31.81	3	1	1	Caffeic acid 3-O-methyltransferase 2; Short=CAOMT-2; Short=COMT-2; AltName: Full=S-adenosysl-L-methionine:caffeic acid 3-O-methyltransferase 2
892	gi|29839421|sp|Q9XGW0.1|COMT1_OCIBA	39529	24.12	3	1	1	Caffeic acid 3-O-methyltransferase 1; Short=CAOMT-1; Short=COMT-1; AltName: Full=S-adenosysl-L-methionine:caffeic acid 3-O-methyltransferase 1
893	gi|844572794|gb|AKN09591.1|	22976	27.18	4	1	1	Basic helix-loop-helix transcription factor [Salvia miltiorrhiza]
894	gi|910312590|ref|YP_009162251.1|	158800	27.01	1	1	1	DNA-directed RNA polymerase subunit beta"UniRule annotation (EC:2.7.7.6UniRule annotation)
895	gi|827345829|gb|AKJ77130.1|	158800	27.01	1	1	1	DNA-directed RNA polymerase subunit beta"UniRule annotation (EC:2.7.7.6UniRule annotation)

No.	Accession Number	Average Mass	Max-10logP	Max Coverage (%)	Max# Peptides	Max# Unique	Description
896	gi|661525316|gb|AIE15765.1|	184302	25.36	1	1	1	Dicer-like protein 3 [Salvia miltiorrhiza]
897	gi|745791003|gb|AJD25210.1|	57675	23.31	2	1	1	Cytochrome P450 CYP89A115 [Salvia miltiorrhiza]
898	gi|521953403|gb|AGQ04160.1|	40132	21.67	3	1	1	Farnesyl diphosphate synthase [Lavandula angustifolia]
899	gi|630058023|gb|AHY94894.1|	51993	21.30	2	1	1	4-coumarate:CoA ligase, partial [Prunella vulgaris]
900	gi|745790929|gb|AJD25173.1|	57680	21.12	1	1	1	Cytochrome P450 CYP73A120 [Salvia miltiorrhiza]
901	gi|725812545|gb|AIY32618.1|	57979	21.12	1	1	1	Cinnamate-4-hydroxylase [Perilla frutescens]
902	gi|762060297|gb|AJQ20620.1|	48394	21.05	2	1	1	Dihydrolipoamide Acetyltransferase [Salvia miltiorrhiza]
903	gi|548918017|gb|AGX15389.1|	56042	20.86	2	1	1	Flavonoid 3' monooxygenase [Plectranthus barbatus]
904	gi|661525320|gb|AIE15767.1|	174990	20.37	1	1	1	Dicer-like protein 4b [Salvia miltiorrhiza]

Chapter 3

Neuroprotective Potential of *Orthosiphon stamineus* Proteins in SH-SY5Y Cell Model Induced by Hydrogen Peroxide

3.1 Introduction

Human neuroblastoma cell line, SH-SY5Y with a stable karyotype consisting of 47 chromosomes, is an *in vitro* model ideal for high-throughput study on neurobiology (Kovalevich & Langford, 2013). SH-SY5Y model provides an efficient platform essential for preliminary drug testing, protein functionality and molecular mechanisms in neurological conditions as well as the pathogenesis of viral infection on the CNS (Shipley, Mangold, & Szpara, 2016).

The present chapter begins with optimizing the SH-SY5Y cell growth at different seeding density. The optimal cell density determined is then used in all the subsequent *in vitro* assays as described in Figure 3.1. Cytotoxic study of OSLP at varying concentrations over two-time points, 24- and 48-hour, are evaluated. The maximal non-toxic dose (MNTD) and the minimal toxic dose (MTD) are also determined. The SH-SY5Y cells are challenged by hydrogen peroxide (H_2O_2) and the half-maximal inhibitory concentration (IC_{50}), as well as the maximal inhibitory concentration (IC_{90}), are determined. The IC_{50} value determined is then used in the evaluation of OSLP protective potential in the H_2O_2-induced SH-SY5Y cell model and the protein expression study. The protective mechanism of OSLP in the H_2O_2-induced SH-SY5Y cell model is also investigated using mass spectrometry-based label-free proteomic quantification (LFQ). LFQ profiles the differentially expressed proteins between the H_2O_2-induced cells and OSLP-treated H_2O_2-induced cells. This thus provides fundamental information to study the functional annotations, the protein-protein interactions, and their gene-disease associations. These enriched biological data help to visualize the molecular interactions, reactions, and relations associated with the anticonvulsive mechanism of OSLP on disease pathway maps. Hence, the objectives of this chapter are:

1. To evaluate the cytotoxic effects of OSLP on SH-SY5Y cells (24- and 48-hour).
2. To establish the H_2O_2-induced SH-SY5Y cell model and determine the IC_{50} value.
3. To evaluate OSLP protective potential in the H_2O_2-induced SH-SY5Y cell model.
4. To elucidate OSLP protective mechanism at protein expression levels in combination with bioinformatics methods.

The flowchart outlining the overview of experimental design to achieve the objectives are summarized Figure 3.1 below:

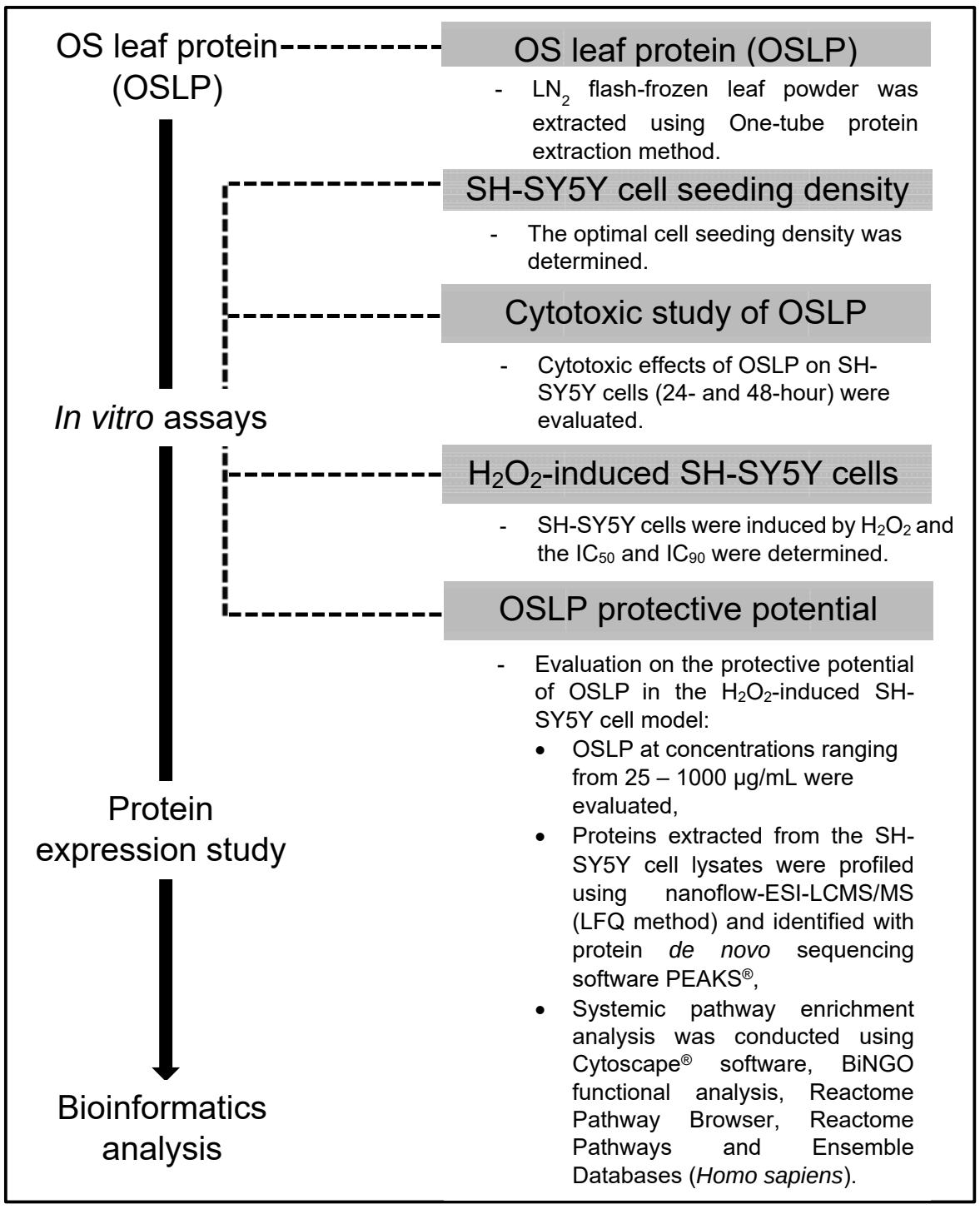

Figure 3.1: Flowchart summarizing the overview of experimental design.

References:

Kovalevich, J., & Langford, D. (2013). Considerations for the use of SH-SY5Y neuroblastoma cells in neurobiology. *Methods Mol Biol, 1078*, 9-21. doi:10.1007/978-1-62703-640-5_2

Shipley, M. M., Mangold, C. A., & Szpara, M. L. (2016). Differentiation of the SH-SY5Y Human Neuroblastoma Cell Line. *Journal of visualized experiments : JoVE*(108), 53193-53193. doi:10.3791/53193

biology

MDPI

Article

Orthosiphon stamineus Proteins Alleviate Hydrogen Peroxide Stress in SH-SY5Y Cells

Yin-Sir Chung [1,2], Pervaiz Khalid Ahmed [3,4], Iekhsan Othman [1,2] and Mohd. Farooq Shaikh [1,4]*

[1] Neuropharmacology Research Laboratory, Jeffrey Cheah School of Medicine and Health Sciences, Monash University Malaysia, Bandar Sunway, Malaysia
[2] Liquid Chromatography-Mass Spectrometry (LCMS) Platform, Jeffrey Cheah School of Medicine and Health Sciences, Monash University Malaysia, Bandar Sunway, Malaysia
[3] School of Business, Monash University Malaysia, Bandar Sunway, Malaysia
[4] Global Asia in the 21st Century (GA21), Monash University Malaysia, Bandar Sunway, Malaysia
* Correspondence: farooq.shaikh@monash.edu

Received: date; Accepted: date; Published: date

Abstract: The neuroprotective potential of extracted *Orthosiphon stamineus* leaf proteins (OSLP) has never been evaluated in SH-SY5Y cells challenged by hydrogen peroxide (H_2O_2). This work thus aimed to elucidate OSLP neuroprotective potential in alleviating H_2O_2 stress. OSLP at varying concentrations were evaluated for cytotoxicity (24- and 48-h) and neuroprotective potential in H_2O_2-induced SH-SY5Y cells (24-h). The OSLP protective mechanism on H_2O_2-induced SH-SY5Y cells was also explored via mass spectrometry-based label-free quantitative proteomics (LFQ) and bioinformatics. OSLP (25, 50, 125, 250, 500 and 1000 μg/mL; 24- and 48-h) were found to be safe. Pre-treatments with OSLP doses (250, 500 and 1000 μg/mL, 24-h) significantly increased the survival of SH-SY5Y cells in a concentration-dependent manner and improved the cell architecture; pyramidal-shaped cells, reduced clumping and shrinkage, and with apparent neurite formations. OSLP pre-treatment (1000 μg/mL, 24-h) had lowered the expressions of two major heat shock proteins, HSPA8 (Heat Shock Protein Family A (Hsp70) Member 8) and HSP90AA1 (Heat shock protein 90), which promote cellular stress signalling under stress conditions. OSLP is therefore suggested to be anti-inflammatory by modulating the "Signaling of Interleukin-4 and Interleukin-13" pathway as the predominant mechanism in addition to regulating the "Attenuation Phase" and "HSP90 Chaperone Cycle for Steroid Hormone Receptors" pathways to counteract heat shock protein (HSP)-induced damage under stress conditions.

Keywords: *Orthosiphon stamineus*; Plant-derived proteins; Neuroprotective; SH-SY5Y cell model; Hydrogen peroxide

1. Introduction

Worldwide, central nervous system (CNS) disorders remain as one of the greatest threats in public health and account for a significant proportion in the picture of global disease burden [1, 2]. These disorders though may involve a wide variety of mechanisms but share some common themes including abnormal protein behaviour, oxidative stress, mitochondrial dysfunction, excitotoxicity, ions imbalance, cellular inflammation, cytotoxicity, necrosis, apoptosis and others [3-7].

Neuroprotection has been explored as a possible treatment strategy [6, 8] that aims to prevent neuronal injury and loss of various brain functions with an ultimate goal to better preserve brain function [9].

Orthosiphon stamineus (OS) or *Orthosiphon aristatus var. aristatus* (OAA) is a medicinal plant belonging to the Lamiaceae family. Often, it is referred to as cat's whiskers or "misai kucing". A

plethora of studies on the crude extracts or secondary metabolites of OS has shown protective effects including antioxidative, anti-inflammatory, antiproliferative, cytotoxic and anti-angiogenic [10, 11]. Added to that, OS has recently been reported for neuroprotective effects [12]. To date, there is no systematic investigation on OS primary metabolites especially their protective potential for the CNS. This thus sees a lack of science-backed evidence to justify the protective potential of OS primary metabolites, let alone its proteins. Using another medicinal plant known as *Nicotiana tabacum* L., Shah, Yoon [13] have found the extracted protein osmotin (24 kDa) shown protection against Alzheimer's disease. The OS proteins, could be similar to the protein osmotin, in that they also possess valuable protective properties for the CNS. Human neuroblastoma cell line, SH-SY5Y with a stable karyotype consisting of 47 chromosomes, is an *in vitro* model ideal for high-throughput study on neurobiology [14]. SH-SY5Y model provide an efficient platform essential for preliminary drug testing, protein functionality and molecular mechanisms in neurological conditions as well as the pathogenesis of viral infection on the CNS [15]. This study was commenced to evaluate the neuroprotective potential of OSLP in SH-SY5Y cells induced by hydrogen peroxide (H_2O_2).

2. Materials and Methods

2.1. Materials, chemicals and apparatuses

Human SH-SY5Y neuroblastoma cells (ATCC®CRL-2266TM) were purchased from the American Type Culture Collection (ATCC, VA, USA). Foetal bovine serum (FBS) and penicillin-streptomycin mixture (Pen/Strep) were purchased from PAA Laboratories (Austria). Haemocytometer BLAUBRAND®Neubauer, Dulbecco's Modified Eagle's Medium (DMEM), 3-(4,5-methylthiazol-2-yl)-2,5-diphenyl-tetrazolium bromide (MTT), cOmplete EDTA-free protease inhibitors, phosphatase inhibitors cocktail 2, Hydrogen peroxide (H_2O_2), TRIS hydrochloride (TRIS-HCl), dithiothreitol (DTT), iodoacetamide (IAA), HPLC-grade methanol (MeOH), ammonium bicarbonate (ABC), trifluoroethanol (TFE), formic acid (FA) and 2,3,5-triphenyltetrazolium chloride (TTC) were purchased from Sigma-Aldrich (USA). Trypsin/Lys-C Mix (Promega, USA), T-25 flask (Corning Inc., MA, USA), 15 mL Falcon tube (BD Biosciences, MA, USA), TrypLE™ Express (Life Technologies, Denmark) and phosphate-buffered saline solution (10XPBS) (Abcam, China). Pierce®trypsin protease, mass spec grade Pierce®Radioimmunoprecipitation assay (RIPA) buffer as well as the Pierce®C18 mini spin columns were purchased from Thermo Scientific Pierce (USA). Protein LoBind microcentrifuge tubes were purchased from (Eppendorf, USA), Quick Start™Bradford Protein Assay Kit from Bio-Rad (USA), trifluoroacetic acid (TFA), acetonitrile (ACN), and mass-spec grade CHAPS (Nacailai Tesque, Japan) were all purchased from Sigma-Aldrich (USA). Milli-Q ultrapure water (MQUP) was from Millipore GmbH (Germany), Dimethylsulfoxide (DMSO) and 37% formaldehyde solution were purchased from Friendemann Schmidt Chemical (Western Australia). Refrigerated centrifuge 5415R (Eppendorf AG, Germany), hydrochloric acid (36%) from Ajax Chemical (Australia) and acetic acid (glacial, 100%) from Merck (Germany). Purified nitrogen gas (99.999%) was supplied by Iwatani Malaysia S/B, liquid nitrogen (LN_2) was purchased from Linde Malaysia, Ultrasonic cell crusher (JY88-II N, China), Eyela SpeedVac Vacuum Concentrator (Thermo Scientific Pierce, USA), precision incubator (Memmert INB200, Germany) and Cole-Parmer™ Stuart™ Orbital Shaker (Thermo Scientific Pierce, USA). All the other chemicals used were of analytical grade.

2.2. Software and equipment

Olympus CKX41 inverted trinocular microscope (Philippines) connected to Olympus UIS2 optical system camera and AnalySIS 1.5 was used for the microscopic examination of SH-SY5Y cells.

In the protein expression study, an Agilent 1200 series HPLC paired with an Agilent 6550 iFunnel Quadrupole Time of Flight (Q-TOF) LC/MS, a C-18 300Å Large Capacity Chip and the Agilent MassHunter data acquisition software (all from Agilent Technologies, USA) were used to determine the differentially expressed proteins. Additionally, Version 8.0 of the PEAKS®Studio software (Bioinformatics Solution, Canada) and the UniProtKB database (Organism: *Homo sapiens*)

were used to analyse the results of the mass spectrometry-based label-free quantitative proteomics (LFQ). The Cytoscape software with version 3.7.2 of the BiNGO plugin was used for Gene Ontology (GO) annotated information (Cytoscape Consortium, USA). Reactome Pathway Browser Version 3.7 and Reactome Database Release 72 (Organism: *Homo sapiens*) were utilised for the investigation into the protein-protein interactions, functional annotations and systemic pathway enrichment analysis.

2.3. Experimental design

2.3.1. SH-SY5Y cells initial culture, sub-culture and seeding conditions

The SH-SY5Y cells obtained were maintained in an initial culture medium (pre-warmed to 37°C) consisting of DMEM supplemented with 10% FBS and 1% Pen/Strep, and kept in incubator at 37°C with 5% CO_2 and 95% air. The initial culture medium was refreshed every 4 – 7 days to remove non-adherent cells and to replenish nutrients and was monitored for cell confluence. When cells reached ≥ 80% confluence, sub-culture was performed. The old initial culture medium was aspirated and the T-25 flask was rinsed with 1 mL of warm 1X PBS (5 s, twice). To lift the cells, 1 mL of TrypLE™ Express was added and the flask was incubated (5 – 10 min, 37°C, 5% CO_2 and 95% air). The flask was removed and observed under a microscope to confirm the detachment of cells (SH-SY5Y cells were seen as "floating"). The cell suspension produced was very gently transferred to a sterile 15 mL Falcon tube containing 1 mL of 1X PBS (37°C). The tube was centrifuged (1000 rpm, 3 min, r. t.). Supernatant produced was gently discarded without disturbing the soft, transparent cell pellet formed at the bottom. The cell pellet was re-suspended in 1 mL fresh growth medium consisting of DMEM supplemented with 1% FBS and 1% Pen/Strep (pre-warmed to 37°C) and was ready for seeding into the plates. In this study, the cells used for each experiment were of less than 20 passage number.

2.3.2. Determination of SH-SY5Y cell growth at different seeding density

A twofold serial dilution of SH-SY5Y cells was carried out to achieve a cell density ranging from 200000, 100000, 50000, 25000, 12500, 6250, 3125 to 1560 cells per well, and the cells were seeded into 96-well plates (n = 3). The cells were incubated for 24-, 48-, 72- and 96-hour respectively (37°C, 5% CO_2, 95% air). Different growth performance over 4 time points were evaluated by MTT assay upon complete incubation at each time point. Absorbance was read at wavelength 570 nm with reference filter set at 690 nm. All experiments were 3 independent biological replicates performed in triplicate.

2.3.3. Evaluation of cytotoxic effects of OSLP on SH-SY5Y cells (24- and 48-hour)

SH-SY5Y cells ($5x10^4$) were seeded into 96-well plates (n = 3). Vacuum-concentrated OSLP was diluted in the growth medium at a concentration range of 25, 50, 125, 250, 500, 1000, 2000, 4000 and 10000 μg/mL. The cells were then treated with OSLP at varying concentrations and incubated for 24 and 48 hours (37°C, 5% CO_2, 95% air). Upon complete incubation, both treatment groups were evaluated for cytotoxic effects using MTT assays. All experiments were 3 independent biological replicates performed in triplicate, and the relative cell viability was expressed as a percentage (%) relative to the untreated control cells (normal control). Also, the maximal non-toxic dose (MNTD) and minimal toxic dose (MTD) of OSLP at 24- and 48-hours were also determined [16].

$$Cell\ viability\ (\%) = \frac{Absorbance\ of\ sample - Absorbance\ of\ blank}{Absorbance\ of\ control - Absorbance\ of\ blank}\ x\ 100$$

2.3.4. Hydrogen peroxide (H_2O_2) induction and determination of half-maximal inhibitory concentration (IC_{50})

SH-SY5Y cells ($5x10^4$) were seeded in 96-well plates (n = 3). SH-SY5Y cells were induced by H_2O_2 at concentrations of 0, 50, 100, 150, 200, 250, 300 and 350 μM. All concentrations of H_2O_2 were freshly prepared by diluting a 30.2% (v/v) stock solution with DMEM. Following that, the H_2O_2-induced cells were incubated at 37°C with 5% CO_2 and 95% air for 24 hours. Upon completion of incubation, cell

viability (%) of SH-SY5Y cells, the half-maximal inhibitory concentration (IC_{50}) and the maximal inhibitory concentration (IC_{90}) were determined using MTT assay. All experiments were 3 independent biological replicates performed in triplicate.

2.3.5. Evaluation of OSLP protective effects on SH-SY5Y cells

SH-SY5Y cells ($5x10^4$) were seeded in 96-well plates (n = 6). Vacuum-concentrated OSLP was diluted in the growth medium at a concentration range of 25, 50, 125, 250, 500 and 1000 μg/mL. The cells were assigned to a total of 8 groups, namely normal control (NC) without H_2O_2 induction and OSLP treatments, negative control (Neg C, H_2O_2) was induced by 150 μM of H_2O_2 and 6 OSLP treatment groups received 6 different concentrations (25 – 1000 μg/mL) (Table 1). All 6 treatment groups were pre-treated with OSLP and incubated for 24-hour at 37°C with 5% CO_2 and 95% air. Following that, all 6 treatment groups were induced by 150 μM of H_2O_2 for another 24-hour at 37°C with 5% CO_2. Upon completion of incubation, all 8 experiment groups were evaluated using MTT assays. All experiments were 6 independent biological replicates performed in triplicate.

Table 1. Experiment groups in the evaluation of OSLP protective effects on SH-SY5Y cells.

Group	Treatment
NC	Normal control (untreated cells)
H_2O_2	H_2O_2 induction (150 μM H_2O_2)
25	OSLP 25 μg/mL + 150 μM H_2O_2
50	OSLP 50 μg/mL + 150 μM H_2O_2
125	OSLP 125 μg/mL + 150 μM H_2O_2
250	OSLP 250 μg/mL + 150 μM H_2O_2
500	OSLP 500 μg/mL + 150 μM H_2O_2
1000	OSLP 1000 μg/mL + 150 μM H_2O_2

Remark: H_2O_2, hydrogen peroxide; OSLP, *Orthosiphon stamineus* leaf proteins.

Microscopic examination using bright-field imaging

Microscopic changes (10X) of the SH-SY5Y cells were studied using bright-field microscopy. The bright-field microscopic images of the normal control (NC), H_2O_2 (induced by 150 μM H_2O_2) and three OSLP treatment groups (250, 500 and 1000 μg/mL) were captured with Olympus CKX41 inverted trinocular microscope connected to Olympus UIS2 optical system camera and AnalySIS 1.5 software.

2.4. Protein expression study

2.4.1. Protein expression profiling with mass spectrometry-based label-free quantitative proteomics (LFQ)

OSLP was prepared in a concentration of 10 mg/mL (as mother stock) and then was twofold diluted to 250, 500, and 1000 μg/mL in fresh growth medium (DMEM with 1% FBS and 1% Pen/Strep). SH-SY5Y cells ($1x10^6$) were seeded in 6-well plates. The cells were assigned to 5 groups (Table 2). The three treatment groups were pre-treated with freshly prepared OSLP and incubated for 24-hour (37°C, 5% CO_2, 95% air). Following that, they were induced by 150 μM of H_2O_2 for another 24-hour and returned to incubation (37°C, 5% CO_2, 95% air). Upon complete incubation, all five experiment groups were subject to cell lysis for protein extraction in order to conduct mass spectrometry-based label-free quantitative proteomics (LFQ). All experiments were 3 independent biological replicates performed.

Table 2. Experiment groups in the protein expression study.

Group	Treatment
NC	Normal control (untreated cells)
H_2O_2	H_2O_2 induction (150 μM H_2O_2)
250	OSLP 250 μg/mL + 150 μM H_2O_2
500	OSLP 500 μg/mL + 150 μM H_2O_2
1000	OSLP 1000 μg/mL + 150 μM H_2O_2

Remark: H_2O_2, hydrogen peroxide; OSLP, *Orthosiphon stamineus* leaf proteins.

2.4.2. Protein extraction from SH-SY5Y cells

After aspirating the media, cells were treated with TrypLE™ Express, incubated and rinsed with pre-cooled 1X PBS. The content was collected into individual sterile ProtLoBind microtubes and centrifuged (500 x g, 4°C; 10 min). The produced supernatant was discarded but the soft, transparent pellet was collected and lysed with ice-cold lysis buffer (200 µL of RIPA, protease inhibitor 20% v/v, phosphatase inhibitor 1% v/v) and incubated (4°C; 20 min). Following that, the cell suspension was homogenised using an ultrasonic cell crusher and then briefly centrifuged (2000 x g, 4°C; 10 min). Proteins extracted were collected into new, individual sterile ProtLoBind microtubes and were concentrated using a speed-vacuum concentrator (300 rpm; 24 h; 60°C) before storage at -152°C for subsequent analysis.

2.4.3. Protein estimation by Bradford protein assay

Protein concentration was estimated using Quick Start™ Bradford Protein Assay following the instructions of the manufacturer. Briefly, 5µL of sample or standard was loaded onto a 96-well plate in triplicate. This was followed by adding 250 µL of dye reagent into each well. The plate was incubated at room temperature (25 - 27°C; 5 min). Absorbance was read at 595 nm with Bio-Rad Benchmark Plus Microplate Reader with Microplate Manager 5.2.1 software. Protein concentrations were determined from the standard curve.

2.4.4. In-solution digestion of proteins

In-solution protein digestion was performed as instructed (Mass Spec Grade Promega, USA). Protein samples were solubilised in 6M urea / 50 mM TRIS-HCl (pH 8.02) followed by the addition of 5 mM DTT (freshly prepared) and incubated in the dark (30 min; 37°C). Next, 15 mM IAA (freshly prepared) was added and incubated in the dark (30 min; r.t.). The reduced and alkylated protein solutions were diluted sixfold with 50 mM TRIS-HCl (pH 8.02). Following that, 20 µg of crude protein was digested by Trypsin/Lys-C Mix (ratio 25 protein:1 protease; w/w) buffered in 50 mM TRIS-HCl (pH 8.02) and then incubated in the dark (overnight; 37°C). Formic acid (1%) was added to halt the enzymatic reaction. Following that, all the samples were subjected to centrifugation (16,000 x g; 4°C; 10 min). The supernatant produced was collected and concentrated using a speed-vacuum concentrator (300 rpm; 24 hr; 60°C). Formic acid (10 µL of 0.1%) was added into all the sample tubes followed by brief vortexing and centrifugation.

2.4.5. De-salting of proteins

Each protein biological replicate was independently de-salted using modified instructions for the Pierce®C18 mini spin column. Every mini spin column was firstly activated using a 50% ACN solution (repeated thrice, r.t.) and equilibrated using a 0.5% solution of TFA in 5% ACN (repeated thrice, r.t.). A 90 µL volume of protein was individually added into a 30 µL solution of sample buffer (2% of TFA in 20% of ACN) and momentarily vortexed at a speed of 2,200 rpm to ensure proper mixing. This step was repeated individually for each protein biological replicate. Next, each them was loaded onto individual sterile mini spin column for de-salting (repeated thrice, r.t.). Subsequently, each protein biological replicate was washed using a 0.5% solution of TFA in 5% ACN (repeated thrice, r.t.). Finally, each protein biological replicate was eluted using a 70% solution of ACN (repeated thrice, r.t.) and all the produced flow-through was collected, vacuum-concentrated (300 rpm; 24 h; 60°C) and was then stored at -20°C for mass spectrometry-based LFQ at a later date.

2.4.6. Mass spectrometry-based label-free quantitative proteomics (LFQ) using Nanoflow-ESI-LCMS/MS

An Agilent C-18 300Å Large Capacity Chip was used to load the previously de-salted peptides. The column was equilibrated using a 0.1% solution of formic acid in water (Solution 1) and the

peptides were eluted using an increasing gradient of 90% acetonitrile in a 0.1% solution of formic acid (Solution 2) using the following gradient, 3-50% Solution B from 0-30 min, 50-95% Solution 2 from 30-32 min, 95% Solution 2 from 32-39 min and 95-3% Solution B from 39-47 min. The Q-TOF settings were as follows: positive polarity, fragmentor voltage at 300 V, capillary voltage at 2050 V, drying gas at a flow rate of 5 L/min and a 300°C gas temperature. Auto MS/MS mode was used to anaylse the intact protein with a range of 110-3000 m/z for the MS scan and a 50-3000 m/z range for the MS/MS scan. The Agilent MassHunter data acquisition software was used to perform the spectrum analysis.

2.4.7. Peptide and protein identification by automated *de novo* sequencing and LFQ analysis

Automated *de novo* sequencing protein identification was carried out with Version 8.0 of PEAKS®Studio. The UniProtKB database (Organism: *Homo sapiens*) (https://www.uniprot.org/proteomes/UP000005640, 163,191 proteins; last modified March 13, 2018) was used to identify the peptides and proteins as well as conduct homology searching via comparison of the *de novo* sequence tag, using the following settings: trypsin cleavage, a parent mass and a precursor mass tolerance of 0.1 Da, minimum ratio count of 2, maximum variable post-translational modification of 3, carbamidomethylation as fixed modification with maximum missed cleavage of 3, mass error tolerance of 20.0 ppm and other parameters as default settings of Agilent. The false discovery rate (FDR) threshold was set at 1% and protein score of -10lgP > 20 was used to filter out proteins that were inaccurate. The PEAKS® software indicated that a protein score of -10lgP> 20 has a relatively high confidence as it targets very few decoy matches above the threshold.

The differentially expressed proteins were identified using LFQ analysis using the following settings: significance score ≥ 13, protein fold change ≥ 1, number of unique peptides ≥ 1 and an FDR threshold of ≤ 1%. PEAKSQ indicated that a significance score of ≥ 13 is equal to a significance value of $p < 0.05$. All other parameters were kept at the default settings set by Agilent.

2.5. Bioinformatics analysis

Using bioinformatics analysis (functional annotations, protein-protein interactions and systemic pathway enrichment analysis) of the identified differentially expressed proteins, the proteins were analysed and matched using the GO Consortium, Ensemble (http://www.ensembl.org/*Homo_sapiens*) and Reactome Database (Release 72; Organism: *Homo sapiens*) online databases.

2.6. Statistical Analysis

Statistical analysis was carried out using version 5.0 of GraphPad Prism. The data obtained from the *in vitro* assays were expressed using the notation of mean ± standard error of the mean (SEM). One-way ANOVA followed by the Dunnett's *post-hoc* test was used to compare data between the control and treated groups using the significance levels of $*p < 0.5$, $**p < 0.01$ and $***p < 0.001$. The built-in statistical tool of PEAKS® software (PEAKSQ statistical analysis) was used to analyse the identified differentially expressed proteins. A 13% significance score of (which is equal to a significance level of 0.05) and an FDR of ≤ 1% was considered to be statistically significant. In the bioinformatics analysis, the hypergeometric test followed by Benjamini & Hochberg FDR correction at a p value < 0.05 (built-in BiNGO statistical tool) was used to correlate the functional annotation of genes with their interacting proteins; overrepresentation analysis of pathways was tested with hypergeometric distribution followed with Benjamani-Hochberg method corrected at p value < 0.05 (Reactome Pathway Browser version 3.7 built-in statistical tool). Overrepresentation analysis of Reactome pathways was used to predict the possible associations of systemic pathways with their interacting proteins and genes [17].

3. Results

3.1. Growth evaluation of SH-SY5Y cells at different seeding density

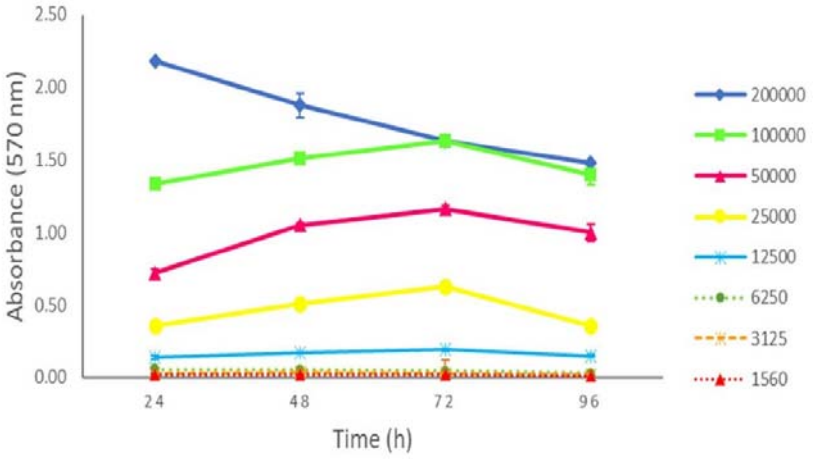

Figure 1. Growth curve of SH-SY5Y cells at different seeding density. Data shown are presented as 3 independent experiments performed in triplicate.

Cell density ranging from 50000 cells per well demonstrated an increased growth pattern from 24-h to 72-h, and came to a steady decrease after 72 hours (Figure 1). Cell density at 25000 cells per well demonstrated an increased growth pattern after 24-h, continued to 48- and 72-h but had a steep decrease after 72 hours. Cell density below 25000 cells per well did not demonstrate increase in the growth pattern after 24-h. Cell density at 200000 cells per well demonstrated a decline in the growth pattern after 24-h. Cell density at 100000 cells per well had shown an absorbance value higher than 1.50. According to ATCC, the number of cells to use in an assay should yield an absorbance of 0.75 - 1.25. Therefore, seeding density at $5x10^4$ cells per well was used in the subsequent viability and neuroprotection assays.

3.2. Evaluation of cytotoxic effects of OSLP on SH-SY5Y cells (24- and 48-hour)

After 24-hr of incubation, significant cytotoxic effects of OSLP were not observed at concentrations below 4000 μg/mL when compared to the NC ($F=251.7$; $p > 0.05$; Figure 2). Cytotoxic effects were apparent when the SH-SY5Y cells were treated with 4000 μg/mL of OSLP (95±1%). This slight reduction however did not attain any statistical significance when compared to the NC ($F=251.7$; $p > 0.05$; Figure 2). In contrast, treatment with 1 mg/mL of OSLP was found to result in a significant decrease, about 52±2%, when compared to the NC ($F=251.7$; ^^^$p < 0.001$; Figure 2).

After 48-hour of incubation, significant cytotoxic effects of OSLP were not observed at concentrations below 2000 μg/mL when compared to the NC ($F=106.6$; $p > 0.05$; Figure 2). Significant cytotoxic effects of OSLP were apparent at concentrations above 2000 μg/mL when compared to the NC ($F=106.6$; $^{**}p < 0.01$; Figure 2). At 2000 μg/mL of OSLP, the cell viability significantly decreased to 84±4% ($F=106.6$; $^{**}p < 0.01$; Figure 2). and declined further to 68±0.5% at 4000 μg/mL of OSLP ($F=106.6$; $^{***}p < 0.001$; Figure 2). A significant plunge, about 84±2%, in SH-SY5Y cell population was observed at 1 mg/mL of OSLP treatment ($F=106.6$; $^{***}p < 0.001$; Figure 2). This indicates that 1 mg/mL of OSLP exerted significant cytotoxic effects on the survival of SH-SY5Y cells.

From the graph plotted (Figure 2), the MNTD of OSLP at 24-h treatment was determined as approximately 2000 μg/mL whilst the MTD of OSLP at 24-h treatment was approximately 4000

μg/mL. In contrast, the MNTD of OSLP at 48-h treatment was determined as approximately 1000 μg/mL whereas the MTD of OSLP at 48-h treatment was approximately 2000 μg/mL.

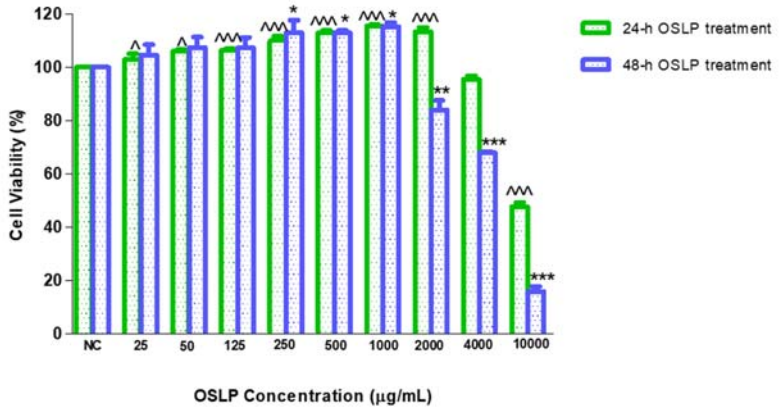

Figure 2. Cytotoxic effects of OSLP on SH-SY5Y cells at 24- and 48-hr. Data shown are presented as mean ± SEM of 3 independent experiments performed in triplicate. ^^^showed $p < 0.001$ against the untreated group (NC, 24-h). ***showed $p < 0.001$ against the untreated group (NC, 48-h). One-way ANOVA with Dunnett's *post-hoc* test.

3.3. Hydrogen peroxide (H_2O_2) induction and determination of half-maximal inhibitory concentration (IC_{50})

As depicted in **Figure 3**, exposure to 50 to 350 μM of H_2O_2 decreased the cell population in a concentration-dependent manner. The cell viability (%) decreased when H_2O_2 concentrations increased. When compared to the NC, 50 - 100 μM of H_2O_2 did not significantly inhibit SH-SY5Y cell growth ($F=105.6$; $p > 0.5$; Figure 3) but 150 - 350 μM of H_2O_2 had significantly inhibit SH-SY5Y cell growth ($F=105.6$; $^{***}p < 0.001$; Figure 3). At about 150 μM of H_2O_2, the cell viability was reduced significantly to 42±6% ($F=105.6$; $^{***}p < 0.001$) and further declined significantly to 34±3% ($F=105.6$; $^{***}p < 0.001$) when the concentration increased to 200 μM growth. Following that, cell viability tumbled steeply to 11±0.4%, 3±0.5% and 5±0.2%, when H_2O_2 induction increased to 250, 300 and 350 μM respectively ($F=105.6$; $^{***}p < 0.001$). From the graph plotted (Figure 3), the IC_{50} of H_2O_2 was determined as approximately 150 μM whilst the IC_{90} of H_2O_2 was determined as 250 μM and above.

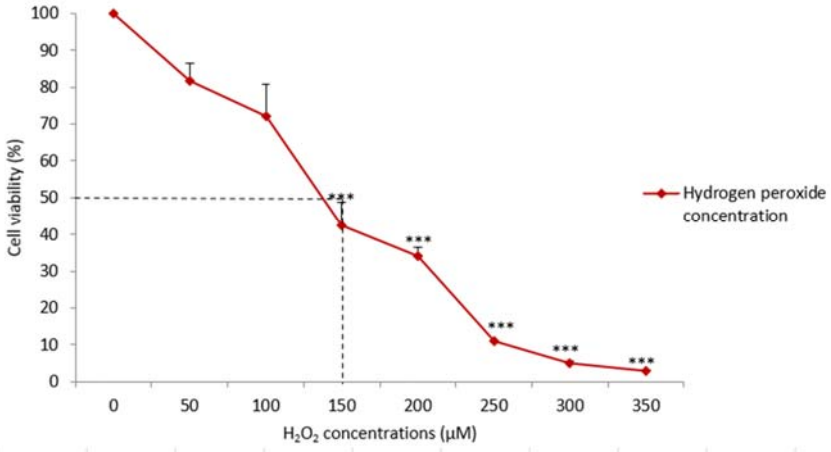

Figure 3. Cell viability of SH-SY5Y cells induced by H_2O_2. SH-SY5Y cells were treated with 0 - 350 μM H_2O_2. Data shown are presented as mean ± SEM of 3 independent experiments performed in triplicate. ***showed $p < 0.001$ against the untreated group (NC, 24-h). One-way ANOVA with Dunnett's *post-hoc* test.

3.4. Evaluation of OSLP protective effects on SH-SY5Y cells

From the graph plotted (Figure 4), H_2O_2 induction (negative control, 150 μM) had significantly declined the SH-SY5Y cell viability (43±5%; F=17.9; ***$p < 0.001$) when compared to the NC. OSLP at these two concentrations, 25 μg/mL (38±2%; F=17.9; $p > 0.5$) and 50 μg/mL (42±5%; F=17.9; $p > 0.5$), did not show significant protection against H_2O_2 induction. At 125 μg/mL, OSLP had increased the cell viability, with about 30% increase when compared to the H_2O_2 group (61±9%; F=17.9; $p > 0.5$). OSLP at 250 μg/mL had significantly increased the SH-SY5Y cell viability (71±12%; F=17.9; *$p < 0.01$) when compared to the H_2O_2 group. An increase of 39% in cell viability was recorded. OSLP at these two concentrations, 500 μg/mL (88±6%; F=17.9; ***$p < 0.001$) and 1000 μg/mL (101±2%; F=17.9; ***$p < 0.001$), had significantly increased the SH-SY5Y cell viability when compared to the H_2O_2 group. OSLP at 500 μg/mL had about 51% increase whilst OSLP at 1000 μg/mL had about 57% increase in the cell viability.

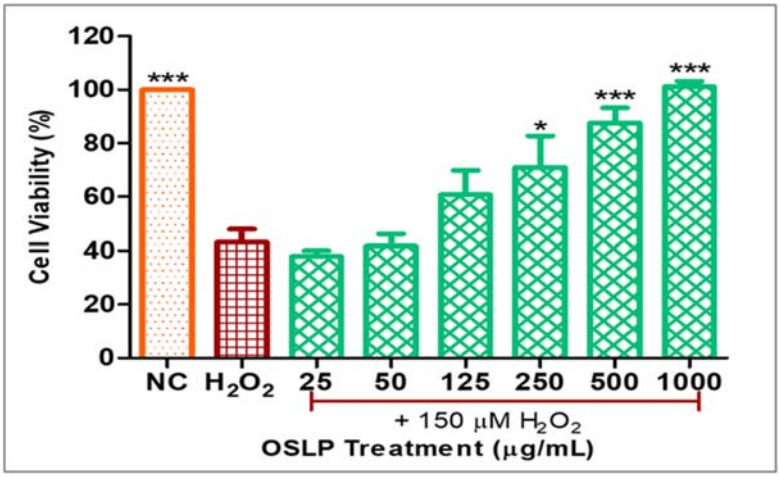

Figure 4. OSLP protective effects on H_2O_2-induced SH-SY5Y cells. Data shown are presented as mean ± SEM of 3 independent experiments performed in triplicate. ***showed $p < 0.001$ against the negative control group (H_2O_2, 150 μM). One-way ANOVA with Dunnett's *post-hoc* test.

3.4.1. Microscopic examination using bright-field imaging

Figure 5 displays the representative bright-field microscopic images of the SH-SY5Y cells. The NC displayed normal cell architecture with pyramidal-shaped cells having apparent neurites (a, blue arrows). SH-SY5Y cells induced by 150 μM of H_2O_2 had shown disrupted cell architecture with clusters of clumping cells and reduced neurites (b, red arrows) compared to the normal control (NC) which received no OSLP treatment and H_2O_2 induction (a, blue arrows). Pre-treatment with OSLP at 250, 500 and 1000 μg/mL had seen improvements in the cell architecture with reduced clumping cells and restored the neuronal cell shapes with clear neurites (c-e, orange arrows) when compared to the negative control (H_2O_2,150 μM). The cell population was also markedly declined in the negative control but pre-treatments with OSLP had increased cell growth.

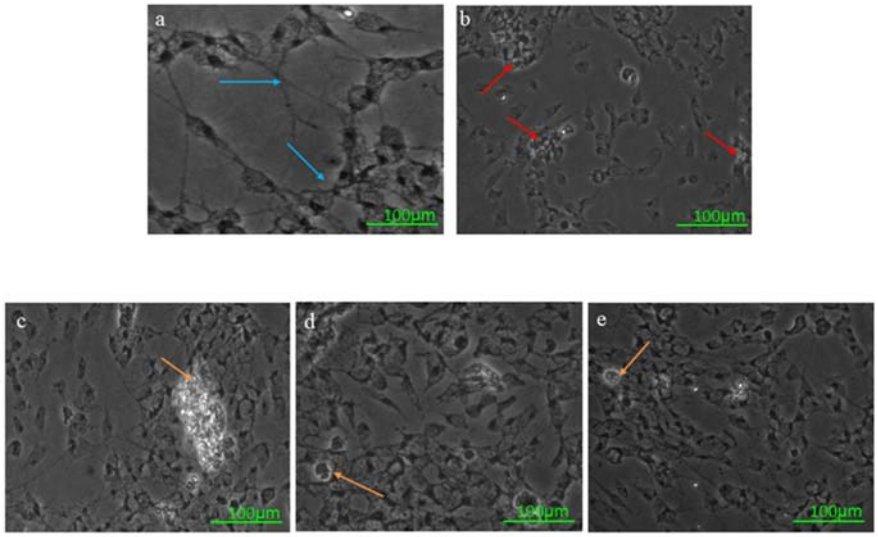

Figure 5. Representative bright-field microscopic images of SH-SY5Y cells. Upper row: (a) Normal Control (NC, without OSLP treatment and H_2O_2 induction) displays pyramidal-shaped cells showing clear neurites (blue arrows) and did not cluster; (b) H_2O_2 (induced by 150 µM of H_2O_2) shows disrupted neuronal cell shapes with many clumping cells (red arrows) and reduced neurites also declined population. Lower row: (c - e) OSLP treatment groups, 250, 500 and 1000 µg/mL respectively. OSLP treatments reduced clumping cells and restored the neuronal cell shapes with clear neurites seen (orange arrows). Scale bar = 100 µm.

3.5. Protein expression study

Proteins were extracted from the normal control (NC, SH-SY5Y cells without OSLP treatment and H_2O_2 induction), H_2O_2 (150 µM H_2O_2 Only) and three OSLP treatment groups (250 µg/mL+150 µM H_2O_2, 500 µg/mL+150 µM H_2O_2 and 1000 µg/mL+150 µM H_2O_2). The protein samples were subjected to mass spectrometry-based label-free quantitative proteomic (LFQ) using nanoflow-ESI-LCMS/MS and subsequent bioinformatics analysis. As for the final results and discussion, only these two pairs were used: Pair A, H_2O_2 (150 µM H_2O_2 Only) versus normal control (without OSLP treatment and H_2O_2 induction) and Pair B, H_2O_2 (150 µM H_2O_2 Only) versus OSLP treatment (OSLP 1000 µg/mL+150 µM H_2O_2). The highest dose of OSLP was chosen to elucidate its maximal protective effects on SH-SY5Y cells induced by H_2O_2.

3.5.1. Protein expression analysis with mass spectrometry-based quantitative label-free proteomics (LFQ)

LFQ has profiled 32 differentially expressed proteins of which 22 were identified in Pair A (H_2O_2 vs. NC) and 10 were identified in Pair B (H_2O_2 vs. Treatment) (Figure 6, Table 3 & 4).

In Pair A (H_2O_2 vs. NC), all the proteins were found expressed at higher levels in the H_2O_2-treated than in the NC. Whereas, in Pair B (H_2O_2 vs. Treatment), seven proteins were expressed at lower levels in the OSLP-treated group than in the H_2O_2-treated. They were keratin, type II cytoskeletal 8 (KRT8, P05787), heat shock cognate 71 kDa protein (HSPA8, P11142), 60S ribosomal protein L14 (RPL14, P50914), beta-galactosidase-1-like protein (GLB1L, Q6UWU2), keratin, type I cytoskeletal 19 (KRT19, P08727), creatine kinase B-type (CKB, P12277) and heat shock protein HSP 90-alpha (HSP90AA1, P07900). The others, namely heterogeneous nuclear ribonucleoprotein U (HNRNPU, Q00839), 60S ribosomal protein L24 (RPL24, P83731) and stathmin (STMN1, P16949) were expressed at higher levels in the OSLP-treated group than in the H_2O_2-treated (Figure 6, Table 3 & 4). Additionally, four proteins were found expressed in both pairs (Figure 7). They were heat shock cognate 71 kDa protein (HSPA8, P11142), keratin, type II cytoskeletal 8 (KRT8, P05787), keratin, type I cytoskeletal 19 (KRT19, P08727) and heat shock protein HSP 90-alpha (HSP90AA1, P07900).

Interestingly, these proteins were found expressed at lower levels in both NC and OSLP-treated groups (Figure 6).

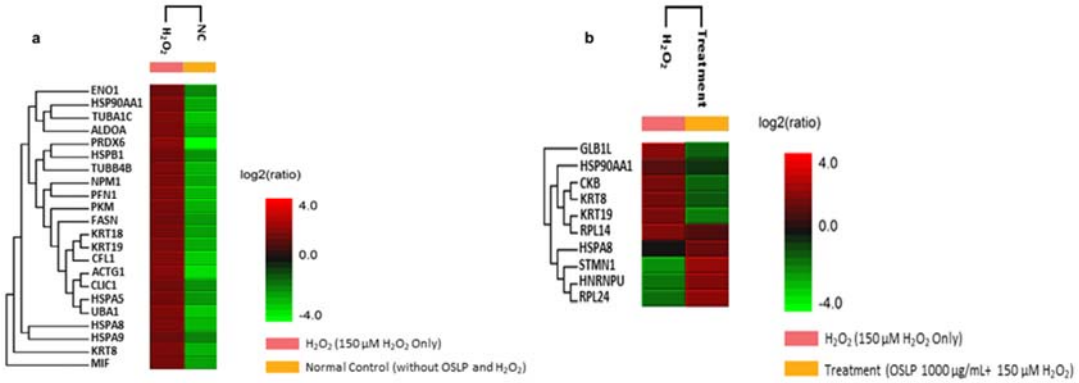

Figure 6. Heat map displays the differentially expressed proteins identified from (a) Pair A: H_2O_2 (150 µM H_2O_2 only) versus NC (normal control without OSLP treatment and H_2O_2 induction) and (b) Pair B: H_2O_2 (150 µM H_2O_2 only) versus OSLP treatment (OSLP 1000 µg/mL+150 µM H_2O_2), n = 3, significance ≥ 13, FDR ≤ 1%, fold change ≥ 1, number of unique peptide ≥ 1. Protein names are listed on the left while experimental groups are indicated on top. The colour key on the bottom right indicates the log2 (ratio) expression levels (green = low, red = high).

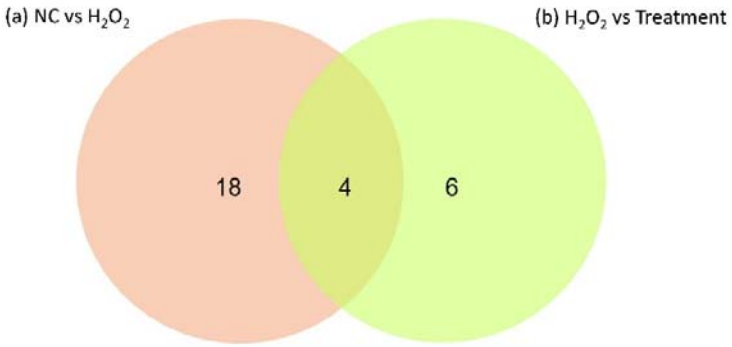

Figure 7. A two-way Venn diagram depicts the differentially expressed proteins identified from (a) Pair A: H_2O_2 (150 µM H_2O_2 only) versus NC (normal control without OSLP treatment and H_2O_2 induction) and (b) Pair B: H_2O_2 (150 µM H_2O_2 only) versus OSLP treatment (OSLP 1000 µg/mL+150 µM H_2O_2), n = 3. As shown, a total of 32 differentially expressed proteins are identified with 4 are overlaps between the two pairs, 18 are identified in Pair A and 6 are in Pair B.

394 **Table 3.** Differentially expressed proteins identified from Pair A (H_2O_2 vs. NC).

Uniprot Accession ID	Uniprot Protein Name	Significance (≥ 13)	Coverage (%)	#Peptides	#Unique	Avg. Mass	Group Profile (ratio of NC/H_2O_2)	Ensembl Protein
P11142	Heat shock cognate 71 kDa protein	34.31	16	7	5	67980	0.34:1.00	HSPA8
P04075	Fructose-bisphosphate aldolase A	24.61	25	5	5	39818	0.20:1.00	ALDOA
P68371	Tubulin beta-4B chain	24.00	15	5	1	49831	0.12:1.00	TUBB4B
P05787	Keratin, type II cytoskeletal 8	23.26	63	31	15	53704	0.20:1.00	KRT8
O00299	Chloride intracellular channel protein 1	23.2	8	1	1	26794	0.02:1.00	CLIC1
P06733	Alpha-enolase	22.22	23	7	7	47169	0.28:1.00	ENO1
P05783	Keratin, type I cytoskeletal 18	20.41	63	19	17	48030	0.16:1.00	KRT18
P38646	Stress-70 protein, mitochondrial	20.12	13	6	6	72401	0.20:1.00	HSPA9
P04792	Heat shock protein beta-1	19.50	40	6	6	22783	0.15:1.00	HSPB1
P23528	Cofilin-1	18.80	28	4	4	22728	0.17:1.00	CFL1
P07737	Profilin-1	18.10	46	5	5	15054	0.25:1.00	PFN1
P14618	Pyruvate kinase PKM	17.35	18	6	3	57937	0.23:1.00	PKM/PK3
P30041	Peroxiredoxin-6	16.95	21	1	1	11161	0.18:1.00	PRDX6
P22314	Ubiquitin-like modifier-activating enzyme 1	16.61	3	2	2	117849	0.10:1.00	UBA1
P63261	Actin, cytoplasmic 2	16.55	33	11	1	41793	0.07:1.00	ACTG1
P49327	Fatty acid synthase	16.33	3	4	4	273424	0.29:1.00	FASN
Q9BQE3	Tubulin alpha-1C chain	15.94	18	7	7	57730	0.26:1.00	TUBA1C
P14174	Macrophage migration inhibitory factor	14.39	10	1	1	12476	0.11:1.00	MIF
P08727	Keratin, type I cytoskeletal 19	13.91	34	10	8	44106	0.15:1.00	KRT19
P07900	Heat shock protein HSP 90-alpha	13.79	12	6	3	68372	0.36:1.00	HSP90AA1
P11021	Endoplasmic reticulum chaperone BiP	13.35	7	3	2	66914	0.17:1.00	HSPA5
P06748	Nucleophosmin	13.27	15	2	2	28400	0.21:1.00	NPM1

395 Remark: Ensembl Human Database (https://asia.ensembl.org/Homo_sapiens/Info/Index, accessed from 09/11/2018) were used to search for the Ensembl protein
396 nomenclatures.

397

398 **Table 4.** Differentially expressed proteins identified from Pair B (H_2O_2 vs. Treatment).

Uniprot Accession ID	Uniprot Protein Name	Significance (≥ 13)	Coverage (%)	#Peptides	#Unique	Avg. Mass	Group Profile (ratio of H_2O_2/treatment)	Ensembl Protein
Q00839	Heterogeneous nuclear ribonucleoprotein U	31.91	2	1	1	67980	1.00:1.72	HNRNPU
P05787	Keratin, type II cytoskeletal 8	25.07	69	41	20	39818	1.00:0.44	KRT8
P11142	Heat shock cognate 71 kDa protein	18.72	21	11	2	49831	1.00:0.94	HSPA8
P83731	60S ribosomal protein L24	16.92	11	1	1	53704	1.00:2.79	RPL24
P50914	60S ribosomal protein L14	16.33	6	1	1	26794	1.00:0.58	RPL14
P16949	Stathmin	15.88	15	2	2	47169	1.00:2.24	STMN1
Q6UWU2	Beta-galactosidase-1-like protein	15.63	2	1	1	48030	1.00:0.38	GLB1L
P08727	Keratin, type I cytoskeletal 19	14.96	43	14	12	72401	1.00:0.27	KRT19
P12277	Creatine kinase B-type	14.25	12	2	2	22783	1.00:0.41	CKB
P07900	Heat shock protein HSP 90-alpha	13.00	20	11	3	22728	1.00:0.49	HSP90AA1

399 Remark: Ensembl Human Database (https://asia.ensembl.org/Homo_sapiens/Info/Index, accessed from 09/11/2018) were used to search for the Ensembl protein
400 nomenclatures.

3.5.2. Bioinformatics analysis

The differentially expressed proteins were also studied using functional annotation analysis to identify and visualise the cellular component, molecular function and biological process of the differentially expressed proteins. The top ten enriched terms in all three categories were selected to elucidate the association between OSLP protection and H_2O_2 stress (Figure 8).

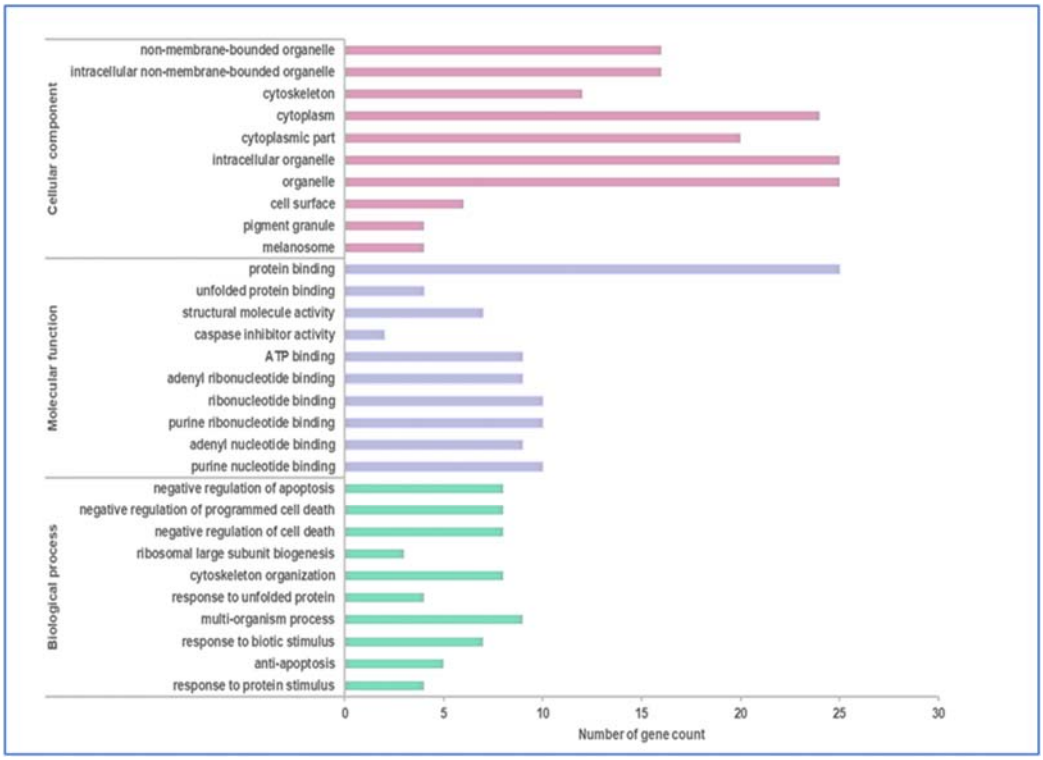

Figure 8. Classification of the top 10 enriched terms in cellular component, molecular function and biological process annotated by BiNGO (Organism: *Homo sapiens*). Hypergeometric test with Benjamini & Hochberg False Discovery Rate (FDR) correction at $p < 0.05$.

The differentially expressed proteins were found to localise at cellular components including non-membrane-bounded organelle (GO:43228), intracellular non-membrane-bounded organelle (GO:43232), cytoskeleton (GO:5856), cytoplasm (GO:5737), cytoplasmic part (GO:44444), intracellular organelle (GO:43229), organelle (GO:43226), cell surface (GO:9986), pigment granule (GO:48770) and melanosome (GO:42470) (Figure 9).

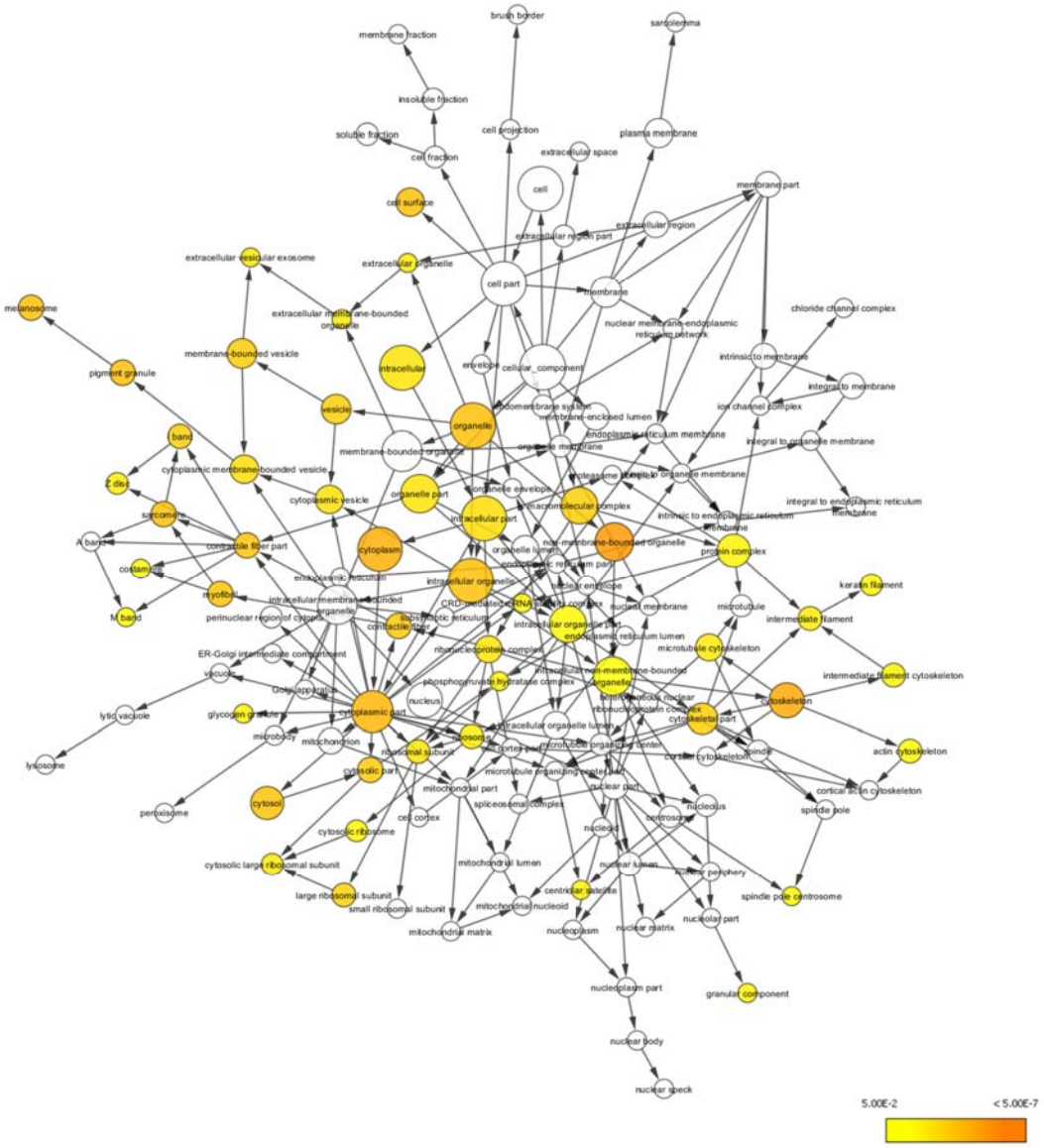

Figure 9. BiNGO result for cellular component as visualised in Cytoscape (Organism: *Homo sapiens*). Coloured nodes indicate significant overrepresentions. White nodes indicate insignificant overrepresention and they are included to show the coloured nodes in the context of the GO hierarchy. Colour key on the bottom right indicates the significance level of overrepresentation.

At these cellular localisations, the interactions of the differentially expressed proteins have been networked to an array of molecular functions involving in protein binding (GO:5515), unfolded protein binding (GO:51082), structural molecule activity (GO:5198), caspase inhibitor activity (GO:43027), ATP binding (GO:5524), adenyl ribonucleotide binding (GO:32559), ribonucleotide binding (GO:32553), purine ribonucleotide binding (GO:32555), adenyl nucleotide binding (GO:30554) and purine nucleotide binding (GO:17076) (Figure 10).

These molecular functions were found to involve in a myriad of biological processes encompassing negative regulation of apoptosis (GO:43066), negative regulation of programmed cell death (GO:43069), negative regulation of cell death (GO:60548), ribosomal large subunit biogenesis (GO:42273), cytoskeleton organisation (GO:7010), response to unfolded protein (GO:6986), multi-organism process (GO:51704), response to biotic stimulus (GO:9607), anti-apoptosis (GO:6916) and response to protein stimulus (GO:51789) (Figure 11).

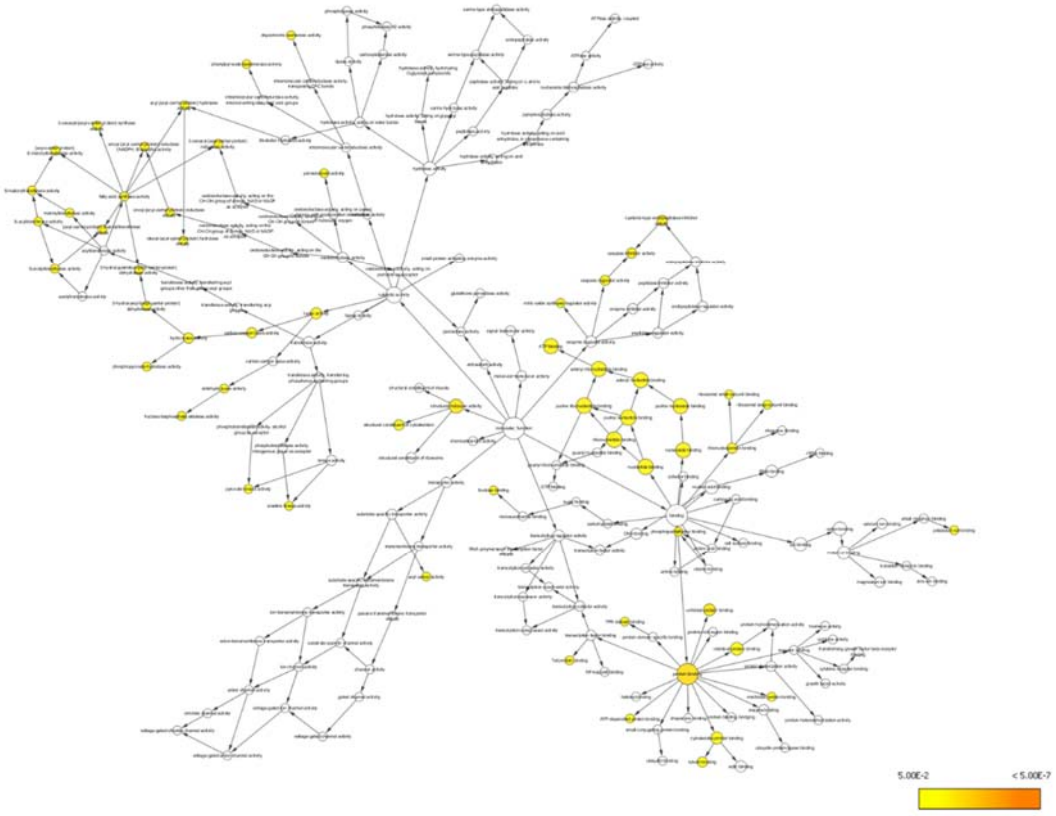

Figure 10. BiNGO results for molecular function as visualised in Cytoscape (Organism: *Homo sapiens*). Coloured nodes indicate significant overrepresentions. White nodes indicate insignificant overrepresention and they are included to show the coloured nodes in the context of the GO hierarchy. Colour key on the bottom right indicates the significance level of overrepresentation.

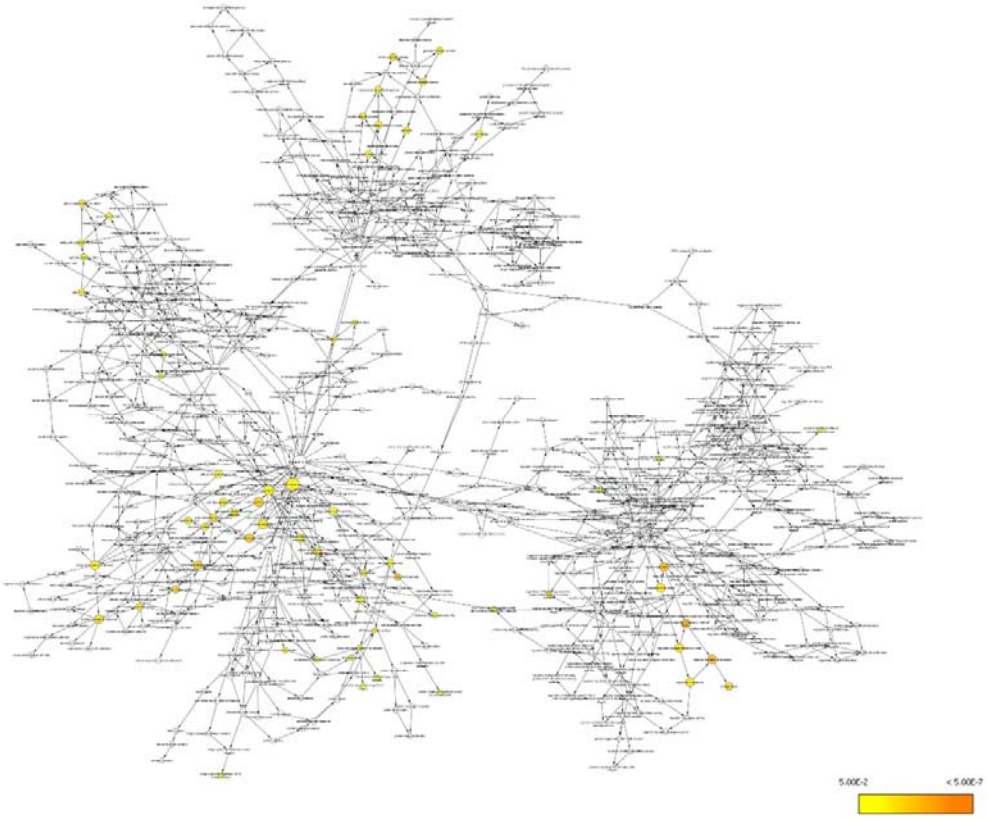

Figure 11. BiNGO results for biological process as visualised in Cytoscape (Organism: *Homo sapiens*). Coloured nodes indicate significant overrepresentions. White nodes indicate insignificant overrepresention and they are included to show the coloured nodes in the context of the GO hierarchy. Colour key on the bottom right indicates the significance level of overrepresentation.

Systematic pathway enrichment analysis

Reactome Pathways has found the differentially expressed proteins to significantly associate with 80 pathways (See Supplementary Data Pair A). Among, 25 pathways are predicted to have the highest relevance ($p < 0.05$, Figure 12). These pathways were associated with 11 top-level pathway hierarchies, namely signal transduction, vesicle-mediated transport, cellular responses to external stimuli, metabolism of proteins, cell cycle, neuronal system, autophagy, metabolism, developmental biology, haemostasis and immune system (Table 5). At sub-level pathway hierarchy, they were seen involved in the signalling by Rho GTPases membrane trafficking, cellular responses to stress and HSF1-dependent transactivation, protein folding and post-translational protein modification, mitotic cell cycle, post NMDA receptor activation events and activation of NMDA receptors and postsynaptic events, macroautophagy, metabolism of glucose and carbohydrates, nervous system development, response to elevated platelet cytosolic Ca^{2+} and innate immune system (Table 5).

In particular, to predict the protective mechanism of OSLP against H_2O_2 stress, the differentially expressed proteins in Pair B (H_2O_2 vs. OSLP treatment) were analysed exclusively by Reactome Pathways. As per the analysis, the protein expression has a significant association with the ten most relevant pathways ($p < 0.05$, Figure 13) out of 56 pathways identified (See Supplementary Data Pair B). They were interleukin-4 and Interleukin-13 signalling (R-HSA-6785807), attenuation phase (R-HSA-3371568), formation of the cornified envelope (R-HSA-6809371), HSF1-dependent transactivation (R-HSA-3371571), HSP90 chaperone cycle for steroid hormone receptors (R-HSA-3371497), keratinisation (R-HSA-6805567), influenza viral RNA transcription and replication (R-HSA-168273), resistance of ERBB2 KD mutants to sapitinib (R-HSA-9665244), resistance of ERBB2 KD mutants to trastuzumab (R-HSA-9665233) and resistance of ERBB2 KD mutants to afatinib (R-HSA-

467 9665249). These pathways were associated with three top-level pathway hierarchies encompassing
468 immune system, cellular responses to external stimuli and developmental biology; two disease
469 pathways namely influenza infection and diseases of signal transduction by growth factor receptors
470 and second messengers (Table 6).

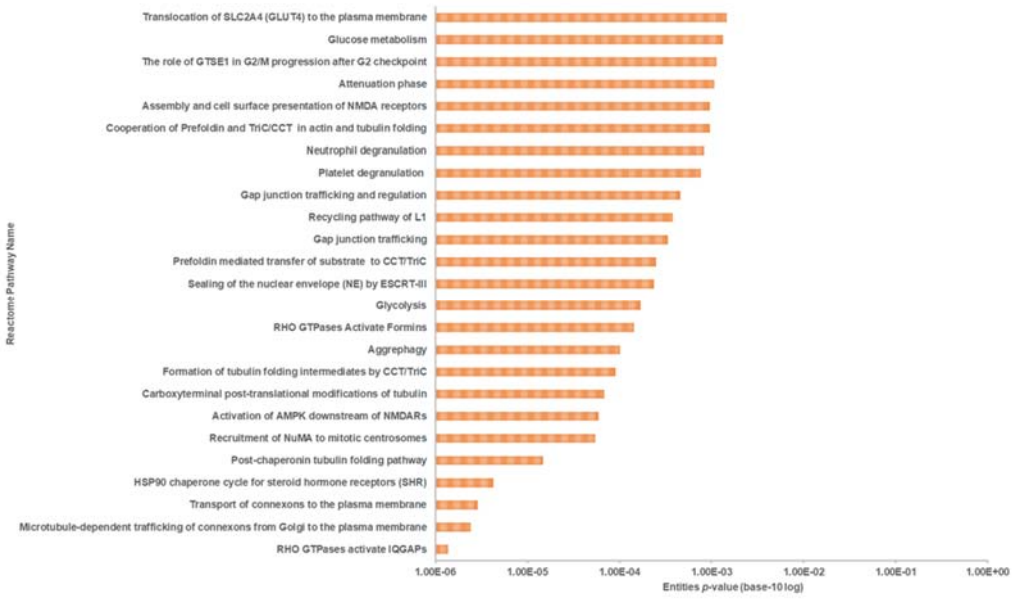

471

472 **Figure 12.** Classification of the 25 most relevant pathways sorted by False Discovery Rate (FDR)
473 correction at $p < 0.05$ in logarithmic scale (base 10) generated by Reactome Pathway Browser
474 (Organism: *Homo sapiens*).

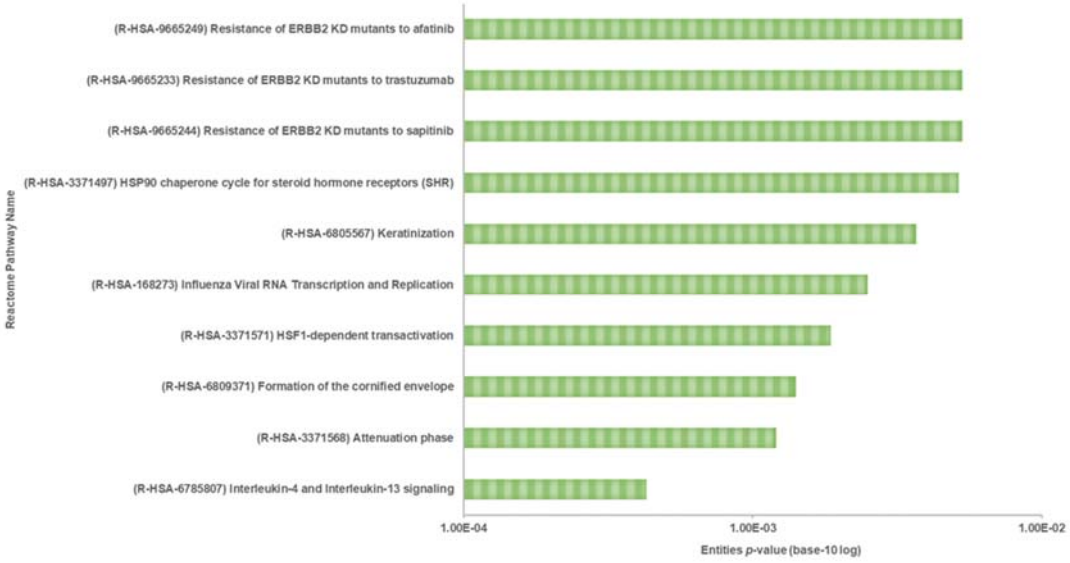

475

476 **Figure 13.** Classification of the 10 most relevant pathways sorted by False Discovery Rate (FDR)
477 correction at $p < 0.05$ in logarithmic scale (base 10) generated by Reactome Pathway Browser
478 (Organism: *Homo sapiens*).

479 **Table 5.** Pathway hierarchy of the 25 most relevant pathways. "Bold" indicates the top-level pathway
480 hierarchy; "bold and italic" indicates the sub-pathway hierarchy.

Reactome Pathway Name	Reactome Pathway Identifier	Entities *p*-value
Signal transduction		
Signalling by Rho GTPases		
RHO GTPases activate IQGAPs	R-HSA-5626467	1.38E-06
RHO GTPases Activate Formins	R-HSA-5663220	1.45E-04
Vesicle-mediated transport		
Membrane trafficking		
Microtubule-dependent trafficking of connexons from Golgi to the plasma membrane	R-HSA-190840	2.41E-06
Transport of connexons to the plasma membrane	R-HSA-190872	2.87E-06
Gap junction trafficking	R-HSA-190828	3.36E-04
Gap junction trafficking and regulation	R-HSA-157858	4.56E-04
Translocation of SLC2A4 (GLUT4) to the plasma membrane	R-HSA-1445148	0.001455
Cellular responses to external stimuli		
Cellular responses to stress		
HSP90 chaperone cycle for steroid hormone receptors (SHR)	R-HSA-3371497	4.24E-06
HSF1-dependent transactivation		
Attenuation phase	R-HSA-3371568	0.001068
Metabolism of proteins		
Protein folding		
Post-chaperonin tubulin folding pathway	R-HSA-389977	1.48E-05
Formation of tubulin folding intermediates by CCT/TriC	R-HSA-389960	9.10E-05
Prefoldin mediated transfer of substrate to CCT/TriC	R-HSA-389957	2.49E-04
Cooperation of Prefoldin and TriC/CCT in actin and tubulin folding	R-HSA-389958	9.66E-04
Post-translational protein modification		
Carboxyterminal post-translational modifications of tubulin	R-HSA-8955332	6.85E-05
Cell cycle		
Cell cycle, mitotic		
Recruitment of NuMA to mitotic centrosomes	R-HSA-380320	5.42E-05
Sealing of the nuclear envelope (NE) by ESCRT-III	R-HSA-9668328	2.37E-04
The role of GTSE1 in G2/M progression after G2 checkpoint	R-HSA-8852276	0.001135
Neuronal system		
Post N-methyl-D-aspartate (NMDA) receptor activation events		
Activation of AMPK downstream of NMDARs	R-HSA-9619483	5.89E-05
Activation of NMDA receptors and postsynaptic events		
Assembly and cell surface presentation of NMDA receptors	R-HSA-9609736	9.66E-04
Autophagy		
Macroautophagy		
Aggrephagy	R-HSA-9646399	1.02E-04
Metabolism		
Glucose metabolism		
Glycolysis	R-HSA-70171	1.70E-04
Metabolism of Carbohydrates	R-HSA-70326	0.001332
Glucose metabolism		
Developmental biology		
Nervous system development		
Recycling pathway of L1	R-HSA-437239	3.81E-04
Haemostasis		
Response to elevated platelet cytosolic Ca^{2+}		
Platelet degranulation	R-HSA-114608	7.68E-04
Immune system		
Innate immune system		
Neutrophil degranulation	R-HSA-6798695	8.23E-04

481
482

Table 6. Pathway hierarchy of the 10 most relevant pathways. "Bold" indicates the top-level pathway hierarchy; "bold and italic" indicates the sub-pathway hierarchy.

Reactome Pathway Name	Reactome Pathway Identifier	Entities *p*-value
Immune system		
Cytokine signalling in immune system		
Interleukin-4 and Interleukin-13 signalling	R-HSA-6785807	4.29E-04
Cellular responses to external stimuli		
Cellular responses to stress		
HSF1-dependent transactivation	R-HSA-3371571	0.001867
Attenuation phase	R-HSA-3371568	0.001204
HSP90 chaperone cycle for steroid hormone receptors (SHR)	R-HSA-3371497	0.005152
Developmental biology		
Keratinisation		
Formation of the cornified envelope	R-HSA-6809371	0.001410
Keratinisation	R-HSA-6805567	0.003672
Disease		
Influenza infection		
Influenza Viral RNA Transcription and Replication	R-HSA-168273	0.002496
Diseases of signal transduction by growth factor receptors & second messengers		
Resistance of ERBB2 KD mutants to sapitinib	R-HSA-9665244	0.0053
Resistance of ERBB2 KD mutants to trastuzumab	R-HSA-9665233	0.0053
Resistance of ERBB2 KD mutants to afatinib	R-HSA-9665249	0.0053

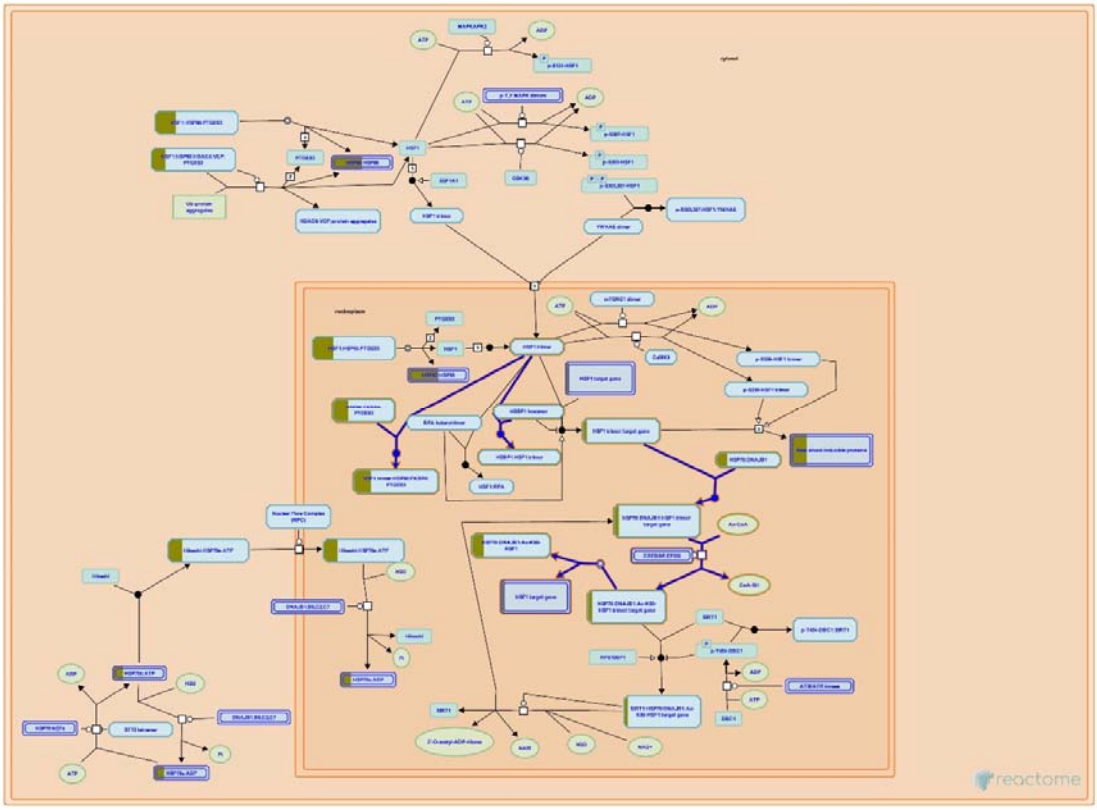

Figure 14. HSP90AA1 (aka Heat shock protein 90) and HSPA8 (aka Heat Shock Protein Family A (Hsp70) Member 8 or HSP70) highlighted in yellow were mapped onto the Attenuation Phase pathway sorted by False Discovery Rate (FDR) correction at $p < 0.05$ in logarithmic scale (base 10) generated by Reactome Pathway Browser (Organism: *Homo sapiens*).

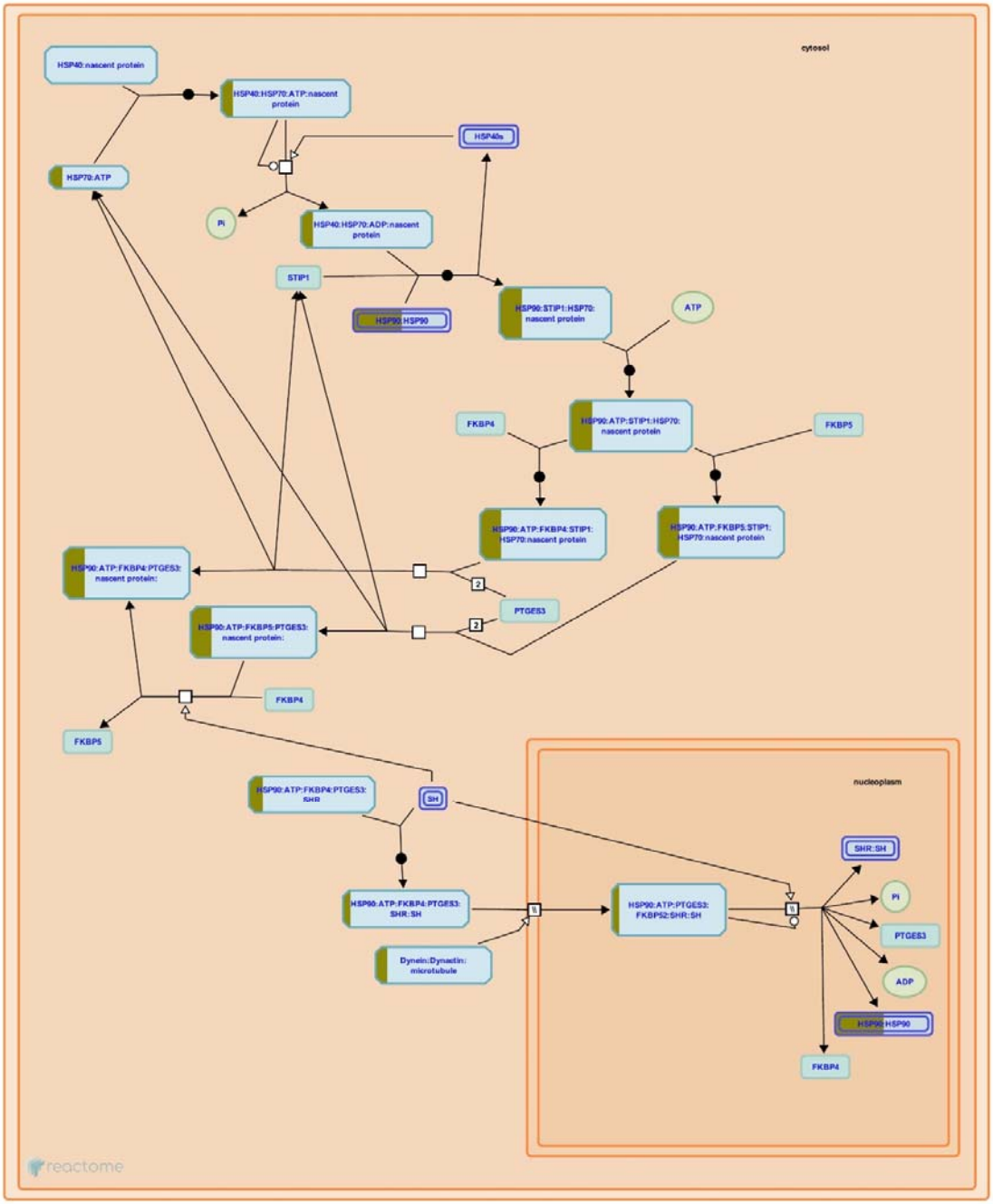

Figure 15. HSP90AA1 (aka Heat shock protein 90) and HSPA8 (aka Heat Shock Protein Family A (Hsp70) Member 8 or HSP70) highlighted in yellow were mapped onto the HSP90 chaperone cycle for steroid hormone receptors (SHR) pathway sorted by False Discovery Rate (FDR) correction at $p < 0.05$ in logarithmic scale (base 10) generated by Reactome Pathway Browser (Organism: *Homo sapiens*).

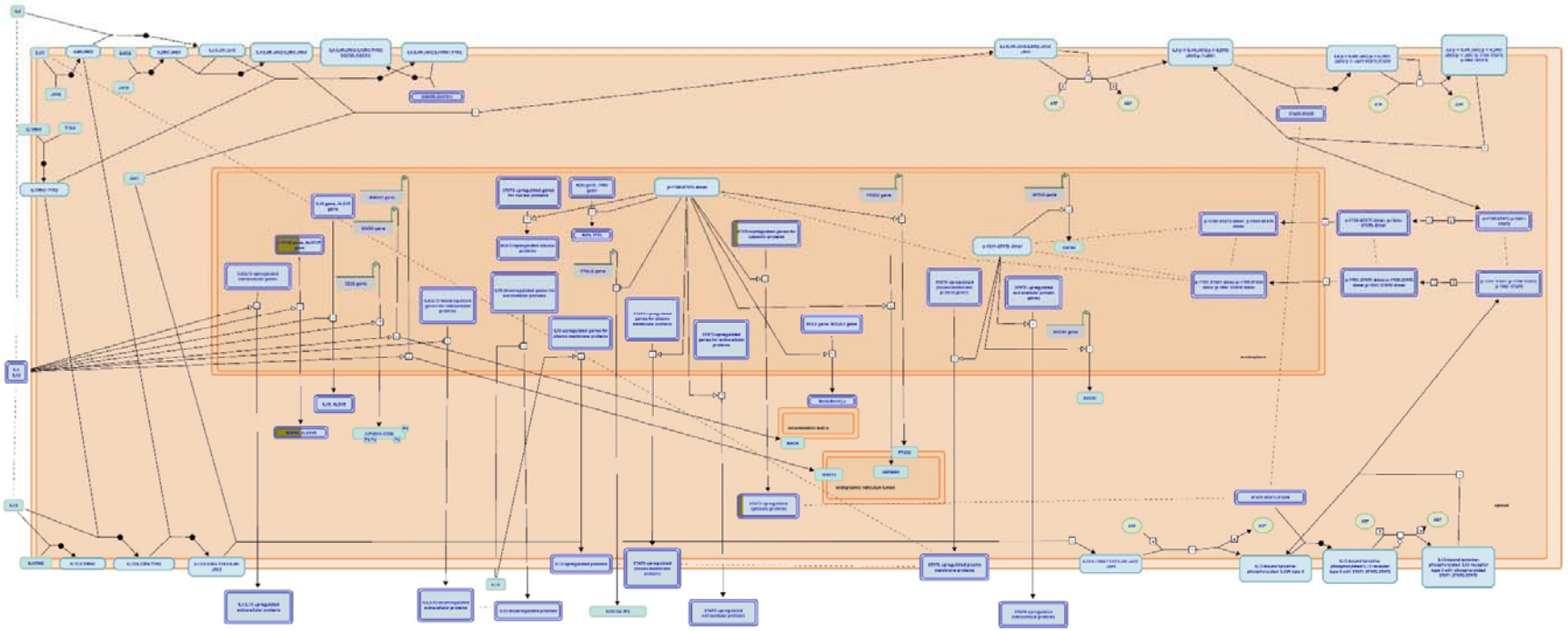

Figure 16. HSPA8 (aka Heat Shock Protein Family A (Hsp70) Member 8 or HSP70) and HSP90AA1 (aka Heat Shock Protein 90, as part of STAT3-upregulated genes for cytosolic proteins and STAT3-upregulated cytosolic proteins) highlighted in yellow were mapped onto the Signalling of Interleukin-4 and Interleukin-13 pathway sorted by False Discovery Rate (FDR) correction at $p < 0.05$ in logarithmic scale (base 10) generated by Reactome Pathway Browser (Organism: *Homo sapiens*).

4. Discussion

Evaluation of cytotoxic effects of OSLP on SH-SY5Y cells (24- and 48-h) in this study has found that OSLP at concentrations of 25, 50, 125, 250, 500 and 1000 μg/mL did not challenge the survival of SH-SY5Y cells. Therefore, OSLP (25, 50, 125, 250, 500 and 1000) is considerably safe in SH-SY5Y cells. In addition, the MNTD and the MTD of OSLP at 24-h treatment was determined as 2000 μg/mL and 4000 μg/mL respectively. In contrast, the MNTD and the MTD of OSLP at 48-h treatment was determined as 1000 μg/mL and 2000 μg/mL respectively. MNTD (the maximal non-toxic dose) represents the highest concentration which does not cause cytotoxic effects in a treated cell population whilst MTD (the minimal toxic dose) represents the lowest concentration which causes cytotoxic effects in a treated cell population [16]. On top of that, OSLP at 1 mg/mL has been found in this study to be potentially cytotoxic to the SH-SY5Y cells. Based on these findings, OSLP (25, 50, 125, 250, 500 and 1000) is used in the evaluation of OSLP protective effects on SH-SY5Y cells.

Hydrogen peroxide (H_2O_2) induction has challenged the survival of SH-SY5Y cells. SH-SY5Y cell survival decreased when H_2O_2 concentrations increased. H_2O_2 at about 150 μM had sufficiently inhibited the cell population by half. Concentrations higher than 250 μM was found to sufficiently inhibit the cell population close to 90%. Based on these findings, the IC_{50} in this study has been determined at 150 μM whereas the IC_{90} is 250 μM and above. The half-maximal inhibitory concentration (IC_{50}) represents the dose which inhibits a cell population by half whilst the maximal inhibitory concentration (IC_{90}) represents the dose which inhibits a cell population by 90% [18]. Therefore, 150 μM of H_2O_2 is used in the following evaluation of protective effects of OSLP on SH-SY5Y cells.

Protective effects of OSLP was evaluated in H_2O_2-induced SH-SY5Y cells. H_2O_2 induction (150 μM) has challenged the survival of SH-SY5Y cells. OSLP treatments have exhibited protection against H_2O_2 induction in a concentration-dependent manner. OSLP at 125 μg/mL has been found to be the lowest treatment dose showing protection against H_2O_2 stress. Pre-treatment with 125 μg/mL of OSLP had increased the survival of SH-SY5Y cells (about 30%) when compared to the H_2O_2 group though it did not attain statistical significance. Pre-treatments with OSLP at these three concentrations, 250, 500 and 1000 μg/mL, had significantly increased the survival of SH-SY5Y cells, with an increase of 39%, 51% and 57% respectively, when compared to the H_2O_2 group. In particular, pre-treatments with 500 and 1000 μg/mL of OSLP have demonstrated apparent inhibitions of H_2O_2. Such observations suggest that OSLP at these concentrations (250 μg/mL or higher) could potentially inhibit the actions of H_2O_2 and additionally, could promote the growth of SH-SY5Y cells. In line with the bright-field microscopic images obtained, OSLP pre-treatments at 250, 500 and 1000 μg/mL has seen improvements in the cell architecture. OSLP-treated H_2O_2-induced SH-SY5Y cells showed reduced clumping and shrinkage (i.e. round up), with apparent neurite formations and pyramidal-shaped cells. In contrast, H_2O_2-treated cells showed shrinkage, round up and clumping, all of which indicative of unhealthy cell appearance, loss of cell viability and progression towards death [15, 19-22]. Additionally, H_2O_2-treated cells has shown a decline in the population but OSLP pre-treatments have shown an increase in the cell population.

Taken together, the outcomes of *in vitro* assays collectively suggest that OSLP (250, 500 and 1000 μg/mL) could be having neuroprotective potential with considerably low cytotoxic effects.

Proteomic analysis has identified a distinct protein expression pattern with all the proteins were highly expressed in H_2O_2 (SH-SY5Y cells induced by 150 μM H_2O_2). compared to NC (SH-SY5Y cells without H_2O_2 induction and OSLP treatment). This observation is not seen in the OSLP-treated SH-SY5Y cells, with the majority of proteins were expressed at lower levels when compared to the H_2O_2-treated. Using functional annotation analysis, the top ten enriched terms in the cellular component, molecular function and biological process were identified (Figure 8). The ten selected enriched terms have seen a significant association with 25 cellular signalling pathways, as suggested by the Reactome Pathways analysis (Figure 12 and Table 5). Additionally, Reactome Pathways analysis has predicted the top ten cellular signalling pathways most likely modulated by OSLP treatment (Figure 13 and Table 6).

553 In the SH-SY5Y cells, H_2O_2 induction could have triggered cellular stress signalling via two main
554 pathways: "Attenuation Phase" and "HSP90 Chaperone Cycle for Steroid Hormone Receptors"
555 (Figures 14 & 15). The modulations of these pathways are particularly related to two major heat shock
556 proteins, HSPA8 (aka Heat Shock Protein Family A (Hsp70) Member 8 or HSP70) and HSP90AA1
557 (aka Heat shock protein 90), act together as a machinery to modulate folding of proteins. Studies have
558 shown that most cellular proteins do not activate the HSP90/HSP70-based chaperone machinery for
559 folding, stabilisation and trafficking under normal physiological conditions; following stress, the
560 function of HSP90/HSP70-based chaperone machinery is disrupted [23-25]. The HSP90/HSP70-based
561 chaperone machinery can influence a wide variety of client proteins and thus, affecting numerous
562 important cellular pathways such as protein conformational cycles, co-chaperone interactions, inter-
563 domain communications, protein conformational stability, trafficking and turnover; signal
564 transduction, intracellular transport [23, 24, 26, 27], synaptic transmissions [28-31] and inflammation
565 [25, 32]. Additionally, studies have shown that activations of HSP70 and HSPB1 (also known as
566 HSP27) following exposure to stress manipulate the heat shock transcriptional response and its client
567 proteins; under normal physiological conditions, these ATP-independent chaperones (HSP70 and
568 HSPB1) provide a wide variety of protections. To name a few, these chaperones prevent the
569 accumulation of improperly folded proteins, participate in the regulated degradation of misfolded
570 proteins, protect the cytoskeleton, involve in cellular metabolism, decrease stress-induced apoptosis
571 [33-35] in addition to preventing synaptic loss and neuronal death [36].
572 In this study, HSP90, HSP70 and HSPB1 had higher expressions in the H_2O_2 (induced by H_2O_2
573 alone) compared to the normal control (without H_2O_2 induction). Therefore, it is suggested that both
574 impaired HSP90/HSP70-based chaperone machinery and HSPB1 activation could have altered, direct
575 or indirectly, a variety of cellular processes in the neuronal cells. In particular, these alterations
576 include neuronal regulation in terms of growth, development and death; neuronal architecture of
577 cytoskeletons, cytoskeletal dynamics and cytoskeletal protein expressions; excitatory postsynaptic
578 transmission activated by NMDA receptors, cellular metabolism especially glucose and proteins,
579 protein conformations, stabilisation and posttranslational modifications as well as inflammatory
580 responses (Figure 12 and Table 5). Alterations as such are some common themes found in
581 neurodegenerative diseases and neurological disorders.
582 In the SH-SY5Y cells, OSLP treatment might help to buffer against cellular stress signalling
583 chiefly via the "Signalling of Interleukin-4 and Interleukin-13" (IL-4/-13 Signalling, R-HSA-6785807)
584 (Figure 16). Within the CNS, HSPs are released from stressed or damaged cells and they act as local
585 "danger signals" that trigger inflammatory responses. OSLP might modulate the expression of IL-
586 4/IL-13 by affecting the interaction of HSP90 with the downstream targets such as HSP8 and the
587 cytoplasmic protein Arachidonate 15-lipoxygenase (ALOX15). In the expression of IL-4/-13, HSP90 is
588 one of the genes for cytoplasmic proteins upregulated by signal transducer and activator of
589 transcription 3 (STAT3); via phosphorylation of STAT3 and signal transducer and activator of
590 transcription 6 (STAT6), HSP8 participates in the down-regulation of extracellular proinflammatory
591 signal transducers including ALOX15. Most likely, by modulating the "IL-4/-13 Signalling" pathway,
592 OSLP could have promoted the neuroprotective effects of IL-4 and IL-13 acting as anti-inflammatory
593 cytokines [37, 38] or IL-4 alone acts directly as a cytoprotective cytokine [39]. For instance, IL-4 and
594 IL-13 induce alternative activation of microglia (aka the M2 state) to protect against neuronal damage
595 in the hippocampus and in the cortex in experimental models of ischaemic stress [40, 41]. Specifically,
596 IL-13 alone has shown anti-inflammatory ability in a mouse model of cerebral ischaemia [42]
597 whereas, a study in humans with multiple sclerosis found high levels of IL-13 enhanced gamma-
598 aminobutyric acid (GABA, the dominant inhibitory neurotransmitter) over glutamate transmission
599 [43]. Otherwise, low levels of IL-4 in epileptic patients have decreased inflammation-related epilepsy
600 [44, 45].
601 Additionally, OSLP treatment might also protect against cellular stress-mediated pathways
602 including "Attenuation Phase" (R-HSA-3371568) and "HSP90 Chaperone Cycle for Steroid Hormone
603 Receptors" (R-HSA-3371497) (Figures 14 & 15). Via the "Attenuation Phase" pathway, OSLP might
604 modulate the downstream interaction of HSP70 and its co-chaperone HSP40 with CoREST

(transcriptional corepressor for repressor element 1-silencing transcription factor) at the negative-feedback loop. This negative feedback loop provides an important mechanism by which cells can regulate the activation and attenuation of Heat Shock Factor 1 (HSF1) via the presence and concentration of HSPs in the cell. OSLP might also regulate SHR-protein interactions via the "HSP90 Chaperone Cycle for Steroid Hormone Receptors" pathway. Upon the upstream activations of HSP40, HSP70 and stress-induced-phosphoprotein 1 (STIP1) respectively, HSP90 binds to the downstream co-chaperones FK506 binding protein 5 (FKBP51 and FKBP52) and Prostaglandin E Synthase 3 (PTGES3). The HSP90 and chaperone-mediated conformational changes are required to keep SHRs in a ligand binding-competent state. In this regard, OSLP could have promoted the cytoprotective functions of HSPs as an alternative of neuroprotection [46]. For instance, HSPs and their respective co-chaperones facilitate native protein stabilisation, translocation, re-folding and degradation in response to stressful stimuli. HSPs-based chaperone machinery not only ensure protein quality control but also prevent protein aggregation that would otherwise overwhelm the cell and lead to programmed cell death (apoptosis) or necrosis in unfavourable conditions [47, 48]. In recent times, HSPs have demonstrated their ability to fine-tune inflammation in the CNS [32]. For instance, HSPs have been shown to assist in the protection of motor neurons and to prevent chronic inflammation after spinal cord injuries in animal models [49, 50].

Last but not least, the changes of both KRT8 and KRT19 were also worthy of mention. They are keratins; KRT8 is a member of the type II keratin family and KRT19 belongs to the of type I family. The intermediate filament (IF) cytoskeleton of all epithelia is built from type I and type II keratins. Keratins not only maintain structural rigidity and stability, they also provide resistance to environmental stress [51]. In the presence of H_2O_2 stress, the keratin network organisation in cytoskeleton could be altered. Altered expression of keratins has an impact on the keratin network organisation and has been associated with inflammation, cellular stress, epithelial barrier defects, and higher sensitivity to tumour necrosis factor (TNF)-induced cell death [51-53].

Taken together, the protein expression study and bioinformatics analysis collectively suggest that OSLP could protect the neuronal cells against inflammation and cellular stress. The neuroprotective potential of OSLP could be attributed to an assortment of proteins present in the crude. For instance, baicalein 7-O-glucuronosyltransferase and its glucoronosylated baicalein have been reported to possess anti-inflammatory, antioxidative and neuroprotective activities [54] as well as anticonvulsive [55]; baicalin biosynthesised by baicalin-beta-D-glucuronidase has shown antioxidant activities [56, 57] whilst, rosmarinic acid biosynthesised by rosmarinate synthase have attracted interest for being anti-inflammatory, anti-oxidant, anti-angiogenic, anti-tumour, anti-microbial [58] and anti-seizure [59].

5. Concluding Remarks

The study suggests that OSLP could be a potential neuroprotective agent. Its neuroprotective potential is attributed to the ability of OSLP to modulate the "Signaling of Interleukin-4 and Interleukin-13" pathway as the predominant mode of action and thereby, activate anti-inflammatory cytokines to protect against pro-inflammatory responses under stress conditions. OSLP also modulates the "Attenuation Phase" and "HSP90 Chaperone Cycle for Steroid Hormone Receptors" pathways to counteract HSP-induced damage under stress conditions. OSLP is therefore worthy of detailed investigations.

Author Contributions: Y.S.C was responsible for the design, execution of all the experiments and data analyses, and writing of the final manuscript; P.K.A aided in supervision and provided critical feedback to the final manuscript; M.F.S and I.O contributed to the conceptualisation, design of the study, supervised all aspects, provided critical feedback and edited the final manuscript as submitted. All authors have read and agreed to the published version of the manuscript.

Funding: This research was funded by the Global Asia in the 21st Century (GA21) Platform, Monash University Malaysia, Research Grant (GA-HW-18-L04) and NKEA EPP#1 Research Grant Scheme (NRGS) (NH1014D066), Ministry of Agriculture and Agro-based Industry, Malaysia

Acknowledgments: The authors would like to thank Drs. Kim-Sang Tang and Jey-Sern Tan for the cell culture knowledge (School of Pharmacy); Dr. Syafiq Asnawi Zainal Abidin for ESI-LCMS/MS technical support (LC-MS laboratory of Jeffrey Cheah School of Medicine and Health Sciences) and Mr. Brandon Kar-Meng Choo for providing critical review to the final manuscript as submitted and unconditional support in this research.

Conflicts of Interest: The authors declare no conflict of interest. The funders had no role in the design of the study; in the collection, analyses, or interpretation of data; in the writing of the manuscript, or in the decision to publish the results.

References

1. WHO, *Neurological Disorders Public Health Challenges.* Scitech Book News, 2007. **31**(3).
2. Feigin, V.L., et al., *Global, regional, and national burden of neurological disorders during 1990–2015: a systematic analysis for the Global Burden of Disease Study 2015.* The Lancet Neurology, 2017. **16**(11): p. 877-897.
3. Jellinger, K.A., *Basic mechanisms of neurodegeneration: a critical update.* Journal of Cellular and Molecular Medicine, 2010. **14**(3): p. 457-487.
4. Vajda, F.J.E., *Neuroprotection and neurodegenerative disease*, in *Alzheimer's Disease*. 2004, Springer. p. 235-243.
5. Lin, X. and N. Zhang, *Berberine: Pathways to protect neurons.* Phytotherapy Research, 2018. **32**(8): p. 1501-1510.
6. Rehman, M.U., et al., *Neuroprotective Strategies for Neurological Disorders by Natural Products: An update.* Current neuropharmacology, 2019. **17**(3): p. 247-267.
7. Clark, I.A. and B. Vissel, *Excess cerebral TNF causing glutamate excitotoxicity rationalizes treatment of neurodegenerative diseases and neurogenic pain by anti-TNF agents.* Journal of Neuroinflammation, 2016. **13**(1): p. 236.
8. Lalkovičová, M. and V. Danielisová, *Neuroprotection and antioxidants.* Neural regeneration research, 2016. **11**(6): p. 865.
9. Schapira, A.H., *Neuroprotection in Parkinson's disease*, in *Blue Books of Neurology*. 2010, Elsevier. p. 301-320.
10. Adnyana, I.K., F. Setiawan, and M. Insanu, *From ethnopharmacology to clinical study of Orthosiphon stamineus Benth.* Int. J. Pharm. Pharm. Sci., 2013. **5**(3): p. 66.
11. Ameer, O.Z., et al., *Orthosiphon stamineus: traditional uses, phytochemistry, pharmacology, and toxicology.* J. Med. Food., 2012. **15**.
12. Chung, Y.-S., et al., *A Systematic Review of the Protective Actions of Cat's Whiskers (Misai Kucing) on the Central Nervous System.* Frontiers in Pharmacology, 2020. **11**(692).
13. Shah, S., et al., *Novel osmotin inhibits SREBP2 via the AdipoR1/AMPK/SIRT1 pathway to improve Alzheimer's disease neuropathological deficits.* Molecular psychiatry, 2017. **22**(3): p. 407.
14. Kovalevich, J. and D. Langford, *Considerations for the use of SH-SY5Y neuroblastoma cells in neurobiology.* Methods Mol Biol, 2013. **1078**: p. 9-21.
15. Shipley, M.M., C.A. Mangold, and M.L. Szpara, *Differentiation of the SH-SY5Y Human Neuroblastoma Cell Line.* Journal of visualized experiments : JoVE, 2016(108): p. 53193-53193.
16. Chevret, S., *Maximum Tolerable Dose (MTD). In Wiley StatsRef: Statistics Reference Online (eds N. Balakrishnan, T. Colton, B. Everitt, W. Piegorsch, F. Ruggeri and J. L. Teugels).* , in *Wiley StatsRef: Statistics Reference Online*. 2014.
17. Fabregat, A., et al., *The Reactome Pathway Knowledgebase.* Nucleic Acids Research, 2017. **46**(D1): p. D649-D655.

18. Marques, J., et al., *Marine organism sulfated polysaccharides exhibiting significant antimalarial activity and inhibition of red blood cell invasion by Plasmodium.* Scientific Reports, 2016. **6**: p. 24368.
19. Encinas, M., et al., *Sequential Treatment of SH-SY5Y Cells with Retinoic Acid and Brain-Derived Neurotrophic Factor Gives Rise to Fully Differentiated, Neurotrophic Factor-Dependent, Human Neuron-Like Cells.* Journal of Neurochemistry, 2000. **75**(3): p. 991-1003.
20. Sree, N.V., P.U. Sri, and N. Ramarao, *Neuro-Protective Properties Of Orthosiphon Staminus (Benth) Leaf Methanolic Fraction Through Antioxidant Mechanisms On SH-SY5Y Cells: An In-Vitro Evaluation.* International Journal of Pharmaceutical Sciences and Research, 2015. **6**(3): p. 1115.
21. Forster, J.I., et al., *Characterization of Differentiated SH-SY5Y as Neuronal Screening Model Reveals Increased Oxidative Vulnerability.* Journal of Biomolecular Screening, 2016. **21**(5): p. 496-509.
22. Zhang, Y., et al., *An Extract from Shrimp Processing By-Products Protects SH-SY5Y Cells from Neurotoxicity Induced by Aβ25–35.* Marine Drugs, 2017. **15**(3): p. 83.
23. Pratt, W.B., et al., *Proposal for a role of the Hsp90/Hsp70-based chaperone machinery in making triage decisions when proteins undergo oxidative and toxic damage.* Experimental Biology and Medicine, 2010. **235**(3): p. 278-289.
24. Picard, D., *Heat-shock protein 90, a chaperone for folding and regulation.* Cellular and Molecular Life Sciences CMLS, 2002. **59**(10): p. 1640-1648.
25. Sevin, M., et al., *HSP90 and HSP70: Implication in Inflammation Processes and Therapeutic Approaches for Myeloproliferative Neoplasms.* Mediators of Inflammation, 2015. **2015**: p. 970242.
26. Li, J., J. Soroka, and J. Buchner, *The Hsp90 chaperone machinery: Conformational dynamics and regulation by co-chaperones.* Biochimica et Biophysica Acta (BBA) - Molecular Cell Research, 2012. **1823**(3): p. 624-635.
27. Stankiewicz, T.R. and D.A. Linseman, *Rho family GTPases: key players in neuronal development, neuronal survival, and neurodegeneration.* Frontiers in cellular neuroscience, 2014. **8**: p. 314-314.
28. Chen, Y., et al., *Hsp90 chaperone inhibitor 17-AAG attenuates Aβ-induced synaptic toxicity and memory impairment.* Journal of Neuroscience, 2014. **34**(7): p. 2464-2470.
29. Garcia, S.M., et al., *Neuronal signaling modulates protein homeostasis in Caenorhabditis elegans post-synaptic muscle cells.* Genes Dev, 2007. **21**(22): p. 3006-16.
30. Gerges, N.Z., et al., *Independent Functions of hsp90 in Neurotransmitter Release and in the Continuous Synaptic Cycling of AMPA Receptors.* The Journal of Neuroscience, 2004. **24**(20): p. 4758-4766.
31. Zhang, Y., et al., *Inhibition of the small GTPase Cdc42 in regulation of epileptic-seizure in rats.* Neuroscience, 2015. **289**: p. 381-91.
32. Dukay, B., B. Csoboz, and M.E. Tóth, *Heat-Shock Proteins in Neuroinflammation.* Frontiers in Pharmacology, 2019. **10**(920).
33. Weeks, S.D., et al., *Characterization of human small heat shock protein HSPB1 α-crystallin domain localized mutants associated with hereditary motor neuron diseases.* Scientific Reports, 2018. **8**(1): p. 688.
34. Etienne-Manneville, S. and A. Hall, *Rho GTPases in cell biology.* Nature, 2002. **420**(6916): p. 629-635.
35. Henstridge, D.C., M. Whitham, and M.A. Febbraio, *Chaperoning to the metabolic party: The emerging therapeutic role of heat-shock proteins in obesity and type 2 diabetes.* Molecular Metabolism, 2014. **3**(8): p. 781-793.
36. Taylor, J.P., J. Hardy, and K.H. Fischbeck, *Toxic proteins in neurodegenerative disease.* Science, 2002. **296**(5575): p. 1991-1995.
37. Mori, S., P. Maher, and B. Conti, *Neuroimmunology of the Interleukins 13 and 4.* Brain sciences, 2016. **6**(2): p. 18.

38. McCormick, S.M. and N.M. Heller, *Commentary: IL-4 and IL-13 receptors and signaling.* Cytokine, 2015. **75**(1): p. 38-50.
39. Walsh, J.T., et al., *MHCII-independent CD4+ T cells protect injured CNS neurons via IL-4.* The Journal of clinical investigation, 2015. **125**(2): p. 699-714.
40. Yu, J.T., et al., *Maintenance of anti-inflammatory cytokines and reduction of glial activation in the ischemic hippocampal CA1 region preconditioned with lipopolysaccharide.* J Neurol Sci, 2010. **296**(1-2): p. 69-78.
41. Zhao, X., et al., *Neuronal Interleukin-4 as a Modulator of Microglial Pathways and Ischemic Brain Damage.* J Neurosci, 2015. **35**(32): p. 11281-91.
42. Kolosowska, N., et al., *Peripheral Administration of IL-13 Induces Anti-inflammatory Microglial/Macrophage Responses and Provides Neuroprotection in Ischemic Stroke.* Neurotherapeutics, 2019. **16**(4): p. 1304-1319.
43. Rossi, S., et al., *Potential role of IL-13 in neuroprotection and cortical excitability regulation in multiple sclerosis.* Multiple Sclerosis Journal, 2011. **17**(11): p. 1301-1312.
44. Strauss, K.I. and K.V. Elisevich, *Brain region and epilepsy-associated differences in inflammatory mediator levels in medically refractory mesial temporal lobe epilepsy.* Journal of Neuroinflammation, 2016. **13**(1): p. 270.
45. Liu, H., et al., *In vivo expression of the interleukin 4 receptor alpha by astrocytes in epilepsy cerebral cortex.* Cytokine, 2000. **12**(11): p. 1656-1661.
46. Wong, H.R., *Endogenous Cytoprotective Mechanisms*, in *NeuroImmune Biology*, L. Bertók and D.A. Chow, Editors. 2005, Elsevier. p. 49-65.
47. Miller, D.J. and P.E. Fort, *Heat Shock Proteins Regulatory Role in Neurodevelopment.* Frontiers in neuroscience, 2018. **12**: p. 821-821.
48. Pratt, W.B., et al., *Targeting Hsp90/Hsp70-based protein quality control for treatment of adult onset neurodegenerative diseases.* Annual review of pharmacology and toxicology, 2015. **55**: p. 353-371.
49. Reddy, S.J., F.L. Marca, and P. Park, *The role of heat shock proteins in spinal cord injury.* 2008. **25**(5): p. E4.
50. Zhou, Z.-b., et al., *Up-regulation of heat shock protein 27 inhibits apoptosis in lumbosacral nerve root avulsion-induced neurons.* Scientific Reports, 2019. **9**(1): p. 11468.
51. Schwarz, N., et al., *Dissection of keratin network formation, turnover and reorganization in living murine embryos.* Scientific reports, 2015. **5**: p. 9007-9007.
52. Schreurs, O., et al., *Expression of keratins 8, 18, and 19 in epithelia of atrophic oral lichen planus.* European Journal of Oral Sciences, 2020. **128**(1): p. 7-17.
53. Moll, R., M. Divo, and L. Langbein, *The human keratins: biology and pathology.* Histochemistry and cell biology, 2008. **129**(6): p. 705.
54. Wang, Z.-L., et al., *A comprehensive review on phytochemistry, pharmacology, and flavonoid biosynthesis of Scutellaria baicalensis.* Pharmaceutical biology, 2018. **56**(1): p. 465-484.
55. Li, P., X. Wang, and J. Zhang, *Baicalein administration protects against pentylenetetrazole-induced chronic epilepsy in rats.* Tropical Journal of Pharmaceutical Research, 2018. **17**(2): p. 293-298.
56. Peng-Fei, L., et al., *Purification and antioxidant activities of baicalin isolated from the root of huangqin (Scutellaria baicalensis gcorsi).* Journal of food science and technology, 2013. **50**(3): p. 615-619.
57. Yin, F., et al., *Baicalin prevents the production of hydrogen peroxide and oxidative stress induced by Aβ aggregation in SH-SY5Y cells.* Neurosci Lett, 2011. **492**(2): p. 76-9.
58. Kim, G.-D., et al., *Production and applications of rosmarinic acid and structurally related compounds.* Applied Microbiology and Biotechnology, 2015. **99**(5): p. 2083-2092.

784 59. Choo, B.K.M., et al., *Orthosiphon stamineus Leaf Extract Affects TNF-α and Seizures in a Zebrafish Model.*
785 Frontiers in Pharmacology, 2018. **9**: p. 139.
786

787

SUPPLEMENTARY DATA PAIR A

Figure SD-1 for Pair A. Genome-wide overview of the 80 significant pathways as visualized in Reacfoam generated by FoamTree (Organism: *Homo sapiens*). Reactome pathways are arranged in a hierarchy. The centre of each of the circular foam is the root of one top-level pathway hierarchy. Each step away from the center represents the next level lower in the pathway hierarchy. Colored foams denote pathways significantly over-represented at $p < 0.05$. Light grey foams denote pathways that are not significantly over-represented. The color key on the top right indicates the significance level of overrepresentation.

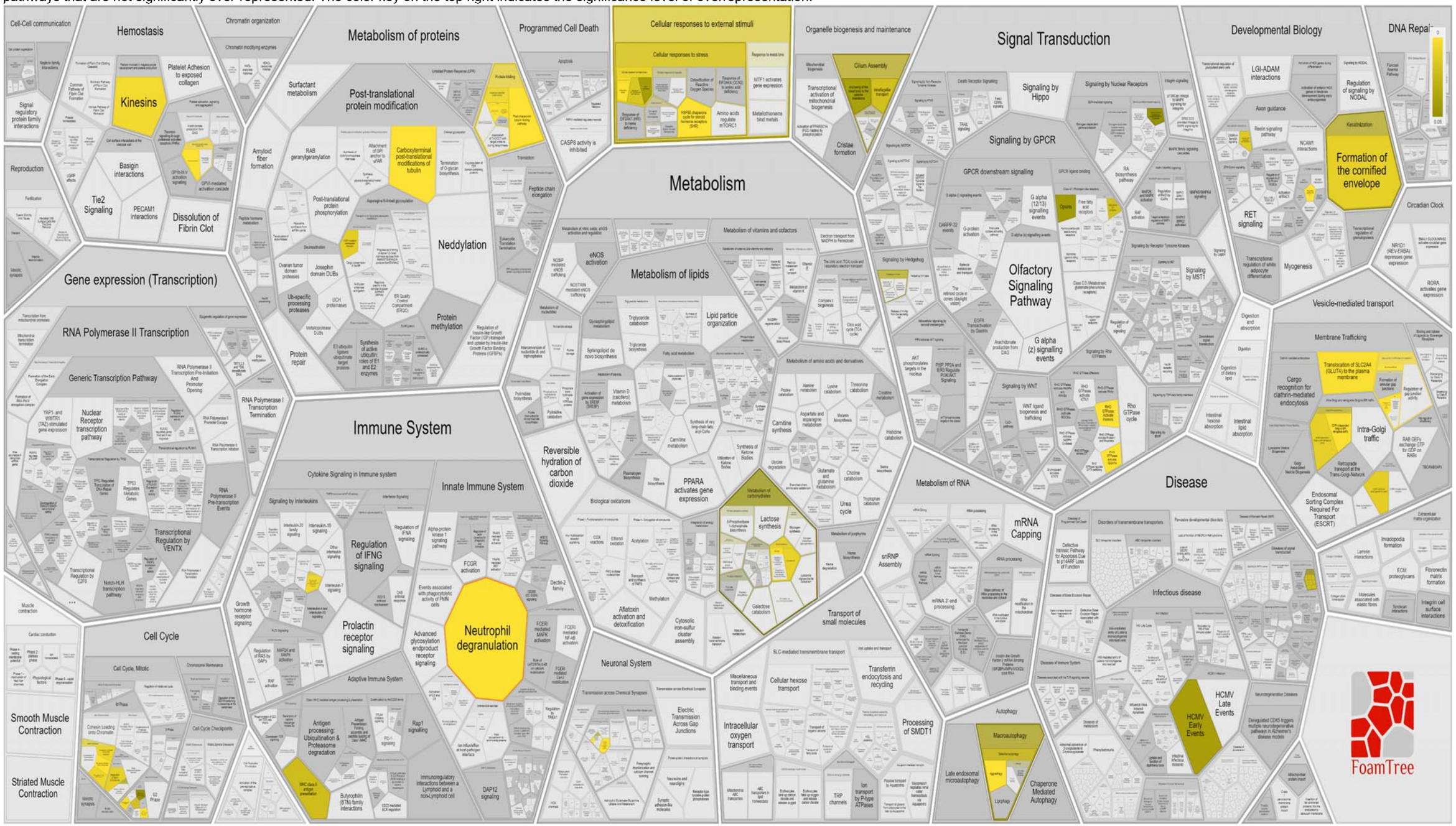

Table SD-1 for Pair A. 80 significant pathways generated by Reactome Pathways. Colorued cells are the top 25 most relevant pathways.

Pathway identifier	Pathway name	#Entities found	#Entities total	#Interactors found	#Interactors total	Entities ratio	Entities pValue	Entities FDR	#Reactions found	#Reactions total	Reactions ratio	Species identifier	Species name	Submitted entities found	Mapped entities	Submitted entities hit interactor	Interacts with	Found reaction identifiers
R-HSA-5626467	RHO GTPases activate IQGAPs	5	36	0	10	0.002480364	1.38E-06	8.09E-04	2	5	3.94E-04	9606	Homo sapiens	TUBA1C;TUBB4B;ACTG1				R-HSA-5626507;R-HSA-5672329
R-HSA-190840	Microtubule-dependent trafficking of connexons from Golgi to the plasma membrane	4	22	0	0	0.001515778	2.41E-06	8.09E-04	1	2	1.57E-04	9606	Homo sapiens	TUBA1C;TUBB4B				R-HSA-190520
R-HSA-190872	Transport of connexons to the plasma membrane	4	23	0	0	0.001584677	2.87E-06	8.09E-04	1	3	2.36E-04	9606	Homo sapiens	TUBA1C;TUBB4B				R-HSA-190520
R-HSA-3371497	HSP90 chaperone cycle for steroid hormone receptors (SHR)	6	70	2	35	0.00482293	4.24E-06	8.94E-04	12	12	9.45E-04	9606	Homo sapiens	TUBA1C;HSPA8;HSP90AA1;TUBB4B	P11142;P07900;P68363;P04350;P68371;Q9BQE3	HSP90AA1;HSPB1	Q13451;Q02790;P31948;Q15185	R-HSA-5618085;R-HSA-3371590;R-HSA-5618080;R-HSA-5618099;R-HSA-5618098;R-HSA-5618093;R-HSA-5618110;R-HSA-5618105;R-HSA-3371503;R-HSA-5618073;R-HSA-3371422;R-HSA-5618107
R-HSA-389977	Post-chaperonin tubulin folding pathway	4	25	0	10	0.001722475	1.48E-05	0.002505556	9	9	7.09E-04	9606	Homo sapiens	TUBA1C;TUBB4B				R-HSA-389956;R-HSA-389972;R-HSA-389974;R-HSA-389969;R-HSA-389955;R-HSA-389964;R-HSA-389976;R-HSA-389963;R-HSA-389978
R-HSA-380320	Recruitment of NuMA to mitotic centrosomes	5	97	0	0	0.006683202	5.42E-05	0.007130186	2	2	1.57E-04	9606	Homo sapiens	TUBA1C;HSP90AA1;TUBB4B				R-HSA-380316;R-HSA-380508
R-HSA-9619483	Activation of AMPK downstream of NMDARs	4	34	0	18	0.002342566	5.89E-05	0.007130186	1	3	2.36E-04	9606	Homo sapiens	TUBA1C;TUBB4B				R-HSA-9619542
R-HSA-8955332	Carboxyterminal post-translational modifications of tubulin	4	52	0	0	0.003582748	6.85E-05	0.00719337	6	6	4.72E-04	9606	Homo sapiens	TUBA1C;TUBB4B				R-HSA-8955706;R-HSA-8955869;R-HSA-8955712;R-HSA-8865774;R-HSA-8867370;R-HSA-8866105
R-HSA-389960	Formation of tubulin folding intermediates by CCT/TriC	4	30	0	26	0.00206697	9.10E-05	0.00854771	2	2	1.57E-04	9606	Homo sapiens	TUBA1C;TUBB4B				R-HSA-389954;R-HSA-389961
R-HSA-9646399	Aggrephagy	5	47	0	67	0.003238253	1.02E-04	0.00854771	6	15	0.001181102	9606	Homo sapiens	TUBA1C;HSP90AA1;TUBB4B				R-HSA-9646354;R-HSA-9646679;R-HSA-9646390;R-HSA-9646347;R-HSA-9646383;R-HSA-9646685
R-HSA-5663220	RHO GTPases Activate Formins	6	149	0	49	0.01026595	1.45E-04	0.0111372	9	27	0.002125984	9606	Homo sapiens	TUBA1C;TUBB4B;PFN1;ACTG1				R-HSA-5665751;R-HSA-5665767;R-HSA-5665809;R-HSA-5666001;R-HSA-5665982;R-HSA-5665802;R-HSA-5665659;R-HSA-203070;R-HSA-5666169
R-HSA-70171	Glycolysis	5	110	0	18	0.007578889	1.70E-04	0.011887748	3	24	0.001889764	9606	Homo sapiens	PKM;ENO1;ALDOA				R-HSA-71670;R-HSA-71496;R-HSA-71660
R-HSA-9668328	Sealing of the nuclear envelope (NE) by ESCRT-III	4	39	0	38	0.002687061	2.37E-04	0.014946677	1	7	5.51E-04	9606	Homo sapiens	TUBA1C;TUBB4B				R-HSA-9668419
R-HSA-389957	Prefoldin mediated transfer of substrate to CCT/TriC	3	29	0	0	0.001998071	2.49E-04	0.014946677	2	2	1.57E-04	9606	Homo sapiens	TUBA1C;TUBB4B				R-HSA-389970;R-HSA-389980

Pathway identifier	Pathway name	#Entities found	#Entities total	#Interactors found	#Interactors total	Entities ratio	Entities pValue	Entities FDR	#Reactions found	#Reactions total	Reactions ratio	Species identifier	Species name	Submitted entities found	Mapped entities	Submitted entities hit interactor	Interacts with	Found reaction identifiers
R-HSA-190828	Gap junction trafficking	5	52	0	98	0.003582748	3.36E-04	0.018842268	7	20	0.001574803	9606	Homo sapiens	TUBA1C;TUBB4B;ACTG1				R-HSA-196017;R-HSA-190519;R-HSA-196026;R-HSA-190520;R-HSA-191737;R-HSA-190877;R-HSA-190829
R-HSA-437239	Recycling pathway of L1	5	55	0	101	0.003789445	3.81E-04	0.019810556	5	14	0.001102362	9606	Homo sapiens	TUBA1C;TUBB4B;ACTG1				R-HSA-445077;R-HSA-443779;R-HSA-445089;R-HSA-445071;R-HSA-373736
R-HSA-157858	Gap junction trafficking and regulation	5	56	0	107	0.003858344	4.56E-04	0.022339072	7	24	0.001889764	9606	Homo sapiens	TUBA1C;TUBB4B;ACTG1				R-HSA-196017;R-HSA-190519;R-HSA-196026;R-HSA-190520;R-HSA-191737;R-HSA-190877;R-HSA-190829
R-HSA-114608	Platelet degranulation	5	137	0	36	0.009439162	7.68E-04	0.036080321	4	11	8.66E-04	9606	Homo sapiens	HSPA5;CFL1;ENO1;ALDOA;PFN1				R-HSA-482775;R-HSA-429157;R-HSA-481007;R-HSA-351323
R-HSA-6798695	Neutrophil degranulation	8	480	0	0	0.033071517	8.23E-04	0.036204833	5	10	7.87E-04	9606	Homo sapiens	HSPA8;HSP90AA1;PKM;FASN;MIF;TUBB4B;ALDOA;PRDX6				R-HSA-6798739;R-HSA-6800434;R-HSA-6798751;R-HSA-6798748;R-HSA-6798745
R-HSA-389958	Cooperation of Prefoldin and TriC/CCT in actin and tubulin folding	4	37	4	69	0.002549263	9.66E-04	0.038640098	5	6	4.72E-04	9606	Homo sapiens	TUBA1C;TUBB4B	P68363;P04350;P68371;Q9BQE3	ACTG1;HSPA8;PFN1;CFL1	P60709	R-HSA-390453;R-HSA-389970;R-HSA-389954;R-HSA-389980;R-HSA-389961
R-HSA-9609736	Assembly and cell surface presentation of NMDA receptors	4	49	1	62	0.003376051	9.66E-04	0.038640098	3	23	0.001811024	9606	Homo sapiens	TUBA1C;TUBB4B	P68363;P04350;P68371;Q9BQE3	KRT18	P07196	R-HSA-9610627;R-HSA-9610408;R-HSA-9610879
R-HSA-3371568	Attenuation phase	3	47	0	1	0.003238253	0.001067984	0.040583377	4	5	3.94E-04	9606	Homo sapiens	HSPA8;HSP90AA1;HSPB1				R-HSA-3371554;R-HSA-5324617;R-HSA-5082369;R-HSA-5082384
R-HSA-8852276	The role of GTSE1 in G2/M progression after G2 checkpoint	5	83	0	112	0.005718617	0.001135296	0.040870667	4	10	7.87E-04	9606	Homo sapiens	TUBA1C;HSP90AA1;TUBB4B				R-HSA-8852306;R-HSA-8852298;R-HSA-8852362;R-HSA-8852280
R-HSA-70326	Glucose metabolism	5	140	0	62	0.009645859	0.001331683	0.046608911	5	50	0.003937008	9606	Homo sapiens	PKM;ENO1;ALDOA				R-HSA-71495;R-HSA-71670;R-HSA-71496;R-HSA-71660;R-HSA-70494
R-HSA-1445148	Translocation of SLC2A4 (GLUT4) to the plasma membrane	5	79	0	126	0.005443021	0.001454593	0.048001553	3	15	0.001181102	9606	Homo sapiens	TUBA1C;TUBB4B;ACTG1				R-HSA-2316352;R-HSA-2316347;R-HSA-2316349
R-HSA-6811436	COPI-independent Golgi-to-ER retrograde traffic	4	63	1	65	0.004340637	0.001621252	0.051880073	2	7	5.51E-04	9606	Homo sapiens	TUBA1C;TUBB4B	P68363;P04350;P68371;Q9BQE3	HSP90AA1	P43034	R-HSA-8849350;R-HSA-8849353
R-HSA-190861	Gap junction assembly	4	41	0	88	0.002824859	0.001823798	0.056537751	3	16	0.001259843	9606	Homo sapiens	TUBA1C;TUBB4B				R-HSA-190520;R-HSA-191737;R-HSA-190877
R-HSA-3371571	HSF1-dependent transactivation	3	59	0	1	0.004065041	0.002013494	0.060404823	5	8	6.30E-04	9606	Homo sapiens	HSPA8;HSP90AA1;HSPB1				R-HSA-3371554;R-HSA-5324617;R-HSA-5082356;R-HSA-5082369;R-HSA-5082384
R-HSA-76005	Response to elevated platelet cytosolic Ca2+	5	144	0	93	0.009921455	0.002914843	0.084530434	4	14	0.001102362	9606	Homo sapiens	HSPA5;CFL1;ENO1;ALDOA;PFN1				R-HSA-482775;R-HSA-429157;R-HSA-481007;R-HSA-351323
R-HSA-8854518	AURKA Activation by TPX2	3	74	0	6	0.005098526	0.004048415	0.113355627	2	2	1.57E-04	9606	Homo sapiens	HSP90AA1;TUBB4B				R-HSA-8853405;R-HSA-8853419
R-HSA-983189	Kinesins	4	68	0	98	0.004685132	0.004491515	0.121270902	2	14	0.001102362	9606	Homo sapiens	TUBA1C;TUBB4B				R-HSA-983259;R-HSA-983266

Pathway identifier	Pathway name	#Entities found	#Entities total	#Interactors found	#Interactors total	Entities ratio	Entities pValue	Entities FDR	#Reactions found	#Reactions total	Reactions ratio	Species identifier	Species name	Submitted entities found	Mapped entities	Submitted entities hit interactor	Interacts with	Found reaction identifiers
R-HSA-390466	Chaperonin-mediated protein folding	4	100	4	75	0.006889899	0.005770767	0.143528908	5	19	0.001496063	9606	Homo sapiens	TUBA1C;TUBB4B	P68363;P04350;P68371;Q9BQE3	ACTG1;HSPA8;PFN1;CFL1	P60709	R-HSA-390453;R-HSA-389970;R-HSA-389954;R-HSA-389980;R-HSA-389961
R-HSA-68877	Mitotic Prometaphase	5	211	0	77	0.014537688	0.00589258	0.143528908	9	20	0.001574803	9606	Homo sapiens	TUBA1C;HSP90AA1;TUBB4B				R-HSA-9648114;R-HSA-9648017;R-HSA-2484822;R-HSA-375302;R-HSA-380316;R-HSA-380508;R-HSA-1638803;R-HSA-2468287;R-HSA-1638821
R-HSA-3371556	Cellular response to heat stress	5	135	2	157	0.009301364	0.005980371	0.143528908	17	29	0.002283465	9606	Homo sapiens	HSPA9;HSPA8;HSP90AA1;HSPA5;HSPB1	P11021;P11142;P07900;ENSG00000106211;P38646	HSP90AA1;HSPB1	P49137;Q15185	R-HSA-5251955;R-HSA-5082409;R-HSA-5251959;R-HSA-5324632;R-HSA-5082369;R-HSA-3371518;R-HSA-3371554;R-HSA-3371586;R-HSA-4793819;R-HSA-5251942;R-HSA-3371467;R-HSA-5324617;R-HSA-5082356;R-HSA-5252041;R-HSA-5082384;R-HSA-4793911;R-HSA-5252079
R-HSA-8950505	Gene and protein expression by JAK-STAT signaling after Interleukin-12 stimulation	6	73	4	334	0.005029627	0.006203243	0.148877824	5	36	0.002834646	9606	Homo sapiens	HSPA9;CFL1;MIF	ENSG00000240972;ENSG00000172757;P14174;P23528;ENSG00000113013;P38646	MIF;ACTG1;HSPB1;HSPA5	P00441;P23528;P14174;P78417	R-HSA-8950732;R-HSA-8950175;R-HSA-8950771;R-HSA-8950389;R-HSA-8950581
R-HSA-9648025	EML4 and NUDC in mitotic spindle formation	4	121	0	68	0.008336778	0.007273065	0.167280493	2	5	3.94E-04	9606	Homo sapiens	TUBA1C;TUBB4B				R-HSA-9648114;R-HSA-9648017
R-HSA-391251	Protein folding	4	106	4	85	0.007303293	0.007826059	0.172173287	14	28	0.002204724	9606	Homo sapiens	TUBA1C;TUBB4B	P68363;P04350;P68371;Q9BQE3	ACTG1;HSPA8;PFN1;CFL1	P60709	R-HSA-389956;R-HSA-389955;R-HSA-389954;R-HSA-389964;R-HSA-389961;R-HSA-389963;R-HSA-390453;R-HSA-389972;R-HSA-389974;R-HSA-389969;R-HSA-389970;R-HSA-389980;R-HSA-389976;R-HSA-389978
R-HSA-2500257	Resolution of Sister Chromatid Cohesion	4	134	0	63	0.009232465	0.007968508	0.175307167	4	8	6.30E-04	9606	Homo sapiens	TUBA1C;TUBB4B				R-HSA-2484822;R-HSA-1638803;R-HSA-2468287;R-HSA-1638821
R-HSA-70263	Gluconeogenesis	3	66	0	45	0.004547334	0.010458059	0.219619242	2	26	0.002047244	9606	Homo sapiens	ENO1;ALDOA				R-HSA-71495;R-HSA-70494
R-HSA-2467813	Separation of Sister Chromatids	4	194	0	28	0.013366405	0.011006381	0.22727882	2	8	6.30E-04	9606	Homo sapiens	TUBA1C;TUBB4B				R-HSA-2467809;R-HSA-2467811
R-HSA-6809371	Formation of the cornified envelope	4	138	0	84	0.009508061	0.011363941	0.22727882	8	27	0.002125984	9606	Homo sapiens	KRT19;KRT18;KRT8				R-HSA-6810357;R-HSA-6811539;R-HSA-6814387;R-HSA-8942224;R-HSA-6814734;R-HSA-6814764;R-HSA-6814298;R-HSA-6810937
R-HSA-6811434	COPI-dependent Golgi-to-ER retrograde traffic	4	107	0	116	0.007372192	0.011728918	0.229925954	2	11	8.66E-04	9606	Homo sapiens	TUBA1C;TUBB4B				R-HSA-6811426;R-HSA-6811423
R-HSA-6807878	COPI-mediated anterograde transport	4	107	0	117	0.007372192	0.012101366	0.229925954	2	12	9.45E-04	9606	Homo sapiens	TUBA1C;TUBB4B				R-HSA-6809006;R-HSA-6809003
R-HSA-9020591	Interleukin-12 signaling	6	84	4	405	0.005787516	0.013797147	0.248348645	5	56	0.004409449	9606	Homo sapiens	HSPA9;CFL1;MIF	ENSG00000240972;ENSG00000172757;P14174;P23528;ENSG00000113013;P38646	MIF;ACTG1;HSPB1;HSPA5	P00441;P23528;P14174;P78417	R-HSA-8950732;R-HSA-8950175;R-HSA-8950771;R-HSA-8950389;R-HSA-8950581
R-HSA-399954	Sema3A PAK dependent Axon repulsion	2	19	2	29	0.001309081	0.01434738	0.258252847	4	6	4.72E-04	9606	Homo sapiens	HSP90AA1;CFL1	P07900;P23528	ACTG1;CFL1	P53667;P23528	R-HSA-399952;R-HSA-399950;R-HSA-419644;R-HSA-419645

Pathway identifier	Pathway name	#Entities found	#Entities total	#Interactors found	#Interactors total	Entities ratio	Entities pValue	Entities FDR	#Reactions found	#Reactions total	Reactions ratio	Species identifier	Species name	Submitted entities found	Mapped entities	Submitted entities hit interactor	Interacts with	Found reaction identifiers
R-HSA-380270	Recruitment of mitotic centrosome proteins and complexes	3	81	0	54	0.005580819	0.017717371	0.264180554	3	3	2.36E-04	9606	Homo sapiens	HSP90AA1;TUBB4B				R-HSA-380311;R-HSA-380455;R-HSA-380283
R-HSA-3371453	Regulation of HSF1-mediated heat shock response	4	113	1	137	0.007785586	0.017885779	0.264180554	8	14	0.001102362	9606	Homo sapiens	HSPA9;HSPA8;HSPA5;HSPB1	P11021;P11142;ENSG00000106211;P38646	HSPB1	P49137	R-HSA-5251955;R-HSA-5251942;R-HSA-5251959;R-HSA-3371467;R-HSA-5252041;R-HSA-3371518;R-HSA-4793911;R-HSA-5252079
R-HSA-380259	Loss of Nlp from mitotic centrosomes	3	71	0	66	0.004891829	0.018067499	0.264180554	2	2	1.57E-04	9606	Homo sapiens	HSP90AA1;TUBB4B				R-HSA-380272;R-HSA-380303
R-HSA-2262752	Cellular responses to stress	13	690	7	1089	0.047540306	0.018214489	0.264180554	45	227	0.017874016	9606	Homo sapiens	HSPA9;TUBA1C;HSPA8;HSP90AA1;HSPA5;FASN;RPL14;RPL24;HSPB1;TUBB4B;PRDX6	P07900;P68363;P30041;P68371;P38646;P11021;P11142;P50914;P83731;P04350;P45985;Q9BQE3;ENSG00000106211	HNRNPU;HSP90AA1;NPM1;HSPA8;KRT18;PKM;HSPB1	P05412;Q16665;Q8N726;P08243;Q13451;Q02790;P31948;P49137;P42771;Q15185;Q9NUX5	R-HSA-5324632;R-HSA-168136;R-HSA-5082369;R-HSA-5618073;R-HSA-3371518;R-HSA-3371554;R-HSA-3229152;R-HSA-4793819;R-HSA-1234177;R-HSA-1791118;R-HSA-3785711;R-HSA-1234181;R-HSA-5324617;R-HSA-5252041;R-HSA-9633742;R-HSA-3371503;R-HSA-5082384;R-HSA-6804998;R-HSA-9633008;R-HSA-5251955;R-HSA-5082409;R-HSA-5618099;R-HSA-5251959;R-HSA-5618098;R-HSA-3343700;R-HSA-3209111;R-HSA-3209114;R-HSA-5618110;R-HSA-5618105;R-HSA-3371422;R-HSA-5618107;R-HSA-5618085;R-HSA-3371586;R-HSA-450292;R-HSA-3371590;R-HSA-5618080;R-HSA-5251942;R-HSA-3371467;R-HSA-5618093;R-HSA-5082356;R-HSA-9645672;R-HSA-9634669;R-HSA-4793911;R-HSA-9633005;R-HSA-5252079
R-HSA-380284	Loss of proteins required for interphase microtubule organization from the centrosome	3	71	0	68	0.004891829	0.01877931	0.264180554	3	3	2.36E-04	9606	Homo sapiens	HSP90AA1;TUBB4B				R-HSA-380294;R-HSA-380272;R-HSA-380303
R-HSA-9665737	Drug resistance in ERBB2 TMD/JMD mutants	1	5	0	0	3.44E-04	0.020321581	0.264180554	1	1	7.87E-05	9606	Homo sapiens	HSP90AA1				R-HSA-9665708
R-HSA-9665244	Resistance of ERBB2 KD mutants to sapitinib	1	5	0	0	3.44E-04	0.020321581	0.264180554	1	1	7.87E-05	9606	Homo sapiens	HSP90AA1				R-HSA-9665304
R-HSA-9665233	Resistance of ERBB2 KD mutants to trastuzumab	1	5	0	0	3.44E-04	0.020321581	0.264180554	1	1	7.87E-05	9606	Homo sapiens	HSP90AA1				R-HSA-9665232
R-HSA-9665247	Resistance of ERBB2 KD mutants to osimertinib	1	5	0	0	3.44E-04	0.020321581	0.264180554	1	1	7.87E-05	9606	Homo sapiens	HSP90AA1				R-HSA-9665280
R-HSA-9665245	Resistance of ERBB2 KD mutants to tesevatinib	1	5	0	0	3.44E-04	0.020321581	0.264180554	1	1	7.87E-05	9606	Homo sapiens	HSP90AA1				R-HSA-9665315
R-HSA-9665251	Resistance of ERBB2 KD mutants to lapatinib	1	5	0	0	3.44E-04	0.020321581	0.264180554	1	1	7.87E-05	9606	Homo sapiens	HSP90AA1				R-HSA-9665284
R-HSA-9665250	Resistance of ERBB2 KD mutants to AEE788	1	5	0	0	3.44E-04	0.020321581	0.264180554	1	1	7.87E-05	9606	Homo sapiens	HSP90AA1				R-HSA-9665278
R-HSA-9665246	Resistance of ERBB2 KD mutants to neratinib	1	5	0	0	3.44E-04	0.020321581	0.264180554	1	1	7.87E-05	9606	Homo sapiens	HSP90AA1				R-HSA-9665286
R-HSA-9665249	Resistance of ERBB2 KD mutants to afatinib	1	5	0	0	3.44E-04	0.020321581	0.264180554	1	1	7.87E-05	9606	Homo sapiens	HSP90AA1				R-HSA-9665311

Pathway identifier	Pathway name	#Entities found	#Entities total	#Interactors found	#Interactors total	Entities ratio	Entities pValue	Entities FDR	#Reactions found	#Reactions total	Reactions ratio	Species identifier	Species name	Submitted entities found	Mapped entities	Submitted entities hit interactor	Interacts with	Found reaction identifiers
R-HSA-417973	Adenosine P1 receptors	1	5	0	0	3.44E-04	0.020321581	0.264180554	1	2	1.57E-04	9606	Homo sapiens	ENO1				R-HSA-418904
R-HSA-9663891	Selective autophagy	6	89	5	454	0.00613201	0.020538095	0.266995241	14	48	0.003779528	9606	Homo sapiens	TUBA1C;HSPA8;HSP90AA1;TUBB4B	P11142;P07900;P68363;P04350;P68371;Q9BQE3	RPL14;PRDX6;HSP90AA1;HSPA8;HSPA9	P21796;P11142;P50542	R-HSA-9646354;R-HSA-9664850;R-HSA-9646679;R-HSA-9646390;R-HSA-5205673;R-HSA-9613530;R-HSA-9646685;R-HSA-9613565;R-HSA-9613666;R-HSA-9646347;R-HSA-9613352;R-HSA-9613513;R-HSA-9646383;R-HSA-5205682
R-HSA-5620924	Intraflagellar transport	3	56	1	108	0.003858344	0.020626356	0.268142626	7	12	9.45E-04	9606	Homo sapiens	TUBA1C;TUBB4B	P04350;P68371;Q9BQE3	HSPA8	Q8TDR0	R-HSA-5624949;R-HSA-5625424;R-HSA-5625426;R-HSA-5625421;R-HSA-5617820;R-HSA-5624952;R-HSA-5625416
R-HSA-8953897	Cellular responses to external stimuli	13	708	7	1107	0.048780488	0.021148268	0.274927488	45	258	0.020314961	9606	Homo sapiens	HSPA9;TUBA1C;HSPA8;HSP90AA1;HSPA5;FASN;RPL14;RPL24;HSPB1;TUBB4B;PRDX6	P07900;P68363;P30041;P68371;P38646;P11021;P11142;P50914;P83731;P04350;P45985;Q9BQE3;ENSG00000106211	HNRNPU;HSP90AA1;NPM1;HSPA8;KRT18;PKM;HSPB1	P05412;Q16665;Q8N726;P08243;Q13451;Q02790;P31948;P49137;P42771;Q15185;Q9NUX5	R-HSA-5324632;R-HSA-168136;R-HSA-5082369;R-HSA-5618073;R-HSA-3371518;R-HSA-3371554;R-HSA-3229152;R-HSA-4793819;R-HSA-1234177;R-HSA-1791118;R-HSA-3785711;R-HSA-1234181;R-HSA-5324617;R-HSA-5252041;R-HSA-9633742;R-HSA-3371503;R-HSA-5082384;R-HSA-6804998;R-HSA-9633008;R-HSA-5251955;R-HSA-5082409;R-HSA-5618099;R-HSA-5251959;R-HSA-5618098;R-HSA-3343700;R-HSA-3209111;R-HSA-3209114;R-HSA-5618110;R-HSA-5618105;R-HSA-3371422;R-HSA-5618107;R-HSA-5618085;R-HSA-3371586;R-HSA-450292;R-HSA-3371590;R-HSA-5618080;R-HSA-5251942;R-HSA-3371467;R-HSA-5618093;R-HSA-5082356;R-HSA-9645672;R-HSA-9634669;R-HSA-4793911;R-HSA-9633005;R-HSA-5252079
R-HSA-2132295	MHC class II antigen presentation	4	148	0	119	0.010197051	0.022838224	0.280494707	1	26	0.002047244	9606	Homo sapiens	TUBA1C;TUBB4B				R-HSA-2213248
R-HSA-380287	Centrosome maturation	3	83	0	68	0.005718617	0.023374559	0.280494707	6	6	4.72E-04	9606	Homo sapiens	HSP90AA1;TUBB4B				R-HSA-380311;R-HSA-380455;R-HSA-380294;R-HSA-380272;R-HSA-380303;R-HSA-380283
R-HSA-8856688	Golgi-to-ER retrograde transport	4	148	1	141	0.010197051	0.026664386	0.319972627	4	18	0.001417323	9606	Homo sapiens	TUBA1C;TUBB4B	P68363;P04350;P68371;Q9BQE3	HSP90AA1	P43034	R-HSA-8849350;R-HSA-6811426;R-HSA-6811423;R-HSA-8849353
R-HSA-438064	Post NMDA receptor activation events	4	96	1	194	0.006614303	0.029854753	0.358257039	2	39	0.003070866	9606	Homo sapiens	TUBA1C;TUBB4B	P68363;P04350;P68371;Q9BQE3	HSP90AA1	P12931	R-HSA-9619542;R-HSA-9612085
R-HSA-5610787	Hedgehog 'off' state	4	124	0	174	0.008543475	0.030185722	0.362228668	2	32	0.002519685	9606	Homo sapiens	TUBA1C;TUBB4B				R-HSA-5610733;R-HSA-5610767
R-HSA-5617833	Cilium Assembly	6	208	1	445	0.014330991	0.03307971	0.365889412	26	50	0.003937008	9606	Homo sapiens	TUBA1C;HSP90AA1;GLB1L;TUBB4B	P07900;P68363;P04350;P08100;P68371;Q9BQE3	HSPA8	Q8TDR0	R-HSA-5625424;R-HSA-5625426;R-HSA-5617820;R-HSA-5623519;R-HSA-5623513;R-HSA-5617816;R-HSA-5618328;R-HSA-5618331;R-HSA-5625421;R-HSA-5625416;R-HSA-5626699;R-HSA-5624949;R-HSA-5626228;R-HSA-5620918;R-HSA-5626227;R-HSA-5620914;R-HSA-5626681;R-HSA-5620921;R-HSA-5624952;R-HSA-5638009;R-HSA-5623525;R-HSA-5623524;R-HSA-5623527;R-HSA-5623521;R-HSA-5626220;R-HSA-5626223
R-HSA-2995410	Nuclear Envelope (NE) Reassembly	4	88	0	224	0.006063111	0.033262674	0.365889412	1	24	0.001889764	9606	Homo sapiens	TUBA1C;TUBB4B				R-HSA-9668419
R-HSA-6805567	Keratinization	4	226	0	84	0.015571173	0.033970526	0.373675782	15	34	0.002677165	9606	Homo sapiens	KRT19;KRT18;KRT8				R-HSA-6806629;R-HSA-6805573;R-HSA-6814734;R-HSA-6814764;R-HSA-6805546;R-HSA-6806613;R-HSA-6810357;R-HSA-6811539;R-HSA-6814387;R-HSA-6806610;R-HSA-6809393;R-HSA-6809663;R-HSA-8942224;R-HSA-6814298;R-HSA-6810937
R-HSA-1632852	Macroautophagy	6	150	5	496	0.010334849	0.038258459	0.420843052	14	87	0.006850394	9606	Homo sapiens	TUBA1C;HSPA8;HSP90AA1;TUBB4B	P11142;P07900;P68363;P04350;P68371;Q9BQE3	RPL14;PRDX6;HSP90AA1;HSPA8;HSPA9	P21796;P11142;P50542	R-HSA-9646354;R-HSA-9664850;R-HSA-9646679;R-HSA-9646390;R-HSA-5205673;R-HSA-9613530;R-HSA-9646685;R-HSA-9613565;R-HSA-9613666;R-HSA-9646347;R-HSA-9613352;R-HSA-9613513;R-HSA-9646383;R-HSA-5205682
R-HSA-9609690	HCMV Early Events	4	215	0	104	0.014813284	0.040342709	0.443769801	2	12	9.45E-04	9606	Homo sapiens	TUBA1C;TUBB4B				R-HSA-9614343;R-HSA-9614367

Pathway identifier	Pathway name	#Entities found	#Entities total	#Interactors found	#Interactors total	Entities ratio	Entities pValue	Entities FDR	#Reactions found	#Reactions total	Reactions ratio	Species identifier	Species name	Submitted entities found	Mapped entities	Submitted entities hit interactor	Interacts with	Found reaction identifiers
R-HSA-5620912	Anchoring of the basal body to the plasma membrane	3	99	0	106	0.006821	0.041031581	0.45134739	8	9	7.09E-04	9606	Homo sapiens	HSP90AA1;TUBB4B				R-HSA-5626228;R-HSA-5626227;R-HSA-5626220;R-HSA-5626223;R-HSA-5626681;R-HSA-5617816;R-HSA-5626699;R-HSA-5638009
R-HSA-3371511	HSF1 activation	2	43	1	40	0.002962657	0.04219468	0.464141476	4	7	5.51E-04	9606	Homo sapiens	HSP90AA1;HSPB1	P07900;ENSG00000106211	HSP90AA1	Q15185	R-HSA-3371586;R-HSA-4793819;R-HSA-5082409;R-HSA-5324632
R-HSA-419771	Opsins	1	10	0	1	6.89E-04	0.044169362	0.479950698	1	2	1.57E-04	9606	Homo sapiens	GLB1L				R-HSA-419841
R-HSA-71387	Metabolism of carbohydrates	6	456	1	195	0.031417941	0.04799507	0.479950698	8	243	0.019133858	9606	Homo sapiens	PKM;GLB1L;ENO1;ALDOA	P13929;P06733;P14618-2;P14618-1;P04075;Q6UWU2	KRT19	Q8IVS8	R-HSA-6799495;R-HSA-2090079;R-HSA-71495;R-HSA-71670;R-HSA-71496;R-HSA-1630306;R-HSA-71660;R-HSA-70494
R-HSA-9665230	Drug resistance in ERBB2 KD mutants	1	12	0	0	8.27E-04	0.048087829	0.480878293	8	8	6.30E-04	9606	Homo sapiens	HSP90AA1				R-HSA-9665315;R-HSA-9665232;R-HSA-9665280;R-HSA-9665286;R-HSA-9665284;R-HSA-9665304;R-HSA-9665311;R-HSA-9665278
R-HSA-9029558	NR1H2 & NR1H3 regulate gene expression linked to lipogenesis	2	17	0	68	0.001171283	0.048089733	0.480897332	2	8	6.30E-04	9606	Homo sapiens	FASN				R-HSA-9605063;R-HSA-9028533
R-HSA-2565942	Regulation of PLK1 Activity at G2/M Transition	3	92	0	112	0.006338707	0.048460857	0.484608571	4	12	9.45E-04	9606	Homo sapiens	HSP90AA1;TUBB4B				R-HSA-3000319;R-HSA-2574845;R-HSA-3000310;R-HSA-2574840

SUPPLEMENTARY DATA PAIR B

Figure SD-2 for Pair B. Genome-wide overview of the 56 significant pathways as visualised in Reacfoam generated by FoamTree (Organism: *Homo sapiens*). Reactome pathways are arranged in a hierarchy. The centre of each of the circular foam is the root of one top-level pathway hierarchy. Each step away from the center represents the next level lower in the pathway hierarchy. Colored foams denote pathways significantly over-represented at $p < 0.05$. Light grey foams denote pathways that are not significantly over-represented. The color key on the top right indicates the significance level of overrepresentation.

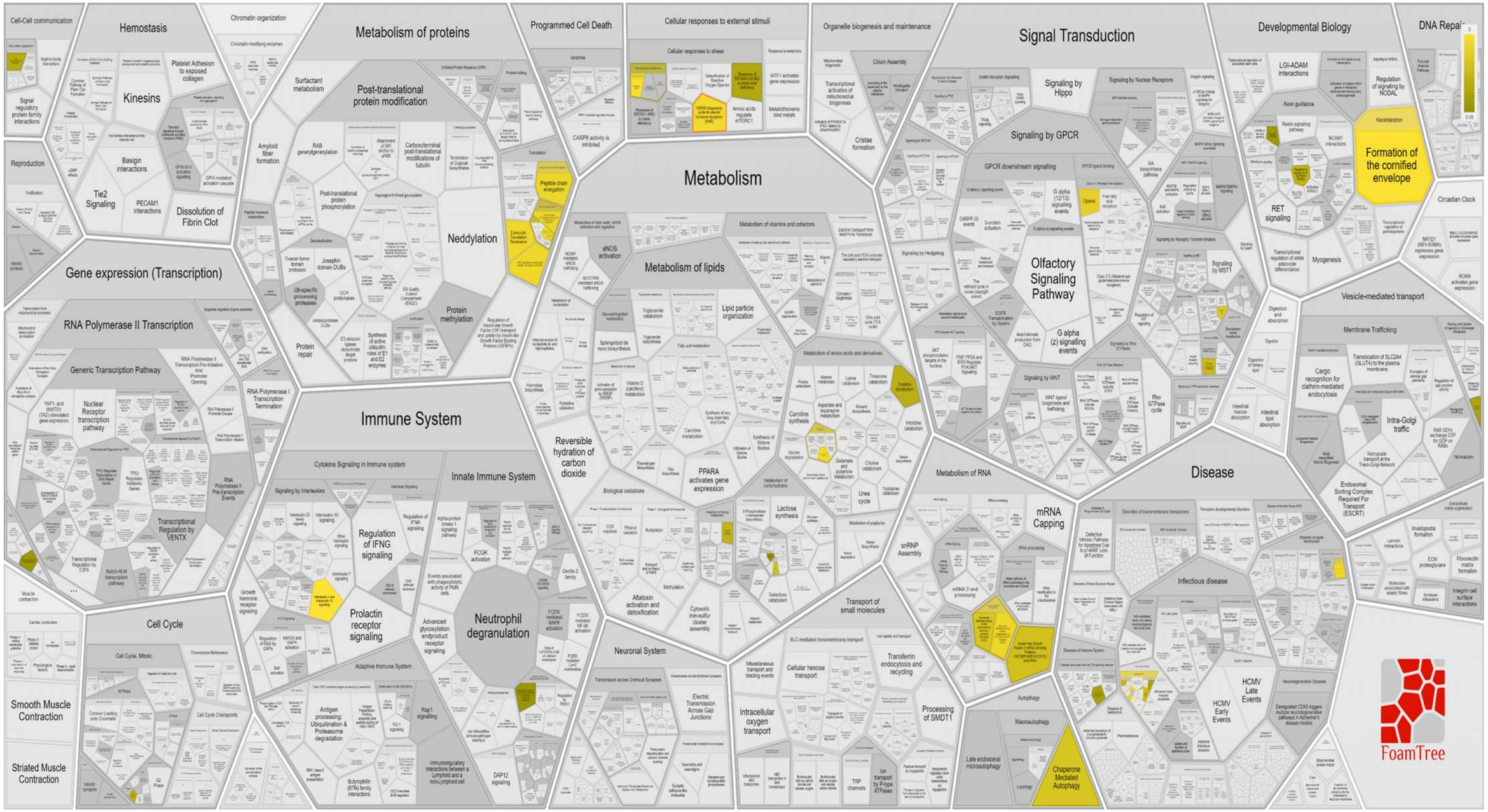

Table SD-2 for Pair B. 56 significant pathways generated by Reactome Pathways. Coloured cells are the top 10 most relevant pathways.

Pathway identifier	Pathway name	#Entities found	#Entities total	#Interactors found	#Interactors total	Entities ratio	Entities pValue	Entities FDR	#Reactions found	#Reactions total	Reactions ratio	Species identifier	Species name	Submitted entities found	Mapped entities	Submitted entities hit interactor	Interacts with	Found reaction identifiers
R-HSA-6785807	Interleukin-4 and Interleukin-13 signaling	4	211	0	143	0.014537688	4.29E-04	0.155759727	2	46	0.003622047	9606	Homo sapiens	HSPA8;HSP90AA1				R-HSA-6797269;R-HSA-6790041
R-HSA-3371568	Attenuation phase	2	47	0	1	0.003238253	0.001203973	0.155759727	4	5	3.94E-04	9606	Homo sapiens	HSPA8;HSP90AA1				R-HSA-3371554;R-HSA-5324617;R-HSA-5082369;R-HSA-5082384
R-HSA-6809371	Formation of the cornified envelope	3	138	0	84	0.009508061	0.001410096	0.155759727	8	27	0.002125984	9606	Homo sapiens	KRT19;KRT8				R-HSA-6810357;R-HSA-6811539;R-HSA-6814387;R-HSA-8942224;R-HSA-6814734;R-HSA-6814764;R-HSA-6814298;R-HSA-6810937
R-HSA-3371571	HSF1-dependent transactivation	2	59	0	1	0.004065041	0.00186676	0.155759727	5	8	6.30E-04	9606	Homo sapiens	HSPA8;HSP90AA1				R-HSA-3371554;R-HSA-5324617;R-HSA-5082356;R-HSA-5082369;R-HSA-5082384
R-HSA-168273	Influenza Viral RNA Transcription and Replication	3	175	2	93	0.012057324	0.002495973	0.155759727	3	14	0.001102362	9606	Homo sapiens	HSP90AA1;RPL14;RPL24	P07900;P50914;P83731	HSP90AA1;HSPA8	P07900	R-HSA-192704;R-HSA-192841;R-HSA-192830
R-HSA-6805567	Keratinization	3	226	0	84	0.015571173	0.00367219	0.155759727	15	34	0.002677165	9606	Homo sapiens	KRT19;KRT8				R-HSA-6806629;R-HSA-6805573;R-HSA-6814734;R-HSA-6814764;R-HSA-6805546;R-HSA-6806613;R-HSA-6810357;R-HSA-6811539;R-HSA-6814387;R-HSA-6806610;R-HSA-6809393;R-HSA-6809663;R-HSA-8942224;R-HSA-6814298;R-HSA-6810937
R-HSA-3371497	HSP90 chaperone cycle for steroid hormone receptors (SHR)	2	70	1	35	0.00482293	0.00515232	0.155759727	12	12	9.45E-04	9606	Homo sapiens	HSPA8;HSP90AA1	P11142;P07900	HSP90AA1	Q13451;Q02790;P31948;Q15185	R-HSA-5618085;R-HSA-3371590;R-HSA-5618080;R-HSA-5618099;R-HSA-5618098;R-HSA-5618093;R-HSA-5618110;R-HSA-5618105;R-HSA-3371503;R-HSA-5618073;R-HSA-3371422;R-HSA-5618107
R-HSA-9665244	Resistance of ERBB2 KD mutants to sapitinib	1	5	0	0	3.44E-04	0.005299788	0.155759727	1	1	7.87E-05	9606	Homo sapiens	HSP90AA1				R-HSA-9665304
R-HSA-9665233	Resistance of ERBB2 KD mutants to trastuzumab	1	5	0	0	3.44E-04	0.005299788	0.155759727	1	1	7.87E-05	9606	Homo sapiens	HSP90AA1				R-HSA-9665232
R-HSA-9665249	Resistance of ERBB2 KD mutants to afatinib	1	5	0	0	3.44E-04	0.005299788	0.155759727	1	1	7.87E-05	9606	Homo sapiens	HSP90AA1				R-HSA-9665311
R-HSA-9665251	Resistance of ERBB2 KD mutants to lapatinib	1	5	0	0	3.44E-04	0.005299788	0.155759727	1	1	7.87E-05	9606	Homo sapiens	HSP90AA1				R-HSA-9665284
R-HSA-9665250	Resistance of ERBB2 KD mutants to AEE788	1	5	0	0	3.44E-04	0.005299788	0.155759727	1	1	7.87E-05	9606	Homo sapiens	HSP90AA1				R-HSA-9665278
R-HSA-9665246	Resistance of ERBB2 KD mutants to neratinib	1	5	0	0	3.44E-04	0.005299788	0.155759727	1	1	7.87E-05	9606	Homo sapiens	HSP90AA1				R-HSA-9665286
R-HSA-9665245	Resistance of ERBB2 KD mutants to tesevatinib	1	5	0	0	3.44E-04	0.005299788	0.155759727	1	1	7.87E-05	9606	Homo sapiens	HSP90AA1				R-HSA-9665315
R-HSA-9665737	Drug resistance in ERBB2 TMD/JMD mutants	1	5	0	0	3.44E-04	0.005299788	0.155759727	1	1	7.87E-05	9606	Homo sapiens	HSP90AA1				R-HSA-9665708
R-HSA-9665247	Resistance of ERBB2 KD mutants to osimertinib	1	5	0	0	3.44E-04	0.005299788	0.155759727	1	1	7.87E-05	9606	Homo sapiens	HSP90AA1				R-HSA-9665280
R-HSA-72689	Formation of a pool of free 40S subunits	2	106	0	6	0.007303293	0.006076314	0.155759727	1	2	1.57E-04	9606	Homo sapiens	RPL14;RPL24				R-HSA-72673
R-HSA-72764	Eukaryotic Translation Termination	2	106	0	6	0.007303293	0.006183332	0.155759727	3	5	3.94E-04	9606	Homo sapiens	RPL14;RPL24				R-HSA-141671;R-HSA-141691;R-HSA-141673
R-HSA-2408557	Selenocysteine synthesis	2	113	0	2	0.007785586	0.006620019	0.155759727	2	7	5.51E-04	9606	Homo sapiens	RPL14;RPL24				R-HSA-2408529;R-HSA-5333615
R-HSA-1799339	SRP-dependent cotranslational protein targeting to membrane	2	119	0	0	0.00819898	0.007070411	0.155759727	5	5	3.94E-04	9606	Homo sapiens	RPL14;RPL24				R-HSA-1799326;R-HSA-1799330;R-HSA-1799329;R-HSA-1799335;R-HSA-1799332
R-HSA-975956	Nonsense Mediated Decay (NMD) independent of the Exon	2	101	0	23	0.006958798	0.00730071	0.155759727	1	1	7.87E-05	9606	Homo sapiens	RPL14;RPL24				R-HSA-927789

Pathway identifier	Pathway name	#Entities found	#Entities total	#Interactors found	#Interactors total	Entities ratio	Entities pValue	Entities FDR	#Reactions found	#Reactions total	Reactions ratio	Species identifier	Species name	Submitted entities found	Mapped entities	Submitted entities hit interactor	Interacts with	Found reaction identifiers
	Junction Complex (EJC)																	
R-HSA-156827	L13a-mediated translational silencing of Ceruloplasmin expression	2	120	0	2	0.008267879	0.00741713	0.155759727	1	3	2.36E-04	9606	Homo sapiens	RPL14;RPL24				R-HSA-156826
R-HSA-156902	Peptide chain elongation	2	97	0	32	0.006683202	0.008133314	0.170799596	4	5	3.94E-04	9606	Homo sapiens	RPL14;RPL24				R-HSA-156915;R-HSA-156912;R-HSA-156923;R-HSA-156907
R-HSA-192823	Viral mRNA Translation	2	114	0	22	0.007854485	0.009006769	0.180135378	2	2	1.57E-04	9606	Homo sapiens	RPL14;RPL24				R-HSA-192704;R-HSA-192841
R-HSA-168255	Influenza Infection	3	199	2	272	0.0137109	0.01133385	0.204191448	7	59	0.004645669	9606	Homo sapiens	HSP90AA1;RPL14;RPL24	P07900;P50914;P83731	HSP90AA1;HSPA8	P07900;P03485	R-HSA-192704;R-HSA-195926;R-HSA-192746;R-HSA-168299;R-HSA-192841;R-HSA-192830;R-HSA-168894
R-HSA-419771	Opsins	1	10	0	1	6.89E-04	0.011624145	0.204191448	1	2	1.57E-04	9606	Homo sapiens	GLB1L				R-HSA-419841
R-HSA-72706	GTP hydrolysis and joining of the 60S ribosomal subunit	2	120	0	47	0.008267879	0.012011262	0.204191448	2	3	2.36E-04	9606	Homo sapiens	RPL14;RPL24				R-HSA-72672;R-HSA-72671
R-HSA-9665230	Drug resistance in ERBB2 KD mutants	1	12	0	0	8.27E-04	0.012674466	0.215465921	8	8	6.30E-04	9606	Homo sapiens	HSP90AA1				R-HSA-9665315;R-HSA-9665232;R-HSA-9665280;R-HSA-9665286;R-HSA-9665284;R-HSA-9665304;R-HSA-9665311;R-HSA-9665278
R-HSA-156842	Eukaryotic Translation Elongation	2	102	0	73	0.007027697	0.013966207	0.223459307	4	9	7.09E-04	9606	Homo sapiens	RPL14;RPL24				R-HSA-156915;R-HSA-156912;R-HSA-156923;R-HSA-156907
R-HSA-9652282	Drug-mediated inhibition of ERBB2 signaling	1	14	0	0	9.65E-04	0.014771912	0.224599153	3	3	2.36E-04	9606	Homo sapiens	HSP90AA1				R-HSA-9652277;R-HSA-9652264;R-HSA-9665726
R-HSA-927802	Nonsense-Mediated Decay (NMD)	2	124	0	79	0.008543475	0.016885091	0.224599153	5	6	4.72E-04	9606	Homo sapiens	RPL14;RPL24				R-HSA-927836;R-HSA-927789;R-HSA-927832;R-HSA-927813;R-HSA-927889
R-HSA-975957	Nonsense Mediated Decay (NMD) enhanced by the Exon Junction Complex (EJC)	2	124	0	79	0.008543475	0.016885091	0.224599153	4	5	3.94E-04	9606	Homo sapiens	RPL14;RPL24				R-HSA-927836;R-HSA-927832;R-HSA-927813;R-HSA-927889
R-HSA-2408522	Selenoamino acid metabolism	2	181	0	15	0.012470718	0.018259218	0.224599153	2	33	0.002598425	9606	Homo sapiens	RPL14;RPL24				R-HSA-2408529;R-HSA-5333615
R-HSA-9613829	Chaperone Mediated Autophagy	2	23	3	179	0.001584677	0.01860999	0.224599153	17	19	0.001496063	9606	Homo sapiens	HSPA8;HSP90AA1	P11142;P07900	HSP90AA1;HSPA8;KRT19	P14136;P11142	R-HSA-9626034;R-HSA-9626256;R-HSA-9626039;R-HSA-9626235;R-HSA-9622840;R-HSA-9626046;R-HSA-9624158;R-HSA-9626242;R-HSA-9625188;R-HSA-9626276;R-HSA-9620197;R-HSA-9615721;R-HSA-9622831;R-HSA-9626060;R-HSA-9625196;R-HSA-9626253;R-HSA-9625197
R-HSA-428359	Insulin-like Growth Factor-2 mRNA Binding Proteins (IGF2BPs/IMPs/VICKZs) bind RNA	0	13	1	7	8.96E-04	0.021038762	0.224599153	1	3	2.36E-04	9606	Homo sapiens			HNRNPU	Q9NZI8	R-HSA-428296
R-HSA-168336	Uncoating of the Influenza Virion	0	18	1	7	0.001240182	0.022079531	0.224599153	1	2	1.57E-04	9606	Homo sapiens			HSPA8	P03485	R-HSA-168299
R-HSA-168270	Fusion and Uncoating of the Influenza Virion	0	18	1	7	0.001240182	0.022079531	0.224599153	1	5	3.94E-04	9606	Homo sapiens			HSPA8	P03485	R-HSA-168299
R-HSA-2022857	Keratan sulfate degradation	1	22	0	0	0.001515778	0.023119243	0.224599153	1	7	5.51E-04	9606	Homo sapiens	GLB1L				R-HSA-1630306
R-HSA-72737	Cap-dependent Translation Initiation	2	130	0	109	0.008956869	0.023621275	0.224599153	3	18	0.001417323	9606	Homo sapiens	RPL14;RPL24				R-HSA-72673;R-HSA-72672;R-HSA-72671
R-HSA-72613	Eukaryotic Translation Initiation	2	130	0	110	0.008956869	0.023816526	0.224599153	4	21	0.001653543	9606	Homo sapiens	RPL14;RPL24				R-HSA-72673;R-HSA-72672;R-HSA-156826;R-HSA-72671
R-HSA-1251985	Nuclear signaling by ERBB4	2	47	1	189	0.003238253	0.024802871	0.224599153	3	34	0.002677165	9606	Homo sapiens	STMN1	P16949;ENSG00000117632	KRT19	P14136	R-HSA-1253321;R-HSA-9612444;R-HSA-9612445
R-HSA-168303	Packaging of Eight RNA Segments	0	17	1	15	0.001171283	0.027267551	0.224599153	1	2	1.57E-04	9606	Homo sapiens			HSPA8	P03485	R-HSA-195926
R-HSA-163680	AMPK inhibits chREBP transcriptional activation activity	0	11	1	16	7.58E-04	0.027267551	0.224599153	1	4	3.15E-04	9606	Homo sapiens			HSP90AA1	Q15831	R-HSA-164151
R-HSA-8854521	Interaction between PHLDA1 and AURKA	0	4	1	24	2.76E-04	0.029335393	0.224599153	2	2	1.57E-04	9606	Homo sapiens			RPL14	Q8WV24	R-HSA-8853429;R-HSA-8853444

Pathway identifier	Pathway name	#Entities found	#Entities total	#Interactors found	#Interactors total	Entities ratio	Entities pValue	Entities FDR	#Reactions found	#Reactions total	Reactions ratio	Species identifier	Species name	Submitted entities found	Mapped entities	Submitted entities hit interactor	Interacts with	Found reaction identifiers
R-HSA-9010553	Regulation of expression of SLITs and ROBOs	2	183	0	81	0.012608516	0.029980948	0.224599153	2	20	0.001574803	9606	Homo sapiens	RPL14;RPL24				R-HSA-9014652;R-HSA-9014610
R-HSA-71288	Creatine metabolism	1	25	0	4	0.001722475	0.030367741	0.224599153	1	6	4.72E-04	9606	Homo sapiens	CKB				R-HSA-200318
R-HSA-446107	Type I hemidesmosome assembly	1	11	0	24	7.58E-04	0.034486659	0.224599153	1	6	4.72E-04	9606	Homo sapiens	KRT19				R-HSA-446077
R-HSA-3371556	Cellular response to heat stress	2	135	1	157	0.009301364	0.035093119	0.224599153	15	29	0.002283465	9606	Homo sapiens	HSPA8;HSP90AA1	P11142;P07900	HSP90AA1	Q15185	R-HSA-5251955;R-HSA-5082409;R-HSA-5251959;R-HSA-5324632;R-HSA-5082369;R-HSA-3371518;R-HSA-3371554;R-HSA-3371586;R-HSA-5251942;R-HSA-3371467;R-HSA-5324617;R-HSA-5082356;R-HSA-5252041;R-HSA-5082384;R-HSA-5252079
R-HSA-9633012	Response of EIF2AK4 (GCN2) to amino acid deficiency	2	115	1	170	0.007923384	0.035322679	0.224599153	5	16	0.001259843	9606	Homo sapiens	RPL14;RPL24	P50914;P83731	HSPA8	P08243	R-HSA-9633008;R-HSA-1791118;R-HSA-9633742;R-HSA-9634669;R-HSA-9633005
R-HSA-3000484	Scavenging by Class F Receptors	1	16	0	20	0.001102384	0.037564882	0.224599153	2	2	1.57E-04	9606	Homo sapiens	HSP90AA1				R-HSA-2247514;R-HSA-2197645
R-HSA-5603027	IKBKG deficiency causes anhidrotic ectodermal dysplasia with immunodeficiency (EDA-ID) (via TLR)	0	3	1	37	2.07E-04	0.038588872	0.224599153	1	1	7.87E-05	9606	Homo sapiens			HSP90AA1	O15111	R-HSA-5262921
R-HSA-168330	Viral RNP Complexes in the Host Cell Nucleus	0	15	1	29	0.001033485	0.039611823	0.224599153	1	3	2.36E-04	9606	Homo sapiens			HSPA8	P03485	R-HSA-192746
R-HSA-399954	Sema3A PAK dependent Axon repulsion	1	19	0	29	0.001309081	0.045727744	0.224599153	2	6	4.72E-04	9606	Homo sapiens	HSP90AA1				R-HSA-419644;R-HSA-419645
R-HSA-5601884	PIWI-interacting RNA (piRNA) biogenesis	1	31	0	13	0.002135869	0.045727744	0.224599153	1	15	0.001181102	9606	Homo sapiens	HSP90AA1				R-HSA-5601883
R-HSA-3134963	DEx/H-box helicases activate type I IFN and inflammatory cytokines production	0	7	1	40	4.82E-04	0.046743443	0.224599153	1	5	3.94E-04	9606	Homo sapiens			HNRNPU	Q08211	R-HSA-3134954
R-HSA-2024096	HS-GAG degradation	1	44	0	1	0.003031556	0.046743443	0.224599153	1	14	0.001102362	9606	Homo sapiens	GLB1L				R-HSA-2090079

Chapter 4

Anticonvulsive Potential of *Orthosiphon stamineus* Proteins in Zebrafish Model Induced by Pentylenetetrazol

4.1 Introduction

Epilepsy is a common neurologic disorder, affecting about 70 million people worldwide (Ngugi, Bottomley, Kleinschmidt, Sander, & Newton, 2010). Among, nearly one-third of the people have epilepsy that is not well controlled by a single antiepileptic drug (AED). Consequently, they often require add-on therapy, a treatment strategy using two or more AEDs (Chen et al., 2019). In the continuous search for effective treatments for epilepsy and its associated complications, the fundamental contribution of medicinal plants must not be understated.

Orthosiphon stamineus (OS) has recently been reported for protective effects on the central nervous system (CNS) (Choo et al., 2018; George et al., 2015; Retinasamy, Shaikh, Kumari, & Othman, 2019; Sree, Sri, & Ramarao, 2015). Typically, these studies focus only on the secondary metabolites of OS. Up to date, there is no systematic study on the primary metabolites of OS. Meanwhile, using another medicinal plant namely *Nicotiana tabacum* L., S. Shah et al. (2017) found protein osmotin (24 kDa) was protective for the CNS. This thus sees a lack of science-backed evidence to justify the therapeutic potential of OS primary metabolites for the CNS, let alone its proteins. OS proteins, could be similar to protein osmotin, also hold valuable protective potential for the CNS. The proteins extracted from OS leaves (OSLP) is therefore worthy of investigation.

In light of the current situation, the anticonvulsive potential of OSLP in an *in vivo* system is worthy of exploration. Zebrafish (*Danio rerio*) is a promising model in the research of epilepsy and drug discovery. Zebrafish shares a genetic profile with about 70% similarity to that of human and about 84% of genes known to human diseases are also expressed in zebrafish (Howe et al., 2013; Norton & Bally-Cuif, 2010). Zebrafish model of seizures can be induced using pentylenetetrazol (PTZ) (Copmans, Siekierska, & de Witte, 2017). PTZ is a tetrazol derivative (Stone, 1970). PTZ exerts its convulsive effects by inhibiting gamma-aminobutyric acid (GABA) activity at $GABA_A$ receptors (R.-Q. Huang et al., 2001; Shaikh, Sancheti, & Sathaye, 2013; Velíšek, 2009). PTZ is well known for its use in screening antiepileptic drugs (Desmond et al., 2012; Kundap, Kumari, Othman, & Shaikh, 2017; Shaikh et al., 2013; Zhao & Holmes, 2006).

The present chapter begins with elucidating the safety study of OSLP in normal adult zebrafish without PTZ induction. The maximum safe starting dose of OSLP determined is then used in the screening against anticonvulsive potential in zebrafish challenged by PTZ injection. Behavioral study based on changes in seizure frequency, seizure onset time, and

locomotor activity is evaluated. Expressions of the two major neurotransmitters, GABA and glutamate (Glu) are analysed using nanoflow-ESI-LCMS/MS. The protective mechanism of OSLP on zebrafish brains at protein levels is also investigated using mass spectrometry-based label-free proteomic quantification (LFQ). LFQ profiles the differentially expressed proteins between the non-seizures and OSLP-treated seizures. This thus provides fundamental information to study the functional annotations, the protein-protein interactions and their gene-disease associations. These enriched biological data provides information to the molecular interactions, reactions and relations associated with the anticonvulsive mechanism of OSLP on disease pathway maps. Hence, the objectives of this chapter are:

1. To elucidate the maximum safe starting dose of OSLP achievable via intraperitoneal (i.p.) route in normal zebrafish
2. To evaluate OSLP anticonvulsive potential in the PTZ-induced zebrafish model
3. To evaluate the anticonvulsive mechanism of OSLP using neurotransmitters and protein expression analysis.

The flowchart outlining the overview of experimental design to achieve the objectives are summarised in Figure 4.1 below:

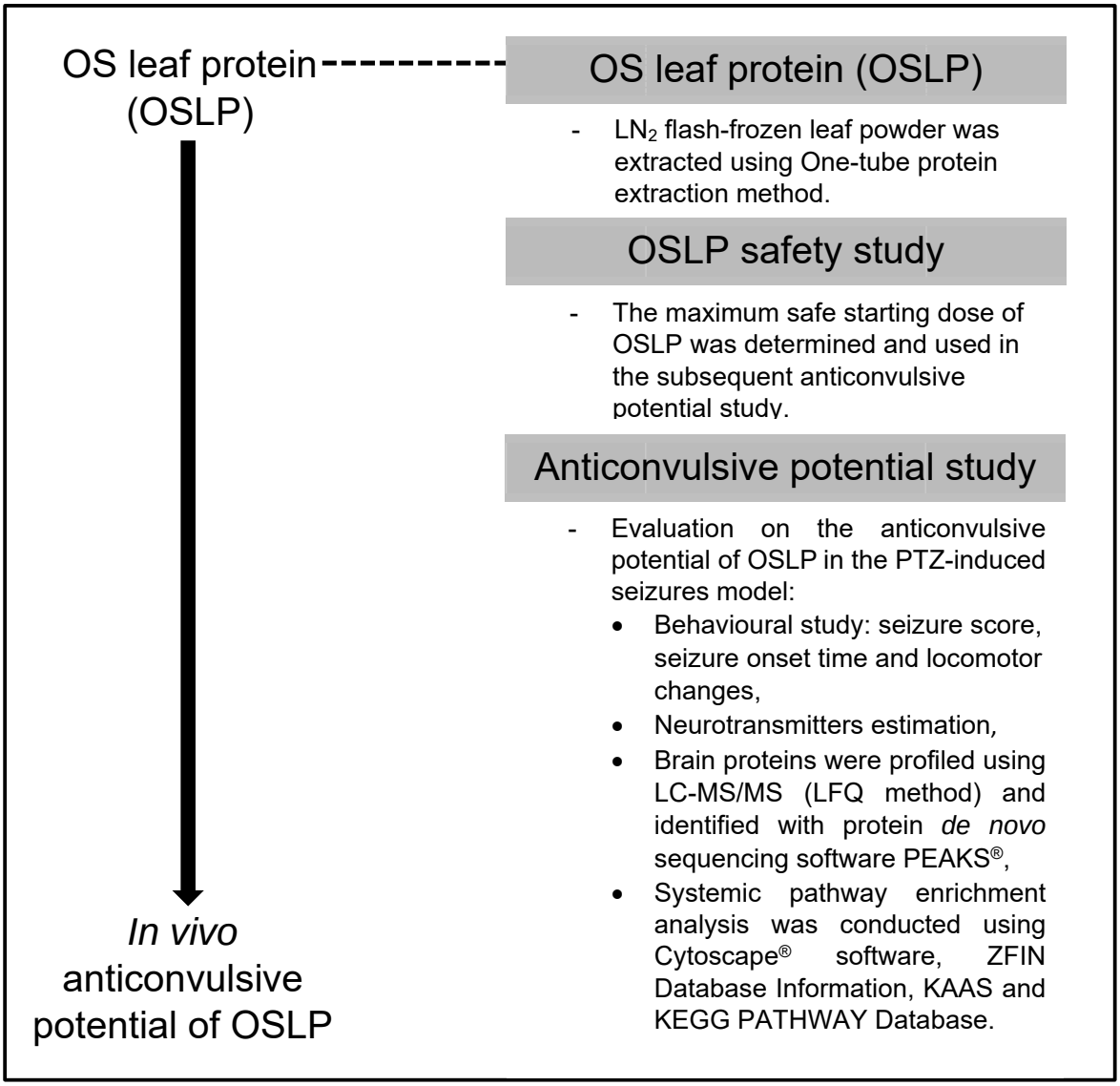

Figure 4.1: Flowchart summarizing the overview of experimental design.

References:

Chen, H., He, H., Xiao, Y., Luo, M., Luo, H., & Wang, J. (2019). Losigamone add-on therapy for focal epilepsy. *Cochrane Database of Systematic Reviews*(12).

Choo, B. K. M., Kundap, U. P., Kumari, Y., Hue, S.-M., Othman, I., & Shaikh, M. F. (2018). Orthosiphon stamineus Leaf Extract Affects TNF-α and Seizures in a Zebrafish Model. *Frontiers in Pharmacology, 9*, 139. doi:10.3389/fphar.2018.00139

Copmans, D., Siekierska, A., & de Witte, P. A. M. (2017). Chapter 26 - Zebrafish Models of Epilepsy and Epileptic Seizures. In A. Pitkänen, P. S. Buckmaster, A. S. Galanopoulou, & S. L. Moshé (Eds.), *Models of Seizures and Epilepsy (Second Edition)* (pp. 369-384): Academic Press.

Desmond, D., Kyzar, E., Gaikwad, S., Green, J., Riehl, R., Roth, A., . . . Kalueff, A. V. (2012). Assessing epilepsy-related behavioral phenotypes in adult zebrafish. In *Zebrafish protocols for neurobehavioral research* (pp. 313-322): Springer.

George, A., Chinnappan, S., Choudhary, Y., Choudhary, V. K., Bommu, P., & Wong, H. J. (2015). Effects of a Proprietary Standardized *Orthosiphon stamineus* Ethanolic Leaf Extract on Enhancing Memory in Sprague Dawley Rats Possibly via Blockade of Adenosine A(2A) Receptors. *J. Evid. Based Complementary Altern. Med. : eCAM, 2015*, 375837. doi:10.1155/2015/375837

Howe, K., Clark, M. D., Torroja, C. F., Torrance, J., Berthelot, C., Muffato, M., . . . Stemple, D. L. (2013). The zebrafish reference genome sequence and its relationship to the human genome. *Nature, 496*(7446), 498-503. doi:10.1038/nature12111

Huang, R.-Q., Bell-Horner, C. L., Dibas, M. I., Covey, D. F., Drewe, J. A., & Dillon, G. H. (2001). Pentylenetetrazole-induced inhibition of recombinant γ-aminobutyric acid type A (GABAA) receptors: mechanism and site of action. *Journal of Pharmacology and Experimental Therapeutics, 298*(3), 986-995.

Kundap, U. P., Kumari, Y., Othman, I., & Shaikh, M. F. (2017). Zebrafish as a Model for Epilepsy-Induced Cognitive Dysfunction: A Pharmacological, Biochemical and Behavioral Approach. *Frontiers in Pharmacology, 8*(515). doi:10.3389/fphar.2017.00515

Norton, W., & Bally-Cuif, L. (2010). Adult zebrafish as a model organism for behavioural genetics. *BMC Neuroscience, 11*(1), 90. doi:10.1186/1471-2202-11-90

Ngugi, A.K., Bottomley, C., Kleinschmidt, I., Sander, J.W. and Newton, C.R. (2010), Estimation of the burden of active and life-time epilepsy: A meta-analytic approach. Epilepsia, 51: 883-890. doi:10.1111/j.1528-1167.2009.02481.x

Retinasamy, T., Shaikh, M. F., Kumari, Y., & Othman, I. (2019). Ethanolic Extract of Orthosiphon stamineus Improves Memory in Scopolamine-Induced Amnesia Model. *Frontiers in Pharmacology, 10*(1216). doi:10.3389/fphar.2019.01216

Shah, S., Yoon, G., Chung, S., Abid, M., Kim, T., Lee, H., & Kim, M. (2017). Novel osmotin inhibits SREBP2 via the AdipoR1/AMPK/SIRT1 pathway to improve Alzheimer's disease neuropathological deficits. *Molecular psychiatry, 22*(3), 407.

Shaikh, M., Sancheti, J., & Sathaye, S. (2013). Effect of Eclipta alba on acute seizure models: a GABAA-mediated effect. *Indian journal of pharmaceutical sciences, 75*(3), 380.

Sree, N. V., Sri, P. U., & Ramarao, N. (2015). Neuro-Protective Properties Of Orthosiphon Staminus (Benth) Leaf Methanolic Fraction Through Antioxidant Mechanisms On SH-SY5Y Cells: An In-Vitro Evaluation. *International Journal of Pharmaceutical Sciences and Research, 6*(3), 1115.

Stone, W. (1970). Convulsant actions of tetrazole derivatives. *Pharmacology, 3*(6), 367-370.

Velíšek, L. (2009). MODELS | Models of Generalized Seizures in Freely Moving Animals. In P. A. Schwartzkroin (Ed.), *Encyclopedia of Basic Epilepsy Research* (pp. 775-780). Oxford: Academic Press.

Zhao, Q., & Holmes, G. L. (2006). CHAPTER 27 - Repetitive Seizures in the Immature Brain**Grant sponsors: NIH NINDS; Grant numbers: NS27984 and NS44295. In A. Pitkänen, P. A. Schwartzkroin, & S. L. Moshé (Eds.), *Models of Seizures and Epilepsy* (pp. 341-350). Burlington: Academic Press.

biomedicines

MDPI

Article

Orthosiphon stamineus Proteins Alleviate Pentylenetetrazol-Induced Seizures in Zebrafish

Yin-Sir Chung [1,2], Brandon Kar Meng Choo [1], Pervaiz Khalid Ahmed [3,4], Iekhsan Othman [1,2] and Mohd. Farooq Shaikh [1,*]

1 Neuropharmacology Research Laboratory, Jeffrey Cheah School of Medicine and Health Sciences, Monash University Malaysia, Bandar Sunway 47500, Malaysia; chung.yinsir@monash.edu (Y.-S.C.); Brandon.Choo@monash.edu (B.K.M.C.); Iekhsan.Othman@monash.edu (I.O.)
2 Liquid Chromatography-Mass Spectrometry (LCMS) Platform, Jeffrey Cheah School of Medicine and Health Sciences, Monash University Malaysia, Bandar Sunway 47500, Malaysia
3 School of Business, Monash University Malaysia, Bandar Sunway 47500, Malaysia; pervaiz.ahmed@monash.edu
4 Global Asia in the 21st Century (GA21), Monash University Malaysia, Bandar Sunway 47500, Malaysia
* Correspondence: farooq.shaikh@monash.edu

Received: 4 June 2020; Accepted: 30 June 2020; Published: 2 July 2020

Abstract: The anticonvulsive potential of proteins extracted from *Orthosiphon stamineus* leaves (OSLP) has never been elucidated in zebrafish (*Danio rerio*). This study thus aims to elucidate the anticonvulsive potential of OSLP in pentylenetetrazol (PTZ)-induced seizure model. Physical changes (seizure score and seizure onset time, behavior, locomotor) and neurotransmitter analysis were elucidated to assess the pharmacological activity. The protective mechanism of OSLP on brain was also studied using mass spectrometry-based label-free proteomic quantification (LFQ) and bioinformatics. OSLP was found to be safe up to 800 µg/kg and pre-treatment with OSLP (800 µg/kg, i.p., 30 min) decreased the frequency of convulsive activities (lower seizure score and prolonged seizure onset time), improved locomotor behaviors (reduced erratic swimming movements and bottom-dwelling habit), and lowered the excitatory neurotransmitter (glutamate). Pre-treatment with OSLP increased protein Complexin 2 (Cplx 2) expression in the zebrafish brain. Cplx2 is an important regulator in the trans-SNARE complex which is required during the vesicle priming phase in the calcium-dependent synaptic vesicle exocytosis. Findings in this study collectively suggests that OSLP could be regulating the release of neurotransmitters via calcium-dependent synaptic vesicle exocytosis mediated by the "Synaptic Vesicle Cycle" pathway. OSLP's anticonvulsive actions could be acting differently from diazepam (DZP) and with that, it might not produce the similar cognitive insults such as DZP.

Keywords: *Orthosiphon stamineus*; plant-derived proteins; epilepsy; seizures; zebrafish

1. Introduction

Epilepsy is a chronic non-communicable disease of the brain that affects around 70 million people of all ages worldwide and accounts for about 1% of the global burden of disease. Epilepsy has a high prevalence and an estimated five million people are diagnosed with epilepsy each year. Epilepsy is characterized by recurrent seizures due to brief disturbances in the electrical functions of the brain. It involves brief episodes of involuntary movement that lead to changes in sensory perception, motor control, behavior, autonomic function, or sometimes loss of consciousness [1]. To date, despite having more than 30 antiepileptic drugs (AEDs) on the market [2,3], there are still difficulties in reaching the goal of treating epilepsy and its associated complications without adverse effects. Globally, epilepsy remains a public health imperative.

People with epilepsy often require lifelong treatment. AEDs are the mainstay of treatment. These conventional drugs bring about clinically worthwhile improvements but have tolerability issues due to their side effects. Many AEDs used in current mainstream clinical practice have been reported to elicit undesired neuropsychological consequences such as depression (24% lifetime prevalence), anxiety (22%), and intellectual disability, particularly in children with epilepsy (30%–40%) [1]. More than one-third of epileptic seizures are not well controlled by a single AED and often require treatment with two or more AEDs (add-on therapy) [1,2]. Furthermore, about 40%–60% of epileptic patients, accounting for both children and adults, develop neuropsychological impairments [3]. This drives a significant portion of epileptic patients to seek alternative interventions, particularly in herbal medicine [4]. Current systematic studies are reporting promising anticonvulsive activities in a constellation of medicinal plants [5,6].

Orthosiphon stamineus (OS) or *Orthosiphon aristatus var. aristatus* (OAA), also commonly known as cat's whiskers or "misai kucing," is an important medicinal plant. Choo et al. (2018) has shown that the ethanolic extract of OS, exhibited anticonvulsive activity in zebrafish Choo, Kundap [7] and Coelho et al. (2015) has demonstrated the anticonvulsant potential of rosmarinic acid in mice, which is an active chemical constituent in OS extract Coelho, Vieira [8]. Nonetheless, until now the protective potential of OS primary metabolites has not been studied, let alone its proteins. The proteins extracted from OS leaves (OSLP) may also hold valuable protective potential for central nervous system (CNS) disorders such as epilepsy. In the research of epilepsy and drug discovery, zebrafish (*Danio rerio*) has been widely recognised as an important and promising vertebrate model. Genetic profile of zebrafish shares approximately 70% similarity with human and about 84% of genes known to human diseases are also expressed in zebrafish [9,10]. This makes the zebrafish model particularly useful as a high-throughput screening system in studying mechanisms of brain functions and dysfunctions [11]. To the best of our knowledge, this is the first study on elucidating the anticonvulsive potential of proteins extracted from OSLP.

2. Experimental Section

2.1. Materials Chemicals and Apparatuses

L-Glutamic acid (Glu), Gamma-Aminobutyric acid (γ-aminobutyric acid), Pentylenetetrazol (PTZ), Diazepam (DZP), Benzocaine, complete EDTA-free protease inhibitors, phosphatase inhibitors cocktail 2, dithiothreitol (DTT), trifluoroethanol (TFE), ammonium bicarbonate (ABC), 2,3,5-triphenyltetrazolium chloride (TTC), formic acid (FA), and methanol (MeOH) of HPLC-grade were purchased from Sigma-Aldrich (St. Louis, MO, USA). Pierce®trypsin protease, Pierce® Radioimmunoprecipitation assay (RIPA) buffer of mass spec grade and Pierce®C18 mini spin columns were purchased from Thermo Scientific Pierce (Rockford, IL, USA). Protein LoBind microcentrifuge tube (Eppendorf, Enfield, CT, USA), acetonitrile (ACN), trifluoroacetic acid (TFA), indoleacetic acid (IAA) and CHAPS (Nacailai Tesque, Kyoto, Japan) of mass spec grade were from Sigma-Aldrich (St. Louis, MO, USA), Quick Start™ Bradford Protein Assay Kit from Bio-Rad (Hercules, CA, USA), Dimethylsulfoxide (DMSO) and 37% formaldehyde solution were from Friendemann Schmidt Chemical (Parkwood, Western Australia), Milli-Q ultrapure (MQUP) water from Millipore GmbH (Darmstad, Germany), acetic acid (glacial, 100%) from Merck (Darmstadt, Germany) and Phosphate buffered saline (PBS) tablets from VWR Life Science AMRESCO® (Radnor, PA, USA). Liquid nitrogen was purchased from Linde Malaysia, Hamilton syringes 25 µL (MICROLITER™ #702) from Hamilton Co. (Reno, NV, USA), 35 gauge needles (PrecisionGlide™) were from Becton, Dickinson and Company (Franklin Lakes, NJ, USA), ultrasonic cell crusher (JY88-II N, Shanghai Xiwen Biotech. Co., Ltd., Shanghai, China), Eyela SpeedVac Vacuum Concentrator (Thermo Scientific Pierce, Rockford, IL, USA), Camry High-Precision Electronic Pocket Scale (Model EHA901, Zhaoqing, China) and Classic pH Pen Tester from Yi Hu Fish Farm Trading Pte. Ltd. (Singapore). The other chemicals of analytical grade were from established suppliers worldwide.

2.2. Software and Equipment

For the behavioral study, SMART V3.0.05 tracking software (Panlab Harvard Apparatus, Barcelona, Spain) was used for the automated tracking of zebrafish swimming patterns. The video recorded using the camcorder was analyzed using the software. The water-filled tank was divided into two halves of the same size; the upper-half was marked as the top zone and the lower-half as the bottom zone as described by Kundap et al. 2017 [12].

For the neurotransmitter analysis, the solvent delivery was performed using Agilent Ultra High-Performance Liquid Chromatography (UHPLC) 1290 Series (Agilent Technologies, Santa Clara, CA, USA) consisting of Agilent 1290 Series High-Performance Autosampler, Agilent 1290 Series Binary Pump and Agilent 1290 Series Thermostatted Column Compartment; the separations were performed using Zorbax Eclipse Plus C18 (Rapid Resolution HD, 2.1 × 150.0 mm with 1.8 µM pore size reverse-phase column) (Agilent Technologies, Santa Clara, CA, USA), and coupled with Agilent 6410B Triple Quadrupole (QQQ) mass spectrometer equipped with an electrospray ionization (ESI) (Agilent Technologies, Santa Clara, CA, USA) to detect the targeted neurotransmitters.

In the protein expression study, Agilent 1200 series HPLC coupled with Agilent 6550 iFunnel Quadrupole Time of Flight (Q-TOF) LC/MS, C-18 300Å Large Capacity Chip (Agilent Technologies, Santa Clara, CA, USA) and Agilent MassHunter data acquisition software were used to identify the differentially expressed proteins (Agilent Technologies, Santa Clara, CA, USA). In addition, PEAKS®Studio software (Version 8.0, Bioinformatics Solution, Waterloo, ON, Canada) and UniProtKB (Organism: *Danio rerio*) database were used for the analysis of mass spectrometry-based label-free proteomic quantification (LFQ). Cytoscape software (Version 3.7.2 plugin BiNGO for Gene Ontology (GO) annotated information, Cytoscape Consortium, San Diego, CA, USA), Zebrafish Information Network (ZFIN) Database Information, KAAS (KEGG Automatic Annotation Server Version 2.1, Kanehisa Lab., Kyoto, Japan) and KEGG PATHWAY Database (Organism: *Danio rerio*) were used to study the functional annotations, protein-protein interactions, and systemic pathway enrichment analysis.

2.3. Zebrafish Maintenance and Housing Conditions

Adult zebrafish (*Danio rerio*; 3–4 months old) of heterogeneous strain wild-type stock (standard short-fin phenotype) were housed in the Animal Facility of Monash University Malaysia and maintained under standard husbandry conditions as follows: standard zebrafish tanks (length of 36 cm × width of 22 cm × height of 26 cm) equipped with circulating water systems to provide constant aeration, controlled water temperature between 26–28 °C and controlled water pH between 6.8–7.1. They were kept in stress-free and hygienic conditions. The zebrafish aquarium was maintained under a 250-lux light intensity with a cycle of 14-h of light to 10-h of darkness controlled by autotimer (light on at 0800 and light off at 2200). Group housing was practiced (10–12 fish per tank) with the females and males separated. The adult zebrafish were fed ad libitum three times a day (TetraMin® Tropical Flakes) and were supplemented with live brine shrimps (Artemia) purchased from Bio-Marine (Aquafauna Inc., Hawthorne, CA, USA). The adult zebrafish were allowed to acclimatize for a period of seven days to reduce stress before commencing the experiments. The Monash University Malaysia Animal Ethics Committee approved all the animal experimental procedures on 17 January 2019.

2.4. Experimental Design

2.4.1. OSLP Safety Study in Adult Zebrafish

A limit test was first performed based on a modified version of the OECD Guidelines for the Testing of Chemicals No. 203 [11,12] and the protocols of Choo et al. [10,13]. Prior to the experimental procedures, all the adult zebrafish were fasted for 24 h. Meanwhile, OSLP powder was completely dissolved in tank water (26–28 °C) and concentrations ranging from 50–1600 µg/kg of zebrafish body weight were freshly prepared. Three-month-old adult zebrafish with an average weight of 0.45–0.50 g

were selected. The zebrafish were then divided into 7 groups (Table 1), with 8 fish per group (n = 8) as follows:

Table 1. Experimental groups in OSLP safety study.

Group	Treatment
VC	Vehicle control (tank water, i.p.)
Treatment Group a	OSLP (50 µg/kg, i.p.)
Treatment Group b	OSLP (100 µg/kg, i.p.)
Treatment Group c	OSLP (200 µg/kg, i.p.)
Treatment Group d	OSLP (400 µg/kg, i.p.)
Treatment Group e	OSLP (800 µg/kg, i.p.)
Treatment Group f	OSLP (1600 µg/kg, i.p.)

A clean observation tank was first set up and filled with 13 L of tank water (Milli-Q filtered water used for keeping the zebrafish; 26–28 °C). One zebrafish from the vehicle control (VC) group was then placed in the observation tank and its behavior was recorded for 10 min using a digital camera (Sony, Japan). After finishing recording, the zebrafish was transferred into a clean individual 1 L tank filled with the same water. This procedure was then repeated for all the other zebrafish in the VC group. For the OSLP-treated groups (II–VII), different concentrations of OSLP were injected intraperitoneally (i.p.) into the zebrafish. Before each IP injection, a zebrafish was individually immersed in anesthesia solution (30 mg/L of Benzocaine) until the cessation of movement [10,13,14]. Immediately, the zebrafish was extracted out to determine the body weight and to calculate the injection volume. The injection volume was calculated at a volume corresponding to 10 microliters per gram of body weight (modified from 15). After injection, the zebrafish was immediately transferred back to the 13 L observation tank. Then, the same recording and tank transfer procedure was repeated, as performed in the VC group. All 56 zebrafish were then kept for 96 h in their respective 1 L tanks. They were checked on every 15 min for the first two hours of exposure and every half an hour thereafter for the first day. On subsequent days, the zebrafish were checked on the morning, afternoon, and evening (3 times per day). Any zebrafish found to exhibit signs of pain, suffering, or anomaly according to our predefined monitoring sheet at any checkpoint were humanely euthanized via an overdose of benzocaine. This protocol deviates from the OECD guidelines in that it does not use mortality as the criterion to determine toxic effects due to the concerns of the MARP-Australia in using death as an endpoint.

2.4.2. Anticonvulsive Potential of OSLP in Adult Zebrafish

The anticonvulsive potential of OSLP was investigated in the pentylenetetrazol (PTZ)-induced seizure model. Seizure score and seizure onset time, were one of the primary evaluation parameters used to examine the anticonvulsive activity. Behavioral changes in the zebrafish were determined by evaluating their swimming patterns, total distance travelled (cm) and time spent in the tank (upper-half versus lower-half, s). Three-month-old adult zebrafish with an average weight of 0.45–0.50 g were selected. Prior to beginning the experiments, the zebrafish were kept in 1 L treatment tanks filled with 1 L of tank water (26–28 °C) normally used to fill the zebrafish tanks. In this study, the zebrafish were divided into 5 groups (n = 10) (Table 2) and procedures of experiment (Figure 1) were as follows:

Table 2. Experimental groups in the evaluation of OSLP anti-convulsive potential.

Group	Treatment
VC	Vehicle control (tank water, i.p. + tank water)
NC	Negative control (tank water + PTZ 170 mg/kg, i.p.)
PC	Positive control (DZP 1.25 mg/kg + PTZ 170 mg/kg, i.p.)
TC	Treatment control (800 µg/kg + tank water, i.p.)
O+P	OSLP-treated PTZ (800 µg/kg + PTZ 170 mg/kg, i.p.)

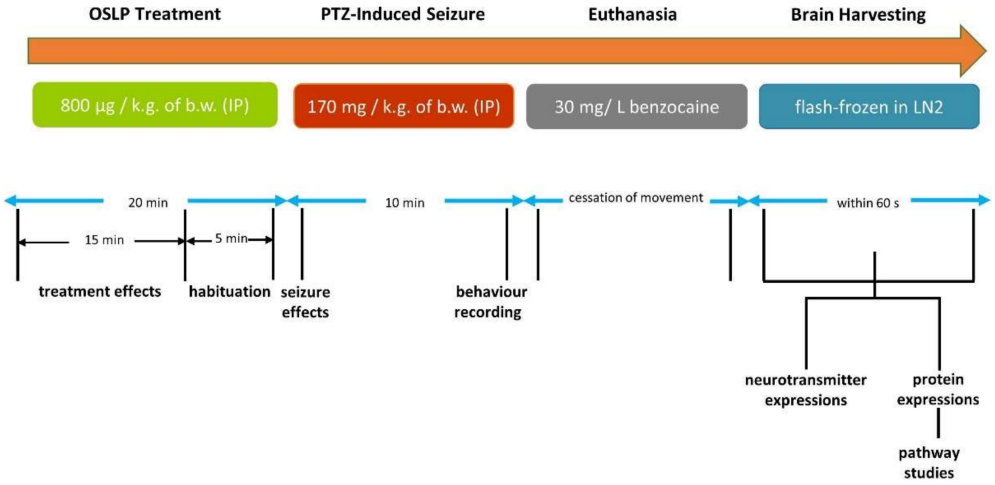

Figure 1. Shows the procedures of experiment.

All the groups were habituated in their treatment tanks for a half hour before the administration of PTZ. Before each i.p. injection, a zebrafish was individually immersed in anesthesia solution (30 mg/L of Benzocaine) until the cessation of movement. When multiple IP injections were required in tandem on the same zebrafish, the injections were given at alternating lateral ends, rather than the midline between the pelvic fins 10, 13, 14. The VC group was injected with tank water twice. The NC group was first pre-treated with tank water and then PTZ (170 mg/kg) whereas the PC group was pre-treated with diazepam (1.25 mg/kg) followed by PTZ (170 mg/kg). The TC group was injected with 800 µg/kg of OSLP and tank water. The O+P group was pre-treated with OSLP (800 µg/kg) followed by PTZ (170 mg/kg). PTZ-induced seizures lasted for approximately 10 min after the PTZ injection [10,13,14]. All the groups were then transferred to a 13 L observation tank filled three quarters of the way with water. Behavioral changes of the zebrafish were then recorded individually (10 min) with a digital camera (Sony, Japan). The PTZ injected zebrafish presented diverse seizure profiles, intensities and latency in reaching the different seizure scores and seizure onset times. In order to determine the seizure score and seizure onset time, the individual video was analyzed using a computer as per the scoring system below (Table 3) [10,13–16]:

Table 3. Seizure scoring system.

Score	Criteria
1	short swim mainly at the bottom of tank
2	increased swimming activity and high frequency of opercular movements
3	burst swimming, left and right movements as well as the erratic movements
4	circular movements

At the end of the experiment, all the groups were sacrificed. The zebrafish were euthanized with 30 mg/L of Benzocaine until the cessation of movement. The brains were then carefully harvested for neurotransmitter analysis, protein expression study and systemic pathway enrichment analysis.

2.5. Extraction of Brains from Zebrafish

At the end of the behavioral studies, the zebrafish brains were carefully harvested from the zebrafish skulls and kept in a sterile Petri dish. Each brain was then immediately transferred into a sterile, pre-chilled 2.0 mL microtube and was flash-frozen in liquid nitrogen (LN_2) before storing them at −152 °C until further analysis.

2.6. Brain Neurotransmitter Analysis Using Nanoflow Liquid Chromatography Coupled with Tandem Mass Spectrometry (Nanoflow-ESI-LC-MS/MS)

The levels of neurotransmitters in the brains, namely gamma-aminobutyric acid (GABA) and glutamate (Glu) were estimated using LC-MS/MS with modifications [13,14,17]. All experiments were performed in 3 independent biological replicates.

A mother stock of neurotransmitter standards was prepared by mixing GABA and Glu in methanol, MQUP water and 0.1% formic acid, to make up a final concentration of 1 mg/mL. Next, serial dilution was performed to prepare 8 points of standard calibrations ranging from 6.25–1000 ng/mL. A blank (methanol, MQUP water in 0.1% formic acid) with a final concentration of 1 mg/mL was also prepared. Together with the 8 points of standard calibrations, they were used for quantifying the levels of GABA and Glu in LC-MS/MS study.

Firstly, each LN_2 flash-frozen zebrafish brain was homogenized in 1 mL ice-cold methanol/MQUP water (3:1, *vol*/*vol*) using an ultrasonic cell crusher (JY88-II N, Shanghai Xiwen Biotech. Co., Ltd., Shanghai, China). The homogenate was then vortex-mixed (2500 rpm, 3 m) and later incubated on an agitating shaker (4 °C, 1 h). The homogenate was then centrifuged (4 °C, 10,000× *g*, 10 min) and the supernatant was carefully transferred into a sterile 2.0 mL microtube. 100 µL of 0.1% formic acid was slowly added, vortex-mixed (2500 rpm, 3 m) and then centrifuged (4 °C, 10,000× *g*, 10 min). The supernatant was carefully transferred into a sterile insert and vial. Finally, all the brain samples were subjected to LC-MS/MS analysis.

LC-MS/MS was run on an Agilent 1290 Infinity UHPLC coupled with an Agilent 6410B Triple Quad MS/MS equipped with an electrospray ionization (ESI). The separations were performed using Zorbax Eclipse Plus C18 (Rapid Resolution HD, 2.1 × 150.0 mm with 1.8 uM pore size reverse-phase column). The flow rate was 0.3 mL/min with the mobile phase consisting of 0.1% formic acid in water (Solvent A) and acetonitrile (Solvent B). The gradient elution used was: (i) 0 min, 5% Solvent B; (ii) 0–3 min, 50% Solvent B and (iii) 3–5 min, 100% Solvent B, with one-minute post time. The injection volume was 1.0 µL per sample with the column compartment temperature and the autosampler temperature set at 25 °C and 4 °C respectively. The total run time for each injection was 5 min. ESI-MS/MS was used in positive ionization mode with a nitrogen gas temperature of 325 °C, gas flow 9 L/min, nebulizer pressure of 45 psi and the capillary voltage of 4000 V. The MS acquisition was scanned in multiple reaction monitoring (MRM) mode. A calibration range of 1.56–200 ng/mL was used for quantifying the targeted neurotransmitters, with a linear plot where $r^2 > 0.99$.

2.7. Protein Expression Profiling Using Mass Spectrometry-Based Label-Free Proteomic Quantification (LFQ)

Brains of these two groups, namely NC (injected with PTZ 170 mg/kg) and O+P (pre-treated with OSLP 800 µg/kg followed by PTZ 170 mg/kg) were subjected to tissue lysis to extract the proteins for mass spectrometry-based label-free proteomic quantification (LFQ). All experiments were performed in 4 independent biological replicates.

2.7.1. Protein Extraction from Zebrafish Brain

The zebrafish brain was lysed with 1 mL of ice-cold lysis buffer (RIPA, protease inhibitor 20% *v*/*v*, phosphatase inhibitor 1% *v*/*v*) in a sterile ProtLoBind microtube and then incubated on an orbital shaker (4 °C; 90 min). Next, the content was homogenized using an ultrasonic cell crusher, briefly centrifuged (18,000 × *g*, 4 °C; 10 min) and the supernatant produced was harvested. The supernatant extracted was collected into a new sterile ProtLoBind microtube. Protein concentration was estimated using the Quick Start™ Bradford Protein Assay as instructed by the manufacturer (Bio-Rad, Hercules, CA, USA). After that, the brain lysates were concentrated in a speed-vacuum concentrator (300 rpm; 24 h; 60 °C).

2.7.2. In-Solution Digestion of Proteins

In-solution protein digestion was carried out according to the instructions (Agilent Technologies, Santa Clara, CA, USA). Briefly, protein samples were re-suspended, denatured and reduced in 25 µL of ABC, 25 µL of TFE and 1 µL of DTT, followed by being vortex-mixed (2500 rpm, 3 m) and then heated in an oven (60 °C, 60 min). Next, the samples were alkylated in 4 µL of IAA and were incubated in the dark (60 min, r.t.). After that, 1 µL of DTT was again added to quench excessive IAA (60 min, r.t., in the dark). 300 µL of MQUP water and 100 µL of ABC were added to dilute and adjust the pH of the protein solutions (pH 7–9). Following that, 1 µL of trypsin was added and was then incubated in an oven (37 °C, 18 h, in the dark). Upon completion of incubation, 1 µL of formic acid was added to terminate the tryptic digestion. Finally, all the samples were concentrated in a speed-vacuum concentrator (300 rpm; 24 h; 60 °C, Eyela SpeedVac Vacuum Concentrator). The dry pellets were kept at −20 °C.

2.7.3. De-Salting of Proteins

De-salting of the protein sample was carried out. Each biological replicate was de-salted independently using a Pierce®C18 mini spin column as instructed (Thermo Scientific Pierce, Rockford, IL, USA), with modifications. Firstly, each mini spin column was activated in 50% ACN (repeated 3 times, r.t.) and equilibrated in 0.5% of TFA in 5% ACN (repeated 3 times, r.t.). Separately, 90 µL of crude protein was added into 30 µL of sample buffer (2% of TFA in 20%) and briefly vortexed at 2200 rpm to mix well. This step was repeated for all the protein samples. Following that, each of the protein samples was loaded onto a mini spin column and was de-salted (repeated 3 times, r.t.). Subsequently, all the protein samples were washed in 0.5% of TFA in 5% ACN (repeated 3 times, r.t.). Lastly, all the protein samples were eluted in 70% ACN (repeated 3 times, r.t.) and all the flow-through produced was collected, vacuum-concentrated (300 rpm; 24 h; 60 °C) and stored at −20 °C prior to mass spectrometry-based LFQ.

2.7.4. Mass Spectrometry-Based Label-Free Proteomic Quantification (LFQ) Using Nanoflow-ESI-LCMS/MS

De-salted peptides were loaded onto an Agilent C-18 300Å Large Capacity Chip. The column was equilibrated by 0.1% formic acid in water (Solution A) and peptides were eluted with an increasing gradient of 90% acetonitrile in 0.1% formic acid (Solution B) by the following gradient, 3%–50% Solution B from 0–30 min, 50%–95% Solution B from 30–32 min, 95% Solution B from 32–39 min and 95%–3% Solution B from 39–47 min. The polarity of Q-TOF was set at positive, capillary voltage at 2050 V, fragmentor voltage at 300 V, drying gas flow 5 L/min and gas temperature of 300 °C. The intact protein was analyzed in auto MS/MS mode from range 110–3000 m/z for MS scan and 50–3000 m/z range for MS/MS scan. The spectrum was analyzed using Agilent MassHunter data acquisition software.

2.7.5. Brain Protein and Peptide Identification by Automated de Novo Sequencing and LFQ Analysis

Protein identification by automated de novo sequencing was performed with PEAKS®Studio Version 8.0. UniProtKB (Organism: *Danio rerio*) database (http://www.uniprot.org/proteomes/UP000000437, 46,847 proteins, accessed on 14 February 2020) was used for protein identification and homology search by comparing the de novo sequence tag, with the following settings: both parent mass and precursor mass tolerance was set at 0.1 Da, carbamidomethylation was set as fixed modification with maximum missed cleavage was set at 3, maximum variable post-translational modification was set at 3, trypsin cleavage, the minimum ratio count set to 2, mass error tolerance set as 20.0 ppm and other parameters were set as default by Agilent. False discovery rate (FDR) threshold of 1% and protein score of −10lgP > 20 were applied to filter out inaccurate proteins. PEAKS® indicated that a −10lgP score of greater than 20 is of relatively high in confidence as it targets very few decoy matches above the threshold.

For LFQ analysis, the differentially expressed proteins between the NC (injected with PTZ 170 mg/kg) and O+P (pre-treated with OSLP 800 µg/kg followed by PTZ 170 mg/kg) groups were

identified with the following settings: FDR threshold ≤ 1%, fold change ≥ 1, unique peptide ≥ 1, and significance score ≥ 20. PEAKSQ indicated that a significance score of greater than 20 is equivalent to significance p value < 0.01. Other parameters were set as default by Agilent.

2.8. Bioinformatics Analysis

Bioinformatics analysis (functional annotations, protein-protein interactions and systemic pathway enrichment analysis) of the differentially expressed proteins were analyzed and matched with the databases obtained from GO Consortium, ZFIN (www.zfin.org) and the KEGG PATHWAY Database (*Danio rerio*) [13]. KAAS provides functional annotation of genes by BLAST or GHOST comparisons against the manually curated KEGG GENES database. The result contains KO (KEGG Orthology) assignments (bi-directional best hit) and automatically generated KEGG pathways. The KEGG pathway maps organism-specific pathways: green boxes are hyperlinked to GENES entries by converting K numbers (KO identifiers) to gene identifiers in the reference pathway, indicating the presence of genes in the genome and also the completeness of the pathway.

2.9. Statistical Analysis

For behavioral study and neurotransmitter estimation, statistical analysis was performed using GraphPad Prism version 8.0. All data were expressed as mean ± standard error of the mean (SEM). One-way analysis of variance (ANOVA) followed with Dunnett's post-hoc test at significance levels of * $p < 0.05$, ** $p < 0.01$ and *** $p < 0.001$ against the negative control group (NC, 170 mg/kg PTZ). PEAKSQ statistical analysis (built-in statistical tool of PEAKS® software) was used in the analysis of differentially expressed proteins identified by LFQ. A significance score of 20% (equivalent to significance level of 0.01) and FDR ≤ 1% was considered statistically significant. In bioinformatics analysis, hypergeometric test followed with Benjamini and Hochberg FDR correction at p value < 0.05 (BiNGO built-in statistical tool) was used to correlate the association between functional annotation of genes and interacting proteins; the built-in statistical tool of KAAS was used to assess the possible association of interacting proteins and systemic pathways in the KEGG PATHWAY Database.

3. Results

3.1. OSLP Safety Study in Adult Zebrafish

3.1.1. Behavioral Study

Swim Path Analysis

As seen in the swim paths generated by PANLAB SMART v3.0 software, the VC group (Figure 2a) swam throughout the whole tank without showing apparent preference for any part of the tank. The OSLP-treated groups, 50, 100, 200, and 400 µg respectively, showed slight preferences for the bottom half of tank when compared to the VC group (Figure 2b–e). In comparison, the OSLP 800 µg group (Figure 2f) showed a similar swimming pattern to the VC group as they swam throughout the whole tank with no apparent preference for any part of the tank. The 1600 µg/kg dose was excluded for causing mortality after an extended duration.

3.1.2. Locomotion Parameters

For the mean total distance travelled, no significant differences ($F = 1.798$, $p > 0.05$) were found between the untreated VC group and all the OSLP-treated groups (50–800 µg/kg) (Figure 3a).

For another locomotion parameter, time spent in upper half of tank (s), no significant differences ($F = 1.408$, $p > 0.05$) were found between the untreated VC group and all the OSLP-treated groups Figure 3b, c). In a similar trend, no significant differences were also found in the mean time spent in

lower half of tank, except in the OSLP 800 µg group. The zebrafish treated with OSLP 800 µg/kg spent a shorter time in the lower half of tank, 328 ± 54 s (F = 6.596, ** $p < 0.01$) than the VC group.

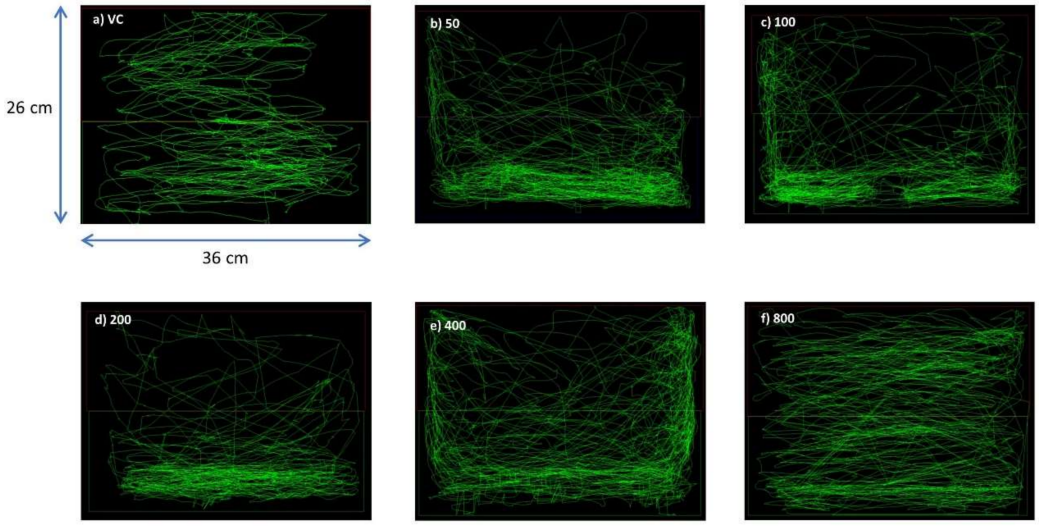

Figure 2. Representative swim paths for the corresponding 6 experimental groups (n = 8). (**a**) VC (tank water only, i.p.), (**b**) OSLP (50 µg/kg, i.p.), (**c**) OSLP (100 µg/kg, i.p.), (**d**) OSLP (200 µg/kg, i.p.), (**e**) OSLP (400 µg/kg, i.p.) and (**f**) OSLP (800 µg/kg, i.p.).

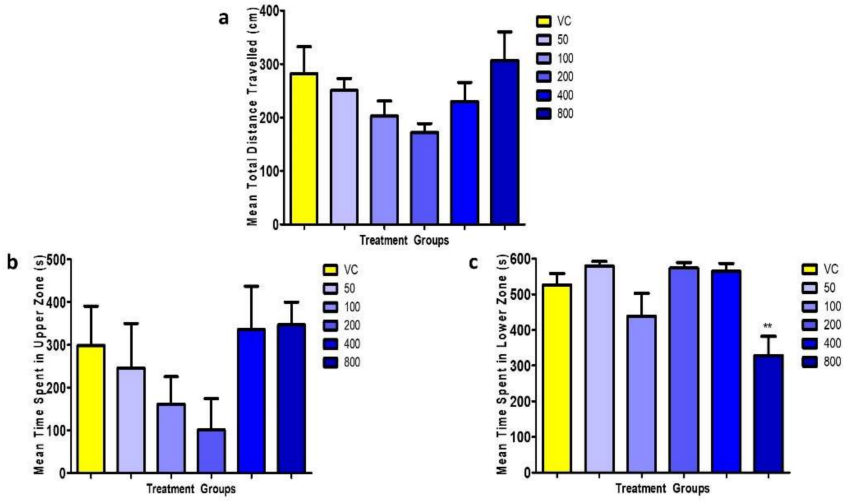

Figure 3. Mean locomotion parameters over 600 s for all the experimental groups. Figure (**a**) represents the mean total distance travelled (cm), Figure (**b**) shows the mean time spent in upper zone (s) and Figure (**c**) displays the mean time spent in lower zone (s). The data are expressed as Mean ± SEM, n = 8 and was analyzed using One-way ANOVA followed with Dunnett's post-hoc test at significance level of ** $p < 0.01$ against the VC group (tank water only, i.p.).

Based on the swim path analysis (Figure 2) and locomotion parameters (Figure 3), OSLP ranging from 50 to 800 µg did not result in any abnormal behavioral changes in the adult zebrafish. These doses were found to be safe for the use in adult zebrafish and did not result in any mortality or morbidity. Considering the maximum protective effects OSLP could possibly exhibit in brain at a safe concentration, 800 µg was fixed as the maximum safe starting dose. Subsequently, OSLP at 800 µg was used as the treatment dose across all further studies in this work. On the other hand, mortality in the adult zebrafish was recorded when treated with 1600 µg of OSLP. Therefore, this dose was considered as unsafe and the findings were not included in this work.

3.2. Evaluation of Anticonvulsive Potential of OSLP

3.2.1. Behavioral Study

Swim Path Analysis

The VC group (Figure 4a) managed to swim throughout the entire tank without showing apparent preference for any part of the tank. In contrast, the NC group showed a more erratic swimming pattern after the PTZ challenge, with the zebrafish dwelling at the bottom half of tank more frequently (Figure 4b). Pre-treatment with DZP (PC group) modified the post PTZ challenge swimming behavior into a swimming pattern comparable to the VC group, with roughly equal amount of time being spent at the top and bottom of the tank (Figure 4c). Pre-treatment with OSLP 800 µg (O+P) also produced a swimming pattern similar to that of the VC group, without showing apparent preference for any part of the tank (Figure 4d). The treatment control group (TC) managed to swim throughout the whole tank without showing erratic swimming pattern (Figure 4e).

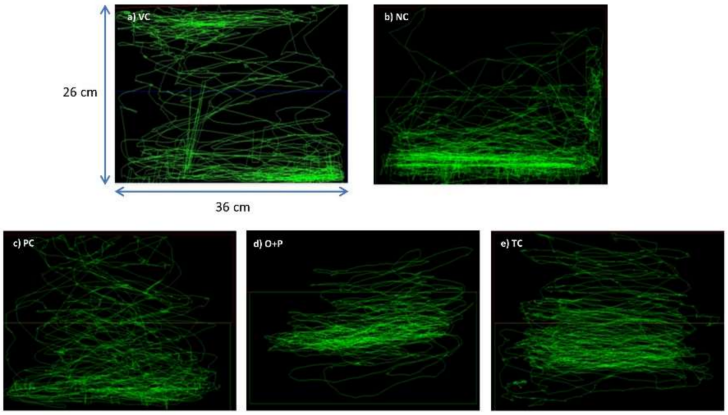

Figure 4. Representative swimming patterns for the corresponding 5 experimental groups (n = 10). VC ((**a**) tank water, i.p.), NC ((**b**) PTZ 170 mg/kg, i.p.), PC ((**c**) DZP 1.25 mg/kg + PTZ 170 mg/kg, i.p.), O+P ((**d**) OSLP 800 µg/kg + PTZ 170 mg/kg, i.p.) and TC ((**e**) OSLP 800 µg/kg + tank water, i.p.).

3.2.2. Seizure Score and Seizure Onset Time

The cutoff time for seizure scoring was 600 s as fish fully recovered from seizures by 600 s. Mean seizure onset time for both the VC group and TC group were set as 600 s and a maximum seizure score of zero was assigned to these groups. They did not receive any PTZ challenges and thus did not show seizures. They served only as the study controls. PTZ injection into the zebrafish resulted in diverse seizure profiles, intensities, and latency in reaching the different seizure scores and onset time.

The NC group injected with PTZ had a significant increase in seizure score to 2.8 ($F = 34.35$ *** $p < 0.001$) and had significantly prompted the seizure onset time to the lowest, 76 s ($F = 49.50$, *** $p < 0.001$), when compared to the VC group. Higher seizure score with a concurrent lower seizure onset time indicated more severe seizures in the PTZ-injected zebrafish. Treatment with 800 µg/kg of OSLP showed a significant decrease in seizure score, to 1.5 ($F = 34.35$, *** $p < 0.001$) and significantly delayed the seizure onset time to 349 s ($F = 49.50$, *** $p < 0.001$) compared to the NC group. As expected, the PC group treated with DZP also showed a significant decrease in seizure score, to < 1 ($F = 34.35$, *** $p < 0.001$) and had significantly delayed the seizure onset time to 564 s ($F = 49.50$, *** $p < 0.001$) compared to the NC group.

In this study, PTZ (170 mg/kg of b.w.) was shown to sufficiently induce seizures in the adult zebrafish, with a high seizure score and a fast seizure onset time. OSLP treatment (800 µg/kg of b.w.) was shown to reduce seizure severity, with a lower seizure score and delayed the onset time to the most serious seizure score 4 (Figure 5).

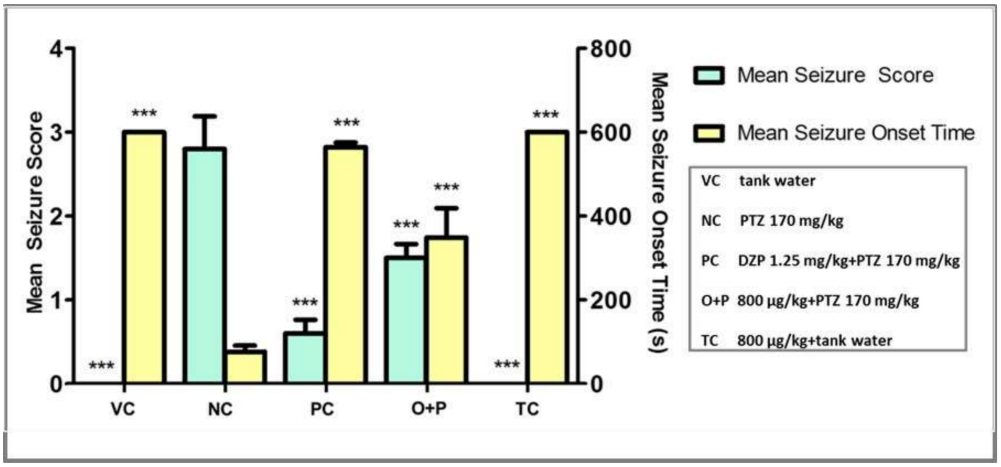

Figure 5. Mean seizure scores and mean seizure onset time (s) for the corresponding 5 experimental groups. Data are mean ± SEM. Experiments were repeated in n = 10, *** showed $p < 0.001$ against negative control. One-way ANOVA with Dunnett's post-hoc test. VC (tank water, i.p.), NC (PTZ 170 mg/kg, i.p.), PC (DZP 1.25 mg/kg + PTZ 170 mg/kg, i.p.), O+P (OSLP 800 µg/kg + PTZ 170 mg/kg, i.p.) and TC (OSLP 800 µg/kg + tank water, i.p.).

3.2.3. Locomotion Parameters

Mean total distance travelled of the VC group was 68±16 cm (F = 4.527, ** $p < 0.01$) and was significantly shorter than the NC group injected with PTZ (172 ± 34 cm, F = 4.527, **$p < 0.01$). The NC group travelled about a 60% longer distance than the VC group (Figure 6a). The PC group treated with DZP had mean total distance travelled of 74 ± 16 cm which was 57% shorter than the PTZ-injected group (F = 4.527, ** $p < 0.01$) (Figure 6a). This significant improvement was also comparable to the VC group (68 ± 16 cm). A reduction was also seen in the O+P group, with mean total distance travelled of 137 ± 22 cm, which was about 20% shorter than the PTZ-induced alone group (Figure 6A).

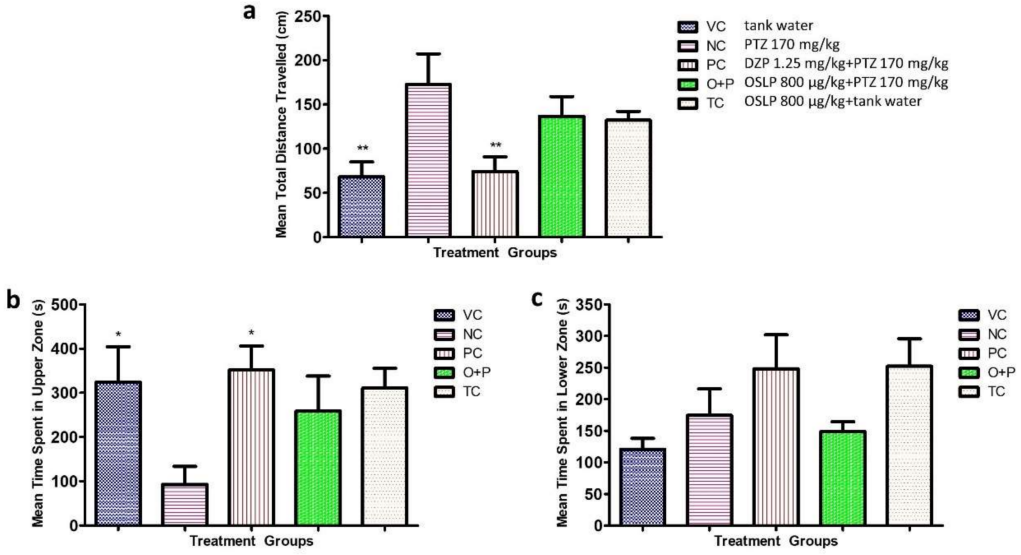

Figure 6. Mean locomotion parameters over 600 s for all the experimental groups. Figure (**a**) represents the mean total distance travelled (cm), Figure (**b**) shows the mean time spent in upper zone (s) and Figure (**c**) displays the mean time spent in lower zone (s). The data are expressed as Mean ± SEM, n = 10 and was analyzed using One-way ANOVA followed with Dunnett's post-hoc test at significance level of * $p < 0.05$ and ** $p < 0.01$ against the negative control group (NC, PTZ 170 mg/kg). VC (tank water, i.p.), PC (DZP 1.25 mg/kg + PTZ 170 mg/kg, i.p.), O+P (OSLP 800 µg/kg + PTZ 170 mg/kg, i.p.) and TC (OSLP 800 µg/kg + tank water, i.p.).

For the parameter of time spent in each half of the tank, only groups VC and PC showed a significant longer time spent in the upper half of tank (324 ± 80 s and 352 ± 54 s respectively, F = 2.716, * $p < 0.05$) and a visibly shorter time spent in the bottom of tank than the NC group (Figure 6b,c). The O+P group (Figure 6b) had a trend of spending a slightly longer time in the upper half of tank (259 ± 78 s) but a slightly shorter time in the bottom half (149 ± 15 s) compared to the NC group (Figure 6c).

It is also worthy to mention that the TC group had displayed a similar trend to the VC group in all three locomotion parameters (Figure 6a–c). OSLP at a dose of 800 µg/kg did not trigger any locomotor manipulations and hence, was considerably safe in the adult zebrafish (Figure 6a–c).

3.2.4. Neurotransmitter Study

Neurotransmitters in the zebrafish brains, namely GABA and glutamate (Glu) and their ratio (GABA/Glu) were evaluated (Figure 7a–c).

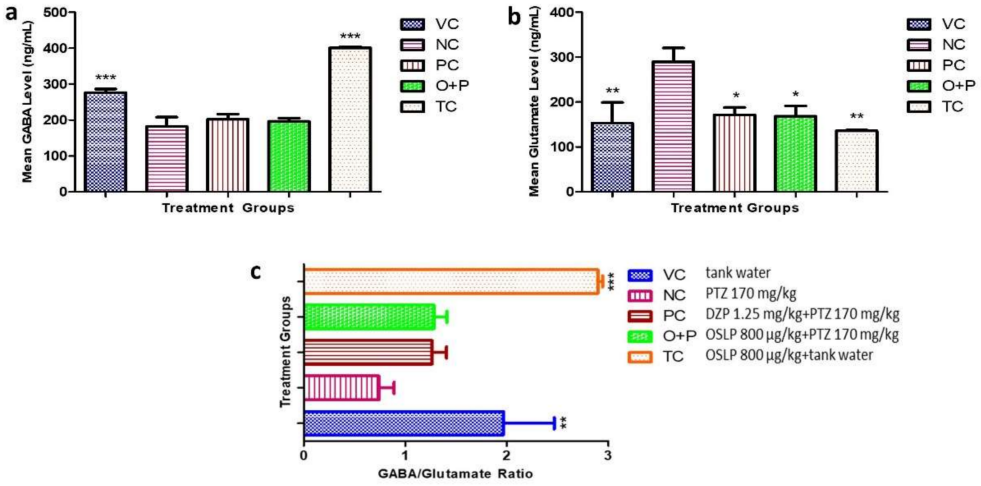

Figure 7. Mean neurotransmitter levels (ng/mL), namely GABA (**a**), glutamate (**b**) and GABA/Glu ratio (**c**) over 600 s for all the experimental groups. The data are expressed as Mean ± SEM, $n = 10$ and was analyzed using One-way ANOVA followed with Dunnett's post-hoc test at significance level of * $p < 0.05$, ** $p < 0.01$ and *** $p < 0.001$ against the negative control group (NC, PTZ 170 mg/kg). VC (tank water, i.p.), PC (DZP 1.25 mg/kg + PTZ 170 mg/kg, i.p.), O+P (OSLP 800 µg/kg + PTZ 170 mg/kg, i.p.) and TC (OSLP 800 µg/kg + tank water, i.p.).

The NC group showed a significant decrease in mean GABA levels (182 ± 26 ng/mL, *** $p < 0.001$) when compared to the VC group (276 ± 10 ng/mL, F = 37.74, *** $p < 0.001$) (Figure 7a). Mean GABA levels of the O+P group was 196 ± 9 ng/mL. Despite attaining about 7% higher GABA levels than the NC group, this treatment however did not attain statistical significance (Figure 7a). DZP treatment also brought about a slight increase in the GABA levels, to 202 ± 14 ng/mL as compared to 182 ± 26 ng/mL in the NC group ($p > 0.05$) (Figure 7a). Similarly, both PC (202 ± 14 ng/mL) and O+P (196 ± 9 ng/mL) had showed just slightly higher GABA levels than the NC group (Figure 7a).

In contrast, NC group showed a significant increase in Glu level (290 ± 30 ng/mL, F = 4.779, ** $p < 0.01$) when compared to the VC and TC groups (153 ± 46 ng/mL and 136 ± 2 ng/mL respectively, F = 4.779, ** $p < 0.01$) (Figure 7b). Meanwhile, DZP treatment brought about a significant decrease to 172 ± 16 ng/mL in the Glu levels, or about 41% lower than the NC group (F = 4.779, * $p < 0.05$) (Figure 7b). Mean Glu levels of the O+P group was 169 ± 22 ng/mL, which was 42% significantly lower than the NC group (F = 4.779, * $p < 0.05$) (Figure 7b). This outcome thus suggests that OSLP treatment could be effectively lower the Glu concentrations, normalizing it to the level comparable to those treated with DZP.

In addition, PTZ injection caused a significant decrease in the GABA/Glu ratio to <1, whereas, both VC and TC groups had a higher GABA/Glu ratio (R > 2, F = 13.81, ** $p < 0.01$ and *** $p < 0.001$, respectively) (Figure 7c). Very noteworthy is that the OSLP-treated and DZP-treated groups had a similar GABA/Glu ratio, though they did not attain statistical significance when compared to the NC (Figure 7c). It is worth mentioning that the TC group (treatment dose control) had higher GABA levels (401 ± 3 ng/mL, F = 37.74, *** $p < 0.001$) (Figure 7a) and lower Glu levels (136 ± 2 ng/mL, F = 4.779, *** $p < 0.001$) (Figure 7b) than the VC group. Also, the GABA/Glu ratio was comparable to the VC group.

3.2.5. Proteins Expression Profiling Using Mass Spectrometry-Based Label-Free Proteomic Quantification (LFQ)

LFQ profiled 29 differentially expressed proteins from the brain samples of PTZ injected zebrafish (NC group) and the OSLP-treated PTZ group (O+P). These proteins were found to be expressed at lower levels in the NC group than in the O+P group (Figure 8 and Table 4). Among them, five proteins, namely hemoglobin subunit alpha (Hbaa1, isoforms Q803Z5 and Q90487), hemoglobin subunit beta-1 (Hbba1, Q90486), fructose-bisphosphate aldolase C-B (Aldocb, Q8JH70), actin beta 2 (Actb2, A8WG05), and complexin 2 (Cplx2, E7FBR8) were found expressed at higher levels.

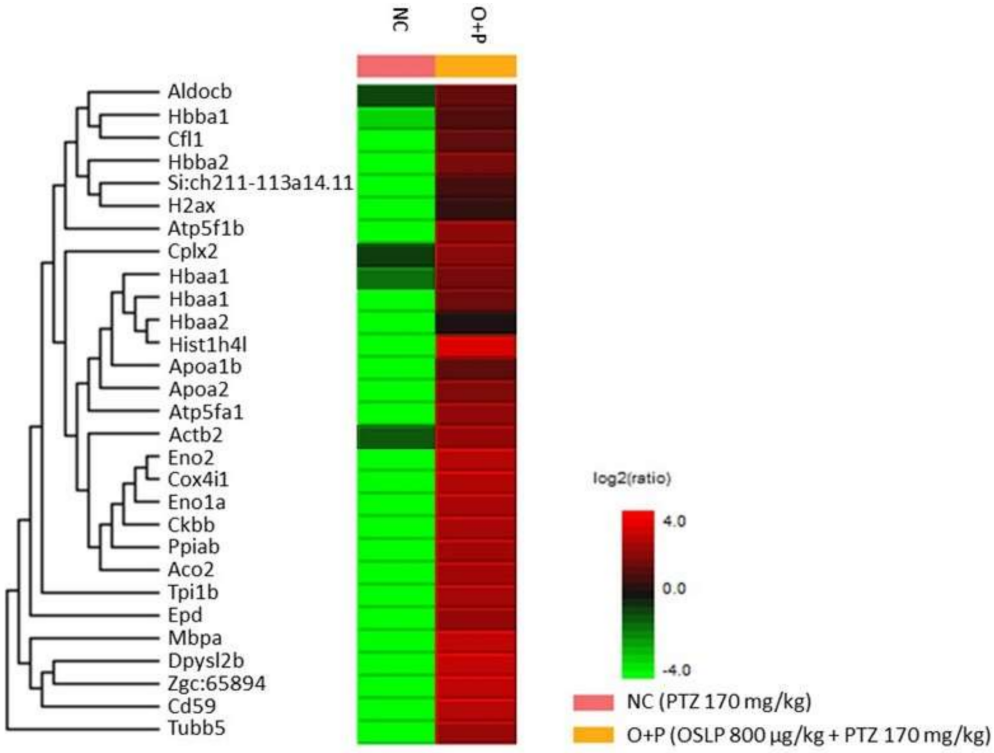

Figure 8. Heat map shows the differentially expressed proteins identified from negative control (NC, PTZ 170 mg/kg only) and O+P (OSLP 800 µg/kg + PTZ 170 mg/kg) zebrafish brains, $n = 4$, significance ≥ 20, FDR ≤ 1%, fold change ≥ 1, unique peptide ≥ 1. Protein names are listed on the left while experimental groups are indicated on top. The color key on the bottom right indicates the log2 (ratio) expression levels (green = low and red = high).

3.2.6. Bioinformatics Analysis

The differentially expressed proteins (Table 4) were searched in the ZFIN Database Information to match the gene ID. The database of InterPro Classification of Protein Families was searched for the respective protein class. The results were presented in Table 5.

Table 4. Differentially expressed proteins identified from negative control (NC, PTZ 170 mg/kg only) and O+P (OSLP 800 μg/kg + PTZ 170 mg/kg) zebrafish brains.

Uniprot Accession ID	Uniprot Protein Name	Significance (≥13)	Coverage (%)	#Peptides	#Unique	Avg. Mass	Group Profile (Ratio of NC/O+P)	ZFIN Protein
Q90487	Hemoglobin subunit alpha	200	49	12	4	15,524	0.00:1.00	Hbaa1
Q803Z5	Hemoglobin subunit alpha	200	49	12	4	15,508	1.00:255.14	Hbaa1
Q90486	Hemoglobin subunit beta-1	200	43	8	8	16,389	1.00:49.49	Hbba1
Q08BA1	ATP synthase subunit alpha	200	15	6	3	59,744	0.00:1.00	Atp5fa1
Q6PC12	Enolase 1	200	12	4	3	47,074	0.00:1.00	Eno1a
Q4VBK0	ATP synthase subunit beta	200	9	3	3	55,000	0.00:1.00	Atp5f1b
Q6ZM12	Hemoglobin beta adult 2	200	13	3	3	16,295	0.00:1.00	Hbba2
E7F2M5	CD59 molecule (CD59 blood group)	200	26	2	2	12,914	0.00:1.00	Cd59
E9QBF0	Triosephosphate isomerase	200	20	4	4	21,811	0.00:1.00	Tpi1b
Q6PC53	Peptidyl-prolyl cis-trans isomerase	200	18	3	3	17,489	0.00:1.00	Ppiab
F8W4M7	Aconitate hydratase mitochondrial	200	4	2	2	85,590	0.00:1.00	Aco2
Q8AY63	Brain-subtype creatine kinase	153.53	7	3	3	42,884	0.00:1.00	Ckbb
Q4VBT9	Cox4i1 protein	126.93	18	2	2	19,443	0.00:1.00	Cox4i1
Q8JH70	Fructose-bisphosphate aldolase C-B	126.51	12	4	4	39,259	1.00:8.14	Aldocb
Q6PE34	Tubulin beta chain	125.32	31	12	3	49,635	0.00:1.00	Zgc:65894
A0A0R4IKF0	Apolipoprotein A-Ib	112	9	2	2	30,140	0.00:1.00	Apoa1b
F8W3W8	Myelin basic protein a	110.44	63	10	2	10,776	0.00:1.00	Mbpa
A3KPR4	Histone H4	104.16	24	2	2	11,367	0.00:1.00	Hist1h4l
B3DFP9	Apolipoprotein A-II	103.56	21	2	2	15,537	0.00:1.00	Apoa2
Q5BJC7	Haemoglobin alpha adult 2	79.54	17	3	2	15,403	0.00:1.00	Hbaa2
Q8AYC4	Tubulin beta chain	76.34	39	13	2	49,826	0.00:1.00	Tubb5
R4GE02	Si:ch211–113a14.11	56.58	21	4	2	27,149	0.00:1.00	Si:ch211–113a14.11
Q7ZUY3	Histone H2AX	56.36	34	4	2	15,001	0.00:1.00	H2ax
Q6TH32	Cofilin 1	44.76	13	2	2	18,771	0.00:1.00	Cfl1
A0A2R8Q2Z0	Ependymin	44.72	12	2	2	23,370	0.00:1.00	Epd
A8WG05	Actin beta 2	43.68	15	6	6	41,753	1.00:9.75	Actb2
E7FBR8	Complexin 2	43.27	24	2	2	15,094	1.00:5.64	Cplx2
A8DZ95	Dihydropyrimidinase-like 2b	43.27	6	2	2	58,285	0.00:1.00	Dpysl2b
Q6GQM9	Eno2 protein	36.01	7	2	1	46,841	0.00:1.00	Eno2

Remark: ZFIN protein nomenclatures were searched in the ZFIN Database Information (*www.zfin.org*) as accessed on 17/02/2020.

Table 5. Protein family of the differentially expressed proteins identified from negative control (NC, PTZ 170 mg/kg only) and O+P (OSLP 800 µg/kg + PTZ 170 mg/kg) zebrafish brains.

Protein Family	ZFIN Protein	ZFIN Gene ID
Globin domain-containing protein		
Belongs to the family of hemoglobin, alpha-type and to the subfamily of hemoglobin, pi	Hbaa1	ZDB-GENE-980526-79
	Hbaa2	ZDB-GENE-081104-38
Member of the hemoglobin, beta-type	Hbba1	ZDB-GENE-990415-18
	Hbba2	ZDB-GENE-040801-164
Plasma protein		
Member of the CD marker	Cd59	ZDB-GENE-030131-7871
Member of the apolipoprotein A/E	Apoa2	ZDB-GENE-030131-1046
Belong to the myelin basic protein	Mbpa	ZDB-GENE-030128-2
Member of the apolipoprotein A/E	Apoa1b	ZDB-GENE-050302-172
Cytoskeletal protein		
Member of the actin family	Actb2	ZDB-GENE-000329-3
Member of the beta tubulin	Tubb5	ZDB-GENE-031110-4
	Zgc:65894	ZDB-GENE-030131-7741
Enzyme protein		
Transferase		
Member of the ATP:guanido phosphotransferase protein	Ckbb	ZDB-GENE-020103-2
Member of the ATP synthase, F1 complex, beta subunit	Atp5f1b	ZDB-GENE-030131-124
Member of the mitochondrial F1-F0 ATP synthase subunit F	Atp5mf	ZDB-GENE-050309-87
Member of the ATP synthase, F1 complex, alpha subunit	Atp5fa1	ZDB-GENE-060201-1
Isomerase		
Member of the cyclophilin-type peptidyl-prolyl cis-trans isomerase	Ppiab	ZDB-GENE-030131-7459
Member of the triosephosphate isomerase	Tpi1b	ZDB-GENE-020416-4
Lyase		
Member of the fructose-bisphosphate aldolase, class-I	Aldocb	ZDB-GENE-030821-1
Member of the enolase	Eno1a	ZDB-GENE-030131-6048
Citric acid cycle related protein		
Belongs to the family of aconitase, mitochondrial-like	Aco2	ZDB-GENE-030131-1390
Member of the enolase	Eno2	ZDB-GENE-040704-27
Histone protein		
Core Histone		
Member of the histone H2A	H2ax	ZDB-GENE-040426-987
	Si:ch211-113a14.11	ZDB-GENE-121214-162
Member of the histone H4	Hist1h4l	ZDB-GENE-070927-10
Intracellular protein-Ependymin		
Member of the ependymin-related protein family (EPDRs)	Epd	ZDB-GENE-980526-111
Cytosolic protein		
Member of the complexin/synaphin family	Cplx2	ZDB-GENE-081113-1
ADF-H domain-containing protein		
Belongs to the family of ADF/Cofilin	Cfl1	ZDB-GENE-030131-215
Transporter protein-Primary active transporter		
Belongs to the cytochrome c oxidase subunit IV family and to the subfamily of cytochrome c oxidase subunit IV	Cox4i1	ZDB-GENE-030131-5175
Amidohydro-rel domain-containing protein		
Belongs to the hydantoinase/dihydropyrimidinase family and to the subfamily of dihydropyrimidinase-related protein 2	Dpysl2b	ZDB-GENE-031105-1

Remark: Protein Families and their respective functions were searched in the InterPro Classification of Protein Families and the ZFIN Database Information (https://www.ebi.ac.uk/interpro/protein/UniProt/ and www.zfin.org accessed on 17 February 2020).

In addition, the differentially expressed proteins were found to localize at 14 different cellular components; mainly at the organelle part (GO:44422) and the macromolecular complex (GO:32991). They were localized at the intracellular non-membrane-bounded organelle (GO:43232), intracellular organelle part (GO:44446), cytoskeletal part (GO:44430), microtubule cytoskeleton (GO:15630), microtubule (GO:5874), protein complex (GO:43234), phosphopyruvate hydratase complex (GO:15), hemoglobin complex (GO:5833), cytosol (GO:5829), cytosolic part (GO:44445), and non-membrane-bounded organelle (GO:43228). The identified proteins were also localized at the nucleus of the cell part (GO:5634) (Figure 9).

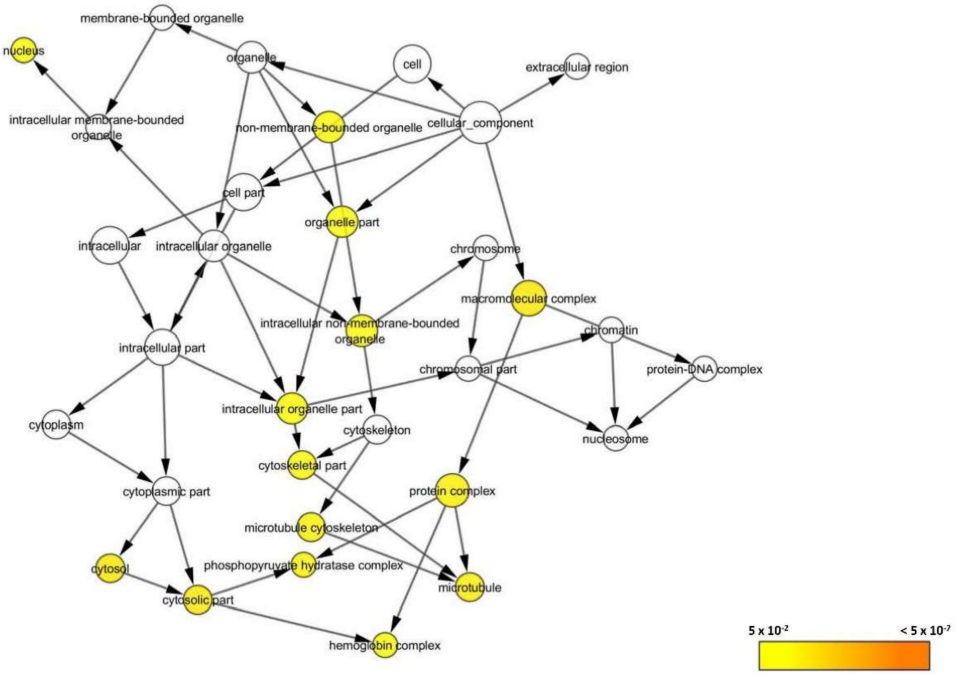

Figure 9. BiNGO result for cellular component as visualized in Cytoscape (Organism: *Danio rerio*). Colored nodes are significantly overrepresented. White nodes are not significantly overrepresented; they are included to show the colored nodes in the context of the GO hierarchy. Color key on the bottom right indicates the significance level of overrepresentation.

The proteins that were found localized at the different cellular components aforementioned have their interactions significantly associated with 14 corresponding molecular functions (Figure 10). Around 12 were involved in catalytic activities of lyase (GO:16829), carbon-oxygen lyase (GO:16835), hydro-lyase (GO:16836), phosphopyruvate hydratase (GO:4634), aconitate hydratase (GO:3994), fructose-bisphosphate aldolase (GO:4332), and aldehyde-lyase (GO:16832); triose-phosphate isomerase (GO:4807), and intramolecular oxidoreductase which interconverts aldoses and ketoses (GO:16861); creatine kinase (GO:4111) and phosphotransferase uses nitrogenous group as acceptor (GO:16775), and GTPase activity (GO:3924). Two protein interactions were particularly noteworthy: the bindings of SNARE (GO:149) and syntaxin (GO:19905) (blue box; Figure 10).

3.2.7. Systematic Pathway Enrichment Analysis

KEGG PATHWAY database (Organism: *Danio rerio*) revealed that the differentially expressed proteins were significantly associated with six major categories of pathways; five of them were associated with metabolism, genetic information processing, environmental information processing, cellular processes, and organismal systems whilst the last one was associated with human diseases (see Table 6).

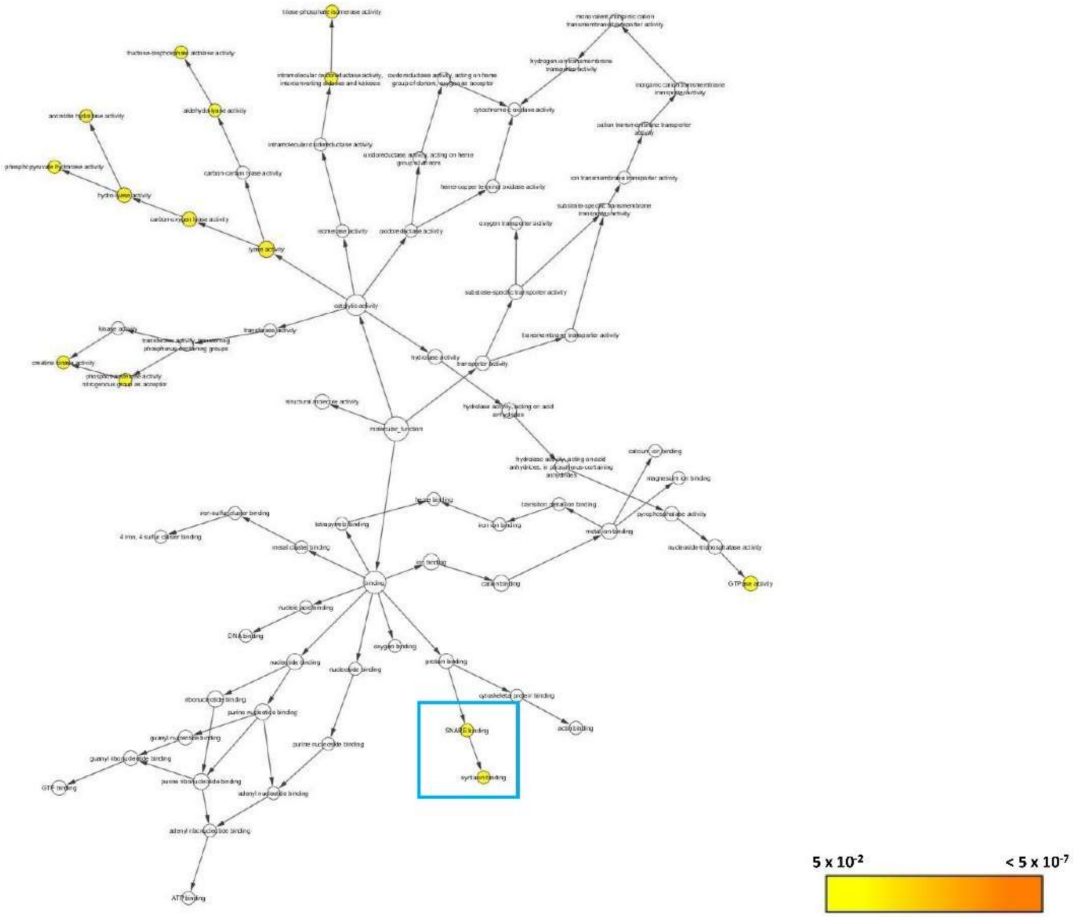

Figure 10. BiNGO result for molecular function as visualized in Cytoscape (Organism: *Danio rerio*). Colored nodes are significantly overrepresented. White nodes are not significantly overrepresented; they are included to show the colored nodes in the context of the GO hierarchy. Color key on the bottom right indicates the significance level of overrepresentation.

Table 6. KEGG pathways (Organism: *Danio rerio*) associated with the differentially expressed proteins identified from negative control (NC, PTZ 170 mg/kg only) and O+P (OSLP 800 µg/kg + PTZ 170 mg/kg) zebrafish brains.

KEGG Pathway ID	Pathway Category	Mapped Protein
	Metabolism	
01100	**Metabolic pathways**	Ckbb, Aldocb, Aco2, Eno1a, Eno2, Tpi1b, Atp5fa1, Atp5f1b, Cox4i1
01110	Biosynthesis of secondary metabolites	Aldocb, Aco2, Eno1a, Eno2, Tpi1b
01120	Microbial metabolism in diverse environments	Aldocb, Aco2, Eno1a, Eno2, Tpi1b
01200	Carbon metabolism	Aldocb, Aco2, Eno1a, Eno2, Tpi1b
01210	2-Oxocarboxylic acid metabolism	Aco2
01230	Biosynthesis of amino acids	Aldocb, Aco2, Eno1a, Eno2, Tpi1b
	Carbohydrate metabolism	
00010	Glycolysis/Gluconeogenesis	Aldocb, Eno1a, Eno2, Tpi1b
00020	Citrate cycle (TCA cycle)	Aco2
00030	Pentose phosphate pathway	Aldocb
00051	Fructose and mannose metabolism	Aldocb, Tpi1b
00630	Glyoxylate and dicarboxylate metabolism	Aco2
00562	Inositol phosphate metabolism	Tpi1b
	Energy metabolism	
00190	Oxidative phosphorylation	Atp5fa1, Atp5f1b, Cox4i1
00710	Carbon fixation in photosynthetic organisms	Aldocb, Tpi1b
00720	Carbon fixation pathways in prokaryotes	Aco2
00680	Methane metabolism	Aldocb, Eno1a, Eno2, Ppiab
	Amino acid metabolism	
00330	Arginine and proline metabolism	Ckbb

Table 6. *Cont.*

KEGG Pathway ID	Pathway Category	Mapped Protein
	Genetic Information Processing	
	Folding, sorting and degradation	
03018	RNA degradation	Eno1a, Eno2
	Environmental Information Processing	
	Signal transduction	
04015	Rap1 signaling pathway	Actb2
04390	Hippo signaling pathway	Actb2
04391	Hippo signaling pathway - fly	Actb2
04066	HIF-1 signaling pathway	Aldocb, Eno1a, Eno2
	Cellular Processes	
	Transport and catabolism	
04145	Phagosome	Actb2, Tubb5, Zgc:65894
	Cell growth and death	
04210	Apoptosis	Actb2
04217	Necroptosis	Ppiab, H2ax
	Cellular community-eukaryotes	
04510	Focal adhesion	Actb2
04520	Adherens junction	Actb2
04530	Tight junction	Actb2
04540	Gap junction	Tubb5, Zgc:65894
	Cell motility	
04810	Regulation of actin cytoskeleton	Actb2, Cfl1
	Organismal Systems	
	Immune system	
04640	Hematopoietic cell lineage	Cd59
04610	Complement and coagulation cascades	Cd59
04611	Platelet activation	Actb2
04666	Fc gamma R-mediated phagocytosis	Cfl1
04670	Leukocyte transendothelial migration	Actb2
	Endocrine system	
04921	Oxytocin signaling pathway	Actb2
04919	Thyroid hormone signaling pathway	Actb2
	Circulatory system	
04260	Cardiac muscle contraction	Cox4i1
	Digestive system	
04971	Gastric acid secretion	Actb2
	Nervous system	
04721	Synaptic vesicle cycle	Cplx2
	Sensory system	
04745	Phototransduction - fly	Actb2
	Development and regeneration	
04360	Axon guidance	Cfl1, Dpysl2b
	Environmental adaptation	
04714	Thermogenesis	Atp5fa1, Atp5f1b, Cox4i1, Actb2
	Human Diseases	
	Cancer: overview	
05205	Proteoglycans in cancer	Actb2
05203	Viral carcinogenesis	Si:ch211-113a14.11, Hist1h4l
	Cancer: specific types	
05225	Hepatocellular carcinoma	Actb2
	Immune disease	
05322	Systemic lupus erythematosus	H2ax, Si:ch211-113a14.11, Hist1h4l
	Neurodegenerative disease	
05010	Alzheimer disease	Atp5fa1, Atp5f1b, Cox4i1, Tubb5
05012	Parkinson disease	Atp5fa1, Atp5f1b, Cox4i1
05016	Huntington disease	Atp5fa1, Atp5f1b, Cox4i1, Tubb5
	Substance dependence	
05034	Alcoholism	H2ax, Si:ch211-113a14.11, Hist1h4l
	Cardiovascular disease	
05418	Fluid shear stress and atherosclerosis	Actb2
05410	Hypertrophic cardiomyopathy (HCM)	Actb2
05412	Arrhythmogenic right ventricular cardiomyopathy (ARVC)	Actb2
05414	Dilated cardiomyopathy (DCM)	Actb2
05416	Viral myocarditis	Actb2
	Endocrine and metabolic disease	
04932	Non-alcoholic fatty liver disease (NAFLD)	Cox4i1

Table 6. *Cont.*

KEGG Pathway ID	Pathway Category	Mapped Protein
	Infectious disease: bacterial	
05110	Vibrio cholerae infection	Actb2
05130	Pathogenic Escherichia coli infection	Actb2, Tubb5, Zgc:65894
05132	Salmonella infection	Actb2
05131	Shigellosis	Actb2
05135	Yersinia infection	Actb2
05133	Pertussis	Cfl1
05100	Bacterial invasion of epithelial cells	Actb2, Cfl1
	Infectious disease: viral	
05164	Influenza A	Actb2
	Drug resistance: antimicrobial	
01503	Cationic antimicrobial peptide (CAMP) resistance	Ppiab

The synaptic vesicle cycle (04721) in the nervous system that is nested under the organismal systems category, was the pathway most likely to play a significant role (Table 6). Complexin 2 (Cplx2) was mapped onto the synaptic vesicle cycle pathway (04721), highlighted in a green box as Complexin (Figure 11). Cplx2 is an isoform of the complexin protein family with four isoforms, Cplx1–4. As shown in a synapse, during priming phase, Cplx2 is bound to the trans-SNARE complex together with synaptotagmin (Syt), vesicle-associated membrane protein (Vamp), syntaxin (Stx), and synaptosomal-associated protein of 25 kDa (Snap25). SNARE binding of complexin is essential for normal priming at the presynaptic plasma membrane, which is known as the active zone, and subsequent Ca^{2+}-evoked neurotransmitter release.

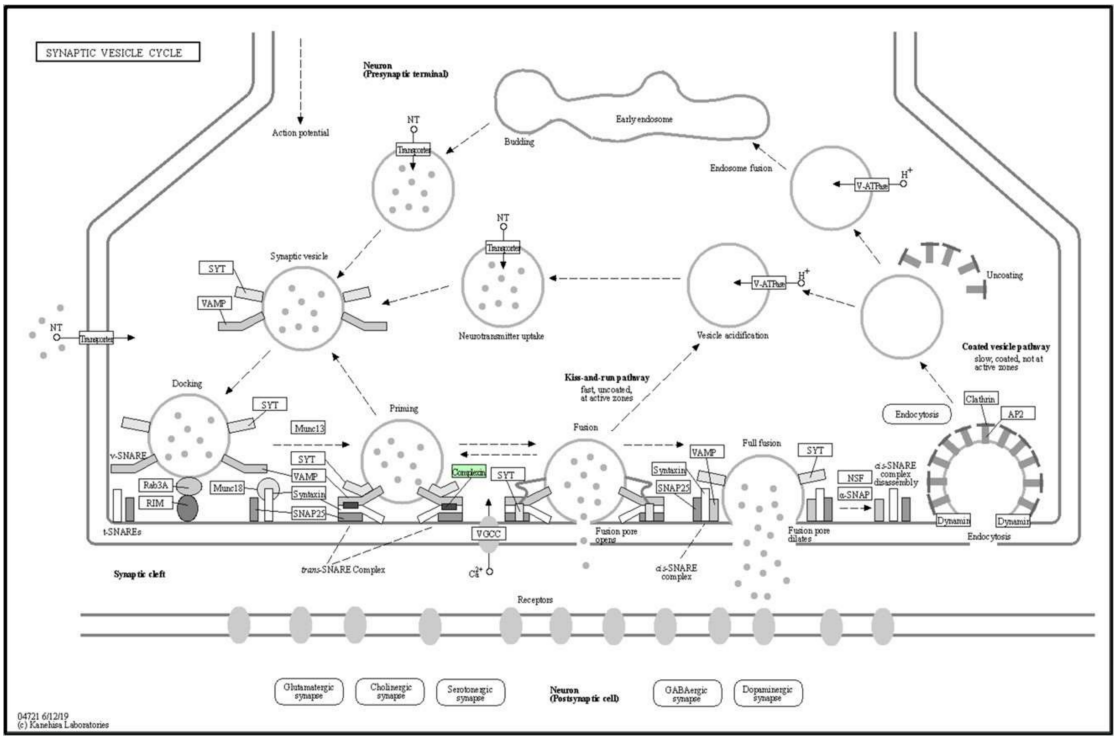

Figure 11. Complexin 2 in green box was mapped onto the synaptic vesicle cycle pathway (04721) generated by KEGG PATHWAY (Organism: *Danio rerio*). Solid arrows represent molecular interactions or relations whereas dashed arrows represent indirect links or unknown reactions.

4. Discussion

This study investigates the maximum safe starting dose of OSLP and elucidates its anticonvulsive potential in PTZ-induced adult zebrafish seizures.

Firstly, the maximum safe starting dose of OSLP to be used for anticonvulsive activity determination in the adult zebrafish [14,18] was evaluated. In this study, OSLP concentrations ranging from 50–1600 μg/kg of b.w. were tested in each assigned group. The zebrafish swimming pattern after exposure to 800 μg of OSLP did not show bottom-dwelling behavior. Diving to the bottom of tank can be a natural reflexive response of zebrafish. However, increased bottom-dwelling behavior has been linked to anxiety in the novel tank test [15,16]. The bottom dwelling frequency has been found reduced in zebrafish when treated with anxiolytic compounds [7,17]. These earlier findings thus lend support to the anxiolytic potential of OSLP in adult zebrafish, at least at a concentration greater than 800 μg/kg of body weight. Noteworthy however, OSLP at a concentration of 1600 μg is capable of causing lethal events in adult zebrafish. This finding has drawn a line to limit the maximum safe dose of OSLP achievable via intraperitoneal route to be not greater than 1600 μg/kg of body weight, at least in the case of zebrafish. This also lends support to the exclusion of 1600 μg OSLP for further analysis in this work. Building on the safety study outcomes and considering the maximum protective effects of OSLP at a safe concentration, 800 μg was chosen as the treatment dose in this study.

The OSLP safety study was crucial as there was no prior published scientific evidence on OSLP in both in vitro and in vivo models, let alone its neuroprotective potential. A prior literature search only yielded two studies on the ethanolic extracts of *Orthosiphon stamineus*; Choo et al. (2018) examined the anticonvulsive potential in adult zebrafish [9] and Ismail et al. (2017) reported on toxicity in zebrafish embryos [19]. As such, this work represents the first of its kind.

In this study, the PTZ-induced seizure model was established [7,12] to investigate the anticonvulsive potential of OSLP (800 μg/kg of b.w.) using adult zebrafish. Pre-treatment with OSLP 800 μg for 30 min brought about significant improvements in the PTZ-injected zebrafish, with a lower seizure score and a prolonged seizure onset time. Pre-treatment with OSLP 800 μg also produced a swimming pattern comparable to that of the untreated VC which received neither PTZ injection nor OSLP treatment (TC). It was seen that the O+P group managed to swim through the whole tank without showing an apparent preference for any spot or apparent bottom-dwelling behavior. Contradictorily, the representative zebrafish swimming pattern showed a bottom-dwelling behavior in the PTZ-injected group, which has been strongly linked to the anxious behavior in seizures [15,16]. A similar observation was also reported in two recent studies using PTZ-induced zebrafish [7,12]. Diazepam (DZP, 1.25 mg/kg) has been found in this study to efficaciously control seizures in the PTZ-injected zebrafish and thus, a swimming pattern comparable to that of the untreated VC was observed. Interestingly, the TC group which received neither PTZ injection nor DZP treatment, produced a swimming pattern comparable to that of the untreated VC group. This finding thus reaffirms that OSLP at 800 μg/kg of body weight does not produce lethal events and with that it could be potentially anticonvulsive. Nevertheless, one of the limitations in this study includes a considerably low yield of OSLP (approximately 0.3%) extracted from OS leaves and hence, based on the safety study (Section 3.1), only the maximal safe dose (800 μg/kg of b.w.) was used.

The PTZ-injected group had the highest mean total distance travelled and travelled about 60% longer distance than the untreated VC group. This uncontrolled movement has been strongly linked to burst neuronal firing in addition to the pass-out phenomenon in seizures [20,21]. A similar observation was also reported in two recent studies using PTZ-induced zebrafish [7,12]. A disruption occurred in the normal balance of excitation and inhibition following the injection of PTZ. Binding of PTZ to $GABA_A$ (γ-aminobutyric acid type A) receptors stimulated excitability in the brains and hence provoked uncontrolled seizures in the zebrafish. This explains the representative swim path of the PTZ-injected group which showed burst swimming activities (i.e., erratic movements, loss of direction) which taken together, contributed to the longest total distance travelled. Moreover, the PTZ-injected group spent a longer time in the lower half of tank, which could possibly be attributed to the bottom-dwelling behavior in seizures [15,16].

In contrast, pre-treatment with DZP significantly alleviated the manipulations of PTZ. A 57% reduction in the total distance travelled was seen in the DZP-treated group and it spent more time in the

upper half of tank in a comparable manner to that of the untreated group. Interestingly however, it also spent a longer time in the bottom half of the tank, but the untreated group did not. This phenomenon could be attributed to the sedative effects of DZP. DZP is an anxiolytic benzodiazepine with fast-acting and long-lasting actions [22]. When administered intravenously, DZP has been shown to act within 1 to 3 min, while oral dosing onset ranges between 15 to 60 min; with a duration of action of more than 12 h. Similar to most benzodiazepines, DZP causes adverse effects including syncope (temporary loss of consciousness), sedation and confusion, to name a few [23]. A similar finding was also reported in three studies using DZP to treat zebrafish [7,12,24]. Pre-treatment with OSLP 800 µg also alleviated the manipulations of PTZ. A 20% reduction in the total distance travelled was seen in the OSLP-treated group and similarly, they spent more time in the upper half of tank compared to the DZP-treated group. Interestingly however, they did not spend a longer time in the bottom half of tank as the DZP-treated group did, but in a pattern more comparable to the untreated VC group. Hence, this outcome suggests that OSLP's anticonvulsive actions could be acting differently from DZP and with that, it might not produce the similar cognitive insults such as DZP. This similar outcome has been reported in Choo's study using *O. stamineus* ethanolic extracts to treat adult zebrafish [7]. On the market, DZP has since been one of the top selling AEDs of all time, well known for its fast onset of action and is often effective in adults [25,26]. However, DZP's high clinical efficacy in treating epilepsy and seizures comes with multiple adverse reactions such as suicidality, paradoxical CNS stimulation, syncope, sedation, depression and dystonia, to name a few [23]. These adverse effects are common in currently available AEDs. Worthy of mention, the TC group did not show any abnormal locomotion parameters and hence, reaffirming that this dose is considerably safe in the adult zebrafish.

Taken together, the outcomes of behavioral study suggest that OSLP at 800 µg/kg of body weight is potentially anticonvulsive. OSLP treatment produced milder anticonvulsant effects in comparison to DZP treatment, which is one of the standard AEDs available today.

In this study, two major neurotransmitters, namely GABA and Glu, were investigated. An interrupted GABA/Glu cycle was seen in the PTZ-injected zebrafish, with a drop in the mean GABA level but a surge in the mean Glu level. Distinctively, such anomalies were not found in the untreated zebrafish which did not receive PTZ injection. Additionally, the GABA/Glu ratio of PTZ-injected group remained the lowest. This thus shows a disruption in the normal balance of excitation and inhibition following the PTZ treatment. PTZ is a tetrazol derivative known to block $GABA_A$ receptor function [27]. PTZ suppresses GABA inhibitory activities which in turn potentiates the Glu excitatory activities in the brain and eventually results in an unbalanced GABA/Glu ratio. This finding has lent more support to the severe seizures seen in the PTZ-injected group. Pre-treatment with DZP, without surprise, significantly suppressed the excitatory neurotransmitter Glu, normalizing it to be comparable to the untreated VC group. Concurrently, the GABA levels in the DZP-treated group saw a slight elevation and this eventually improved the GABA/Glu ratio. A similar finding has been reported earlier [28]. DZP inhibits Glu release to suppress glutamatergic hyperactivity and hence, restores the balance between GABA and Glu to promptly arrest neuroexcitation [29,30]. Pre-treatment with OSLP has also improved the neurotransmitters profile, with significantly lower excitatory Glu levels. More interestingly, OSLP treatment brings the GABA/Glu ratio close to the DZP treatment. Although to a lesser degree than the pure drug control, taken together, these findings show that OSLP has GABA potentiating actions and antiglutamatergic effects. Moreover, the finding that TC group had a neurotransmitters profile comparable to the untreated VC group, has also buttressed the proposal of OSLP could be having neuroprotective potential.

The present protein expression study is useful in helping to predict the anticonvulsive mechanism of OSLP. The main findings are the following. First, mass spectrometry-based LFQ analysis compared the differentially expressed proteins in the seizure group (NC, induced by PTZ 170 mg/kg only) and the OSLP-treated seizure group (OSLP 800 µg/kg + PTZ 170 mg/kg). This identified a distinct protein expression profile of 29 differentially expressed proteins that had higher expressions in the O+P group than in the NC group. Second, functional annotation analysis found the protein bindings

of SNARE (GO:149) and syntaxin (GO:19905) at intracellular localizations that were particularly interesting, given the fundamental role they play in the regulation of membrane fusion during presynaptic vesicle exocytosis. Third, KEGG pathway mapping proposed the synaptic vesicle cycle (04721) as the most probable pathway, in line with the strong association between SNARE and syntaxin proteins. These proteins are required in calcium (Ca^{2+})-dependent synaptic vesicle exocytosis. As shown, the trans-SNARE complex was assembled in the presence of SNARE proteins including complexin (Cplx), syntaxin (Stx), synaptotagmin (Syt), synaptosomal-associated protein of 25 kDa (Snap25) and vesicle-associated membrane protein (Vamp). According to ZFIN (https://zfin.org/ZDB-GENE-081113-1), gene cplx2 is predicted to orthologous to human gene CPLX2.

Complexin is an important regulator of synaptic vesicle exocytosis. Complexins, also called synaphins, are small cytosolic proteins. They form a small protein family with four isoforms, Cplx1–4 [31]. Cplx1 and Cplx2 are highly homologous. In particular, they bind to the SNARE complex which are expressed at presynaptic sites [32–35]. SNARE binding is a highly specialized regulation that is strictly regulated by synaptic fusion machinery. The basic components of a synaptic fusion machinery are the SNARE proteins namely Cplx, Stx, Syt, Snap25, Vamp, and two mammalian uncoordinated proteins (Munc13 and Munc18) [36]. The formation of the trans-SNARE complex is required in the vesicle priming phase. As the trans-SNARE complex forms, the vesicle is pulled close to the plasma membrane, where it is ready to fuse in response to the Ca^{2+} influx that is triggered by an action potential, usually in less than a millisecond. Complexin binds to the trans-SNARE complex and modulates the fusion process by either increasing or decreasing the height of the energy barrier for fusion. The height of the energy barrier for fusion is not only important for evoked release but also determines how likely vesicles are to fuse spontaneously in the absence of a Ca^{2+}-triggering signal. After fusion, the vesicle is retrieved by endocytosis and reloaded for another round of exocytosis [13,32,33,36]. Therefore, the binding of complexin to the SNARE complex is crucial for the normal priming and subsequent Ca^{2+}-evoked neurotransmitter release during presynaptic vesicle exocytosis.

The findings of protein expression study have suggested that synaptic vesicle cycle pathway could play a significant role in modulating the anticonvulsive mechanism of OSLP. OSLP could be regulating the release of GABA and Glu via calcium-dependent synaptic vesicle exocytosis. Similar findings have been reported by studies using samples from rats and patients [32,34,35]. Decreased expressions of complexin 2 have also been associated with neurodegenerative diseases including Alzheimer's, Huntington's, and Parkinson's; psychiatric disorders including schizophrenia and bipolar disorder [37–40], with seizures and epilepsy being common comorbidities [41–46].

OSLP could be a potential anticonvulsant. Found in OSLP, baicalein 7-*O*-glucuronosyltransferase and baicalin-beta-D-glucuronidase are responsible for the biosynthesis of baicalein and baicalin, respectively. Baicalein and baicalin have been reported to have anxiolytic activity and acting on GABA and glutamic acid in rat brains [47], binding to the benzodiazepine site of the $GABA_A$ receptor to potentiate GABA-mediated inhibition [48–50] and anticonvulsive action in the PTZ-induced seizure rat model [51]. Beta-mycrene synthase and R-linalool synthase are proteins responsible for the biosynthesis of myrcene and linalool respectively. Linalool has been reported to have antiepileptiform and antiseizure properties in PTZ-treated rats [52–54] whereas beta-mycrene has also been reported for sedative effects in human [55] and anticonvulsive effects in PTZ-treated rats [56]. Beta-mycrene synthase and R-linalool synthase might not directly act on cannabinoid receptors but could be producing synergic effects with future cannabinoid-based AEDs. The postulated synergistic contribution on both GABA and Glu neurotransmitters can increase the efficacy of future cannabinoid-based AEDs in managing epilepsy and seizures [57–60]. Rosmarinate synthase is involved in the biosynthesis of rosmarinic acid Choo, Kundap [7] suggested that rosmarinic acid (in an ethanolic extract of OS) is one of the probable antiepileptic components of the extract in adult zebrafish whereas similar findings in PTZ-induced seizures in mice have also been reported earlier [10,61].

5. Conclusions

The study suggests that OSLP could be a potential anticonvulsant. OSLP most likely regulates the release of the neurotransmitters, GABA and Glu, via calcium-dependent synaptic vesicle exocytosis mediated by the "synaptic vesicle cycle" pathway. To the best of our knowledge, this study is the first to show that OSLP can safely ameliorate epilepticeizures in adult zebrafish.

Author Contributions: Y.-S.C. designed, performed all the experiments and prepared the final manuscript; B.K.M.C. helped in the behavioral experiments and edited the final manuscript; P.K.A. aided in supervision and helped edit the final manuscript; M.F.S. and I.O. contributed to the design of research, supervised all aspects of the study and edited the final manuscript as submitted. All authors have read and agreed to the published version of the manuscript.

Funding: This research was funded by the NKEA EPP#1 Research Grant Scheme (NRGS) (NH1014D066), Ministry of Agriculture and Agro-based Industry, Malaysia and Global Asia in the 21st Century (GA21) Platform, Monash University Malaysia, Research Grant (GA-HW-18-L04).

Acknowledgments: The authors would like to thank Syafiq Asnawi Zainal Abidin and Nurziana Sharmilla Binti Nawawi for ESI-LCMS/MS technical support (LC-MS laboratory of Jeffrey Cheah School of Medicine and Health Sciences).

Conflicts of Interest: The authors declare no conflict of interest. The funders had no role in the design of the study; in the collection, analyses, or interpretation of data; in the writing of the manuscript, or in the decision to publish the results.

References

1. World Health Organisation. *Epilepsy: A Public Health Imperative: Summary*; World Health Organization: Geneva, Switzerland, 2019.
2. Jacob, S.; Nair, A.B. An updated overview on therapeutic drug monitoring of recent antiepileptic drugs. *Drugs R D* **2016**, *16*, 303–316. [CrossRef] [PubMed]
3. Luft, J.G.; Steffens, L.; Morás, A.M.; Da Rosa, M.S.; Leipnitz, G.; Regner, G.G.; Pflüger, P.F.; Gonçalves, D.; Moura, D.J.; Pereira, P. Rosmarinic acid improves oxidative stress parameters and mitochondrial respiratory chain activity following 4-aminopyridine and picrotoxin-induced seizure in mice. *Naunyn-Schmiedeberg's Arch. Pharmacol.* **2019**, *392*, 1347–1358. [CrossRef]
4. Chen, Z.; Brodie, M.J.; Liew, D.; Kwan, P. Treatment outcomes in patients with newly diagnosed epilepsy treated with established and new antiepileptic drugs: A 30-year longitudinal cohort study. *JAMA Neurol.* **2018**, *75*, 279–286. [CrossRef]
5. Helmstaedter, C.; Witt, J.-A. Chapter 28—Clinical neuropsychology in epilepsy: Theoretical and practical issues. In *Handbook of Clinical Neurology*; Stefan, H., Theodore, W.H., Eds.; Elsevier: Amsterdam, The Netherlands, 2012; Volume 107, pp. 437–459.
6. World Health Organisation. *WHO Traditional Medicine Strategy 2014–2023*; World Health Organisation: Geneva, Switzerland, 2013.
7. Zhu, H.-L.; Wan, J.-B.; Wang, Y.-T.; Li, B.-C.; Xiang, C.; He, J.; Li, P. Medicinal compounds with antiepileptic/anticonvulsant activities. *Epilepsia* **2014**, *55*, 3–16. [CrossRef] [PubMed]
8. Rabiei, Z. Anticonvulsant effects of medicinal plants with emphasis on mechanisms of action. *Asian Pac. J. Trop. Biomed.* **2017**, *7*, 166–172. [CrossRef]
9. Choo, B.K.M.; Kundap, U.P.; Kumari, Y.; Hue, S.-M.; Othman, I.; Shaikh, M.F. Orthosiphon stamineus leaf extract affects TNF-α and seizures in a zebrafish model. *Front. Pharmacol.* **2018**, *9*, 139. [CrossRef]
10. Coelho, V.R.; Vieira, C.G.; De Souza, L.P.; Moysés, F.; Basso, C.; Papke, D.K.M.; Pires, T.R.; Siqueira, I.R.; Picada, J.N.; Pereira, P. Antiepileptogenic, antioxidant and genotoxic evaluation of rosmarinic acid and its metabolite caffeic acid in mice. *Life Sci.* **2015**, *122*, 65–71. [CrossRef]
11. Howe, K.; Clark, M.D.; Torroja, C.F.; Torrance, J.; Berthelot, C.; Muffato, M.; Collins, J.E.; Humphray, S.; McLaren, K.; Matthews, L.; et al. The zebrafish reference genome sequence and its relationship to the human genome. *Nature* **2013**, *496*, 498–503. [CrossRef]
12. Norton, W.; Bally-Cuif, L. Adult zebrafish as a model organism for behavioural genetics. *BMC Neurosci.* **2010**, *11*, 90. [CrossRef]

13. Stewart, A.M.; Braubach, O.; Spitsbergen, J.; Gerlai, R.; Kalueff, A.V. Zebrafish models for translational neuroscience research: From tank to bedside. *Trends Neurosci.* **2014**, *37*, 264–278. [CrossRef]
14. OECD (Organisation for Economic Co-operation). *Development Test No. 203: Fish, Acute Toxicity Test*; OECD Publishing: Paris, France, 1992.
15. Blaser, R.E.; Rosemberg, D.B. Measures of anxiety in zebrafish (danio rerio): Dissociation of black/white preference and novel tank test. *PLoS ONE* **2012**, *7*, e36931. [CrossRef]
16. Kysil, E.V.; Meshalkina, D.A.; Frick, E.E.; Echevarria, D.J.; Rosemberg, D.B.; Maximino, C.; Lima, M.G.; Abreu, M.S.; Giacomini, A.C.; Barcellos, L.J. Comparative analyses of zebrafish anxiety-like behavior using conflict-based novelty tests. *Zebrafish* **2017**, *14*, 197–208. [CrossRef] [PubMed]
17. Gebauer, D.L.; Pagnussat, N.; Piato, Â.L.; Schaefer, I.C.; Bonan, C.D.; Lara, D.R. Effects of anxiolytics in zebrafish: Similarities and differences between benzodiazepines, buspirone and ethanol. *Pharmacol. Biochem. Behav.* **2011**, *99*, 480–486. [CrossRef]
18. OECD (Organisation for Economic Co-operation). *Development Test No. 203: Fish, Acute Toxicity Test*; OECD Publishing: Paris, France, 2018.
19. Ismail, H.F.; Hashim, Z.; Soon, W.T.; Ab Rahman, N.S.; Zainudin, A.N.; Majid, F.A.A. Comparative study of herbal plants on the phenolic and flavonoid content, antioxidant activities and toxicity on cells and zebrafish embryo. *J. Tradit. Complementary Med.* **2017**, *7*, 452–465. [CrossRef]
20. Kundap, U.P.; Kumari, Y.; Othman, I.; Shaikh, M.F. Zebrafish as a model for epilepsy-induced cognitive dysfunction: A pharmacological, biochemical and behavioral approach. *Front. Pharmacol.* **2017**, *8*, 515. [CrossRef] [PubMed]
21. Mormann, F.; Jefferys, J.G. Neuronal firing in human epileptic cortex: The ins and outs of synchrony during seizures: Dissociation of synchronization of neurons and field potentials. *Epilepsy Curr.* **2013**, *13*, 100–102. [CrossRef]
22. Scharfman, H.E. The neurobiology of epilepsy. *Curr. Neurol. Neurosci. Rep.* **2007**, *7*, 348–354. [CrossRef]
23. Griffin, C.E., 3rd; Kaye, A.M.; Bueno, F.R.; Kaye, A.D. Benzodiazepine pharmacology and central nervous system-mediated effects. *Ochsner J.* **2013**, *13*, 214–223. [PubMed]
24. Dhaliwal, J.S.; Saadabadi, A. Diazepam [Updated 2019 January 30]. In *StatPearls [Internet]*; StatPearls Publishing: Treasure Island, CA, USA, 2019.
25. Gupta, P.; Khobragade, S.B.; Shingatgeri, V.M.; Rajaram, S.M. Assessment of locomotion behavior in adult Zebrafish after acute exposure to different pharmacological reference compounds. *Drug Dev. Ther.* **2014**, *5*, 127–133. [CrossRef]
26. Calcaterra, N.E.; Barrow, J.C. Classics in chemical neuroscience: Diazepam (valium). *ACS Chem. Neurosci.* **2014**, *5*, 253–260. [CrossRef]
27. Kelly, T.H.; Delzer, T.A.; Martin, C.A.; Harrington, N.G.; Hays, L.R.; Bardo, M.T. Performance and subjective effects of diazepam and d-amphetamine in high and low sensation seekers. *Behav. Pharmacol.* **2009**, *20*, 505–517. [CrossRef] [PubMed]
28. Velíšek, L. Models of Generalized Seizures in Freely Moving Animals. In *Encyclopedia of Basic Epilepsy Research*; Philip, A.S., Ed.; Academic Press: Cambridge, MA, USA, 2009; pp. 775–780. [CrossRef]
29. Bernasconi, R.; Klein, M.; Martin, P.; Portet, C.; Maitre, L.; Jones, R.; Baltzer, V.; Schmutz, M. The specific protective effect of diazepam and valproate against isoniazid-induced seizures is not correlated with increased GABA levels. *J. Neural Transm.* **1985**, *63*, 169–189. [CrossRef] [PubMed]
30. Perks, A.; Cheema, S.; Mohanraj, R. Anaesthesia and epilepsy. *BJA Br. J. Anaesth.* **2012**, *108*, 562–571. [CrossRef] [PubMed]
31. Cao, L.; Bie, X.; Huo, S.; Du, J.; Liu, L.; Song, W. Effects of diazepam on glutamatergic synaptic transmission in the hippocampal CA1 area of rats with traumatic brain injury. *Neural Regen. Res.* **2014**, *9*, 1897–1901. [PubMed]
32. Trimbuch, T.; Rosenmund, C. Should I stop or should I go? The role of complexin in neurotransmitter release. *Nat. Rev. Neurosci.* **2016**, *17*, 118–125. [CrossRef] [PubMed]
33. Acuna, C.; Guo, Q.; Burré, J.; Sharma, M.; Sun, J.; Südhof, T.C. Microsecond Dissection of Neurotransmitter Release: SNARE-Complex Assembly Dictates Speed and Ca2+ Sensitivity. *Neuron* **2014**, *82*, 1088–1100. [CrossRef]
34. Li, Y.C.; Kavalali, E.T. Synaptic vesicle-recycling machinery components as potential therapeutic targets. *Pharm. Rev.* **2017**, *69*, 141–160. [CrossRef]

35. Snead, D.; Eliezer, D. Chapter Nine—Spectroscopic Characterization of Structure–Function Relationships in the Intrinsically Disordered Protein Complexin. In *Methods in Enzymology*; Rhoades, E., Ed.; Academic Press: Cambridge, MA, USA, 2018; Volume 611, pp. 227–286.
36. Tang, J. Complexins. In *Encyclopedia of Neuroscience*; Squire, L.R., Ed.; Academic Press: Oxford, UK, 2009; pp. 1–7.
37. Ungermann, C.; Langosch, D. Functions of SNAREs in intracellular membrane fusion and lipid bilayer mixing. *J. Cell Sci.* **2005**, *118*, 3819–3828. [CrossRef]
38. Moriya, Y.; Itoh, M.; Okuda, S.; Yoshizawa, A.C.; Kanehisa, M. KAAS: An automatic genome annotation and pathway reconstruction server. *Nucleic Acids Res.* **2007**, *35*, W182–W185. [CrossRef]
39. Roncon, P.; Soukupovà, M.; Binaschi, A.; Falcicchia, C.; Zucchini, S.; Ferracin, M.; Langley, S.R.; Petretto, E.; Johnson, M.R.; Marucci, G. MicroRNA profiles in hippocampal granule cells and plasma of rats with pilocarpine-induced epilepsy–comparison with human epileptic samples. *Sci. Rep.* **2015**, *5*, 141–143. [CrossRef]
40. Chen, X.; Tomchick, D.R.; Kovrigin, E.; Araç, D.; Machius, M.; Südhof, T.C.; Rizo, J. Three-dimensional structure of the complexin/snare complex. *Neuron* **2002**, *33*, 397–409. [CrossRef]
41. Scarmeas, N.; Honig, L.S.; Choi, H.; Cantero, J.; Brandt, J.; Blacker, D.; Albert, M.; Amatniek, J.C.; Marder, K.; Bell, K.; et al. Seizures in alzheimer disease: Who, when, and how common? *Arch. Neurol.* **2009**, *66*, 992–997. [CrossRef] [PubMed]
42. Son, A.Y.; Biagioni, M.C.; Kaminski, D.; Gurevich, A.; Stone, B.; Di Rocco, A. Parkinson's disease and cryptogenic epilepsy. *Case Rep. Neurol Med.* **2016**, *2016*, 3745631. [CrossRef] [PubMed]
43. Sipilä, J.O.T.; Soilu-Hänninen, M.; Majamaa, K. Comorbid epilepsy in Finnish patients with adult-onset Huntington's disease. *BMC Neurol.* **2016**, *16*, 24. [CrossRef]
44. Mendez, M.F.; Grau, R.; Doss, R.C.; Taylor, J.L. Schizophrenia in epilepsy. *Seizure Psychos. Var.* **1993**, *43*, 1073.
45. Cascella, N.G.; Schretlen, D.J.; Sawa, A. Schizophrenia and epilepsy: Is there a shared susceptibility? *Neurosci. Res.* **2009**, *63*, 227–235. [CrossRef]
46. Knott, S.; Forty, L.; Craddock, N.; Thomas, R.H. Epilepsy and bipolar disorder. *Epilepsy Behav.* **2015**, *52*, 267–274. [CrossRef]
47. Awad, R.; Arnason, J.T.; Trudeau, V.; Bergeron, C.; Budzinski, J.W.; Foster, B.C.; Merali, Z. Phytochemical and biological analysis of skullcap (scutellaria lateriflora l.): A medicinal plant with anxiolytic properties. *Phytomedicine* **2003**, *10*, 640–649. [CrossRef]
48. Awad, R.; Levac, D.; Cybulska, P.; Merali, Z.; Trudeau, V.; Arnason, J. Effects of traditionally used anxiolytic botanicals on enzymes of the γ-aminobutyric acid (GABA). *Can. J. Physiol. Pharmacol.* **2007**, *85*, 933–942. [CrossRef]
49. Hanrahan, J.R.; Chebib, M.; Johnston, G.A.R. Flavonoid modulation of GABA(A) receptors. *Br. J. Pharmacol.* **2011**, *163*, 234–245. [CrossRef]
50. Wang, H.; Hui, K.-M.; Chen, Y.; Xu, S.; Wong, J.T.-F.; Xue, H. Structure-activity relationships of flavonoids, isolated from scutellaria baicalensis, binding to benzodiazepine site of GABAA receptor complex. *Planta Med.* **2002**, *68*, 1059–1062. [CrossRef] [PubMed]
51. Zhang, Z.; Lian, X.-y.; Li, S.; Stringer, J.L. Characterization of chemical ingredients and anticonvulsant activity of american skullcap (scutellaria lateriflora). *Phytomedicine* **2009**, *16*, 485–493. [CrossRef] [PubMed]
52. Jones, N.A.; Hill, A.J.; Smith, I.; Bevan, S.A.; Williams, C.M.; Whalley, B.J.; Stephens, G.J. Cannabidiol displays antiepileptiform and antiseizure properties in vitro and in vivo. *J. Pharm. Exp. Ther.* **2010**, *332*, 569–577. [CrossRef] [PubMed]
53. Hill, A.; Mercier, M.; Hill, T.; Glyn, S.; Jones, N.; Yamasaki, Y.; Futamura, T.; Duncan, M.; Stott, C.; Stephens, G. Cannabidivarin is anticonvulsant in mouse and rat. *Br. J. Pharm.* **2012**, *167*, 1629–1642. [CrossRef] [PubMed]
54. Hill, T.D.M.; Cascio, M.-G.; Romano, B.; Duncan, M.; Pertwee, R.G.; Williams, C.M.; Whalley, B.J.; Hill, A.J. Cannabidivarin-rich cannabis extracts are anticonvulsant in mouse and rat via a CB1 receptor-independent mechanism. *Br. J. Pharm.* **2013**, *170*, 679–692. [CrossRef] [PubMed]
55. Karniol, I.G.; Shirakawa, I.; Takahashi, R.N.; Knobel, E.; Musty, R.E. Effects of Δ^9-Tetrahydrocannabinol and Cannabinol in Man. *Pharmacology* **1975**, *13*, 502–512. [CrossRef] [PubMed]
56. De Barros, G.S.; Silva, C.M.M.; De Abreu Matos, F.J. Anticonvulsant activity of essential oils and active principles from chemotypes of Lippia alba (Mill.) NE Brown. *Biol. Pharm. Bull.* **2000**, *23*, 1314–1317.
57. Russo, E.B. Taming THC: Potential cannabis synergy and phytocannabinoid-terpenoid entourage effects. *Br. J. Pharmacol.* **2011**, *163*, 1344–1364. [CrossRef]

58. Reddy, D.S.; Golub, V.M. The pharmacological basis of cannabis therapy for epilepsy. *J. Pharmacol. Exp. Ther.* **2016**, *357*, 45–55. [CrossRef]
59. Perucca, E. Cannabinoids in the treatment of epilepsy: Hard evidence at last? *J. Epilepsy Res.* **2017**, *7*, 61–76. [CrossRef]
60. Katona, I. Cannabis and endocannabinoid signaling in epilepsy. In *Endocannabinoids*; Springer: Berlin/Heidelberg, Germany, 2015; pp. 285–316.
61. Grigoletto, J.; De Oliveira, C.V.; Grauncke, A.C.B.; De Souza, T.L.; Souto, N.S.; De Freitas, M.L.; Furian, A.F.; Santos, A.R.S.; Oliveira, M.S. Rosmarinic acid is anticonvulsant against seizures induced by pentylenetetrazol and pilocarpine in mice. *Epilepsy Behav.* **2016**, *62*, 27–34. [CrossRef] [PubMed]

SUPPLEMENTARY DATA

Table SD-1 KO (KEGG Orthology) generated KEGG pathways.

UniProt ID	KO ID
tr|Q7SZV9|Q7SZV9_DANRE	K13826
tr|Q803Z5|Q803Z5_DANRE	K13826
tr|Q8AYC4|Q8AYC4_DANRE	K07375
sp|Q90485|HBB2_DANRE	K13825
tr|Q6PE34|Q6PE34_DANRE	K07375
tr|F8W3W8|F8W3W8_DANRE	K17269
tr|Q08BA1|Q08BA1_DANRE	K02132
tr|A8WG05|A8WG05_DANRE	K05692
sp|Q7ZUY3|H2AX_DANRE	K11251
tr|A3KPR4|A3KPR4_DANRE	K11254
tr|Q6PC12|Q6PC12_DANRE	K01689
tr|Q4VBK0|Q4VBK0_DANRE	K02133
tr|Q6ZM12|Q6ZM12_DANRE	K13825
sp|Q8JH70|ALDCB_DANRE	K01623
tr|E7F2M5|E7F2M5_DANRE	K04008
tr|R4GE02|R4GE02_DANRE	K11252
tr|Q5BJC7|Q5BJC7_DANRE	K13826
tr|E9QBF0|E9QBF0_DANRE	K01803
tr|Q8AY63|Q8AY63_DANRE	K00933
tr|B3DFP9|B3DFP9_DANRE	no data
tr|Q6TH32|Q6TH32_DANRE	K05765
tr|Q6PC53|Q6PC53_DANRE	K03767
tr|A0A0R4IKF0|A0A0R4IKF0_DANRE	no data
tr|Q6GQM9|Q6GQM9_DANRE	K01689
tr|F8W4M7|F8W4M7_DANRE	K01681
tr|A8DZ95|A8DZ95_DANRE	K07528
tr|A0A2R8Q2Z0|A0A2R8Q2Z0_DANRE	no data
tr|E7FBR8|E7FBR8_DANRE	K15294
tr|Q4VBT9|Q4VBT9_DANRE	K02263

Chapter 5

Anticonvulsive Potential of *Orthosiphon stamineus* Proteins in a Zebrafish Model of Hypoxia-associated Seizures Model

5.1 Introduction

Specifically, cerebral hypoxia occurs when there is a decreased supply of oxygen to the brain. Cerebral hypoxia can lead to hypoxic-ischaemic injury (McKenna, Scafidi, & Robertson, 2015). Hypoxic-ischaemic encephalopathy (HIE), a form of hypoxic-ischaemic injury, has been linked to the incidence of epilepsy (Sutter, Marsch, Fuhr, & Rüegg, 2013; Vintila, Roman, & Rociu, 2010; Weinhouse, Young, & Morrison, 2015). In HIE, seizures signal the secondary injury phase which can further decline cognitive functions of the Central Nervous System (CNS) (Scully, 2014).

Zebrafish (*Danio rerio*) is a cost-effective model ideal for high-throughput study on stress adaptation in a vertebrate system (Kokel et al., 2010; Piato et al., 2011; Steenbergen, Richardson, & Champagne, 2011; Yu & Li, 2011). It provides fundamental information for neurological, physiological and behavioral responses. Therefore, this makes zebrafish a potential alternative for studying the complex mechanism underlying hypoxic-ischaemia, seizures and epilepsy.

To date nonetheless, there remains no systematic study on the primary metabolites of OS, particularly in the CNS. As a primary metabolite, proteins extracted from OS leaves (OSLP) may hold novel protection for managing HIE and epilepsy.

The present chapter begins with establishing an adult zebrafish model of double challenge – hypoxia induction followed by PTZ injection. The model reminiscent the hypoxic-ischaemic insults on a mammalian brain. This model is then used to evaluate OSLP anticonvulsive potential under a hypoxic condition. The maximum safe starting dose of OSLP determined (See Chapter 4) is then used. The behavioral study including seizure score, seizure onset time, and locomotor activity are evaluated. Expressions of the two major neurotransmitters, gamma-Aminobutyric acid (GABA) and glutamate (Glu) are analysed using nanoflow-ESI-LCMS/MS. The protective mechanism of OSLP on zebrafish brains at the protein level is also investigated using mass spectrometry-based label-free proteomic quantification (LFQ). LFQ profiles the differentially expressed proteins between the four treatment groups: hypoxia-induced alone, hypoxia+PTZ-induced, OSLP-treated hypoxia, and OSLP-treated hypoxia+PTZ-induced. This thus provides fundamental information to study the functional annotations, the protein-protein interactions, and their gene-disease associations. These enriched biological data help to visualize the molecular interactions, reactions, and relations associated with the anticonvulsive mechanism of OSLP under hypoxia on disease pathway maps. Hence, the objectives of this chapter are:

1. To establish an adult zebrafish model of double challenge – hypoxia induction followed by PTZ induced seizures
2. To evaluate OSLP for its anticonvulsive potential under a hypoxic condition.
3. To study the potential of OSLP on neurotransmitters and protein expression levels

The flowchart outlining the overview of experimental design to achieve the objectives are summarized in Figure 5.1 below:

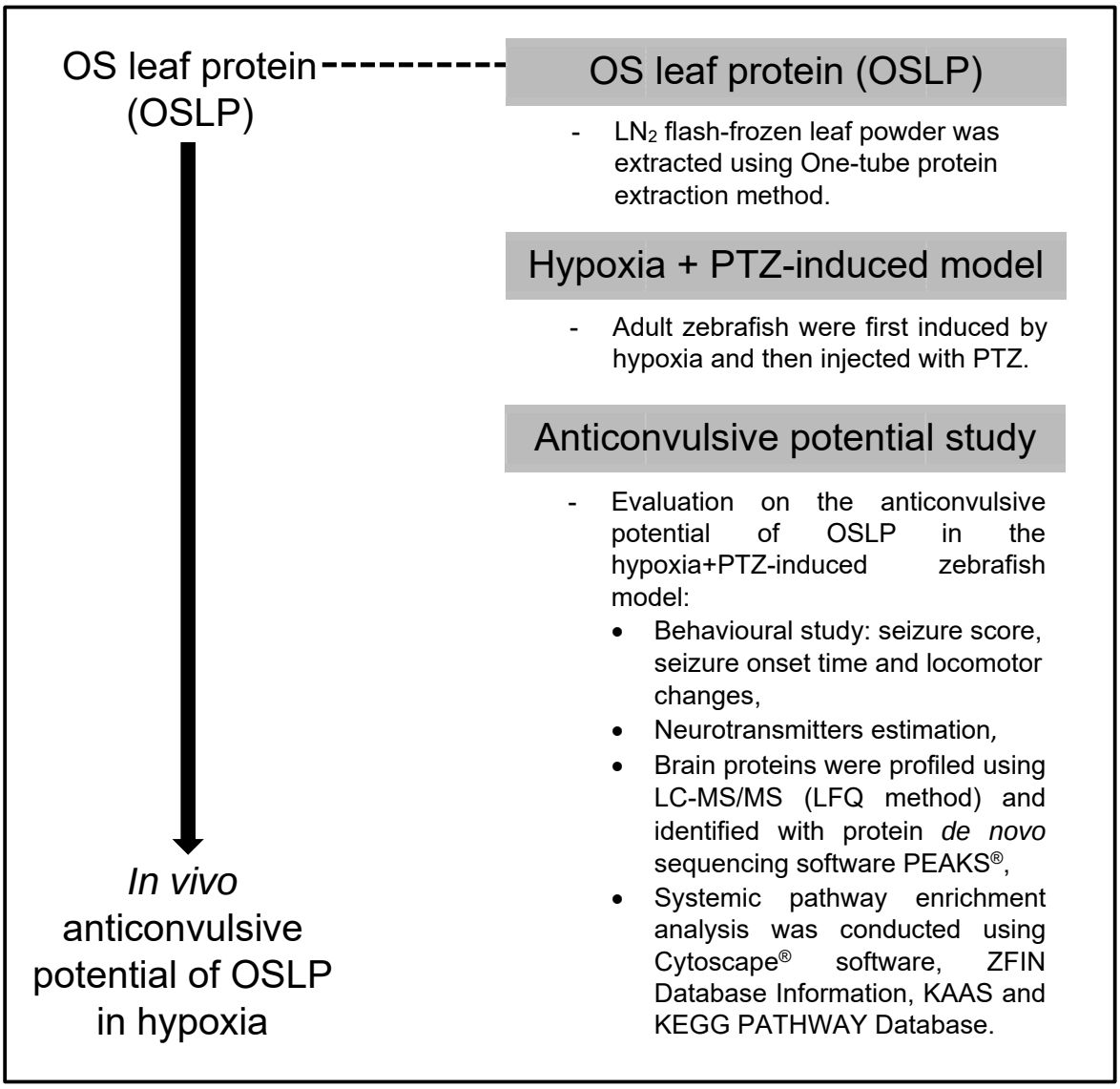

Figure 5.1: Flowchart summarizing the overview of experimental design.

References:

Kokel, D., Bryan, J., Laggner, C., White, R., Cheung, C. Y. J., Mateus, R., . . . Peterson, R. T. (2010). Rapid behavior-based identification of neuroactive small molecules in the zebrafish. *Nature Chemical Biology, 6*(3), 231-237. doi:10.1038/nchembio.307

McKenna, M. C., Scafidi, S., & Robertson, C. L. (2015). Metabolic Alterations in Developing Brain After Injury: Knowns and Unknowns. *Neurochemical research, 40*(12), 2527-2543. doi:10.1007/s11064-015-1600-7

Piato, Â. L., Capiotti, K. M., Tamborski, A. R., Oses, J. P., Barcellos, L. J. G., Bogo, M. R., . . . Bonan, C. D. (2011). Unpredictable chronic stress model in zebrafish (Danio rerio): Behavioral and physiological responses. *Progress in Neuro-Psychopharmacology and Biological Psychiatry, 35*(2), 561-567. doi:https://doi.org/10.1016/j.pnpbp.2010.12.018

Scully, C. (2014). 13 - Neurology. In C. Scully (Ed.), *Scully's Medical Problems in Dentistry (Seventh Edition)* (pp. 345-392). Oxford: Churchill Livingstone.

Steenbergen, P. J., Richardson, M. K., & Champagne, D. L. (2011). The use of the zebrafish model in stress research. *Progress in Neuro-Psychopharmacology and Biological Psychiatry, 35*(6), 1432-1451.

Sutter, R., Marsch, S., Fuhr, P., & Rüegg, S. (2013). Mortality and recovery from refractory status epilepticus in the intensive care unit: a 7-year observational study. *Epilepsia, 54*(3), 502-511.

Vintila, I., Roman, C., & Rociu, C. (2010). Hypoxic-ischemic encephalopathy in adult. *Acta Medica Transilvanica, 2*, 189-192.

Weinhouse, G. L., Young, G. B., & Morrison, R. S. (2015). Hypoxic-ischemic brain injury in adults: Evaluation and prognosis. *UpToDate [Internet]. Waltham, MA: UpToDate Inc.; c2019 [cited 2019 Feb 10]. Available from: https://www. uptodate. com/contents/hypoxic-ischemic-brain-injury-in-adults-evaluation-and-prognosis*.

Yu, X., & Li, Y. V. (2011). Zebrafish as an alternative model for hypoxic-ischemic brain damage. *International Journal of Physiology, Pathophysiology and Pharmacology, 3*(2), 88-96. Retrieved from http://www.ncbi.nlm.nih.gov/pmc/articles/PMC3134003/

biology

MDPI

Article

Orthosiphon stamineus Proteins Provide Hypoxic-Ischaemic Tolerance to Zebrafish Challenged by Hypoxia and Pentylenetetrazol-Induced Seizures

Yin-Sir Chung [1,2], Brandon Kar Meng Choo [1], Pervaiz Khalid Ahmed [3,4], Iekhsan Othman [1,2] and Mohd. Farooq Shaikh [1,*]

[1] Neuropharmacology Research Laboratory, Jeffrey Cheah School of Medicine and Health Sciences, Monash University Malaysia, Bandar Sunway, Malaysia
[2] Liquid Chromatography-Mass Spectrometry (LCMS) Platform, Jeffrey Cheah School of Medicine and Health Sciences, Monash University Malaysia, Bandar Sunway, Malaysia
[3] School of Business, Monash University Malaysia, Bandar Sunway, Malaysia
[4] Global Asia in the 21st Century (GA21), Monash University Malaysia, Bandar Sunway, Malaysia
* Correspondence:Correspondence: farooq.shaikh@monash.edu

Received: 07 July 2020; Accepted: date; Published: date

Abstract: Hypoxic-ischaemic encephalopathy (HIE) is a form of hypoxic-ischaemic injury capable of eliciting epilepsy. This study thus aims to elucidate the the anticonvulsive potential of proteins extracted from OS leaves (OSLP) in hypoxic zebrafish. Hypoxia induction (15 -18 min per fish) followed by pentylenetetrazol (PTZ) injection (170 mg/kg of body weight) was sufficiently induced hypoxia and provoked seizures in the adult zebrafish. Physical changes under hypoxic conditions (seizure intensity and onset duration, swimming behaviour, locomotor) and neurotransmitter analysis (gamma-aminobutyric acid, GABA; glutamate, Glu) were elucidated to assess the pharmacological activity. The protective mechanism of OSLP on brain was also studied using mass spectrometry-based label-free proteomic quantification (LFQ) and bioinformatics. OSLP pre-treatment (800 μg/kg, i.p., 30 min) had demonstrated subtle anticonvulsive effect in the zebrafish model of double challenge. OSLP showed subtle improvements in the seizure profile, swimming and locomotor behaviours; lowered the excitatory Glu and increased brain protein glutamine synthetase (Glula) expression. Glula is required to keep the GABA-Glu-Gln (glutamine) cycle in check. OSLP also increased the brain proteins (Enolase 2 and Isocitrate dehydrogenase 2) in the hypoxic but seizure-free zebrafish. These proteins promote anaerobic metabolism in neurons under hypoxic conditions. Taken together, this study suggests that OSLP is most likely to influence the synaptic transmission by providing hypoxic-ischaemic tolerance to the synapses via the "Glutamatergic Synapse" and "GABAergic Synapse" pathways, in addition to modulating cellular energy metabolism in neurons via the "Hypoxia-inducible factors (HIF)-1 Signalling" and "Citrate Cycle" pathways.

Keywords: *Orthosiphon stamineus*; plant-derived protein; hypoxic-ischaemic encephalopathy; epilepsy; zebrafish; seizures

1. Introduction

Cerebral hypoxia is a form of hypoxia affecting the brain and is a condition in which oxygen is not available in sufficient amounts to maintain adequate homeostasis. This can result from inadequate oxygen delivery to the brain either due to low blood supply or low oxygen content in the blood (hypoxaemia). Cerebral hypoxia can vary in intensity from mild to severe and can present in acute or chronic forms [1, 2], depending on the degree and duration of oxygen deprivation [3, 4]. Cerebral hypoxia can starve the neurons of oxygen and glucose that triggers a series of biochemical and

molecular events [4, 5], all of which eventually leads to hypoxic-ischaemic injuries such as variable inflammation, damage or death of the neural tissues of the brain [6, 7].

Hypoxic-ischaemic encephalopathy (HIE) is a form of hypoxic-ischaemic injury capable of eliciting epilepsy [8, 9]. HIE challenges the cellular metabolism and energy production in neurotransmitters and thereby, disrupts their synthesis, release and uptake [6]. This provokes seizures. In HIE, seizures signal the secondary injury phase to further cause a decline in sensory perception, motor control, behaviour, memory, autonomic function and syncope. Consequently, HIE can result in severe brain damage and permanent disabilities. On a global scale, HIE remains as one of the most challenging neurological disorders in adults [10].

In terms of genetic profile, zebrafish (*Danio rerio*) are close to 70% similar to humans and zebrafish also express approximately 84% of known human disease related genes [11, 12], providing fundamental information for neurological, physiological and behavioural responses. With this, zebrafish have become a promising species in studying stress adaptation in a vertebrate system [13-16]. The zebrafish model is therefore a potential alternative for studying the complex mechanism underlying hypoxic-ischaemia, seizures and epilepsy.

Various Orthosiphon stamineus (OS) crude extracts have been studied for their antioxidative [17] and anticonvulsive activities individually [18]. The proteins extract from OS leaves (OSLP) however, has not been explored yet. OSLP has been shown to be potentially anticonvulsive in adult zebrafish given the pro-convulsant pentylenetetrazol (PTZ) [19]. The anticonvulsive potential of OSLP in the face of hypoxia remains unstudied. Seeing the interplay between cerebral hypoxia and epilepsy, this study was thus commenced to elucidate the anticonvulsive potential of OSLP under a hypoxic condition.

2. Materials and Methods

2.1. Materials, chemicals and apparatuses

2.1.1. Materials & Chemicals

From Sigma-Aldrich (USA), phosphatase inhibitors cocktail 2, trifluoroethanol (TFE), L-Glutamic acid (Glu), HPLC-grade methanol (MeOH), 2,3,5-triphenyl tetrazolium chloride (TTC), γ-aminobutyric acid, formic acid (FA), diazepam (DZP), ammonium bicarbonate (ABC), Pentylenetetrazol (PTZ), iodoacetamide (IAA), cOmplete EDTA-free protease inhibitors, Benzocaine and dithiothreitol (DTT) were purchased. Mass-spec-grade acetonitrile (CAN), trifluoroacetic acid (TFA) and CHAPS (Nacailai Tesque, Japan) were also purchased from Sigma-Aldrich (USA)

Of the remaining materials & chemicals, 37% formaldehyde solution and dimethylsulfoxide (DMSO) were purchased from Friedemann Schmidt Chemical (Western Australia), phosphate buffered saline (PBS) tablets from VWR Life Science AMRESCO® (USA), mass-spec-grade Pierce®Radioimmunoprecipitation assay (RIPA) buffer and Pierce®trypsin protease from Thermo Scientific Pierce (USA), acetic acid (glacial, 100%) from Merck (Germany) and hydrochloric acid (36%) from Ajax Chemical (Australia).

Additionally, liquid nitrogen (LN_2) was purchased from Linde Malaysia, purified nitrogen gas (99.999%) was supplied by Iwatani Malaysia S/B and Milli-Q ultrapure water (MQUP) was from Millipore GmbH (Germany). Any other unlisted chemicals were analytic grade and were sourced from established supplier worldwide.

2.1.2. Apparatus

The apparatus used for the study include the Quick Start™Bradford Protein Assay Kit (Bio-Rad, USA), Pierce®C18 mini spin column (Thermo Scientific Pierce, USA), Protein LoBind microcentrifuge tube from (Eppendorf, USA), Cole-Parmer™ Stuart™ Orbital Shaker (Thermo Scientific Pierce, USA), 35 gauge needles (PrecisionGlide™, Becton, Dickinson and Company, USA), Hamilton syringes 25 μL (MICROLITER™ #702, Hamilton Co. USA), refrigerated centrifuge 5415R (Eppendorf AG, Germany), classic pH Pen Tester (Yi Hu Fish Farm Trading Pte. Ltd., Singapore), Camry High-Precision Electronic

Pocket Scale (Model EHA901, China), ultrasonic cell crusher (JY88-II N, China), Sera O_2 Test Kit (Sera GmbH, Germany), precision incubator (Memmert INB200, Germany) and the Eyela SpeedVac Vacuum Concentrator (Thermo Scientific Pierce, USA).

2.2. Software and equipment

Automated tracking of zebrafish swimming patterns was acomplished using the SMART V3.0.05 tracking software from Panlab Harvard Apparatus, Spain in combination with a camcorder from Sony, Japan to record video for software analysis. As described by Kundap, Kumari [20], the tank containing the swimming zebrafish was equally divided into two and designated as the top and bottom zones respectively.

To detect the targeted neurotransmitters, an Agilent Ultra-High-Performance Liquid Chromatography (UHPLC) 1290 Series (Agilent Technologies, USA) was used for solvent delivery. The chromatography system consists of the Agilent 1290 Series Thermostatted Column Compartment, Agilent 1290 Series High-Performance Autosampler and the Agilent 1290 Series Binary Pump. The Zorbax Eclipse Plus C18 (Rapid Resolution HD, 2.1 x 150.0 mm with a 1.8 μM pore size reverse-phase column) (Agilent Technologies, USA) together with an electrospray ionisation (ESI) equipped Agilent 6410B Triple Quadrupole (QQQ) mass spectrometer (Agilent Technologies, USA) was used to perform the separations.

To identify the proteins being differentially expressed, an Agilent 1200 series HPLC coupled with an Agilent 6550 iFunnel Quadrupole Time of Flight (Q-TOF) LC/MS, C-18 300Á Large Capacity Chip (Agilent Technologies, USA) and the Agilent MassHunter data acquisition software (Agilent Technologies, USA) was used. To analyse mass spectrometry-based label-free proteomic quantification (LFQ), the PEAKS®Studio software (Version 8.0, Bioinformatics Solution, Canada) together with the UniProtKB (Organism: *Danio rerio*) database was used. To study protein-protein interactions and functional annotations as well as analyse systemic pathways, the Zebrafish Information Network (ZFIN) database, KAAS (KEGG Automatic Annotation Server Version 2.1, Kanehisa Lab., Japan), KEGG PATHWAY Database (Organism: *Danio rerio*) and Cytoscape software (Version 3.7.2 plugin BiNGO for Gene Ontology (GO) annotated information, Cytoscape Consortium, USA) were used.

2.3. Zebrafish maintenance and housing conditions

Heterogenous wild-type three to four month old adult zebrafish (*Danio rerio*) with a short-fin phenotype were maintained under standard husbandry conditions [21] in the Monash University Malaysia animal facility. Standardised zebrafish housing tanks (36 cm long x 26 cm tall and 22 cm wide) were connected to a water circulation system which aerates the water as well as controls the water temperature (26 - 28°C) and pH (6.8 – 7.1) to provide a hygenic and low stress environment. The tanks were maintained under a light intensity of 250 lux with a 14-h to 10-h light-dark cycle with the lights being regulated by an automatic timer that turns on the light at 0800 and turns off the light at 2200. Up to ten to twelve zebrafish were housed in one tank, with only male or female zebrafish being in any one tank at a time. The zebrafish were fed *ad libitum* with TetraMin® Tropical Flakes three times a day and their diet was supplemented with live brine shrimps (*Artemia*) (Bio-Marine, Aquafauna Inc., USA). The zebrafish were accorded a 7-day acclimatisation period to reduce any stress before commencement of the experiments. All the animal experimentations conducted in this study (MUM/2018/14) were approved by the Monash Animal Research Platform (MARP) Animal Ethics Committee (Australia).

140 *2.4. Experimental design*

141 2.4.1. Anticonvulsive potential of OSLP in hypoxic animals

142 The anticonvulsive potential of OSLP under a hypoxic condition was investigated. In this study,
143 the adult zebrafish received a double challenge: first with hypoxia induction and immediately
144 followed by an intraperitoneal (i.p.) injection of PTZ. The treatment dose of OSLP was determined to
145 be 800 µg/kg of body weight as determined by an initial safety study [19]. Seizure score as well as
146 onset time were the two parameters used to quantify convulsive activity. Zebrafish behavioural
147 changes were evaluated by taking into account their time spent in the tank (upper- versus lower-half,
148 s), total distance travelled (cm) as well as swimming pattern. Before beginning the experiments, adult
149 zebrafish weighing between 0.45 – 0.50 g were selected and kept in 1 L treatment tanks filled with 1 L
150 of the tank water (26 - 28ºC) normally used to fill the tanks. The seven zebrafish groups (n = 10) (Table
151 1) as well as the experimental procedure were as follows (Figure 1):

152 **Table 1.** Experimental groups.

Group	*Treatment*
VC	Vehicle control (tank water + tank water, i.p.)
NC 1	Negative control 1 (tank water + hypoxia-induced + tank water, i.p.)
NC 2	Negative control 2 (tank water + hypoxia-induced + PTZ 170 mg/kg, i.p.)
PC	Positive control (DZP 1.25 mg/kg + hypoxia-induced + PTZ 170 mg/kg, i.p.)
TC	Treatment control (OSLP 800 µg/kg + tank water, i.p.)
O+H	OSLP-treated hypoxia (OSLP 800 µg/kg + hypoxia-induced + tank water, i.p.)
O+P	OSLP-treated hypoxia + PTZ (OSLP 800 µg/kg + hypoxia-induced + PTZ 170 mg/kg, i.p.)

153

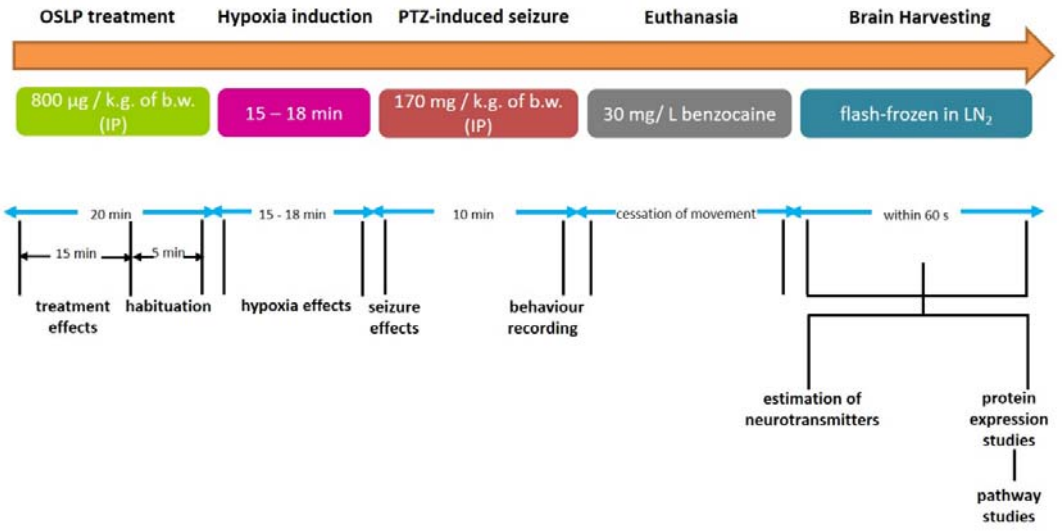

154

155 **Figure 1.** Procedures of the experiment.

156 All the groups were habituated for half hour before the hypoxia induction (except the VC and TC
157 groups) and before the administration of PTZ (except the VC, NC 1 and TC groups). Before giving each
158 individual IP injection, the zebrafish was individually immersed in benzocaine, at a concentration of
159 30 mg/L, until it ceased moving. For all the groups receiving hypoxia induction (NC1, NC2, PC, O+H
160 and O+H+P), the zebrafish did not again undergo anaesthesia before the injection of PTZ. If more than
161 a single IP injection was required consecutively on the individual zebrafish, the injections were not
162 given at the midline between the pelvic fins but rather at alternating lateral ends [20, 22].

163 Setting up the hypoxia chamber

164 The hypoxia chamber was made of thick, transparent acrylic with dimensions of 20 cm (L) x 20 cm
165 (W) x 20 cm (H). It had a thick, black rubber band running around the bottom side of the lid to produce
166 an air-tight condition. There were two small ports on both left and right sides (about 5 cm away from
167 the top) of the chamber; the left port was connected from the air space inside the container to the
168 outside open air, allowing oxygen exchange and the right port was connected to purified nitrogen gas
169 (99.999% N_2) tank (Figure 2). Prior to creating a systemic hypoxia environment, approximately 80 % of
170 the total chamber space was filled up with tank water (26 - 28ºC) normally used to fill the zebrafish
171 tanks while leaving about 20 % air space for controlling oxygen exchange. Purified N_2 was flushed at a
172 constant flow rate of 10 mg/L into the chamber water for 20 min and then sealed immediately after
173 stopping N_2 perfusion. Once sealed, this produced a systemic hypoxia condition and the dissolved
174 oxygen (DO_2) concentration in the chamber was determined to be near to 2 mg/L (modified from Yu
175 and Li [16], Cao, Jensen [23]). A hypoxic condition is defined as when DO_2 level is near to or below 2
176 mg/L, according to the Committee on Environment and Natural Resources [24, 25].

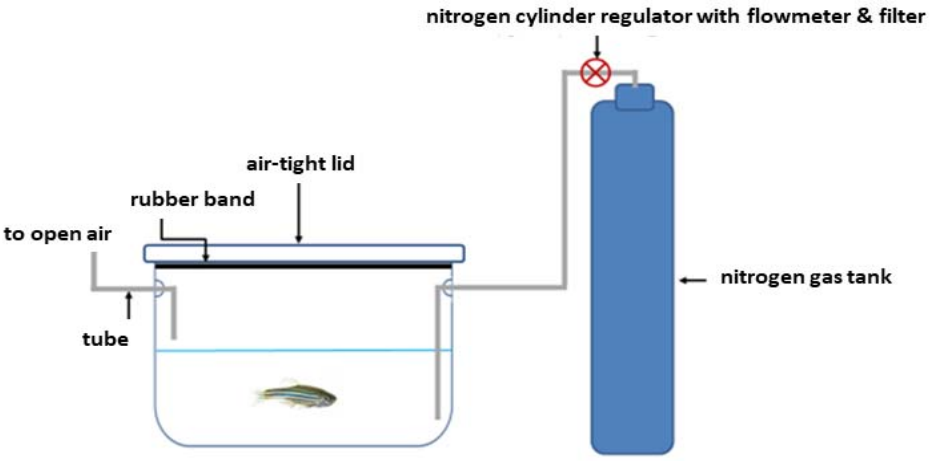

177
178 **Figure 2.** Diagram of the hypoxia chamber.

179 Hypoxia induction

180 When the chamber was hypoxia-ready, a zebrafish from each group (except the VC and TC
181 groups) was transferred into the hypoxic chamber and the water was continuously perfused with a
182 steady stream of purified N_2 at a constant flow rate of 2 mg/L. The end-point of the time a zebrafish in
183 the hypoxic chamber was determined as follows (Table 2) [16, 23]:

184 **Table 2.** Hypoxia measurement.

No.	Criteria
1	Lying motionless except for occasionally opercular movements for 40 s and above
2	Lying on one side or with abdomen up for 40 s and above

**Remark:* *This measurement is not accumulative, any motionless or staying still status less than 40 s is ignored.*

185 In this protocol, the hypoxia induction required an average of 15 – 18 min per zebrafish. After the
186 termination of hypoxia induction, all the zebrafish were hypoxic but remained alive and were not
187 vegetative. Behavioural changes of the hypoxic zebrafish were individually recorded using a
188 camcorder.

PTZ injection

Once a zebrafish was hypoxic, it was immediately extracted out of the hypoxia chamber and was immediately injected with PTZ. The NC 1 group did not receive a 170 mg/kg injection of PTZ. The NC 2 group was injected with 170 mg/kg of PTZ. The PC group was pre-treated with 1.25 mg/kg of DZP followed by 170 mg/kg of PTZ. The O+H group was pre-treated with 800 μg/kg of OSLP but did not receive the 170 mg/kg PTZ injection whereas the O+H+P group was pre-treated with 800 μg/kg of OSLP followed by 170 mg/kg of PTZ. Both VC and TC did not receive hypoxia induction or PTZ injection because they served as the experimental controls. The VC group was IP injected with only tank water whereas the TC group was injected with 800 μg/kg of OSLP and also injected with tank water. After that, all the zebrafish were individually transferred to a 13 L observation tank filled three-quarters of its volume with tank water. Any zebrafish behavioural changes were individually recorded (10 min) using a camcorder. The hypoxic and PTZ injected zebrafish presented various seizure scores and onset times. To determine the seizure score and onset time, the individual video was analysed using a computer as per the defined scoring system that is given in Table 3 [18, 20, 22, 26, 27].

Table 3. Seizure scoring system.

Score	*Criteria*
1	short swim mainly at the bottom of the tank
2	increased swimming activity and high frequency of opercular movements
3	burst swimming; left and right movements as well as the erratic movements
4	circular movements

2.5. Extraction of brains from zebrafish

After concluding the experiment, all the zebrafish used were sacrificed by euthanising them in benzocaine at a concentration of 30 mg/L. The brains of the zebrafish were carefully removed from their skulls and temporarily kept individually on a sterile petri dish before being transferred as quickly as possible to a sterile, pre-chilled 2.0 mL microtube and flash-frozen in liquid nitrogen (LN_2) before storage at -152ºC until further protein expression study and systemic pathway enrichment analysis as well as neurotransmitter analysis.

2.6. Neurotransmitter analysis using nanospray liquid chromatography coupled with tandem mass spectrometry (Nanospray-ESI-LC-MS/MS)

The levels of two major brain neurotransmitters, glutamate (Glu) and gamma-Aminobutyric acid (GABA) were determined using LC-MS/MS with some modifications to the method used in previous studies [19, 20, 22, 28]. All experiments were performed as three independent biological replicates.

A mother stock containing the neurotransmitter standards was prepared by mixing Glu and GABA in MQUP water, MeOH and 0.1% FA and, and the final concentration was adjusted to 1 mg/mL. Next eight standard calibration points (6.25 - 1000 ng/mL) was prepared by serial dilution. A blank was also prepared by mixing MeOH and MQUP water into 0.1% FA, and the final concentration was adjusted to 1 mg/mL. The blank together with the eight standard calibration points was used to quantify the levels of Glu and GABA.

Each LN_2 flash-frozen zebrafish brain was firstly homogenised in 1 mL of MeOH/MQUP water (3:1 vol/vol, ice-cold) using an ultrasonic cell crusher. The homogenate was then vortex-mixed (2500 rpm, 3 m) and incubated afterwards on an agitated shaker (4°C, 1 h). Next, the homogenate was centrifuged (4°C, 10,000 x g, 10 min) and the produced supernatant was carefully transferred into a 2.0 mL sterile microtube before slowly adding 100 μL of 0.1 % formic acid, followed by vortex-mixing (2500 rpm, 3 m) and then centrifuging (4°C, 10,000 x g, 10 min). The supernatant produced was then carefully transferred into a sterile insert fixed in a sterile mass spec grade vial. Finally, all the neurotransmitter samples were subjected to nanospray-ESI-LC-MS/MS analysis.

Nanospray-ESI-LC-MS/MS analysis was run using an Agilent 1290 Infinity UHPLC coupled to the electrospray ionisation equipped Agilent 6410B Triple Quad MS/MS. The separations were performed using the Zorbax Eclipse Plus C18 reverse-phase column (Rapid Resolution HD, 2.1 x 150.0 mm with a 1.8 uM pore size). The flow rate was set at 0.3 mL/min with the mobile phase consisting of 0.1% FA in MQUP water (Solvent 1) and ACN (Solvent 2). The gradient elution used was as follows: (i) 0 min, 5% Solvent 2; (ii) 0 - 3 min, 50% Solvent 2 and (iii) 3 - 5 min, 100% Solvent 2, with one-minute post time. The injection volume was 1.0 uL per sample with the autosampler temperature and the column compartment temperature set at 4°C and 25°C respectively. Every injection had a total run time of 5 min. ESI-MS/MS was used in positive ionisation mode with a nitrogen gas temperature of 325°C, a gas flow of 9 L/min, nebuliser pressure of 45 psi and a capillary voltage of 4000 V. The MS acquisition was scanned in Multiple Reaction Monitoring (MRM) mode. Quantification of the targeted neurotransmitters was done using a calibration range of 1.56 - 200 ng/mL, with a linear plot in which $r^2 > 0.99$.

2.7. Protein expression profiling using mass spectrometry-based label-free proteomic quantification (LFQ)

The brains of these two pairs, namely Negative Control 1 versus OSLP-treated hypoxia (Pair 1, NC1 vs. O+H) and Negative Control 2 versus OSLP-treated hypoxia + PTZ (Pair 2, NC2 vs. O+H+P) were subjected to tissue lysis to extract the proteins for mass spectrometry-based LFQ. All experiments were performed as four independent biological replicates.

2.7.1. Protein extraction from zebrafish brain

Ice-cold lysis buffer (1 mL, RIPA, protease inhibitor 20% v/v, phosphatase inhibitor 1% v/v) was used to lyse the zebrafish brain inside a sterile ProtLoBind microtube before incubating on an orbital shaker (4°C; 90 min). Next, the contents of the microtube were homogenised using an ultrasonic cell crusher and briefly centrifuged (18000 x g, 4°C; 10 min) to harvest the supernatant produced and collect it into a new sterile ProtLoBind microtube. Using the Quick Start™ Bradford Protein Assay as instructed by the manufacturer, protein concentration was estimated. Subsequently, the brain lysates were concentrated using a speed-vacuum concentrator (300 rpm; 24 h; 60°C).

2.7.2. In-solution digestion of proteins

In-solution protein digestion was carried out as instructed by the manufacturer (Agilent Technologies, USA). In brief, the protein samples were re-suspended, denatured and reduced in 25 µL of TFE, 25 µL of ABC and 1 µL of DTT before being vortex-mixed (2500 rpm, 3 m) and oven heated (60°C, 60 min). The samples were then alkylated in 4 µL of IAA and then incubated in darkness (60 min, r.t.). Next, excessive IAA was quenched with 1 µL of DTT (60 min, r.t., in darkness). 100 µL of ABC and 300 µL of MQUP water were then added to dilute and to adjust the final pH of the protein solutions to between pH 7 and pH 9. 1 µL of trypsin was then added before incubating in an oven (37°C, 18 h, in darkness). After the incubation, 1 µL of FA was added to cease the tryptic digestion. Lastly, every sample was vacuum-concentrated using a speed-vacuum concentrator (300 rpm; 24 h; 60°C,). The dry pellets were then kept at -20°C.

2.7.3. De-salting of protein samples

Each biological replicate was independently de-salted using a Pierce®C18 mini spin column as according to the manufacturer's instructions (Thermo Scientific Pierce, USA) though with several modifications. Each mini spin column was firstly activated in 50% of ACN (three-time repetition, r.t.) and equilibrated using 0.5% of TFA in 5% ACN (three-time repetition, r.t.). Separately, 90 µL of crude protein sample was individually added into 30 µL of sample buffer (2% of TFA in 20% ACN) and mixed well by briefly vortexing at 2,200 rpm. Each of the protein samples were then individually loaded onto a mini spin column for de-salting (three-time repetition, r.t.). Subsequently, all protein samples were washed using 0.5% of TFA in 5% ACN (three-time repetition, r.t.). Lastly, all the protein

samples were eluted using 70% ACN (repeated 3 times, r.t.) and all the produced flow-through was collected, vacuum-concentrated (300 rpm; 24 h; 60°C) and stored at -20°C before mass spectrometry-based LFQ.

2.7.4. Mass spectrometry-based label-free proteomic quantification (LFQ) using Nanospray-ESI-LCMS/MS

An Agilent C-18 300Å Large Capacity Chip was used to load the de-salted peptides. The column was equilibrated using 0.1% of FA in MQUP water (Buffer A) and the peptides were eluted with an increasing gradient of 90% ACN in 0.1% of FA (Buffer B) by the following gradients: 3-50% Buffer B from 0-30 min, 50-95% Buffer B from 30-32 min, 95% Buffer B from 32-39 min and 95-3% Buffer B from 39-47 min. Q-TOF was set as follow: positive polarity, capillary voltage at 2050 V, fragmentor voltage at 300 V, nitrogen gas temperature of 300°C and drying gas flow at 5 L/min. The intact protein was analysed in auto MS/MS mode from a range of 110-3000 m/z for MS scan and 50-3000 m/z range for MS/MS scan. The spectrum was analysed using the Agilent MassHunter data acquisition software.

2.7.5. Brain protein and peptide identification by automated *de novo* sequencing and LFQ analysis

Automated *de novo* sequencing using the PEAKS®Studio software (Version 8.0) was performed for protein identification. Protein identification and homology search was done by comparing the *de novo* sequence tag using the UniProtKB (Organism: *Danio rerio*) database (http://www.uniprot.org/proteomes/UP000000437, 46,847 proteins, accessed on 16/04/2020). The settings applied were: trypsin cleavage, carbamidomethylation was set as fixed modification with maximum missed cleavage was set at 3, the maximum variable post-translational modification was set at 3, the minimum ratio count set to 2, mass error tolerance set as 20.0 ppm with both parent mass and precursor mass tolerance were set at 0.1 Da. The other parameters were set as default by Agilent. To filter out the inaccurate proteins, a false discovery rate (FDR) threshold of 1% and a protein score of -10lgP > 20 were applied. PEAKS® indicated that a -10lgP score of greater than 20 is of relatively high in confidence as very few decoy matches above the threshold are targeted.

For LFQ analysis, the differentially expressed proteins between the two pairs, NC1 versus O+H (Pair 1) and NC2 versus O+H+P (Pair 2) were identified using the following filters: number of unique peptide ≥ 1, protein fold change ≥ 1, significance score ≥ 13, and FDR threshold ≤ 1% PEAKSQ indicated that a significance score of greater than 13 is equivalent p-value < 0.05. The other parameters were set as default by Agilent.

2.8. Bioinformatics analysis

Bioinformatics analysis (protein-protein interactions, functional annotations, and systemic pathway enrichment analysis) of the differentially of the expressed proteins was matched to databases obtained from ZFIN (www.zfin.org), the GO Consortium and the KEGG PATHWAY database (*Danio rerio*) [29]. KAAS allows functional annotation of genes by GHOST or BLAST comparisons against a manually curated KEGG GENES database. The result contains automatically generated KEGG pathways and KO (KEGG Orthology) assignments (bi-directional best hit). Organism-specific pathways are mapped by KEGG pathways: GENES entries are hyperlinked by green boxes by converting K numbers (KO identifiers) to gene identifiers in the reference pathway, indicating the completeness of the pathway and also the presence of genes in the genome [30].

2.9. Statistical Analysis

For behavioural study and the estimation of neurotransmitter levels, statistical analysis was performed using GraphPad Prism version 8.0. All data were expressed as mean ± standard error of the mean (SEM). One-way analysis of variance (ANOVA) followed with Tukey's post-hoc test at significance levels of $*p < 0.05$, $**p < 0.01$ and $***p < 0.001$ against the negative control 1 (NC1, hypoxia-induced alone) whereas $^{\#}p < 0.05$, $^{\#\#}p < 0.01$ and $^{\#\#\#}p < 0.001$ against the negative control 2

(NC 2, Hypoxia + PTZ-induced). For the analysis of differentially expressed proteins identified by ms-based LFQ, PEAKSQ statistical analysis (built-in statistical tool of PEAKS® software) was used. An FDR ≤ 1% and a significance score of 13% (equivalent to the significance level of 0.05) was considered as statistically significant. In the bioinformatics analysis, the hypergeometric test followed by the Benjamini & Hochberg FDR correction at p-value < 0.05 (BiNGO built-in statistical tool) was used to correlate the associations between the functional annotation of genes and interacting proteins; the built-in statistical tool of KAAS was used to assess the possible association of interacting proteins and systemic pathways using the KEGG PATHWAY Database.

3. Results

3.1. OSLP safety study in adult zebrafish

OSLP safety study conducted previously [19] found that the maximal safe starting dose of OSLP achievable via intraperitoneal (i.p.) route was 800 μg/kg of body weight. Therefore, 800 μg of OSLP was chosen in this study as the treatment dose.

3.2. Evaluation of the anticonvulsive potential of OSLP in hypoxic animals

3.2.1. Behavioural study

3.2.2. Swim path analysis

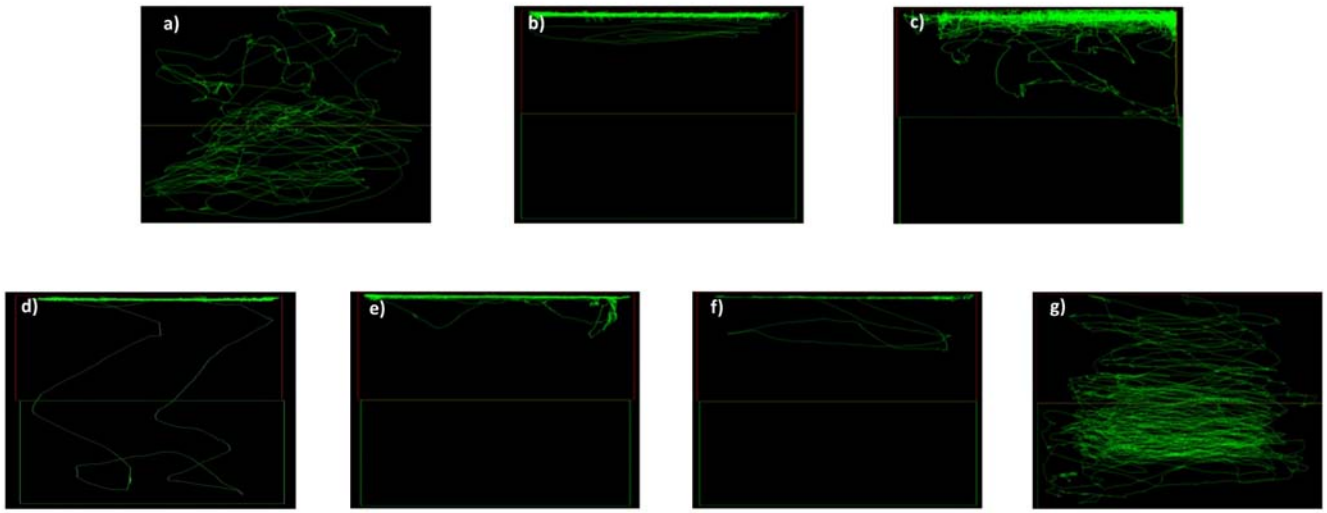

Figure 3. Representative swimming patterns for the corresponding 7 experimental groups (n = 10). VC (a, tank water, i.p.), NC 1 (b, hypoxia-induced alone), NC 2 (c, Hypoxia + PTZ 170 mg/kg, i.p.), O+H (d, OSLP 800 μg/kg + hypoxia, i.p.), O+H+P (e, OSLP 800 μg/kg + hypoxia + PTZ 170 mg/kg, i.p.) , PC (f, DZP 1.25 mg/kg + PTZ 170 mg/kg, i.p.) and TC (g, OSLP 800 μg/kg + tank water, i.p.).

The automated tracking software analysed the zebrafish swimming patterns, and one representative swimming pattern was selected for each group from among the n = 10 zebrafish per group (Figure 3). The VC group (Panel a) swam throughout the entire tank without showing a clear preference for any part of the tank. In contrast, the NC 1 (Panel b) group did not swim throughout the whole tank but showed an evident preference for the upper half of the tank, particularly close to the water surface, whilst the NC 2 group showed apparent twitching and a more erratic swimming pattern, with the zebrafish dwelling at the upper half of the tank more frequently (Panel c). The O+H group also did not manage to swim throughout the entire tank when compared to the untreated VC and showed a similar swimming pattern to that of the NC 1, with an apparent preference for the upper half of the tank (Panel d). The O+H+P group (Panel e) managed to swim through the whole tank with reduced twitching and a less erratic swimming pattern compared to the NC 2. The PC group did not produce a swimming pattern comparable to that of the untreated VC but still showed an evident preference for the upper half of the tank (Panel f). The TC group (Panel g) showed a swimming pattern comparable to that of the untreated VC.

3.2.3. Seizure score and seizure onset time

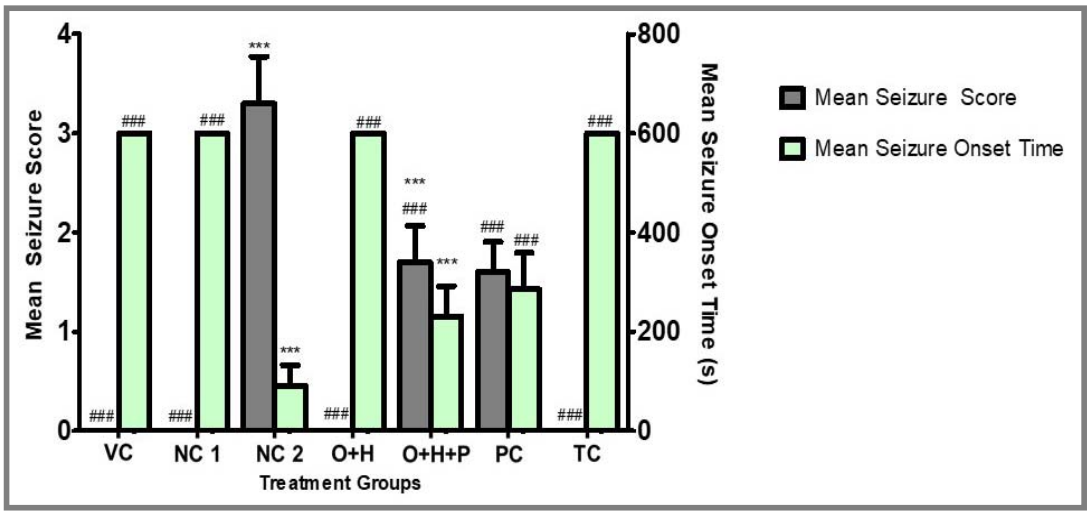

Figure 4. Mean seizure scores and mean seizure onset time (s) for the corresponding 7 experimental groups. Data are mean ± SEM. Experiments were repeated in n = 10, ***showed $p < 0.001$ against the NC1 (Hypoxia-induced alone) whereas ### $p < 0.001$ against the NC2 (Hypoxia + PTZ-induced). One-way ANOVA with Tukey's *post-hoc* test was used. VC (tank water, i.p.), O+H (OSLP 800 μg/kg + hypoxia, i.p.), O+H+P (OSLP 800 μg/kg + hypoxia + PTZ 170 mg/kg, i.p.) , PC (DZP 1.25 mg/kg + PTZ 170 mg/kg, i.p.) and TC (OSLP 800 μg/kg + tank water, i.p.).

The cutoff time for seizure scoring was 600 seconds (s) as fish recover from seizures after around 600 seconds and thus, any seizures beyond that time point was not considered. Mean seizure onset time for both the untreated vehicle control (VC group) and OSLP treatment dose control (TC group) was set as 600 s and a maximum seizure score of zero (0) was assigned to these groups (Figure 4). They did not receive any PTZ injection and thus did not show seizures, serving only as the study controls. The NC 1 also did not receive any PTZ injection but was observed for the development of seizures. These groups received PTZ injections: NC 2, O+H+P and PC. PTZ injection into the zebrafish resulted in different seizure scores and onset times, particularly in the face of hypoxia.

The NC 2 group, induced by hypoxia and injected with PTZ, had a significant increase in seizure score to 3.3 ($F = 26.17$, $^{###}p < 0.001$) and had a significantly reduced seizure onset time to the lowest, 91 s ($F = 31.52$, $^{###}p < 0.001$), when compared to the VC group. Treatment with 800 μg/kg of OSLP (O+H+P) significantly decreased the seizure score to 1.7 ($F = 26.17$, $^{###}p < 0.001$) and significantly delayed the

seizure onset time to 231 s (F = 31.52, $^{###}p < 0.001$) compared to the NC 2 group. The PC group treated with DZP also showed a significant decrease in seizure score to 1.6 (F =26.17, $^{###}p < 0.001$) and had a significantly delayed seizure onset time to 286 s, (F = 31.52, $^{###}p < 0.001$), when compared to the NC 2 group.

In this study, hypoxia induction (15 -18 min per fish) sufficiently induced hypoxic insults. However, the hypoxic adult zebrafish (NC 1) did not exhibit any significant seizure behaviour and thus, the seizure score and seizure onset time remained unchanged. OSLP treatment (800 μg/kg of b.w.) did not show significant protection in the hypoxic adult zebrafish (O+H). On the other hand, PTZ (170 mg/kg of b.w.) sufficiently induced seizures in the adult zebrafish under a hypoxic condition (NC 2). OSLP treatment (800 μg/kg of b.w.) was shown to significantly alleviate seizures in hypoxic adult zebrafish (O+H+P), with seizure score and seizure onset time comparable to the PC group.

3.2.4. Locomotion parameters

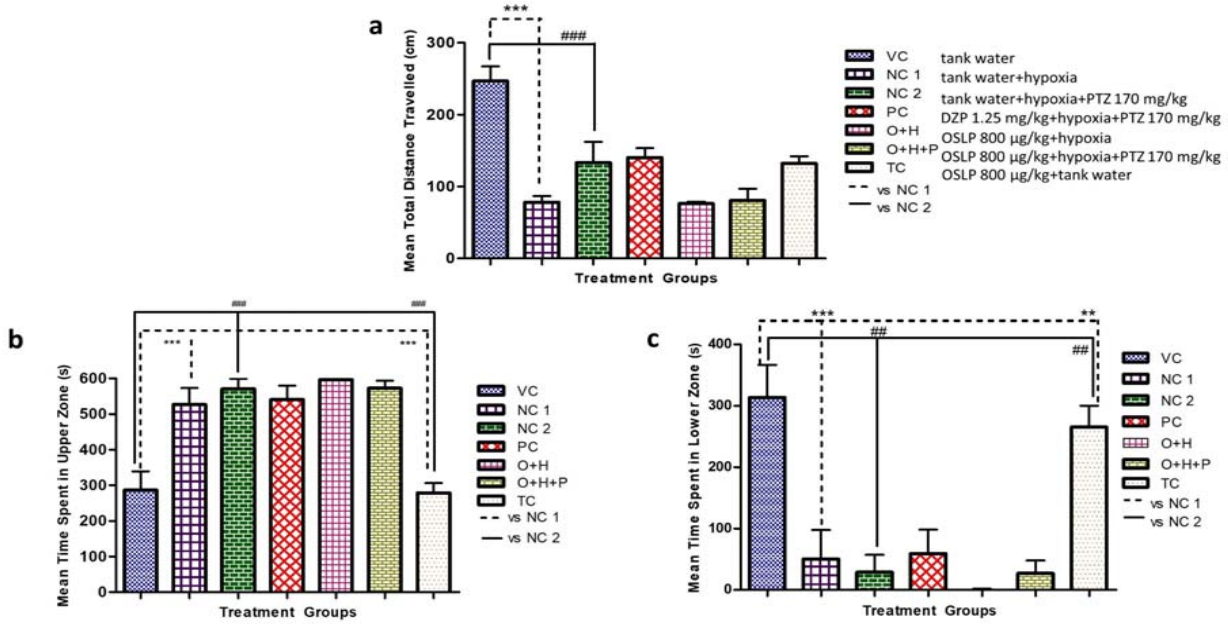

Figure 5. Mean locomotion parameters over 600 s for all the experimental groups. Figure a represents the mean total distance travelled (cm), Figure b shows the mean time spent in upper zone (s) and Figure c displays the mean time spent in lower zone (s). Data are mean ± SEM. Experiments were repeated in n = 10, ***showed $p < 0.001$ against the NC 1(Hypoxia-induced alone) whereas ### $p < 0.001$ against the NC 2 (Hypoxia + PTZ-induced). One-way ANOVA with Tukey's *post-hoc* test was used. VC (tank water, i.p.), O+H (OSLP 800 µg/kg + hypoxia, i.p.), O+H+P (OSLP 800 µg/kg + hypoxia + PTZ 170 mg/kg, i.p.) , PC (DZP 1.25 mg/kg + PTZ 170 mg/kg, i.p.) and TC (OSLP 800 µg/kg + tank water, i.p.).

Both negative control groups, NC 1 (78±8 cm, F = 17.99, $^{***}p < 0.001$) and NC 2 (133±29 cm, F = 17.99, $^{###}p < 0.001$) showed a significant reduction in the mean total distance travelled when compared to the VC group (247±20 cm) (Figure 5a). When compared between the two negative controls, the NC 2 group had travelled about a 41% longer mean total distance than the NC 1 group. This outcome, however, did not attain statistical significance ($p > 0.05$). Whereas, mean total distance travelled of the O+H group was 76±2 cm and was insignificantly lower than the NC 1 group. Mean total distance travelled of the O+H+P group was 81±16 cm and was insignificantly lower than the NC 2 group. The PC group, treated with DZP, had a mean total distance travelled of 141±13 cm when compared to the NC 2 group.

For the parameter of time spent in each half of the tank, both negative control groups, NC 1(F = 15.50, $^{***}p < 0.001$) and NC 2 (F = 15.50, $^{###}p < 0.001$) showed increased time spent in the upper half of tank when compared to the VC (287±53 s) and TC (279±28 s) (Figure 5b). Both VC (314±53 s) and TC (265±35 s) had showed a significantly longer time spent in the bottom half of tank than both NC 1 (F = 12.17, $^{***}p < 0.001$) and NC 2 (F = 12.17, $^{###}p < 0.001$) (Figure 5c). When compared between the two negative controls, NC 2 had spent about 8% longer time in the upper half of tank but spent a shorter time in the lower half of tank (about 57 %) than NC 1. This outcome however did not attain statistical significance ($p > 0.05$). Both OSLP-treated groups, O+H and O+H+P, did not show a trend of overcoming the adverse effects when compared to both NC groups ($p > 0.05$) for the parameter of time spent in each half of the tank. The PC group was seemed to reduce the time spent in the upper half of tank and correspondingly increase time spent in the bottom half of tank. This outcome however did not attain statistical significance ($p > 0.05$). Worthy of mention is that the TC group had displayed a similar trend to the VC group in the parameter of time spent in each half of the tank (Figures 5b and 5c).

3.2.4. Neurotransmitter study

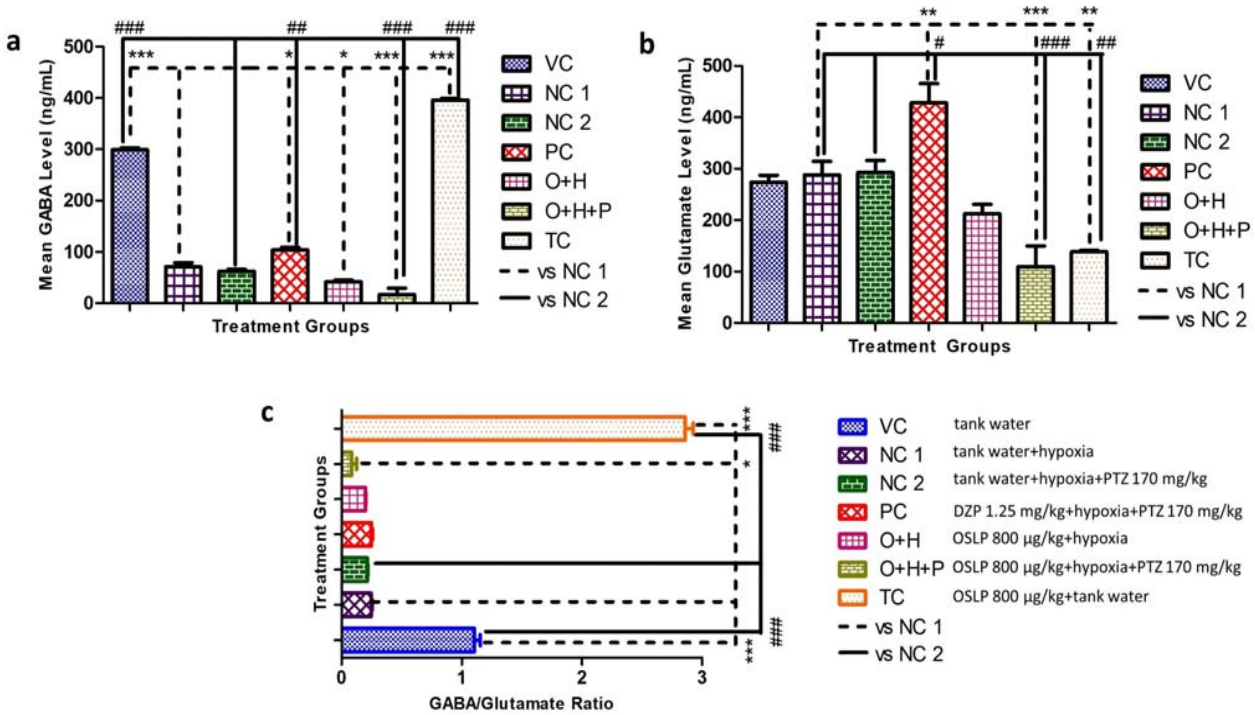

Figure 6. Mean neurotransmitter levels (ng/mL), namely GABA (a), glutamate (b) and GABA/Glu ratio (c) over 600 s for all the experimental groups. Data are mean ± SEM. Experiments were repeated in n = 10, ***showed $p < 0.001$ against the NC 1 (Hypoxia-induced alone) whereas ### $p < 0.001$ against the NC 2 (Hypoxia + PTZ-induced). One-way ANOVA with Tukey's *post-hoc* test was used. VC (tank water, i.p.), O+H (OSLP 800 µg/kg + hypoxia, i.p.), O+H+P (OSLP 800 µg/kg + hypoxia + PTZ 170 mg/kg, i.p.) , PC (DZP 1.25 mg/kg + PTZ 170 mg/kg, i.p.) and TC (OSLP 800 µg/kg + tank water, i.p.).

Neurotransmitters, namely GABA and Glu, and their ratio (GABA/Glu) were evaluated. Both negative control groups, NC 1 (71±8 ng/mL, F = 486.7, $^{***}p < 0.001$) and NC 2 (62±4 ng/mL, F = 486.7, $^{###}p < 0.001$) showed a significant decrease in the mean GABA levels when compared to the VC group (299±4 ng/mL) (Figure 6a). Mean GABA levels of the O+H group was 42±3 ng/mL (F = 486.7, $^{*}p < 0.05$) and was about 41% lower when compared to NC 1. Mean GABA levels of the O+H+P group was 17±13 ng/mL which was about 76% lower than the NC 1 group (F = 486.7, $^{***}p < 0.001$) and was about 73% lower than the NC 2 group (F = 486.7, $^{###}p < 0.001$). The PC group had a significant increase in the mean GABA levels to 104±5 ng/mL when compared to both NC 1 (71±8 ng/mL, F = 486.7, $^{*}p < 0.05$) and NC 2 (62±4 ng/mL, F = 486.7, $^{##}p < 0.01$).

In contrast, both NC 1 (288±27 ng/mL, F = 16.98, $p > 0.05$) and NC 2 and (293±23 ng/mL, F = 16.98, $p > 0.05$) showed slightly higher mean Glu levels than the VC (273±14 ng/mL) whereas, mean Glu levels of the O+H group was 212±18 ng/mL which was about 26 % lower than the NC 1 group (Figure 6b). Mean Glu levels of the O+H+P group was 110±39 ng/mL, which was about 62 % significantly lower than both NC 1 (F = 16.98, $^{***}p < 0.001$) and NC 2 (F = 16.98, $^{###}p < 0.001$). Surprisingly, the PC group treated with DZP saw a spike in the mean Glu levels (428±37 ng/mL) when compared to NC 1 (F = 16.98, $^{**}p < 0.01$) and NC 2 (F = 16.98, $^{#}p < 0.05$). The TC group displayed a similar trend to the VC group in the neurotransmitter analysis (Figure 6b).

The GABA/Glu ratio showed a significant decrease in both negative control groups, NC 1 (R < 1, F = 813.6, $^{***}p < 0.001$) and NC 2 (R < 1, F = 813.6, $^{###}p < 0.001$) when compared to the VC group (R > 1) (Figure 6c). Meanwhile, the O+H+P group had a lower GABA/Glu ratio (R < 1, F = 813.6, $^{*}p < 0.5$) when compared to the NC 1 group but had no significant difference when compared to the NC 2 group. The O+H group did not display a significant difference in the GABA/Glu ratio when compared to both negative control groups. Neither the PC group show a significant difference in the GABA/Glu ratio when compared to both negative control groups (Figure 6c). Interestingly, the TC group had a significant difference in the GABA/Glu ratio when compared to the NC 1 (R > 2, F = 813.6, $^{***}p < 0.001$) and NC 2 (R > 2, F = 813.6, $^{###}p < 0.001$) (Figure 6c).

3.3. Protein expression study

3.3.1. Proteins expression profiling using mass spectrometry-based label-free proteomic quantification (LFQ)

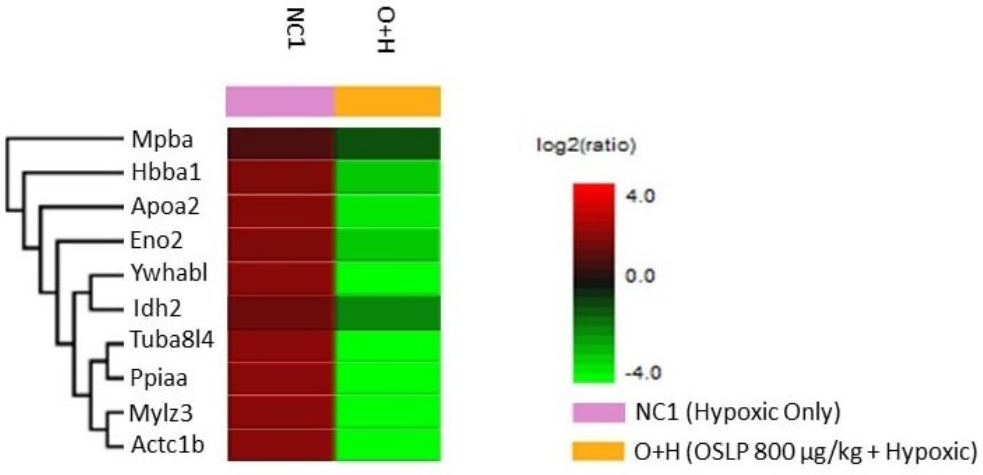

Figure 7. Heat map shows the differentially expressed proteins identified from NC 1 (hypoxic only) and O+H (OSLP 800 µg/kg + hypoxic), n = 4, significance ≥ 13, FDR ≤ 1%, fold change ≥ 1, unique peptide ≥ 1. Protein names are listed on the left while experimental groups are indicated on top. The colour key on the bottom right indicates the log2 (ratio) expression levels (green = low and red = high).

In the LFQ analysis, the −10lgP value (significance level) signifies that the higher the score, more confident the detection of the protein is. The peptide value (#peptides) denotes the number of peptides belonging to a particular identified protein and the unique value (#unique) signifies its resemblance with the identified protein. The coverage (%) means that out of the identified peptides, only a particular % belongs to the identified protein as mentioned in the protein description (Tables 4 and 5).

LFQ profiled 10 differentially expressed proteins from the hypoxia-induced group (NC 1) versus the OSLP-treated hypoxia group (O+H). These proteins were found to be expressed at higher levels in the NC1 group than in the O+H group (Figure 7 & Table 4). Interestingly, haemoglobin subunit beta-1 (Hbba1, Q90486), eno 2 protein (Eno2, Q6GQM9), apolipoprotein A-II (Apoa2, B3DFP9), isocitrate dehydrogenase [NADP] (Idh2, Q7ZUP6) and myelin basic protein a (Mbpa, F8W3W8) were expressed slightly higher compared to the other proteins.

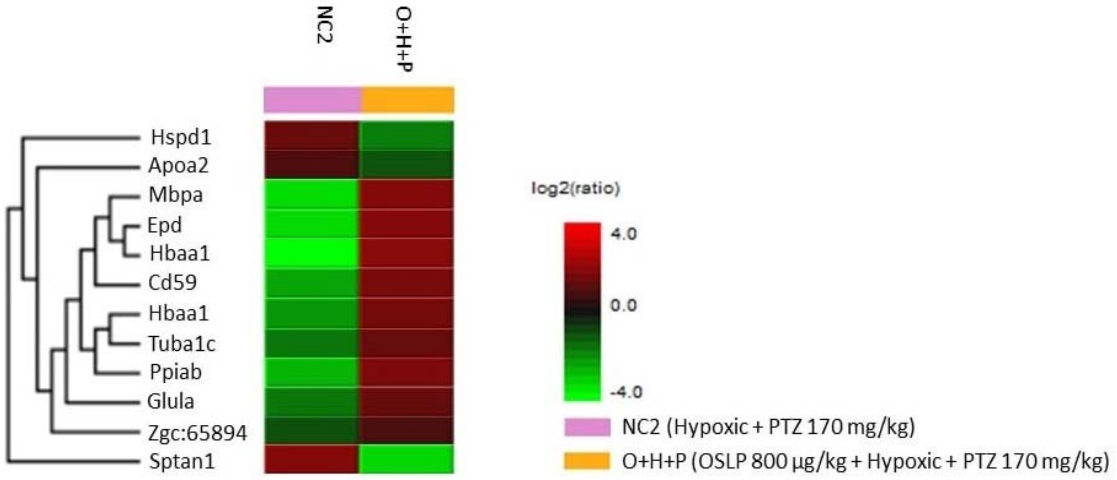

Figure 8. Heat map shows the differentially expressed proteins identified from NC 2 (hypoxic + PTZ 170 mg/kg) and O+H+P (OSLP 800 µg/kg + hypoxic + PTZ 170 mg/kg), n = 4, significance ≥ 13, FDR ≤ 1%, fold change ≥ 1, unique peptide ≥ 1. Protein names are listed on the left while experimental groups are indicated on top. The colour key on the bottom right indicates the log2 (ratio) expression levels (green = low and red = high).

LFQ profiled 12 differentially expressed proteins from the hypoxia- and PTZ-induced (NC 2, hypoxic + PTZ 170 mg/kg) versus O+H+P (OSLP 800 µg/kg + hypoxic + PTZ 170 mg/kg) groups (Figure 8 & Table 5). Among them, nine proteins were expressed at lower levels in the NC2 group than in the O+P+H group. They were novel alpha-globin (Hbaa1, isoforms Q7SZV9 and Q90487), myelin basic protein a (Mbpa, F8W3W8), ependymin (Epd, A0A2R8Q2Z0), peptidyl-prolyl cis-trans isomerase (Ppiab, Q6PC53), CD59 molecule (Cd59, A0A0B5JW41), tubulin alpha chain (Tuba1c, isoforms A0A2R8RZK5 and Q6PE34) and glutamine synthetase (Glula, Q7T2P7). The other three proteins namely haemoglobin subunit alpha (Hbaa1, isoforms Q803Z5 and Q90487), spectrin alpha non-erythrocytic 1 (Sptan1, F1R446), apolipoprotein A-II (Apoa2, B3DFP9) and heat shock 60 protein 1 (Hspd1, Q803B0) were found to be expressed at higher levels in the NC 2 group than in the O+P+H group.

484 **Table 4.** Differentially expressed proteins identified from negative control 1 (NC 1, Hypoxic Only) and O+H (OSLP 800 μg/kg + Hypoxic).

Uniprot Accession ID	Uniprot Protein Name	Significance (≥ 13)	Coverage (%)	#Peptides	#Unique	Avg. Mass	Group Profile (ratio of NC1/O+H)	ZFIN Protein
B8JKH7	Myosin light polypeptide 3 skeletal muscle	200	9	1	1	13758	1.00:0.00	Mylz3
Q90486	Haemoglobin, beta adult 1	200	28	3	3	16389	1.00:0.10	Hbba1
Q9I8V1	Actin alpha cardiac muscle 1b	200	12	1	1	41973	1.00:0.00	Actc1b
Q6NWJ5	Tubulin alpha chain	200	8	2	2	50034	1.00:0.00	Tuba8l4
B3DFP9	Apolipoprotein A-II	200	21	2	2	15537	1.00:0.05	Apoa2
Q6P5J4	Peptidyl-prolyl cis-trans isomerase	200	8	1	1	19472	1.00:0.00	Ppiaa
Q6GQM9	Eno2 protein	200	4	1	1	46841	1.00:0.10	Eno2
Q6P102	Tyrosine 3-monooxygenase/tryptophan 5-monooxygenase activation protein beta polypeptide-like	200	6	1	1	27907	1.00:0.00	Ywhabl
Q7ZUP6	Isocitrate dehydrogenase [NADP]	136.71	3	1	1	50397	2.89:1.00	Idh2
F8W3W8	Myelin basic protein a	19.1	13	1	1	10776	1.00:0.71	Mbpa

485 Remark: ZFIN protein nomenclatures were searched in the ZFIN Database Information (*www.zfin.org)* accessed from 16/04/2020.

486

487 **Table 5.** Differentially expressed proteins identified from negative control 2 (NC 2, Hypoxic + PTZ 170 mg/kg) and O+H+P (OSLP 800 μg/kg + Hypoxic + PTZ 170
488 mg/kg).

Uniprot Accession ID	Uniprot Protein Name	Significance (≥ 13)	Coverage (%)	#Peptides	#Unique	Avg. Mass	Group Profile (ratio of NC2/O+H+P)	ZFIN Protein
Q7SZV9	Novel alpha-globin	200	41	6	3	15524	0.00:1.00	Hbaa1
F8W3W8	Myelin basic protein a	200	65	12	12	10776	1.00:14.30	Mbpa
Q90487	Haemoglobin subunit alpha	200	41	6	3	15522	1.00:3.77	Hbaa1
A0A2R8Q2Z0	Ependymin	200	25	3	3	23370	1.00:13.66	Epd
Q6PC53	Peptidyl-prolyl cis-trans isomerase	200	26	3	3	17489	1.00:6.38	Ppiab
A0A0B5JW41	CD59 molecule (CD59 blood group)	200	34	2	2	10145	1.00:4.82	Cd59
A0A2R8RZK5	Tubulin alpha chain	87.27	23	7	4	48534	1.00:2.30	Tuba1c
Q7T2P7	Glutamine synthetase	83.70	14	3	3	41613	1.00:2.26	Glula
F1R446	Spectrin alpha non-erythrocytic	20.61	1	1	1	284928	1.00:0.08	Sptan1
B3DFP9	Apolipoprotein A-II	20.32	39	3	3	15537	1.00:0.68	Apoa2
Q6PE34	Tubulin beta chain	18.59	41	13	3	49635	1.00:1.41	Zgc:65894
Q803B0	Heat shock 60 protein 1	15.74	4	1	1	61196	1.00:0.40	Hspd1

489 Remark: ZFIN protein nomenclatures were searched in the ZFIN Database Information (www.zfin.org) accessed from 16/04/2020.

490 3.3.1. Bioinformatics analysis

491 The differentially expressed proteins (Table 4 and Table 5) were searched using the ZFIN
492 Database Information to match the ID of the gene. The InterPro Classification of Protein Families
493 database was searched for the respective protein class. The results are presented in Table 6 and Table 7.
494 The differentially expressed proteins were also examined using functional annotation analysis.
495 For Pair 1 (NC1 vs. O+H), they were found to localise at seven different cellular components
496 encompassing intracellular non-membrane-bounded organelle (GO:43232), non-membrane-bounded
497 organelle (GO:43228), protein complex (GO:43234), phosphopyruvate hydratase complex (GO:15),
498 cytosolic part (GO:44445), cytosol (GO:5829) and cytoskeleton (GO:5856) (Figure 9). At these cellular
499 localisations, the interactions of the differentially expressed proteins have significantly been associated
500 with four corresponding molecular functions. Three were involved in the catalytic activities of
501 isocitrate dehydrogenase (NADP+) (GO:4450), isocitrate dehydrogenase (GO:4448) and
502 phosphopyruvate hydratase (GO:4634) whilst one was involved in magnesium ion binding (GO:287).
503 Among them, the enzymatic activity of phosphopyruvate hydratase was particularly interesting (pink
504 box; Figure 10).
505 For Pair 2 (NC2 vs. O+H+P), the differentially expressed proteins were found to localise at four
506 cellular components mainly at mitochondrial lumen (GO: 31980), mitochondrial matrix (GO:5759),
507 haemoglobin complex (GO:5833) and cytoskeleton (GO:5856) (Figure 11). Found localised at these
508 cellular components, their interactions have significantly been associated with eight corresponding
509 molecular functions. Three were involved in the catalytic activities of glutamate-ammonia ligase
510 (GO:4356), ammonia ligase (GO:16211) and acid-ammonia (or amide) ligase (GO:16880). Four were
511 involved in the bindings of ribonucleotide (GO:32553), purine ribonucleotide (GO:32555), purine
512 nucleotide (GO:17076) and oxygen (GO:19825) whilst the last molecular function was seen in oxygen
513 transporter activity (GO:5344). Among them, the enzymatic activity of glutamate-ammonia ligase was
514 particularly noteworthy (purple box; Figure 12).

515 **Table 6.** Protein family of the differentially expressed proteins identified from negative control 1 (NC 1, Hypoxic Only) and O+H (OSLP 800 μg/kg + Hypoxic).

Protein Family	ZFIN Protein	ZFIN Gene ID
Globin domain-containing protein		
Member of the haemoglobin, beta-type	Hbba1	ZDB-GENE-990415-18
Plasma protein		
Member of the CD marker	Cd59	ZDB-GENE-030131-7871
Member of the apolipoprotein A/E	Apoa2	ZDB-GENE-030131-1046
Belongs to the myelin basic protein	Mbpa	ZDB-GENE-030128-2
Cytoskeletal protein		
Belongs to the actin family	Actc1b	ZDB-GENE-000322-1
Belongs to the tubulin family; subfamily of the alpha tubulin	Tuba8l4	ZDB-GENE-040426-860
14-3-3 protein		
Belongs to the 14-3-3 family	Ywhabl	ZDB-GENE-030131-448
Enzyme protein		
Isomerase		
Member of the cyclophilin-type peptidyl-prolyl cis-trans isomerase	Ppiaa	ZDB-GENE-030131-7459
Isocitrate dehydrogenase		
Member of the isocitrate dehydrogenase NADP-dependent	Idh2	ZDB-GENE-031118-95
Citric acid cycle related protein		
Member of the enolase	Eno2	ZDB-GENE-040704-27
Motor protein		
Belongs to the family of myosin	Mylz3	ZDB-GENE-000322-6

516 Remark: Protein Families and their respective functions were searched in the InterPro Classification of Protein Families, ZFIN Database Information and KEGG Brite
517 databases (*https://www.ebi.ac.uk/interpro/protein/UniProt/*, *www.zfin.org* and *https://www.genome.jp/kegg/brite.html* accessed from 16/04/2020).

518

519 **Table 7.** Protein family of the differentially expressed proteins identified from negative control 2 (NC 2, Hypoxic + PTZ 170 mg/kg) and O+H+P (OSLP 800 μg/kg +
520 Hypoxic + PTZ 170 mg/kg).

Protein Family	ZFIN Protein	ZFIN Gene ID
Globin domain-containing protein		
Belongs to the family of haemoglobin, alpha-type and to the subfamily of haemoglobin, pi	Hbba1	ZDB-GENE-980526-79
Plasma protein		
Member of the CD marker	Cd59	ZDB-GENE-030131-7871
Member of the apolipoprotein A/E	Apoa2	ZDB-GENE-030131-1046
Belongs to the myelin basic protein	Mbpa	ZDB-GENE-030128-2
Cytoskeletal protein		
Belongs to the tubulin family; subfamily of the alpha tubulin	Tuba1c	ZDB-GENE-061114-1
Belongs to the tubulin family; subfamily of the beta tubulin	Zgc:65894	ZDB-GENE-030131-7741
A filamentous cytoskeletal protein	Sptan1	ZDB-GENE-051113-60
Enzyme protein		
Isomerase		
Member of the cyclophilin-type peptidyl-prolyl cis-trans isomerase	Ppiab	ZDB-GENE-030131-7459
Mitochondrial enzyme		
Belongs to the glutamine synthetase family	Glula	ZDB-GENE-030131-688
Chaperonin protein - Cpn60/TCP-1 family		
Member of the chaperonin Cpn60	Hspd1	
Intracellular protein - Ependymin		
Member of the ependymin-related protein family (EPDRs)	Epd	ZDB-GENE-980526-111

521 Remark: Protein Families and their respective functions were searched in the InterPro Classification of Protein Families, ZFIN Database Information and KEGG Brite
522 databases (https://www.ebi.ac.uk/interpro/protein/UniProt/, www.zfin.org and https://www.genome.jp/kegg/brite.html accessed from 16/04/2020).

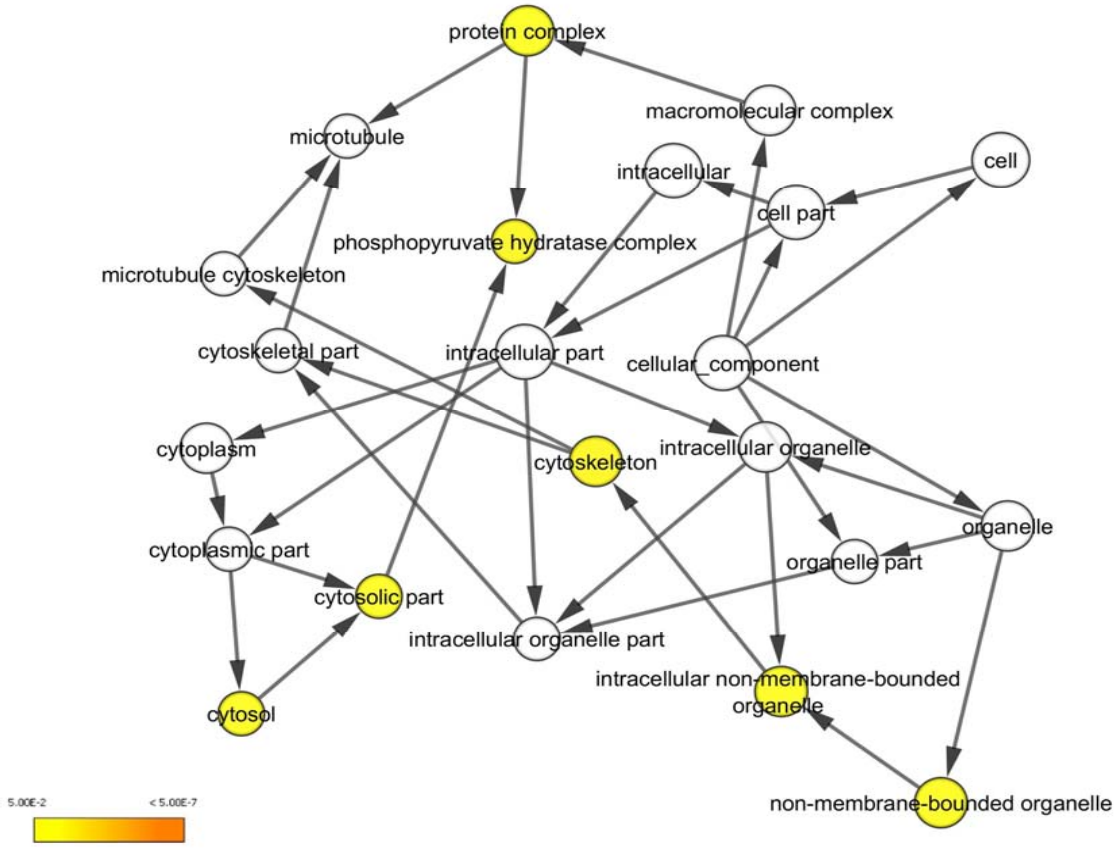

Figure 9. BiNGO result for cellular component as visualised in Cytoscape (Group: NC1 vs. O+H; Organism: *Danio rerio*). Coloured nodes are significantly overrepresented. White nodes are insignificantly overrepresented, they are included to show the coloured nodes in the context of the GO hierarchy. Colour key on the bottom left indicates the significance level of overrepresentation.

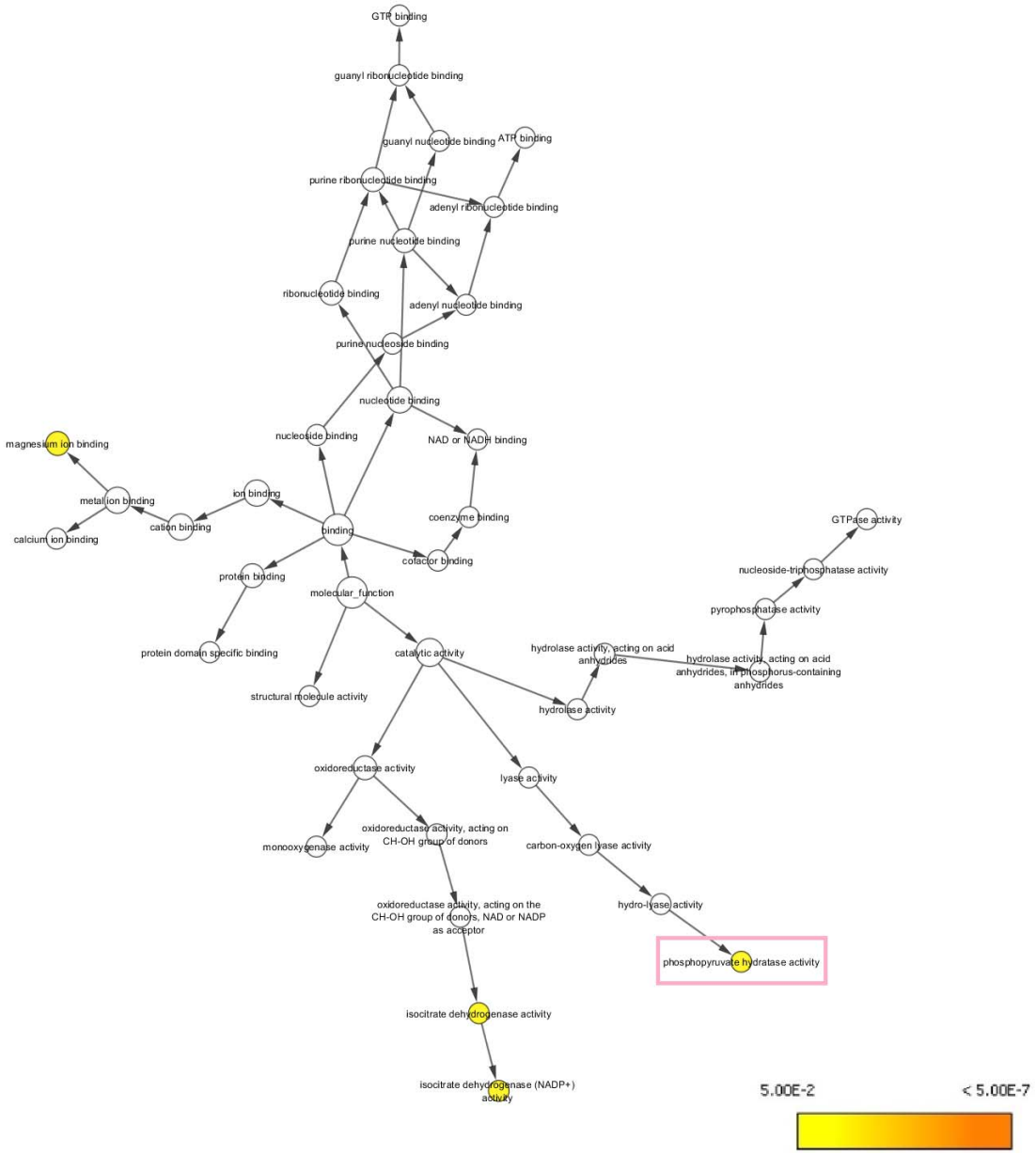

527

528 **Figure 10.** BiNGO result for molecular function as visualised in Cytoscape (Group: NC1 vs. O+H;
529 Organism: *Danio rerio*). Coloured nodes are significantly overrepresented. White nodes are
530 insignificantly overrepresented, they are included to show the coloured nodes in the context of the GO
531 hierarchy. Colour key on the bottom right indicates the significance level of overrepresentation. .

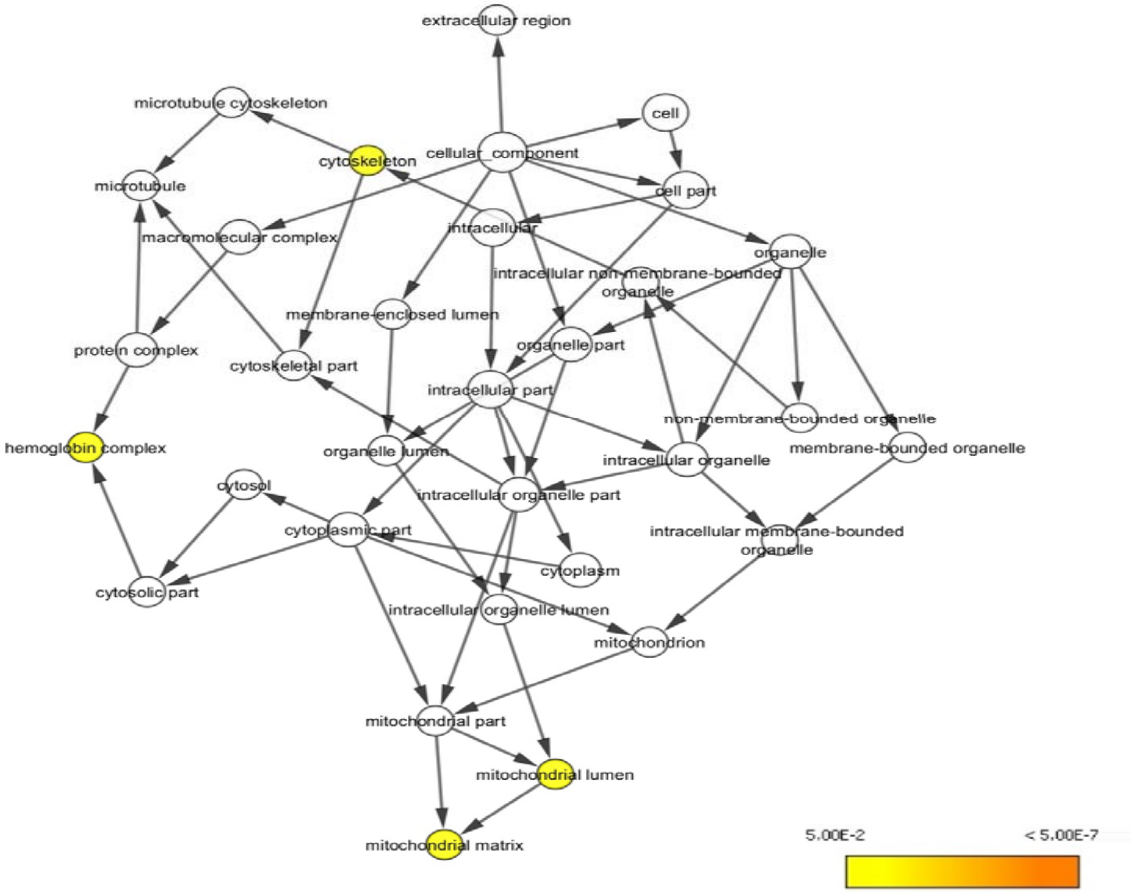

Figure 11. BiNGO result for cellular component as visualised in Cytoscape (Group: NC2 vs. O+H+P; Organism: *Danio rerio*). Coloured nodes are significantly overrepresented. White nodes are insignificantly overrepresented, they are included to show the coloured nodes in the context of the GO hierarchy. Colour key on the bottom right indicates the significance level of overrepresentation. .

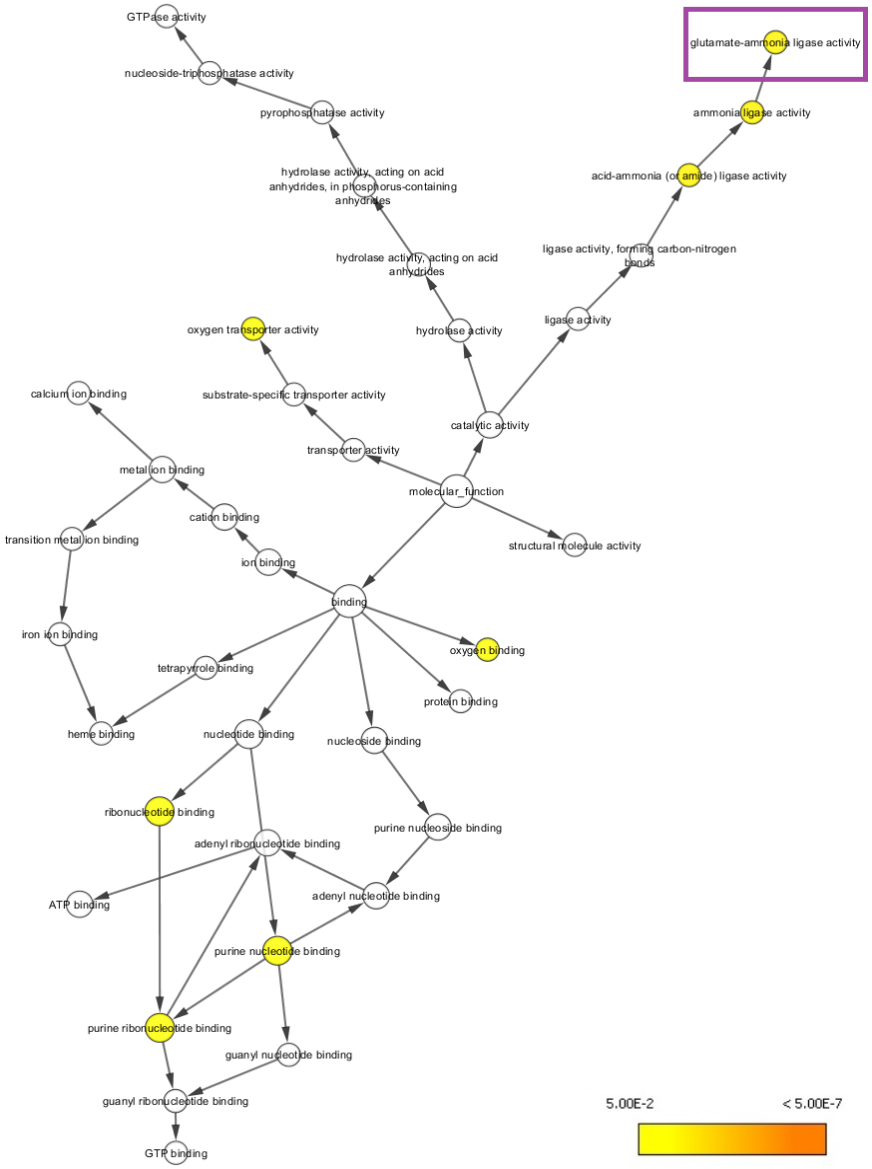

Figure 12. BiNGO result for molecular function as visualised in Cytoscape (Group: NC2 vs. O+H+P; Organism: *Danio rerio*). Coloured nodes are significantly overrepresented. White nodes are insignificantly overrepresented, they are included to show the coloured nodes in the context of the GO hierarchy. Colour key on the bottom right indicates the significance level of overrepresentation.

Systematic pathway enrichment analysis

For Pair 1 (NC1 vs. O+H), the differentially expressed proteins were found to be significantly associated with six major pathway categories; five of them were associated with metabolism, genetic information processing, environmental information processing, cellular processes and organismal systems whilst the last one was associated with human diseases (Table 8). Among them, the hypoxia-inducible factor 1 (HIF-1) signalling pathway (04066) in signal transduction nested under the environmental information processing category and the citrate cycle (TCA cycle, 00020) in carbohydrate metabolism nested under the metabolism category, were two most probable pathways (Table 8).

Enolase 2 (Eno2) was mapped onto the HIF-1 signalling pathway (as ENO 1 in green box; Figure 13). Enolase has three isoenzymes namely Eno1, Eno2 and Eno3. Eno2, also known as neuron-specific enolase (NSE) and is particularly highly expressed in neurons and neural tissues.

According to ZFIN (https://zfin.org/ZDB-GENE-040704-27), Eno2 is orthologous to human ENO2. As shown in the HIF-1 signalling pathway, Eno2 interacted with the other proteins to promote anaerobic metabolism in the mitochondria under hypoxic conditions. Also seen in this pathway was the citrate cycle. The citrate cycle was part of the metabolic cycle in the HIF-1 signalling pathway under hypoxic conditions.

The citrate cycle, also known as the tricarboxylic acid (TCA) cycle or the Krebs cycle, occurs in the mitochondrial matrix. Isocitrate dehydrogenase 2 (Idh2) was mapped onto the citrate cycle pathway (as EC 1.1.1.42 in the green box; Figure 14). Idh2 is an isoform of the isocitrate dehydrogenase enzyme family with three isoforms, Idh1 – 3. According to ZFIN (https://zfin.org/ZDB-GENE-031118-95), Idh2 is orthologous to human IDH2. As shown in the citrate cycle pathway, Idh2 catalyses reversible reactions, either decarboxylating isocitrate to 2-oxoglutarate (2OG) while reducing $NADP^+$ to NADPH or acting in the reductive carboxylation reaction to convert 2OG to isocitrate while oxidising NADPH to $NADP^+$. In particular, under hypoxic conditions, the citrate cycle was shifted to the reductive carboxylation reaction. As seen, the citrate cycle was part of the metabolic programme in the HIF-1 signalling pathway (04066).

For Pair 2 (NC2 vs. O+H+P), the differentially expressed proteins were found to be significantly associated with six major pathway categories; five of them were associated with metabolism, genetic information processing, environmental information processing, cellular processes and organismal systems whilst the last one was associated with human diseases (Table 9). Among them, glutamatergic synapse (04724) and GABAergic synapse (04727) were two pathways most likely to play a significant role in the regulation of neurotransmitters under hypoxia. They all were grouped in the subsection of the nervous system under the organismal systems category. Glutamine synthetase (Glula) was mapped onto the glutamatergic synapse and the GABAergic synapse respectively (as GLNS in the green box, 04724; as GS in the green box, 04727; Figure 15 and Figure 16).

Glutamine synthetase (EC 6.3.1.2 or GS or glutamate-ammonia ligase) is encoded by the gene *glula*. According to ZFIN (https://zfin.org/ZDB-GENE-030131-688), Glula is orthologous to human GLUL (glutamate-ammonia ligase). GS catalyses glutamate (Glu) to glutamine (Gln). As shown in the glutamatergic synapse pathway, GS directly converted Glu to Gln, which was then transported to the presynaptic terminal and released into the synaptic cleft. After being released into the synaptic cleft, Glu was removed from the synaptic cleft and transported back into glial cell where it was again converted back to Gln. Whilst, in the GABAergic synapse, GS was involved in the GABA shunt to produce and conserve the supply of GABA via the transamination of α-ketoglutarate, formed from glucose metabolism in the citrate cycle and by GABA α-oxoglutarate transaminase (GABA-T) into Glu which is then converted to Gln by GS in glial cells. Glu was transported out and deposited in the presynaptic terminal where it was catalysed by glutamate decarboxylase (aka glutamic acid decarboxylase, GAD) to form GABA.

Table 8. KEGG pathways (Organism: *Danio rerio*) associated with the differentially expressed proteins identified from negative control 1 (NC1, Hypoxic Only) and O+H (OSLP 800 μg/kg + Hypoxic).

KEGG Pathway ID	Pathway Category	Mapped Protein
	Metabolism	
01100	**Metabolic pathways**	Idh2, Eno2
01110	Biosynthesis of secondary metabolites	Idh2, Eno2
01120	Microbial metabolism in diverse environments	Idh2, Eno2
01200	Carbon metabolism	Idh2, Eno2
01210	2-Oxocarboxylic acid metabolism	Idh2
01230	Biosynthesis of amino acids	Idh2, Eno2
	Carbohydrate metabolism	
00010	Glycolysis / Gluconeogenesis	Eno2
00020	Citrate cycle (TCA cycle)	Idh2

KEGG Pathway ID	Pathway Category	Mapped Protein
	Energy metabolism	
00720	Carbon fixation pathways in prokaryotes	Idh2
00680	Methane metabolism	Eno2
	Metabolism of other amino acid	
00480	Glutathione metabolism	Idh2
	Genetic Information Processing	
	Folding, sorting and degradation	
03018	RNA degradation	Eno2
	Environmental Information Processing	
	Signal transduction	
04013	MAPK signalling pathway - fly	Ywhabl
04390	Hippo signalling pathway	Ywhabl
04391	Hippo signalling pathway - fly	Ywhabl
04066	HIF-1 signalling pathway	Eno2
04020	Calcium signalling pathway	Ppiaa
04022	cGMP-PKG signalling pathway	Ppiaa
04151	PI3K-Akt signalling pathway	Ywhabl
	Cellular Processes	
	Transport and catabolism	
04145	Phagosome	Actc1b, Tuba8l4
04146	Peroxisome	Idh2
	Cell growth and death	
04110	Cell cycle	Ywhabl
04114	Oocyte meiosis	Ywhabl
04210	Apoptosis	Tuba8l4
	Cellular community - eukaryotes	
04530	Tight junction	Tuba8l4
04540	Gap junction	Tuba8l4
	Organismal Systems	
	Circulatory system	
04260	Cardiac muscle contraction	Actc1b
04261	Adrenergic signalling in cardiomyocytes	Actc1b
	Aging	
04212	Longevity regulating pathway - worm	Ywhabl
	Human Diseases	
	Cancer: overview	
05203	Viral carcinogenesis	Ywhabl
	Neurodegenerative disease	
05010	Alzheimer disease	Tuba8l4, Ppiaa
05012	Parkinson disease	Ppiaa
05016	Huntington disease	Tuba8l4, Ppiaa
	Cardiovascular disease	
05410	Hypertrophic cardiomyopathy (HCM)	Actc1b
05414	Dilated cardiomyopathy (DCM)	Actc1b
	Infectious disease: bacterial	
05130	Pathogenic Escherichia coli infection	Tuba8l4
	Infectious disease: viral	
05161	Hepatitis B	Ywhabl
05160	Hepatitis C	Ywhabl

KEGG Pathway ID	Pathway Category	Mapped Protein
	Infectious disease: parasitic	
05145	Toxoplasmosis	Ppiaa

593 **Table 9.** KEGG pathways (Organism: Danio rerio) associated with the differentially expressed
594 proteins identified from negative control 2 (NC2, Hypoxic + PTZ 170 mg/kg) and O+H+P (OSLP 800
595 μg/kg + Hypoxic + PTZ 170 mg/kg).

KEGG Pathway ID	Pathway Category	Mapped Protein
	Metabolism	
01100	Metabolic pathways	Glula
01120	Microbial metabolism in diverse environments	Glula
01230	Biosynthesis of amino acids	Glula
	Carbohydrate metabolism	
00630	Glyoxylate and dicarboxylate metabolism	Glula
	Energy metabolism	
00910	Nitrogen metabolism	Glula
	Amino acid metabolism	
00250	Alanine, aspartate and glutamate metabolism	Glula
00220	Arginine biosynthesis	Glula
	Genetic Information Processing	
	Folding, sorting and degradation	
03018	RNA degradation	Hspd1
	Environmental Information Processing	
	Signal transduction	
02020	Two-component system	Glula
	Cellular Processes	
	Transport and catabolism	
04145	Phagosome	Tuba1c, Zgc:65894
	Cell growth and death	
04210	Apoptosis	Sptan1, Tuba1c
04217	Necroptosis	Glula, Ppiab
	Cellular community - eukaryotes	
04530	Tight junction	Tuba1c
04540	Gap junction	Tuba1c, Zgc:65894
	Organismal Systems	
	Immune system	
04640	Haematopoietic cell lineage	Cd59
04610	Complement and coagulation cascades	Cd59
	Nervous system	
04724	Glutamatergic synapse	Glula
04727	GABAergic synapse	Glula
	Aging	
04212	Longevity regulating pathway - worm	Hspd1
	Human Diseases	
	Neurodegenerative disease	
05010	Alzheimer disease	Tuba1c, Zgc:65894
05016	Huntington disease	Tuba1c, Zgc:65894
	Endocrine and metabolic disease	
04940	Type I diabetes mellitus	Hspd1
	Infectious disease: bacterial	

KEGG Pathway ID	Pathway Category	Mapped Protein
05130	Pathogenic Escherichia coli infection	Tuba1c, Zgc:65894
05134	Legionellosis	Hspd1
05152	Tuberculosis	Hspd1
	Infectious disease: viral	
05144	Malaria	Hbba1
05143	African trypanosomiasis	Hbba1
	Drug resistance: antimicrobial	
01503	Cationic antimicrobial peptide (CAMP) resistance	Ppiab

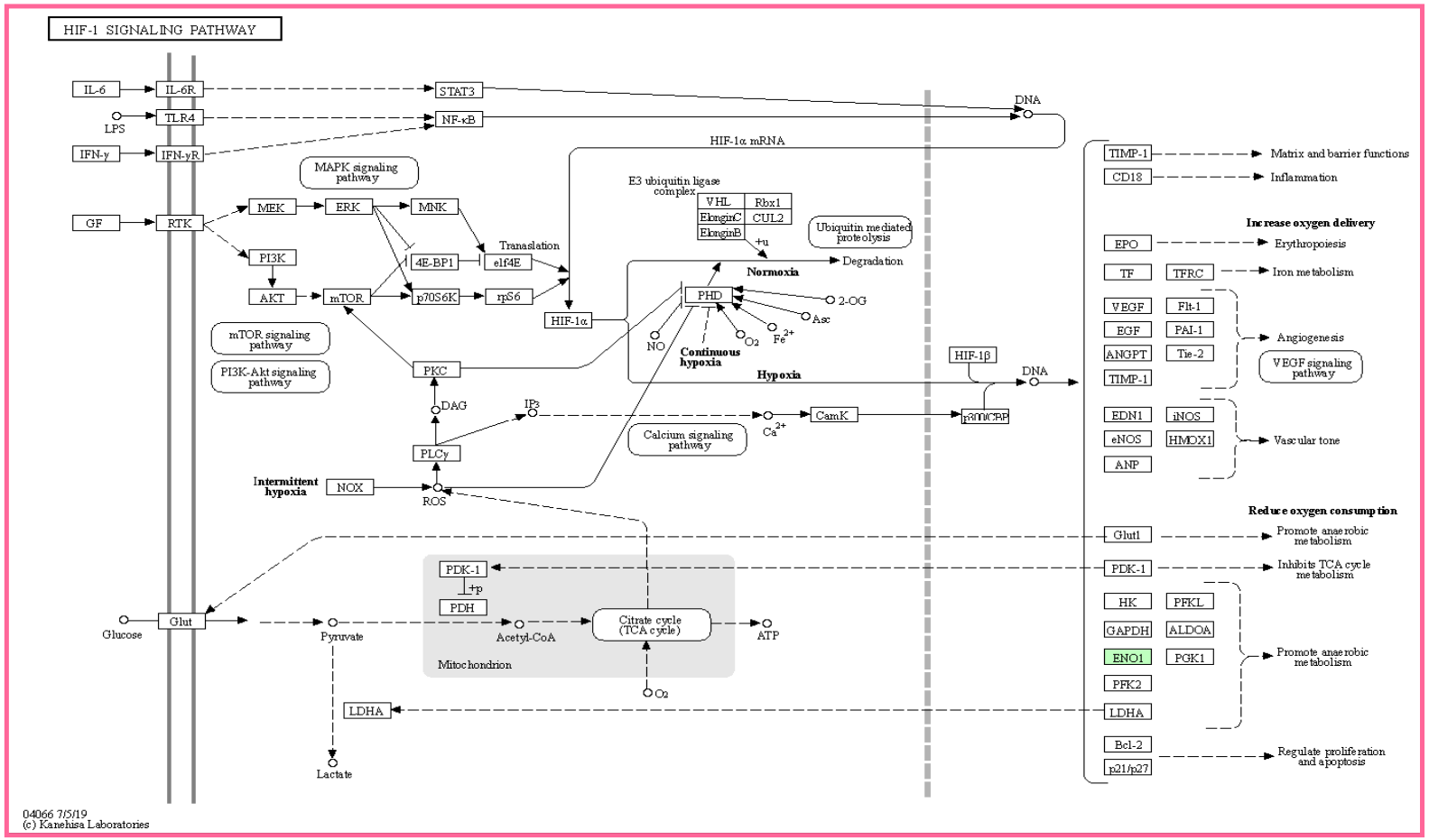

596

597 **Figure 13.** Enolase 2 in the green box was mapped onto the HIF-signalling pathway (04066) generated by KEGG PATHWAY (Organism: *Danio rerio*).

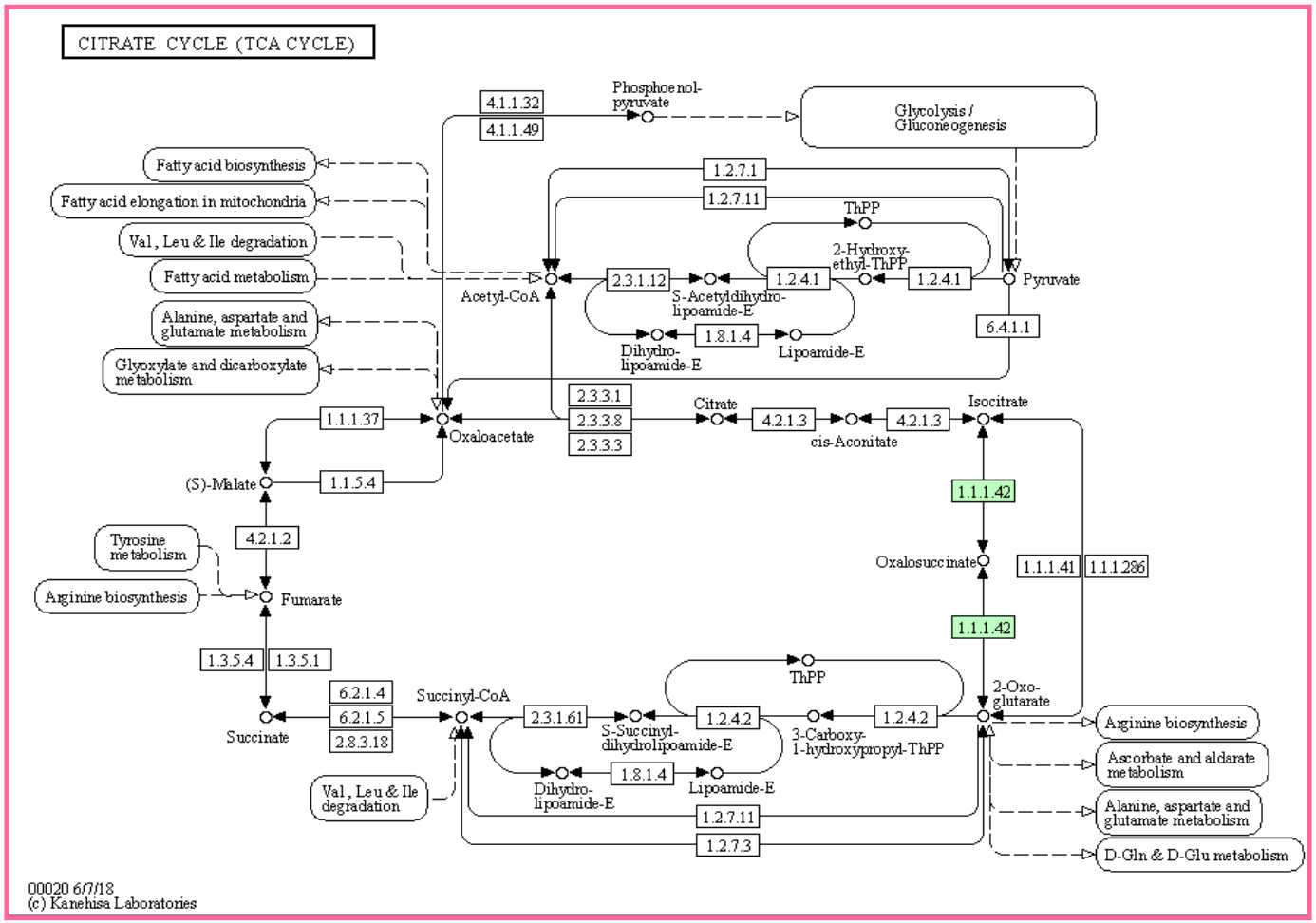

Figure 14. Isocitrate dehydrogenase 2 (Idh2) in the green box was mapped onto the citrate cycle (TCA cycle) pathway (00020) generated by KEGG PATHWAY (Organism: *Danio rerio*).

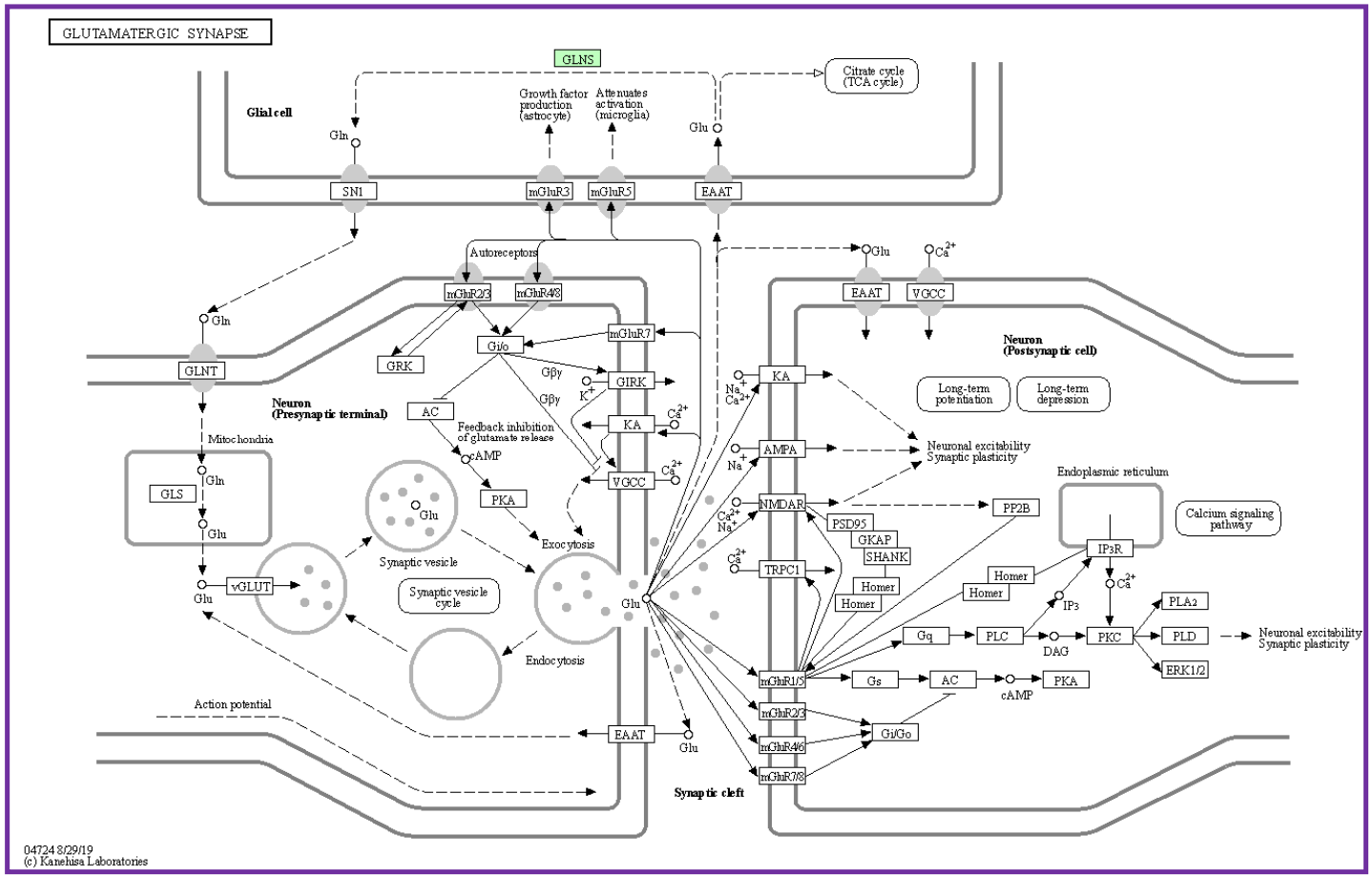

Figure 15. Glutamine synthetase (Glula) in the green box was mapped onto the glutamatergic synapse pathway (04724) generated by KEGG PATHWAY (Organism: *Danio rerio*).

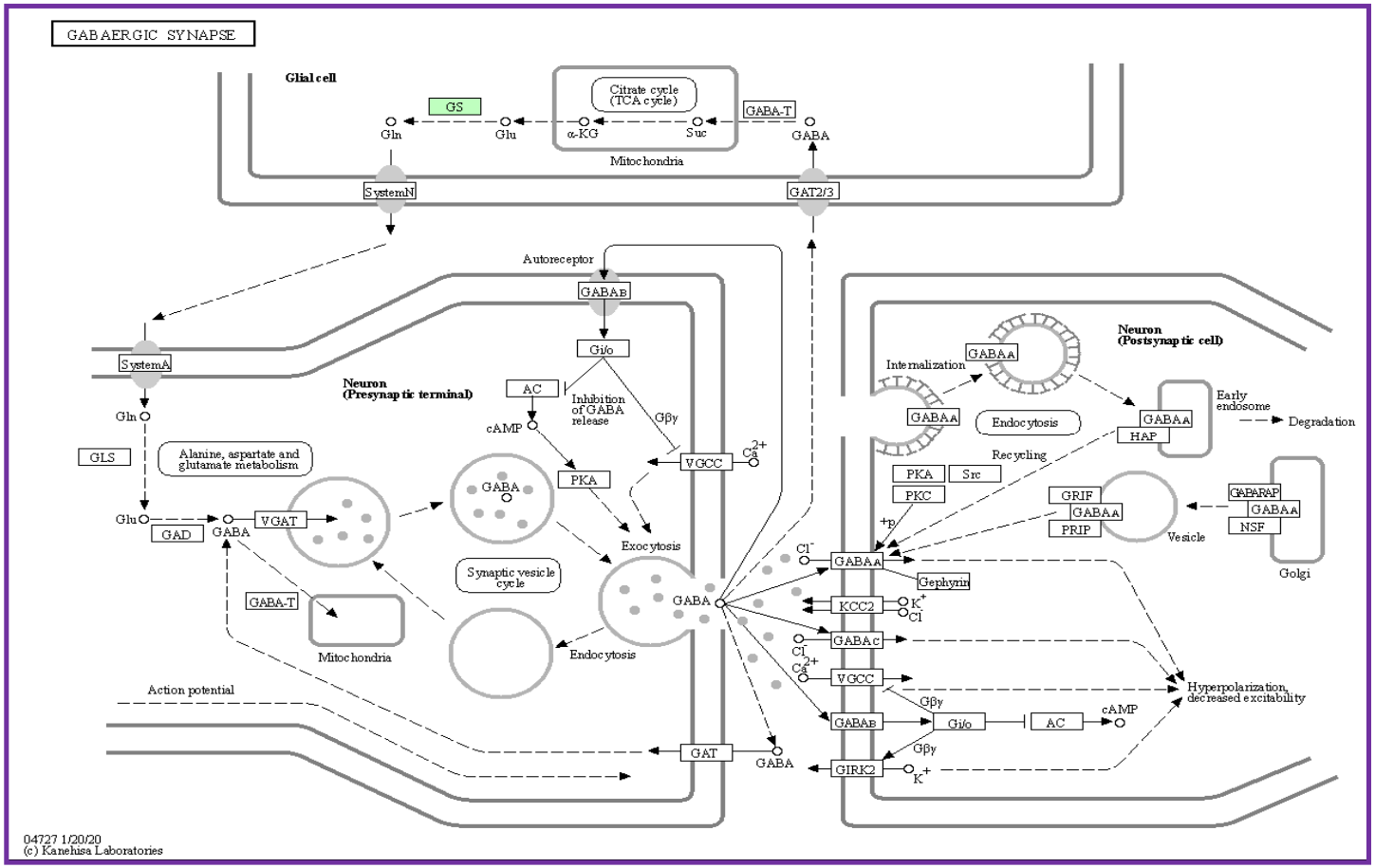

Figure 16. Glutamine synthetase (Glula) in the green box was mapped onto the GABAergic synapse pathway (04727) generated by KEGG PATHWAY (Organism: *Danio rerio*).

4. Discussion

In this study, the anticonvulsive potential of OSLP (800 μg/kg of b.w.) in adult zebrafish under a hypoxic condition was investigated. The OSLP safety study [19] conducted previously, limits the maximum zebrafish intraperitoneal route safe dose of OSLP achievable to 800 μg/kg of body weight.

Firstly, an adult zebrafish model of double challenge – hypoxia induction followed by PTZ injection was established. Findings obtained from the behavioural study have suggested that hypoxia induction for 15 -18 min sufficiently resulted in hypoxic insults. The adult zebrafish were hypoxic but remained alive at the end of the hypoxia induction. This is crucial as it permits the second challenge using PTZ (170 mg/kg of b.w., i.p.). However, the hypoxic adult zebrafish (NC 1) were not observed to have seizures. Based on this outcome, it is therefore suggested that the timing might be insufficient to elicit seizures in the adult zebrafish. Kubová and Mareš [31] have reported a similar finding in a rat model. On the other hand, the adult zebrafish were hypoxic and epileptic (NC 2) following the double challenge. It is therefore suggested that, in this study, hypoxia induction followed by PTZ injection can provoke seizures.

This zebrafish model has never been established before as there is no prior published scientific evidence. A prior literature search only yielded one study; Kubová and Mareš [31] established an immature Wistar albino rat model using a simulation of hypobaric hypoxia and PTZ injection. As such, this work represents the first of its kind.

Swim path analysis in this study has shown that the hypoxia-induced group (NC 1) did not manage to swim through the whole tank but rather, showed an apparent preference for the upper half of the tank, particularly close to the water surface. The NC 2 group (hypoxia + PTZ-induced) showed apparent twitching and erratic movements. Additionally, the NC 2 group saw a higher seizure score and a delayed seizure onset time when compared to the VC group. Such observations suggest that PTZ is sufficient to elicit seizures in the hypoxic zebrafish. PTZ inhibits GABA actions particularly at the $GABA_A$ receptors [32-34] and hence suppresses GABA inhibitory activities which in turn potentiates Glu excitatory activities. Decreased GABA contributes to promoting excitability in the brains and hence, provoked uncontrolled movements (i.e. kindling or twitching) in the zebrafish. This explains the representative swim path of NC 2 group showing erratic swimming patterns. The NC 2 group, though showing erratic swimming patterns, however, also did not manage to swim throughout the whole tank. Similarly, it was seen that both negative controls showed strong preferences for the upper half of the tank, which allows them to be closer to the water surface. When encountering hypoxic conditions, fish in most cases will respond by escaping to oxygenated environments [35]. It is perhaps by doing so, the zebrafish could restore the exchange of oxygen and carbon dioxide in blood and pH, as a means to quickly provide tolerance to counteract the effects of hypoxia. Previous studies have reported that acute inadequate oxygen supply can trigger anaerobic metabolism and increased respiration in an attempt to increase oxygen intake [35-38].

Meanwhile, these two groups, OSLP-treated hypoxia (O+H) and OSLP-treated hypoxia + PTZ (O+H+P) received pre-treatment with OSLP 800 μg for 30 min before hypoxia induction or double challenge, respectively. The O+H+P group saw subtle improvements (lower seizure score, prolonged seizure onset time and less erratic swimming pattern) compared to the NC 2 group. This observation suggests that OSLP 800 μg could exert anticonvulsive effects but at a lower degree under hypoxia. The O+H group did not observe a swimming pattern comparable to that of the untreated VC. Rather, it showed a similar swimming pattern with an apparent preference for the upper half of the tank and both OSLP-treated groups did not manage to swim through the whole tank. This observation suggests that OSLP 800 μg could not efficaciously oppose the hypoxia insults. Meanwhile, the PC group pre-treated with Diazepam (DZP, 1.25 mg/kg) was also found in this study to mildly improve seizures (lower seizure score, prolonged seizure onset time and less erratic swimming pattern) compared to the NC 2 group. Nonetheless, the DZP-treated zebrafish still showed an apparent preference for the upper half of the tank and did not produce a swimming pattern comparable to that of the untreated VC and TC. Such observations suggest that DZP could still exert anticonvulsive effects under hypoxic conditions. Goswami, Singh [39] and Kubová and Mareš [31] have reported

659 similar findings. DZP, however, could not efficaciously oppose the hypoxia insults because DZP is
660 not a drug used in clinical settings to treat hypoxia or hypoxemia.
661 Locomotion parameter analysis in this study showed that the NC 1 group had a lower mean
662 total distance travelled and travelled about a 68 % shorter distance than the untreated VC group.
663 Such lower locomotor activity has been strongly linked to the disruption of cerebral blood flow
664 which starves neurons of oxygen and glucose and thereby affects energy metabolism under hypoxic
665 conditions [4, 40]. The NC 2 group also had a lower mean total distance travelled and travelled about
666 a 46 % shorter distance than the untreated VC group. However, when compared to the NC 1 group,
667 the NC 2 group had a higher mean total distance travelled, which was about a 41 % longer distance.
668 Such uncontrolled movements could be rendered by burst neuronal firing in addition to the pass-out
669 phenomenon in seizures [31, 41, 42] after PTZ injection. PTZ disrupted the balance of excitation and
670 inhibition in the brains and hence elicited uncontrolled movements (i.e. kindling or twitching, erratic
671 swimming, loss of direction) which taken together, contributed to a longer mean total distance
672 travelled in NC 2.
673 Pre-treatment with OSLP 800 μg was found to insufficiently mitigate the hypoxia insults as the
674 O+H group still had a lower mean total distance travelled than the NC 1 and untreated VC groups at
675 the end of the experiment. The O+H+P group showed a reduction in mean total distance travelled,
676 which was about a 39 % shorter distance than the NC 2 group. This observation suggests that OSLP
677 could exert anticonvulsive effects. Interestingly, the PC group saw only a subtle improvement in the
678 mean total distance travelled, which was insignificantly different from the NC 2 group and still had
679 a lower mean total distance travelled than the untreated VC group at the end of the experiment. This
680 could be related to adverse effects including sedation, hypnosis, syncope (temporary loss of
681 consciousness), confusion [43] and respiratory suppression due to the anxiolytic action of DZP
682 [44-46] which might be worsened by a hypoxic blackout, a common condition in hypoxia [47, 48].
683 Moreover, the DZP-treated group spent a long time in the upper half of the tank, which possibly is
684 attributed to the starvation of oxygen in the zebrafish following hypoxia induction. Overall, it was
685 seen that all the hypoxia-treated groups displayed a trend of spending a long time in the upper half
686 of the tank whereas, the non-hypoxic groups, VC and TC, did not show a strong preference for any
687 spot in the tank but managed to swim throughout the whole tank.
688 Taken together, the outcomes of the behavioural study suggest that hypoxia induction for 15 -18
689 min per adult zebrafish is sufficient to cause cerebral hypoxia though this acute hypoxia induction is
690 insufficient to provoke convulsive activity. The double challenge with hypoxia induction and PTZ
691 injection is sufficient to cause cerebral hypoxia and provoke seizures. The anticonvulsive effect of
692 OSLP (800 μg/kg of b.w.) could be milder under a hypoxic condition.
693 In this study, GABA and Glu, were investigated as two of the major neurotransmitters. An
694 interrupted GABA/Glu cycle was seen in all the hypoxia-treated groups, with a lower mean GABA
695 level but a higher mean Glu level when compared to the untreated VC and TC groups. Both negative
696 controls saw an interrupted GABA/Glu cycle, with a decrease in GABA levels but an increase in Glu
697 levels. GABA/Glu synthesis in the glia involves intermediates of the citric acid cycle that are
698 regulated by oxygen availability. When oxygen becomes limiting, GABA/Glu synthesis in the glia is
699 shifted to reductive carboxylation in the citrate cycle, with α-ketoglutarate (aka 2-oxoglutarate, 2OG)
700 as the key intermediate [49-51]. Consequently, Glu competes for α-ketoglutarate with GABA to
701 continuously support a normal synthesis under hypoxia [52-54]. This ultimately disrupted the
702 GABA/Glu cycle in the CNS. This explains a lower GABA/Glu ratio in all the hypoxia-treated
703 groups.
704 The NC 2 group saw a lower GABA/Glu ratio than the NC 1 group. The PTZ injection could
705 have exacerbated the GABA/Glu cycle in the face of hypoxia. As aforementioned, PTZ suppresses
706 GABA which in turn favours Glu accumulation. In this regard, glial Glu uptake is necessary to
707 prevent the accumulation of Glu at the synaptic terminals [55-58]. However, Glu uptake could
708 become impaired by disrupted cerebral blood flow in hypoxia. Additionally, seizures provoked by
709 PTZ have been linked to alteration of ion channel functions involving the six major known ions,
710 namely potassium (K^+), sodium (Na^+), chloride (Cl^-), calcium (Ca^{2+}), hydrogen (H^+) and bicarbonate

711 (HCO^{-3}) [59]. Altered ion channel functions (i.e. clearance and release, depolarisation and
712 hyperpolarisation) could be further affected by hypoxia as a possible result of alterations in reactive
713 oxygen species levels [60-62]. As such, it has possibly resulted in an unbalanced GABA/Glu ratio.
714 Pre-treatment with OSLP 800 μg has been found to mildly alleviate seizures as the O+H+P
715 group showed a lower mean Glu level when compared to the NC 2 group and therefore a subtle
716 improvement in the GABA/Glu ratio, though, such improvement was lower when compared to the
717 untreated VC group. Hypoxia might decrease the activity of OSLP. Hypoxia can decrease the
718 synthesis, release and uptake of neurotransmitters; as well as alter ionic gradients, redox status and
719 metabolic rate in the brain [6, 63].
720 Unexpectedly, the PC group (pre-treated with DZP) had a surge in mean Glu level when
721 compared to all the hypoxia-treated groups. This might be related to the alteration of ion channel
722 functions under hypoxia. DZP is a benzodiazepine derivative that binds to an allosteric site in the
723 $GABA_A$ receptor (Cl^-) channels to enhance the efficacy of inhibitory synapses [64]. However,
724 hypoxia could alter ion channel functions as aforementioned [60-62] and such alterations might have
725 partially affected the binding of DZP and its subsequent efficacy. Studies have found the chloride
726 (Cl^-) channel influences the efficacy and polarity of synaptic transmission mediated by GABA [65]
727 and the formation [66] as well as functional maintenance of glutamatergic synapses [67].
728 Additionally, Hertle, Werhahn [68] have linked the reduction of functional recovery and neuronal
729 survival in rats to sedative effects as sedation is one of the known side effects of DZP [43]. These
730 studies have lent support to the observations seen in the present study. DZP could be still exerting
731 anticonvulsive effects under hypoxic conditions but its efficacy might be reduced under hypoxia.
732 The PC group showed an interrupted GABA/Glu cycle at the end of the experiment. A similar trend
733 was seen in all the hypoxia-treated groups.
734 Interestingly, the TC group neither showed interrupted mean GABA nor mean Glu activity and
735 consequently, displayed a balance in the GABA/Glu ratio at the end of the experiment. Taken
736 together, the neurotransmitter study suggests that hypoxia induction alone or together with PTZ
737 injection could disrupt the GABA/Glu balance. OSLP could be potentially anticonvulsive but its
738 effect was milder under a hypoxic condition.
739 The protein expression study was performed to predict the anticonvulsive mechanism of OSLP.
740 The main findings are the following.
741 For Pair 1 (NC 1 vs. O+H), mass-spectrometry-based LFQ analysis compared the differentially
742 expressed proteins in the hypoxic group (NC1, induced by hypoxia only) and the OSLP-treated
743 hypoxia group (O+H, OSLP 800 μg/kg + hypoxia). This identified a distinct protein expression
744 profile of 10 differentially expressed proteins. They had higher expressions in the NC 1 group than
745 in the O+H group. Functional annotation analysis found that the enzymatic activity of
746 phosphopyruvate hydratase (aka Eno2; GO:4634) localised at the phosphopyruvate hydratase
747 complex (GO:15) was particularly interesting, given the important role Eno2 plays in the adaptation
748 to hypoxic insults in neurons. In line with this, KEGG pathway mapping has proposed
749 hypoxia-inducible factor 1 (HIF-1) signalling (04066) as the most probable pathway. As shown, the
750 citrate cycle was part of the metabolic cycle in the HIF-1 signalling pathway under hypoxic
751 conditions., implying a strong association between Eno2 and Idh2. The enzymatic activities of
752 isocitrate dehydrogenase (NADP+) (GO:4450) and isocitrate dehydrogenase (GO:4448) regulate
753 energy supply which can influence the biosynthesis of neurotransmitters under hypoxia. In line with
754 this, KEGG pathway mapping also proposed the citrate cycle (00020) as another relevant pathway.
755 Enzyme Eno2, also known as neuron-specific enolase (NSE), is produced by neurons and
756 neuroendocrine cells, particularly the cells of the amine precursor uptake and decarboxylation
757 lineage [69, 70]. As shown, Eno2 is one of the hypoxia-inducible proteins in the HIF-1 signalling
758 pathway in neurons [71]. The HIF-1 signalling pathway, predominantly governed by HIF-1
759 stabilisation [72, 73], is activated in response to hypoxia, a condition in which there is a decrease in
760 the oxygen supply to a neuron. Under hypoxia, HIF-1 (in particular HIF-1α) is rapidly stabilised and
761 its downstream target genes are promptly increased [72]. Eno2 is one of the downstream target
762 genes. Eno2 is activated to promote anaerobic metabolism by switching from oxidative

phosphorylation (aerobic) to the citrate cycle (anaerobic), as a means to reduce oxygen consumption [74] through metabolic depression and to maintain normal cellular metabolism, proliferation and apoptosis, under hypoxia [35, 37]. HIF-1 elicits a wide range of adaptive responses, which mainly focus on the upregulation of transcriptional cascades that are important for tissue protection and adaptation [72, 73].

When oxygen becomes limiting, cerebral blood flow can be disrupted. Sensing the disruption, neurons swiftly elicit adaptive responses by resetting their cellular metabolism to a low oxygen consumption mode. Hence, the reductive carboxylation reaction (in the reverse citrate cycle direction) is triggered as the primary way of energy production (in the form of adenosine triphosphate, ATP). As shown, reductive carboxylation reaction is catalysed by Idh2 to convert 2-oxoglutarate (2OG) to isocitrate while oxidising NADPH to $NADP^+$. 2OG (aka α-ketoglutarate, 2-ketoglutaric acid, oxoglutaric acid), and is a key intermediate of the citrate cycle [49]. It is a precursor for the synthesis of the neurotransmitters Gln and Glu [75, 76]. Neurons can then refill Gln from the citrate cycle via the conversion of Glu and α-ketoglutarate catalysed by glutaminase and glutamate dehydrogenase, respectively. Gln or Glu is then used as fuel by neurons [75, 77, 78] to continuously support a normal cellular metabolism with an optimal energy supply in hypoxia.

The findings of Pair 1 (NC 1 vs. O+H) suggested that OSLP could be modulating the energy metabolism in neurons via HIF-1 signalling and citrate cycle pathways and thereby, indirectly influencing the synthesis of neurotransmitters under hypoxia. Hypoxia can disrupt cerebral blood flow which in turn starves the neurons of oxygen and glucose while also reducing the clearance of toxic waste products such as acids, reactive oxygen species and dead cellular components [40, 72, 74]. A study by van der Meer, van den Thillart [79] found that genes encoding enzymes for glycolysis and fermentation are expressed more strongly after long-term hypoxia in adult zebrafish whereas Ton, Stamatiou [80] reported a similar finding in zebrafish embryos after 24-h of anoxia (0% O_2). It is perhaps by acting on these pathways, that the neurons find metabolic support to provide hypoxic-ischaemic tolerance to the disrupted cerebral blood flow and energy substrates [49, 72, 75, 76].

For Pair 2 (NC 2 vs. O+H+P), mass-spectrometry-based LFQ analysis compared the differentially expressed proteins in the hypoxic and epileptic (NC2, hypoxic + PTZ 170 mg/kg) versus OSLP-treated hypoxia + PTZ (O+H+P, OSLP 800 μg/kg + hypoxic + PTZ 170 mg/kg) groups. This has identified a unique protein expression profile of 12 differentially expressed proteins. Among them, protein glutamine synthetase (Glula, Q7T2P7, lowly expressed in NC 2 but highly expressed in O+H+P) was particularly noteworthy. Functional annotation analysis found the enzymatic activity of glutamate-ammonia ligase (GO:4356; aka glutamine synthetase, GS) to be particularly interesting, given the fundamental role Glula plays in the regulation of neurotransmitter synthesis in the glia. In line with this, KEGG pathway mapping proposed the glutamatergic synapse (04724) and the GABAergic synapse (04727) pathways as most likely to play a significant role in the synaptic transmission under hypoxia.

Glutamine (Gln) acts as a precursor for glutamate (Glu) in the glutamatergic synapse. In the glutamatergic synapse, Glu is converted to Gln by GS or enters the citrate cycle in glia. Glu acts on postsynaptic ionotropic Glu receptors (iGluRs) to mediate fast excitatory synaptic transmission [57]. After its action on these receptors, Glu is removed from the synaptic cleft and is transported back into glial cells where it is again converted back to Gln. A small portion of Glu is oxidatively metabolised, thus making *de novo* synthesis of Glu necessary to maintain adequate Glu levels [81], as shown in the glutamatergic synapse pathway. Gamma-aminobutyric acid (GABA), a dominant inhibitory neurotransmitter, is either reutilised as an inhibitory neurotransmitter or metabolised predominantly via the GABA shunt in glial cells where Glu is converted to Gln by GS [52-54], as shown in the GABAergic synapse pathway.

Under hypoxia, GABA and Glu synthesis and subsequently GABA and Glu concentrations can be profoundly altered. In particular, Glu synthesis in glial cells in the glutamatergic synapse is shifted to reductive carboxylation in the citrate cycle, with α-ketoglutarate (aka 2OG) as the key intermediate [49-51]. α-ketoglutarate is then catalysed by glutamate dehydrogenase to form Glu

which is then converted to Gln by GS, refilling the Gln pool. This is crucial because Gln is the precursor of Glu in glial cells [82]. GABA is predominantly formed from the transamination of α-ketoglutarate produced in the citrate cycle by GABA α-oxoglutarate transaminase (GABA-T) into Glu [52-54]. α-ketoglutarate is catalysed by glutamate dehydrogenase to form Glu via the GABA shunt in glial cells in the GABAergic synapse, which is then converted to Gln by GS, refilling the Gln pool. This is critical for conserving the supply of GABA in glial cells [52-54]. Therefore, following the shift to reductive carboxylation in the glutamatergic synapse, Glu competes for α-ketoglutarate with GABA to continuously support a normal energy metabolism under hypoxia. This ultimately disrupted the GABA-Glu-Gln cycle in the CNS [50, 82].

The GABA-Glu-Gln cycle could also be exacerbated by PTZ in the face of hypoxia. PTZ, a tetrazole derivative [83], is known to be capable of inhibiting GABA actions particularly at the $GABA_A$ receptors [32-34]. PTZ inhibits GABA inhibitory activities at GABAergic synapses which in turn potentiates Glu excitatory activities on glutamatergic synapses. In this regard, the removal of Glu from synaptic terminals is crucial as Glu is not only an excitatory neurotransmitter but is also an excitotoxic agent which, in high concentrations, has the potential to cause neuronal death [56]. The excessive amount of Glu is removed from the synaptic terminals via glial Glu uptake and is then converted back to Gln by GS [55-58]. This might further elevate metabolic demand in glial cells at a time when energy supplies are inadequate and thus exacerbates the GABA-Glu-Gln cycle.

The findings of Pair 2 (NC 2 vs. O+H+P) suggested that OSLP could be modulating the synthesis of GABA and Glu in glial cells via the "Glutamatergic synapse" and "GABAergic synapse" pathways and thereby, influencing the regulation of neurotransmission. It is perhaps by acting on these pathways, the neurons keep the GABA-Glu-Gln cycle in check to provide hypoxic-ischaemic tolerance to disrupted synaptic transmission as a result of hypoxia induction and PTZ injection [50, 51, 53, 57, 58]. The double challenge saw a more direct impact on the synaptic transmission compared with the Pair 1 (NC 1 vs. O+H).

In the brain, hypoxic stress can contribute to hypoxic-ischaemic insults which can also alter the metabolism of cellular energy and neurotransmitters. For instance, hypoxic-ischaemic encephalopathy (HIE), a neuro-vascular and neuro-metabolic syndrome caused by a shortage of supply of oxygen and glucose or their metabolites in the brain. HIE results from a global hypoperfusion or oxygenation deficiency rather than from infarction in a specific vascular or cerebral territory [10]. In particular, Eno2 is one of the key biomarkers in clinical settings to assess HIE. Elevations of Eno2 have been reported in adult patients with cerebrovascular incidents [84-86] and in animal models with traumatic brain injuries [87]. Additionally, HIE can also alter the neurotransmitter metabolism which can affect the synaptic transmission and thereby causes aberrant neuronal activities. For instance, Goldberg, Monyer [88] have reported impaired energy metabolism in the synaptic transmitter pools in cortical cell cultures during experimental hypoxia or ischaemia. Wang, Wu [89] have demonstrated that brain hypoxia-ischaemia can induce early-onset convulsive seizures in ageing mice. Sutter, Marsch [8] have reported HIE as one of the main presumed etiologies of refractory status epilepticus in patients in a 7-year observational study. HIE has also been recognised as a common cause of seizures in term neonates [90, 91]. Vintila, Roman [10] have described HIE as one of the most frequent and dramatic urgency found in neurological diseases of adults.

Based on the present protein expression study, OSLP most likely modulates the anticonvulsive mechanism by acting on the HIF-1 signalling and citrate cycle pathways to slow the metabolic processes in an attempt to maintain the cellular energy metabolism in neurons under hypoxia; as well as glutamatergic and GABAergic synapse pathways to regulate the synthesis of GABA and Glu in glial cells with optimal energy supply under a hypoxic-ischaemic condition.

Last but not least, the present protein expression study profiled a limited number of proteins. This observation could be linked to the denaturation of proteins as a result of the depletion of energy-rich compounds following hypoxia induction or the double challenge. For instance, as energy-dependent membrane pumps fail, neuronal and glial cell membranes depolarise and allow the influx of Ca^{2+} ions. Elevated intracellular Ca^{2+} and other second messengers activate lipases and

867 proteases, which release membrane-bound free fatty acids that denature proteins in the ischaemic
868 cascade [5]. This lends support to the detection of higher expressions of protein Apoa2
869 (apolipoprotein A-II) in both negative controls (NC 1 and NC 2) in this study.

870 **5. Conclusions**

871 OSLP most likely influences synaptic transmission by providing hypoxic-ischaemic tolerance to
872 the synapses. This potential is most likely attributed to the ability of OSLP to regulate the synthesis
873 of GABA and Glu in glial cells via the "Glutamatergic Synapse" and "GABAergic Synapse"
874 pathways, in addition to modulating cellular energy metabolism in neurons via the "HIF-1
875 Signalling" and "Citrate Cycle" pathways. OSLP can safely alleviate seizures in an adult zebrafish
876 model of double challenge – hypoxia induction followed by PTZ injection and could be a potential
877 candidate for further investigation and development.

878 **Author Contributions:** Y.S.C took lead in the design, execution of all the experiments and data analyses, and
879 the writing and editing of the final manuscript; B.K.M.C helped in the experiments and data analyses as well as
880 edited the final manuscript; P.K.A aided in supervision and reviewed the final manuscript; M.F.S and I.O
881 contributed to the design of research, supervised all aspects of the study and edited the final manuscript. All
882 authors have read and agreed to the published version of the manuscript.

883 **Funding:** This research was funded by the NKEA EPP#1 Research Grant Scheme (NRGS) (NH1014D066),
884 Ministry of Agriculture and Agro-based Industry, Malaysia and Global Asia in the 21st Century (GA21)
885 Platform, Monash University Malaysia, Research Grant (GA-HW-18-L04).

886 **Acknowledgments:** The authors would like to thank Dr. Syafiq Asnawi Zainal Abidin and Nurziana Sharmilla
887 Binti Nawawi for ESI-LCMS/MS technical support (LC-MS laboratory of Jeffrey Cheah School of Medicine and
888 Health Sciences).

889 **Conflicts of Interest:** The authors declare no conflict of interest.

890 **References**

891 1. Gossman, W., F. Alghoula, and I. Berim, *Anoxia (Hypoxic Hypoxia)*, in *StatPearls [Internet]*. 2019,
892 StatPearls Publishing.
893 2. Watts, E.R. and S.R. Walmsley, *Inflammation and hypoxia: HIF and PHD isoform selectivity.* Trends in
894 molecular medicine, 2019. **25**(1): p. 33-46.
895 3. Turetz, M.L. and R.G. Crystal, *62 - Mechanisms and Consequences of Central Nervous System Hypoxia*, in
896 *Neurobiology of Disease*, S. Gilman, Editor. 2007, Academic Press: Burlington. p. 681-688.
897 4. Lacerte, M. and F.B. Mesfin, *Hypoxic Brain Injury.* 2019.
898 5. Zivin, J.A., *413 - Approach to Cerebrovascular Diseases*, in *Goldman's Cecil Medicine (Twenty Fourth*
899 *Edition)*, L. Goldman and A.I. Schafer, Editors. 2012, W.B. Saunders: Philadelphia. p. 2304-2310.
900 6. McKenna, M.C., S. Scafidi, and C.L. Robertson, *Metabolic Alterations in Developing Brain After Injury:*
901 *Knowns and Unknowns.* Neurochemical research, 2015. **40**(12): p. 2527-2543.
902 7. Dodrill, P., *Chapter 13 - Disorders Affecting Feeding and Swallowing in Infants and Children*, in *Dysphagia*
903 *(Second Edition)*, M.E. Groher and M.A. Crary, Editors. 2016, Mosby: St. Louis. p. 271-304.
904 8. Sutter, R., et al., *Mortality and recovery from refractory status epilepticus in the intensive care unit: a 7-year*
905 *observational study.* Epilepsia, 2013. **54**(3): p. 502-511.
906 9. Scully, C., *13 - Neurology*, in *Scully's Medical Problems in Dentistry (Seventh Edition)*, C. Scully, Editor.
907 2014, Churchill Livingstone: Oxford. p. 345-392.
908 10. Vintila, I., C. Roman, and C. Rociu, *Hypoxic-ischemic encephalopathy in adult.* Acta Medica
909 Transilvanica, 2010. **2**: p. 189-192.
910 11. Howe, K., et al., *The zebrafish reference genome sequence and its relationship to the human genome.* Nature,
911 2013. **496**(7446): p. 498-503.
912 12. Norton, W. and L. Bally-Cuif, *Adult zebrafish as a model organism for behavioural genetics.* BMC
913 Neuroscience, 2010. **11**(1): p. 90.
914 13. Steenbergen, P.J., M.K. Richardson, and D.L. Champagne, *The use of the zebrafish model in stress*
915 *research.* Progress in Neuro-Psychopharmacology and Biological Psychiatry, 2011. **35**(6): p. 1432-1451.

14. Kokel, D., et al., *Rapid behavior-based identification of neuroactive small molecules in the zebrafish.* Nature Chemical Biology, 2010. **6**(3): p. 231-237.
15. Piato, Â.L., et al., *Unpredictable chronic stress model in zebrafish (Danio rerio): Behavioral and physiological responses.* Progress in Neuro-Psychopharmacology and Biological Psychiatry, 2011. **35**(2): p. 561-567.
16. Yu, X. and Y.V. Li, *Zebrafish as an alternative model for hypoxic-ischemic brain damage.* International Journal of Physiology, Pathophysiology and Pharmacology, 2011. **3**(2): p. 88-96.
17. Sree, N.V., P.U. Sri, and N. Ramarao, *Neuro-Protective Properties Of Orthosiphon Staminus (Benth) Leaf Methanolic Fraction Through Antioxidant Mechanisms On SH-SY5Y Cells: An In-Vitro Evaluation.* International Journal of Pharmaceutical Sciences and Research, 2015. **6**(3): p. 1115.
18. Choo, B.K.M., et al., *Orthosiphon stamineus Leaf Extract Affects TNF-α and Seizures in a Zebrafish Model.* Frontiers in Pharmacology, 2018. **9**: p. 139.
19. Chung, Y.-S., et al., *Orthosiphon stamineus Proteins Alleviate Pentylenetetrazol-Induced Seizures in Zebrafish.* Biomedicines, 2020. **8**(7): p. 191.
20. Kundap, U.P., et al., *Zebrafish as a Model for Epilepsy-Induced Cognitive Dysfunction: A Pharmacological, Biochemical and Behavioral Approach.* Frontiers in Pharmacology, 2017. **8**(515).
21. Westerfield, M., *The Zebrafish Book. A Guide for The Laboratory Use of Zebrafish (Danio rerio)*. Vol. 385. 2000.
22. Choo, B.K.M., et al., *Effect of newer anti-epileptic drugs (AEDs) on the cognitive status in pentylenetetrazol induced seizures in a zebrafish model.* Progress in Neuro-Psychopharmacology and Biological Psychiatry, 2019. **92**: p. 483-493.
23. Cao, Z., et al., *Hypoxia-induced retinopathy model in adult zebrafish.* Nature Protocols, 2010. **5**: p. 1903.
24. Science, N., T.C.C.o. Environment, and N. Resources, *Integrated assessment of hypoxia in the northern Gulf of Mexico*. 2000: National Science and Technology Council, Committee on Environment and ….
25. Eby, L.A. and L.B. Crowder, *Hypoxia-based habitat compression in the Neuse River Estuary: context-dependent shifts in behavioral avoidance thresholds.* Canadian Journal of Fisheries and Aquatic Sciences, 2002. **59**(6): p. 952-965.
26. Banote, R.K., et al., *Oral gabapentin suppresses pentylenetetrazole-induced seizure-like behavior and cephalic field potential in adult zebrafish.* Epilepsy & Behavior, 2013. **27**(1): p. 212-219.
27. Mussulini, B.H.M., et al., *Seizures Induced by Pentylenetetrazole in the Adult Zebrafish: A Detailed Behavioral Characterization.* PLOS ONE, 2013. **8**(1): p. e54515.
28. Kanwal, S. and A. Incharoensakdi, *Extraction and Quantification of GABA and Glutamate from Cyanobacterium Synechocystis sp. PCC 6803.* Bio-protocol, 2016. **6**(18): p. e1928.
29. Moriya, Y., et al., *KAAS: an automatic genome annotation and pathway reconstruction server.* Nucleic Acids Research, 2007. **35**(suppl_2): p. W182-W185.
30. Kanehisa, M., *Toward understanding the origin and evolution of cellular organisms.* Protein Science, 2019. **28**(11): p. 1947-1951.
31. Kubová, H. and P. Mareš, *Hypoxia-induced changes of seizure susceptibility in immature rats are modified by vigabatrin.* Epileptic Disorders, 2007. **9**(5): p. 36-43.
32. Shaikh, M., J. Sancheti, and S. Sathaye, *Effect of Eclipta alba on acute seizure models: a GABAA-mediated effect.* Indian journal of pharmaceutical sciences, 2013. **75**(3): p. 380.
33. Huang, R.-Q., et al., *Pentylenetetrazole-induced inhibition of recombinant γ-aminobutyric acid type A (GABAA) receptors: mechanism and site of action.* Journal of Pharmacology and Experimental Therapeutics, 2001. **298**(3): p. 986-995.
34. Velíšek, L., *MODELS | Models of Generalized Seizures in Freely Moving Animals*, in *Encyclopedia of Basic Epilepsy Research*, P.A. Schwartzkroin, Editor. 2009, Academic Press: Oxford. p. 775-780.
35. Chen, N., et al., *Effects of Acute Hypoxia and Reoxygenation on Physiological and Immune Responses and Redox Balance of Wuchang Bream (Megalobrama amblycephala Yih, 1955).* Frontiers in physiology, 2017. **8**: p. 375-375.
36. Roman, M.R., et al., *Interactive Effects of Hypoxia and Temperature on Coastal Pelagic Zooplankton and Fish.* Frontiers in Marine Science, 2019. **6**(139).
37. Douxfils, J., et al., *Physiological and proteomic responses to single and repeated hypoxia in juvenile Eurasian perch under domestication–clues to physiological acclimation and humoral immune modulations.* Fish & shellfish immunology, 2012. **33**(5): p. 1112-1122.

38. Barrionuevo, W., M. Fernandes, and O. Rocha, *Aerobic and anaerobic metabolism for the zebrafish, Danio rerio, reared under normoxic and hypoxic conditions and exposed to acute hypoxia during development.* Brazilian Journal of Biology, 2010. **70**: p. 425-434.
39. Goswami, S., I.S. Singh, and J.J. Ghosh, *Effect of pre- and post-treatments with diazepam on the rat brain GABAergic system during anoxic stress and recovery.* Neurochemistry International, 1991. **18**(1): p. 107-113.
40. Ali, Z. and L.D. Jensen, *Hypoxia-Induced Retinal Angiogenesis in Adult Zebrafish*, in *Handbook of Vascular Biology Techniques*. 2015, Springer. p. 173-183.
41. Mormann, F. and J.G. Jefferys, *Neuronal Firing in Human Epileptic Cortex: The Ins and Outs of Synchrony during Seizures: Dissociation of synchronization of neurons and field potentials.* Epilepsy currents, 2013. **13**(2): p. 100-102.
42. Scharfman, H.E., *The neurobiology of epilepsy.* Current neurology and neuroscience reports, 2007. **7**(4): p. 348-354.
43. Dhaliwal, J.S. and A. Saadabadi, *Diazepam [Updated 2019 January 30]. In:*, in *StatPearls [Internet]*. 2019, StatPearls Publishing: Treasure Island, United States.
44. Manna, S.S. and S.N. Umathe, *Transient receptor potential vanilloid 1 channels modulate the anxiolytic effect of diazepam.* Brain research, 2011. **1425**: p. 75-82.
45. Liu, X., et al., *Restricted access magnetic core-mesoporous shell microspheres with C8-modified interior pore-walls for the determination of diazepam in rat plasma by LC-MS.* Talanta, 2013. **106**: p. 321-327.
46. Sirven, J.I. and E. Waterhouse, *Management of status epilepticus.* American family physician, 2003. **68**(3): p. 469-476.
47. Pallais, J.C., et al., *Fainting, swooning, and syncope.* The primary care companion for CNS disorders, 2011. **13**(4): p. PCC.11f01187.
48. Aminoff, M.J., *Chapter 3 - Electroencephalography: General Principles and Clinical Applications*, in *Aminoff's Electrodiagnosis in Clinical Neurology (Sixth Edition)*, M.J. Aminoff, Editor. 2012, W.B. Saunders: London. p. 37-84.
49. Huergo, L.F. and R. Dixon, *The Emergence of 2-Oxoglutarate as a Master Regulator Metabolite.* Microbiology and Molecular Biology Reviews, 2015. **79**(4): p. 419-435.
50. Waagepetersen, H.S., U. Sonnewald, and A. Schousboe, *1 Glutamine, Glutamate, and GABA: Metabolic Aspects*, in *Handbook of Neurochemistry and Molecular Neurobiology: Amino Acids and Peptides in the Nervous System*, A. Lajtha, et al., Editors. 2007, Springer US: Boston, MA. p. 1-21.
51. Cox, O.H. and R.S. Lee, *Chapter 8 - Behavioral Medical Epigenetics*, in *Medical Epigenetics*, T.O. Tollefsbol, Editor. 2016, Academic Press: Boston. p. 127-146.
52. Olsen, R.W. and G.-D. Li, *Chapter 18 - GABA*, in *Basic Neurochemistry (Eighth Edition)*, S.T. Brady, et al., Editors. 2012, Academic Press: New York. p. 367-376.
53. Deutch, A.Y., *Chapter 6 - Neurotransmitters*, in *Fundamental Neuroscience (Fourth Edition)*, L.R. Squire, et al., Editors. 2013, Academic Press: San Diego. p. 117-138.
54. Olsen RW, D.T., *GABA Synthesis, Uptake and Release.* Basic Neurochemistry: Molecular, Cellular and Medical Aspects. 6th edition., ed. A.B. In: Siegel GJ, Albers RW, et al., editors. 1999, Philadelphia: Lippincott-Raven.
55. Anderson, C.M. and R.A. Swanson, *Astrocyte glutamate transport: review of properties, regulation, and physiological functions.* Glia, 2000. **32**(1): p. 1-14.
56. Sills, G.J., *Excitable but lacking in energy: contradictions in the human epileptic hippocampus.* Epilepsy currents, 2006. **6**(1): p. 6-7.
57. Hassel, B. and R. Dingledine, *Chapter 17 - Glutamate and Glutamate Receptors*, in *Basic Neurochemistry (Eighth Edition)*, S.T. Brady, et al., Editors. 2012, Academic Press: New York. p. 342-366.
58. Kasischke, K.A., *Activity-dependent metabolism in glia and neurons.* 2015.
59. Raimondo, J.V., et al., *Ion dynamics during seizures.* Frontiers in Cellular Neuroscience, 2015. **9**(419).
60. Fujiwara, N., et al., *Effects of hypoxia on rat hippocampal neurones in vitro.* The Journal of physiology, 1987. **384**: p. 131-151.
61. Shimoda, L.A. and J. Polak, *Hypoxia. 4. Hypoxia and ion channel function.* American journal of physiology. Cell physiology, 2011. **300**(5): p. C951-C967.
62. Hertz, L. and Y. Chen, *Importance of astrocytes for potassium ion (K+) homeostasis in brain and glial effects of K+ and its transporters on learning.* Neuroscience & Biobehavioral Reviews, 2016. **71**: p. 484-505.

63. Roesner, A., T. Hankeln, and T. Burmester, *Hypoxia induces a complex response of globin expression in zebrafish (Danio rerio).* Journal of Experimental Biology, 2006. **209**(11): p. 2129-2137.
64. Bergmann, R., et al., *A unified model of the GABA(A) receptor comprising agonist and benzodiazepine binding sites.* PloS one, 2013. **8**(1): p. e52323-e52323.
65. Chamma, I., et al., *Role of the neuronal K-Cl co-transporter KCC2 in inhibitory and excitatory neurotransmission.* Frontiers in cellular neuroscience, 2012. **6**: p. 5-5.
66. Li, H., et al., *KCC2 interacts with the dendritic cytoskeleton to promote spine development.* Neuron, 2007. **56**(6): p. 1019-1033.
67. Gauvain, G., et al., *The neuronal K-Cl cotransporter KCC2 influences postsynaptic AMPA receptor content and lateral diffusion in dendritic spines.* Proceedings of the National Academy of Sciences, 2011. **108**(37): p. 15474-15479.
68. Hertle, D., et al., *Depression of neuronal activity by sedatives is associated with adverse effects after brain injury.* Brain Research, 2013. **1510**: p. 1-9.
69. Sunwoo, H.H. and M.R. Suresh, *Cancer markers*, in *The Immunoassay Handbook*. 2013, Elsevier. p. 833-856.
70. Berger, R.P., et al., *Trajectory analysis of serum biomarker concentrations facilitates outcome prediction after pediatric traumatic and hypoxemic brain injury.* Developmental neuroscience, 2010. **32**(5-6): p. 396-405.
71. Miura, N., et al., *Spatial reorganization of Saccharomyces cerevisiae enolase to alter carbon metabolism under hypoxia.* Eukaryotic cell, 2013. **12**(8): p. 1106-1119.
72. Lee, J.W., et al., *Hypoxia signaling in human diseases and therapeutic targets.* Experimental & Molecular Medicine, 2019. **51**(6): p. 1-13.
73. Mukandala, G., et al., *The Effects of Hypoxia and Inflammation on Synaptic Signaling in the CNS.* Brain sciences, 2016. **6**(1): p. 6.
74. Lendahl, U., et al., *Generating specificity and diversity in the transcriptional response to hypoxia.* Nature Reviews Genetics, 2009. **10**(12): p. 821-832.
75. McDonald, T., M. Puchowicz, and K. Borges, *Impairments in Oxidative Glucose Metabolism in Epilepsy and Metabolic Treatments Thereof.* Frontiers in cellular neuroscience, 2018. **12**: p. 274-274.
76. Chinopoulos, C., *Which way does the citric acid cycle turn during hypoxia? The critical role of α-ketoglutarate dehydrogenase complex.* Journal of Neuroscience Research, 2013. **91**(8): p. 1030-1043.
77. Divakaruni, A.S., et al., *Inhibition of the mitochondrial pyruvate carrier protects from excitotoxic neuronal death.* Journal of Cell Biology, 2017. **216**(4): p. 1091-1105.
78. Sonnewald, U., *Glutamate synthesis has to be matched by its degradation–where do all the carbons go?* Journal of neurochemistry, 2014. **131**(4): p. 399-406.
79. van der Meer, D.L., et al., *Gene expression profiling of the long-term adaptive response to hypoxia in the gills of adult zebrafish.* American Journal of Physiology-Regulatory, Integrative and Comparative Physiology, 2005. **289**(5): p. R1512-R1519.
80. Ton, C., D. Stamatiou, and C.-C. Liew, *Gene expression profile of zebrafish exposed to hypoxia during development.* Physiological Genomics, 2003. **13**(2): p. 97-106.
81. Hampe, C.S., H. Mitoma, and M. Manto, *GABA and Glutamate: Their Transmitter Role in the CNS and Pancreatic Islets*, in *GABA And Glutamate-New Developments In Neurotransmission Research*. 2017, IntechOpen.
82. Kvamme, E., *Synthesis of glutamate and its regulation*, in *Progress in brain research*. 1998, Elsevier. p. 73-85.
83. Stone, W., *Convulsant actions of tetrazole derivatives.* Pharmacology, 1970. **3**(6): p. 367-370.
84. Mondello, S., et al., *Towards translating research to clinical practice: Novel Strategies for Discovery and Validation of Biomarkers for Brain Injury*. 2015: Frontiers Media SA.
85. Hay, E., et al., *Cerebrospinal fluid enolase in stroke.* Journal of Neurology, Neurosurgery & Psychiatry, 1984. **47**(7): p. 724-729.
86. Heinz, U.E. and J.D. Rollnik, *Outcome and prognosis of hypoxic brain damage patients undergoing neurological early rehabilitation.* BMC research notes, 2015. **8**: p. 243-243.
87. Costine, B.A., et al., *Neuron-specific enolase, but not S100B or myelin basic protein, increases in peripheral blood corresponding to lesion volume after cortical impact in piglets.* Journal of neurotrauma, 2012. **29**(17): p. 2689-2695.

88. Goldberg, M.P., H. Monyer, and D.W. Choi, *Hypoxic neuronal injury in vitro depends on extracellular glutamine.* Neuroscience Letters, 1988. **94**(1): p. 52-57.
89. Wang, J., et al., *Early-Onset Convulsive Seizures Induced by Brain Hypoxia-Ischemia in Aging Mice: Effects of Anticonvulsive Treatments.* PloS one, 2015. **10**(12): p. e0144113-e0144113.
90. Kharoshankaya, L., et al., *Seizure burden and neurodevelopmental outcome in neonates with hypoxic–ischemic encephalopathy.* Developmental Medicine & Child Neurology, 2016. **58**(12): p. 1242-1248.
91. Srinivasakumar, P., et al., *Treating EEG seizures in hypoxic ischemic encephalopathy: a randomized controlled trial.* Pediatrics, 2015. **136**(5): p. e1302-e1309.

SUPPLEMENTARY DATA

Table SD-1. NC 1 (hypoxic only) and O+H (OSLP 800 µg/kg + hypoxic). KO (KEGG Orthology) generated KEGG pathways.

UniProt ID	KO ID
tr|B8JKH7|B8JKH7_DANRE	no data
tr|B3DG37|B3DG37_DANRE	K13825
tr|Q9I8V1|Q9I8V1_DANRE	K12314
tr|Q6NWJ5|Q6NWJ5_DANRE	K07374
tr|B3DFP9|B3DFP9_DANRE	no data
tr|F8W3W8|F8W3W8_DANRE	K17269
tr|Q6P5J4|Q6P5J4_DANRE	K09565
tr|Q6GQM9|Q6GQM9_DANRE	K01689
tr|Q6P102|Q6P102_DANRE	K16197
tr|Q7ZUP6|Q7ZUP6_DANRE	K00031

Table SD-2. NC 2 (hypoxic + PTZ 170 mg/kg) and O+H+P (OSLP 800 µg/kg + hypoxic + PTZ 170 mg/kg). KO (KEGG Orthology) generated KEGG pathways.

UniProt ID	KO ID
tr|Q7SZV9|Q7SZV9_DANRE	K13822
tr|Q6PE34|Q6PE34_DANRE	K07375
tr|F8W3W8|F8W3W8_DANRE	K17269
sp|Q90487|HBA_DANRE	K13826
tr|B3DFP9|B3DFP9_DANRE	no data
tr|A0A2R8RZK5|A0A2R8RZK5_DANRE	K07374
tr|A0A2R8Q2Z0|A0A2R8Q2Z0_DANRE	no data
tr|Q6PC53|Q6PC53_DANRE	K03767
tr|Q7T2P7|Q7T2P7_DANRE	K01915
tr|A0A0B5JW41|A0A0B5JW41_DANRE	K04008
tr|Q803B0|Q803B0_DANRE	K04077
tr|F1R446|F1R446_DANRE	K06114

Chapter 6

Integrated Discussion and Conclusion

6.1 Integrated Discussion

Proteins from *Orthosiphon stamineus* have never been extracted before as per the available literature. Saidan and colleagues (Saidan et al., 2015) had extracted a mixture of primary metabolites (not proteins alone) from OS leaves but they did not investigate its neuroprotective potential. As such, this study represents the first of its kind. The first step in this study was to establish an optimal protein extraction method achievable at a laboratory scale. One-Tube Protein Extraction Method (OTM) has successfully extracted OSLP out of the many attempts tried (not included in this thesis). OTM extracted OSLP from LN_2-flash-frozen OS leaves. The total protein yield of OTM was about 3 mg/g which was equivalent to approximately 0.3% out of 1 g of LN_2-flash-frozen leaf sample. At a laboratory scale, this yield was considered optimal. Studies on various protein extraction methods using various plant materials reported elsewhere collectively lend support to this finding. Hence, OTM was used as the routine extraction method in this study. Prior to the subsequent experiments in this study, OSLP extracted was analyzed by mass spectrometry-based proteomics. Proteomics analysis has identified the different protein compositions present in OSLP. Functional annotation analysis was employed to characterise the different protein compositions of OSLP. They were categorised into 49 protein families. The protein compositions present at 21 cellular components, from extracellular to intracellular compartments. They involved in 23 types of molecular function, protein homeostasis, trafficking, signalling, metabolic processes, energy metabolism, defence responses and gene transcriptions. The proteomic profiling of OSLP has never been reported elsewhere and hence, the present finding also represents the first of its kind. This information may provide important clues to further explore the protective potential of OSLP in different aspects. For example, rosmarinic acid biosynthesized by rosmarinate synthase has been reported for anti-inflammatory, antioxidative, anti-angiogenic, anti-tumor, anti-microbial (Kim, Park, Jin, & Park, 2015) and anti-seizure (Choo et al., 2018).

Before screening for OSLP protective potential, it is important to find out if the OSLP extracted from OTM possesses biological activity. Therefore, a high-throughput screening approach is necessary. *In vitro* screening is a high-throughput approach ideal for both time and cost efficiencies. The human neuroblastoma cell line (SH-SY5Y) was used in this study. Prior to screening for OSLP protective potential, its cytotoxic activity was evaluated. The selected OSLP doses (25, 125, 250, 500 and 1000 µg/mL; 24- and 48-h) have demonstrated considerably low cytotoxic effects on the neuronal cells. Moreover, OSLP has demonstrated protective potential in SH-SY5Y cells challenged by hydrogen peroxide (H_2O_2). H_2O_2 is a

chemical stress inducer. H_2O_2 insults have been prevalently reported in different neurological disorders including neuroexcitation, neuroinflammation, and neurotoxicity, just to name a few (Feeney et al., 2008; van der Vliet & Janssen-Heininger, 2014; Wittmann et al., 2012). OSLP pre-treatments (250, 500, 1000 µg/mL; 24-h) has increased the survival of cells (39%, 51% and 57%) induced by 150 µM H_2O_2 (IC_{50} value determined). Bright-field imaging has also captured microscopic images of improved cell architecture (pyramidal-shaped cells with apparent neurite formations) and reduced dead cells (as round-shaped, clustered cells). Cell lysis extracted the proteins from the H_2O_2-induced cells pre-treated with OSLP (250, 500, 1000 µg/mL; 24-h). The proteins were analyzed by mass spectrometry-based label-free quantitative proteomic technique (LFQ). LFQ provides a fast and low-cost measurement of protein expression levels in complex biological samples in the area of discovery proteomics (Zhu, Smith, & Huang, 2010). In combinations with functional analysis and systemic pathway enrichment analysis, the neuroprotective mechanism of OSLP (1000 µg/mL, 24-h) was elucidated. Findings obtained have shown that OSLP is potentially neuroprotective by acting as an anti-inflammatory agent and antioxidant. In this study, it is suggested that the predominant neuroprotective action of OSLP is modulated via the “Signalling of Interleukin-4 and Interleukin-13” pathway. It is also suggested that OSLP could exert its antioxidative potential by modulating “Attenuation Phase” and “HSP90 Chaperone Cycle for Steroid Hormone Receptors” pathways. Last but not least, it is shown that OTM has not only successfully extracted OSLP but it has also preserved the biological activity of OSLP extracted and this permits further explorations for OSLP biological activity.

Additionally, this study also investigated the neuroprotective potential of OSLP in a vertebrate system using adult zebrafish (*Danio rerio*). Two different zebrafish models were used; PTZ injection (170 mg/kg, i.p.) and double challenge (hypoxia induction for 15 - 18 min on average) followed by PTZ injection (170 mg/kg, i.p.), a new zebrafish model which was not studied before. The zebrafish model has been widely used as an *in vivo* high-throughput model in studying mechanisms of CNS functions and dysfunctions important for drug discovery (Stewart, Braubach, Spitsbergen, Gerlai, & Kalueff, 2014). It is a promising species because the genetic profile of zebrafish share approximately 70% similarity with humans and express approximately 84% of known human disease related genes (Howe et al., 2013; Norton & Bally-Cuif, 2010). OSLP safety profile was evaluated before screening for its anticonvulsive potential. The selected OSLP doses administered via intraperitoneal route (50 - 800 µg/kg of b.w., i.p.; 96-h) in zebrafish were found safe and thereby, the maximal safe starting dose of OSLP (800 µg/kg of b.w.) was used as the

treatment dose in both zebrafish models. The selection was based on three reasons: (1) safety study of OSLP has found concentration greater than 800 µg was lethal, (2) to achieve the maximum protective potential of OSLP at a safe concentration, 800 µg is an optimal treatment dose and (3) the limit of considerably low yield of OSLP (approximately 0.3%) in a laboratory doing fundamental research.

In the PTZ-injected seizures model, OSLP pre-treatment (800 µg/kg, i.p.; 30 min) has demonstrated improvements in the behavioral profiles; seizure profile (lower score and prolonged onset time), locomotor activity (reduced erratic swimming movements and bottom-dwelling habit) and neurotransmitter profile (decreased excitatory glutamate, Glu; increased inhibitory gamma-Aminobutyric acid, GABA). Tissue lysis extracted the brain proteins and was analyzed by mass spectrometry-based LFQ. OSLP pre-treatment has increased the protein expression of Complexin 2 (Cplx2), an ortholog to human CPLX2 protein. Cplx2 binds to the SNARE complex to modulate normal calcium-evoked neurotransmitter release during presynaptic vesicle exocytosis. Bioinformatics analysis has proposed that OSLP is most likely to regulate the release of neurotransmitters, GABA and Glu, via the calcium-dependent synaptic vesicle exocytosis mediated by the “Synaptic Vesicle Cycle” pathway. Taken together, the findings collectively suggest the neuroprotective potential of OSLP as an anticonvulsant.

In the double challenge model, hypoxia induction followed by PTZ injection has created a hypoxic-ischaemic condition that can lead to hypoxic-ischaemic injury capable of eliciting epilepsy (Scully, 2014; Sutter et al., 2013). This zebrafish model has never been established before as there is no prior published scientific evidence; Kubová and Mareš (2007) established an immature Wistar albino rats model using a simulation of hypobaric hypoxia followed by PTZ injection. As such, this study represents the first of its kind. In this study, hypoxia induction followed by PTZ injection has sufficiently provoked convulsive activity in the zebrafish. More so, the double challenge has influenced the efficiency of OSLP pre-treatment (800 µg/kg i.p., 30 min), with a subtle anticonvulsive effect seen. OSLP pre-treatment has demonstrated improvements in the behavioral profiles; seizure profile (lower score and prolonged onset time), locomotor activity (less erratic swimming patterns) and neurotransmitter profile (lower excitatory glutamate, Glu). Tissue lysis extracted the brain proteins and was analyzed by mass spectrometry-based LFQ. OSLP pre-treatment has increased the protein expression of glutamine synthetase (Glula), an ortholog to human GLUL protein. Glula encodes for the mitochondrial enzyme glutamine synthetase which is required to keep the GABA-Glu-Gln (glutamine) cycle in check. Whereas, OSLP pre-

treatment also increased the protein expressions of Enolase 2 (Eno2) and Isocitrate dehydrogenase 2 (Idh2) in the hypoxic but seizure-free zebrafish. These proteins promote anaerobic metabolism in neurons under hypoxic conditions. Taken together, this study suggests that OSLP is most likely to influence the synaptic transmission by providing hypoxic-ischaemic tolerance to the synapses via the “Glutamatergic Synapse” and “GABAergic Synapse” pathways, in addition to modulating cellular energy metabolism in neurons via the “HIF-1 Signalling” and “Citrate Cycle” pathways. Taken together, the findings collectively suggest that OSLP is capable to provide hypoxic-ischaemic tolerance to disrupted synaptic transmission. The neuroprotective potential of OSLP as an anticonvulsant has seen a subtle effect in a hypoxic-ischaemic condition.

6.1.1 Conclusion

The findings in this study provide new insights into (1) the protein extraction method from OS leaf sample using OTM achievable at laboratory scale, (2) the neuroprotective potential of OSLP against H_2O_2 stress, (3) the anticonvulsive potential of OSLP under a normal condition and a hypoxic-ischemic condition. It is postulated that the OSLP may be an interesting candidate for future investigation as a dietary supplement or adjuvant in CNS disorders.

6.1.2 Future Directions:

There are recommendations for future studies.

OSLP is a mixture of active proteins. Due to the complexity, the protective action of an isolated protein may not be well elucidated. Fractionation and purification will be good strategies to reduce the intricacy of OSLP. The selected fractions can be screened for their biological activities, not limited only to neuroprotective potential; characterized for their molecular functions and further purified to isolate a specific protein target which holds accountable for a specific protection. For this purpose, a reverse-phase high-performance liquid chromatography (RP-HPLC) is recommended. RP-HPLC is particularly useful for peptides and protein analysis with advantages such as excellent resolution of molecules separation, experimentally easy to manipulate mobile phase changes, high recovery and productivity and good reproducibility. Using analytical RP-HPLC, the purify of a protein can be evaluated. The purified protein can further be estimated for peptide and protein masses using nanospray ESI-LC-MS/MS. These strategies allow the quantification and identification of a protein within a specific time frame.

Protein docking, a molecular modeling method, represents another powerful approach. Assisted by computer science algorithms and techniques, it aims to predict the mutual orientation and position of two molecules forming a complex. One of the molecules is a protein, the other could be another protein, a nucleic acid chain or a smaller molecule. Using the protein-ligand docking approach, the structures of proteins can be predicted with high accuracy regardless of the types of ligands, such as protein-protein docking and protein-small molecule docking. The proteins purified from OSLP can therefore be elucidated more efficiently, in terms of (1) 3-dimensional structures of molecules, (2) hydrophobicity or hydrophilicity, (3) binding affinity calculated through scoring functions and (4) flexibility or rigidity of the backbone. This will allow the identification of a specific protein target with its specific activity after purification by RP-HPLC.

Gene expression study will be another interesting aspect for more in-depth insights into the neuroprotective actions of OSLP elucidated in this study. Microarray analysis extremely powerful to efficiently detect the expression of thousands of genes at the same time. The data gathered through microarrays can be used to create gene expression profiles that show simultaneous changes in the expression of many genes in response to a particular experimental condition. In combination with systemic pathway analysis, this strategy will allow the identification and visualization of specific gene targets with their respective molecular actions in diverse cellular pathways.

In the past, the OS leaves were only used to extract for their rich small molecules (secondary metabolites) and then were disposed. This study has revealed the neuroprotective actions of OSLP at pre-clinical stages extracted using the OTM protocol. OTM is a scalable and reproducible protein extraction protocol. The final yield of OSLP can be adjusted according to the amount of LN_2-flash-frozen leaf sample and the volume of solvents. The production of OSLP on a large scale is therefore achievable. OTM is not only applicable for the extraction of protein alone, it can also be used to extract diverse materials encompassing primary metabolites (i.e. starch and plant cell wall components), small molecules and lipids, from a single sample. Therefore, OTM will be useful to maximize the extractable and identifiable materials from the OS leaves without the demand of additional inputs. This will also contribute to reducing the wastage of natural resources, which may be reused in healthcare instead of disposed after a single use (only extract for small molecules). In the long run, OTM may be considered as an extraction strategy with decent economic efficiency alongside environmental sustainability.

References:

Choo, B. K. M., Kundap, U. P., Kumari, Y., Hue, S.-M., Othman, I., & Shaikh, M. F. (2018). Orthosiphon stamineus Leaf Extract Affects TNF-α and Seizures in a Zebrafish Model. *Frontiers in Pharmacology, 9*, 139. doi:10.3389/fphar.2018.00139

Howe, K., Clark, M. D., Torroja, C. F., Torrance, J., Berthelot, C., Muffato, M., . . . Stemple, D. L. (2013). The zebrafish reference genome sequence and its relationship to the human genome. *Nature, 496*(7446), 498-503. doi:10.1038/nature12111

Kim, G.-D., Park, Y. S., Jin, Y.-H., & Park, C.-S. (2015). Production and applications of rosmarinic acid and structurally related compounds. *Applied Microbiology and Biotechnology, 99*(5), 2083-2092. doi:10.1007/s00253-015-6395-6

Kubová, H., & Mareš, P. (2007). Hypoxia-induced changes of seizure susceptibility in immature rats are modified by vigabatrin. *Epileptic Disorders, 9*(5), 36-43.

Norton, W., & Bally-Cuif, L. (2010). Adult zebrafish as a model organism for behavioural genetics. *BMC Neuroscience, 11*(1), 90. doi:10.1186/1471-2202-11-90

Saidan, N. H., Hamil, M. S. R., Memon, A. H., Abdelbari, M. M., Hamdan, M. R., Mohd, K. S., . . . Ismail, Z. (2015). Selected metabolites profiling of Orthosiphon stamineus Benth leaves extracts combined with chemometrics analysis and correlation with biological activities. *BMC Complementary and Alternative Medicine, 15*, 350. doi:10.1186/s12906-015-0884-0

Stewart, A. M., Braubach, O., Spitsbergen, J., Gerlai, R., & Kalueff, A. V. (2014). Zebrafish models for translational neuroscience research: from tank to bedside. *Trends in neurosciences, 37*(5), 264-278. doi:10.1016/j.tins.2014.02.011

Zhu, W., Smith, J. W., & Huang, C.-M. (2010). Mass Spectrometry-Based Label-Free Quantitative Proteomics. *Journal of Biomedicine and Biotechnology, 2010*, 840518. doi:10.1155/2010/840518

Appendices

Appendix I

	Methods	Descriptions
	Non-freeze-dried	Slurry paste, sticky
	Freeze-dried	Fine powder, dry
	Liquid nitrogen (LN_2) flash-frozen	Very fine powder, frozen

Figure 1 shows different leaf samples of OS.

Appendix II

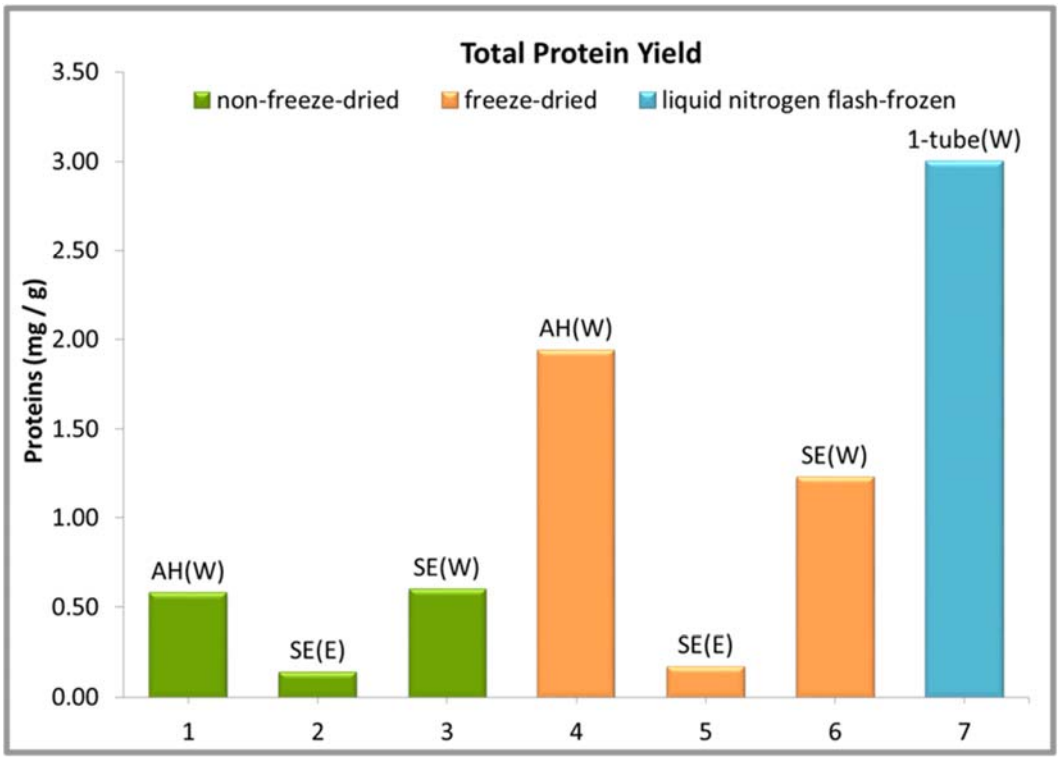

Figure 2 Comparison of protein yields using different leaf samples and extraction methods (Chapter 2). AH, acetone/water; SE, sequential extraction; E, ethanol; W, water; 1-tube, OTM.

Appendix III

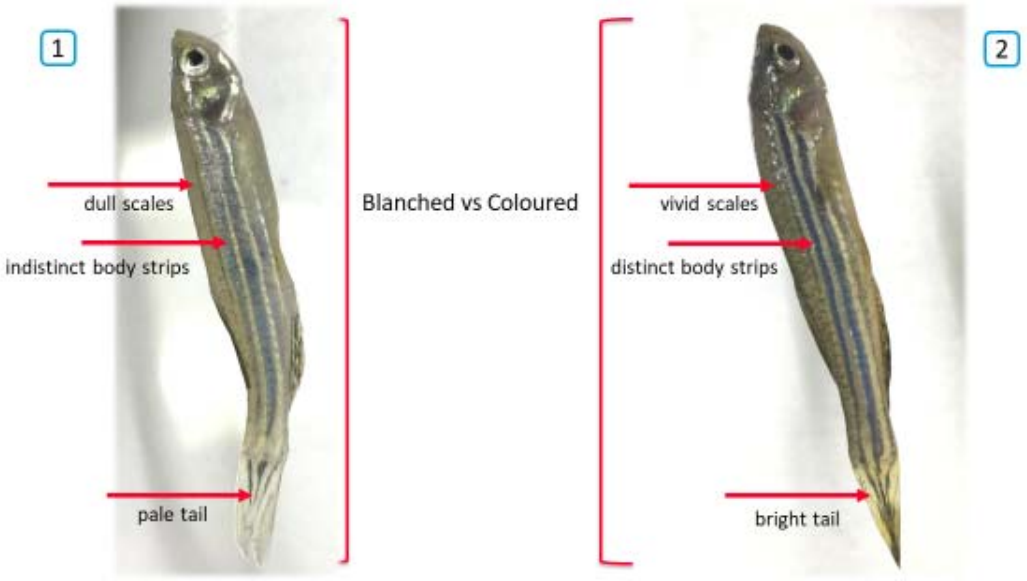

Figure 3 (1) shows a hypoxic zebrafish. As seen, the hypoxic zebrafish had indistinct body strips when compared to the non-hypoxic zebrafish in **Figure 3 (2)**. The hypoxic zebrafish displayed a pale tail and dull scales but in contrast, the non-hypoxic zebrafish had a bright tail with vivid scales. Overall, the non-hypoxic zebrafish displayed vibrantly colored physical but the hypoxic zebrafish were blanched (Chapter 5).

Appendix IV

International Journal of
Molecular Sciences

MDPI

Review

Treatment, Therapy and Management of Metabolic Epilepsy: A Systematic Review

Vanessa Lin Lin Lee, Brandon Kar Meng Choo, Yin-Sir Chung, Uday P. Kundap, Yatinesh Kumari and Mohd. Farooq Shaikh *

Neuropharmacology Research Laboratory, Jeffrey Cheah School of Medicine and Health Sciences, Monash University Malaysia, Bandar Sunway, 47500 Subang Jaya, Selangor, Malaysia; vanessa.lee1@monash.edu (V.L.L.L.); brandon.choo@monash.edu (B.K.M.C.); chung.yinsir@monash.edu (Y.-S.C.); uday.kundap@monash.edu (U.P.K.); yatinesh.kumari@monash.edu (Y.K.)
* Correspondence: farooq.shaikh@monash.edu; Tel.: +60-355-14-4483

Received: 20 February 2018; Accepted: 13 March 2018; Published: 15 March 2018

Abstract: Metabolic epilepsy is a metabolic abnormality which is associated with an increased risk of epilepsy development in affected individuals. Commonly used antiepileptic drugs are typically ineffective against metabolic epilepsy as they do not address its root cause. Presently, there is no review available which summarizes all the treatment options for metabolic epilepsy. Thus, we systematically reviewed literature which reported on the treatment, therapy and management of metabolic epilepsy from four databases, namely PubMed, Springer, Scopus and ScienceDirect. After applying our inclusion and exclusion criteria as per the Preferred Reporting Items for Systematic Reviews and Meta-Analyses (PRISMA) guidelines, we reviewed a total of 43 articles. Based on the reviewed articles, we summarized the methods used for the treatment, therapy and management of metabolic epilepsy. These methods were tailored to address the root causes of the metabolic disturbances rather than targeting the epilepsy phenotype alone. Diet modification and dietary supplementation, alone or in combination with antiepileptic drugs, are used in tackling the different types of metabolic epilepsy. Identification, treatment, therapy and management of the underlying metabolic derangements can improve behavior, cognitive function and reduce seizure frequency and/or severity in patients.

Keywords: metabolic epilepsy; metabolic disorders; antiepileptic drugs; dietary therapy; seizures; cognitive function

Appendix V

Awards

• AOCN Travel Grant		USD 500.00
• MSN Education Grant	Chapter General Neurology	MYR1,500.00
• MSN Education Grant	Chapter Epilepsy	MYR1,500.00
• MUM Graduate Research Travel Subsidy		MYR3,000.00

Conferences / Seminars

- 16th Asian Oceanian Congress of Neurology
  Date of Event: 08-11 November 2018
  Poster Presentation: Protective Potential of *Orthosiphon Stamineus* Leaf Protein against Hydrogen Peroxide-Induced Neurotoxicity
  Venue of Event: Seoul, South Korea

- Cure Epilepsy Seminar and Research Meeting (as Organising Committee)
  Date of Event: 28 February 2018
  Venue of Event: Monash University, Malaysia

- 3rd Malaysian Zebrafish Workshop
  Date of Event: 27 November 2019
  Poster Presentation: *Orthosiphon stamineus* Proteins Alleviate Pentylenetetrazol-Induced Epileptic Seizure in Zebrafish
  Venue of Event: Universiti Malaya, Malaysia

Workshop

- Agilent's Integrated Biology Workshop 2018
  Date of Event: 05-06 December 2018
  Venue of Event: Monash University, Malaysia